The role of *Drosophila* Golgi matrix proteins in the early exocytic pathway

Evangelos Kondylis

PhD

The University of Edinburgh

2004

Abstract

The relationship between the stacked architecture of the Golgi apparatus and the transitional ER (tER) organisation has recently been subject of intense research and has influenced our view on how the Golgi apparatus is formed. The proposed model of *de novo* formation of the Golgi complex, together with comparative studies in yeast have suggested that the organisation and integrity of the tER is reflected in the Golgi architecture. Additionally, a group of proteins, the Golgi matrix proteins, have also been implicated in the formation and maintenance of the Golgi apparatus.

During the course of this study, the role of *Drosophila* homologues of Golgi matrix proteins in the organisation of the early exocytic pathway (tER and Golgi) was investigated. dp115, dGM130 and dGRASP were depleted from *Drosophila* S2 cells by RNA interference. Using electron and immunofluorescence microscopy, dp115 depletion was shown to result in Golgi stack breakdown and tER dispersion. The effect on tER organisation was specific for dp115, as depletion of the other Golgi matrix proteins did not have a similar effect. Although, single depletion of dGRASP or dGM130 did not lead to a quantitative disruption of the Golgi morphology, dGM130/dp115 and dGM130/dGRASP double depletions pointed to genetic interactions for building and/or maintenance of the Golgi stacks.

Considering the key role of the Golgi apparatus in protein transport along the exocytic pathway, anterograde transport of plasma membrane protein Delta, from its site of synthesis (ER) to its final destination, was monitored in cells depleted of the above mentioned Golgi matrix proteins. Surprisingly, none of the depletions, including dp115 that alters considerably the organisation of the exocytic pathway, led to a significant inhibition of intracellular transport.

Anterograde intracellular transport in the absence of Golgi stacks exists physiologically during *Drosophila* development. In a morphological study performed in imaginal discs during the transition from early 3rd instar larva to white pupa, the biogenesis of the Golgi stacks from vesicular-tubular larval clusters was described. These larval clusters were shown to contain several Golgi-specific markers and, therefore seem capable of carrying out proper Golgi functions. This biogenetic event is regulated by 20-hydroxyecdysone, through alteration in expression of Golgi-related genes. Overall, this study suggests that at specific developmental stages and tissues, a functional Golgi apparatus may not exhibit a stacked architecture and, this may explain why only a marginal inhibition of transport was observed in the absence of Golgi stacks in cultured S2 cells.

When setting out upon your way to Ithaca,
wish always that your course be long,
full of adventure, full of knowledge.

...

...

...

For Ithaca has given you the lovely trip.
Without her you would not have set your course.
There is no more that she can give.

If Ithaca seems then too poor, you have not been deceived.
As wise as you are now become, of such experience,
you will have understood what Ithaca stands for.

Constantinos P. Cavafis

Extracted from "Ithaka", 1911

Αφιερωμένο
στους γονείς μου

Contents

1. Chapter 1: Introduction

Chapter 2: Materials and Methods

Chapter 8: Discussion and future prospects

Chapter One

Introduction

1.1 The early exocytic pathway

The exocytic pathway of eukaryotic cells consists of distinct membrane-bound organelles, which are involved in protein and lipid biosynthesis and transport to endosomes/lysosomes, the plasma membrane or the extracellular medium. The endoplasmic reticulum, the transitional ER, the ER-Golgi intermediate compartment and the Golgi apparatus compose collectively the early exocytic pathway (Figure 1.1), and transport through them is a compulsory route followed by all secretory proteins, plasma membrane glycoproteins and lysosomal enzymes. Moreover, many of the resident proteins of these organelles follow the same route until reaching the correct compartment, where they are retained via different retention mechanisms. During their trafficking along the early exocytic pathway, these proteins are subjected to a number of post-translational modifications, which help them being properly sorted or activate their function. Finally, when they reach the trans-Golgi network (TGN), the different classes of proteins are sorted and exit from the Golgi apparatus leaving for their final destination. The exit from the TGN and subsequent forward transport is referred to as the late exocytic pathway (Farquhar and Hauri, 1997; Sanderfoot and Raikhel, 1999).

1.1.1 Endoplasmic Reticulum (ER)

The endoplasmic reticulum is single membrane organelle that forms an extensive maze-like network enclosing a single continuous lumen. It is one of of the subcellular organelles occupying the largest relative volume within a eukaryotic cell, and comprises discrete subdomains, such as the rough ER, the smooth ER and the nuclear envelope (Voeltz et al., 2002).

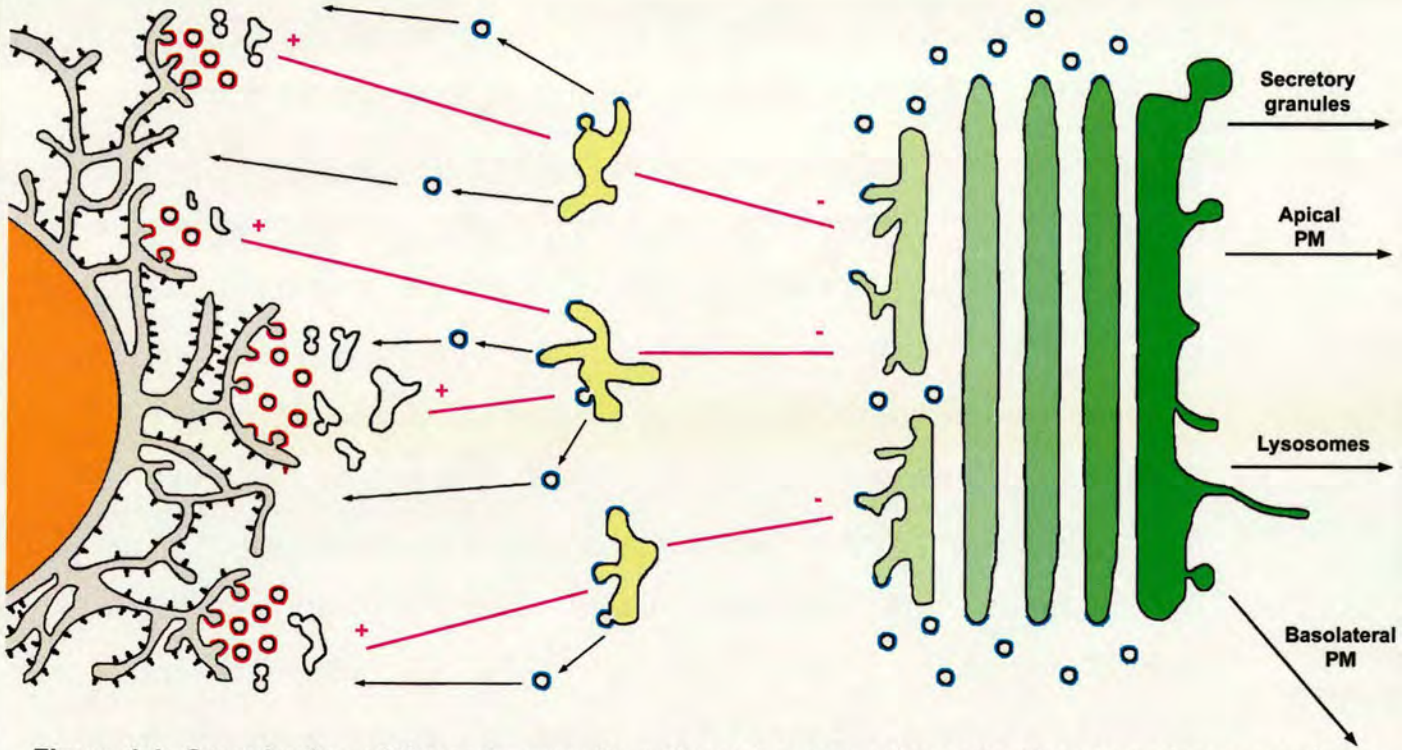

Figure 1.1: Organisation of the early exocytic pathway in mammalian cells. Secretory, plasma membrane and endosomal/lysosomal proteins are synthesised on ribosomes of the rough ER, translocated into the continuous ER lumen (grey), where they start being modified. Exit from ER takes place at specialised domains, the tER sites, and is mediated by COPII-coated vesicles (red). Soon after their budding, COPII vesicles fuse either homotypically or with pre-existing membranes forming the intermediate compartment (IC) elements (yellow). The IC membranes move towards the minus (-) end of microtubules (pink), transporting the cargo molecules to the Golgi apparatus (green shaded). During this movement, the IC elements are populated by COP I coats that form COP I-coated vesicles (blue), which mediate retrograde transport of ER resident proteins. Anterograde cargo proteins enter the Golgi apparatus at the CGN (light green), are modified as they pass through the Golgi stack, and finally, they are sorted at the TGN (dark green) and transported to their final destination. COP I vesicles bud also at the rims of the Golgi cisternae mediating retrograde and possibly anterograde traffic, although the latter is still debatable. The nucleus is labelled in orange. This simplified scheme represents the sequence of transport steps taking place along the exocytic pathway and does not depict the actual position of the different organelles in a mammalian cell. See text for more details.

The rough ER is defined by the associated ribosomes, where translation of secretory, transmembrane and lysosomal proteins takes place (Voeltz et al., 2002). The translation of these proteins starts on free ribosomes, which become associated with the ER membranes through the signal recognition particle that binds to the signal peptide of these proteins (Nagai

et al., 2003). During their translation on rough ER membranes, the proteins are translocated through the translocon complex into the ER lumen, where they start undergoing modifications, including folding and N-linked glycosylation by ER resident enzymes (Roth, 1997). As an exception to this process, a group of integral membrane proteins, the C-tail anchored proteins, are synthesised and released in the cytosol and then become anchored to the ER membranes via a hydrophobic C-terminal domain. These proteins are modified and carry out their functions at the cytosolic face of all membranes they are bound to (Borgese et al., 2003).

1.1.2 Transitional ER sites (tER sites)

Once the ER-related modifications have been completed, the newly synthesised proteins leave the ER. This occurs at ER subdomains, known as transitional ER (tER) sites. "ER transitional elements" was the first term used to describe this compartment in pioneering studies following the transport of secretory proteins in pancreatic cells using a combination of electron microscopy and autoradiography (Palade, 1975). This term reflected the morphology of the tER sites, as small, tubular ER regions, which are devoid of ribosomes and give rise to transport vesicles carrying proteins to the Golgi apparatus. More recently, other terms, such as "ER export complexes" and "ER exit sites" were used in an attempt to include the functional role of this compartment (Bannykh et al., 1996; Cole et al., 1996). However, the definition of ER export complexes encompasses both the ER budding profiles and the vesicular-tubular clusters (VTCs), which are situated in close vicinity to the tER sites (Figure 1.2; Bannykh et al., 1996; 1998). This has caused some confusion in the bibliography since the VTCs have been characterised as a separate intermediate compartment between the ER and the Golgi apparatus, at least in mammalian cells (see section 1.1.3). Furthermore, although tER

sites and VTCs are often very closely associated and exhibit convoluted membrane organisation, they can be distinguished by their content of different molecular markers (Klumperman, 2000).

Figure 1.2: Organisation of ER export sites according to Bannykh et al (1996). Three-dimensional reconstruction of a peripheral ER export site from serial thin sections. ER export sites comprise ER-associated buds (blue) characterised by the presence of COPII coats and facing the central region, and a collection of vesicular and tubular elements (VTCs) containing COPI coats (red). Green denotes the ER cisternae, while the intensity of each colour reflects distance from the top section (most intense). The fact that this description of ER export sites includes two distinct compartments (tER and IC) with different molecular markers (COPII and COPI) can be misleading. For example, a protein localisation at ER export sites does not necessarily refer to membranes still attached to ER cisternae. Instead, it could represent membranes completely dissociated from the ER. The picture is taken from Bannykh et al (1996).

The feature that has been widely used during the last decade to define the tER compartment is the presence of COPII protein coat. COPII protein coat was originally described in yeast to form coated vesicles that mediate exit of cargo from tER sites (Barlowe et al., 1994; Schekman, 2002), although other types of carriers have recently been proposed to exist *in vivo* (Aridor et al., 2001; Mironov et al., 2003).

The formation of the COPII coat involves the recruitment of at least 5 cytosolic components, the small GTPase Sar1p and two hetero-dimeric protein complexes, Sec23p-Sec24p and Sec13p-Sec31p (Barlowe et al., 1994; Barlowe, 2002). The coat assembly takes place in a stepwise fashion (Figure

1.3). Initially, Sec12p[1], a guanine nucleotide exchange factor (GEF) that is concentrated at the tER sites, converts cytosolic GDP-bound Sar1p to Sar1p-GTP. This promotes its association with the tER membranes. Sar1p-GTP recruits in turn the Sec23p-Sec24p sub-complex. Binding on Sar1p takes place through an interaction with Sec23p, while Sec24p selects different transmembrane protein cargos for subsequent transport. In the next stage of coat formation, Sec13p-Sec31p sub-complex is recruited and this leads to polymerisation of the coat and induces membrane curvature, driving the vesicle budding. Moreover, Sec13p-Sec31p binding increases the GTPase-activating (GAP) function of Sec23p, which triggers the GTP hydrolysis of Sar1p, and eventually the uncoating of the vesicles (Antonny et al., 2001; Barlowe, 2002).

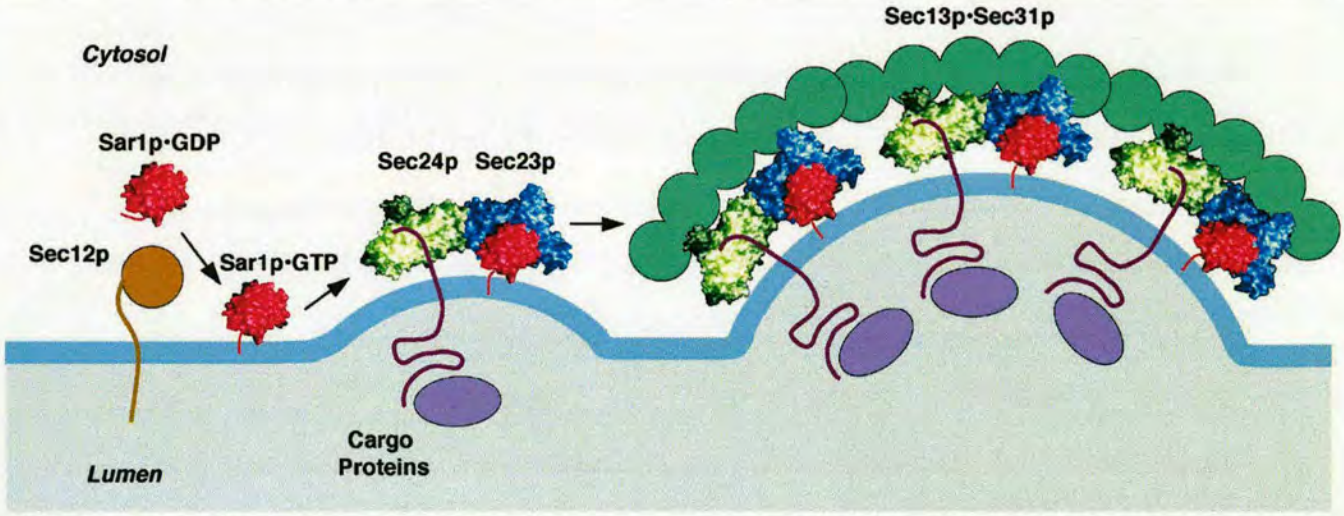

Figure 1.3: COPII coat assembly. Cytosolic Sar1p is activated when the associated GDP is exchanged for GTP by transmembrane protein Sec12p. Activated Sar1p becomes membrane bound and recruits Sec23p-Sec24p subcomplex, through its interaction with Sec23p. Sec24p is involved in transmembrane cargo protein selection. Finally, Sec13p-Sec31p subcomplex associates with the ternary complex leading to the polymerisation of the coat, deformation of the membrane and eventually, COPII vesicle budding. The depictions of Sar1p, Sec23p and Sec24p are surface representations from the crystal structure of these proteins (Bi et al., 2002). Taken from Bonifacino and Glick, 2004.

[1] After the submission of this thesis, a report by Soderholm et al. (2004) was published showing that contrary to the general belief, the concentration of yeast Sec12p at the tER sites is not essential for their organisation and the COPII coat assembly. See discussion for more details

The cargo molecules that leave the ER in COPII-coated vesicles need to be sorted from ER resident proteins. The sorting mechanism depends on the nature of each cargo molecule. Most transmembrane cargo proteins seem to exit the ER by being concentrated at the tER sites through direct interactions with COPII subunits, while some transmembrane and the majority of soluble cargo proteins are sorted by interacting with membrane receptors, such as members of p24 family (Bonifacino and Glick, 2004). The sorting signals recognised by COPII coat comprise di-acidic, di-basic and short hydrophobic motifs, longer sequences, or combinations of these motifs (Barlowe, 2003; Giraudo and Maccioni, 2003). The variety of sorting signals for the same sorting step can be sustained only if there are multiple binding sites on one COPII subunit, or a family of recognition proteins exists (Bonifacino and Glick, 2004). In support of this hypothesis, Sec24p, which seems to be the major COPII sorting subunit (Figure 1.3), contains at least three distinct sites for the recognition of different signal (Miller et al., 2003; Mollessova et al., 2003). Furthermore, three and four Sec24p paralogues exist in yeast and mammalian cells, respectively (Roberg et al., 1999; Kurihara et al., 2000; Tang et al., 1999). An additional mechanism has also been proposed, where soluble cargo molecules exit from tER sites without prior selection and become concentrated only in downstream compartments of the exocytic pathway (Martinez-Menarguez et al., 1999). However, this mechanism is more likely to apply for abundant secretory cargo (Klumperman, 2000).

Despite the fact that the molecular mechanism of COPII coat formation is an evolutionarily conserved feature of the tER sites, their organisation (size, number and distribution within the cells) varies significantly among the eukaryotes. For example, a typical mammalian cell exhibits about 200 small ER exit sites that distribute throughout the

cytoplasm and concentrate at the perinuclear area (Paccaud et al., 1996; Hammond and Glick, 2000). On the other hand, yeast *Pichia pastoris* has only 2-5 discrete tER sites at steady state (Rossanese et al., 1999). In marked contrast, in *S. cerevisiae*, the most common budding yeast and closely related to *Pichia*, tER sites have been visualised in light microscopy as many small dots scattered throughout the entire ER (Rossanese et al., 1999). Finally, the nature of tER sites in plant cells is not clear, as no direct visualisation has been performed to date. One model has proposed that the whole ER surface is able to produce COPII vesicles, whereas more recent models support that tER sites are formed at specific ER domains, but there is a disagreement whether these are fixed export sites or highly mobile (Neumann et al., 2003).

The visualisation of tER sites in mammalian cells (Stephens et al., 2000) and *Pichia pastoris* (Bevis et al., 2002) by live cell imaging has made clear that these sites exhibit very restricted movement once they are formed. This finding suggests that a tER matrix could be involved in the formation and maintenance of these apparently long-lived sites. Several key proteins have been identified in yeast, which are involved in COPII coat assembly and could be components of this putative matrix. One of these proteins is Sec12p, a type II transmembrane protein exhibiting GEF activity for Sar1p (Barlowe and Schekman, 1993). However, a recent study on *S. cerevisiae* and *P. pastoris* homologues of Sec12p (Soderholm et al., 2004) suggested that this Sar1p GEF is unlikely to be a crucial component of the tER matrix (see chapter 8 for more details). Sec16p, a peripheral protein tightly associated to the ER membranes has also been proposed to act as a putative scaffold protein at ER exit sites (Espenshade et al., 1995). Finally, Sed4p is a Sec12p homologue lacking its GEF activity for Sar1p, and unlike Sec12p, it binds to Sec16p (Gimeno et al., 1995; Saito-Nakano and Nakano, 2000). Furthermore, Sed4p has been suggested to function as a potential inhibitor of Sar1p GTP

hydrolysis (Saito-Nakano and Nakano, 2000). In mammalian cells, only a homologue for Sec12p has been identified, while the existence of Sec16p and Sed4p homologues remains unknown (Bonifacino and Glick, 2004). Therefore, it is likely that more proteins related to the organisation of the tER sites are bound to be discovered.

1.1.3 Intermediate Compartment (IC)

Once COPII coated vesicles containing cargo molecules bud from the tER sites, they rapidly shed their coat (Antonny et al., 2001) and fuse either homotypically to form *de novo* the IC compartment, or with a pre-existing IC compartment near the tER site (Figure 1.1; Stephens et al., 2000). Other commonly used terms for the IC are vesicular-tubular clusters (VTC) (Bannykh et al., 1996) or ER to Golgi intermediate compartment (ERGIC) (Hauri and Schweizer, 1992), which reflect the morphological features and its position in the exocytic pathway. At the molecular level, the most widely used IC marker is ERGIC53/58, a transmembrane protein that actively cycles between the ER, ERGIC and the cis-Golgi, but at steady state its majority localises in the IC (Hauri et al., 2000). ERGIC53/58 exhibits lectin-binding properties, and was shown to act as receptor for sorting and transport of N-linked glycosylated proteins from ER to IC (Appenzeller et al., 1999).

In terms of function, the IC is the first place along the exocytic pathway, where segregation between anterograde and retrograde transport occurs (Stephens and Pepperkok, 2001). An important role in this cargo segregation step is mediated by another protein coat, the COP I coat (Duden, 2003). Similar to COPII coat, COP I coat formation is initiated by a small GTPase called Arf1 (ADP ribosylation factor 1). Membrane association of Arf1 triggers the recruitment of seven other coat subunits (α-, β-, β'-, γ-, δ-, ε- and ζ-COP). The established function of COP I in the IC is the sorting of

retrograde cargo (e.g. KDEL-receptor ERD2 or proteins containing a di-lysine motif) and its transport back to the ER (Cosson and Letourneur, 1994; Duden, 2003). Co- visualisation of fluorescently labelled anterograde cargo and COP I subunits has revealed a progressive segregation of COP I-rich and cargo-rich domains on IC elements (Shima et al., 1999). This is also supported by EM data showing that secretory proteins were excluded from COP I-coated tips of the IC membranes, where KDEL receptor and recycling components of the transport machinery localise (Martinez-Menarguez et al., 1999). This active selection of retrograde cargo by COP I has also been proposed to contribute in concentration of anterograde soluble cargo (Martinez-Menarguez et al., 1999). Time-lapse confocal microscopy has demonstrated a sequential mode of action between the COPII- and COP I-coated membrane structures (Stephens et al., 2000). This has permitted to use the localisation of subunits of the two coats as markers for the tER sites and the IC (Martinez-Menarguez et al., 1999), which are often not easily distinguishable by morphology due to their close proximity and vesicular-tubular appearance (Figure 1.2).

The distribution of the intermediate compartment is similar to that of tER sites with some of them located at the cell periphery, while the majority is concentrated in the juxtanuclear area (Hammond and Glick, 2000; Stephens et al., 2000). However, contrary to the stable nature and restricted movement of tER sites, IC elements are very dynamic (Presley et al., 1997; Scales et al., 1997). In fact, the dynamic and transient nature of this compartment is probably the reason why only few IC resident proteins have been found and its boundaries are still unclear (Bannykh et al., 1998; Farquhar and Palade, 1998). Peripheral IC elements have been described to move soon after their formation towards the perinuclear area, where the Golgi apparatus is found (Figure 1.1; see next paragraph). This rapid, centripetal, long-distance

movement of IC membrane structures is dependent on the microtubule minus-end directed motor complex of dynein-dynactin (Presley et al., 1997). This necessity for long-range transport from peripheral tER sites to the Golgi apparatus seems to be the reason for the identification and characterisation of IC as a separate compartment, in mammalian cells. In other eukaryotes that do not seem to need long-distance carriers for ER to Golgi transport, a compartment equivalent to IC has not been defined (Glick, 2000).

1.1.4 Golgi apparatus

The post-IC station in the exocytic pathway is the Golgi apparatus (Figure 1.1). Since its discovery by Camilio Golgi, more than a century ago, Golgi is probably the most hotly debated organelle concerning the relationship between its structural organisation and the functions it performs (Farquhar and Palade, 1998; Marsh and Howell, 2002).

1.1.4.1 Structural organisation

The Golgi apparatus is one of the most striking intracellular organelles of a eukaryotic cell due to its unique architecture. In a typical mammalian cell, the Golgi apparatus consists of a series of flattened membrane compartments, called cisternae, which are closely apposed and aligned in parallel to form a stack (Figure 1.4; Rambourg and Clermont, 1997; Ladinsky et al., 1999). On either side of the Golgi stack lays a tubular-vesicular network; the cis-Golgi network (CGN) that makes up the entry side for the exocytic cargo and, the trans-Golgi network (TGN), which is situated at the exit side (Figure 1.4). The existence of two functionally distinct sides gives the Golgi stack a polarised organisation and arranges the cisternae in cis-, medial- and trans-cisternae. Mammalian cells exhibit dozens of Golgi stacks per cell, which in three-dimensional reconstructions appear to be interconnected between the equivalent cisternae by thin tubules (Figure 1.4).

As a result, the mammalian Golgi apparatus is organised as a single–copy reticulum, also known as Golgi ribbon (Rambourg and Clermont, 1997).

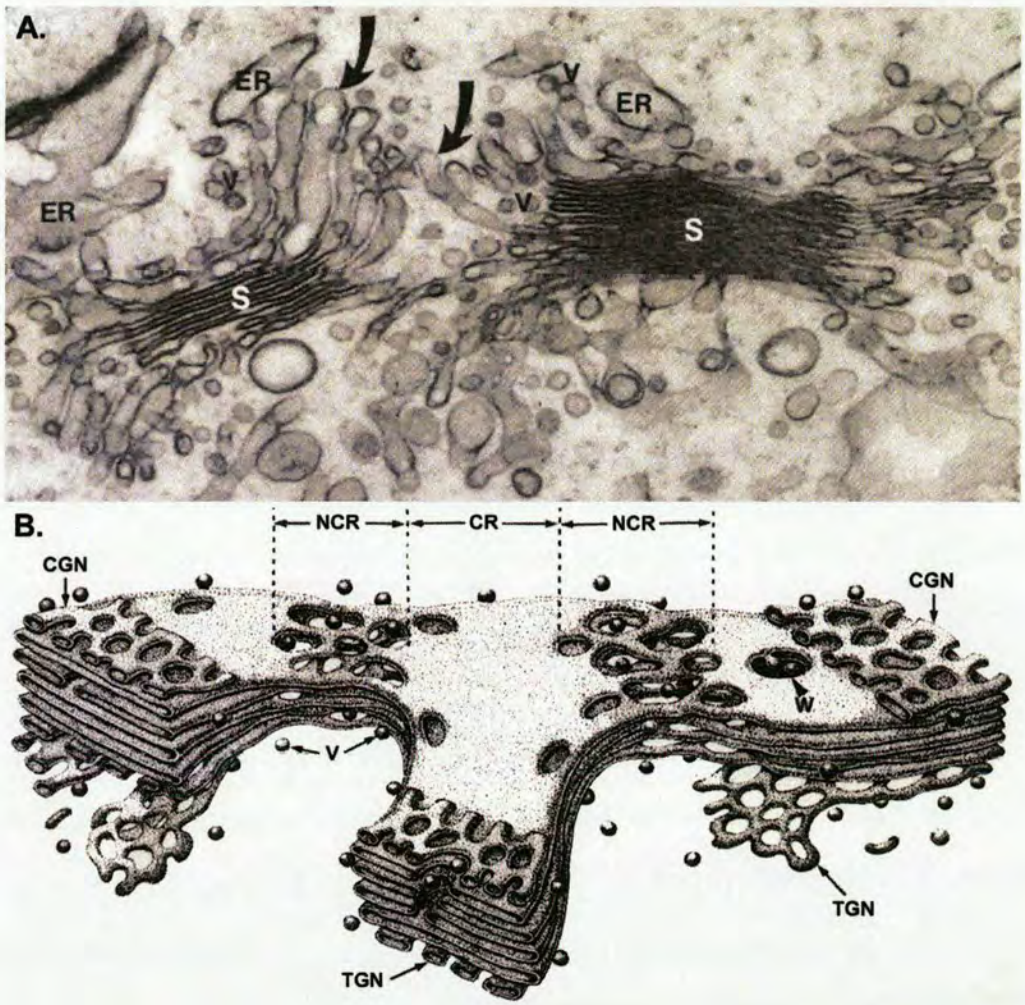

Figure 1.4: Organisation of the mammalian Golgi apparatus. A. Electron micrograph showing two Golgi stacks (S) out of dozens that form the mammalian Golgi ribbon. Vesicles (V) are found all around the Golgi stacks and the associated tubules (curved arrows) connect the cisternae of neighbouring Golgi stacks. Taken from Clermont et al., 1994. B. Three-dimensional diagram of a small part of the Golgi ribbon from a spinal ganglion cell. Two types of regions are illustrated; the compact regions (CR) that comprise stacked, poorly fenestrated Golgi cisternae and the non-compact regions (NCR) that are composed of fenestrated tubular membranes interconnecting the adjacent Golgi stacks. Parts of the cis-Golgi network (CGN) and trans-Golgi network (TGN) are also illustrated. TGN appears highly fenestrated and at a final stage, it is detached from the Golgi stack. Small vesicles are seen in compact regions, where the cisternae are perforated forming wells (W), and also at the rims of the Golgi ribbon and in non-compact areas. Adapted from Rambourg and Clermont, 1997.

The subcellular localisation of the mammalian Golgi ribbon is very characteristic. It occupies a central part of the cell, capping the nucleus and close to the centrosome, which serves as a microtubule-organizing centre (MTOC) (Rios and Bornens, 2003). This does not seem to be a coincidence, as the existence of the Golgi apparatus as a single copy organelle depends on microtubule integrity. Treatment of mammalian cells with microtubule depolymerisation drugs induces fragmentation of the Golgi ribbon into small Golgi stacks that are dispersed in the cytoplasm (Thyberg and Moskalewski, 1999; see also section 1.4.2.2). In addition to microtubules, the actin cytoskeleton has also been implicated in the integrity of the Golgi apparatus (Valderrama et al., 1998; Babia et al., 1999; di Campli et al., 1999). A plausible candidate for linking the cytoskeleton elements with the Golgi membranes is spectrin and its associated proteins, which form a skeleton surrounding the Golgi apparatus (Beck and Nelson, 1998). Spectrin skeleton is thought to facilitate Golgi membrane anchoring to the microtubule and microfilament networks through its interactions with motor proteins, including cytoplasmic dynein, kinesin and myosins. In this way, cytoskeleton elements could control the membrane organisation, stability and shape of the Golgi apparatus (de Matteis and Morrow, 2000).

The minimal organisation of the Golgi apparatus (a Golgi stack with the abutting networks) has been conserved throughout the evolution of eukaryotes, from diplomonad *Giardia lamblia* to mammals (Shorter and Warren, 2002). However, the organisation of the Golgi ribbon seems to be a specific feature developed in mammalian cells. In plants and lower animal cells, like yeast and *Drosophila*, Golgi apparatus appears under the form of many discrete Golgi stacks remaining dispersed throughout the cytoplasm (Rossanese et al., 1999; Rabouille et al., 1999; Neumann et al., 2003).

Furthermore, parameters, such as the number of Golgi stacks per cell or the cisternae per stack, seem to be organism and tissue specific.

1.1.4.2 Functions

Besides its remarkable architecture, the Golgi apparatus also performs important functions. First, it is involved in post-translational processing of newly synthesised proteins and lipids (e.g. glycosylation, phosphorylation, sulphation) carried out by Golgi resident enzymes. Protein glycosylation is the best-characterised modification and comprises the N-linked and O-linked glycosylation, where the oligosaccharide side-chain is bound on an asparagine or a serine/threonine residue, respectively (Roth, 1997). The two types of glycosylation seem to differ significantly. N-glycosylation starts already during the translocation of nascent proteins into the ER lumen, while for O-glycosylation, the localisation of the initial reaction in the Golgi apparatus suggests that it occurs exclusively in this organelle (Deschuyteneer et al., 1988; Roth, 1997). Moreover, N-glycosylation comprises first the *en bloc* addition on the protein of a lipid-bound, high-mannose oligosaccharide, which is then trimmed, before additional glycan residues are added. In contrast, O-glycosylation involves the sequential biosynthesis of sugars with classical glycosyltransferase reactions, without the addition of lipid-linked preassembled oligosaccharide (Roth, 1997). The topology of N-glycosylation enzymes by immuno-electron microscopy has shown that their distribution is usually confined to 2 adjacent cisternae (Rabouille et al., 1995c), and is cell-type dependent (Velasco et al., 1993). This localisation of the glycosylation enzymes could sustain partly their sequential mode of action, since enzymes participating in early N-glycosylation reactions localise in earlier Golgi cisternae than those enzymes involved in the final glycosylation steps (Kornfeld and Kornfeld, 1985). Although this could provide a reason for the organisation of Golgi apparatus in stacks, it cannot explain the observed

overlapping enzyme distribution on the same cisterna (Rabouille et al., 1995c). Nevertheless, this overlap may create a unique biochemical composition in different Golgi cisternae, which could also be related to the mechanism of cisternal stacking (Rabouille and Nilsson, 1995).

In the Golgi apparatus, and particularly in TGN, precursor proteins undergo limited proteolysis, a process that is completed later in the secretory vesicles. This function is carried out by the family of proprotein convertases, and results in production of biologically active proteins and peptides destined for secretion or transport to the plasma membrane (Steiner, 1998). Polypeptides involved in a broad range of developmental events are substrates for these convertases, including neuropeptides (e.g. enkephalins), peptide hormones (e.g. insulin), growth factors, receptors, adhesion molecules, and many more (Taylor et al., 2003). The best-studied member of this family is furin, which exhibits a steady state localisation at the TGN and is often used as a molecular marker for it. Nevertheless, despite its TGN localisation, furin may not perform all its proteolytic activities in this compartment. Instead, TGN could serve as a pool of furin molecules, which become activated in post-TGN compartments (Thomas, 2002). Moreover, Rhomboid-1, a member of another conserved family of intramembrane serine proteases, called Rhomboids, was localised on the Golgi apparatus (Lee et al., 2001; Urban et al., 2001). This protease was shown to be important for the proteolytic cleavage of Spitz, a ligand for the *Drosophila* EGF receptor, providing a link between the Golgi functions and signalling events.

Another crucial Golgi function is the sorting of different groups of anterograde and retrograde protein cargo (Short and Barr, 2000). The CGN and the cis-Golgi cisterna could be viewed as an extension of the intermediate compartment in terms of sorting activity, because there, the sorting of anterograde cargo from cargo receptors (e.g. ERGIC53/58) and

transport machinery that need to be recycled back to the ER is completed (Duden, 2003). Like in the intermediate compartment, COP I coat is believed to mediate this retrograde transport step. In agreement with this proposal, COP I coat subunits have been localised predominantly at the cis side of the Golgi (Oprins et al., 1993). Additionally, COP I coated areas exist at the rims of the Golgi cisternae and on vesicles found in close proximity to the Golgi stack (Oprins et al., 1993; Orci et al., 1997). Whether these COP I-coated vesicles are involved both in anterograde and retrograde transport through the Golgi stack is a matter of intense debate (Marsh and Howell, 2002; see models of Golgi biogenesis). Finally, the major station for active sorting of anterograde cargo molecules is the trans-Golgi cisterna and the TGN. The sorting of lysosomal enzymes, as well as the segregation of regulated from constitutively secreted proteins and apical from basolateral plasma membrane proteins in polarised cells take place at this Golgi sub-compartment (Farquhar and Hauri, 1997). Once they are properly sorted, the different groups of cargo are packaged into distinct vesicular or tubular carriers and transported to their final destination (Lippincott-Schwartz et al., 2000).

1.2 Golgi biogenesis: models and debates

1.2.1 Vesicular transport stable compartment versus cisternal maturation

Intracellular transport to and through the Golgi apparatus, especially in the anterograde direction, has been one of the long-standing debates concerning this organelle (Marsh and Howell, 2002). This debate is related to how cargo moves from the intermediate compartment to the cis-Golgi and whether the COP I-coated vesicles move both in anterograde and retrograde direction or only in a retrograde fashion (Schekman and Mellman, 1997).

Two main mechanisms have been proposed for forward movement of cargo. The first one is the **vesicular transport stable compartment model** (Figure 1.5A), which considers the Golgi apparatus as a stable compartment and suggests that anterograde cargo transport from one Golgi cisterna to the next is performed by vesicles (Elsner et al., 2003). These vesicles were proposed to be a population of COP I-coated vesicles, which participate in the anterograde transport and are distinct from those COP I vesicles that are involved in retrograde recycling of the transport machinery (Orci et al., 1997). According to this static view of the Golgi stack, a need for recycling of Golgi resident enzymes is not predicted, since they are not meant to move. The problem with the vesicular transport stable compartment model begins in the attempt to reconcile the predictions deriving from it and the obtained experimental data. Immuno-electron microscopy studies have tried to investigate the content of the peri-Golgi COP I-coated vesicles generating controversial results, even when the experimental conditions were identical. One report showed that anterograde cargo VSV-G (vesicular stomatitis virus G-protein) was included in COP I vesicles (Orci et al., 1997), while resident enzyme α-Mannosidase II was largely excluded (Cosson et al., 2002). On the other hand, an independent report using the same cell line, approach and reagents demonstrated that VSV-G was largely absent from peri-Golgi vesicles, whereas α-Mannosidase II and transport machinery proteins were concentrated in cisternal rims and COP I-coated vesicles (Martinez-Menarguez et al., 2001). Until recently, another caveat in the model of bi-directional movement of COP I vesicles was the presence of only one species of COP I coat. However, this restriction could be overcome, at least theoritically, since 2 isotypes of γ (γ1 and γ2) and ζ (ζ1 and ζ2) subunits of COP I coat were discovered (Wegmann et al., 2004). The combinations of these two subunits together with the 5 remaining COP I subunits form three

COP I coat isoforms that could potentially be involved in different transport steps. A question, though, to which this model has not provided an adequate answer is how large macromolecular complexes, can be transported through the Golgi stack in vesicles of much smaller diameter. One possibility could be the VTC-like structures that have been obverved close to the Golgi stacks in tomographic studies (Ladinsky et al., 1999; Glick, 2000), although this is still hypothetical. Furthermore, it has been shown that large engineered protein aggregates traverse rapidly through the Golgi stack in megavesicles (Volchuk et al., 2000). Nevertheless, these conditions are non-physiological and the observed huge carriers may have been artificially induced. Under physiological conditions, such as the transport of procollagen aggregates or scales in algae, similar megavesicles have not been reported (Melkonian et al., 1991; Bonfanti et al., 1998).

On the other hand, the alternative mechanism of anterograde cargo movement, the **cisternal maturation model** (Figure 1.5B), can provide an explanation on how oversized molecules, like procollagen aggregates and scales, are transported through the exocytic pathway (Elsner et al., 2003). The cisternal maturation model proposes that at a late stage, the intermediate compartment arrives *en bloc* in the CGN, where it acquires the flattened shape of a cisterna and is populated with cis-specific proteins transported back from the downstream cisterna. In this way, the new cisterna gets the identity of the first cis-Golgi cisterna. In its original version, this model implies the necessity for COP I-coated vesicles only in retrograde movement of Golgi resident enzymes and transport machinery proteins back to "younger" cisternae (Glick, 2000). However, this continuous retrograde movement of the Golgi residents should be coupled to their gradient along the Golgi stack. In order to account for this polarity, it has been proposed that the various enzymes are incorporated into COP I vesicles with different

relative efficiencies (the more cis-localised are recycled more efficiently). This could reflect different binding affinities of the enzymes for a receptor or involve their differential partitioning into membrane subdomains or differences in their oligomerisation state (Glick et al., 1997; Munro, 1998; Glick and Malhotra, 1998). Compared to the vesicular transport stable compartment model, cisternal maturation model emphasises more the dynamic organisation of the Golgi apparatus. Such a dynamic behaviour is evident during mitosis when the Golgi ribbon undergoes a disassembly-reassembly cycle, but also in interphase, when many Golgi residents proteins are actively recycling between the Golgi membranes and the cytosol, or

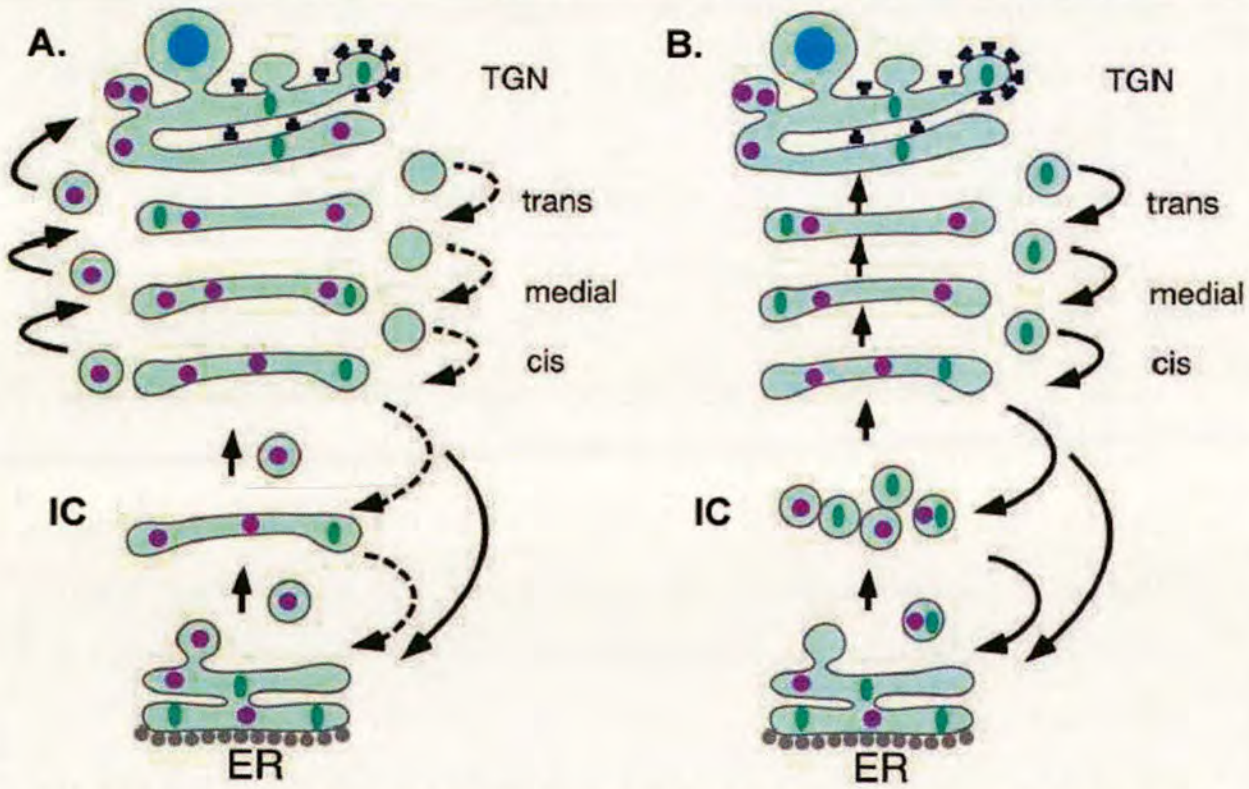

Figure 1.5: Two major models for anterograde transport through the Golgi stack. A. Vesicular transport stable compartment. According to this model, anterograde transport of newly synthesised cargo is mediated by vesicles, while each cisterna is viewed as a stable compartment that does not change over time. **B. Cisternal maturation.** In this model, each cisterna moves from cis to trans direction carrying forward the newly synthesized cargo. The Golgi associated vesicles mediate only the retrograde movement of Golgi resident proteins like the Golgi glycosylation enzymes. Newly synthesised proteins and resident proteins of each compartment are depicted in purple circles and green ellipsoids, respectively. ER, endoplasmic reticulum; IC, intermediate compartment; TGN, trans-Golgi network. Adapted from Elsner et al., 2003.

between the Golgi and earlier exocytic compartments (see later; Shorter and Warren, 2002; Lippincott-Schwartz et al., 2000).

Although the static view of the first model seems no longer the most favourable among the researchers in the field, the bi-directionality of COP I vesicles is still ambiguous. In an attempt to unify both models in a hybrid one, Pelham and Rothman (2000) have proposed the **percolating vesicle model**, which predicts that slow moving anterograde cargo is transported in maturing Golgi cisternae, while fast moving cargo is packaged in forward-directed COP I vesicles. Despite the fact that it could explain the slow movement of collagen and mucins through the Golgi stack compared to the fast movement of VSV-G, this alternative model is at odds with other experimental data testing the predictions deriving from this model. These data concern the kinetics of anterograde transport of different cargos and the localisation of proteins of transport machinery (Elsner et al., 2003).

Finally, a more provocative model proposes that cargo moves forward by tubular connections that form between the Golgi cisternae. Such intra-cisternal tubular connections seem to be very transient and were demonstrated very recently by electron tomography in insulin secreting cells after glucose stimulation (Marsh et al., 2004). All models seen from a historic perspective are reviewed in Elsner et al (2003). It remains to be seen whether the whole truth lies in one of these models or life will turn out to be once more based on synthesis and variety.

1.2.2 *De novo* formation versus stable Golgi matrix

Another more recent debate related to the Golgi apparatus is how it acquires and maintains its highly complex architecture. Again, two principal models have been put forward. One model has proposed the building of the Golgi apparatus around a **stable Golgi matrix**. The Golgi matrix is envisaged as a

structural template that orchestrates the formation of the Golgi complex and determines the Golgi identity. In this view, Golgi represents an autonomous organelle, always distinct from the ER (Shorter and Warren, 2002; Lowe, 2002). On the other side, the ***de novo* formation of the Golgi apparatus** has been proposed. This model implies that Golgi can be formed from scratch by its molecular constituents without the need for a pre-existing template. Thus, the Golgi apparatus is considered as an ER outgrowth, rather than an independent organelle defined by a stable Golgi matrix (Zaal et al., 1999; Bevis et al., 2002; Lowe, 2002).

The definition of *de novo* biogenesis of a membrane organelle, especially when this organelle exhibits such a complex architecture as the Golgi apparatus does, is difficult and tricky. The *de novo* formation of a cellular structure is intrinsically linked with its capacity for self-organisation, which describes the ability of its components to determine its architectural and functional features, although each component individually is not functional (Misteli, 2001). Self-organisation would require that this structure have a stable steady-state organization, while its constituents display dynamic behaviour and continuous cycling on and off the structure. Applying this general definition of the self-organisation on the Golgi apparatus, Benjamin Glick (2002) has suggested that Golgi formation should be considered to take place *de novo*, if the membrane vesicles deriving from the ER were able to fuse creating cisternae, which would then recruit peripheral Golgi proteins (membrane vesicles and peripheral membrane proteins would comprise the fundamental Golgi units; see Figure 1.6). In contrast, a template-directed Golgi organisation would require additionally a scaffold to drive these reactions (Glick, 2002).

Nevertheless, two key features of the *de novo* formation model could stir up new debates and should be clarified. One question is whether it is

possible that ER-derived vesicles are able to create a cisterna with flattened shape just by their homotypic fusion and without an earlier assembly of a template that will aid the membrane shaping. Second, the *de novo* Golgi biogenesis predicts that all Golgi resident proteins should recycle back to the ER. However, it seems rather difficult to prove experimentally that trace amounts of proteins do not remain in the cytoplasm and act as a nucleating matrix for the Golgi formation.

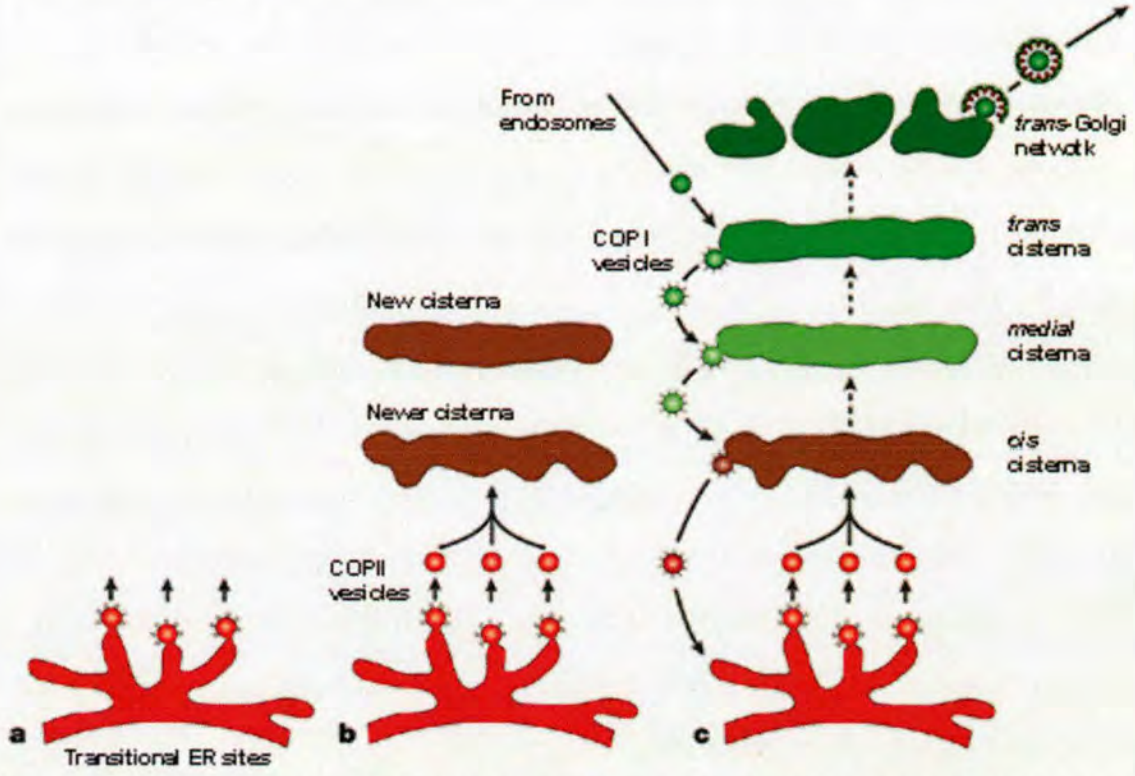

Figure 1.6: Hypothetical mechanism for *de novo* Golgi formation. a. The process begins when a transitional ER site, not functionally connected to a Golgi stack, produces COPII-coated vesicles. Such a tER site could arise in several ways: by *de novo* formation, as in yeast *Pichia pastoris*; by reactivation of an inactivated tER site during mitosis in vertebrate cells; or may represent a peripheral tER site that has lost its connection to the perinuclear located Golgi apparatus due to microtubule depolymerisation (for more details, see later in the text). **b.** The COPII vesicles fuse homotypically to form a new cisterna. Once the first cisterna is assembled, a second can be formed. **c.** Further rounds of cisternae production take place and the resulting cisternal stack acquires its polarity by COP I-mediated retrograde transport between the cisternae and from the cisternae back to the ER. At the same time, peripheral proteins are recruited to the Golgi membranes from the cytosol (not shown) and other membrane components are delivered by vesicles from downstream compartments, like endosomes. The final result is a functional Golgi stack. Taken from Glick, 2002.

1.3 Golgi matrix proteins

1.3.1 Golgi matrix and its components

The presence of a Golgi matrix was originally postulated by electron microscopy studies visualising an inter-cisternal, electron-dense material (Mollenhauer, 1965). In biochemical isolation experiments, the Golgi stacks remained intact and still exhibited this inter-cisternal material (Cluett and Brown, 1992). However, both these features were disrupted upon treatment with certain proteases, suggesting that the material that was responsible for the stacking of Golgi cisternae was of proteinaceous nature. Upon Triton X-100 and low salt extraction of Golgi stacks, a proteinaceous putative Golgi structural skeleton that retained the ultrastructural characteristics of the stack was left behind, and it was called the Golgi matrix (Slusarewicz et al., 1994). The Golgi matrix was largely devoid of Golgi enzymes with the exception of two medial-Golgi enzymes. Antibodies raised against the Golgi matrix led to the characterisation of GM130 (Golgi matrix protein of 130kD; Nakamura et al., 1995). Subsequently, a combination of biochemical approaches with an *in vitro* Golgi reassembly assay from mitotic Golgi fragments (Rabouille et al., 1995b) resulted in the identification of several other proteins, which are known as **Golgi matrix proteins.**

The best-characterised Golgi matrix proteins are GM130 (Nakamura et al., 1995; 1997), p115 (Rabouille et al., 1995a), giantin (Linstedt et al., 1995), GRASP65 (Barr et al., 1997) and GRASP55 (Shorter et al., 1999). GM130 is a rod-like protein comprising 6 coiled-coil domains (Nakamura et al., 1995), and it localises in the cis-Golgi by interacting with GRASP65 through its C-terminus (Barr et al., 1998). p115 is a homodimeric protein with a myosin II-like structure comprising a N-terminal globular head, a coiled-coil tail and a short acidic C-terminal domain (Sapperstein et al., 1995; Yamakawa et al.,

1996). Through this C-terminal acidic tail, p115 has been shown to interact with GM130 and giantin (Dirac-Svejstrup et al., 2000; Linstedt et al., 2000). The p115 binding sites were narrowed down to the 75 N-terminal amino acids of GM130 (Nakamura et al., 1997) and the 448 N-terminal amino acids of giantin (Lesa et al., 2000). Giantin, like GM130 and p115, is also a long coiled-coil protein, but in contrast to these two proteins, it is a transmembrane protein that is inserted in ER membranes through the C-tail anchoring mechanism (Linstedt et al., 1995). Its Golgi localisation through the C-terminal part leaves almost the whole molecule projecting in the cytoplasm, and since it is at least partially present on COP I-coated vesicles, it was proposed to hold these vesicles close to the Golgi cisternae (Linstedt et al., 1995; Sönnichsen et al., 1998). GRASP65 is anchored on the Golgi membranes through myristoylation of glycine residue at the position 2 (Barr et al., 1997) and it serves as a Golgi receptor for GM130 through a PDZ-like domain around the middle of the molecule (Barr et al., 1998). GRASP55, like GRASP65, was identified by the *in vitro* functional assay, as an important factor for the cisternal stacking (Shorter et al., 1999). Localisation of GRASP65 and GRASP55 by cryo-electron microscopy has revealed a distinct distribution on the cis- and medial-Golgi, respectively (Shorter et al., 1999).

1.3.2 Characteristics of the Golgi matrix proteins

The Golgi matrix proteins are characterised by their predominant localisation to the Golgi apparatus (Barr and Short, 2003). They are subdivided into two protein families: the golgins and the GRASPs. To date, the GRASP family comprises only GRASP65 and GRASP55, while the number of golgins has increased significantly (Gillingham and Munro, 2003). A common feature among the members of the golgin family is the long coiled-coil domains they exhibit, which form extended rod-like structures (Barr and Short, 2003;

Gillingham and Munro, 2003). Additionally, GRASP65, GRASP55 and most of the golgins have been shown to interact with Rabs, a family of small GTPases that is involved in intracellular transport between the different membrane compartments (see section 1.5). Despite these shared characteristics, golgins appear to be a relatively divergent group of proteins in terms of sequence and size (Gillingham and Munro, 2003). They comprise integral membrane proteins (e.g. giantin, golgin-84, CASP), but mostly peripherally associated proteins. For some of these proteins, it has been shown that they are targeted to the Golgi membranes through a conserved C-terminal GRIP domain (Munro and Nichols, 1999). However, other peripheral golgins, like p115, GM130 or golgin-45, do not have recognisable common targeting or other motifs.

1.4 Does a Golgi matrix exist?

This question seems strange especially because, as it was mentioned previously, the Golgi matrix was described morphologically and biochemically. However, the issue was brought up when the behaviour of the Golgi matrix proteins was studied in more detail and the model of *de novo* Golgi formation was proposed.

Despite the fact that the debate between the Golgi matrix and the *de novo* Golgi formation models has begun only about 5 years ago, many experimental data have already been generated supporting either model. The issue has been addressed experimentally under conditions where the Golgi apparatus was disassembled reversibly, and then its subsequent biogenesis was studied. Two main experimental lines have been followed: one makes use of the physiological disassembly-reassembly cycle of the Golgi apparatus during mitosis in mammalian cells and, the other triggers the disassembly of

the interphase Golgi ribbon by use of drugs or overexpression of dominant negative mutant proteins.

1.4.1 Golgi matrix proteins during mitosis

The fate of the Golgi apparatus during mitosis is only briefly described, because it is not directly relevant to the subject of this thesis, but the issue has been extensively reviewed by Shorter and Warren (2002) and Rabouille and Jokitalo (2003).

As a mammalian cell enters mitosis, the Golgi ribbon has been described to undergo gradual fragmentation into a collection of vesicles and tubules, which were called Golgi clusters (Lucocq et al., 1987). These clusters were shown to contain Golgi enzymes and Golgi matrix proteins (Shima et al., 1997; Seemann et al., 2002) and were considered to be the units for the partitioning of the Golgi apparatus in the two dividing cells (Shima et al., 1997; Shorter and Warren, 2002).

This model was challenged by a study demonstrating that a Golgi enzyme fused with triple GFP tag was rapidly absorbed back to the ER upon enter of the cells into mitosis (Zaal et al., 1999). As an alternative model for Golgi inheritance, it was proposed that the components of the Golgi apparatus merge back to the ER during prometaphase and emerge from it at telophase. In this view, the partitioning units are not the mitotic Golgi clusters, but the ER membranes (Zaal et al., 1999; Lippincott-Schwartz et al., 2000). Although this report could provide support to the model of *de novo* formation of the Golgi apparatus at the end of each mitotic division, it did not address the behaviour of the Golgi matrix proteins that should also recycle back to the ER to sustain this model.

Attempts to reproduce the proposed recycling of the Golgi resident proteins (enzymes and matrix proteins) back to the ER both by biochemical

and morphological means were proven mostly unsuccessful, as ER and Golgi markers could always be distinguished (Jesch and Linstedt, 1998; Jokitalo et al., 2001; Prescott et al., 2001; Jesch et al., 2001; Seemann et al., 2002). Moreover, it is suspected that the localisation of the tagged Golgi enzyme in the ER during mitosis did not reflect the active recycling of the enzyme, but its retention there due to misfolding caused by the triple GFP tag that was used for the visualisation of the enzyme (Shorter and Warren, 2002). Finally, the more recent evidence against this model came from an elegant trapping assay, where a Golgi and an ER resident protein were tagged with 2 polypeptides that interact only in the presence of rapamycin (Pecot and Malhotra, 2004). If the Golgi marker were indeed returning to the ER membranes during mitosis, it would be expected to interact with the ER proteins in the presence of rapamycin and be retained to the ER. However, such an ER entrapping was not observed arguing against the mitotic ER recycling of the Golgi resident proteins.

Finally, a quantitative live cell imaging study in sea urchin dividing blastomeres has suggested that the truth could stand somewhere in the middle. More specifically, at least 20% of a Golgi enzyme chimera was estimated to redistribute back to the ER during the mitotic divisions. However, this study could not resolve where the rest of the Golgi enzyme was located during mitosis and therefore, could not exclude the possibility of being present in vesicles (Terasaki, 2000).

In conclusion, most experimental data suggest that at least the majority of both the Golgi enzymes and the Golgi matrix proteins remain in membranes distinct from ER during mitosis, which argues against a mechanism of *de novo* formation of the Golgi apparatus at the end of each mitotic division.

1.4.2 Golgi matrix proteins upon induced disassembly of the Golgi apparatus

1.4.2.1 Brefeldin A treatment and Sar1p mutants

A set of experimental observations that has stirred up the controversy on whether the Golgi matrix exists or the Golgi apparatus is formed *de novo*, has derived from the use of the fungal metabolite Brefeldin A (BFA). BFA has been shown to block activation of Arf1 GTPase by inhibiting the GDP exchange activity of a subset of Sec7-type GEF proteins (Peyroche et al., 1999), and its action induces a rapid breakdown of the Golgi apparatus, which can be reversed after the drug is washed out (Klausner et al., 1992).

Upon BFA treatment, the Golgi ribbon disappears rapidly and most Golgi membranes are absorbed in the ER (Lippincott-Schwartz et al., 1989). The Golgi resident enzymes have been demonstrated to relocate back to the ER. By live cell imaging, this process was shown to take place initially via tubules emanating from the Golgi apparatus and later with a sudden diffusion of the fluorescent signal into the ER, a phenomenon known as Golgi blinkout (Sciaky et al., 1997). On the other hand, Golgi matrix proteins were described to persist in specific tubular and vesicular membrane structures, as it was assessed by EM (Seemann et al., 2000a). These tubular-vesicular structures were thought to be Golgi remnants, which serve as a template for the organelle reassembly after BFA removal. However, these Golgi remnants did not exhibit a clear cisternal morphology similar to this observed in the original description of the putative Golgi matrix (Slusarewitz et al., 1994). An effect analogous to BFA treatment was reported when a GTP-restricted, dominant-negative form of Sar1p ($Sar1^{DN}$) was microinjected in NRK or HeLa cells (Seemann et al., 2000a; Prescott et al., 2001). This GTP-locked Sar1p does not affect the formation of the COPII-coated vesicles, but it blocks their uncoating and subsequent fusion (Aridor et al., 1995; Pepperkok

et al., 1998). Finally, in the presence of Sar1^{DN}, BFA washout led to a re-organisation of the Golgi matrix proteins in the peri-nuclear area, while the Golgi enzymes remained in the ER membranes due to the ER exit block (Seemann et al., 2000a).

Surprisingly, subsequent studies tackling the same issue, sometimes using the same reagents, have provided evidence suggesting a more dynamic nature for the Golgi matrix proteins. First, fluorescence recovery after photobleaching (FRAP) analysis of GRASP65 tagged with GFP revealed that the protein is rapidly exchanged between membranes and cytosol (Ward et al., 2001), although this is contradictory to biochemical fractionation data that failed to detect GRASP65 in the cytosolic fraction (Barr et al., 1997). Addition of BFA led to a redistribution of GRASP65-GFP to peripheral structures earlier than the observed recycling of Golgi enzymes, arguing against the proposal that these structures are remnants left behind after Golgi breakdown (Ward et al., 2001). Instead, their partial co-localisation with Sec13p suggested that they might represent part of tER sites or the intermediate compartment. Experiments using the GTP-bound mutant form of Sar1p also indicated that the structures, where the Golgi matrix proteins accumulated, represented ER exit sites (Ward et al., 2001). Upon injection of higher concentration of GTP-locked Sar1p in HeLa cells, it was shown that a portion of Golgi matrix proteins display ER distribution, in addition to ER exit site granular pattern (Miles et al., 2001). Moreover, overexpression of a GDP-restricted Sar1p mutant that disrupts ER exit by completely preventing the COPII coat formation resulted in total redistribution of all Golgi residents back to the ER (Ward et al., 2001). Additionally, when Sar1p-GTP or Sar1p-GDP mutants were used in combination with BFA, they prevented the rebuilding of the Golgi after BFA washout, indicating that Golgi reassembly is dependent on Sar1p activity (Ward et al., 2001; Miles et al., 2001; Stroud et

al., 2003). Along the same line, in a recent report (Puri and Linstedt, 2003), ER exit block was imposed on mammalian cells using the drug H89, a protein kinase inhibitor that interferes with Sar1p recruitment to the ER membranes (Aridor and Balch, 2000). Upon prior or concomitant redistribution of the Golgi proteins by BFA, the presence of H89 inhibited the rebuilding of the Golgi ribbon upon BFA washout, suggesting the importance of ER export for the perinuclear localisation of both the Golgi enzymes and the Golgi matrix proteins (Puri and Linstedt, 2003). However, a caveat of the experiments using Sar1p mutants or drugs that block ER exit is that it has been shown that cessation of ER to Golgi transport alone can cause disassembly of the Golgi apparatus (Seemann et al., 2000a; Prescott et al., 2001). Therefore, the fact that the Golgi apparatus cannot reassemble upon an ER exit block by Sar1p mutants does not prove that all Golgi residents recycle back to the ER or that their ER export block is the crucial factor for the Golgi reassembly. Instead, the ER export of another newly synthesised factor may be essential for the reassembly/maintenance of the Golgi apparatus (Rabouille and Jokitalo, 2003).

Although the observations mentioned above have provided support to the model of *de novo* Golgi formation, another elegant study has directly tested this model. Pelletier et al. (2000) have created microsurgically peripheral cytoplasts deprived of Golgi membranes, but still containing significant amount of ER membranes. In these cytoplasts, no Golgi apparatus was observed to form for as long as 4 hours, arguing against the capacity of the Golgi to form *de novo* from the ER. On the contrary, when BFA-induced redistribution of Golgi matrix proteins was performed prior to microsurgery, the cytoplasts were able to give rise to Golgi stacks capable of mediating proper transport of a plasma membrane reporter protein (Pelletier et al., 2000). These results suggested that Golgi assembly cannot occur in the

absence of a template, but it could also reflect the absence of molecules that are required for ER-Golgi transport and may have inhibited the Golgi biogenesis (Lowe, 2002).

1.4.2.2 Nocodazole treatment

Additional evidence for the dynamic recycling of Golgi proteins between ER and Golgi has been obtained from experiments using the microtubule depolymerising drug, nocodazole, in mammalian cells. Upon nocodazole treatment, the Golgi ribbon undergoes fragmentation, giving rise to small Golgi stacks next to tER sites (Rogalski and Singer, 1984; Cole et al., 1996; Hammond and Glick, 2000). In the absence of microtubule network, anterograde transport in initially arrested, but recovers back to normal levels, as soon as the small Golgi stacks appear, 1.5-2 hours after the addition of nocodazole (Rogalski et al., 1984; Cole et al., 1996). The small Golgi stacks were thought to originate from the dissociation of the Golgi stacks that form the Golgi ribbon (Thyberg and Moskalewski, 1999). However, live cell imaging of Golgi residents enzymes in nocodazole-treated cells has failed to track Golgi fragments moving outward from the juxtanuclear Golgi complex towards the cell periphery (Storrie et al., 1998). Instead, scattered mini-Golgi stacks appeared abruptly supporting a *de novo* formation of the Golgi stacks through the continuous recycling of the Golgi residents to the ER. The ER recycling of the Golgi enzymes was again confirmed by blocking the ER exit with $Sar1^{DN}$. In this case, the Golgi enzymes accumulated gradually in the ER and hardly any peripheral Golgi elements were observed (Storrie et al., 1998).

A similar study for the Golgi matrix proteins has not been reported. Indirect immunofluorescence experiments monitoring the distribution of giantin in nocodazole-treated cells have postulated that the Golgi matrix protein could follow a similar behaviour to that of Golgi resident enzymes (Hammond and Glick, 2000). Giantin was first redistributed in the ER

membranes with BFA and then its localisation was examined upon BFA washout in the presence of nocodazole. Like Golgi enzymes, giantin was localised initially close to the tER sites and then to intermediate-sized Golgi structures that were described to form upon microtubule depolymerisation in this report (Hammond and Glick, 2000). However, in a recent study, where the dynamics of endogenous giantin was visualised with a recombinant antibody tagged with GFP or YFP in nocodazole-treated cells, it was demonstrated that giantin did not rapidly recycle through ER to the newly formed mini-stacks (Nizak et al., 2003). Contrary to other Golgi matrix proteins, such as GM130, which were confined to the newly formed mini-stacks, giantin remained on the slowly fragmenting "old Golgi". The slow dynamics of giantin suggested that this Golgi matrix protein might define a more stable Golgi matrix (Nizak et al., 2003).

Despite the fact that a considerable amount of experimental data obtained using drugs, or mutant forms of Sar1p sustain the notion that the Golgi apparatus is capable of self-organisation, the same may not hold true under physiological conditions, for example during cell division (Lowe, 2002). Concerning mitosis, two kinetic parameters could be important to determine whether *de novo* Golgi formation takes place. First, the time it would take for the Golgi self-organisation to occur at the end of mitosis should be short. If this is a slow process, it would be more advantageous for the cells to keep their Golgi residents into small vesicles and tubules that could nucleate the Golgi reassembly more efficiently. Second, the Golgi proteins should recycle quickly back to the ER. If the recycling rate were not fast enough, the Golgi proteins would not accumulate in the ER (Lowe, 2002). This raises also the possibility that, even in the drug-based experiments, the Golgi proteins may not be fully recycled back to the ER, which would be a prerequisite in order to support *de novo* Golgi formation. Many studies

exploiting GFP fluorescence microscopy techniques have often interpreted a diffused pattern as ER redistribution. However, light microscopy is not suitable to resolve small structures, and a recent study has shown that protein diffusion could also represent small vesicular or tubular structures dispersed in the cytoplasm (Axelsson and Warren, 2004; Barr, 2004).

1.4.3 The question of *de novo* formation in non-mammalian cells

Although the question of the *de novo* Golgi formation in mammalian cells is under debate, the most direct evidence comes from the yeast species, *Pichia pastoris*. A typical *Pichia* cell contains 2-5 tER sites, as it was visualised by tagging Sec13p with GFP (Rossanese et al., 1999). In close association with these discrete tER sites, there are polarised Golgi stacks (Mogelsvang et al., 2003). Using video confocal microscopy, Bevis at al. (2002) have demonstrated the sudden appearance of tER sites (marked by Sec13-GFP) both in mother cell and in the bud. Adjacent to these newly formed tER sites, a Golgi structure appears with a short lag in time. Late peripheral Golgi protein, Sec7, and transmembrane medial Golgi protein, Gos1, were used as Golgi markers. Therefore, it has been suggested that the daughter cell in *Pichia* does not inherit pre-existing Golgi stacks from the mother cell, but instead it is able to build its own by a mechanism of *de novo* formation from the tER sites. The tER sites themselves have also been proposed to display self-organising properties, and when their fundamental molecules exceed a critical concentration in an ER domain, they nucleate a new tER site. When this site has reached the proper size, it gives rise to a new Golgi stack (Bevis et al., 2002). Study of the dynamics of the tER sites has supported the self-organising tER properties by showing that they are able to control their size and number by growth or shrinkage when they are formed or fuse (Bevis et al., 2002). Nevertheless, these observations cannot exclude that the seemingly

de novo formation of the tER and the Golgi stacks could take place on templates that control the organisation of the two compartments and are invisible in the above mentioned experiments. Additionally, although the membranes of the newly formed Golgi stacks were proposed to derive from the neighbouring tER sites, the possibility that components of the old Golgi stacks are also needed to be recruited to build a functional new Golgi has not been ruled out. This seems to be the case in *Trypanosoma brucei*, where it was recently shown that the newly formed Golgi stacks require material that is supplied, at least in part, from the old Golgi, despite its close spatial relationship to a new tER site (He et al., 2004).

The example of the *de novo* Golgi formation in *Pichia* is not the only way to inherit Golgi apparatus (Munro, 2002). The most common budding yeast, *S. cerevisiae*, exhibits single cisternae surrounded by vesicles and tubules instead of the typical Golgi stacks (Preuss et al., 1992). These cisternae are populated by early or late Golgi markers and are believed to function as cis- or trans-Golgi elements (Glick, 2002). Although the early cisternae were proposed to be inherited through *de novo* formation from ER membranes, the late Golgi cisternae are transported from the mother to the daughter cell along actin microfilaments (Rossanese et al., 2001).

A third way for Golgi inheritance has been observed in many algae and protozoa, which split their single Golgi stack in half (Munro, 2002). Live imaging of the Golgi stack in *Toxoplasma gondii* demonstrated that Golgi grows laterally to subsequently undergo two rounds of medial fission. Each pair of stacks is then segregated to the two daughter cells, where they coalesce to produce the single Golgi stack of the protozoon (Pelletier et al., 2002). This suggests that *de novo* Golgi formation could perhaps represent one of the alternative mechanisms for the organelle division and inheritance during mitosis.

1.5 Functions of the Golgi Matrix proteins

Parallel to the issue of the existence of a Golgi matrix or not, which seems far from being settled, the functions of the components of this putative matrix in the structural and functional maintenance of the Golgi apparatus have been investigated.

1.5.1 Involvement in Golgi architecture

In order to investigate the involvement of Golgi matrix proteins in the structural organisation of the Golgi apparatus, a combination of *in vitro* and *in vivo* studies have been performed. p115 was suggested to promote Golgi cisternal regrowth and stacking *in vitro* (Rabouille et al., 1995a; Shorter and Warren, 1999) and act as a tethering factor (see section 1.5.2) for COP I vesicles in the peri-Golgi area, by interacting with giantin on COP I vesicles and with GM130 on the Golgi membranes (Figure 1.7; Sönnichsen et al., 1998). Except for its role in transport, the same tripartite complex was also proposed to facilitate the initial alignment and tethering of neighbouring Golgi cisternae initiating the stack formation (Figure 1.7; Shorter and Warren, 1999; Linstedt, 1999). The importance of this tripartite complex for the Golgi stacked architecture has been examined further *in vivo*, generating some controversial results. Microinjection of a peptide comprising the 73 N-terminal amino acids of GM130 that competes with the endogenous GM130 for p115 binding (see section 1.3.1), or overexpression of a GM130 lacking this N-terminal peptide was shown to cause vesiculation of the Golgi apparatus and transport inhibition in NRK cells (Seemann et al., 2000b). In a different approach, injection of antibodies targeted against p115 led to Golgi ribbon breakdown in WIF-B or HeLa cells, confirming that p115 function is essential for the Golgi architecture (Alvarez et al., 1999; Puthenveedu and Linstedt, 2001). However, injection of anti-GM130 antibodies that disrupt

p115-GM130 interaction did not have any effect on Golgi organisation (Puthenveedu and Linstedt, 2001). Moreover, injection of antibodies that targeted giantin for degradation did not lead to any obvious alteration of the Golgi ribbon, at least by immunofluorescence (Puthenveedu and Linstedt, 2001).

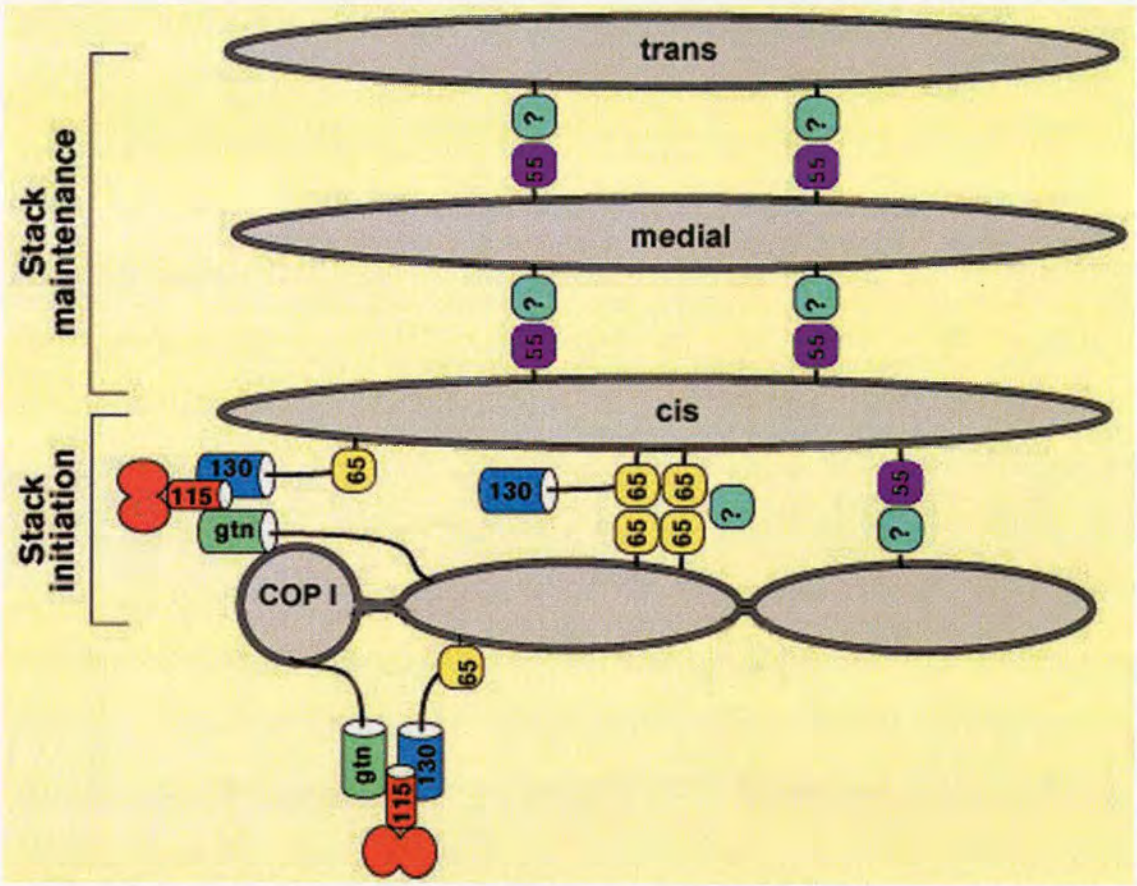

Figure 1.7: Involvement of Golgi matrix proteins in Golgi architecture. GRASP65 (yellow) is anchored on the Golgi membranes through a myristoylation site and serves as receptor for GM130 (blue). p115 (red) tethers the COP I vesicles by interacting simultaneously with giantin (green) on the vesicles and GM130-GRASP65 on the Golgi cisterna facilitating their subsequent docking and fusion. The same complex was proposed to tether a newly formed cisterna to the cis-Golgi cisterna initiating cisternal stacking. A GM130-independent role for GRASP65 in cisternal stacking at the cis-side of the Golgi stack has also been proposed through the formation of trans oligomers in neighbouring cisternae. Finally, GRASP55 (purple) is thought to be involved in maintaining the linking of the cisternae due to its broader distribution throughout the Golgi stack. Interacting partners for GRAS65 and GRASP55 concerning their role in cisternal stacking have not been identified thus far. Adapted from Linstedt, 1999.

The role of GM130 for Golgi architecture became even more doubtful when the characterisation of the conditional lethal mutant cell line ldlG was performed (Vasile et al., 2003). At the permissive temperature, this cell line contains no detectable GM130; nevertheless, it exhibits a Golgi apparatus with apparently normal morphology and function. The absence of GM130 seems to become crucial only after imposing stress conditions on the cells by shifting them at the non-permissive temperature.

The two GRASP proteins (GRASP65 and GRASP55) are both required for cisternal stacking of mitotic Golgi fragments *in vitro* (Barr et al., 1997; Shorter et al., 1999). GRASP65 role in stacking was proposed to be independent of its function as receptor for GM130 on Golgi membranes (Figure 1.7; Shorter and Warren, 1999), since addition of a soluble form of GRASP65 blocked stacking without causing GM130 release from membranes or affecting the GM130-dependent cisternal regrowth (Barr et al., 1997; Shorter et al., 1999). However, it is not yet clear whether the observations that have derived from this *in vitro* assay reflect the situation *in vivo* or recapitulate only one aspect of the Golgi stack building (Shorter et al., 1999; Linstedt, 1999). Recent *in vivo* observations showed that injection of anti-GRASP65 antibodies in mitotic cells prevent the proper cisternal stacking without though affecting the overall organisation of the Golgi ribbon (Wang et al., 2003). Considering that GRASP65 forms homodimers, this study has postulated that the formation of GRASP65 trans oligomers mediate stacking of the Golgi cisternae *in vivo* (Figure 1.7).

Additionally, golgin-45 and golgin-84 were shown to be important for the Golgi architecture *in vivo*. Golgin-45 was demonstrated to interact with GRASP55 and its depletion by RNA interference (RNAi) resulted in a disruption of the Golgi ribbon organisation (Short et al., 2001). On the other hand, the role of golgin-84 was studied by two groups independently. One

group localised golgin-84 throughout the Golgi ribbon and showed that is required for the Golgi reassembly *in vitro* (Satoh et al., 2003). The other group, however, localised the protein predominantly at the cis-side of the Golgi and the tubular interconnections that attach the Golgi stacks together. In agreement with this localisation, golgin-84 depletion by RNAi led to fragmentation of the Golgi ribbon into very small stacks accompanied by an enlargement of the ER, but did not affect the stacking itself, while protein transport was reduced but not blocked (Diao et al., 2003).

1.5.2 Involvement in intracellular transport

Although the term "Golgi matrix proteins" suggests a role for these proteins in the structural integrity of the Golgi apparatus, there is mounting evidence showing that they also play a significant role in intracellular transport.

Independently of the nature of anterograde transport carriers, both forward and backward membrane traffic steps along the exocytic pathway involve a donor and an acceptor compartment. Once a cargo transport carrier has budded from the donor compartment, it needs to recognise the correct acceptor compartment and fuse with it. The recognition of the acceptor compartment is thought to be a two-step process.

First comes a tethering step that might provide the specificity or increase the efficiency of the initial loose anchoring of the carrier (Figure 1.8; Warren and Mellman, 2000; Whyte and Munro, 2002). The tethering step has been proposed to be carried out either by multi-subunit complexes, like COG and TRAPP complexes (White and Munro, 2002), or/and by Rab small GTPases in combination with the golgins (Figure 1.8; Barr and Short, 2003). Activated Rab proteins (GTP-bound) are thought to bind first on the membranes and subsequently regulate the recruitment of specific golgins (Barr and Short, 2003). Golgins, due to their long, coiled-coil structure, are

good candidates to serve as tethering factors, performing the initial, long-distance capturing of transport carriers (Gillingham and Munro, 2003).

The second step is the docking that tightly secures the carrier on the acceptor compartment and possibly drives its subsequent fusion (Gillingham and Munro, 2003). The docking step is performed by SNAREs (soluble NSF-attachment protein receptors). More specifically, a monomeric v-SNARE on the vesicle carrier binds to an oligomeric t-SNARE complex on the target membrane, forming a stable four-helix bundle (Figure 1.8). This SNARE complex brings the two membrane bilayers in close proximity promoting their fusion, possibly with the participation of other downstream factors (Warren and Mellman, 2000; White and Munro, 2002; Bonifacino and Glick, 2004). After fusion, the SNARE complex is separated through the action of NSF ATPase and SNAPs (soluble NSF-attachment proteins) (Sollner et al., 1993), and finally, the v-SNARE is recycled to the donor compartment and the t-SNAREs are primed for a new round of docking and fusion. (Warren and Mellman, 2000).

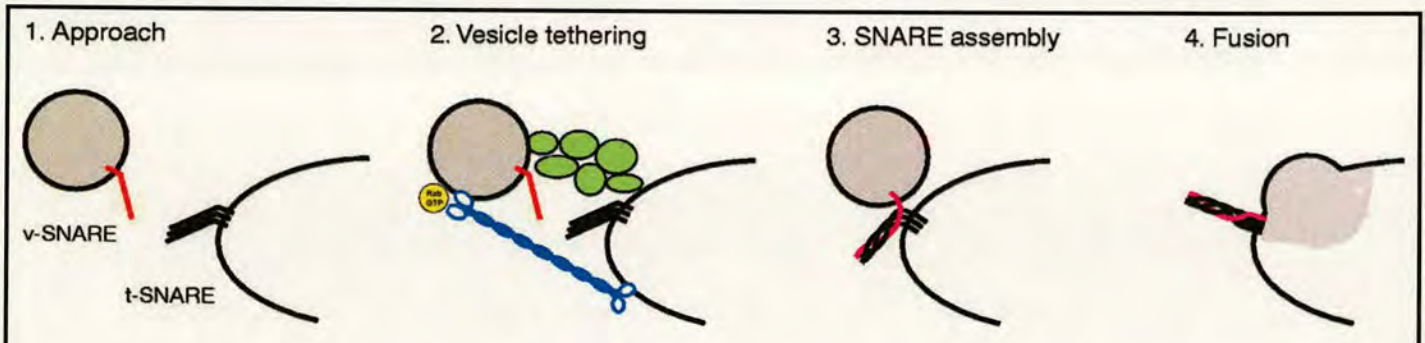

Figure 1.8: Steps of vesicle targeting and fusion to the correct organelle. (1) A vesicle approaches its target membrane either by diffusion or by directed transport along cytoskeleton filaments. **(2)** The vesicle is proposed to be tethered to the acceptor membrane via multi-subunit protein complexes (green) or by long coiled-coil proteins (blue) in combination with Rab GTPases (yellow). **(3)** A v-SNARE (red) on the vesicle interacts with three t-SNARE molecules (black) on the target compartment, leading to the formation of a stable four-helix bundle. The SNARE assembly brings the two membrane bilayers in close proximity, (4) driving their fusion and delivering the vesicle content in the acceptor compartment. The same principles could apply also for non-vesicular carriers. Adapted from Whyte and Munro, 2002.

The role of Golgi matrix proteins as tethering factors has been suggested by many experimental results. p115 is one of the golgins that appear to act at multiple steps along the early exocytic pathway. In mammalian cells, it localises predominantly to the cis-Golgi and peripheral structures that could represent tER sites or the intermediate compartment (Nelson et al., 1998). In accordance with this distribution, p115 has been assigned a role at a pre-Golgi compartment (Alvarez et al., 1999; 2001), which is distinct from its role at the Golgi apparatus in tethering COP I vesicles, together with GM130 and giantin (Sönninchen et al., 1998). The pre-Golgi p115 role in transport was established, when p115 was found to be an effector of activated Rab1 on COPII-coated vesicles and, proposed to prime these vesicles for fusion with other COPII vesicles or with the intermediate compartment (Allan et al., 2000). However, because Rab1 is also found in the intermediate compartment and the Golgi complex, it is plausible that it may recruit p115 in these compartments, as well.

Along this line, it has been proposed that p115 may facilitate interactions between components of the ER to Golgi transport machinery, such as SNAREs and GBF1, which is a GEF protein for Arf GTPase (Garcia-Mata and Sztul, 2003). Interactions between p115 and Gos-28 (v-SNARE), syntaxin-5 (t-SNARE) and other SNAREs have been described, and p115 was shown to promote the SNARE complex assembly in a catalytic fashion (Shorter et al., 2002).

Finally, the multi-functional nature of p115 is further exemplified from data on its yeast homologue, Uso1p. First, Uso1p through its interaction with Ypt1p (yeast Rab1 homologue) was shown to be involved in the initial tethering of COPII vesicles to the Golgi membranes, which does not require SNARE molecules (Cao et al., 1998). However, the need for Uso1p tethering function can be surpassed upon overexpression of v-SNARE proteins

(Sapperstein et al., 1996). In addition, Uso1p has recently been implicated in proper sorting of glycosylphosphatidyl inositol (GPI)-anchored proteins at the tER sites (Morsomme and Riezman, 2002). The suggestion is that Ypt1p recruits Uso1p and other tethering factors on the ER membranes, where they interact with v-SNAREs and probably other molecules, which ensure correct sorting and packaging of soluble cargo molecules in COPII-coated vesicles. Independently, the recruited tethering factors confer also their function in targeting these vesicles to their acceptor compartment (Morsomme and Riezman, 2002; Morsomme et al., 2003).

GM130 has also been implicated in transport due to its reported biochemical interactions with several Rab proteins (Barr and Short, 2003). The complex of GM130 with GRASP65 has been identified as another effector of Rab1-GTP, independent of the Rab1 interaction with p115 (Moyer et al., 2001), and the Rab1 binding site was mapped on the coiled-coil domain 3 of GM130 (Weide et al., 2001). Considering the reported interaction between p115 and GM130, the fact that the two proteins are distinct effectors of the same Rab protein has led to the proposal that Rabs might cooperate with specific golgins to ensure the membrane specificity during transport (Moyer et al., 2001; Barr and Short, 2003).

Visualisation of GM130 by time-lapse confocal microscopy has shown that the GM130-GRASP65 complex seems to cycle between the cis-Golgi and a late IC subdomain via transient tubules. These GM130-positive tubules were suggested to play a role in capturing cargo-containing carriers deriving from earlier exocytic compartments (Marra et al., 2001). This transport step could represent the GM130-requiring step in ER-Golgi trafficking of VSV-G, which was shown to follow the p115-requiring step (Alvarez et al., 2001).

Furthermore, GM130 was shown to interact with Rab2 (Short et al., 2001) and Rab33b (Valsdottir et al., 2001) that has been localised in the medial Golgi (Zheng et al., 1998).

Finally, a recent article has implicated GM130 in signalling events that seem to take place in the Golgi apparatus (Preisinger et al., 2004). More specifically, it was shown to recruit two members of Ste20 kinase family on the Golgi and increase significantly their kinase activity. Interference with one of these two kinases led to cell migration defects and to a breakdown of the Golgi ribbon. Interestingly, a substrate of this kinase has been involved in signalling pathways regulating cell migration, but also in the ER-Golgi transport of multimeric membrane protein complexes, providing a possible link between the Golgi apparatus and cell migration (Preisinger et al., 2004).

The two mammalian GRASP proteins have been further involved in intracellular transport. GRASP55 was found to bind indirectly to Rab2 through its interaction with golgin-45, which upon depletion led to block in anterograde protein transport (Short et al., 2001). Moreover, both GRASP65 and GRASP55 have been demonstrated to directly interact with members of p24 family, which function as cargo receptors (Barr et al., 2001). Furthermore, both proteins have been reported to interact with the transmembrane protein TGF-α, regulating its deposition to the plasma membrane (Kuo et al., 2000; Barr et al., 2001). Mutations in the GRASP binding site on p24a receptors or TGF-α resulted in mistargeting to the plasma membrane or decrease transport to the cell surface, respectively. These data have suggested a role for GRASPs in retention of integral Golgi proteins and their sequestration from the associated cargo molecules (Kuo et al., 2000; Barr et al., 2001).

In conclusion, the Golgi matrix proteins seem to be implicated in the structural organisation of the Golgi apparatus, as well as in the intracellular transport. In most *in vivo* experiments, at least in mammalian cells, when the

interference with the function of a Golgi matrix protein has led to disorganisation of the Golgi apparatus, then it has also resulted in the impairment of intracellular transport. This has rendered the dissociation between the two processes not possible. Thus, it is uncertain whether intracellular transport and Golgi organisation can be affected independently.

1.6 Relationship between tER sites and the Golgi apparatus

Despite the ongoing controversy about the autonomous or ER-dependent nature of the Golgi apparatus, many of the observations mentioned earlier seem to point to a close relationship between the tER sites and the Golgi apparatus not only concerning their function in the exocytic pathway, but also in terms of their spatial association. First of all, in mammalian cells, a fraction of the numerous tER sites is concentrated at the peri-nuclear area, where the Golgi apparatus is located. The tER concentration in this location has been attributed, at least in part, to a mutual feedback relationship between tER and Golgi (Hammond and Glick, 2000). Another indication has come from the nocodazole experiments showing that Golgi stacks re-emerge next to the tER sites (Cole et al., 1996; Storrie et al., 1998; Hammond and Glick, 2000). A similar close association between the two compartments is also reported in *Pichia* (Bevis et al., 2002). Moreover, the important role of the tER sites in regulating the Golgi organisation is implied by observations in *Pichia* and *Toxoplasma*, where events of Golgi stack fusion or fission always follow similar events at tER sites (Bevis et al., 2002; Sheffield and Melton, 1968).

The notion that the organisation of tER sites influences the morphology of the Golgi apparatus has been further exemplified by a comparative study between two budding yeasts *P. pastoris* and *S. cerevisiae* (Rossanese et al., 1999). In contrast to *P. pastoris* that has typical Golgi stacks,

S. cerevisiae exhibits single cisternal Golgi elements (Figure 1.9; Preuss et al., 1992). Interestingly, this difference in Golgi architecture between the two yeasts is reflected in the different organisation of their tER sites, marked by Sec13p or Sec12p (Rossanese et al., 1999). While in *P. pastoris*, Sec13-GFP is concentrated in few spots within the cell, in *S. cerevisiae*, it appears as multiple dots dispersed throughout the cell (Figure 1.9).

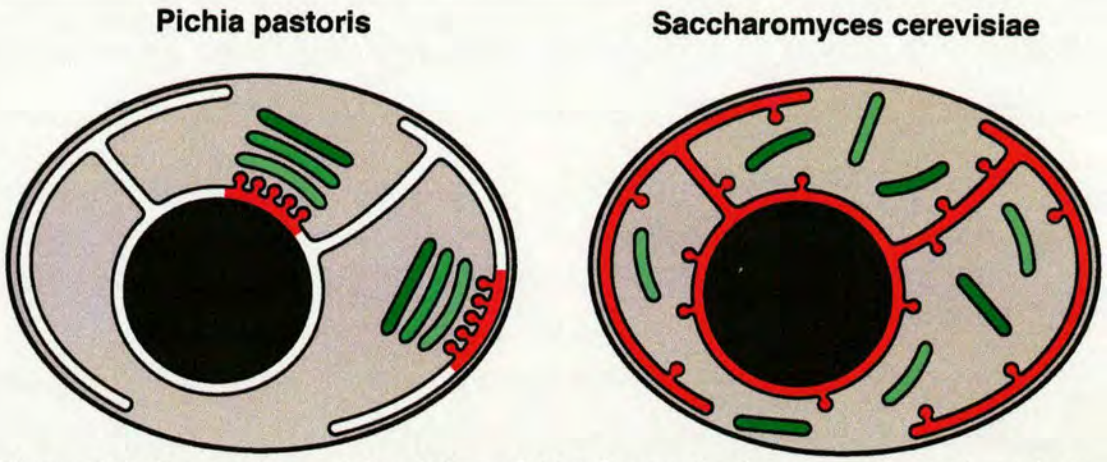

Figure 1.9: Comparison of the tER and Golgi organisation in *P. pastoris* and *S. cerevisiae*. *P. pastoris* exhibits discrete tER sites (red) that give rise to polarised Golgi stacks (green). *S. cerevisiae* produces COPII vesicles from the entire ER network (red), while only Golgi cisternae dispersed in the cytoplasm can be observed. Cis-Golgi (early) cisternae are indicated with light green, whereas trans-Golgi (late) cisternae have dark green colour. Adapted from Rossanese et al., 1999.

Based on these findings, it was proposed that the tER organisation correlates with the Golgi structure. According to this model, the focused tER sites of *P. pastoris* seem to produce COPII-coated vesicles with a local concentration high enough to allow cisternal formation and stacking. On the other hand, COPII vesicles budding from the dispersed tER sites of S. *cerevisiae* reach probably a too low local concentration, and therefore, they can only sustain formation of single cisternae, and not their subsequent stacking. Alternatively or additionally to this kinetic view of Golgi stack formation, the existence of a t-ER matrix in *P. pastoris* could organise the tER

sites at specific regions of the ER (Rossanese et al., 1999). This would not exclude the presence of a Golgi matrix, distinct or common with the putative tER matrix, which could correspond to the ribosome-excluded region that surrounds the tER sites and Golgi stacks observed in electron microscopy and tomographic studies (Mollenhauer and Morre, 1978; Mogelsvang et al., 2003).

All these observations, in combination with the reported cycling of Golgi matrix proteins between the tER and the Golgi apparatus in mammalian cells (Barr, 2002), are indicative of an existing cross-talk between the tER sites and the Golgi apparatus.

1.7 Drosophila: A model organism for genetic, developmental and cell biology studies

Drosophila melanogaster has been for many decades one of the most popular organisms for genetic and developmental studies for multiple reasons. First of all, its culture is easy and inexpensive, while it is not harmful to humans. The generation time is relatively short, and the development from an embryo to the adult fly takes about 10 days at 25°C. Under ideal conditions, the *Drosophila* life span is about two months (Ashburner, 1989). Second, D. *melanogaster* has been used as a genetic model for the last 100 years due to the ease that mutations can be isolated and studied. This has resulted in the identification of important biological processes and the creation of thousands of transgenic cell lines. Third, a big advantage of using *Drosophila* as experimental model is the fact that its development has been described in detail. It exhibits a complex development that includes the formation of all the major cell types found in higher animals. This facilitates the extension into development of findings at the genetic or cell biology level, which is not possible in unicellular organisms like yeast, or very difficult in mammals. The cell biology of the flies is also well known, although not as extensively as

this of the mammalian cells. However, the subcellular organisation of *Drosophila* cells seems to share similar characteristics with the higher eukaryotes. Finally, since March 2000, the entire *Drosophila* genome has been sequenced (Adams et al., 2000) providing a valuable tool in the search for gene and protein homologues between the flies and other organisms, which will promote the study of cell biological processes throughout evolution.

1.7.1 Life cycle

The *Drosophila* life cycle comprises four stages: embryo, larva, pupa, and adult. After fertilization the zygotic embryo undergoes 14 rapid mitotic divisions without cytokinesis, leading to the formation of a syncytial blastoderm containing about 6000 nuclei. Cellularisation of the blastoderm takes place by synchronous deposition of membrane between the nuclei. During gastrulation, the peripherally located cells migrate inwards forming the 3 primary cell types (ectoderm, mesoderm, endoderm). Subsequent complex cell movements and cell differentiation generates the internal and external structures of the larval body, before the embryo hatches, about 24 hours after being laid (Foe et al., 1993).

Upon hatching, the fly enters the larval period, which lasts a total of 5-7 days, and is divided into three instars (stages). During the transitions from one instar to the next (molting periods), the larva sheds its cuticle, mouth hooks, and spiracles. Throughout the duration of the three instars, larva is continuously feeding and increases in size (Ashburner, 1989).

The end of the third instar larval stage is characterised by the eversion of the anterior spiracles and the formation of the puparium (pupal case), due to the retraction of the epidermis and the hardening of the larval skin. From this point and until the adult has emerged, the animal is, technically, a pupa. The entire metamorphosis takes place inside the puparium (Bainbridge and

Bownes, 1981). During this remarkable process, all the organs of the adult fly are formed from precursor groups of cells, known as imaginal discs (see 1.7.2) and histoblasts. When metamorphosis is completed, the adult male or female fly emerges from the pupal case (eclosion). Few hours after eclosion, the adult fly becomes sexually mature.

1.7.2 Imaginal discs

The third instar larval stage is one of the best studied during *Drosophila* development, because at this stage, larvae are large and can be manipulated easily. Moreover, at this developmental stage, many interesting morphogenetic events take place. One of these events is the initial phase of imaginal disc elongation, which occurs between the stages of early third-instar larvae and puparium formation (white pupa stage).

Imaginal discs begin as small groups of 2-20 precursor cells, which are specified during the embryonic development. In the following 3 larval instars, the imaginal discs, which are located at specific parts of the larval body, proliferate without being differentiated. In 3rd instar larvae, they appear as flat, concentrically folded, sac-like structures. They comprise two epithelial cell layers: one is a squamous thin epithelium (peripodial membrane), and the other is folded and comprises columnar cells (5μm in diameter and up to 30μm in height) (Fristrom and Fristrom, 1993). During late 3rd-instar larval development, the more peripheral epithelial cell folds constrict, pushing the central folds toward the peripodium. As a consequence, the imaginal discs lose their flattened shape and expand or elongate, depending on the shape of the organ that they are programmed to generate (Fristrom and Fristrom, 1993). This first phase of disc elongation is completed at the puparium formation. In the subsequent stages of pupal development, the imaginal discs continue their morphogenesis, and

eventually will give rise to all adult appendages (Fristrom and Fristrom, 1993).

Puparium formation and all the morphogenetic events taking place at the late 3rd instar are tightly controlled by the steroid hormone 20-hydroxyecdysone (ecdysone) (Fristrom and Fristrom, 1993). One of the three highest peaks of ecdysone during *Drosophila* development occurs 6-8 hours prior to puparium formation (the other two occur during the embryonic and the pupal stage) (Richards, 1981). The prepupal ecdysone peak has been shown to activate the expression of the "early puff genes" via the heterodimeric receptor complex comprising the ecdysone receptor, EcR, and the gene product of *ultraspiracle* (Koelle *et al.*, 1991). At least three of these "early genes" encode transcription factors, such as Broad complex (DiBello *et al.*, 1991; Andres *et al.*, 1993), E74 (Burtis *et al.*, 1990), and E75 (Segraves and Hogness, 1990). These transcription factors self-attenuate their own transcription and activate the transcription of more than a hundred "late puff genes" that are involved in a variety of developmental events.

1.7.3 The early exocytic pathway in *Drosophila*

As it was mentioned before, the cell biology of *Drosophila* is not as extensively studied as in mammalian cells. Although morphological studies in different *Drosophila* tissues have shown that the organisation of the exocytic pathway resembles this of the mammalian cells, information about the molecular aspects the pathway has only been fragmentary.

The general morphology of the Golgi apparatus in *Drosophila* cells and tissues is similar to that of the mammalian cells. The most striking difference is the lack of interconnections between the individual Golgi stacks, which in mammalian cells form the Golgi ribbon. In contrast, the *Drosophila* Golgi stacks do not exhibit a pericentriolar distribution, and they remain usually

dispersed throughout the cytoplasm (Ripoche et al., 1994; Stanley et al., 1997; Rabouille et al., 1999). Moreover, it is worth mentioning that in certain developmental stages and tissues, such as the pre-cellularised and gastrulating embryos, and the salivary glands of early 3rd instar larvae, no Golgi stacks appear to be present in the cells. Instead, vesicular-tubular clusters are observed, which have been suggested to represent the Golgi membranes (Fullilove and Jacobson, 1971; Thomopoulos et al., 1992; Ripoche et al., 1994; Stanley et al., 1997).

The observed similarity in the basic morphological features between *Drosophila* and mammalian Golgi apparatus indicates that most proteins involved in Golgi architecture and functions are likely to be conserved in flies. Our lab has conducted an extensive database search, which indeed has shown that most Golgi-related proteins found in mammalian cells have putative homologues in *Drosophila* (Figure 1.10; Dunne and Rabouille, 2001). The cytogenetic map of a fraction of the *Drosophila* homologues of genes associated with the structural and functional organisation of the Golgi apparatus shows that the genes associated with the Golgi structure and functions are distributed in all three major *Drosophila* chromosomes (Figure 1.10).

Nevertheless, there are also examples of some mammalian proteins for which no obvious homologues have been found in the *Drosophila* genome. Considering the golgins, it has to be pointed out that, although their majority is conserved in flies, two out of the three golgins with a transmembrane domain (giantin and CASP) do not have a clear homologue and only golgin-84 seems to be present in *Drosophila* (Dunne and Rabouille, 2001; Gillingham and Munro, 2003). The same is true for GGAs (Golgi-localizing, gamma-adaptin ear homology domain, ARF-binding proteins), which function as adaptors for the formation clathrin-coated vesicles at the TGN (Bonifacino,

2004). *Drosophila* has only one GGA homologue instead of three that exist in mammalian cells. Furthermore, an apparent homologue for TGN38/46, an integral membrane protein commonly used as a marker for the TGN in the mammalian cells (Luzio et al., 1990), does not exist in *Drosophila* (Dunne and Rabouille, 2001).

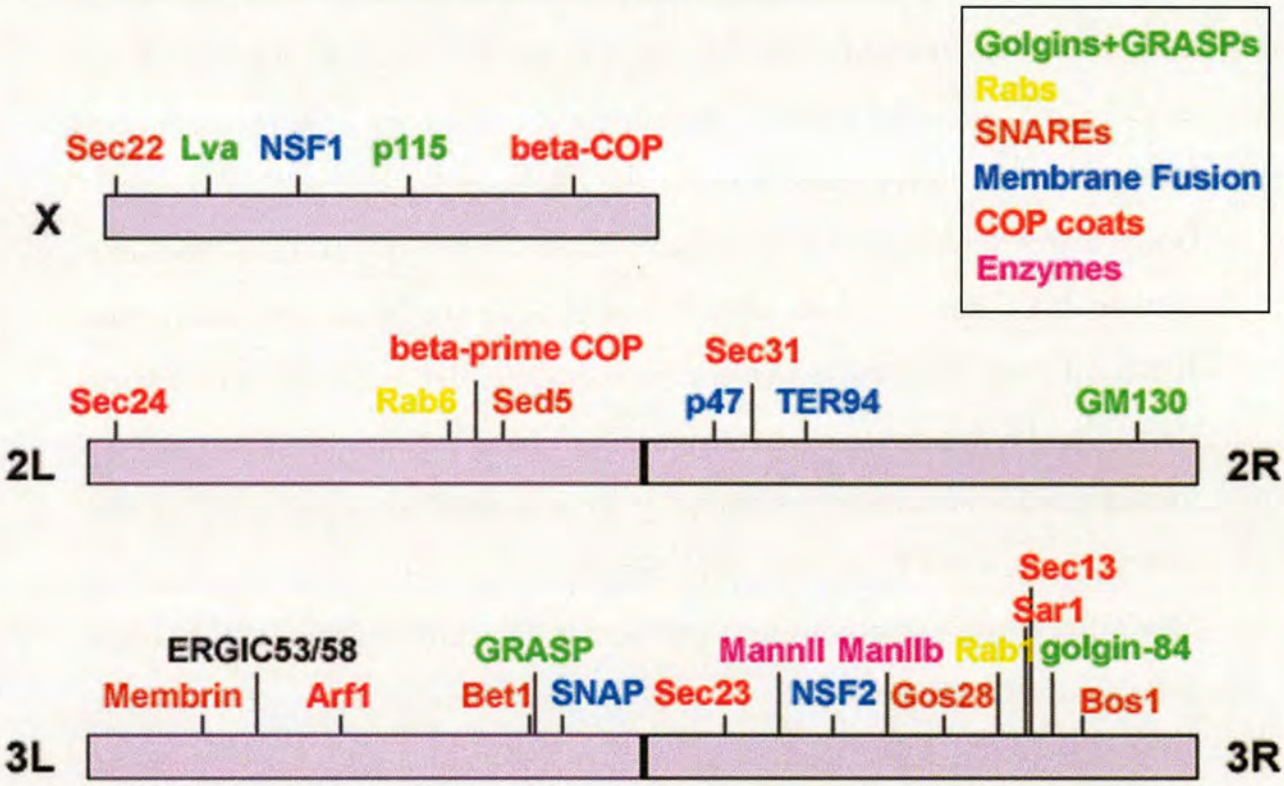

Figure 1.10: Distribution of Golgi-related genes in *Drosophila* genome. *Drosophila* homologues of mammalian genes related to functional or structural aspects of the early exocytic pathway are depicted in a simplified map of the three major *Drosophila* chromosomes (X, 2nd and 3rd) of the fly genome. Different colours have been used to mark the different functions of the proteins encoded by these genes. The black line in the middle of the 2nd and 3rd chromosome represents the centromere. L, left chromosome arm; R, right chromosome arm.

Despite the identification of putative homologues for most proteins related to the early exocytic pathway, the functional characterisation for the majority of them still needs to be performed. β-COP, one of the COP I coat subunits, has been localised in the Golgi membranes in *Drosophila* embryos

and tissue culture cells (Ripoche et al., 1994). Using β-COP and another integral Golgi protein of 120kd as Golgi markers (Stanley et al., 1997), it was demonstrated that the Golgi membranes in the beginning of cycle 14 (precellularised embryos) are located apically relative to the nuclei. Subsequently, cellularisation takes place, which comprises an initial "slow phase" followed by a "fast phase". During the slow phase, Golgi membranes move basally in a saltatory fashion and then, individual Golgi elements move apically and associate with the advancing furrow front. Finally, when the furrow front has progressed beyond the nuclei at the end of "fast phase", Golgi membranes move again rapidly towards the cell surface (Foe and Alberts, 1983; Ripoche et al., 1994; Sisson et al., 2000; Dunne and Rabouille, 2001). All these Golgi movements, as well as Golgi-derived membranes, were shown to be essential for the furrow progression that leads to plasma membrane formation, and eventually to successful cellularisation of the embryo (Lecuit and Wieschaus, 2000; Sisson et al., 2000).

The relationship between anterograde transport through the exocytic pathway and cell division has been further exemplified by two recent studies. Flies bearing a mutation in dSed5, the *Drosophila* homologue of t-SNARE Syntaxin 5 (Banfield et al., 1994) that is involved in ER-Golgi transport (Hardwick and Pelham, 1992), were shown to have impaired anterograde transport to the plasma membrane and cytokinesis defects during spermatogenesis (Xu et al., 2003). In the second case, mutation in dCOG5 was also shown to affect cytokinesis of developing spermatids (Farkas et al., 2003). dCOG5 is the *Drosophila* homologue of the mammalian COG5, which is a subunit of the octameric COG complex (Sec34/35 complex in yeast). This complex has been implicated in vesicle tethering during transport through the Golgi apparatus (Ungar et al., 2002; Whyte and Munro, 2001).

Concerning the role of Golgi matrix proteins in *Drosophila*, the available information is very limited. An interesting protein is Lava lamp (Lva), which exhibits long coiled-coil structure and localises in the Golgi membranes, both characteristics of the golgin protein family (Sisson et al., 2000). Lva does not have obvious homologues in other organisms and was identified in a screen for microfilament/microtubule–associated proteins from *Drosophila* embryo extracts (Sisson et al., 2000). Additionally, Lva was shown to interact with spectrins that have been proposed to form a scaffold around the Golgi preserving its structural organisation and regulating membrane transport through it (De Matteis and Morrow, 2000). These interactions together with the observed impairment of transport upon interference with Lva function, has led to the suggestion that it might be part of a Golgi-based scaffold, similar to the Golgi matrix that has been proposed to exist in the mammalian cells.

Despite the limited knowledge on the molecular and functional organisation of the *Drosophila* exocytic pathway, the sequence of *Drosophila* genome in combination with the easy genetic manipulation of the flies and the advent of the recently developed technique of RNA interference (RNAi) are bound to accelerate our understanding on this aspect of fly cell biology.

1.8 RNA interference (RNAi)

Until recently, the question of a protein function was addressed by most cell biologists, using the transient expression of full-length or truncated mutant forms of this protein. However, this approach can lead to ambiguous results, as the expressed protein may have additional functions or interact with its endogenous counterpart (Hudson et al., 2002). A better way to answer this question, avoiding complications in the interpretation, is to deplete the protein of interest and then study the effect of its absence *in vivo*. This is the

principle of a reverse genetic approach, which was immensely facilitated by the discovery of RNA interference few years ago.

The phenomenon of RNA interference (RNAi) in animal cells was described for the first time in *Caenorhabditis elegans* by Fire et al (1998). Soon after that, it became clear that this process is ancient and exists from protozoa to humans. As a term, RNAi has been used to describe the process of post-transcriptional gene silencing in worms, flies and mammals. Related phenomena in plants and Neurospora are known as co-suppression and quelling or meiotic silencing by unpaired DNA (MSUD), respectively (Zamore, 2002).

1.8.1 Mechanism and biological functions of RNAi

Our understanding on how RNAi works has derived from genetic and biochemical studies in *C. elegans*, plants and *Drosophila* (Hannon, 2002). Gene silencing can be triggered by *in vitro* synthesized double-stranded RNA (dsRNA), dsRNA from replicating viruses or transposons, and dsRNA from transcribed transgenes or nuclear genes (Denli and Hannon, 2003). In all cases, the dsRNAs are recognised by an evolutionary conserved RNAse III-type enzyme family, named Dicer enzymes, which cleave them into 21-25 nucleotide small interfering RNAs (siRNAs) (Figure 1.11). These siRNAs are then transferred to a nuclease complex called RISC (RNA-induced silencing complex). RISC is activated by unwinding the dsRNA (Nykanen et al., 2001) and subsequently, is guided by the anti-sense strand to find and degrade mRNAs with complementary sequence or to inhibit their translation (Hannon, 2002; Figure 1.11). Moreover, in plants and fungi, RISC activation can promote methylation of homologous DNA inducing stable and inheritable transcriptional gene silencing (Martienssen and Colot, 2001). Finally, in plants and *C. elegans*, but not yet in *Drosophila* and mammalian

cells, it has also been shown that dsRNA silencing signal needs to be amplified (transitive RNAi). This is carried out by an RNA-directed RNA polymerase (RdRP), which may be included in the RISC complex or form a distinct complex (Hannon, 2002).

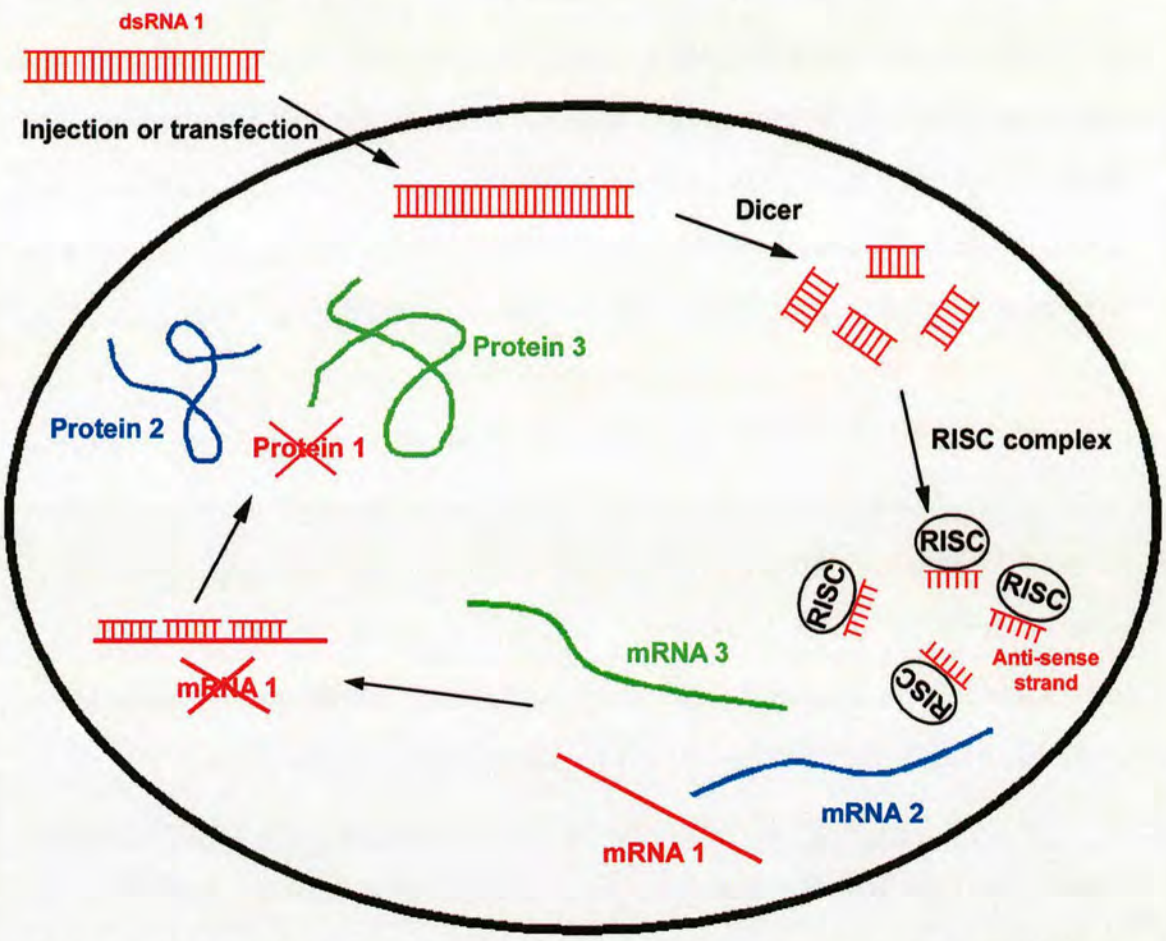

Figure 1.11: Principle of RNA interference. Long (0.5-1.0 kb) synthetic dsRNAs are introduced in *Drosophila* or *C. elegans* cells by injection or transfection. Dicer enzyme recognises the dsRNAs and cleaves them into small interfering RNAs (siRNAs). The siRNAs are transferred to RISC nuclease complex, which becomes activated by unwinding them. Having as a guide the anti-sense strand of siRNAs, the activated RISC complex recognises and binds to the mRNA with complementary sequence (mRNA 1), but not to other mRNAs with unrelated sequence (mRNAs 2 and 3). The binding of RISC on the target mRNA promotes its degradation. As a consequence, the protein encoded by this mRNA (Protein 1) stops being produced, while the translation of all the other proteins (Proteins 2 and 3) remains unaffected. In differentiated mammalian cells, long dsRNAs induce sequence-independent cytotoxicity, which can be bypassed, if the cells are transfected directly with synthetic siRNAs.

The RNAi mechanism is involved in several biological processes. First, it is believed to act as a defence mechanism for viral infections (Zamore, 2002). In fact, the reason why RNAi experiments were not possible in mammalian tissue culture cells until recently (Elbashir et al., 2001), was because the long synthetic dsRNA introduced into the cells induced the activation of such an anti-viral mechanism (Williams, 1999). Second, RNAi has been linked to the repression of DNA transposition and the removal of aberrant non-functional RNAs from nucleus or cytoplasm (Tijsterman et al., 2002). In this way, RNAi may stabilise the genome by preventing the jump of transposons and restricting the repetitive elements that lead to recombination events and chromosome translocations (Hannon, 2002). Furthermore, RNAi-related mechanisms regulate gene expression at the transcriptional and translational level. Examples of transcriptional regulation include DNA-methylation, transposon silencing and co-suppression. The latter refers to the silencing of an endogenous gene following the introduction of a homologous transgene (Sharp, 2001). At the translation level, RNAi is thought to be related to development (Tijsterman et al., 2002). In *C. elegans*, mutation in Dicer gene, DCR-1, causes sterility and further developmental abnormalities during larval growth or the transition of larvae to adults (Grishok et al., 2001; Ketting et al., 2001). In addition, small temporal RNAs (stRNAs) produced from lin-4 and let-7 genes, are post-transcriptionally processed from ~70-nucleotide precursors to ~21-nucleotide mature form. These stRNAs act as negative regulators of specific protein-coding genes by inhibition of translation and not mRNA degradation. Similar to DCR-1 mutants, mutations in lin-4 and let-7 genes affect larval transitions in worms (Hannon, 2002).

1.8.2 Methodology

The methodology for performing RNAi varies between the different organisms. In *C. elegans*, long dsRNAs can be injected, used to soak the worms in or added in the food (Zamore, 2002). One of the fascinating aspects of RNAi in *C. elegans* is its systemic nature (Tijsterman et al., 2002). That means that even if a small quantity of dsRNA is injected to a particular part of the worm, the silencing effect will spread to other tissues. Only neuronal cells seem to be resistant to systemic silencing (Winston et al., 2002). Systemic acquired silencing is also observed in plants (Palauqui et al., 1997).

In *Drosophila* tissue culture cells, RNAi simply requires the addition of dsRNA (usually 0.5-1 kilobases in length), corresponding to the coding region, or/and the 5′ and 3′ UTRs of the gene of interest, into the culture medium. A big advantage of RNAi in *Drosophila* is that it allows the study of a gene function during development. For example, by injecting embryos with a specific dsRNA, it is possible to investigate the function of the targeted protein during embryogenesis (Kennerdell and Carthew, 1998). In this way, maternal contribution problems can be overcome. However, the most powerful innovation of RNAi technology in *Drosophila* is the possibility of creating transgenic flies with inducible expression of dsRNA (Tavernarakis et al., 2000; Kennerdell and Carthew, 2000; Lam and Thummel, 2000; Kalidas and Smith, 2002). The methodology behind the inducible RNAi is to generate a transgene, where two complementary cDNA copies of the target gene are inverted and connected with a non-palindromic sequence. This construct is placed under the control of a UAS transcription element. A cross between this transgenic fly and a fly having a GAL4 transgene will result in F1 progeny that produces RNA transcripts with a hairpin-loop conformation. The expression of the dsRNA and the subsequent RNAi-mediated silencing will only be conferred to those cells that activate the specific GAL4 driver

that has been used in the cross (Kennerdell and Carthew, 2000). Instead of cDNA, genomic sequences have also been used for the transgene construction. In this case, the hairpin-loop is formed after splicing of the genomic sequence, and this modification seems to improve the efficiency of silencing (Kalidas and Smith, 2002). Inducible RNAi provides a means of studying the role of a protein at a specific developmental stage and tissue by using different GAL4 drivers. Thus, it gives the opportunity to study later functions of genes that cause early lethality and, essentially, it permits the generation of dominant temperature-sensitive alleles for any gene (Lam and Thummel, 2000).

Performing RNAi in mammalian cells also involves different strategies. In embryonic cultured cells, oocytes and early embryos, it is possible to obtain silencing by transfecting or injecting the cells with long dsRNAs, like in *C. elegans* and *Drosophila* (Zamore, 2002). However, gene silencing in differentiated cultured cells can only be done by transfecting them with 21-23 nucleotide siRNAs (Elbashir et al., 2001). Due to the high cost of siRNA chemical synthesis, DNA plasmid vectors were developed, which are capable of producing short hairpin-loop RNAs, when transfected in cultured cells (Paddison et al., 2002; Brummelkamp et al., 2002). Nevertheless, because both chemically synthesised siRNAs and plasmid-based hairpin siRNAs have to be introduced in the cells by transfection, this restricts their use only to those cell lines that can be transfected and even then, problems of low transfection efficiency or inconsistency can be encountered (Devroe and Silver, 2002). To deal with these difficulties, the latest development in the field is the delivery of hairpin siRNAs into the cells using retrovirus vectors (Barton and Medzhitov, 2002; Devroe and Silver, 2002). This method makes RNAi possible in most cell lines and primary cell types. Furthermore, as retroviral vectors integrate into the genome, they

produce stable mutant cell line, overcoming the transient effect of RNAi, observed in normal transfections (Barton and Medzhitov, 2002).

1.8.3 Specificity

A reason why RNAi is considered to be a powerful technique is that the post-translational silencing is specific for the mRNA that exhibits identical sequence with that of the siRNA. Single nucleotide mismatch between siRNA and target mRNA does not confer RNAi-mediated silencing (Brummelkamp et al., 2002). However, the existence of RNAi-related mechanisms that may lead to general translation inhibition or DNA remodelling makes the use of sufficient controls in RNAi experiments very important. For instance, recently, it was shown that some siRNAs can induce a decrease in the expression of proteins with sequences unrelated to that of the target gene (Scacheri et al., 2004).

The issue of controlling the RNAi specificity has been discussed in the editorial of Nature Cell Biology (June, 2003) proposing a list of controls for RNAi experiments. As basic controls, the expression of both the mRNA and the protein should be monitored. This will rule out the possibility of a general translation arrest in case only protein levels are reduced. Another good control is to obtain the same effect using at least another siRNA that targets a different domain of the gene of interest. Finally, the ultimate control is a functional one, where the RNAi phenotype should be rescued by introducing the targeted gene back to the cells. This can be done in two ways: either by expressing the target gene containing one or more silent mutations in the targeted site or, by expressing the wild-type target gene but use a siRNA directed against the 5′ or 3′ UTR of the gene. In both cases, only the mRNA from the endogenous gene should be degraded.

1.8.4 Applications

The extremely fast development of the RNAi methodology has initiated a new era in functional genomics, reducing the required time between the identification of a gene and the discovery of its function. An application that is bound to dominate the future of cell biology is the use of genome-wide genetic screens by RNAi (Gartner, 2003). Libraries of bacteria have already been made that correspond to about 90% of the predicted genes in *C. elegans* (Kamath and Ahringer, 2003) and *Drosophila* (Boutros et al., 2004), while this will soon be true for the human genome (Brummelkamp et al., 2003). Genes involved in basic biological processes, like body fat regulation, maintenance of genome stability or cell growth and viability, have been identified in such high-throughput screens (Ashrafi et al., 2003; Pothof et al., 2003; Boutros et al., 2004). An additional potential application of RNAi technology is in therapeutics of cancer and diseases caused by point mutations in different genes. Taking advantage of the absolute match between the dsRNA and the target mRNA to obtain RNAi-mediated silencing, the expression of a mutated gene can be targeted without affecting the wild-type gene (Brummelkamp et al., 2002; 2003). Finally, another interesting RNAi application is also in identifying gene targets for drugs or biochemical pathways in which a drug or pesticide is involved (O'Neil et al., 2001; Brummelkamp et al., 2003).

Chapter Two
Materials and Methods

2.1 Materials

2.1.1 Chemicals

General purpose chemicals were purchased from Sigma-Aldrich, BDH, Fisher Scientific and Merck. In case of a different supplier, the company's name is mentioned in the text.

2.1.2 Buffers and Solutions

All buffers and solutions were prepared with double distilled water (ddH_2O). Sterilisation, when required, was achieved by autoclaving for 30 minutes at 15 psi. Solutions were stored at room temperature (RT, 23-25°C), unless otherwise stated. General solutions and buffers are listed in Table 2.1, buffers for gel electrophoresis in Table 2.2 and, buffers and solutions for electron microscopy in Table 2.3.

Table 2.1: General solutions and buffers

Solution	Components/Preparation	Final concentration
DEPC-ddH_2O	0.5ml Diethyl Pyrocarbonate (DEPC) Adjust the volume to 500ml with ddH_2O. Autoclave to deactivate DEPC.	0.1%
Phosphate Buffer Saline (PBS, 10x) pH 7.4	80g NaCl (Mw: 58.44) 2g KCl (Mw: 74.55) 14.4g $Na_2HPO_4.2H_2O$ (Mw: 178) 2.3g $NaH_2PO_4.H_2O$ (Mw: 138) Adjust the volume to 1l with ddH_2O. Dilute 1:10 prior to use.	1.37M 26.8mM 80.9mM 16.7mM
0.2M Phosphate Buffer (PB) pH 7.4	Buffer A: 27.6g $NaH_2PO_4.H_2O$ (Mw: 138) in 1l ddH_2O Buffer B: 35.7g $Na_2HPO_4.2H_2O$ (Mw: 178) in 1l ddH_2O Mix 19ml of buffer A with 81ml of buffer B.	0.2M 0.2M

TE pH 8.0	1ml 1M Tris-HCl, pH 8.0 200µl 0.5M EDTA, pH 8.0 Adjust the volume to 100ml with ddH_2O	10mM 1mM
Drosophila Ringer	8g NaCl (Mw: 58.44) 0.2g KCl (Mw: 74.55) 1g $NaHCO_3$ (Mw: 84.01) 0.04g $NaH_2PO_4.H_2O$ (Mw: 138) 0.2g $CaCl_2.2H_2O$ (Mw: 147) 0.05g $MgCl_2$ (Mw: 95.21) 1g glucose Adjust the volume to 1l with ddH_2O	13.7mM 2.7mM 11.9mM 0.3mM 1.4mM 0.5mM 0.1%

Table 2.2: Solutions for SDS-PAGE and agarose gel electrophoresis

Buffer	Components/Preparation	Final concentration
Homogenisation Buffer	200µl 1M Tris-HCl pH 7.5 20µl 0.5M EDTA pH 8.0 100µl 1M MgCl2 100µl 1M KCl 25µl 4M NaCl 100µl 100mM DTT 1ml 2.3M sucrose 2 complete mini protease inhibitor cocktail tablets (Roche) Adjust the volume to 10ml with ddH_2O. Aliquots of 0.5ml were frozen at -20°C and were defrosted prior to use.	20mM 1mM 10mM 10mM 10mM 1mM 0.23M
SDS-PAGE Migration Buffer (5x)	15g Tris base (Mw: 121.1) 72g glycine (Mw: 75.07) 2.5g SDS (Mw: 288.38) Adjust the volume to 500ml with ddH_2O. Dilute 1:5 prior to use.	250mM 1.92M 0.5%
Blotting Buffer	40ml 5x SDS-PAGE migration buffer 100ml Methanol 0.25ml 20% SDS	1x 20% 0.01%

	Adjust the volume to 500ml with ddH_2O	
Ponceau S (10x)	2g Ponceau S	2%
	30g trichloracetic acid (Mw: 163.39)	184mM
	30g 5-Sulfosalicylic acid dihydrate (Mw: 254.22)	118mM
	Adjust the volume to 100ml with ddH_2O.	
	Dilute 1:10 prior to use.	
Membrane Stripping Buffer	690µl Mercaptoethanol	100mM
	2g SDS	2%
	6.25ml 1M Tris-HCl pH 6.5	62.5mM
	Adjust the volume to 100ml with ddH_2O.	
DNA Sample Buffer (6x)	0.25g bromophenol blue (Mw: 669.96)	0.37mM
	0.25g xylene cyanol (Mw: 538.6)	0.46mM
	50ml glycerol	50%
	1ml 1M Tris-HCl pH 8.0	10mM
	Adjust the volume to 100ml with ddH_2O.	
TAE Buffer (50x)	121g Tris base (Mw: 121.14)	1M
	28.55ml glacial acetic acid	5.7%
	50ml 0.5M EDTA pH 8.0	50mM
	Adjust the volume to 500ml with ddH_2O.	
	Dilute 1:50 with ddH_2O prior to use.	

Table 2.3: Solutions for electron microscopy

Solution	Components/Preparation
0.1M Cacodylate buffer pH 7.4	0.69g Cacodylic acid (Mw: 138)
	Adjust the volume to 50ml with ddH_2O.
	Adjust pH.
Agar 100 Epoxy Resin (Agar scientific)	12g Agar 100 epoxy resin
	8g DDSA hardener
	5g MNA hardener
	0.75g BDMA accelerator
	Mix thoroughly before use.
4% aqueous Uranyl Acetate	2g uranyl acetate
	Adjust the volume to 50ml with ddH_2O.
	Store at 4°C for maximum 2 months.

	Filter before use through a 0.22μm filter.
7% Uranyl Acetate in 70% methanol	3.5g uranyl acetate 35ml methanol Adjust the volume to 50ml with ddH_2O. Store at 4°C for maximum 2 months. Filter before use through a 0.22μm filter.
Lead Citrate (Reynolds, 1963)	1.33g $Pb(NO_3)_2$ 1.76g $Na_3C_6H_5O_7.2H_2O$ Add 30ml ddH_2O and mix well. Leave for 30 minutes. Add 8ml 1N NaOH. Adjust the volume to 50ml with ddH_2O. The final pH should be around 12.

2.1.3 Cell lines

S2 cells are a *Drosophila* embryonic cell line of mesodermal origin and were obtained from Margarete Heck's lab (Edinburgh, UK).

Delta WTNdeMyc S2 cells, (referred to as Delta S2 cells), are stably transfected to express the full-length Delta protein with a C-terminal MYC epitope tag (Klueg et al., 1998), and were kindly provided by Dr. Kristin Klueg (Bloomington, Indiana).

ScAb-S20 is a stable S2 cell line expressing a secreted recombinant monoclonal antibody (scFv) tagged with the human kappa-light chain domain (Ck). scFv-S20 cell line expresses the same scFv molecule tagged with a MYC epitope in its C-terminus (Reavy et al., 2000). Both cell lines were a kind gift from Brian Reavy (SCRI, Dundee, UK).

2.1.4 Fly stocks

Genotypes of all fly stocks used in the present thesis are listed in table 2.4. Additional information about the experiments where they were used are provided in the relevant chapters.

Table 2.4 Common wild type and balancer fly stocks

Stock	Genotype	Comments / Donor
Oregon R	Wild type	Red eyed wild type, Andrew Jarman
w^{1118}	Wild type	White eyed wild type, Andrew Jarman
MF919	yw; P [w^+, UAS-Fringe 5 (ADD)]	Myc tagged Fringe abolishing glycosyltransferase activity but retaining its Golgi localisation Matthew Freeman
hsGAL4 / Elp, Bc, Gla		Appearance of black cells after late first instar larval stage and ellipsoid eyes in adults Petra zur Lage

2.1.5 Antibodies

All primary and secondary antibodies used during this project are listed in table 2.5 and 2.7, respectively. Information about the recognizing antigen, as well as the working concentrations for western blotting (WB), immuno-fluorescence (IF) and immuno-electron microscopy (IEM), is given. Table 2.6 contains additional information about the part of the protein against which each primary antibody is raised and its lab of origin together with the reference where it was first described.

Table 2.5 List of primary antibodies[1]

Antibody name	Recognising Protein	Working concentration		
		WB	IF	IEM
MLO7	GM130 / dGM130	1:250	1:200-250	1:30
NN7	p115 / dp115	nd	1:200	1:100
dp115/584	dp115	1:20-75	nd	1:3-10
GRASP65	GRASP65 / dGRASP	1:150	Not working	1:30-50
COPII [2]	Sec23 / dSec23p	1:750	1:300-400	1:300-400
Sec23 [2]	Sec23 / dSec23p	nd	1:150	nd
a-Drosophila Golgi	120kd Golgi	1:500	1:200	1:80-100
JSEE1	Syntaxin 5 / dSed5p	1:300	nd	nd
C594.9B *	Delta	1:500	1:50	1:250
dGMII	dGMII	1:200	1:150	1:50
9E10 *	MYC epitope	1:250-400	1:150	1:100
Sec31p	Sec31p / dSec31p	nd	1:100	nd
δAP3	δAP3	nd	1:150	nd
1D3*	Protein disulfide	nd	1:150	nd
Cκ	scAb-S20 protein	1:250	nd	nd
α-tubulin *	α-tubulin	nd	1:2000	nd

[1] Primary antibodies were rabbit polyclonal antibodies except for those marked with an asterisk which were mouse monoclonal antibodies.

[2] Both anti-COPII and Sec23 antibodies will be referred to in the results as anti-Sec23 antibodies. The first has been used in all RNAi experiments (chapters 3-6), while the second was used in chapter 7.

Table 2.6 Characterisation of primary antibodies

Antibody name	Antigen	Source / Reference
MLO7	73 N-terminal amino acids of rat GM130	M. Lowe Nakamura et al., 1997
NN7	Full-length rat p115 protein	M. Lowe Nakamura et al., 1997
dp115/584	dp115-specific peptide (G)CSKLAEVSRHEAYSRA	Rabouille lab Kondylis and Rabouille, 2003
GRASP65	Recombinant GRASP65	F. Barr Shorter et al., 1999
a-COPII	Peptide MTTYLEFIQQNEERDGVR	Affinity Bioreagents, Inc.
Sec23	41-361 amino acids of human Sec23	J.P. Paccaud Paccaud et al., 1996
a-Drosophila Golgi	The immunogen was purified Golgi membranes from Drosophila embryos	Calbiochem Stanley et al., 1997
JSEE1	Full-length rat Syntaxin 5	M. Lowe Lowe et al., 2004
C594.9B	*Drosophila* Delta extracellular domain	DSHB, IA Generated in the lab of S.Artavanis-Tsakonas
dGMII	14 C-terminal amino acids of Drosophila Golgi α-mannosidase II (CPMETAAYVSSHSS)	D. Roberts Rabouille et al., 1999
9E10	MYC epitope	T. Nilsson Nilsson et al., 1993
Sec31p	323-436 amino acids of human Sec31	F. Gorelick Shugrue et al., 1999
δAP3	22-756 amino acids of δ-subunit of human AP3	M.S. Robinson Simpson et al., 1997
1D3	C-terminal peptide KDDDQKAVKDEL of human PDI	D. Vaux Fricker et al., 1997
Cκ	Cκ domain of human IgG	B. Reavy Reavy et al., 2000
α-tubulin	Microtubules from chicken embryo brain	Sigma Blose et al., 1984

Table 2.7 List of secondary antibodies

Antigen	Host	Conjugate	Working concentration		Source, Product number
			WB	IF	
Mouse IgG	Horse	HRP	1:1000	--	Vector, PI-2000
Mouse IgG	Sheep	HRP	1:2000	--	Amersham Biosciences, NA931V
Mouse IgG	Horse	Texas Red	--	1:150	Vector, TI-2000
Mouse IgG	Goat	Alexa-568	--	1:200	Molecular Probes, A-11031
Rabbit IgG	Goat	HRP	1:1000	--	Vector, PI-1000
Rabbit IgG	Donkey	HRP	1:2000	--	Amersham Biosciences, NA934V
Rabbit IgG	Goat	FITC	--	1:150	Vector, FI-1000
Rabbit IgG	Goat	Alexa-488	--	1:200	Molecular Probes, A-11034

2.1.6 cDNAs and genomic clones for dsRNA production

Clone name	Containing gene	Preparation method / comments
1P2C1	dp115	Screening an embryonic cDNA library with a DNA probe made from EST LD41079
p5.6KK	dGM130	Genomic clone (gift from T. Orr-Weaver) containing the MeiS32 gene (Kerrebrock et al, 1995) and the coding sequence of dGM130 (C. Rabouille, unpublished results)
Clone 3.5	dGRASP	RT-PCR amplification from total RNA isolated from Drosophila Kc cells and subsequent cloning into TOPOII vector (Invitrogen) and sequencing

2.1.7 Primers

The primers used to amplify the DNA fragments, which were subsequently used as templates for dsRNA production in RNA interference (RNAi) experiments, are listed in table 2.8. Information about the primers that were used for RT-PCR, are mentioned in table 2.9.

In RNAi primers an additional sequence was added to the 5′ end of each primer, which corresponds to the promoter sequence of T_7 or T_3 RNA polymerase. Either of these two enzymes was used to transcribe the DNA template into RNA. The T_7-specific sequence corresponds to TTA ATA CGA CTC ACT ATA GGG AGA, while the T_3-specific sequence corresponds to AAT TAA CCC TCA CTA AAG GGA GA.

Table 2.8 Primers for RNAi

Primer name	Sequence in 5' > 3' direction	Length (nt)	Tm (°C)
dGRASP/19.5' *	T_7-AGC CAC AGC ATC CAT	39	70.5
dGRASP/556.3' *	T_7-GCG GTA TTC GGC TTG AT	41	71.4
dGM130/21.5' **	T_7-CGC CAG CAA CAA CAA	39	112
dGM130/749.3' **	T_7-TGC TCC TTG TCC TGC GTT	42	122
dp115/86.5' **	T_7-ACC CAG AAT AGA C	37	110
dp115/768.3' **	T_7-TCA AAA AGG CGG TCA	39	104
dEGFP/144.5' ***	T_7-TAA ACG GCC ACA AGT TCA G	43	ND
dEGFP/730.3' ***	T_3-GTG ATC GCG CTT CTC GTT G	42	ND
dSed5/894.5' ***	T_7-GCT TAT TTG ATG ACA GAT	42	ND
dSed5/1578.3' ***	T_3-AAT ATG AGA ACG CCG AAG	41	ND

Table 2.9 Primers for RT-PCR

Primer name	Sequence in 5' > 3' direction	Length (nt)	Tm (°C)
dp115/5.5' **	AGT TCC TGA AGA GTG GCA TCA A	22	64
dp115/395.3' **	ATC GTA TTC GTC CAG ATA GC	20	58
dGM130/307.5' **	GAA CGG TCA GAC AGC GAG AT	20	62
dGM130/677.3' **	TGT AGC AGT TGT GCC TGG AGT T	22	66
dH2A/61.5' **	GTG GAA AAG GTG GCA AAG TGA A	22	64
dH2A/274.3' **	TTC TTG TTG TCA CGA GCA GCA T	22	64

* Primers purchased by MWG Biotech AG, UK, ** Primers purchased by Bioline, UK, ***Primers were a gift from Thomas Vaccari and Anne Ephrussi, EMBL, Heidelberg, Germany.

2.1.8 Inhibitors

The inhibitors used in this study were purchased from Sigma, except H89, which was bought from Calbiochem. Stock solutions of the reagents were made as follows: Nocodazole (6.7mM in DMSO), Colchicine (25mM in 70% ethanol), Cytochalasin D (2mM in DMSO), Brefeldin A (18mM in 70% ethanol) and H89 (10mM in DMSO). Each reagent was stored in aliquots at -20°C and diluted to final concentration in culture medium just before use.

2.2 Molecular Biology Methods

2.2.1 dsRNA preparation

To prepare dsRNA, cDNA or genomic clones containing the targeted genes (see 2.1.6) were used to amplify a fragment of each gene by PCR. The primers used in each case with flanking T7- or T3-RNA polymerase binding sites are listed in table 2.8. The amplified fragments ranged in length between 600-800bp (table 2.10). The PCR products were separated on a 0.8% agarose II gel (Amresco, Solon, OH) and the appropriate band was recovered from the gel (see 2.2.7). About 0.5μg of the purified PCR products were used as templates to produce dsRNA with MEGASCRIPT T7 or T3 transcription kit (Ambion, Austin, TX), according to the manufacturer's protocol. The dsRNA products were ethanol- or lithium chloride precipitated and resuspended in 40μl DEPC-treated water. dsRNAs were incubated at 65°C for 30 minutes to denature the RNA and then were left to cool slowly for correct pairing of sense and anti-sense strands. 0.5μl was analysed by 0.8% agarose gel electrophoresis to ensure that the majority of the dsRNA existed as a single band at the appropriate length (Figure 2.1). dsRNA concentration was estimated by UV spectrophotometry (see 2.2.4) and adjusted to 3μg/μl. The dsRNA was stored at -20°C.

Table 2.10: Amplified DNA fragments for dsRNA preparation

Gene target	First and last nucleotide of the amplified fragment (cDNA sequence accession number)	Length in bp including the RNA pol promoter sequence
dp115	86 – 768 (AJ272048)	731
dGM130	213 – 956 (NM137798)	792
dGRASP	10 – 548 (NM140903)	587
dSed5	894 – 1578 (NM078858)	731
EGFP	144 – 730 (AJ566337)	633

Figure 2.1: Examination of dsRNA integrity on 0.8% agarose gel

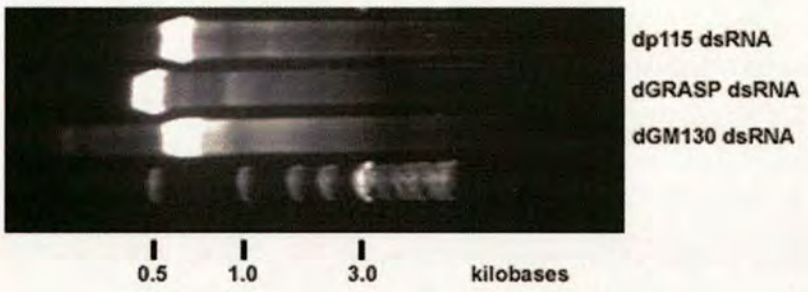

2.2.2 RNA precipitation

dsRNA was precipitated by adding 0.1 volume of 3M potassium acetate and 2.5 volume absolute EtOH. Alternatively, the 20µl of dsRNA transription reaction was mixed with 30µl nuclease-free ddH_2O and 25µl of lithium chloride (LiCl) precipitation solution (Ambion). In both cases, the solutions were mixed thoroughly and placed in -20°C for at least 1 hour. dsRNA was then pelleted by centrifugation at 13,000 rpm for 20 minutes at 4°C. The translucent pellet was washed once with 70% EtOH and centrifuged at 13,000 rpm for 15 minutes at 4°C. Finally, the RNA pellet was air dried and resuspended in RNAse free (DEPC-treated) ddH_2O.

2.2.3 Agarose gel electrophoresis

Horizontal agarose gel electrophoresis was used to separate DNA or RNA molecules according to their size. Typically, 0.8% agarose gels containing ethidium bromide to a final concentration of 1μg/ml were prepared in 1xTAE buffer. Agarose I was used for simple check of the electrophoretic motility, while highly purified agarose II was used in gels from which DNA bands needed to be purified. The samples were premixed with loading buffer (Table 2.2) to a final concentration of 1x, loaded on the gel, and electrophoresed at 100 Volts in 1xTAE buffer until being separated as appropriate.

To determine the size of the nucleic acid fragments, 0.5μg of 1kb or 100bp DNA ladder (New England Biolabs, Beverly, MA) was applied in each gel (Figure 2.2). The DNA or RNA bands were visualised on a long-wavelength UV transilluminator (365nm). The images were either saved directly as JPG files or were printed on thermal paper and subsequently scanned.

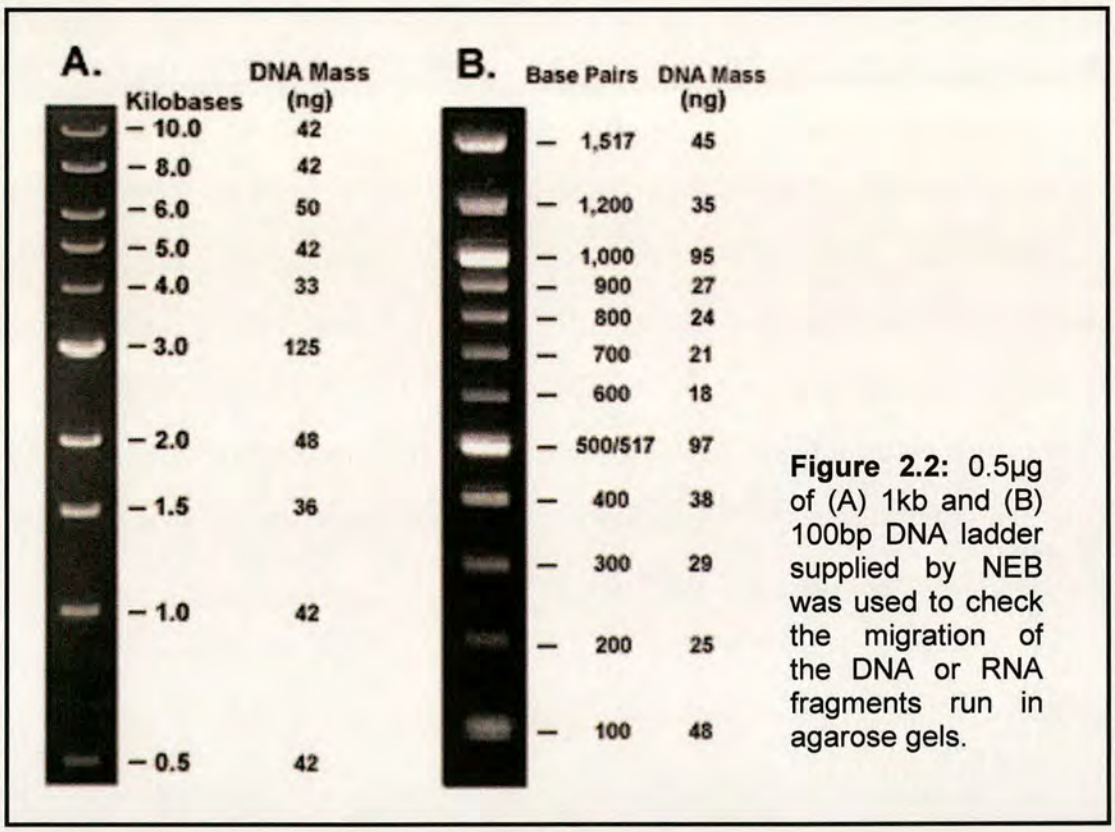

Figure 2.2: 0.5μg of (A) 1kb and (B) 100bp DNA ladder supplied by NEB was used to check the migration of the DNA or RNA fragments run in agarose gels.

2.2.4 Estimation of nucleic acid concentration

When a rough estimation of the DNA concentration was needed, the intensity of the band of interest on the agarose gel was compared with a similar size band in the DNA ladder and the DNA mass was estimated by reference to the manufacturer's guide (Figure 2.2).

When precise determination of the concentration and purity of nucleic acids was necessary, UV spectrophotometry was used. The DNA/RNA absorbance was measured at 260nm and 280nm using a Beckman DU-64 spectrophotometer and the concentration of the sample was calculated using the following equation:

$$\text{DNA/RNA Concentration in } \mu g/\mu l = \frac{A_{260} \times DF \times Sc}{1000},$$

DF: Dilution Factor, Sc: Spectrophotometric conversion (50 for double stranded DNA and 40 for RNA or single stranded DNA).

The purity of DNA was estimated by calculating the ratio A_{260}/A_{280}. DNA was considered to be sufficiently free of protein at ratio greater than 1.8 (2.0 for RNA).

2.2.5 Reverse transcription and PCR (RT-PCR)

Total RNA was isolated from 1 million S2 cells using the PURESCRIPT RNA isolation kit (Flowgen, UK) and following the supplier's protocol. The RNA concentration in each sample was estimated by measuring the OD_{260} and equalized by adding RNA hydration solution (supplied in the kit). Typically, the RNA yield was around 0.5 μg/μl.

Reverse transcription was carried out in a 20μl reaction volume according to the following protocol: 1μg total RNA was mixed with 100ng

random hexamers (Invitrogen) and 0.5mM of each dNTP (dATP, dCTP, dGTP, and TTP). DEPC-treated ddH_20 was added up to 12µl and the tube was incubated at 65°C for 5 minutes and quickly cooled on ice. After adding 10mM DTT and 1x RT buffer, the tubes were incubated at 25°C for 10 minutes and at 42°C for 2 minutes. Finally, 200U of Superscript II reverse transcriptase was added and the RT mix was incubated for 50 minutes at 42°C followed by heat inactivation of the enzyme at 70°C for 15 minutes. The RT products were diluted 1/20 before used as a template for subsequent PCR amplification. PCR conditions are described in the following paragraph.

2.2.6 Polymerase Chain Reaction (PCR)

PCR reactions were carried out in a Techgene Thermal Cycler (Techne, Cambridge, UK). A standard PCR included the following components: 50pmol of the 5′ and 3′ primers, 0.2mM of dATP, dCTP, dGTP, and TTP (Abgene), 1x Taq polymerase buffer, 2.5-5mM $MgCl_2$ and 2U Taq polymerase (Qiagen or Roche), 5-50ng of DNA template and ddH_20 to a final volume of 25µl. The amplification profile for each reaction was within the following limits:

1. Initial denaturing step: 95°C for 10-15 minutes;
2. 35 cycles with the following parameters:
    - Denaturation step at 94°C for 30 seconds,
    - Annealing step at 47-60°C (depending on the annealing temperature of the primers used) for 30 seconds and,
    - Extension step at 72°C for 1-3 minutes (1 minute per 1kb of the amplified product).
3. Final extension step: 72°C for 10-15 minutes.

2.2.7 Recovery of DNA fragments from agarose gel

The DNA fragments were excised and recovered from agarose gels using the QIAquick® Gel Extraction Kit (Qiagen) and according to manufacturer's protocol. The final elution of DNA from the column was performed by adding 30µl of DEPC-treated ddH20 to obtain more concentrated samples.

2.3 Protein Biochemistry Methods

2.3.1 Preparation of protein extract from cells and tissues

Total protein extracts from S2 cells were prepared in the following way. The number of cells was first calculated using a Neubauer haemocytometer, and the cells were then pelleted and dissolved directly in 60µl 1x SDS-sample buffer (New England Biolabs) containing 7mM DTT. The samples were boiled for 5 minutes, passed 15 times through a Hamilton syringe to sheer the DNA and boiled for additional 3 minutes. Alternatively, the cell pellet was homogenised in 25µl homogenisation buffer (Table 2.2) supplemented with 1% Triton X-100 using a motorised pestle. After centrifugation at 13000 rpm for 3 minutes (4°C) to remove the nuclei and unbroken cells, the supernatant was mixed with 14µl 3x SDS-sample buffer (1x final concentration) and 3µl 100mM DTT (7mM final concentration) and boiled for 5 minutes. The samples were stored at -20°C.

All *Drosophila* tissues were dissected in *Drosophila* Ringer and homogenised in the appropriate volume of 1x SDS-sample buffer or homogenisation buffer as described previously for the S2 cells. Third instar larvae were transected in Drosophila Ringer to the anterior/posterior midline and the two parts were everted so that the internal organs were exposed to the buffer.

2.3.2 Membrane / Cytosol fractionation of S2 cells

Ten million S2 cells were pelleted and resuspended in 600-700µl homogenisation buffer containing protease inhibitors. The cells were cracked by passing them 20 times through a 30g needle. After centrifugation at 2500 rpm for 2 minutes (4°C) to remove cell debris and nuclei, the post-nuclear supernatant was spun for 1 hour at 100,000g to separate the cytosolic from the membrane fraction. The membrane pellet was recovered in 50µl of 1x SDS-Sample buffer.

2.3.3 SDS - Polyacrylamide gel electrophoresis (SDS-PAGE)

SDS-PAGE was carried out using a Mini-PROTEAN 3 Cell apparatus (BioRad). The composition of separation and stacking gels is mentioned in table 2.11.

Before each use, the glass plates, spacers and combs were cleaned with 70% ethanol and dH_20. Approximately 4ml of separation gel mix was poured between the plates and overlaid with absolute ethanol to even the surface. The gel was allowed to set, the ethanol was discarded and the remnants were washed away with stacking gel mix without APS and TEMED. About 0.6ml of stacking gel mix was poured on the top of the separation gel before the comb was fixed. After polymerisation, the comb was removed and the gel was placed in the electrophoresis tank and migration buffer added (table 2.2). Protein samples were loaded and the gel run at 90 V for about 2 hours.

Table 2.11 SDS-PAGE separation and stacking gel composition

	Reagents/Preparation
Separation gel 10% Acrylamide	For 10ml of final volume 4.6ml ddH_2O 2ml 2M Tris-HCl, pH 8.8 3.3ml 30% Acrylamide/Bis-acrylamide stock solution (w/v)(37.5:1) 100µl 10% SDS 75µl 10% (w/v) APS 15µl TEMED
Stacking gel 3.6% Acrylamide	For 2.5ml of final volume 1.83ml ddH_2O 350µl 0.5M Tris-HCl, pH 6.8 300µl 30% Acrylamide/Bis-acrylamide stock solution (w/v)(37.5:1) 25µl 10% SDS 35µl 10% (w/v) APS 6.5µl TEMED

2.3.4 Western Blot

Proteins were transferred from the polyacrylamide gel to Hybond-C nitrocellulose membrane (Amersham Biosciences) in blotting buffer (table 2.2) at 100V for 1 hour using BioRad's Mini Trans-Blot Cell.

A piece of nitrocellulose membrane of the same size as the gel was cut and prewet in blotting buffer together with 6 whatman filter papers (slightly bigger than the gel), the gel after the removal of the stacking gel and the 2 sponges supplied with the apparatus. The "sandwich" assembly was performed but placing in turn from anode (+): a sponge, 3 filter papers, the membrane, the gel, 3 filter papers, a sponge. After placing each filter paper or the membrane, the trapped air bubbles were removed with a glass rod.

The efficiency of transfer was monitored by staining the proteins on the membrane with Ponceau S for 5 minutes. After destaining with dH_2O, the non-specific binding sites were blocked by immersing the membrane in 5% non-fat milk diluted in PBS supplemented with 0.1% Tween20 (v/v) (PBT) for 2 hours at RT. The membrane was put in a plastic bag containing the primary antibody diluted appropriately (see 2.1.5) in the blocking buffer and incubated overnight at 4°C. Subsequently, the membrane was washed 2 times in 5% milk in PBT for 30 minutes each on a shaker and incubated again in a plastic bag with the appropriate secondary antibody conjugated to horseradish peroxidase (HRP) for 2 hours at RT. During both incubations with the primary and the secondary antibody, the membranes were being rotated on a wheel. After the incubation with the secondary antibody, the membrane was washed 2 times in 5% milk in PBT for 30 minutes each on a shaker and then 6 x 5 minutes in PBS.

The protein bands were visualised with the ECL detection kit (Amersham Biosciences) according to the company's protocol. The membrane was then covered with Saran wrapping membrane, placed in an autoradiography cassette with intensifying screens, and exposed to a Kodak XAR-5 film for 30 seconds and up to 20 minutes.

2.3.5 Membrane Stripping

When a membrane needed to be re-blotted for another primary antibody, it was washed 2 x 10 minutes in PBT, immersed in stripping buffer (table 2.2), incubated at 60-65°C for 30 minutes with agitation, and washed again 2 x 10 minutes in PBT. Before the new immunodetection, the membrane should be blocked anew.

2.3.6 Affinity purification of dp115/584 antibody

2.3.6.1 Column equilibration

Approximately 0.5ml of EAH-Sepharose (Amersham Biosciences) was placed in a small, sealed glass column, which was connected to an aspirator. The matrix was washed with 80ml 0.5M NaCl and 30ml 10mM P1 buffer (Na-Phosphate-buffer, pH 7.2).

2.3.6.2 Column activation

While the column was filled with 3ml of P1, 8mg Sulfo-MBS crosslinker (Pierce) dissolved in 100µl P1 were added and the column was sealed with parafilm and rotated for 1 hour at RT. After the incubation, the matrix was left to settle and washed with 20ml 50mM Tris, pH 7.2 to quench the unbound crosslinker on the column. Washing steps with 30ml 10mM P1, 30ml 50mM Na-Phosphate-buffer, pH 6.0 and 20ml PBS followed, and finally the column material was resuspended as much as possible using a glass pipette.

2.3.6.3 Peptide addition

Six micrograms of the dp115 specific peptide (G)CSKLAEVSRHEAYSRA were dissolved in 600µl ddH_2O and lyophilised under SpeedVac. The dry pellet was dissolved in 400µl PBS and centrifuged for 10 minutes. The supernatant was added to the activated column material and the column was rotated overnight at 4°C. About 5µl of the peptide solution were kept as a control of the peptide input concentration. The next day, the column material was left to settle, and the supernatant was removed and kept for calculating the efficiency of the peptide binding. The column was washed with 1ml PBS that was also kept for the same reason.

To determine the peptide binding efficiency, 1:1000 dilutions of the peptide solutions before and after the incubation with the column were made and their absorbance was measured at 280nm against PBS ($O.D_{280}$=3.0

represents a peptide concentration of 1mg/ml). If less than 50% of the peptide had bound, a saturation step of the cross-linker with cysteine (8mg cysteine in 20ml of 50mM Tris, pH 7.2) was necessary.

Once the binding of the peptide on column was satisfactory, the column was washed with 15ml PBS and 10ml of 1M NaCl in PBS. At this step the column could be stored at 4°C by adding 3mM NaN_3 (0.02%) as a preservative.

2.3.6.4 *Incubation with antiserum*

Before incubation with the antiserum, the column was washed with 10ml PBS. Subsequently, the column material was removed from the glass tube and placed in a 15ml falcon tube, where 7ml of the anti-dp115 serum (last bleeding) were added, and the tube was incubated overnight on rotation at 4°C. The next day, the column material was transferred back to the glass tube, let settle and the eluate was removed. All following steps were carried out at 4°C. The column material was washed with 10ml PBS, 10 volumes of 0.5M NaCl in PBS, 3 volumes 0.1M Na-acetate, pH 4.8 (5.8ml CH3COOH-conc/l of 0.5M NaCl) to reduce the non-specific binding of serum components, and finally with 3 volumes of 0.5M NaCl in PBS.

2.3.6.5 *Antibody Elution*

The column was left run almost dry of liquid. The antibody was eluted with 4M $MgCl_2$, by applying 9 times 900µl on the column and collecting the fractions separately at the bottom. In the end, the column was washed with 0.5M NaCl in PBS and stored at 4°C by adding 3mM NaN_3.

The antibody concentration in each fraction was determined by measuring the optical density at 280nm (the mean OD_{280} was approximately 0.25). The most concentrated fractions were combined and BSA (Sigma) was added to a final concentration of 0.8 mg/ml. The purified antibody was

placed in a dialysis tube and was dialysed overnight against 2 litres of PBS containing 3mM NaN_3. The PBS-NaN_3 was replaced twice.

2.4 Cell Biology Methods

2.4.1 Cell cultures

Wild type, Delta and scAb-C_k S2 cells were cultured in Schneider's insect medium with L-glutamine and sodium bicarbonate (Sigma), supplemented with 10% (v/v) heat-inactivated and insect tested foetal bovine serum (FBS) (Sigma). Additionally, for selection purposes, $2x10^{-6}$M Methotrexate (ICN Biomedicals) was added to Delta S2 cell culture medium, while scAb-C_k cell culture medium was supplemented with 500μM Hygromycin-B (Sigma).

2.4.2 RNAi experiments

RNA interference (RNAi) was performed in all cell lines in the same way according to Clemens et al (2000). The cells were separated from culture media and diluted to a final concentration of $1x10^6$ cells/ml in Drosophila expression system (DES) serum-free medium (Invitrogen) or Schneider's insect medium (Sigma). One millilitre of cells was plated per well of a six-well cell culture dish (1 million cells/well). About 30μg of the various dsRNA (for dsRNA of about 700 bp, this corresponds to a final concentration of 74mM) were added followed by vigorous agitation. The dsRNA was incubated with the S2 cells for 40 minutes at RT followed by addition of 2ml of Schneider's insect medium containing 10% FBS and the appropriate drug when stable transformed cell lines were used.

Mock-treated and mock-depleted cells were treated in the same way except that no dsRNA or ds EGFP was added, respectively.

2.4.3 Indirect Immunofluorescence microscopy (IF)

2.4.3.1 Cells

S2 cells prepared for IF were grown and subjected to RNAi or BFA treatments on coverslips of 13 or 15mm in diameter. After each treatment, the cells were fixed for 20 minutes in 3% paraformaldehyde (PFA) (Polysciences) in PBS at RT, rinsed 3 times in PBS and stored in PBS at 4°C.

The samples were processed for IF as follows: Petri dishes containing coverslips with cells were incubated for 10 minutes in 50mM NH_4Cl in PBS to quench their aldehyde groups, rinsed in PBS, permeabilised for 5 minutes in 0.1% Triton X-100 in PBS, rinsed in PBS and blocked in 0.2% fish skin gelatin (Sigma) in PBS (FSG-PBS) (2 x 10 minutes). Coverslips with attached cells were inverted on a 40µl drop of the primary antibody diluted in the blocking buffer (for dilutions, see table 2.5), incubated for 25 minutes at RT, transferred again in petri dishes and rinsed 3 times in FSG-PBS. The same procedure was repeated for the secondary antibodies that were also diluted in FSG-PBS (table 2.6). For detection of mouse monoclonal antibodies, anti-mouse IgGs were used coupled either to Texas Red (Vector) or Alexa-568 (Molecular Probes). In contrast, for rabbit polyclonal primary antibodies, anti-rabbit IgGs coupled to FITC (Vector) or Alexa-488 (Molecular Probes) were used. After the incubation with the secondary antibodies, the coverslips were rinsed in FSG-PBS and dH_20, drained, mounted in Vectashield containing Dapi (Vector) and were viewed with a Leica TCS-NT confocal microscope. In case only surface labelling of Delta S2 cells was performed, Triton X-100 incubation was omitted from the protocol.

When stronger fixation was required, cells were fixed in 2% PFA and 0.2% glutaraldehyde (GA) (Polysciences) for 2 hours at RT and processed for immunofluorescence as described above, after an incubation of 10 minutes

with 0.1% NaBH4 (Merck) in PBS to quench non-reacted GA, thus reducing its autofluorescence.

2.4.3.2 *Imaginal discs*

Third instar larvae of different stages and white pupae (for stage distinction see 2.5.2) were "semi-dissected" and fixed at room temperature for 20 minutes in 3% PFA in 0.2M PB pH 7.4 supplemented with 0.1% Triton X-100, followed by three to four times rinsing in PBS and storage at 4°C, if necessary. The term "semi-dissection" describes the trans-section of larva or pupa in the anterior/posterior midline and the subsequent eversion of the anterior portion so that the imaginal discs were exposed and visible under the dissecting stereoscope.

Semi-dissected leg and wing imaginal discs that were processed for IF, were placed in an eppendorf tube and blocked for 30 minutes in FSG-PBS supplemented with 0.1% Triton X-100. Subsequently, they were incubated for 3 hours with the primary antibodies diluted in the blocking buffer, rinsed 3 times over 1 hour with FSG-PBS-Triton and incubated for 2 hours with secondary antibodies conjugated with FITC or Texas Red (Vector) in the dark, rinsed 3 times in FSG-PBS-Triton and stored overnight in PBS. All incubations were carried out on a rotation wheel at RT. The discs were dissected out of the carcasses and mounted in Vectashield containing Dapi.

2.4.3.3 *Confocal microscopy*

The samples that were processed for IF were examined with a Leica TCS-NT confocal microscope. When projection pictures are presented, it means that a series of 25-30 confocal sections through the cells were collected (step size of 300-450nm) and their projections were reconstituted and presented. The pictures were processed in Adobe Photoshop.

2.4.4 Electron microscopy (EM)

2.4.4.1 Conventional EM

Pelleted S2 cells, testes from newly eclosed male flies or semi-dissected third instar larvae were fixed for 2 hours in 1% GA in 0.2M PB at RT and rinsed three times in 0.2M PB. Imaginal discs were finely dissected from the carcasses and stored in PB until further processed. The cells or tissues were washed in 0.1M cacodylate buffer pH 7.4 (2x10min) and post-fixed in 1% OsO_4 in cacodylate buffer supplemented with 1.5% cyanoferrate for 1 hour on ice. After washing in cacodylate buffer, they were dehydrated in ethanol solutions of increasing concentration (50%, 70%, 95% and 100%) for 15 minutes in each one and 2 times in 100% ethanol. Subsequently, they were placed in 1:1 mixture of propylene oxide:epon resin (table 2.3) for 30 minutes. The propylene oxide/epon mix was replaced by 100% epon for 2 hours, and then, new resin was added and the samples were left for 24 hours at RT with the lids open to let the traces of propylene oxide evaporate. Finally, the blocks were polymerised at 65°C for 16 hours.

80-90nm ultrathin sections were cut on a Reichert FC4E or a Leica Ultracut S4 ultramicrotome and placed on 150-mesh copper grids. The section staining was performed by inverting the grids over drops of the staining solutions, using one of the following protocols:

1. Lead citrate for 5 minutes, 4% uranyl acetate in ddH_20 for 1 hour and lead citrate for 10 minutes (all washes in ddH_20).
2. 7% uranyl acetate in 70% methanol for 6 minutes (washes in 70% methanol) and lead citrate for 2 minutes (washes in ddH_20).

The stained sections were viewed under a Philips Biotwin or a Jeol 1200 EX electron microscope.

2.4.4.2 Stereology

The **Golgi area** is defined by the Golgi stacked cisternae and immediate surrounding vesicles and tubules. When Golgi stacks were not observed, the Golgi area was defined as the clusters of vesicles and tubules occupying the position where Golgi stacks are normally found, nested near an ER cisterna in most of the cases. To be counted as a **Golgi cluster**, at least 10 vesicles or tubules needed to be present, not more than 100nm apart. A **Golgi stack** is defined by the occurrence of at least two cisternae overlapping by at least 50% of their length. A **cisterna** had a width equal or less than 30nm and was at least 200nm long. When dilated rims were linked to cisternal elements, they were considered as part of the cisternae. **Vesicles** were defined as having an axial ratio of 1 to 1.5. Most were 50-70nm in diameter with the exception of a small number that were 2 to 3 times larger. A **tubule** was defined as having an axial ratio higher than 1.5 and a width of ≥70nm. The **cytoplasm** was defined as the volume enclosed by the plasma membrane and excluding the nucleus (but including all other organelles).

The boundaries of the Golgi apparatus were defined by the interface between the outmost membrane profiles and either the more amorphous cytoplasm or the cup-shaped ER cisternal membrane when present.

The percentage of cell profiles exhibiting at least one Golgi stack was estimated by randomly analysing under the transmission electron microscope more than 100 cell profiles taken from at least two grids and two different experiments. The cell profiles taken into account exhibited a section of their nucleus and a Golgi area containing either a stack or a cluster of vesicles and tubules. The cell profiles that did not exhibit either were not taken into account. Typically, about 20% of the cell profiles were excluded.

As "control" Golgi stacks were considered all stacks having a cross sectional diameter not less than 50% shorter than the average diameter of

0.368μm, observed in mock-treated cells or mock incubated cells. That is to say that Golgi stacks with cisternal diameter shorter than 0.184μm were counted as "non-control" Golgi stacks. This variation in the definition of Golgi stacks was introduced to distinguish the short stacks observed in dp115-dGM130 and dGRASP-dGM130 double depletions and better describe the effect of these depletions on Golgi architecture (see chapter 3).

To estimate the percentage of membrane in cisternae (total, single and stacked), tubules or vesicles per Golgi area, the intersection method was applied in 10-15 randomly selected pictures from each experiment printed at the magnification of about 100K (Rabouille, 1999). A 4-mm line grid was laid over printed images and each intersection crossing the membrane of each profile was scored. The percentage of intersections corresponding to each membrane profile was then calculated as $N_{\text{intersections in profile}} / N_{\text{total intersections}}$ and expressed as a percentage of total Golgi membrane. The ratio of stacked cisternae over total cisternae was determined by the same method taking into account only the cisternal profiles. Results were expressed ±SD.

The surface density of the Golgi (Golgi stacks or Golgi clusters) within the cytoplasm (SD_{Go}) is dependent on two distinct parameters: the surface density of the Golgi membranes within the volume they occupy (S_{Go}/V_{Go}) multiplied by the volume density of the organelle within the cytoplasm volume (V_{Go}/V_{cyt}).

To estimate the S_{Go}/V_{Go}, the boundaries of the Golgi area as well as all membranes within these boundaries were drawn in printed pictures at a magnification of about 90 K. S_{Go} was estimated with the use of the intersection method by counting the number of intersections (ΣI) between the lines of a 3mm grid and all membranes comprised within the organelle boundaries. V_{Go} was determined by the point-hit method in counting the

number of point hits falling within the Golgi boundaries (ΣP) with the use of a 3mm grid (Rabouille, 1999). S_{Go}/V_{Go} was calculated by the following equation:

$$S_{Go}/V_{Go} = \frac{\Sigma I}{\Sigma P} \times \text{mag (in } \mu m^{-1}),$$

mag is the final magnification of the each printed picture.

Vcyt was estimated by the point-hit method with the use of pictures of cells at a magnification of about 10K and a 4mm grid. The results were expressed ±SD.

2.4.4.3 Immuno - EM

A. Cryo-EM (Cells, Salivary glands)

Cells or dissected tissues were fixed in 2% PFA and 0.2% GA in 0.2M PB for 3 hours at RT or in 4% PFA in 0.2M PB for 3 hours at RT and then overnight at 4°C.

Once the fixative was washed away with 0.2M PB, the samples were infiltrated with 10% gelatin in PB for 30 minutes at 37°C. Subsequently, the cells were pelleted and transferred on ice to solidify the gelatin. Each gelatin block with cells was cut with a razor blade in small squares of <1x1 mm under the stereoscope at 4°C. For better penetration of gelatin in the tissue, the infiltration was carried out in three steps by placing successively the tissue in 2%, 5% and 10% gelatin for 20 minutes at 37°C. Each salivary gland was placed on a warm drop of gelatin on a glass slide, covered with a piece of parafilm to make the layer of gelatin as thin as possible and the glass slide was transferred on ice. After the gelatin was jellified, gelatin blocks were prepared at 4°C.

The blocks of cells or tissue were immersed in vials with 2.3M sucrose in 0.1M PB and incubated overnight on a rotating table at 4°C. Sucrose

infusion of the samples is important to prevent ice crystal formation during freezing. To increase the visibility of the cells or tissue, a drop of methylene blue was sometimes added in sucrose without that affecting the efficiency of immuno-cytochemistry.

In the next step, the blocks were fished out of the sucrose vials and mounted on aluminium specimen holders removing the excess of sucrose but leaving enough to glue the block at the basal side of the holder. The mounted blocks were then put in aluminium cans filled with LN_2, where they were stored until further use.

Using a Leica Ultracut S microtome with cryo-attachment at -120°C, each sample was trimmed to create a rectangular block face. Ultrathin sections of 50-70 nm were cut. Ribbons of 3-4 sections were picked up from the knife using a stainless steel loop (diameter 3 mm) with a thin layer of 1:1 mixture of 2.3M sucrose in PB and 2% methyl cellulose in dH_2O. The layer of sucrose/methyl cellulose (Sigma) with the attached sections was deposited on hexagonal copper grids covered with a carbon-coated Formvar film (Merck). The sections were stored at 4°C until being used for immuno-cytochemistry.

B. Unicryl-embedded material (imaginal discs)

Leg and wing imaginal discs were semi-dissected out of induced Fringe-DXD-myc mid third instar larvae (table 2.4), fixed in 2% PFA and 0.2% GA in 0.2M PB at RT for 3 hours and embedded in Unicryl (British Biocell International) according to the standard protocol proposed by the manufacturer. Ultrathin sections of 50-60nm were cut, labelled as described in section 2.4.4.4, using 0.5% fish skin gelatin in PBS as a blocking buffer and anti-mouse or anti-rabbit IgGs coupled to gold particles as secondary antibodies. The sections were stained as described in section 2.4.4.1.

2.4.4.4 *Immuno-labelling*

Grids with sections were put on petri dishes containing 2% gelatin in PB (the sections touching the gelatin) and the gelatin was melted under a lamp for about 5 minutes. The grids on melted gelatin were placed at 37°C. After an incubation of 20 minutes, the grids were transferred on drops of 0.1% glycine in PBS (5x2min), 1% BSA in PBS (1x3min) and on a 10µl drop of the primary antibody diluted in 1% BSA in PBS for 60 minutes at RT (for primary antibody dilutions see 2.1.5). Subsequently, the grids were washed in drops of 0.1% BSA in PBS (5x2min) and incubated for 20 minutes on a 15µl drop of Protein A coupled to gold particles of different sizes (PAG) diluted in 1% BSA in PBS. In case a mouse monoclonal antibody was used as a primary antibody, the grids were incubated in a drop of rabbit anti-mouse IgG diluted in 1% BSA in PBS for 20 minutes and washed in 0.1% BSA in PBS, before being transferred to PAG. After incubation with PAG, the grids were rinsed in PBS (7x2min), put in 1% GA in PBS for 15 minutes to fix the immuno-reagents on the sections before the staining procedure and washed in fresh dd$H_2$0 (10x1min). In case of double labelling, after the GA incubation, the grids were washed in drops of PBS (5x2min) and all the steps were repeated starting from glycine in PBS. In case of increased background labelling, blocking and dilution of primary antibodies and PAG was performed in 0.5% FSG and 0.1% BSA-C (Aurion) in PBS.

The staining of the grids aims to increase the contrast of the cells or tissues and was performed by transferring the grids in a drop of uranyl-acetate pH 7 for 5 minutes and then to a 9:1 mixture of 2% methyl cellulose and 4% uranyl acetate pH 4 for 10 minutes on ice. Each grid was picked up with a wire loop (diameter of 3.5-4mm) and the excess of the methyl cellulose/uranyl acetate was removed by touching the loop on a filter paper.

The grids were allowed to dry for few minutes at RT, detached from the loop with fine tweezers and viewed with a Jeol 1200 EX electron microscope.

2.4.4.5 Quantitation of Gold Labelling

Relative distribution of the gold particles (RD) in each organelle gives an indication of the subcellular localisation of a specific antigen without reflecting the concentration of this particular antigen into each organelle, as it does not take into account the organelle size (Rabouille, 1999). The RD is calculated as the percentage of the gold particles in each compartment out of the total number of specific gold particles measured. Gold particles labelling the nucleus or the mitochondria were considered as background.

Linear density determines the density of gold particles per μm of organelle membrane, when the antigen under study is membrane bound (Rabouille, 1999). It takes into account two parameters: the number of specific gold particles N_{org} associated with each organelle membrane within a distance of 20nm, and the length of organelle membrane L_{org}. The L_{org} was estimated by applying the intersection method (see 2.4.4.2) and using the equation:

$$L_{org} = I \times d / mag \text{ (in } \mu m),$$

where I is the number of intersections of the grid with the organelle membrane, d is the distance between two consecutive lines of the grid and mag is the final magnification of the each printed picture. The linear density is estimated by the equation:

$$\text{Linear Density} = N_{org} / L_{org} \text{ (in gold particles/}\mu m)$$

2.4.5 Delta protein transport assay

2.4.5.1 *General description*

Delta S2 cells, plated on glass coverslips, were treated with dsRNA for given time periods to deplete the protein of interest. The synthesis of Delta protein

was then induced by adding 1mM $CuSO_4$ (final concentration) to the culture medium. After 25-120 minutes of induction at 27°C, the $CuSO_4$-containing medium was replaced by new Schneider's medium without $CuSO_4$. Delta was then chased to the plasma membrane for a period ranging from 45 minutes to 4 hours (for different induction and chase periods, see section 2.4.5.2).

2.4.5.2 Kinetic measurement of Delta transport

To estimate the initial transport of Delta to the plasma membrane, Delta S2 cells were induced with $CuSO_4$ for 25 minutes and then chased for 45, 60 and 90 minutes. The combination of induction for 25 minutes and chase for 45 minutes was the minimum induction and chase periods to obtain detectable Delta labelling at the plasma membrane in at least 10% of the cell population.

The steady state transport of Delta to the plasma membrane was estimated by two different conditions: 2 hours induction + 4 hours chase, or 60 minutes induction + 90 minutes chase. In both conditions, the total intensity of fluorescence measured at the plasma membrane was comparable and the same held true for the average fluorescence intensities of the 3 labelling categories that the cells were ranked into (see 2.4.5.4). This signifies that already after 60 minutes induction and 90 minutes chase, Delta transport to the plasma membrane has reached its maximum plateau and therefore represents indeed the steady state situation.

2.4.5.3 Delta transport in presence of inhibitors

The efficiency of Delta transport to the plasma membrane was measured in the presence of different inhibitors. In Brefeldin A (BFA) experiments, Delta S2 cells were pre-incubated with 50μM brefeldin A for 30 minutes at 37°C. Subsequently, the cells were transferred at 27°C, where Delta transport assay was performed (see 2.4.5.2). The 30-minute pre-incubation of cells with BFA at 37°C was included in the protocol, because the block in anterograde

transport was less efficient if the BFA treatment was carried out exclusively at 27°C. This is probably because BFA acts optimally at 37°C. Nevertheless, the heat-shock from the incubation at 37°C imposed on S2 cells could be the reason for the observed transport block upon BFA treatment (see chapter 3). However, control cells (no drug or 0.5% DMSO) that were treated under the same conditions transported Delta at the plasma membrane as efficiently as non heat-shocked cells.

Microtubule depolymerisation drugs, nocodazole and colchicine, were used at a final concentration of 50μM or 75μM, respectively, and the cells were incubated for 2 hours or overnight at 27°C. This treatment was preceded by a 45-minute incubation on ice to destabilise the microtubules. Finally, H89, and actin polymerisation inhibitor, cytochalasin D, were added in the cell medium for 2 hours at a final concentration of 50μM (for cytochalasin D, a concentration of 20μM in overnight incubation was also used). After treatment of cells with each inhibitor, Delta was induced with $CuSO_4$ for 45 minutes and its transport to the plasma membrane was chased for 60 minutes at 27°C, always in the presence of the inhibitors.

2.4.5.4 Quantitation of transport

The quantitation of the intensity of Delta labelling at the plasma membrane was performed on cells permeabilised or not with Triton X-100.

Randomly selected fields of cells from each sample and equatorial sections of the cells were captured with a Leica TCS-NT confocal microscope and using a 63x water lens. Sections of mock-treated or mock-depleted cells were captured first so that the highest intensity of labelling was within the dynamic range of the laser. These settings were maintained for the entire analysis of the RNAi-depleted cells.

The labelling intensity of the plasma membrane was estimated using the Leica software, which is able to measure and display the intensity of

labelling along a line drawn perpendicular to the plasma membrane. In this way, the intensity peak as well as the thickness of the labelled plasma membrane was estimated (Figure 2.3). Typically, the intensity around the perimeter of each cell did not vary a lot, and two independent measurements per plasma membrane profile were performed to ensure more accurate intensity representation within each cell population.

When Delta S2 cells were assessed for steady state transport of Delta to the plasma membrane (60min+90min, or 2h+4h protocol), they displayed a large range of fluorescence intensity at the plasma membrane and were ranked into three categories:

1. Cells displaying labelling of 210±45 intensity units per plasma membrane cross-section (high intensity),
2. Cells displaying plasma membrane labelling of 130±35 intensity units per plasma membrane cross-section (medium intensity) and,
3. Cells displaying plasma membrane labelling of 75±20 intensity units per plasma membrane cross-section (low intensity).

When cells were permeabilised with Triton X-100, the intracellular pool of Delta was also visible, and therefore a fourth category of cells, where Delta was retained intracellularly, was added to the previous three. Moreover, this allowed the estimation of the total number of induced cells, which was essentially constant between the experiments (≥70% of the cells).

The same type of intensity measurements were carried out in samples, where initial rate of Delta transport was estimated, and the three categories of cell populations exhibited average plasma membrane intensity of 180±40, 105±35 and 55±15 IU per plasma membrane cross-section, respectively.

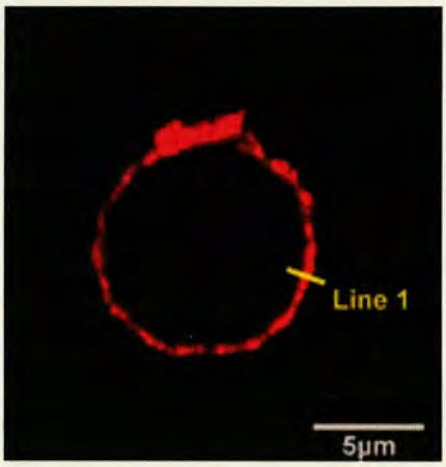

Figure 2.3: Estimation of fluorescence intensity per plasma membrane cross section. When a line (line 1) is drawn perpendicular to the labelled plasma membrane, Leica TCS-NT software was able to display the intensity profile along this line. From this profile, it was able to extract information, such as the maximum and mean fluorescence intensity along the line.

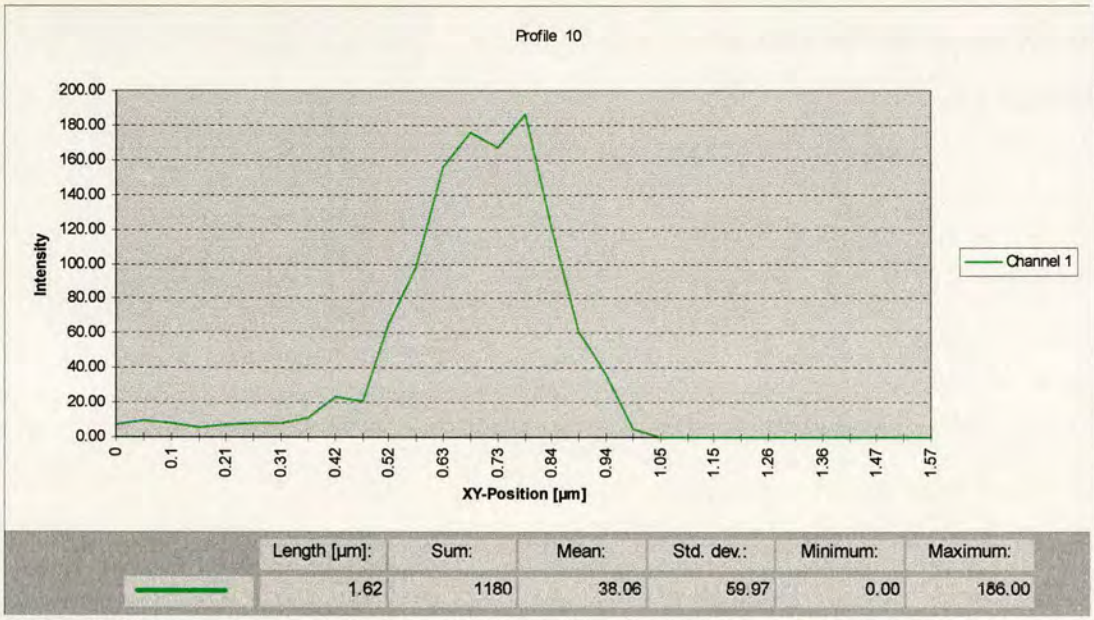

Length [µm]:	Sum:	Mean:	Std. dev.:	Minimum:	Maximum:
1.62	1180	38.06	59.97	0.00	186.00

To estimate the total intensity per experimental condition, about 300-500 randomly selected cells were distributed to one of the four cell population categories mentioned above and the results were expressed as a percentage of cells in each category of intensity. The total intensity in each condition was calculated using the following equation

$$\text{Total intensity} = \Sigma\, I \times N \times p \text{ (in arbitrary units AU)},$$

where I is the average fluorescent intensity per plasma membrane cross-section for each category (cells displaying Delta only intracellularly have I=0), N is the percentage of cells exhibiting high, medium, low or no staining

intensity at their plasma membrane, and p is the perimeter length of the plasma membrane. The perimeter length was not taken into account because both control and depleted cells had similar mean diameters and their almost spherical shape did not change. The total intensity was considered as 100% for the control cells, while the efficiency of intracellular transport in treated/depleted cells was expressed as ratio of their total intensity versus that of the control cells. This approach is comparable to a FACS analysis.

2.4.6 ScFv-Ck transport assay

After being treated with the dsRNA of interest for a given time, scAb-S20 cells were induced to produce and secrete scAb-Ck in the 3ml culture medium by adding 1mM $CuSO_4$ for 16h. At the end of the incubation time cells were separated from the medium. An extract made from 2 million cells, and 40µl aliquot from the medium were processed for Western blotting. To detect the scAb-Ck on the nitrocellulose, an anti-human Ck domain antibody conjugated to alkaline phosphatase was used (table 2.5). Blots were developed using SigmaFast NBT/BCIP substrate (Sigma).

2.5 Drosophila Methods and Genetics

2.5.1 Maintenance of Drosophila stocks

All fly stocks were maintained in vials with cornmeal food (2.5% corn flour, 5% sugar, 1.75% lyophilised yeast, 1% agar and 0.005% Nipagin in 95% ethanol) either at 18°C or at 24°C, in case they showed reduced viability. Fly stock genotypes are given in table 2.4.

2.5.2 Developmental staging of 3rd instar larvae and white pupae

Third instar larvae can be distinguished from the first and second instar larvae by several morphological characteristics. Relative body size and the appearance of mouthparts and anterior spiracles were used in this study. Third instar larvae exhibit larger body size, higher number of "teeth" in their mouth hooks compared to first and second instar larvae and their anterior spiracles have a "fanned" appearance.

Early third instar larvae were considered larvae with third instar characteristics that were still feeding, burrowed in the food. Mid third instar larvae were considered third instar larvae that left the food and began to wander actively on the vial walls, while the nearly motionless larvae were considered as late third instar larvae. Additionally, to distinguish mid from late third instar larvae, the morphology of salivary glands was also examined. Salivary glands of mid third instar larvae swell gradually, their surface become enlarged and bumpy and the cell borders become highly visible (see figure 2.4A-B). This results from glue synthesis taking place in response to the slow ecdysone titre increase (Boyd and Ashburner, 1977; Biyasheva et al., 2001). At late third instar, the prepupal ecdysone pulse triggers the rapid expulsion of the glue product into the lumen of the gland. This causes a swelling of the entire salivary gland and a concomitant stretching of the gland cells such that they become flattened and smooth. The cell borders become considerably less visible at this stage (see figure 2.4C-D). Finally, white pupae exhibited everted anterior spiracles and a soft white pupal case (puparium).

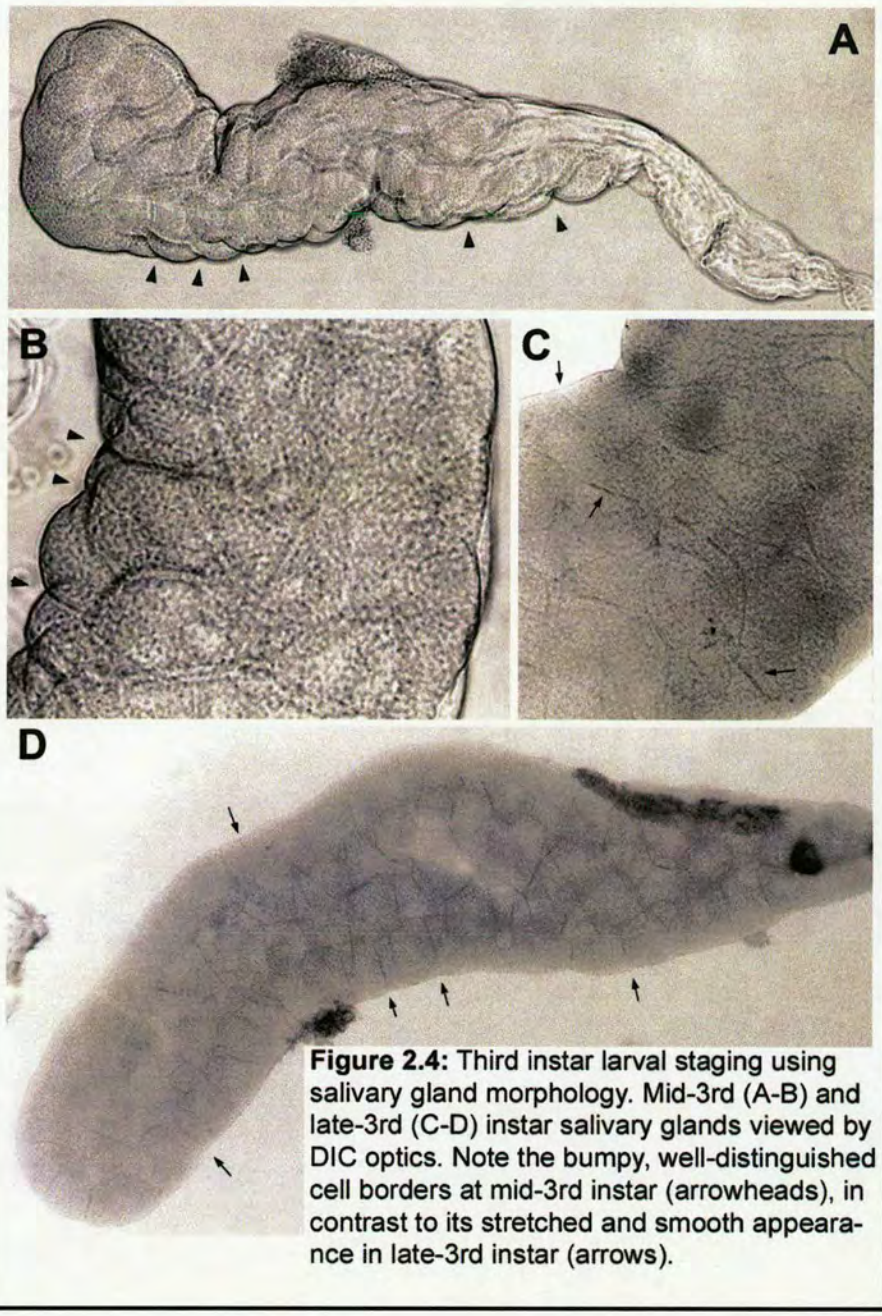

Figure 2.4: Third instar larval staging using salivary gland morphology. Mid-3rd (A-B) and late-3rd (C-D) instar salivary glands viewed by DIC optics. Note the bumpy, well-distinguished cell borders at mid-3rd instar (arrowheads), in contrast to its stretched and smooth appearance in late-3rd instar (arrows).

2.5.3 Collection of virgin females and crosses

Virgin female flies were collected in the following way. Every morning the fly vials were emptied from any eclosed flies, and the newly eclosed female flies were then collected every 4 hours (vials maintained at 24°C). Virgin females were also recognised by their pale pigmentation and the presence of a dark spot in their translucent abdomen. After collection,

virgin flies were transferred together into vials with fresh fly food until being used for crosses.

Generally, fly crosses were carried out by transferring 2-3 virgin females and 2-3 male flies into the same vial, containing fresh fly food, supplemented with dry yeast. The flies were incubated at 24°C for 10 days, before being removed to avoid mixing the parents with the F1 progeny.

Chapter Three

Characterisation of the Early Exocytic Pathway in *Drosophila* S2 Cells

The early exocytic pathway in *Drosophila* has not been described as extensively as in other organisms, like mammals or yeast. Nevertheless, it seems to be organised in a similar fashion and comprise the equivalent compartments that exist in these organisms. The Golgi apparatus in *Drosophila* shares common morphological characteristics with those of the mammalian cells, exhibiting stacked flattened cisternae with abutting tubular/vesicular networks (Rabouille et al., 1999). However, the *Drosophila* Golgi stacks appear smaller in diameter and not linked into a large ribbon (Stanley et al., 1997; Rabouille et al., 1999). Instead, they remain dispersed in the cytoplasm. This scattered distribution of the *Drosophila* Golgi stacks is reminiscent of the distribution of tER sites in mammalian and yeast cells (Rossanese et al., 1999; Murshid and Presley, 2004), and made it interesting to investigate the possible relationship between the tER and the Golgi apparatus. Moreover, a recent comparative study in yeast species *S. cerevisiae* and *P. pastoris,* proposing a direct correlation between the structure of the Golgi apparatus and the organisation of the tER sites (Rossanese et al., 1999), provided an additional incentive for a better characterisation of the *Drosophila* early exocytic compartments. For these reasons, the organisation of the tER sites and the Golgi apparatus was examined in *Drosophila* S2 cells under physiological conditions during the cell cycle and upon treatment with certain inhibitors.

3.1 Early exocytic compartment markers

3.1.1 Transitional ER (tER)

Transitional ER sites and their synonyms (ER exit sites and ER export complexes) have generated confusion in the bibliography, since the term has been used sometimes based on morphological criteria and sometimes based on the functional aspect of the compartment (see introduction). In the present

thesis, tER sites are defined as these membrane structures, released or still connected to the ER, which are positive for the COPII coat subunit Sec23p and colocalise with anterograde transport cargo. To identify the tER sites in *Drosophila*, an antibody raised against the first 18 amino acids of rat Sec23 was used (MTTYLEFIQQNEERDGVR). This peptide is 90% conserved in *Drosophila* Sec23p (dSec23p; MTTYEEFIQQNEDRDGVR). When ultrathin cryosections of S2 cells and salivary glands were labelled, the majority of gold particles decorated pleiomorphic membrane structures comprising 50-70 nm vesicular profiles, ER coated buds, as well as larger vesicular and tubular membrane structures, often found in the concavity of an ER cisterna (Figure 3.1A-C). Whether these larger structures are still connected to ER or not can only be answered by combining IEM with electron tomography, in order to obtain the 3D-organisation of these structures. The labelling density of tER sites was six to seven times higher that of the surrounding cytoplasm, while from the membrane-associated gold particles, only 10±3% labelled the rough ER cisternae. By immunofluorescence (IF), S2 cells exhibited 20±8 discrete spots throughout their cytoplasm, which were positive for dSec23p and corresponded to tER sites (Figure 3.1D). A large, less bright spot, positive for dSec23p, was often seen in the nucleus, but it was not taken into account (see arrows in figure 3.1D).

3.1.2 Golgi apparatus

The *Drosophila* Golgi apparatus was identified using as a marker a monoclonal antibody raised against a Golgi membrane antigen of 120kd (d120kd) from *Drosophila* embryos. This antibody has been characterised previously, and the 120kd antigen colocalises with *Drosophila* β-COP by IF (Stanley et al., 1997). Nevertheless, to confirm this result, the antibody was also tested by IEM. The gold labelling was specifically confined to the Golgi

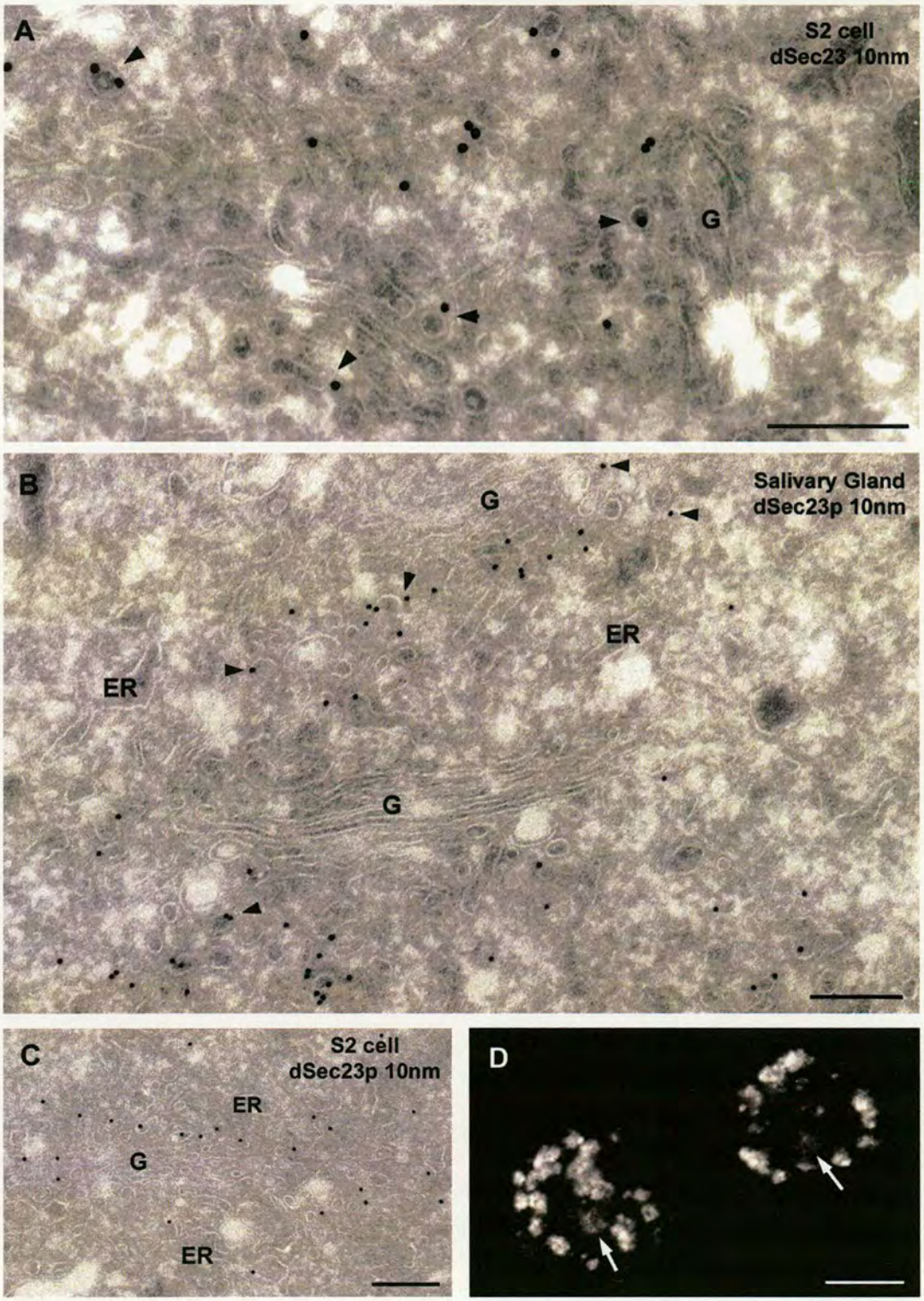

Figure 3.1: Transitional ER defined by the COPII coat subunit, dSec23p. S2 cells (A, C, D) and salivary glands (B), were processed for IEM (A-C) or IF (D), and labelled with anti-Sec23p antibody. Note in A and B the coated membranes, which are labelled for dSec23p and are marked by arrowheads. In D, arrows point to a large and less bright dSec23p-positive spot appearing in the nucleus. G, Golgi stacks; ER, endoplasmic reticulum. Bars: (A-C) 200nm; (D) 5μm.

apparatus (Figure 3.1 A-B). The labelling quantification showed that 55% of the gold particles was on the Golgi stacks, 35% labelled vesicles and small tubules very close to the Golgi stacks, while the remaining 10% was found on other membranes, like ER. This result is in agreement with the IF labelling (Figure 3.1C) and makes d120kd antibody a reliable Golgi marker.

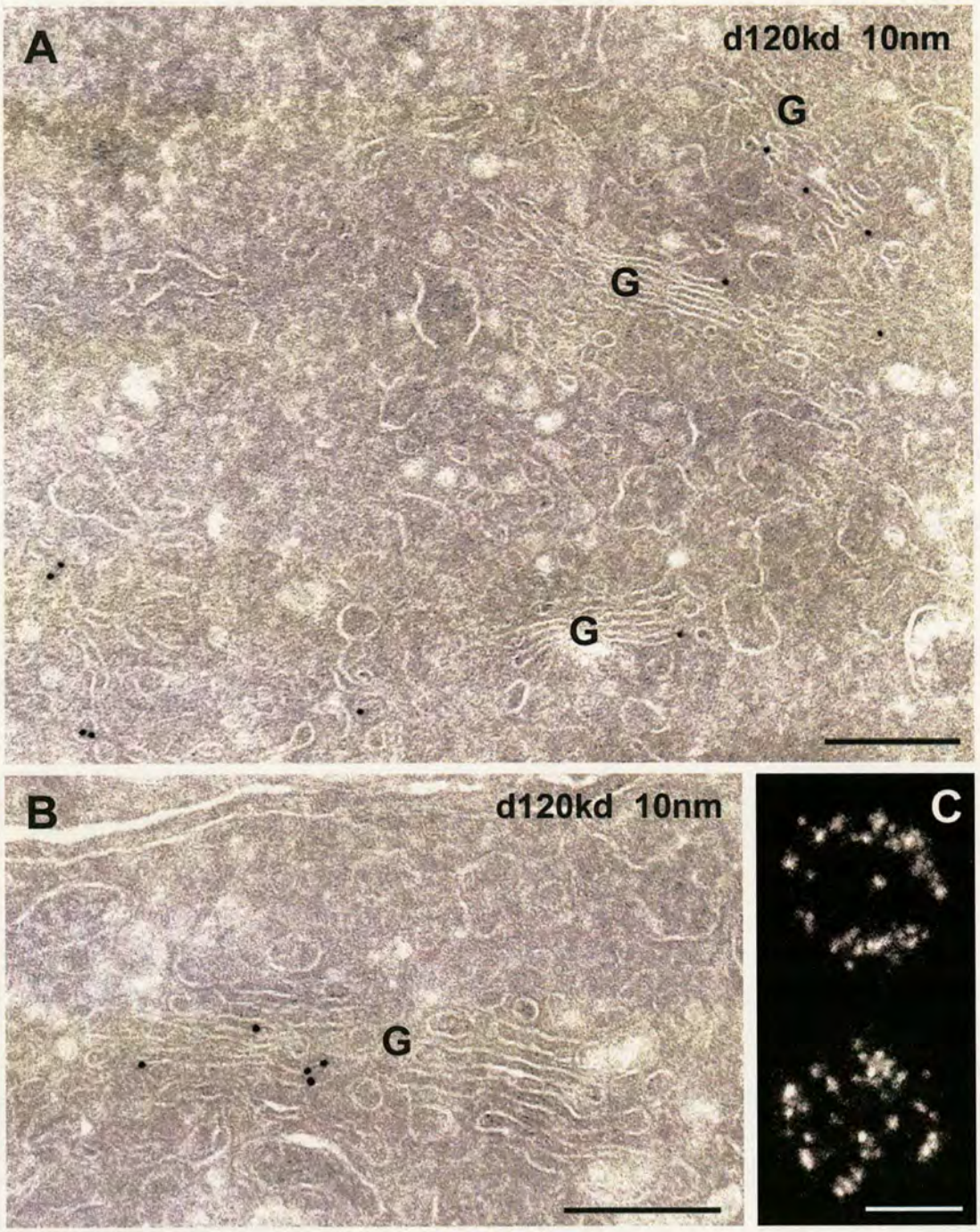

Figure 3.2: Localisation of *Drosophila* Golgi marker of 120kd. S2 cells were processed for IEM (A and B) or IF (C) and labelled with the monoclonal antibody against d120kd. Golgi stacks are indicated by G. Bars: (A-B) 200nm; (C) 5μm.

When S2 cells were double labelled for IF with d120kd and dSec23p antibodies, tER sites appeared to overlap partially with the Golgi apparatus (Fig 3.3A). By IEM, it was confirmed that the overlapping region corresponded to the interface between the Golgi stack and the tER sites (Figure 3.3B-C). Therefore, although the two compartments are in close proximity, they can be clearly distinguished, at least by the high resolution of EM. In addition, this tight spatial association between the tER sites and the Golgi stacks raises the possibility that IC structures, which in mammalian cells appear to form a functional and morphological intermediate compartment, do not exist in *Drosophila* S2 cells. However, the absence of a morphologically distinct intermediate compartment from S2 cells does not mean that its functions are missing from *Drosophila* cells (see discussion in chapter 8).

Figure 3.3: The Golgi apparatus and tER sites are found in close proximity. S2 cells were processed for IF (A) or IEM (B-C) and labelled for d120kd (red or 15nm gold) and dSec23p (green or 10nm gold). G, Golgi stacks; ER, endoplasmic reticulum. Bars: (A) 5µm; (B-C) 200nm.

3.2 Organisation of the early exocytic pathway during the cell cycle

The organisation of the tER sites and the Golgi apparatus was first investigated during the mitotic cycle. In mammalian cells, intracellular transport is known to be inhibited during mitosis by an ER to Golgi block (Featherstone et al., 1985; Farmaki et al., 1999). One reason for this transport arrest was shown to be the significant reduction in budding activity from ER exit sites (Prescott et al., 2001) and the dissociation of COPII coat components from ER membranes and their redistribution in the cytosol (Farmaki et al., 1999; Stephens, 2003). However, transport arrest during mitosis is not a universal feature in all eukaryotic cells. In plants, intracellular transport does not cease (Andreeva et al., 1998), as Golgi-derived vesicles are necessary for the formation of the cell plate, which upon maturation gives rise to the new cell wall and the plasma membrane needed for cell division (Staehelin and Hepler, 1996). Likewise, in yeast, secretion during mitosis is not affected as well (Makarow, 1988), and the reason is also thought to be the need of large amounts of new membrane and cell wall material to complete the division (Munro, 2002). However, a recent work in fission yeast has challenged this notion by showing that mutants of COPII components were able to divide, although transport from the ER was blocked (Matynia et al., 2002). The observed cell cycle arrest was attributed to defects in nuclear envelope organisation caused by the inhibition of protein export from ER.

To address the question of the fate of *Drosophila* tER sites during mitosis, an unsynchronised population of S2 cells was labelled for dSec23p and α-tubulin, in order to visualise the tER and the microtubule network, respectively (Figure 3.4). The organisation of the microtubule network was used to distinguish mitotic from interphase cells, as well as the different

stages of mitosis (Figure 3.4, middle column). The chromosome condensation and distribution within the cells was also monitored with Dapi staining to confirm the mitotic stage (not shown). In **interphase** S2 cells, microtubules are organised mainly as a network parallel to the cell cortex, while tER sites are organised in 20±8 focused areas in the cytoplasm (Figure 3.4). As cells enter into **prophase**, the two centrosomes separate and move to the opposite ends of the cell, where they organise the mitotic spindle. tER sites appear to become already dispersed even in early prophase, when centrosomes cannot yet be distinguished as two different microtubule organising sites, while only few smaller dSec23p-positive spots still persist (Figure 3.4). In **metaphase**, the mitotic spindle is formed (Figure 3.4) and the condensed chromosomes line up in metaphase plate (not shown). At this stage, dSec23p labelling diffuses significantly with very small puncta remaining discernible (Figure 3.4). A similar punctate pattern has also been reported in mammalian metaphase cells (Farmaki et al., 1999; Hammond and Glick, 2000; Prescott et al., 2001). These puncta could represent small clusters of COPII-coated membranes (Prescott et al., 2001) or non-membrane associated pools of COPII coat subunits (Martinez-Menarguez et al., 1999). Alternatively, it has been proposed that these dots could be an artefact of the IF procedure, since in a study following the fate of mammalian tER sites during mitosis using life cell imaging of Sec23-YFP, such small spots could not be distinguished (Stephens, 2003). In **anaphase**, the sister chromatids have separated and moved to the spindle poles (not shown), while tER sites have already begun to get reorganised in a seemingly random fashion, relative to the mitotic spindle (Figure 3.4). At **telophase** (see the formation of spindle mid-zone microtubule bundles in figure 3.4) and subsequently, during **cytokinesis** (see mid-body formation and plasma membrane constriction in figure 3.4), the

tER sites are fully formed and distribute equally in the 2 daughter cells (Figure 3.4). In general, these data show that tER sites behave similarly to mammalian ER exit sites during mitosis. A slight difference may be that in S2

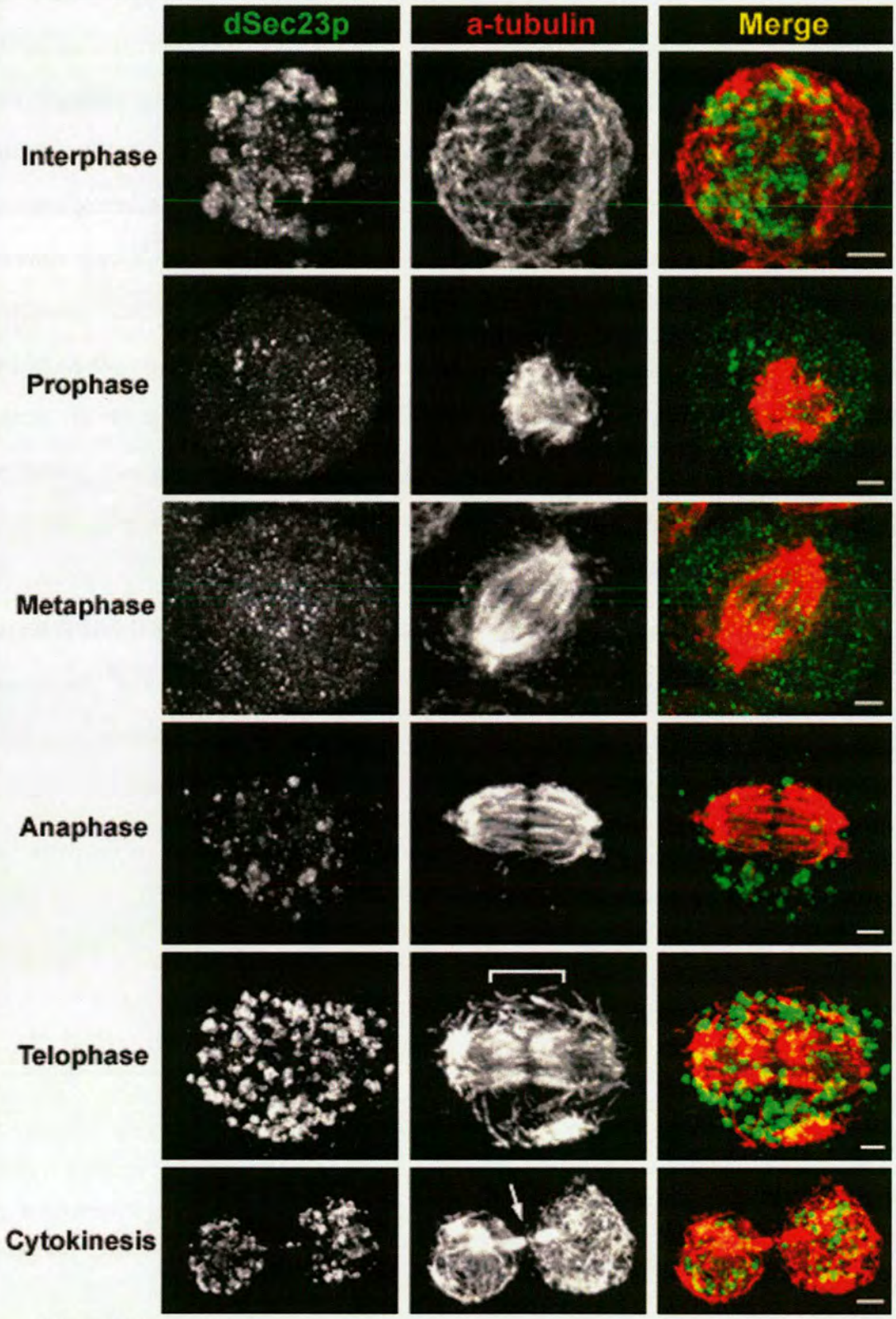

Figure 3.4 See following page for legend

cells, the tER sites start to re-organise at anaphase, whereas in CHO cells this does not happen before telophase, although such slight differences seem to exist also between mammalian cell lines (Hammond and Glick, 2000).

Another mitotic feature that is shared between the *Drosophila* S2 and mammalian tissue culture cells is the fragmentation of the Golgi stacks, as it has already been described by IF (Stanley et al., 1997). The absence of distinguishable Golgi stacks from metaphase S2 cells was also confirmed by EM (Figure 3.5). Interestingly, though, during *Drosophila* embryogenesis (Stanley et al., 1997) or spermatogenesis (Figure 3.6; Tates, 1971), Golgi stacks of dividing cells do not undergo fragmentation (see arrows and inset in figure 3.6), and the same is true for the nuclear envelope (arrowheads in figure 3.6; Stafstrom and Staehelin, 1985). This is similar to yeast, where both the Golgi stacks and the nuclear envelope remain intact during cell division (Hurt et al., 1992). Thus, it seems that in *Drosophila* cells both the mammalian and the yeast mechanism of mitotic division can take place. In conclusion, it seems that during mitosis, features such as the organisation of the tER sites and the presence of Golgi stacks differ between the organisms, but may also vary among the tissues of the same organism.

Figure 3.4: tER site organisation during the cell cycle in *Drosophila* S2 cells. Cells were processed for IF and labelled for dSec23p (tER marker, left column) and α-tubulin (microtubule network, middle column). In the merged pictures (right column), tER sites are labelled in green and microtubules in red. The cell cycle stage is mentioned on the left. Bracket in telophase cell indicates the spindle mid-zone microtubules, and arrow points to the plasma membrane constriction site and mid-body formation during cytokinesis. Bars: 3μm

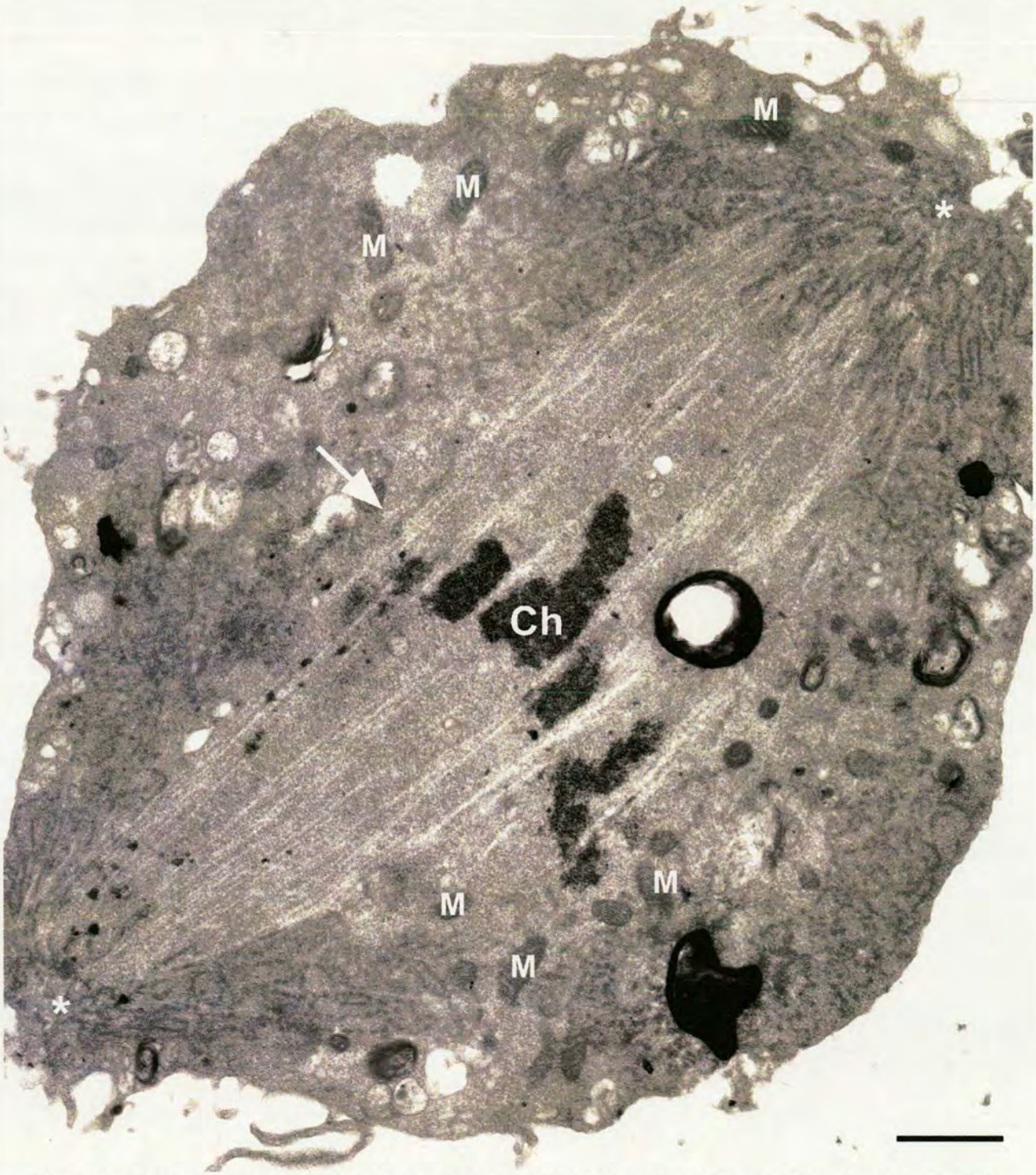

Figure 3.5: *Drosophila* S2 cell in metaphase visualised by EM. Metaphase in S2 cells exhibits similar features to those observed in mammalian tissue culture cells, such as nuclear envelope breakdown, chromosome alignment in metaphase plate (arrow) and absence of distinguishable Golgi stacks. Note that ER membranes are dispersed throughout the cytoplasm, but they are more concentrated in the spindle poles (asterisks). Ch, chromosomes; M, mitochondria. Bar: 1µm

Figure 3.6: *Drosophila* primary spermatocyte during metaphase to anaphase transition of the 1st meiotic division. In contrast to *Drosophila* S2 cells, during spermatogenesis, the nuclear envelope remains intact (arrowheads), and the Golgi stacks do not undergo fragmentation (arrows). Two of the Golgi stacks are presented in higher magnification in insets. Note that chromosomes have just begun to separate and move to the spindle poles. C, centriole; M, mitochondria. Bar: 2μm

3.3 tER and Golgi behaviour upon treatment with different inhibitors

The behaviour of *Drosophila* tER sites and Golgi stacks was studied after treatment of S2 cells with inhibitors that interfere with ER to Golgi transport, or disrupt actin and microtubule cytoskeleton.

3.3.1 Brefeldin A treatment

Brefeldin A (BFA) is a fungal metabolite having as primary target a subset of Sec7-type GTP exchange factors that catalyse the activation of Arf1 (Jackson and Casanova, 2000). BFA is known to induce the redistribution of the Golgi enzymes back to the ER (Lippincott-Schwartz et al., 1990), while Golgi matrix proteins are localised in punctate structures that may represent Golgi remnants (Seemann et al., 2000a) or ER exit sites (Ward et al., 2001). However, the organisation of the tER sites visualised with Sec13-YFP does not seem to change upon treatment of mammalian cells with BFA, at least at the morphological level (Ward et al., 2001).

On the contrary, when S2 cells were treated with 50μM BFA for 30-40min, their tER sites lost their focused organisation and the large dSec23p-positive spots were reduced in number (arrowheads in figure 3.7). Instead, dSec23p appeared mostly in small and dispersed puncta. On the other hand, the integral Golgi membrane protein, d120kd, behaved similar to Golgi resident enzymes in mammalian cells, as it seemed to be transported at least in part back to the ER, judging from the nuclear envelope staining (arrow in figure 3.7). The persisting d120kd-positive spots could represent BFA-resistant Golgi membranes or an ER-Golgi hybrid compartment induced by BFA treatment (Nebenfuhr et al., 2002).

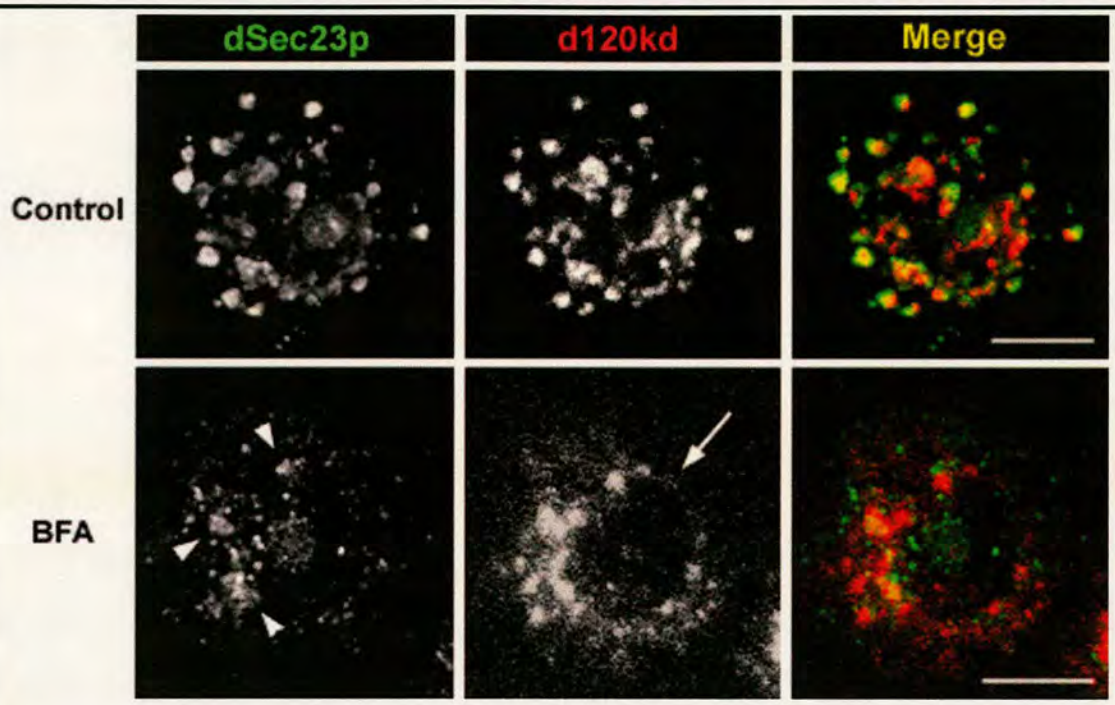

Figure 3.7: tER site organisation of S2 cells upon BFA treatment. Cells incubated without (upper panel) or with 50µM BFA for 30min (lower panel), were processed for IF and labelled for dSec23p (left column) and d120kd (middle column). In the merged pictures (right column), tER sites are labelled in green and the Golgi marker in red. Note the reduced number of focused tER sites in BFA-treated cells indicated by arrowheads. Arrow points to the nuclear envelope, which is labelled for d120kd suggesting that d120kd recycles at least in part back to the ER upon incubation with BFA. Bars: 5µm

3.3.2 H89 treatment

H89 is an isoquinolinesulfonamide that has been shown to block both anterograde and retrograde transport between ER and Golgi in mammalian cells (Aridor and Balch, 2000; Lee and Linstedt, 2000; Cabrera et al., 2003). Although H89 is considered a kinase inhibitor, its precise target kinase is unknown. However, H89-dependent block in anterograde transport occurs via an inhibition of Sar1 recruitment on the ER membranes (Aridor and Balch, 2000), which leads to a cytosolic redistribution of COPII subunit Sec13 (Lee and Linstedt, 2000).

In *Drosophila* S2 cells, the use of 50μM H89 for the suggested time of 10 minutes (Lee and Linstedt, 2000) did not affect the organisation of tER sites (not shown). Nevertheless, an incubation of S2 cells with the inhibitor for 2 hours led to a partial diffusion of the labelling, presumably in the cytosol, while dSec23p-positive spots were smaller in size and increased in number (Figure 3.8, middle and lower panel). The reduction in the size of the tER sites seemed to take place gradually, as, at this time point, half of the cells had lost all their focused tER sites (Figure 3.8, lower panel), while the other half exhibited an intermediate phenotype between the control cells and those H89-treated cells with completely disorganised tER sites (Figure 3.8, middle

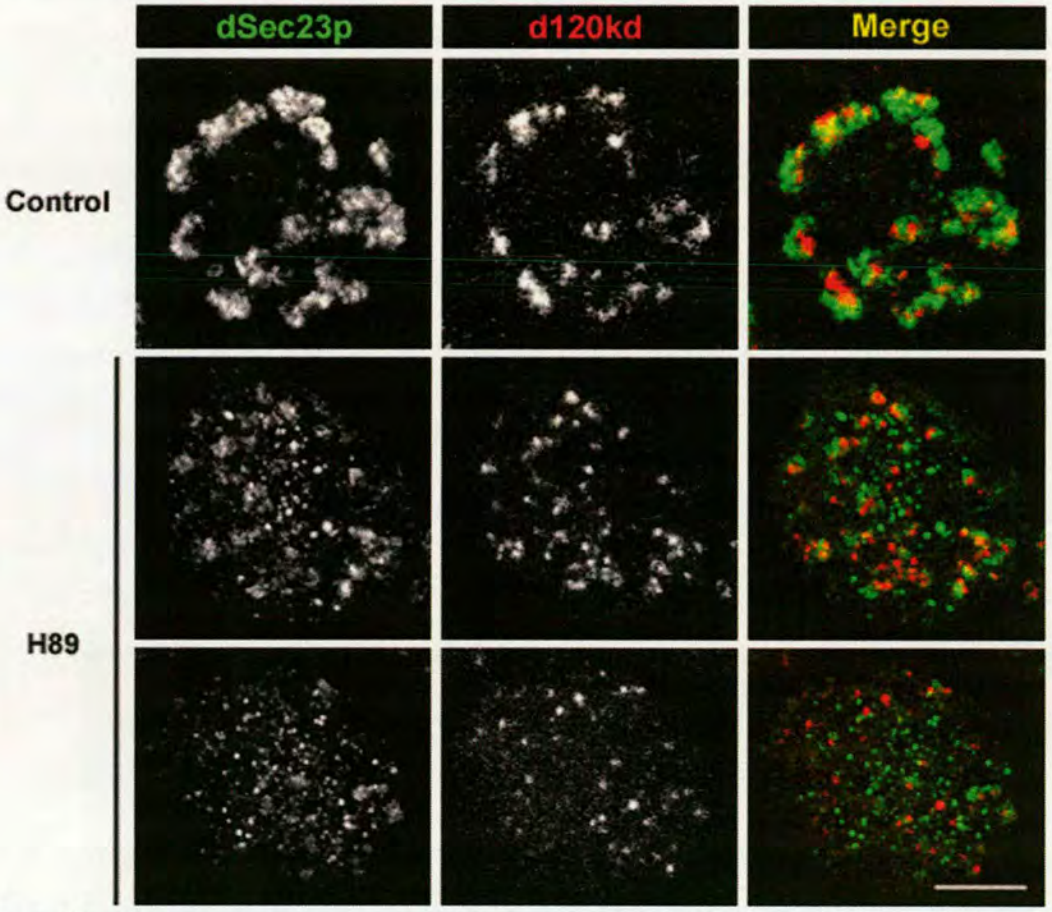

Figure 3.8: tER site organisation of S2 cells upon H89 treatment. Cells incubated without (upper panel) or with 50μM H89 for 2h (middle and lower panel), were processed for IF and labelled as described in figure 3.7. Note that upon treatment with H89, some cells have fully fragmented tER sites (lower panel), while other show moderately disturbed tER organisation (middle panel). Also, d120kd-positive puncta retain a distinct cytoplasmic localisation and do not relocate to the ER membranes. Bar: 5μm

panel). The punctate pattern of the Golgi marker d120kd was dispersed as well (Figure 3.8, middle and lower panel), but it was not redistributed to the ER, as in BFA-treated cells. This could be in agreement with the proposed role for H89 in blocking a subset of the constitutive Golgi-ER transport (Lee and Linstedt, 2000). Whether d120kd dots in H89-treated cells represent Golgi stacks or tubulo-vesicular Golgi clusters requires examination by EM.

3.3.3 Microtubule depolymerisation

The dependence of tER organisation on the presence of intact microtubule network was also investigated in S2 cells. In mammalian cells, microtubule depolymerisation by nocodazole was shown to leave the ER exit sites unaffected, except that it causes their partial clustering into the peri-nuclear area after 2 hours of treatment (Hammond and Glick, 2000). This coincides with the rapid fragmentation of the Golgi ribbon and the appearance of mini Golgi stacks after 90-120 minutes (Cole et al., 1996).

Nocodazole was initially used to depolymerise microtubules in S2 cells, but this did not turn out to be effective. Even after an overnight incubation of the cells with 50μM of the drug (3 times higher than what is normally used in mammalian cells), it was not possible to demonstrate a disruption in the microtubule network (Figure 3.9). Moreover, metaphase

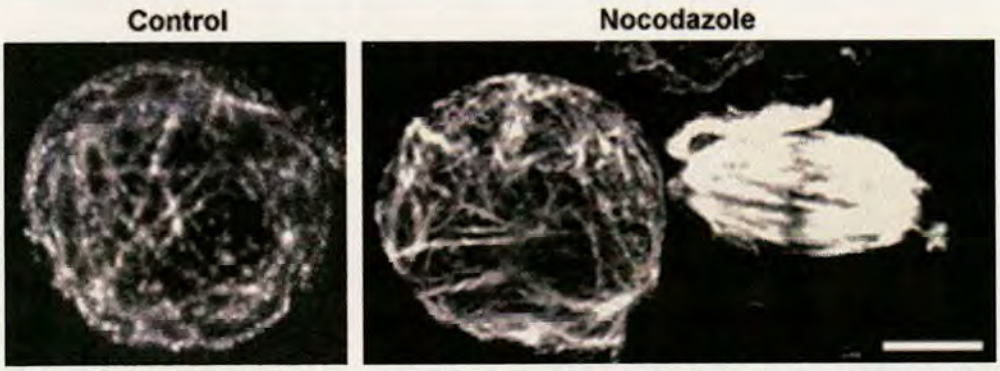

Figure 3.9: Nocodazole does not depolymerise microtubules in *Drosophila* S2 cells. Cells incubated in the presence or absence of 50μM Nocodazole for 15h were processed for IF and labelled for α-tubulin. Note that the microtubule network in nocodazole-treated cells is similar to that in non-treated cells and that the mitotic spindle is not disrupted. Bar: 5 μm

cells with apparently normal mitotic spindle could be observed among the cell population (Figure 3.9). The non-effectiveness of nocodazole in disrupting the microtubule network has also been reported in yeast (Walker, 1982; Ayscough et al., 1992). To overcome this problem, another microtubule depolymerisation reagent, colchicine, was applied at a concentration of 75μM for 2 hours. Upon this treatment, S2 cells exhibited significantly disrupted microtubule network compared to non-treated cells (Figure 3.10, middle column). These cells exhibited only few short microtubules with high concentration at one part of the cytoplasm, presumably where the centrosome is located (arrow in figure 3.10). Additionally, no cell was observed to assemble a mitotic spindle, suggesting that the drug inhibits its formation. This effect was further exemplified when a 15 hour incubation of the S2 cells with 30μM colchicine led to an accumulation of cells arrested in prometaphase, as it was assessed by Dapi staining (not shown). When tER

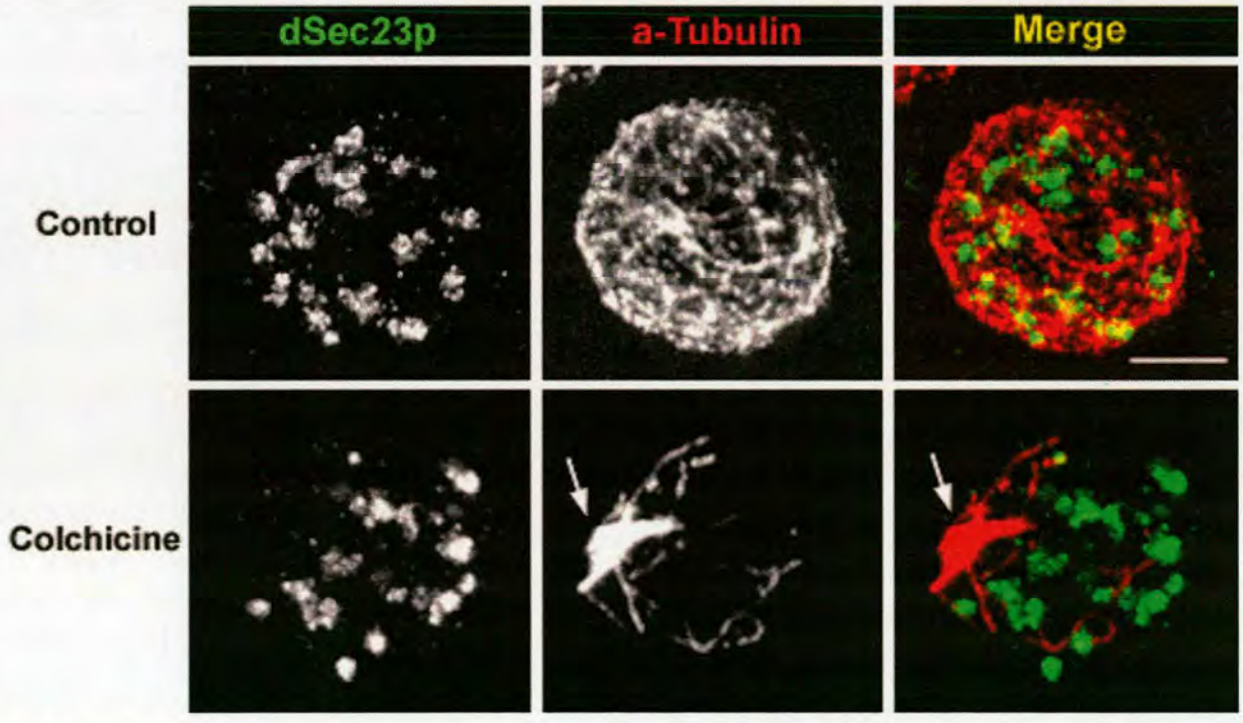

Figure 3.10: tER site organisation of S2 cells upon microtubule depolymerisation. Cells incubated without (upper panel) or with 75μM colchicine for 2h (lower panel), were processed for IF and labelled for dSec23p (left column) and α-tubulin (middle column). In the merged pictures (right column), tER sites are labelled in green and microtubules in red. Arrows in colchicine-treated cell point to a place of locally high concentration of microtubules, where the centrosome is probably situated. Bar: 5μm

organisation was examined by looking at dSec23p localisation, it was found essentially unchanged (Figures 3.10 and 3.11). Furthermore, microtubule depolymerisation does not seem to affect the distribution of d120kd-positive Golgi membranes or to disrupt their close spatial association with the tER sites (Figure 3.11).

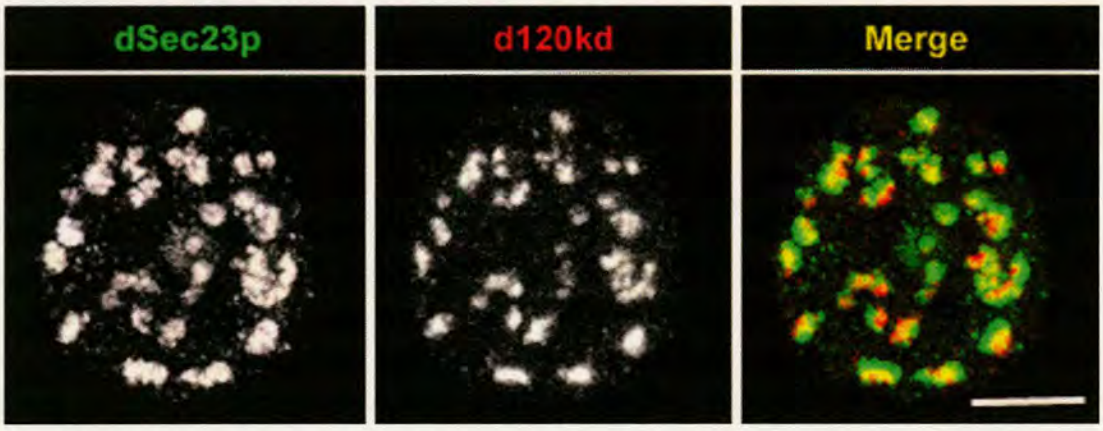

Figure 3.11: No disruption in tER-Golgi close spatial relationship upon microtubule depolymerisation. Cells incubated with 75μM colchicine for 2h were processed for IF and labelled for dSec23p (left) and d120kd (middle). In the merged picture (right), tER sites are labelled in green and Golgi membranes in red. Note the partial overlap of nearly all dSec23p- and d120kd-positive spots in a similar fashion to non-treated S2 cells. Bar: 5μm

3.3.4 Actin filament depolymerisation

Finally, the importance of actin cytoskeleton in the organisation of early exocytic pathway was studied in cells treated with the actin depolymerisation drug, cytochalasin D. Actin depolymerisation in mammalian cells was shown to alter the morphology of the Golgi apparatus, which acquired a more compact juxtanuclear position when visualised by IF (Valderrama et al., 1998; di Campli et al., 1999). At the ultrastructural level, the Golgi stacks did not appear fragmented, but the cisternae were swollen increasing significantly the cisternal volume (Valderrama et al., 1998).

After incubating S2 cells with 50μM cytochalasin D for 2 hours, the efficiency of the drug treatment was assessed by labelling the cells with

phalloidin conjugated to TRITC (Sigma), which binds to F-actin (Figure 3.12, A and D). In non-treated cells, actin filaments are localised at the cell cortex and form spiky extensions, which are known as stress fibres (Figure 3.12A). Stress fibres are bundles of actin filaments that help the cultured cells adhere to a surface through the formation of focal adhesions (Petit and Thiery, 2000). Therefore, as expected, they were mostly seen at the side, with which the cells were attached on the coverslip (Figure 3.12A). In contrast, cytochalasin D-treated cells exhibited a reduction of cortical labelling for F-actin and loss of the stress fibres observed in the control cells. Instead, the cytoplasm was full of F-actin spots (Figure 3.12E) that could correspond to actin aggregates, which have been described to form *de novo* upon cytochalasin D treatment (Rotsch and Radmacher, 2000; Mortensen and Larson, 2003). As an additional support for the inhibitor's effective action, an increase in the number of bi-nucleated cells was observed, suggesting a defect in actin-dependent process of cytokinesis.

Subsequently, control and cytochalasin D-treated cells were examined for their tER and Golgi organisation (Figure 3.12, B-D and F-H). Upon actin depolymerisation, dSec23p labelling appeared more diffused and dispersed in small puncta, although focused tER sites were largely present (Figure 3.12, compare B with F). On the other hand, d120kd-positive structures appeared smaller in size and their number increased by about 50% compared to the non-treated cells, but they did not appear to cycle back to the ER, as upon BFA treatment (Figure 3.12, C and G). In merged pictures, contrary to non-treated cells, several d120kd-positive spots were not in close association with focused tER sites (arrowheads in figure 3.12H), and the converse was also true (Figure 3.12, compare D and H). Therefore, it seems that the integrity of actin microfilaments plays an important role in the organisation of the early

exocytic pathway, and especially of the Golgi stacks, since their depolymerisation led to fragmentation of the d120kd-positive structures. Whether these d120kd spots represent Golgi stacks or clusters will need further investigation by EM.

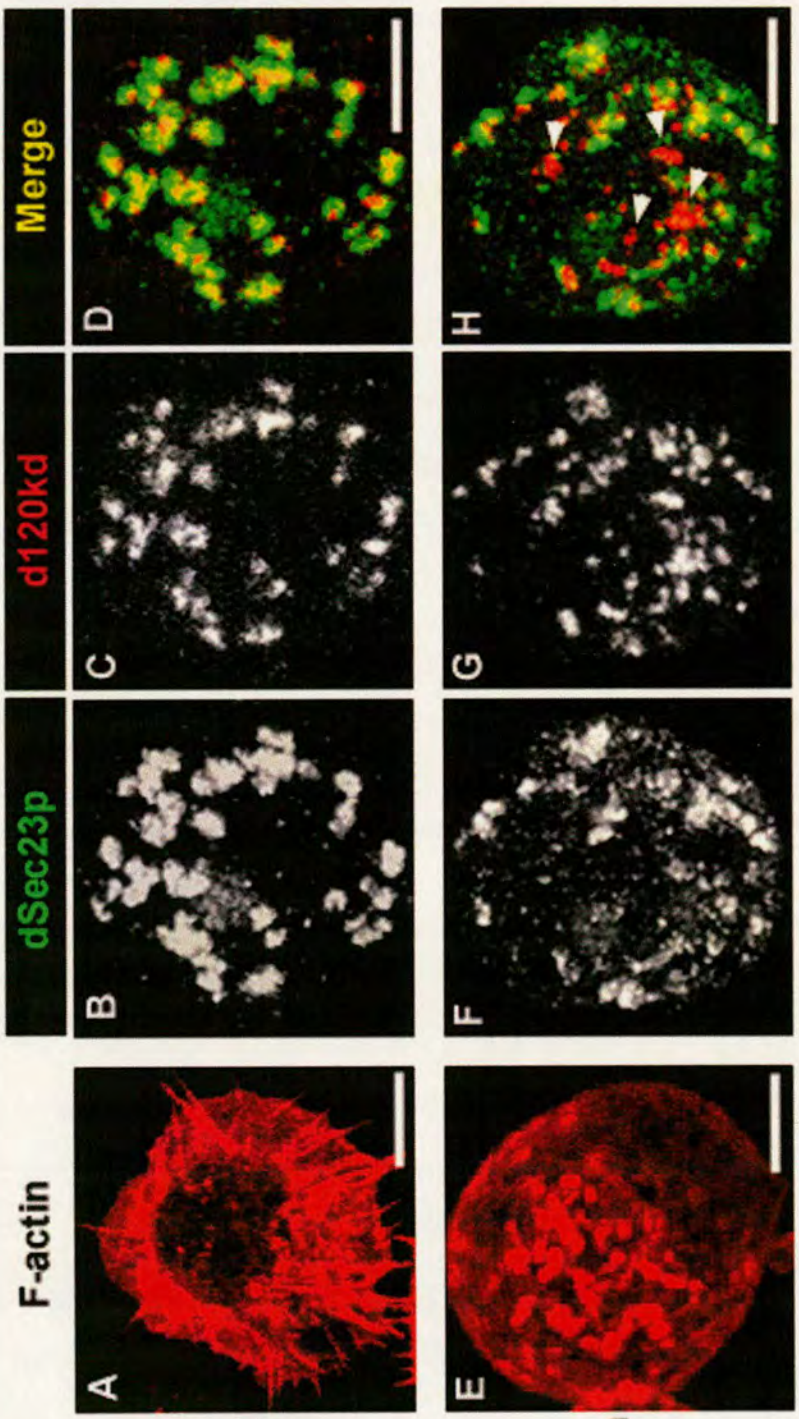

Figure 3.12: Effect of actin depolymerisation on tER and Golgi organisation in S2 cells. Cells incubated without (A-D) or with 50µM cytochalasin D for 2h (E-H), were processed for IF and either labelled for F-actin using phalloidin conjugated to TRITC (A and E), or double labelled for dSec23p (B and F) and d120kd (C and G). In the merged picture (D and H), tER sites are labelled in green and Golgi membranes in red. Note that the stress fibres of actin filaments in non-treated cells are replaced by F-actin aggregates in cytochalasin D-treated cells. In H, arrowheads point to d120kd-positive structures that are not associated with a focused tER site, something that is almost never observed in control cells. Bars: 5µm.

3.4 Anterograde intracellular transport through the early exocytic pathway

The early exocytic compartments play an essential role in transport of secretory, plasma membrane and endosomal/lysosomal proteins to their final destination (see introduction). In order to correlate the organisation of the early exocytic pathway with anterograde protein transport in *Drosophila* S2 cells, Delta protein was used as a reporter for transport to the plasma membrane (PM).

3.4.1 Characterisation of Delta as a reporter for anterograde transport

Delta is one of the *Drosophila* ligands for Notch (Rebay et al., 1991) and like its receptor, it is a substrate for O-glycosylation. More specifically, Fringe, a glycosyltranferase localised in the Golgi apparatus (Munro and Freeman, 2000), has been shown to catalyse the addition of N-acetylglucosamine on O-fucose glycans of Delta (Panin et al., 2002). Delta was also reported to be cleaved, producing several isoforms (Klueg et al., 1998). These proteolytic cleavage events of Delta seem to take place after the protein has reached the plasma membrane (Schlöndorff and Blobel, 1999). For example, metalloprotease Kuzbanian was shown to cleave Delta on the cell surface releasing an extracellular fragment, which is involved in Notch signalling pathway (Qi et al., 1999).

A useful tool that allowed the monitoring of Delta transport through the exocytic pathway was a stable S2 cell line (Delta S2 cells) expressing the full length Delta protein (Figure 3.13A), which was a kind gift from Kris Klueg (Bloomington, Indiana). The expression of Delta in this cell line is under the control of a metallothionein promoter that is switched on by the addition of 1mM $CuSO_4$ in the culture medium. Initially, Delta transport to

the PM was visualised using the 9E10 antibody (anti-MYC, see table 2.6), since the expressed Delta molecule has a MYC tag in its cytosolic C-terminus (Figure 3.13A). After 2 hours induction and 4 hours chase (see 2.4.5), the induced cells exhibited labelling at their PM and in some intracellular structures (Figure 3.13B). Double labelling with 9E10 and an anti-GM130 antibody (MLO7, see table 2.6) showed that these internal structures do not colocalise with the Golgi marker (not shown), suggesting that they probably represent endosome/lysosome compartments.

One problem of using 9E10 to visualise Delta was that permeabilisation of the cells with Triton was necessary, as the MYC epitope is in the cytosolic side. This made it difficult to assess the intensity of fluorescence at the PM (see 2.4.5.4). Furthermore, it has been shown that in Delta S2 cells, almost the entire cytosolic part of Delta can be cleaved and generate a fragment of ~22kD that is detectable by anti-MYC antibodies (Klueg et al., 1998). To test whether the amount of this C-terminal fragment was high enough to influence the quantitation of Delta transport, a Western blotting using 9E10 was performed on cells induced with $CuSO_4$ for different periods (Figure 3.13C). The amount of this 22kD fragment increases parallel to the increasing level of full length Delta and after 4 hours induction the two bands are almost equal. Therefore, the C-terminal fragment was not negligible and its potential localisation in the endosomal/lysosomal system could lead to a misinterpretation of Delta transport efficiency. For this reason, another monoclonal antibody was applied (C594.9B). This antibody recognises an epitope in Delta EGF-like repeats 4 and 5 (Klueg et al., 1998), which are located in the extracellular part of the protein (Figure 3.13A). Thus, the requirement for permeabilisation of the cells was bypassed (Figure 3.14), and the measurement of fluorescence intensity at the PM was facilitated.

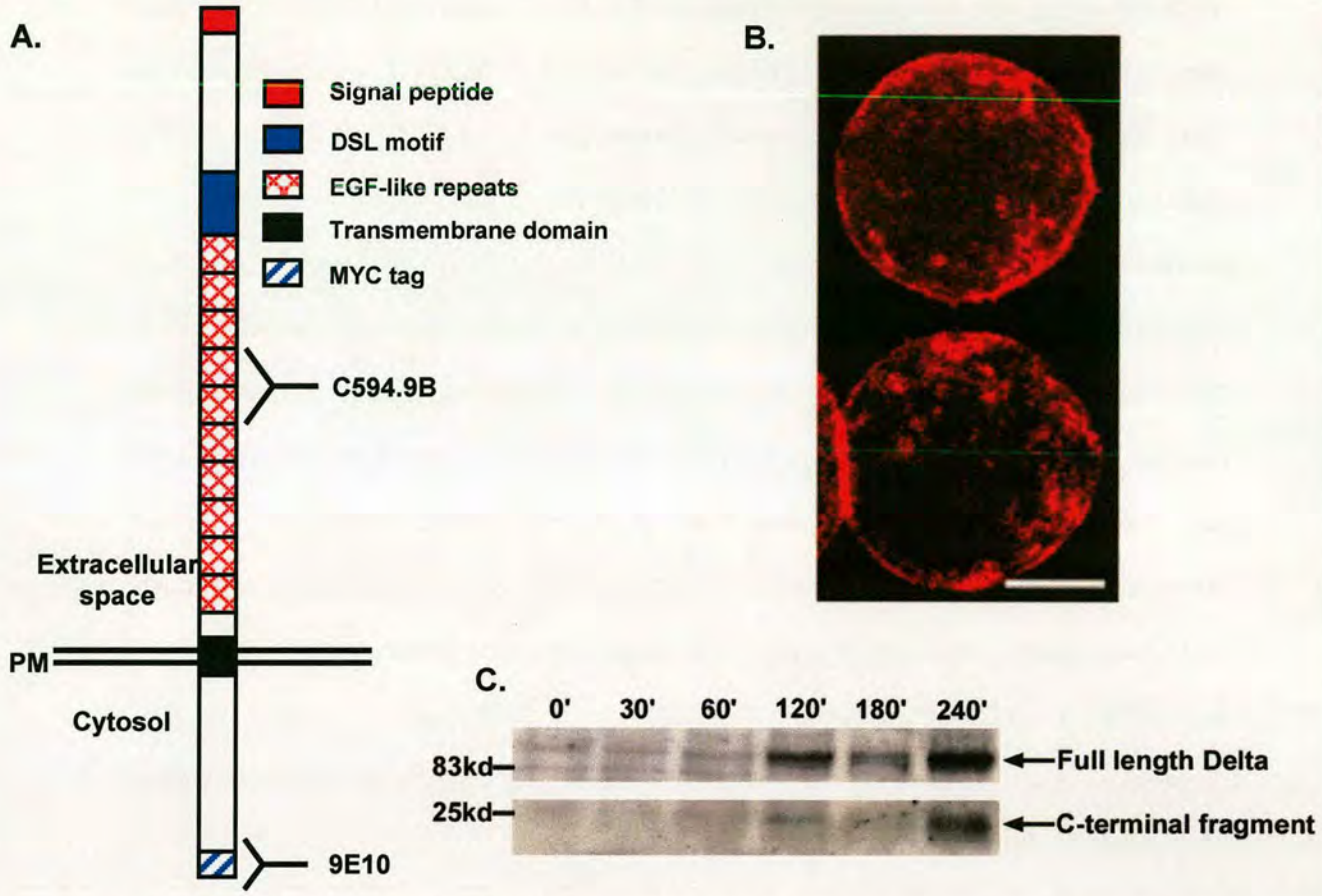

Figure 3.13: A. Structure of Delta protein expressed in Delta S2 cells. In its extracellular (lumenal) part, Delta contains a DSL motif (common in transmembrane ligands of Notch), 10 epidermal growth factor (EGF) repeats and the signal peptide that is cleaved in the ER. In its cytosolic part, it comprises a MYC tag associated with the C-terminus. Note the parts of the molecule that are recognised by 9E10 and C594.9B antibodies that were used. Adapted from Klueg et al., 1998. **B.** Delta S2 cells were induced for 2h followed by a 4h chase, and processed for IF. Cells were labelled with 9E10 (anti-MYC) to visualise Delta. Note the numerous internal structures labelled for Delta. The picture represents a confocal section. **C.** Delta S2 cells were induced for different periods and the level of Delta expression was assessed by Western blotting using the 9E10 antibody. Note that after 120min of induction, a significant amount of the 22kD fragment corresponding almost to the entire cytosolic domain of Delta is present in the cells. Bar: 5μm

In order to confirm that Delta is transported to the PM following the classical exocytic pathway, the protein was visualised by IEM in Delta S2 cells induced for 90 minutes with $CuSO_4$. Since Delta S2 cells are not a clonal cell population, the induction efficiency and transport of Delta was not synchronous in all cells (Figure 3.14). For example, some cells seemed to have

responded in the $CuSO_4$ induction earlier than other cells. Consequently, these "early responding" cells transported Delta to the PM before those with "late response". Due to glutaraldehyde sensitivity of C594.9B antibody, the cells were fixed only with paraformaldehyde, resulting in increasing cell extraction (Figure 3.15). Despite the less optimal cell preservation, Delta was clearly found to localise in all compartments of the exocytic pathway (ER, tER, Golgi apparatus and PM; Figure 3.15A and B), suggesting that it follows the typical anterograde transport route. Moreover, it was verified that Delta also reaches the endosomes (see inset in figure 3.15A). However, it is not transported to the endosomes directly from the TGN, but it first reaches the PM and then it is endocytosed. This was apparent in cells with "delayed response" to $CuSO_4$ induction, where although Delta had arrived at the PM, there was not enough time to be endocytosed during the 90 minutes of the experiment (Figure 3.15B).

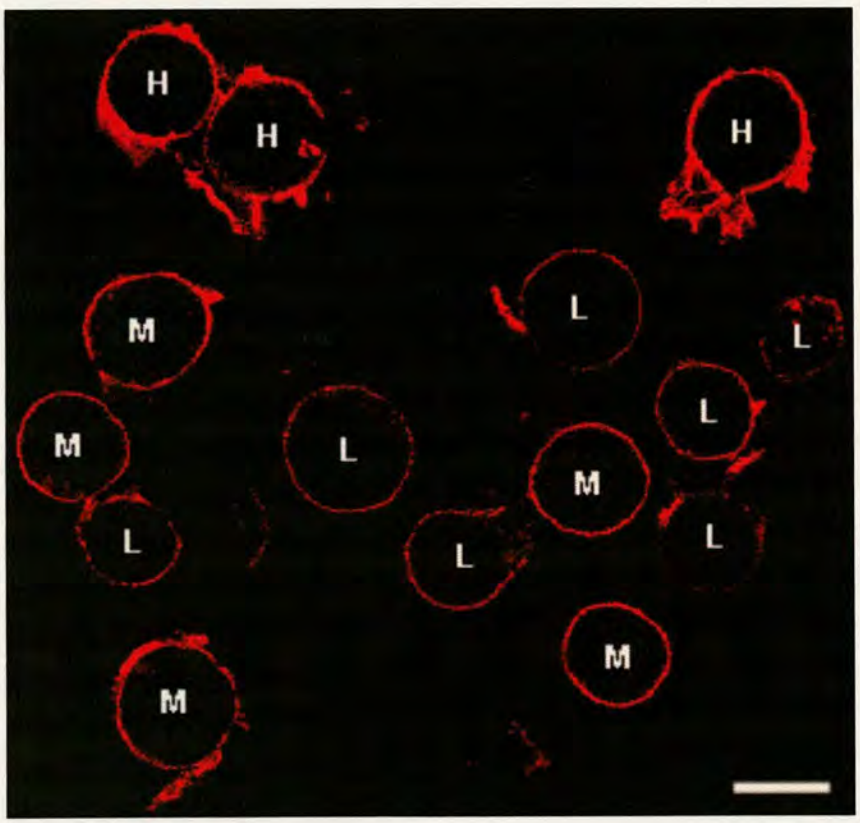

Figure 3.14: Differential "response" of Delta S2 cells upon induction with $CuSO_4$. Cells were induced with $CuSO_4$ for 1h followed by 90min chase and processed for IF without permeabilisation with Triton X-100. The cells were labelled for Delta using C594.9B antibody. A confocal section of a randomly selected area of the sample is captured. Based on the fluorescence intensity at the PM, the cells were categorised in those displaying high (H), medium (M) or low (L) intensity (see paragraph 2.4.5). Bar: 5μM.

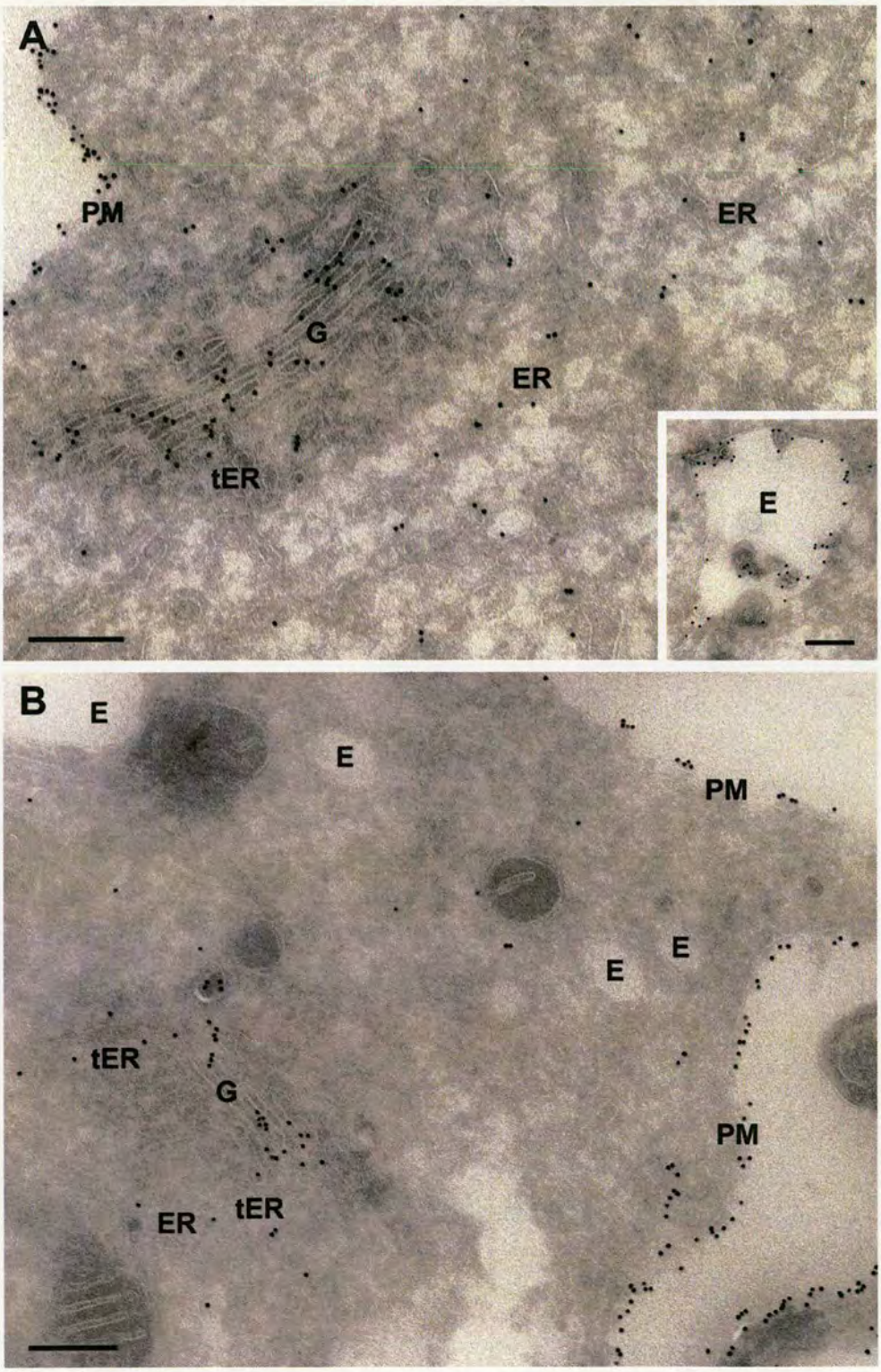

Figure 3.15: Immunolocalisation of Delta throughout the exocytic pathway in S2 cells. A-B. Cells were induced with for 90min, fixed in 4% PFA, processed for IEM, and labelled with C594.9B followed by Protein A coupled to 10nm gold. All the compartments of the classical exocytic pathway contain Delta. Note that the endosome (E) illustrated in the inset in A is labelled for Delta, while the endosomes in B are not, although the protein has reached the PM. This shows the differential response of Delta S2 cells in $CuSO_4$ induction and suggests that Delta needs to be transported to PM before being endocytosed and delivered to endosomes. ER, endoplasmic reticulum; tER, transitional ER; G, Golgi stacks; PM, plasma membrane. Bars: 200nm

3.4.2 Description and testing of Delta intracellular transport assay

In order to use transport of Delta to the PM as an assay for monitoring anterograde intracellular transport through the tER sites and the Golgi apparatus, it was important to optimise the parameters of its expression and transport. First of all, the time-dependent expression of Delta was investigated by Western blotting (Figure 3.16). Full-length Delta is detectable in trace amount after 30 minutes induction with $CuSO_4$. Only after 60 minutes, a significant amount of the full-length protein is detected and it seems to reach its maximal level after 120 minutes (Figure 3.16). Furthermore, the two intermediate and the short Delta isoforms, which have been described to derive from the cleavage of the full-length molecule (Klueg et al., 1998), appear 90-120 and 180 minutes after induction, respectively (Figure 3.16). This is in agreement with the Western blot detection of Delta using 9E10 (Figure 3.13C), and suggests that it is only after 2 hours induction that considerable Delta processing takes place.

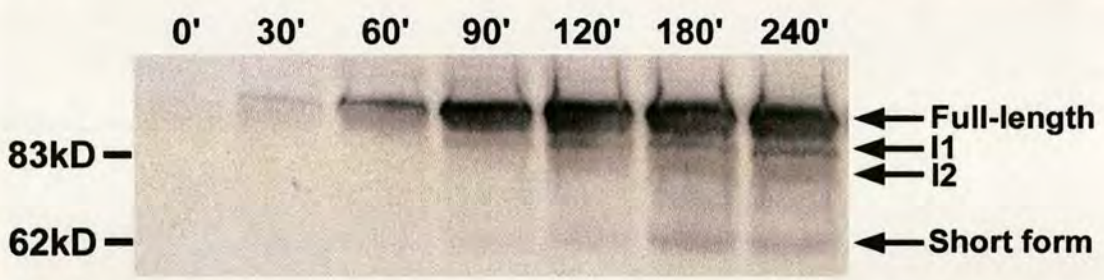

Figure 3.16: Time course examination of Delta induction. Delta S2 cells were induced with $CuSO_4$ for different time periods and extracts from 3 million cells were processed for Western blotting using C594.9B antibody. Note that the intermediate truncated isoforms of Delta (I1 and I2) become detectable 90-120 min after induction, while the short isoform of about 65kD is clearly seen after 180min.

The transport of Delta to the PM was assessed by estimating the total fluorescence intensity at the PM after inducing Delta synthesis and chasing its transport for certain time periods. Shortly, in each sample, the percentage

of cells exhibiting high, medium and low PM intensity or exclusive intracellular staining was calculated (Figure 3.18). These figures were multiplied by the average intensity for each labelling category under the specific experimental conditions, and were summed up (see also section 2.4.5.4).

By applying this quantitation method, the kinetics of Delta transport was initially examined for 3 different induction periods (15, 30 and 60 min) and 3 different chase periods (45, 60, 90 min). The total fluorescence intensity at the PM was calculated for each condition (Figure 3.17). From the results of this experiment the following conclusions can be drawn:

a. The 60-minute induction protocol (Figure 3.17, blue line) produced the maximal fluorescence intensity at the PM after 90 minutes chase. Prolonged induction periods (e.g. 120 minutes) did not increase further the measured total fluorescence (not shown). This means that the "60min induction + 90min chase" protocol reflects the steady state transport of Delta.
b. The 15-minute incubation with $CuSO_4$ induced only a limited amount of Delta, since the total fluorescence intensity was low even after a chase period of 90 minutes (Figure 3.17, green line). The inefficient induction of Delta was already predicted from the time course experiment monitoring the induction of Delta (Figure 3.16).
c. An interesting curve was that corresponding to 30-minute induction (Figure 3.17, red line). Although after 45-minute chase the total fluorescence intensity was low, longer chase periods led to a rapid increase of the total fluorescence, which reached finally a figure comparable to that of steady state condition curve (Figure 3.17, compare

blue and red lines). Thus, this 30-minute induction curve could be used to study the initial rate of Delta transport to the PM.

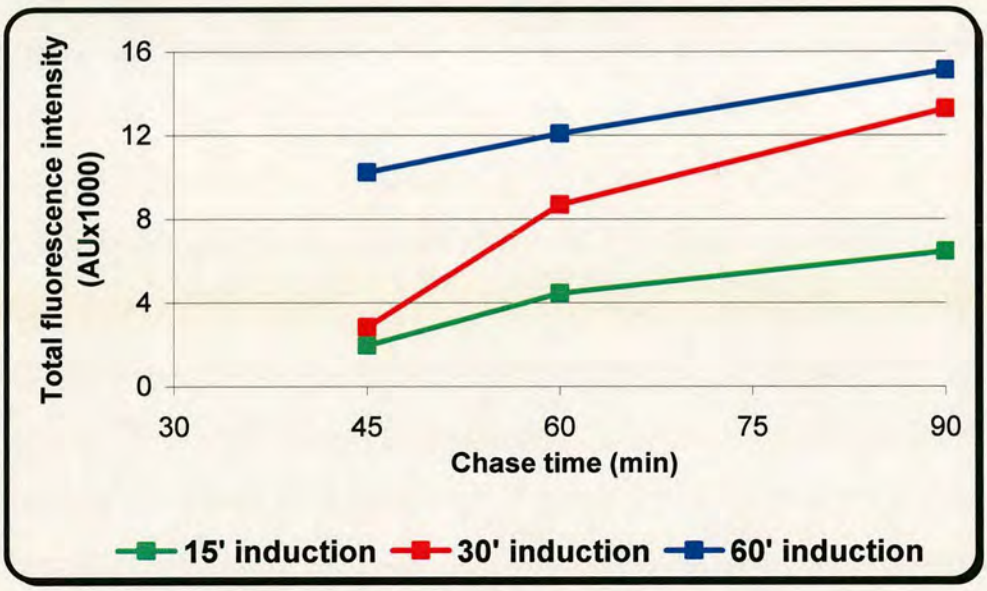

Figure 3.17: Kinetic study of Delta transport to the PM. Delta S2 cells were induced for 15 (green), 30 (red) or 60min (blue) with $CuSO_4$, and Delta transport to the PM was chased for 45, 60 or 90min. Note that 15min induction is not adequate, as only 40% of the maximal amount of Delta is produced. In contrast, the 30min-induction curve shows that the induced amount of Delta is ~90% of the maximal (compare red and blue lines after 90min chase), and also indicates that in these conditions, the arrival of the majority of Delta to the PM can be captured.

Next, the sensitivity of this Delta transport assay was tested. As a positive control BFA was chosen, since it is a known inhibitor of anterograde transport in mammalian cells (Fujiwara et al., 1988; Lippincott-Schwartz et al., 1989) and it was shown earlier in this chapter to have a similar effect in *Drosophila* S2 cells (see section 3.3.1). Delta S2 cells were treated with 50μM BFA for 30 minutes at 37°C, followed by a 45-minute induction and a 60-minute chase of Delta at 27°C, always in the presence of the drug. In parallel, non-treated cells were induced and chased under the same conditions, and their total PM fluorescence intensity was set as 100% transport efficiency (Figure 3.19). As expected, in BFA-treated cells, Delta was retained

intracellularly in 85% of the cells (Figure 3.18). The transport block seemed to occur mostly in the ER export of Delta, judging from the reticular and nuclear envelope staining observed by light microscopy (Figure 3.20). However, it cannot be excluded that at least some of the observed structures where Delta is concentrated might represent persisting Golgi membranes. The efficiency of Delta transport upon BFA treatment was calculated to be 11.3±2.0% (Figure 3.19).

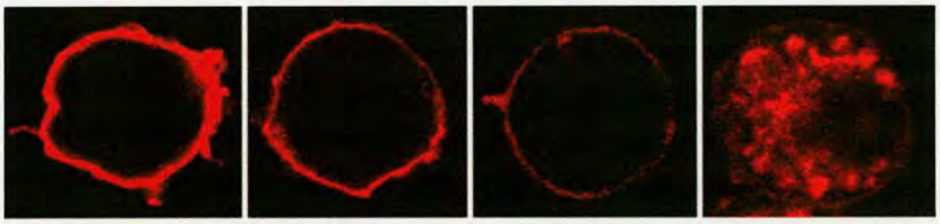

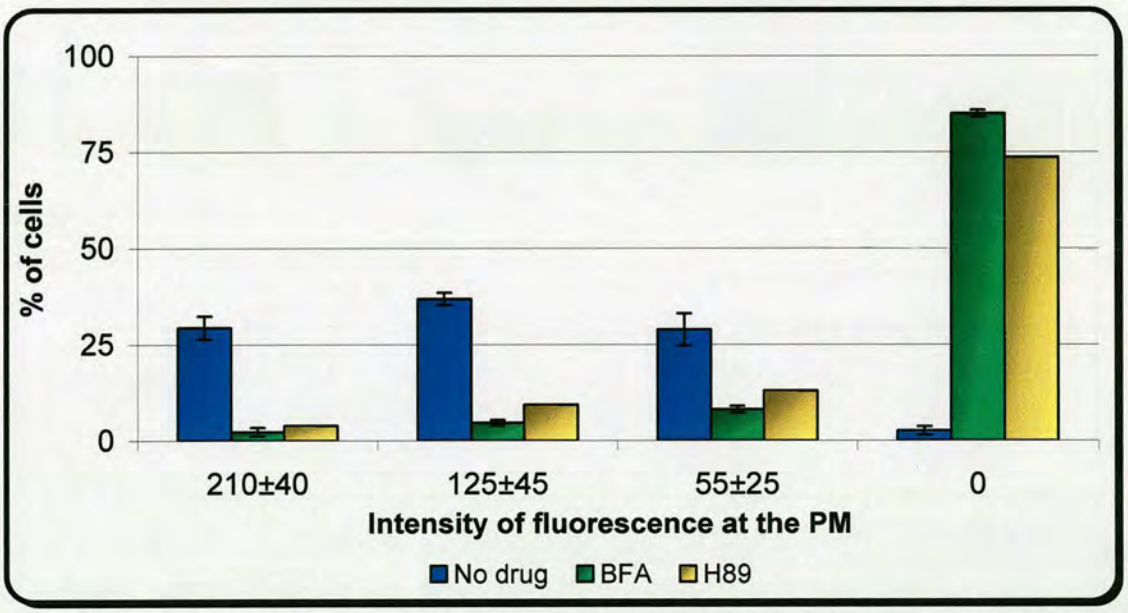

Figure 3.18: Quantification of the effect of anterograde transport inhibitors on Delta transport to the PM. Delta S2 cells were incubated with the BFA and H89 for time periods mentioned in 2.4.5.3, and subsequently were induced for 45min with $CuSO_4$ followed by chase of 60min. After being processed for IF and labelled for Delta, the percentage of cells exhibiting the three different intensities of plasma membrane or exclusive intracellular labelling was scored (examples of the 4 labelling categories are shown above the graph). In these conditions, the average fluorescence intensity for each of the three categories is indicated in the x-axis. Results are expressed as a percentage of total number of cells examined (500 for each condition). The error bars represent the SD. Note the high percentage of cells showing intracellular staining after BFA and H89 treatment compared to the non-treated cells.

H89 was used as an additional anterograde transport inhibitor. Under the same experimental conditions used for BFA (45min induction and 60min chase), 73.7% of the H89-treated cells exhibited intracellular staining for Delta (Figure 3.18), and the transport efficiency was estimated to be only 20.2% relative to non-treated cells (Figure 3.19).

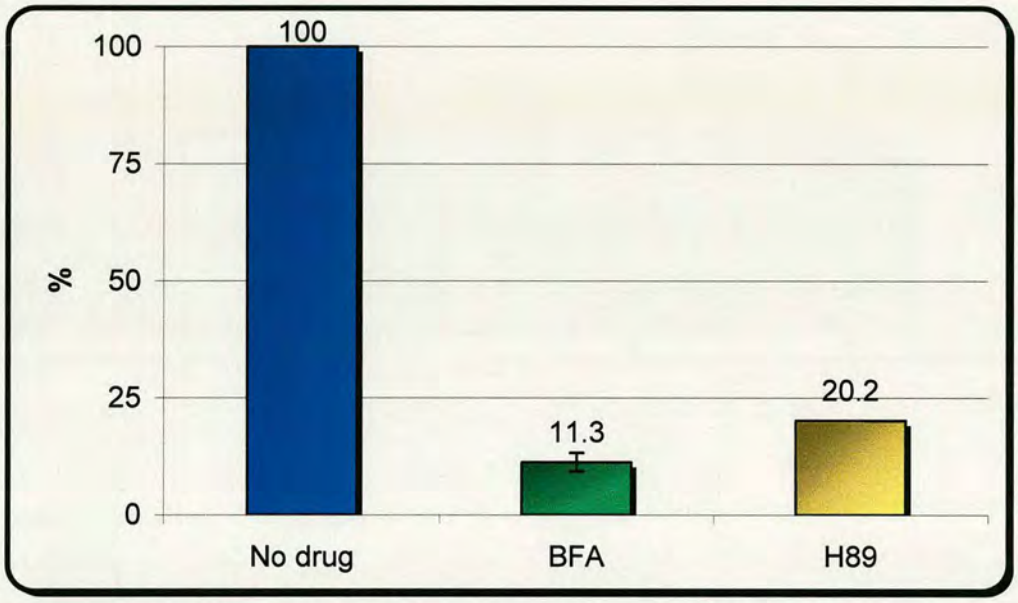

Figure 3.19: Efficiency of anterograde transport of Delta to the PM upon treatment with ER-Golgi transport inhibitors. Total fluorescence intensity was calculated for cells treated with BFA and H89 and it was expressed as a percentage over the non-treated cells. The error bars represent the SD.

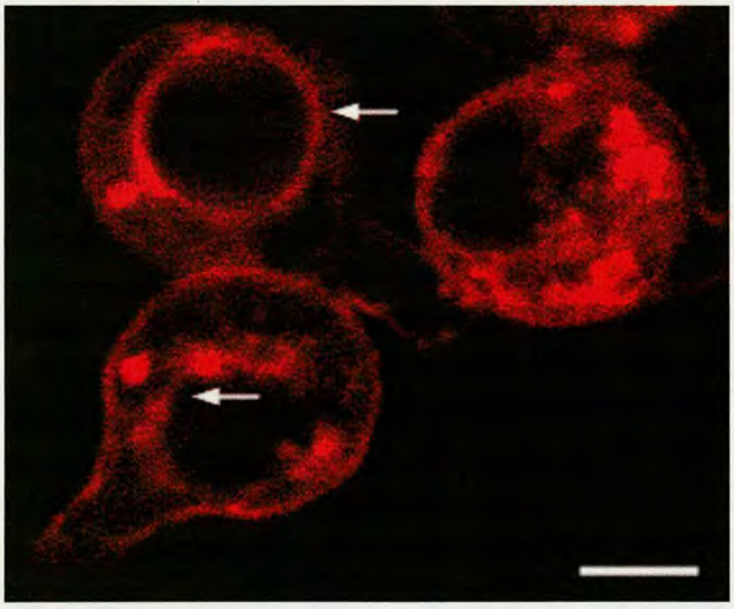

Figure 3.20: The bulk of Delta is blocked in the ER upon treatment of Delta S2 cells with BFA. Note the labelling of the nuclear envelope pointed by arrows and the continuous structure labelled in the cell on the right, which are reminiscent of the ER distribution. Both patterns are characteristic of an ER localisation of Delta. The image represents a confocal section. Bar: 5μM.

3.4.3 The role of the cytoskeleton in intracellular transport in S2 cells

3.4.3.1 Microtubules

The role of the cytoskeleton in transport of Delta to the PM was also investigated. In mammalian cells, the role of microtubules in transport of cargo-containing ERGIC structures from the cell periphery to the Golgi apparatus and from the Golgi apparatus to the cell surface is well established (Presley et al., 1997; Hirschberg et al., 1998). However, several earlier reports have shown that upon microtubule depolymerisation with nocodazole for more than 90 minutes, anterograde transport is moderately or hardly affected (Rogalski et al., 1984; Van de Moortele et al., 1993; Cole et al., 1996). This coincides with the redistribution of Golgi stacks at the periphery of the cells (Cole et al., 1996; see introduction). After the appearance of the peripheral Golgi stacks, the integrity of the microtubule network seems to be important only for apical transport in polarised epithelial cells (Thyberg and Moskalewski, 1999), where apical membrane proteins are missorted to the basolateral surface (Eilers et al., 1989).

In *Drosophila* S2 cells, cargo does not need to cover a long distance to reach the Golgi, as the tER sites are situated next to the Golgi apparatus (Figure 3.3). Furthermore, the disruption of microtubule cytoskeleton did not affect the organisation of the early exocytic pathway (Figures 3.10 and 3.11). Nevertheless, the efficiency of Delta transport was examined upon treatment with both potentially microtubule depolymerising agents. As mentioned before, nocodazole was not effective in depolymerising the microtubules (Figure 3.9), and not surprisingly, treatment of Delta S2 cells with the drug did not affect their competence in transporting Delta to the PM (Figure 3.21). Only a small reduction of 8.3% in transport efficiency was detected (Figure 3.22). Colchicine, the other strong microtubule inhibitor (50μM for 2 hours),

was shown to disrupt significantly the microtubule organisation in *Drosophila* S2 cells (Figure 3.10), but similar to nocodazole, its effect on Delta transport was estimated to a 10% inhibition (Figure 3.22). The incubation of Delta S2 cells with colchicine was also prolonged to 15 hours, but the result concerning Delta transport was identical. Therefore, this experiment suggests that, at least in *Drosophila* S2 cells, the integrity of the microtubule network is not necessary for anterograde protein transport at steady state.

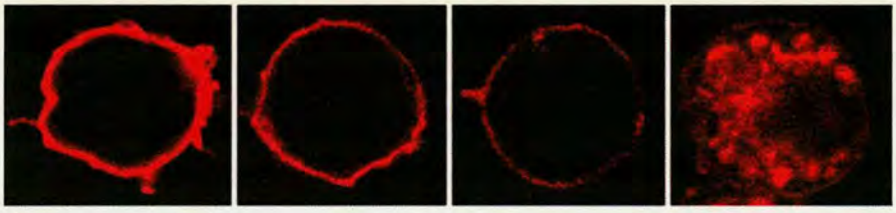

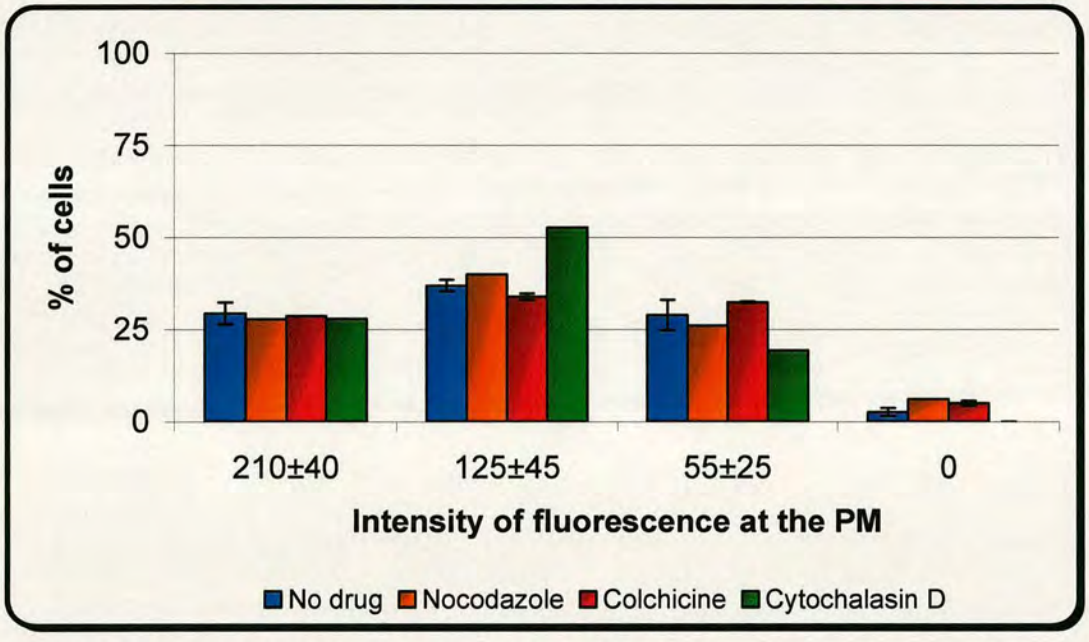

Figure 3.21: Quantification of the effect of cytoskeleton depolymerising drugs on Delta transport to the PM. Delta S2 cells were incubated with nocodazole, colchicine or cytochalasin D for 2h at concentrations mentioned in 2.4.5.3, and subsequently were induced for 45min using $CuSO_4$ followed by chase of 60min. Processing for IF and quantitation was performed as described in figure 3.18. Note the similar labelling distribution of cells with disrupted cytoskeleton and the non-treated cells.

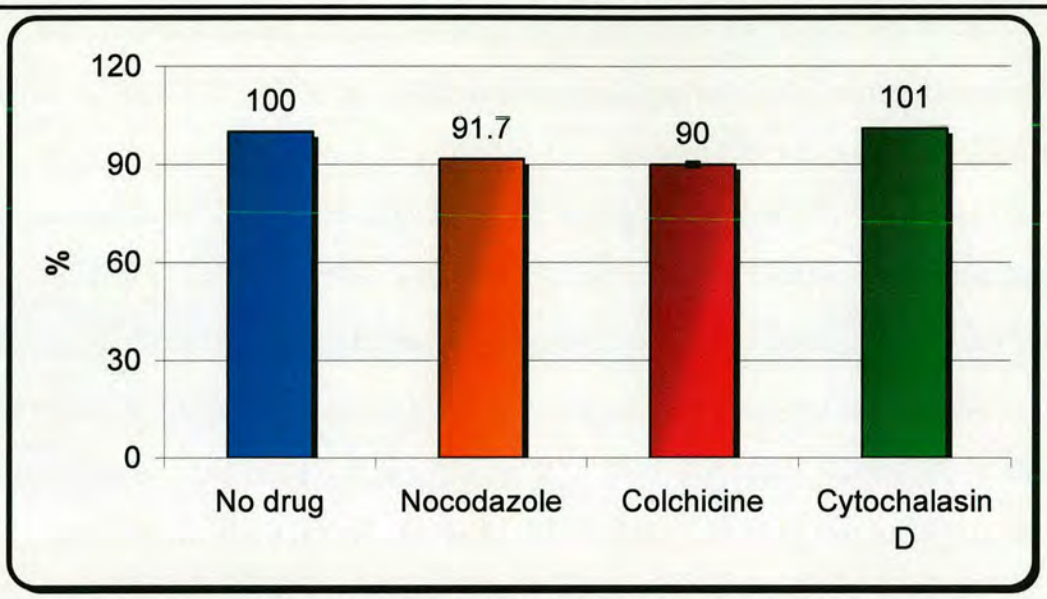

Figure 3.22: Efficiency of anterograde transport of Delta to the PM upon treatment with microtubule and microfilament inhibitors. Total fluorescence intensity was calculated for cells treated with nocodazole, colchicine and cytochalasin D, and was expressed as a percentage over the non-treated cells. The error bars represent the SD.

As a way to test whether transport is inhibited during mitosis in S2 cells, cells treated with colchicine for 15 hours were examined. As it was mentioned in paragraph 3.3.3, when Delta S2 cells were incubated with colchicine for this prolonged period, an increased percentage of them were arrested in pro-metaphase, unable to complete their mitosis due to the lack of mitotic spindle. Sixty arrested cells were examined concerning the expression of Delta, and 90% of them were devoid of any detectable amount of Delta labelling, while only 10% exhibited Delta labelling. Given that normally about 60% of the total cell population is induced under the conditions used (45min induction and 60min chase), this result suggests that protein synthesis may be shut down during mitosis. However, it could also imply an ER exit block in transport of Delta, which could be too dispersed in the ER to

be detected by IF. This would then correlate with the disorganisation of the tER sites and the Golgi stacks during mitosis (Figure 3.4).

3.4.3.2 Actin microfilaments

The role of actin cytoskeleton in Delta transport was tested in cytochalasin D-treated cells after 45 minutes induction followed by 60 minutes chase. Under these conditions in non-treated cells, Delta had time to be synthesised, transported to the PM and endocytosed to endosomes (Figure 3.23, left). In cells with disrupted F-actin filaments, anterograde transport was not affected, since PM was labelled for Delta (Figure 3.23, right). However, Delta endocytosis was significantly inhibited, since only few internal Delta-positive structures were observed (Figure 3.23, right).

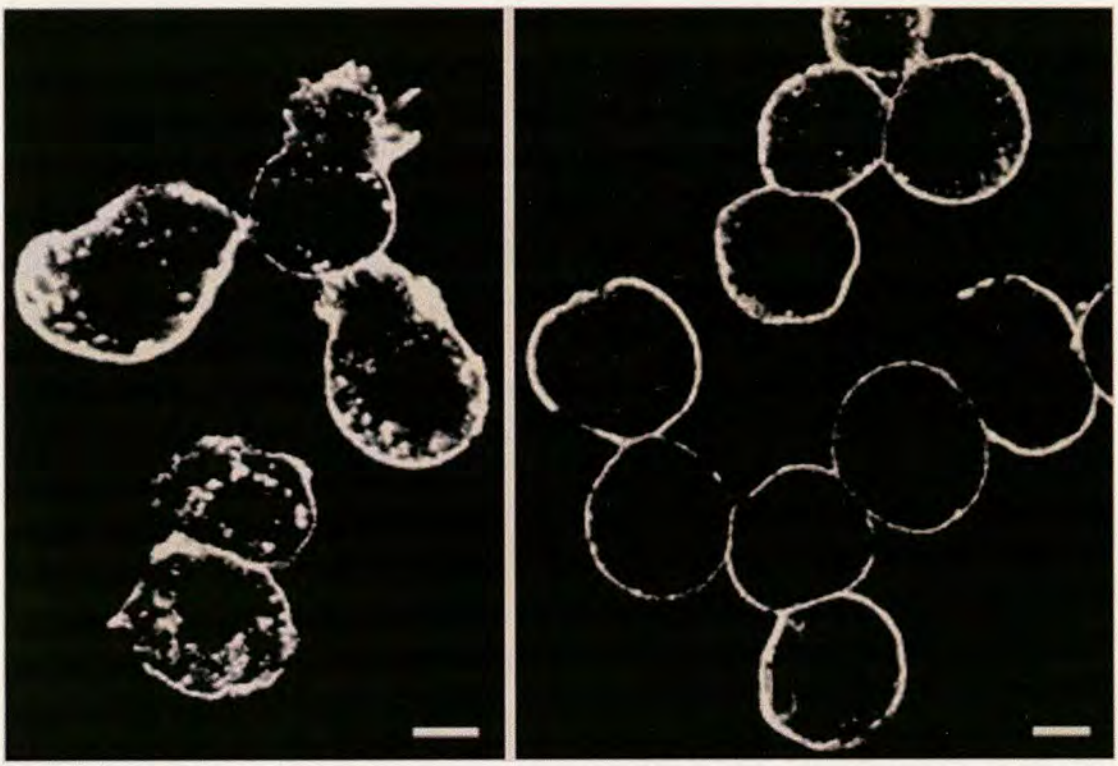

Figure 3.23: Effect of actin depolymerisation on Delta intracellular transport. Delta S2 cells were incubated in the absence (left) or presence (right) of 50μM cytochalasin D for 2h, processed for the Delta transport assay (45min induction / 60min chase), and labelled with C594.9B antibody. Note the depletion of labelling in intracellular structures in cytochalasin D-treated cells. Bars: 5 μM

The lack of any effect in anterograde transport by cytochalasin D treatment suggests that actin microfilaments are not essential for ER-Golgi and Golgi-PM transport, at least in *Drosophila* S2 cells. These results are in agreement with data from mammalian cells showing that ER-Golgi traffic of VSV-G (Valderrama et al., 1998; 2001), as well as the post-Golgi constitutive transport of VSV-G and glycosaminoglycans to the PM (Hirschberg et al., 1998; di Campli et al., 1999), are not inhibited in the absence of filamentous F-actin. This is seemingly contradictory to other studies reporting that myosin motors use actin cables as tracks for the transport of vesicles to the cell surface (DePina and Langford, 1999 and references therein). However, these results could reflect the distinct requirement of the different types of vesicle transport from TGN to PM for the actin filaments (i.e. constitutive vs. regulated exocytosis). On the other hand, the observed inhibition of Delta endocytosis is corroborative of the well-established role of actin cytoskeleton in the endocytic pathway (Engqvist-Goldstein and Drubin, 2003).

Taking into account that anterograde transport of Delta is not affected upon actin depolymerisation, the observed disruption in tER organisation (Figure 3.11) is unlikely to stem from an ER-Golgi transport arrest. In contrast, this effect could be a result of an alteration in the retrograde transport from Golgi to ER. This has been suggested by the implication of actin filaments in Golgi-ER retrograde traffic of Shiga toxin, KDEL receptor and the Golgi enzymes upon BFA treatment (Valderrama et al. 2001). Finally, the Golgi fragmentation upon cytochalasin D treatment is also not likely to be due to a transport defect. Instead, the reason for this effect could be that depolymerised F-actin might cause a disruption in the spectrin membrane skeleton, which has been proposed to form a scaffold responsible for the localisation and maintenance of the Golgi apparatus, and has been shown to

interact with cytoskeleton-related proteins (De Matteis and Morrow, 2000 and references therein).

3.5 Summary

A synopsis of the characterisation of the exocytic pathway in *Drosophila* S2 cells is shown in table 3.1. Three basic features of this pathway, namely the architecture of the Golgi apparatus, the organisation of the tER sites and the anterograde transport during cell cycle and upon treatment with certain inhibitors are compared between *Drosophila* and mammalian cultured cells.

A common feature between the S2 and mammalian cells is that they display similar behaviour during mitosis considering the organisation and probably the function of their exocytic pathway. However, it should be noted that in certain *Drosophila* tissues, dividing cells do not exhibit a Golgi stacks disassembly, which resembles the situation in yeast and plants.

The use of anterograde transport inhibitors Brefeldin A and H89 led to a disorganisation of the early exocytic pathway in S2 cells comparable to that observed in mammalian cells. The only difference was that the focused tER sites in S2 cells appeared also dispersed.

In contrast to mammalian cells, in S2 cells, the integrity of the microtubule network does not seem to be essential for the architecture of the early exocytic pathway, as well as the anterograde transport, at least of constitutively transported proteins, like Delta.

Finally, the actin filaments seem to be important for the organisation of the early exocytic pathway in S2 cells, since their disruption leads to a fragmentation of both the tER sites and the Golgi stacks. However, this did not affect anterograde transport of Delta to the PM, but only impaired its endocytosis.

		Golgi stack organisation		tER organisation (COPII coat markers)		Anterograde Transport	
		Drosophila S2 cells	Mammalian cells	Drosophila S2 cells	Mammalian cells	Drosophila S2 cells	Mammalian cells
Cell Cycle	Interphase	18±7 Golgi stacks dispersed in the cytoplasm[1, 2, 3]	Stacks interconnected into a perinuclear Golgi ribbon[4,5]	20±8 focused sites per cell[3]	~200 spots per cell[10,11]	Normal[3]	Normal[14,15]
	Prophase	Disassembly[1]	Fragmentation into individual Golgi stacks[4,5]	Dispersed[3]	Disorganisation COPII cytosolic[12]	?	Blocked[14,15]
	Metaphase	Disassembly [1,3]	Disassembly[4,5]	Dispersed[3]	Disorganisation COPII cytosolic[12]	?	Blocked[14,15]
	Anaphase	Begin to reassemble[1]	Disassembly[4,5]	Dispersed[3]	Disorganisation COPII cytosolic[12]	?	Blocked[14,15]
	Telophase	Reassembly[1]	Reassembly of individual Golgi stacks[4,5]	Focused[3]	Reorganisation[12]	?	Normal[14,15]
	Cytokinesis	Reassembly [1]	Pericentriolar Golgi ribbon[4,5]	Focused[3]	Reorganisation[12]	?	Normal[14,15]
Inhibitors	BFA	Absorbed in the ER at least in part[3]	Absorbed in the ER[6]	Dispersed[3]	Not changed[13]	Blocked[3]	Blocked[16]
	H89	Dispersal[3]	Disassembly[7]	Dispersed[3]	Disorganisation COPII cytosolic[7]	Blocked[3]	Blocked[7]
	Nocodazole	No effect[3]	Small dispersed stacks[8]	Focused[3]	Not changed but clustered[11]	Normal[3]	Initially blocked but recovers after ~2h[17]
	Colchicine	No effect[3]	Small dispersed stacks[8]	Focused[3]	?	Normal[3]	Dependent on the protein[8]
	Cytochalasin D	Fragmentation[3]	More compact Golgi ribbon[9]	Dispersal and fragmentation[3]	?	Normal, but block in endocytosis[3]	ER-Golgi normal[9] TGN-PM varies[18]

[1] Stanley et al., 1997; [2] Rabouille et al., 1999; [3] This study; [4] Lucocq and Warren, 1987; [5] Shima et al., 1997, [6] Lippincott-Schwartz et al., 1989; [7] Lee and Linstedt, 2000; [8] Thyberg and Moskalewski, 1985; [9] Valderamma et al., 1998; [10] Paccaud et al., 1996; [11] Hammond and Glick, 2000; [12] Prescott et al., 2001; [13] Ward et al., 2001; [14] Featherstone et al., 1985; [15] Farmaki et al., 1999; [16] Misumi et al., 1986; [17] Cole et al., 1996; [18] DePina and Langford, 1999

Chapter Four

Effect of dGM130 and dGRASP depletion in the organisation of the exocytic pathway in Drosophila S2 Cells

4.1 Drosophila Golgi Matrix protein homologues

The presence of a Golgi matrix that orchestrates the organisation of the Golgi apparatus has been a long-standing debate in mammalian cells (see introduction). GM130 is considered to be a major component of this matrix (Nakamura et al., 1995), together with GRASP65, which was shown to act as its receptor on the Golgi membranes (Barr et al., 1998). Recently, several experimental data have suggested that these Golgi matrix proteins do not form a stable scaffold, but they cycle between the ER membranes and the Golgi apparatus (see section 1.4). Considering that the Golgi stacks observed in *Drosophila* cells exhibit common morphological characteristics to the mammalian cells, the existence of a similar Golgi matrix was investigated by depleting S2 cells from the *Drosophila* putative homologues of these two proteins by RNA interference (RNAi).

dGM130 is the *Drosophila* putative homologue of the mammalian GM130, which has been shown to interact with p115 (Nakamura et al., 1997). At the amino acid level, it exhibits only 23% homology and 40% similarity to its rat counterpart (EMBOSS-Align program), and it is 191 amino acids shorter. Despite this low sequence homology, dGM130 shows similar overall coiled-coil structure and content in basic amino acids, like lysine, glutamine and asparagine (Kondylis et al., 2001). Furthermore, the homology between the 73 N-terminal amino acids of rat GM130 and the equivalent domain of dGM130 is higher, when compared to the overall homology between the two proteins, especially in the first 25 amino acids (Figure 4.1) This N-terminal domain has been shown to contain the binding domain for p115 (Nakamura et al., 1997). In addition, the MLO7 antibody, which was used in the present study and was raised against this 73 amino acid peptide of GM130,

recognises a specific band corresponding to dGM130 (see section 4.3), showing that the molecule is highly conserved at least in its N-terminal part.

Mammalian GM130 is also known to interact with the PDZ domain of GRASP65, and the important amino acids for this interaction were mapped to the sequence xxNDxxxIMVI in its C-terminus (Barr et al., 1998). However, a similar motif was not identified in the C-terminal part of dGM130.

```
rGM130     1 MSEETRQS---KLAAAKKKLREYQQK--NSPGVPAGAKKKKKIKNGHSPERTSASD- 51
dGM130     1 MPDDTQDAKAQKLAAARKKLKEYQQRASNNNGQPGAEEPVAATTQSHSSTVSISSNL 57

rGM130    52 ---CQSAENV---PTDHTAPAPPS---TAAA 73
dGM130    58 SERSDSEINVNGGGAGGTQPPEQSALPTAAS 88
```

Figure 4.1: Alignment of rat and Drosophila GM130 N-terminal part (p115 binding site) with EMBOSS-Align program. The first 73 amino acids of rat GM130 were aligned with the homologous domain of dGM130 (first 88 amino acids). Note that there is 33% identity and 48% similarity between the N-terminal parts of the two proteins. The identity and similarity increases to 50% and 77% respectively, when the aligned part is narrowed down to the first 25 amino acids, figures that are much higher than the overall similarity between the two proteins. Conserved amino acids are black shaded, while equivalent amino acids are shaded in grey.

Drosophila, like all eukaryotes except mammals, has only one homologue of GRASP protein family (dGRASP, CG7809). This is in contrast to GRASP65 and GRASP55 that exist in mammalian cells. dGRASP consists of 460 amino acids and is highly homologous to both mammalian GRASPs especially in the first 203 amino acids, where it exhibits 89% and 79% similarity to GRASP55 and GRASP65, respectively (Figure 4.2A). The second half of the GRASP homologues is very diverse, even between GRASP65 and GRASP55. Functionally important sites of GRASP proteins conserved in dGRASP are the glycine residue at position 2 (myristoylation site), the cysteine at position 191 (possibly responsible for GRASP sensitivity to sulphydryl modifying agents, like NEM; Barr et al., 1997) and the PDZ-like domain (Barr et al., 1998) (Figure 4.2B). The PDZ-like domain of GRASP65

has been shown to contain the GM130 binding site (Barr et al., 1998). Despite that GRASP55 also contains the same PDZ-like domain, it does not seem to interact with GM130, *in vivo* (Shorter et al., 1999). In dGRASP, this PDZ-like domain is conserved, as well (Figure 4.2B). This, together with its similar level of homology to both GRASP65 and GRASP55, leaves open the possibility for dGRASP to represent a homologue of only one of the 2 mammalian GRASPs, or to carry out the functions of both.

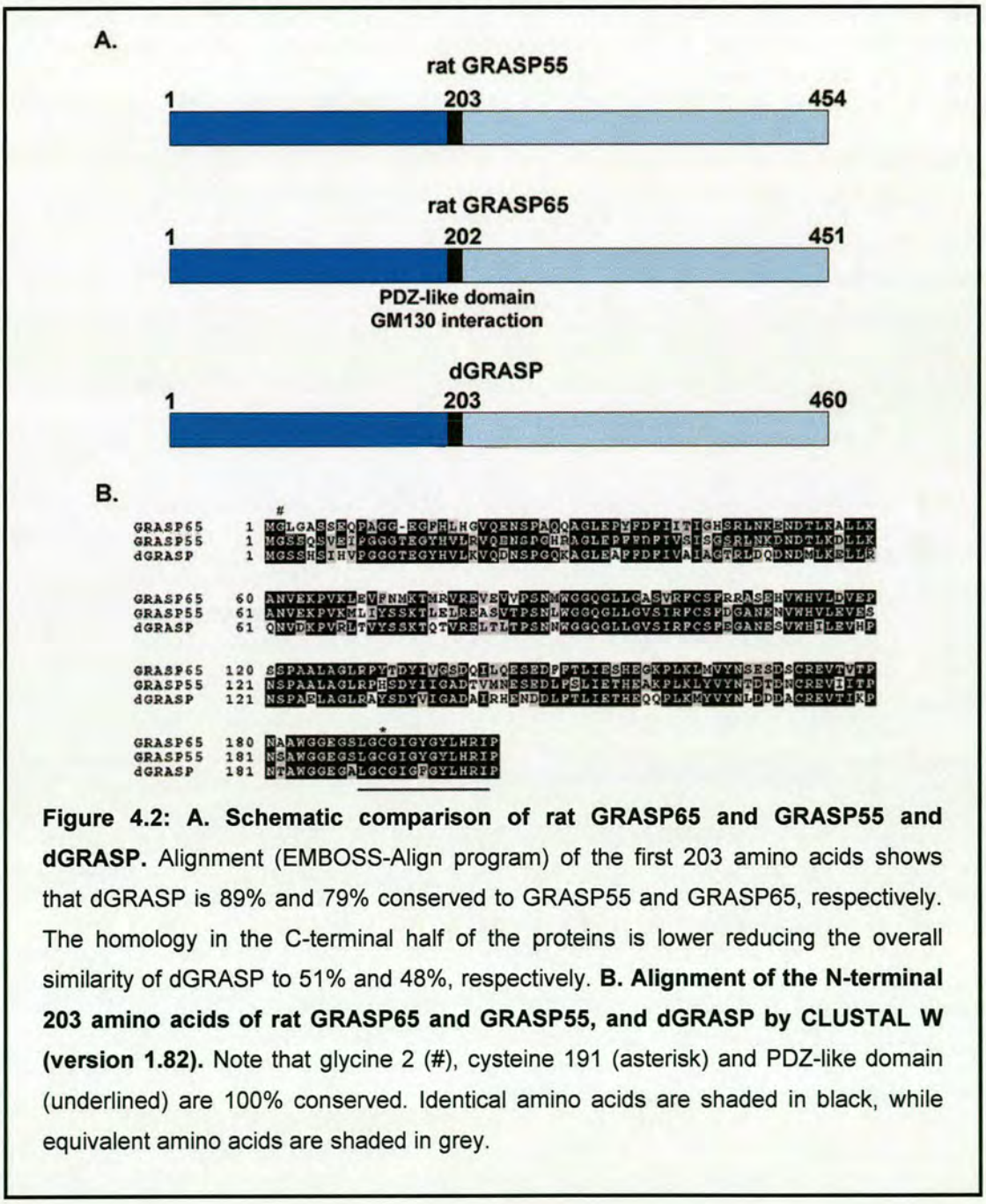

Figure 4.2: A. Schematic comparison of rat GRASP65 and GRASP55 and dGRASP. Alignment (EMBOSS-Align program) of the first 203 amino acids shows that dGRASP is 89% and 79% conserved to GRASP55 and GRASP65, respectively. The homology in the C-terminal half of the proteins is lower reducing the overall similarity of dGRASP to 51% and 48%, respectively. **B. Alignment of the N-terminal 203 amino acids of rat GRASP65 and GRASP55, and dGRASP by CLUSTAL W (version 1.82).** Note that glycine 2 (#), cysteine 191 (asterisk) and PDZ-like domain (underlined) are 100% conserved. Identical amino acids are shaded in black, while equivalent amino acids are shaded in grey.

4.2 Localisation of dGM130 and dGRASP

In order to confirm that dGM130 and dGRASP are true homologues of the respective mammalian Golgi proteins, the immuno-localisation was performed. dGM130 was localised using MLO7 antibody that has been raised against the first 73 amino acids of rat GM130 (Tables 2.5 and 2.6). Both in S2 cells and in 3rd instar larval salivary glands the distribution of the gold labelling was similar (Figure 4.3), and the relative distribution was calculated using both samples. From the membrane-associated gold particles, 41.5% were confined in the Golgi stacks and the closely associated vesicles and tubules, 31.0% in ER cisternae, and 27.5% in pleiomorphic structures that were confirmed to be tER sites by double labelling with dSec23p antibody (Figure 4.3C-D). It is worth mentioning that the gold particles corresponding to dGM130, which were distributed in the Golgi apparatus, were mostly associated with the vesicles and tubules surrounding the Golgi stack and rarely with the cisternae themselves (arrowheads in figure 4.3). Moreover, they did not seem to localise specifically at the cis-side of the Golgi stack, as the mammalian GM130 was shown to do (Nakamura et al., 1995).

The localisation of dGRASP on S2 cell and salivary gland cryosections was determined using an antibody recognising mammalian GRASP65 (Tables 2.5 and 2.6). In S2 cells, the background labelling in compartments such as mitochondria, endosomes/lysosomes or the nucleus was high, compared to the specific labelling (Figure 4.4A). This, combined with the overall low labelling, rendered the estimation of the relative distribution of gold particles difficult. In salivary glands (Figure 4.4B-C), although background labelling was still present, the specific labelling on the early exocytic compartments was enhanced, facilitating the quantification. In addition, salivary gland cells are specialised secretory cells. As a

consequence, the compartments of the exocytic pathway are more developed compared to S2 cells and therefore, proteins that are involved in their structure and function are also highly expressed. In these cells, 22.9±3.0% of the total gold particles were found in the cytoplasm and the rest was membrane-associated. From the membrane-associated gold, 33.9±2.5% decorated the Golgi stacks and the surrounding vesicles and tubules, 26.1±1.7% the ER cisternae and 40±1.3% the tER pleiomorphic membranes (Figure 4.4B-C). To account for the different membrane surface of these three compartments, the linear density was estimated and found to be 0.84 gold particles/μm on the Golgi membranes, 0.53 on tER membranes and 0.12 on ER cisternae. It should be underlined that from the Golgi-associated labelling, 88.2% of the gold particles were localised in the CGN and the cis-most Golgi cisternae. The cis side of the Golgi stack was determined by its proximity to the dSec23p-positive membranes (arrow in figure 4.4B). Moreover, unlike dGM130, dGRASP is found between the cisternae in addition to the Golgi-associated vesicles and tubules (arrowheads in figure 4.4). According to these data, dGRASP distribution seems to resemble more that of mammalian GRASP65.

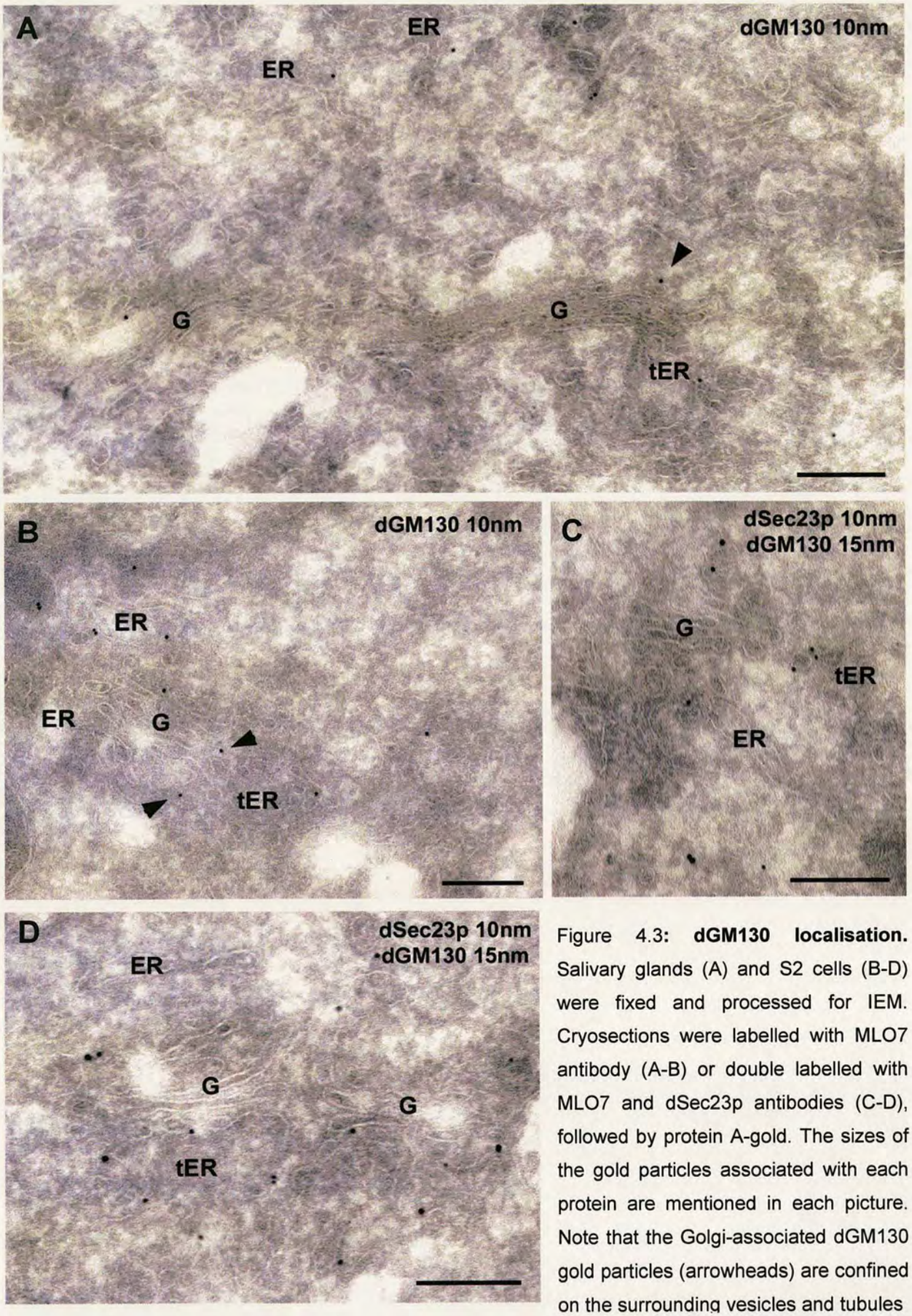

Figure 4.3: **dGM130 localisation.** Salivary glands (A) and S2 cells (B-D) were fixed and processed for IEM. Cryosections were labelled with MLO7 antibody (A-B) or double labelled with MLO7 and dSec23p antibodies (C-D), followed by protein A-gold. The sizes of the gold particles associated with each protein are mentioned in each picture. Note that the Golgi-associated dGM130 gold particles (arrowheads) are confined on the surrounding vesicles and tubules than the Golgi stack itself. G, Golgi stacks; ER, endoplasmic reticulum. Bars, 200nm.

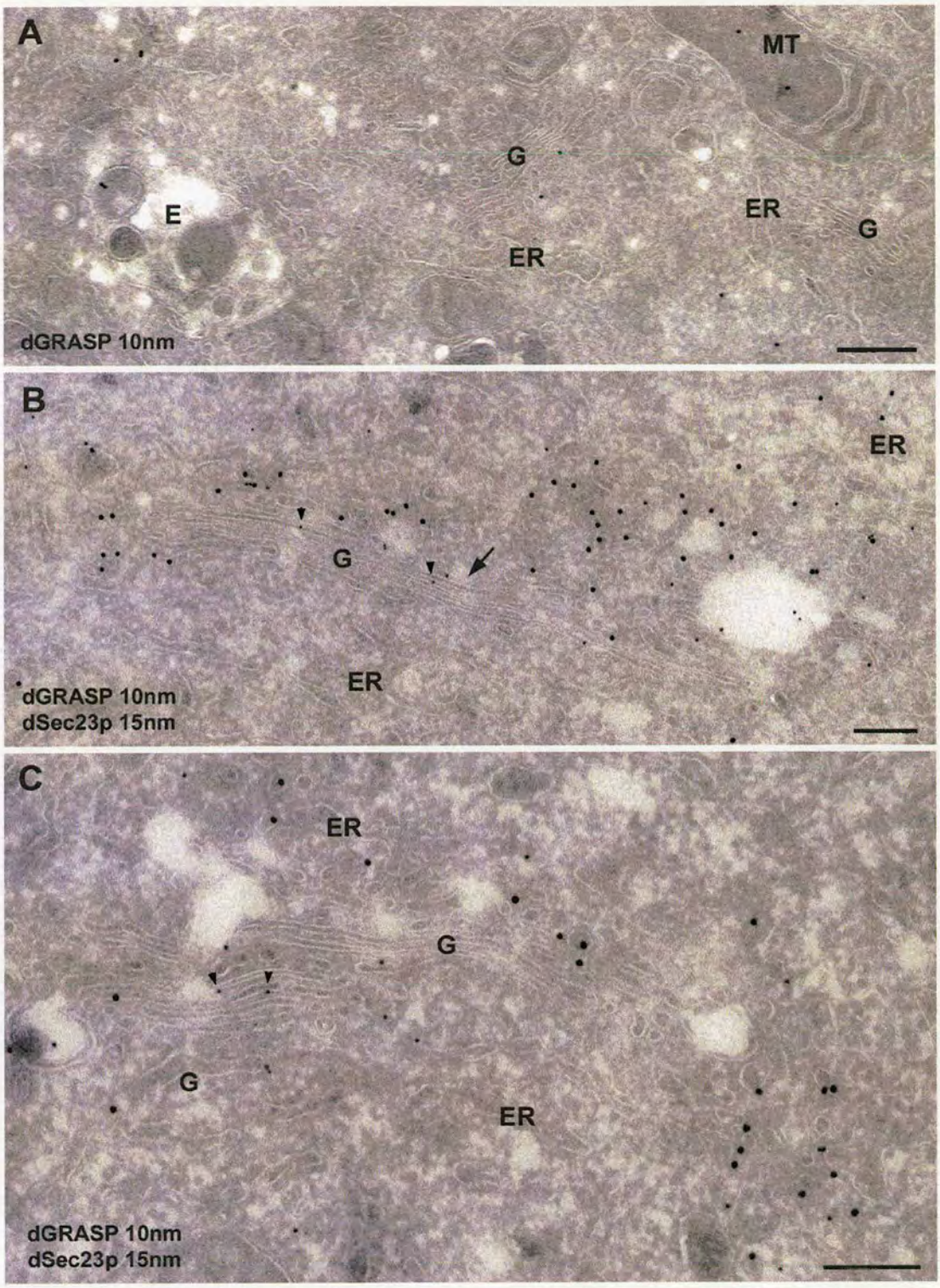

Figure 4.4: dGRASP localisation. S2 cells (A) and salivary glands (B-C) were fixed and processed for IEM. Cryosections were labelled with an anti-GRASP65 antibody (A) or double labelled with GRASP65 and dSec23p antibodies (B-C), followed by protein A-gold. The sizes of the gold particles associated with each protein are mentioned in each picture. Arrow in B points to CGN, where most of the Golgi-assossiated dGRASP is localised. Note that gold particles are found in the intercisternal space (arrowheads). G, Golgi stacks; ER, endoplasmic reticulum, MT, mitochondria; E, endosomes. Bars, 200nm.

4.3 Effect of dGM130 depletion on Golgi architecture

S2 cells were depleted from dGM130 by incubating them for up to 120 hours with dsRNA corresponding to the second exon of the dGM130 gene (CG11061). The cell growth was monitored and was not affected significantly by the dsRNA addition compared to the mock-treated cells (-dsRNA; Figure 4.5A). The protein expression in mock- and RNAi-treated cell samples was analysed by Western blotting using MLO7 antibody. dGM130 protein level was found substantially reduced, already after 24h of ds dGM130 addition, and it was below detection from 48h and up to 120h (Figure 4.5B).

Control and dGM130-depleted cells were processed for conventional EM, but the depletion of dGM130 did not seem to lead to any apparent disruption of the Golgi stack morphology (Figure 4.6). To describe this effect quantitatively, the percentage of cell sections exhibiting at least one Golgi stack per cell profile was scored in mock-treated and dGM130-depleted cells (for EM quantification, see 2.4.4.2), but no significant difference was found between the two samples (Figure 4.7A). Similarly, the number of cisternae per stack (3.5±1.6) and the mean diameter of the stacked cisternae (0.347±0.078μm) were comparable to the figures obtained for mock-treated cells (3.7±0.8 cisternae per stack and cross sectional diameter of 0.368±0.047μm). Furthermore, stereological analysis performed on random micrographs confirmed the morphological findings. The relative distribution of Golgi membranes into total cisternae (single and stacked), vesicular profiles and tubules showed no significant variation between dGM130-depleted and mock-treated cells (Figure 4.7B).

Although the lack of an effect on the Golgi morphology by dGM130 depletion was initially surprising, this result has been supported by recent

data deriving from the study of its mammalian homologue (see discussion). Moreover, this experiment served as a good control for the specificity of the effects observed in the other RNAi depletions that were performed (see this and next chapter).

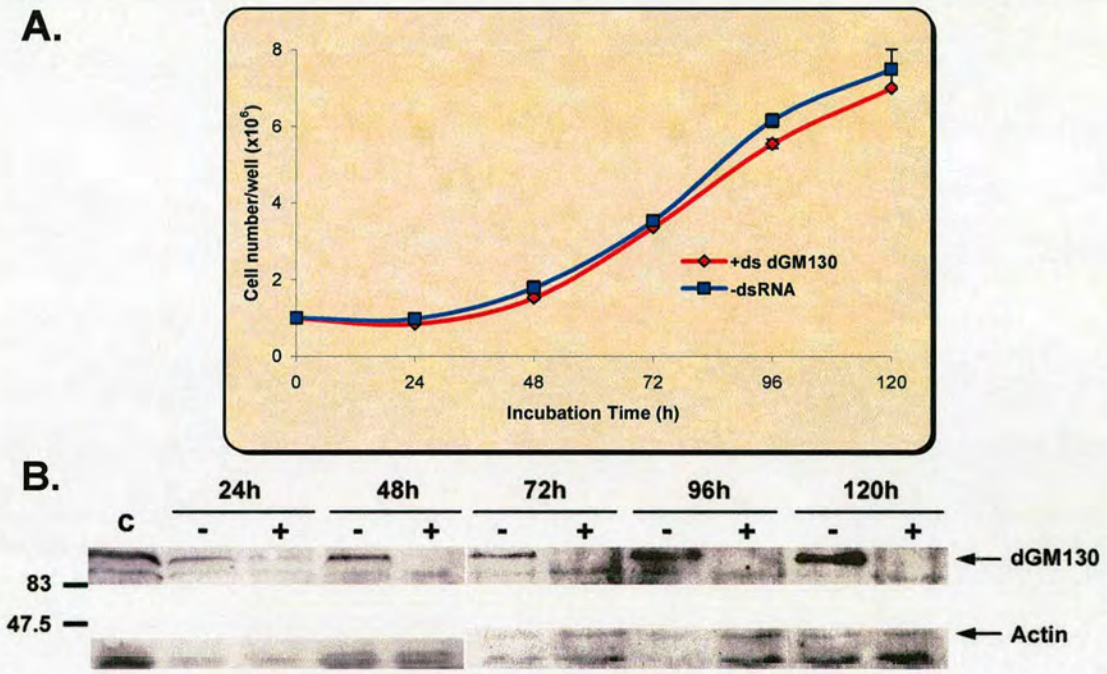

Figure 4.5: A. Growth rate of S2 cells in the presence or absence of dGM130 dsRNA. B. Depletion of dGM130 protein. Total extract from S2 cells incubated with (+) or without (-) ds dGM130 for increasing length of time was analysed by Western blotting using MLO7 antibody. C corresponds to time 0. In lanes 24h-72h, 1.5 million cells were used to prepare the samples, while 2.5-3 million cells were used for the extracts loaded in lanes C, 96h and 120h. MLO7 antibody recognises one major band at 130kD, which is specifically depleted in RNAi-treated cells, and a faint band at 120kD that was not taken into acount. A non-specific band at 35kD was used as a loading control. Additionally, in 72-120h samples, blotting with an anti-actin polyclonal antibody (gift from Heck lab, Edinburgh) was used to detect actin (~42kD) as a loading control.

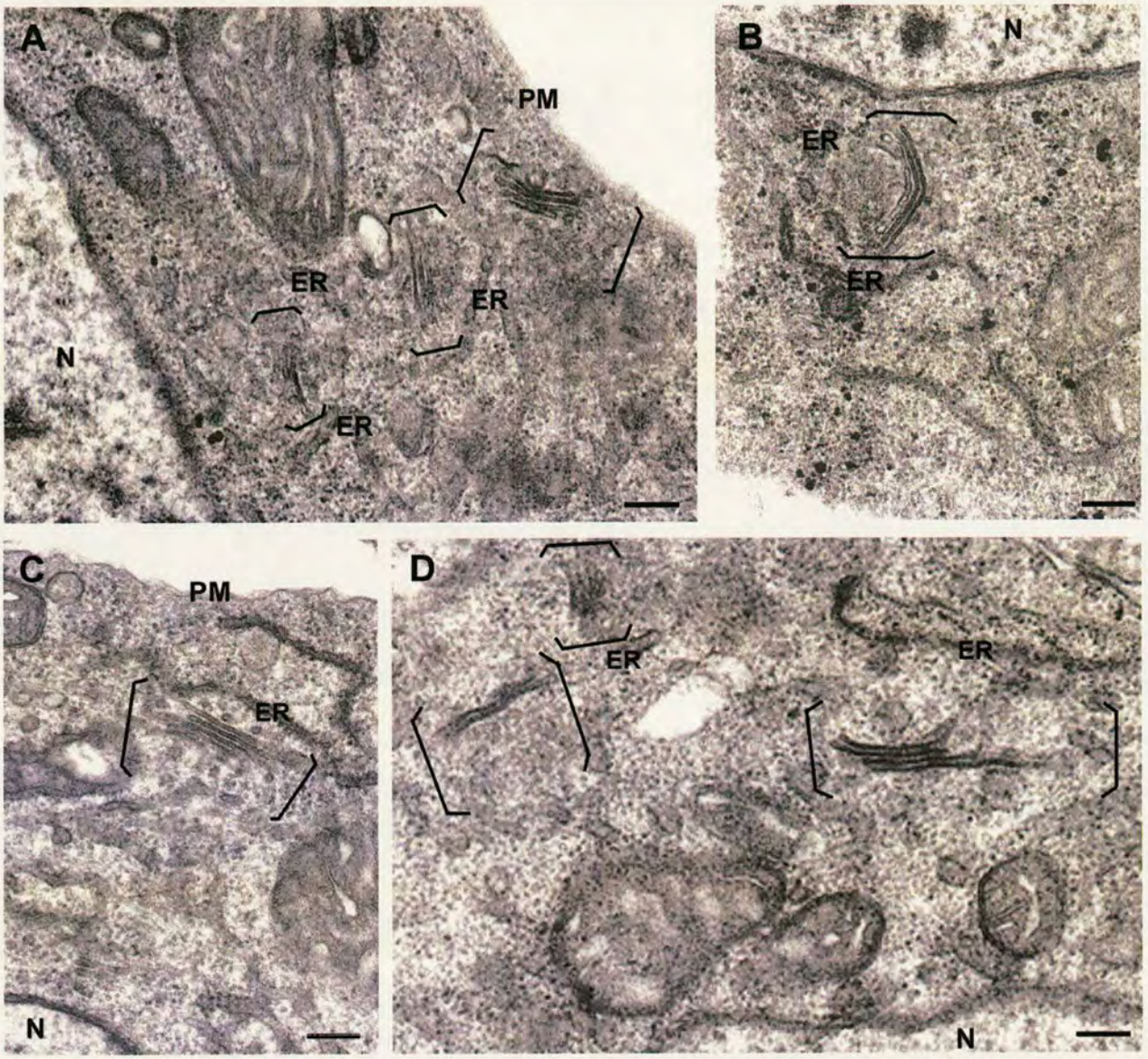

Figure 4.6: Effect of dGM130 depletion on Golgi stack morphology. S2 cells were cultured in the absence (A and C) or presence of ds dGM130 (B and D) for 72h (A and B) or 96h (C and D). Golgi areas are marked between brackets. Note dGM130 depleted cells exhibit normal Golgi stacks. N, nucleus; ER, endoplasmic reticulum; PM, plasma membrane. Bars, 200nm.

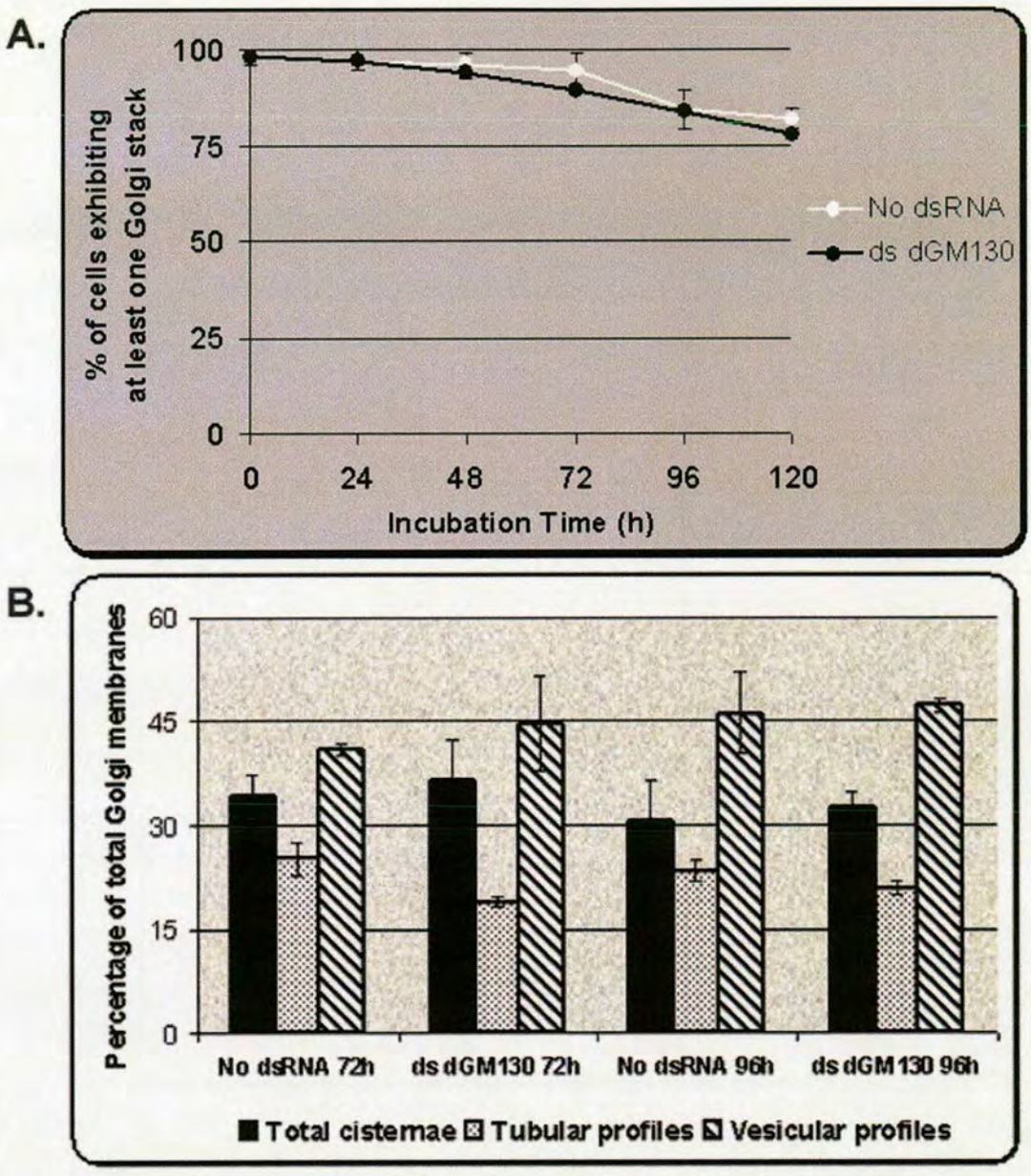

Figure 4.7: Quantitative analysis of the effect on Golgi morphology after dGM130 depletion. **A.**The percentage of S2 cell profiles exhibiting at least one Golgi stack per cell section was scored on ultrathin epon sections from mock-treated (white circles) and dGM130-depleted cells (black circles). The results are presented as a percentage of the total number of cells examined for each condition (~300). **B.** Random EM pictures of mock-treated cells and dGM130-depleted cells at 72h and 96h were used to estimate the percentage of Golgi membrane in total cisternae (black bars), tubular (dotted bars) and vesicular profiles (lined bars). The error bars represent the SD.

4.4 Effect of dGRASP depletion on Golgi architecture

Similar RNAi experiments were performed for dGRASP, the sole *Drosophila* homologue of mammalian GRASP65 and GRASP55, using dsRNA corresponding to the second exon of dGRASP gene (CG7809).

Cell growth was monitored and was found identical to that of mock-treated cells (Figure 4.8A). dGRASP depletion was assessed by Western blotting using an anti-GRASP65 antibody (Table 2.5). Although more than one bands appeared on the blot, only that migrating approximately at 62kD, which is the predicted molecular weight for dGRASP, was specifically depleted from the RNAi-treated cells from 48h and up to 120h (Figure 4.8B).

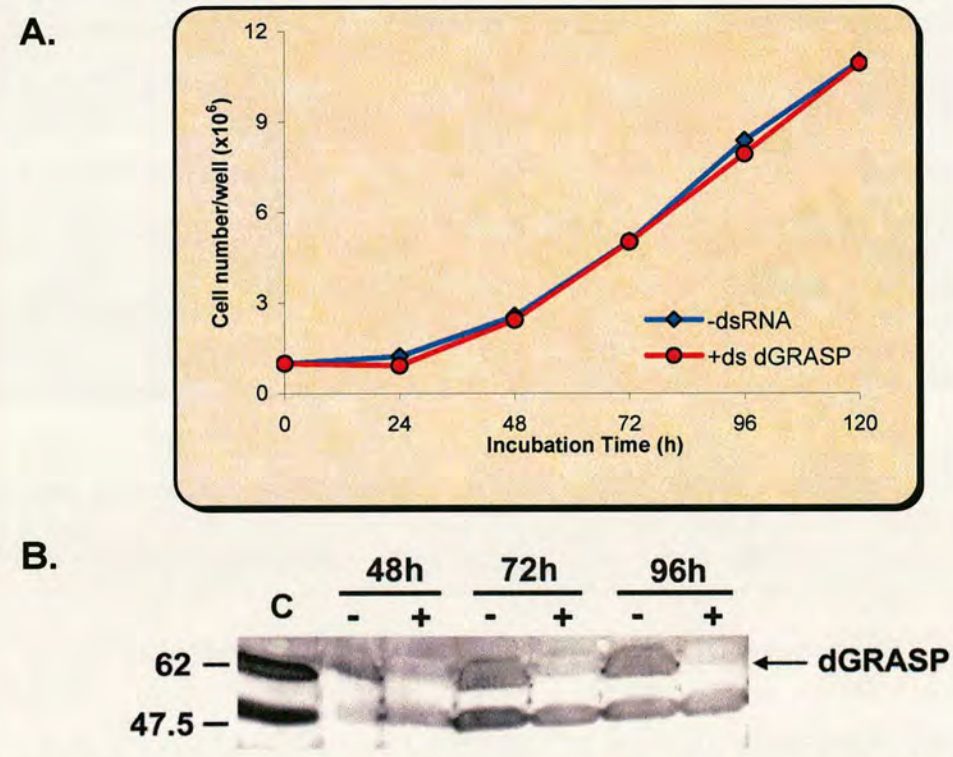

Figure 4.8: A. Growth rate of S2 cells in the presence or absence of dGRASP dsRNA. B. Depletion of dGRASP protein. Total extract from S2 cells incubated with (+) or without (-) ds dGRASP for 48-96h was analysed by Western blotting using the GRASP65 antibody. C corresponds to time 0. The extract loaded on 48h sample corresponds to 1.5 million cells, while 2.5-3 million cells were used for the extracts loaded in lanes C, 72h and 96h. Among the bands appearing on the blot, the one running at 62kD (predicted molecular weight for dGRASP), was the only one to be specifically depleted in RNAi-treated cells.

When examined by EM, the majority of dGRASP-depleted cells still exhibited Golgi stacks in their cytoplasm, occasionally of smaller diameter compared to mock-treated cells (Figure 4.9A, arrow). However, about 20% of the cell profiles at 96h and 120h were observed to contain vesiculated Golgi (Figure 4.9B), and more importantly, a small, but significant percentage of cells exhibited single cisternae (Figure 4.9C, arrowhead) embedded in clusters of vesicles and tubules, a feature very rarely observed in control cells or upon RNAi depletion of other Golgi matrix proteins.

The quantification of the percentage of cells with at least one Golgi stack revealed that dGRASP depletion caused a statistically significant, but non-penetrant Golgi stack breakdown, as Golgi stacks could still be identified in 65.4±4.3% of the cell sections after 120 hours of RNAi treatment (Figure 4.10A). More detailed stereological analysis of random micrographs showed that the percentage of Golgi membranes in total cisternae decreased by 23.3% at 96h, and this reduction was counterbalanced by a 25.6% increase in tubular profiles, leaving unaffected the vesicular profiles (Figure 4.10B). Strikingly, about 20% of the cisternal membranes in dGRASP-depleted cells represented single cisternae. This represents a 6- and 3-fold increase in the percentage of Golgi membranes in single cisternae, when compared to mock-treated and dGM130- or dp115-depleted cells (see chapter 5), respectively (Figure 4.13C). The specificity of this feature for the dGRASP-depleted cells suggested a role of this protein in the process of cisternal stacking *in vivo*.

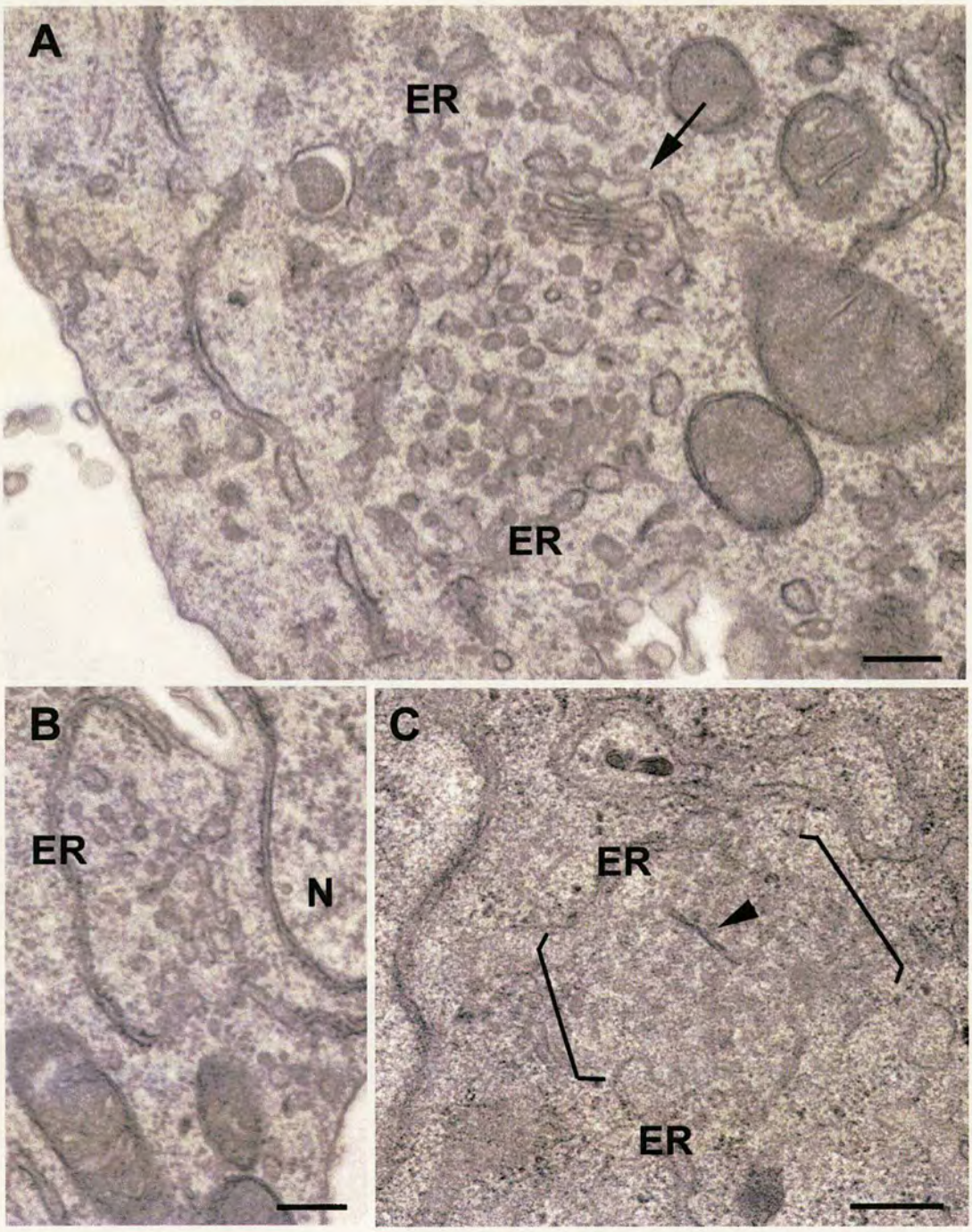

Figure 4.9: Effect of dGRASP depletion on Golgi stack architecture. S2 cells cultured in the presence of ds dGRASP for 96h were processed for conventional EM. Golgi area in C is marked between brackets. Although the majority of cells have apparently normal Golgi stacks, a significant number of dGRASP depleted cells exhibit short Golgi stacks (arrow in A), vesiculated Golgi (B) or interestingly, single cisternae (arrowhead in C). N, nucleus; ER, endoplasmic reticulum. Bars, 200nm.

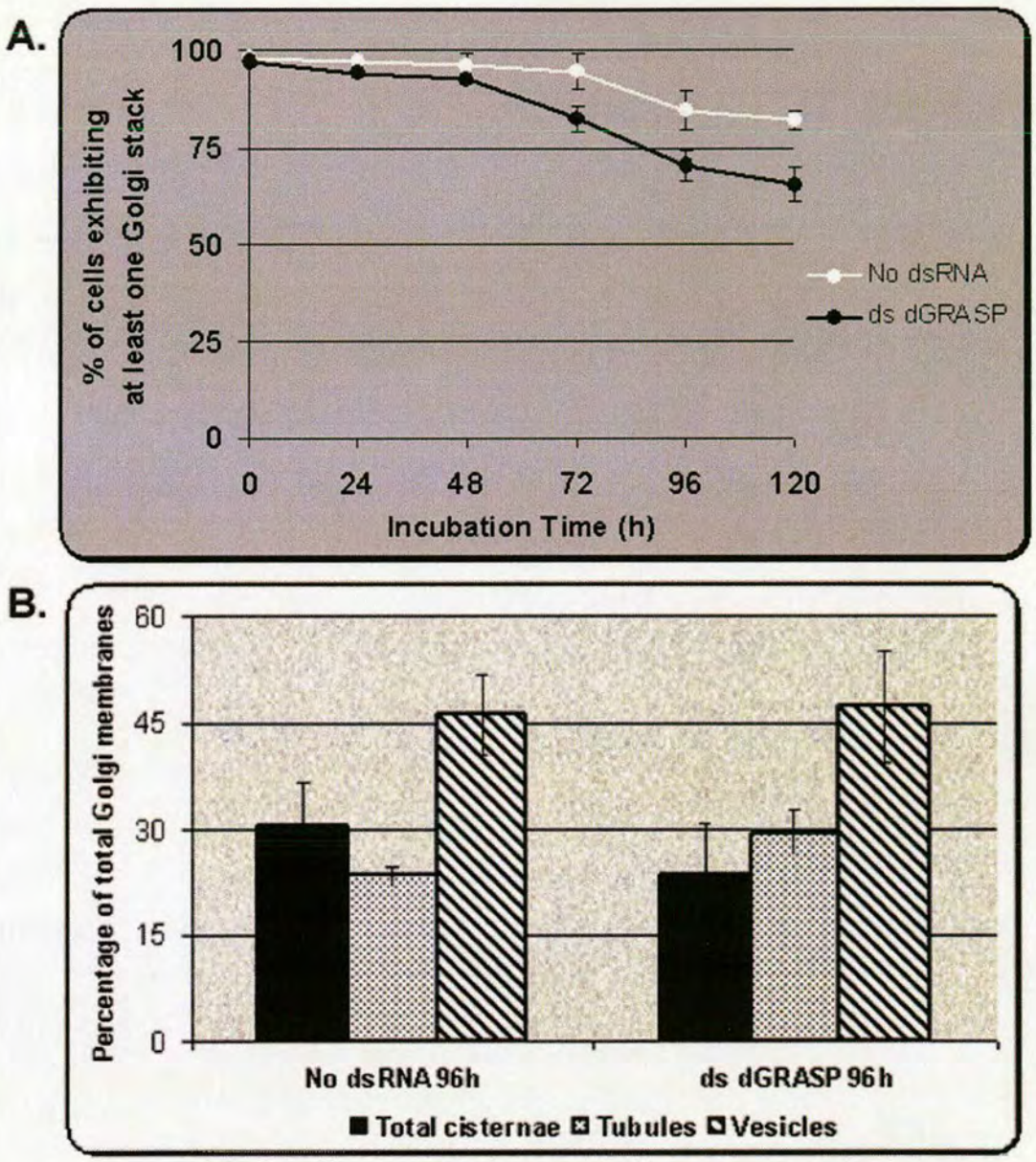

Figure 4.10: Quantitative analysis of dGRASP depletion on Golgi morphology. **A.**The percentage of S2 cell profiles exhibiting at least one Golgi stack in their cytoplasm was scored on ultrathin epon sections from mock-treated (white circles) and dGRASP-depleted cells (black circles). **B.** Random EM pictures of mock-treated and dGRASP-depleted cells at 96h were used to estimate the percentage of Golgi membrane in total cisternae (black bars), tubular (dotted bars) and vesicular profiles (lined bars). The error bars represent the SD.

4.5 dGRASP-dGM130 double depletion

Despite that their mammalian homologues have been suggested to play an important role for the Golgi stacked structure (Barr et al., 1997; Shorter and Warren, 1999), individual depletion of dGRASP or dGM130 from S2 cells did not lead to a penetrant Golgi stack breakdown. Thus, the double depletion of dGRASP in conjunction with its potential interactor dGM130 was carried out in an attempt to enhance this mild phenotype.

Both dGRASP and dGM130 were confirmed to be depleted at least 72h after dsRNA addition by Western blotting (Figure 4.11). Furthermore, it was confirmed that each single depletion does not affect the expression of the other protein (Figure 4.11, last two lanes).

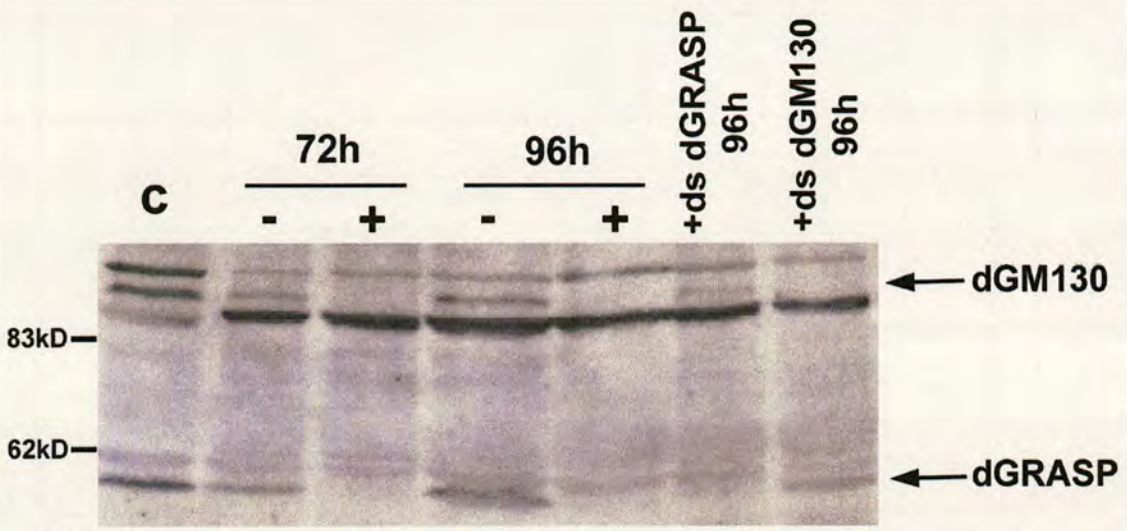

Figure 4.11: Double depletion of dGRASP and dGM130. Total extract from S2 cells were incubated with (+) or without (-) dsRNAs corresponding to dGM130 and dGRASP for 72 and 96h was analysed by Western blotting using MLO7 and anti-GRASP65 antibodies. Single depletion of either protein for 96h was also performed (last two lanes). C corresponds to time 0 and total extract from 2.5 million cells. All the other lanes were loaded with extracts from 2 million cells.

EM analysis of the double depleted samples unravelled a more penetrant Golgi stack breakdown compared to the single depletions (Figure

4.12 and 4.13A). After 72 hours of dGRASP/dGM130 RNAi, 34.5% of the cells exhibited vesiculated Golgi (vs. 13.3% for dGRASP single depletion). This figure increased to 42.5% and 45.3% at 96 and 120h time points, respectively. The single cisterna phenotype, observed in dGRASP depletion, was also reproduced (Figure 4.12B). After 72h, 13.4% of the double depleted cells exhibited single cisternae. This percentage rose to 18.9% and 20.4% after 96 and 120h dsRNA incubation, respectively. Interestingly, from the remaining cells exhibiting Golgi stacks, it was often observed, that these stacks were rather short and contained only 2 cisternae (Figure 4.12C). For example, at 120 hours after the dsRNA addition, 58% of the Golgi stack containing cells exhibited 2 cisterna-stacks with a mean diameter 37% shorter than in control cells.

The stereological analysis of dGRASP/dGM130 depleted cells revealed that the percentage of Golgi membranes in total cisternae decreased by 50% and 30%, when compared to dGM130- or dGRASP-depleted cells, respectively (Figure 4.13B). The percentage of Golgi membranes in vesicles remained essentially unchanged, while tubular profiles rose by 95% or 38% (Figure 4.13B).

Because of the described function for mammalian GRASP proteins in cisternal stacking, the percentage of Golgi membranes in total cisternal membranes was further analysed by being divided into single and stacked cisternae for all the performed RNAi experiments (Figure 4.13C). This confirmed that in dGRASP- and dGRASP/dGM130 depleted cells, the percentage of Golgi membrane found as single cisternae exhibited at least a 3- and 9-fold increase, respectively, when compared to dGM130-depletion. Similar figures were obtained when the percentage of membranes in single cisternae in dGRASP- and dGRASP/dGM130 depleted cells was compared

with dp115- or dp115/dGM130 depletions, despite that these depletions led to an extensive breakdown of the Golgi stacks (see chapter 5). Moreover, in dGRASP-dGM130 double depleted cells, single cisternal membranes accounted for 60% of the total cisternal membranes, resulting in the seemingly high percentage of total Golgi cisternae. Overall, these results are suggestive of a specific dGRASP role in cisternal stacking *in vivo*.

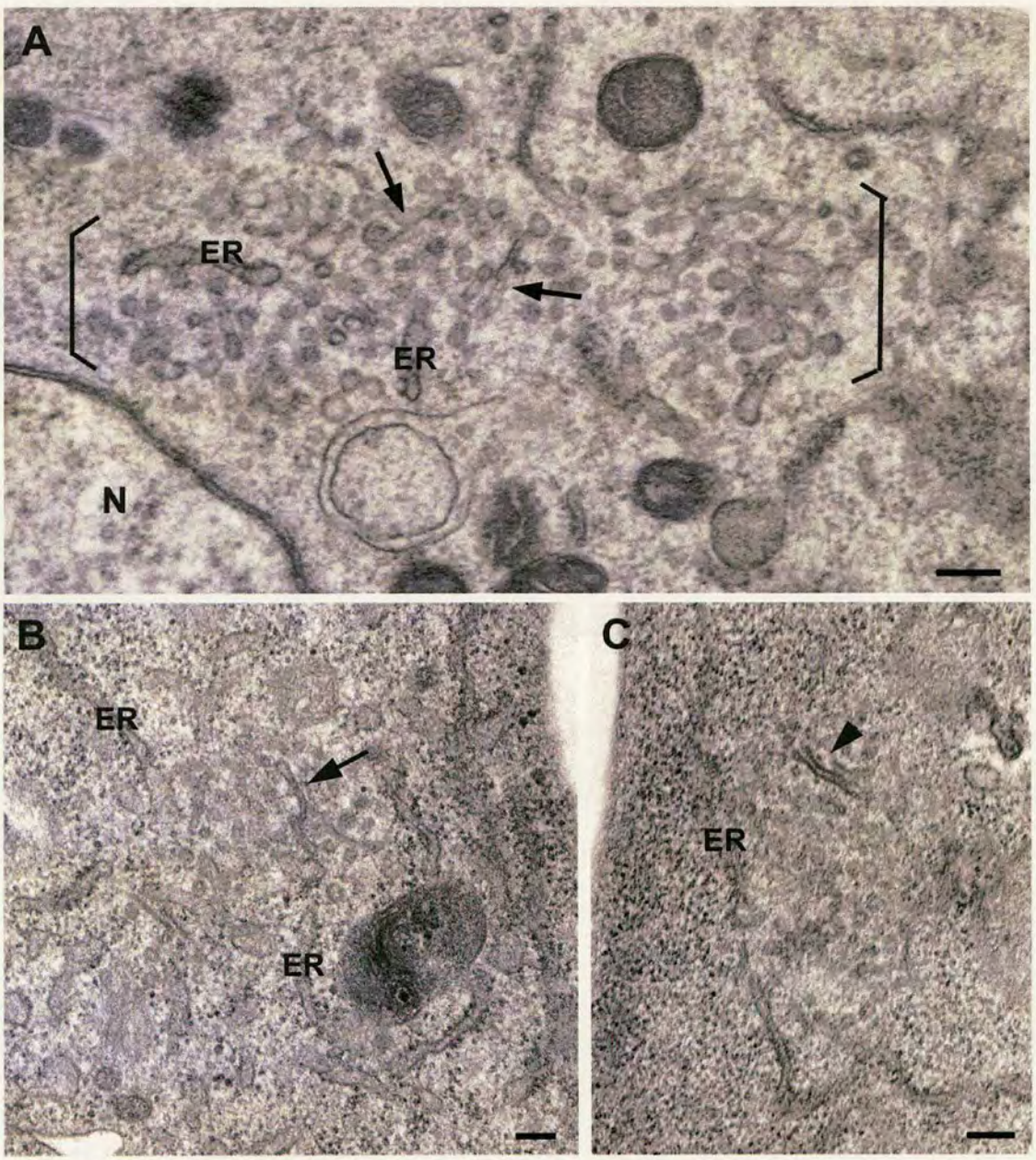

Figure 4.12: Significant Golgi stack breakdown by dGRASP/dGM130 double depletion. S2 cells were cultured in the presence of ds dGRASP and dGM130 for 96h (A and B) or 120h (C). Vesiculated Golgi areas (between brackets in A), single cisternae (arrows in A and B) and short 2 cisterna stacks (arrowhead in C) were common features of the double depletion. N, nucleus; ER, endoplasmic reticulum. Bars, 200nm.

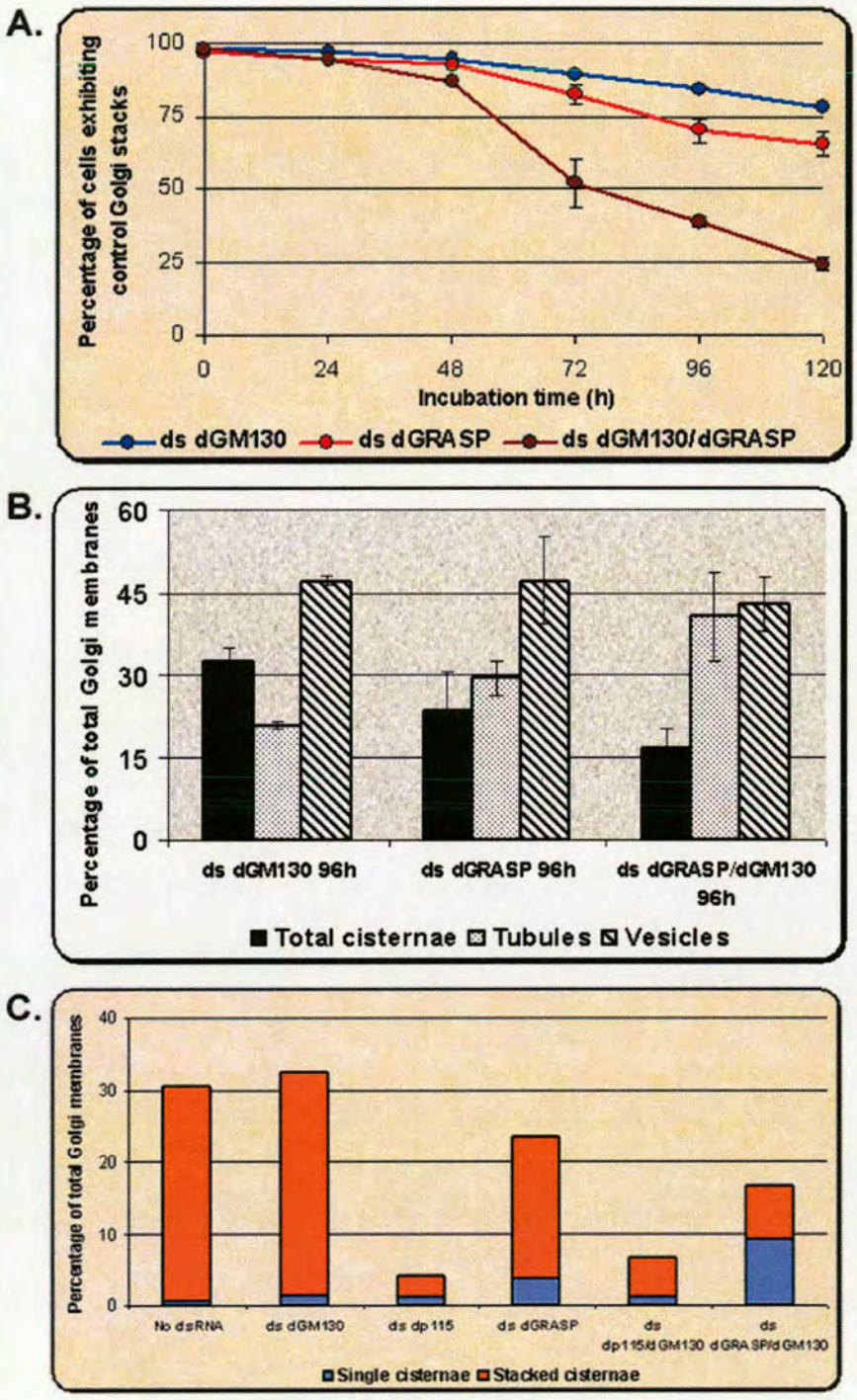

Figure 4.13: Quantitative analysis of dGRASP/dGM130 depletion on Golgi morphology.

A.The percentage of S2 cell profiles exhibiting at least one control Golgi stack in their cytoplasm was scored on ultrathin epon sections from dGM130- (blue), dGRASP- (red) and dGRASP/dGM130-depleted cells (brown).

B. Random EM pictures of dGM130-, dGRASP- and dGRASP/dGM130-depleted cells for 96h were used to estimate the percentage of Golgi membrane in total cisternae (black bars), tubular (dotted bars) and vesicular profiles (lined bars). The error bars represent the SD.

C. The percentage of total cisternal membranes was divided in single cisternae (purple bars) and stacked cisternae (orange bars) in mock-treated and single or double RNAi depleted cells. Note the significantly higher percentage of single cisternal membranes in dGRASP and dGRASP/dGM130 depleted cells.

4.6 Effect of dGM130 and dGRASP depletion on the tER organisation

In recent studies using BFA or reagents blocking ER exit, the mammalian putative homologues of dGM130 and dGRASP, GM130 and GRASP65, were suggested to cycle between the ER and Golgi membranes (see introduction section 1.4.2). These observations together with the immuno-localisation experiments (see paragraph 4.2) demonstrating at least a partial localisation of the two proteins on dSec23p-positive pleiomorphic membranes implied that these proteins could have a role in the tER organisation. Therefore, although dGM130 and dGRASP single depletions did not lead to a penetrant disruption of the Golgi stack architecture, their effect on the focused organisation of the tER sites was also investigated.

In order to address this question, S2 cells were depleted of dGM130 or dGRASP by adding the respective dsRNA for 96 hours, labelled for dSec23p, and the distribution of the tER marker was assessed by confocal microscopy. Nevertheless, both dGM130- and dGRASP-depleted cells mostly exhibited a dSec23p pattern indistinguishable from non-treated cells (Figure 4.14). A disruption in tER organisation could not be detected in more than 10% of the total cell number counted.

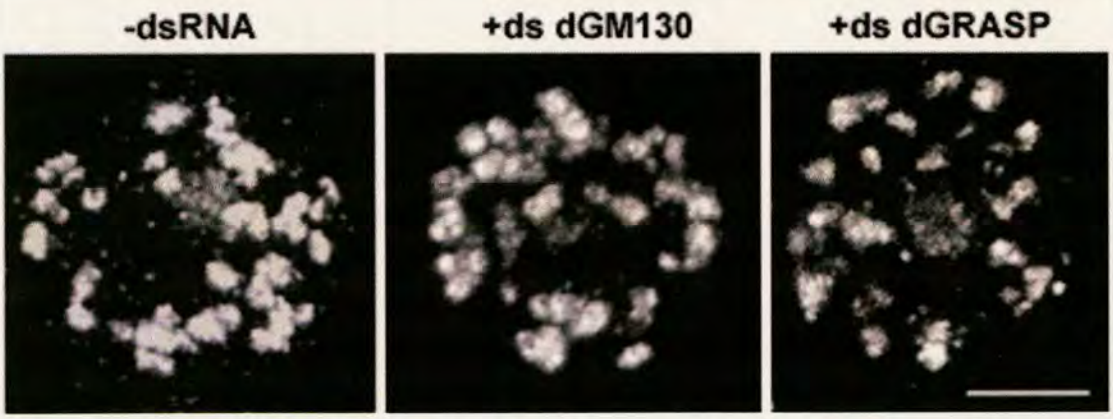

Figure 4.14: dGM130 or dGRASP depletion does not affect the organisation of the tER sites. tER organization was monitored by IF using the anti-dSec23p antibody in mock-treated (left), dGM130-depleted (middle), and dGRASP-depleted cells (right) for 96h. Bar: 5µm.

Finally, to test the hypothesis of whether tER and Golgi stack organisation are linked as it has been proposed in yeast (Rossanese et al., 1999), the integrity of the tER sites was also examined in dGM130/dGRASP double depleted S2 cells, which exhibited a quantitative Golgi stack breakdown. However, similar to single dGRASP and dGM130 depletions, 84.5±1.1% of the double depleted cells appeared normal in terms of their tER organisation, at least at the light microscopy level (Figure 4.15, top panel). A small difference from the mock-depleted cells could be that few of dSec23p-positive dots were not in proximity to a d120kd–positive structure (arrows in figure 4.15). On the other hand, d120kd staining appeared to be more diffused around the d120kd-positive spots, when compared to mock-depleted cells (compare d120kd labelling in figures 4.15 and 3.3). This could support a role of dGM130 and dGRASP in a matrix that keeps Golgi elements together. Nonetheless, d120kd-positive spots are still distinguishable and this is an example demonstrating that at the low resolution of IF, the presence of Golgi stacks, cisternae or clusters cannot be determined in *Drosophila* cells.

Thus, this result indicates that the integrity of the tER sites in S2 cells may not dictate necessarily the appearance of the Golgi apparatus, since the presence of tER sites with apparently normal organisation generated a Golgi apparatus with disrupted stacked architecture.

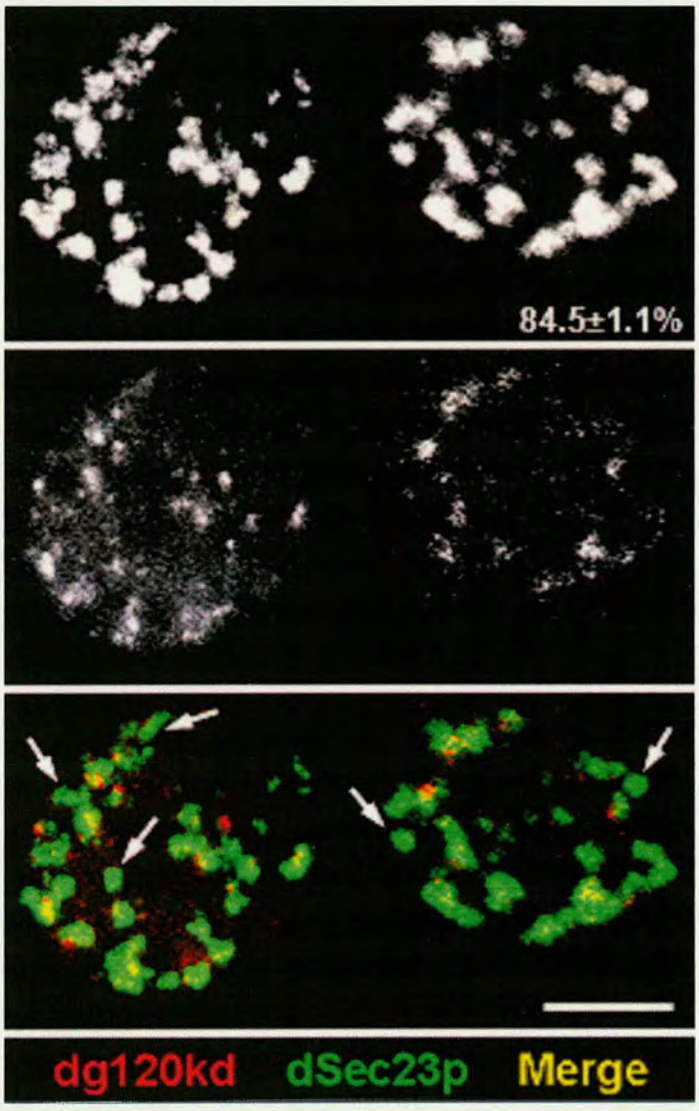

Figure 4.15: Golgi stack breakdown does not require disorganisation of the tER sites. dGM130 and dGRASP double-depleted S2 cells were processed for IF, and labelled for dSec23p (upper panel) and d120kd (middle panel). In the merged picture (lower panel), tER sites are labelled in green, Golgi membranes in red and overlapping areas in yellow. Arrows point to dSec23p-positive structures that are not located close to a Golgi membrane. Note the increased haze of d120kd labelling that could reflect the disruption in Golgi architecture seen by EM. The number in the top panel represents the percentage of the total cell population exhibiting the typical dSec23p distribution. Bar: 5µm

Chapter Five

Effect of dp115 depletion by RNAi in the organisation of the exocytic pathway in *Drosophila* S2 Cells

As it was described in the previous chapter, the single depletions of dGM130 or dGRASP did not affect the organisation of the Golgi stacks in a quantitative manner. This result was unexpected, because the mammalian homologues of these two Golgi matrix proteins have been proposed to be part of a scaffold, important for the building and maintenance of the Golgi apparatus. Therefore, the *Drosophila* homologue of p115, another long, coiled-coil golgin, was depleted by RNAi.

Mammalian and yeast p115 has been implicated in different functions in the ER exit sites, the intermediate compartment and the Golgi apparatus, and due to its multiple interactions with other proteins, it is thought as an orchestrating molecule for the organisation of the early exocytic pathway (see section 1.5). For this reason, it was anticipated that the *Drosophila* homologue of p115 would be a likely candidate to have a strong effect on the structure of the Golgi apparatus.

5.1 Drosophila p115 homologue

The *Drosophila* homologue of p115 (dp115) consists of 837 amino acids and exhibits 42% identity and 57% similarity to its rat counterpart (EMBOSS-Align program). Despite this relatively high homology, dp115 does not possess the acidic C-terminal domain that, in mammalian p115, contains the binding site for GM130 and giantin (Linstedt et al., 2000; Dirac-Svejstrup et al., 2000) (Figure 5.1A). This characteristic of dp115 molecule is obvious when its C-terminal part is aligned with the p115 homologue from 6 other species using the CLUSTAL W program (version 1.82) (Figure 5.1B). The domain of dp115 that is aligned with the acidic stretch of mammalian p115 homologues (underlined sequence in figure 5.1B) does not contain any acidic amino acids, while along the last 100 amino acids, dp115 contains only 13 scattered acidic amino acids. The acidic stretch is also shorter in *C. elegans*

and *Arabidopsis* compared to mammalian p115 (5 and 10 acidic amino acids, respectively; Figure 5.1B). In addition, serine at position 942 of human p115, which is thought to be important for p115 function (Dirac-Svejstrup et al., 2000), is not conserved in p115 homologues of non-vertebrate eukaryotes (Figure 5.1B). Although dp115 seems to lack the GM130 binding described in mammalian cells, the p115-binding site is highly conserved in the *Drosophila* homologue of GM130 (dGM130; Figure 4.1). Taking this into consideration, whether dp115 and dGM130 interact, as their mammalian homologues do,

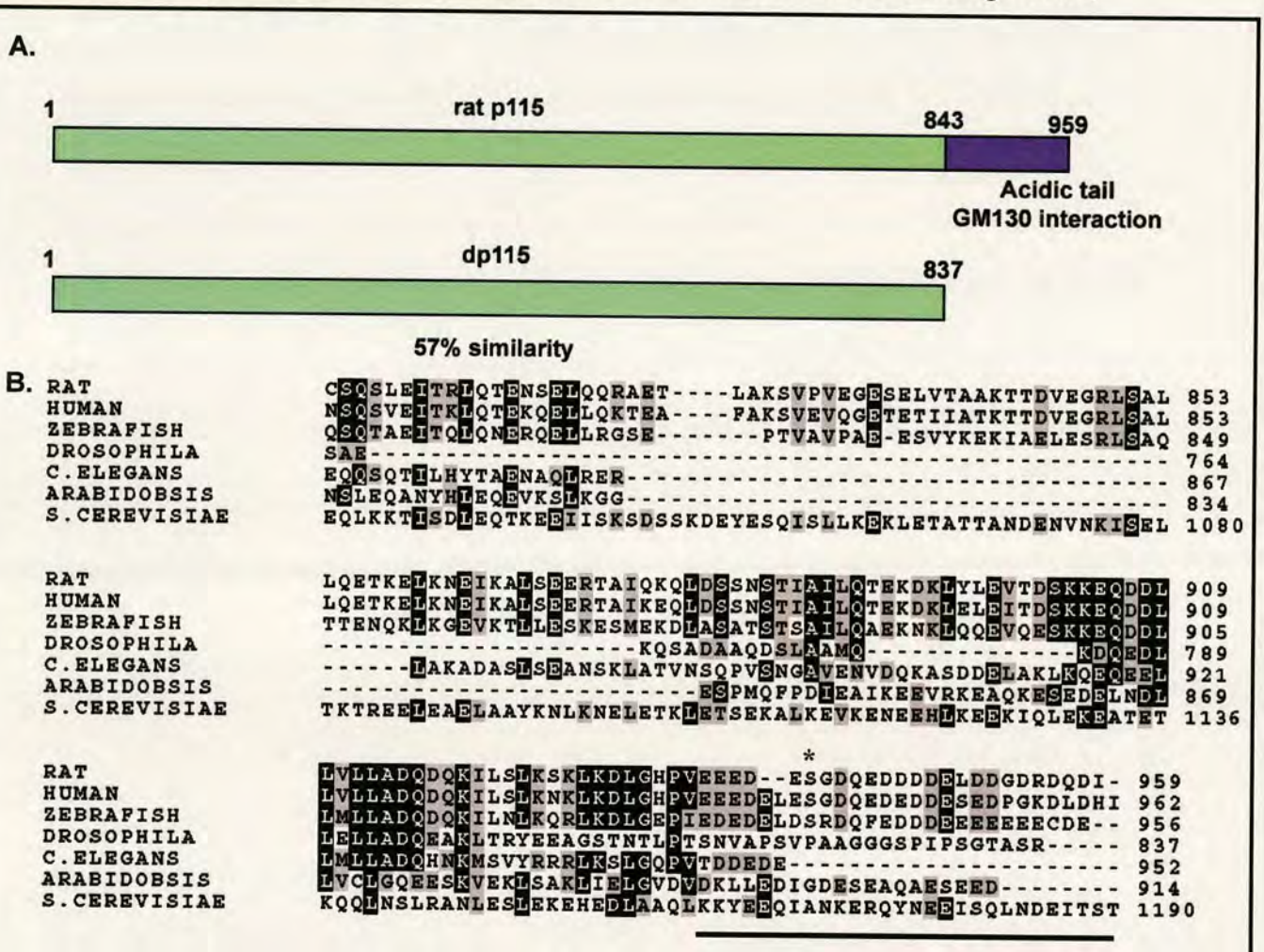

Figure 5.1: A. Schematic comparison of rat p115 and dp115. Similarity was calculated with the EMBOSS-Align program. Note that the lacking C-terminal acidic domain required for GM130 binding in mammalian cells. **B. Alignment of dp115 C-terminal part with p115 homologues from 6 other eukaryotes with sequenced genome with CLUSTAL W program (version 1.82).** Note that the C-terminal acidic stretch (underlined), which is involved in GM130 interaction and is absent from dp115, is also shorter in *C.elegans* and *Arabidopsis* p115 homologues. The functionally important serine 941 (asterisk) is conserved only in mammalian and zebrafish p115 homologues. Highly concerved and equivalent amino acids are black and grey shaded, respectively.

remains still a question. This is theoretically possible, albeit through a different domain of dp115.

On the contrary, the p115 domains that are involved in interactions of the protein with Rab1 (Allan et al., 2000), members of the SNARE family (Shorter et al., 2002) and GBF1 (Garcia-Mata and Sztul, 2003) are well conserved in dp115 amino acid sequence.

5.2 Generation and characterization of an anti-dp115 antibody

In order to localise dp115, an antibody was raised against dp115-specific peptide GCSKLAEVSRHEAYSRA (Bio-synthesis, Lewisville, TX). In Western blotting analysis, anti-dp115 serum recognised a band slightly above 83kd (predicted molecular weight for dp115), but also many additional bands (Figure 5.2, lane 1). To reduce the background, the serum was affinity purified against the dp115-specific peptide (see 2.3.6). The first batch of affinity-purified antibody (dp115/584-1) recognised besides the expected band for dp115, two additional bands one around 40kD and one at 65kD (Figure 5.2, lane 2). Both these bands were considered non-specific for several reasons. Unlike dp115-specific band, they were not consistently present in every blot. The 40kD band was probably a result of the secondary antibody, as it was present even in the absence of the primary antibody. The 65kD band could be a degradation product, despite the use of protease inhibitor cocktail in the preparation of the extracts. However, it is more likely to represent also a background band, because in each individual blot, its intensity was the same independent of the intensity of dp115-specific band or the amount of protein loaded in each lane. The second batch of purified antibody (dp115/584-2), probably due to more efficient purification, recognises only one band at 90kD (Figure 5.2, lane 3). dp115 is very strongly

expressed in third instar larvae (Figure 5.2, lane 4), while it could not be detected in extract from 80 *Drosophila* embryos (not shown). In adult male and female flies, the band corresponding to dp115 is faint but detectable. An additional band around 30kD was also observed (Figure 5.2, lanes 5-6).

The association of dp115 with membranes at steady state was also investigated by performing fractionation of a post nuclear supernatant into a membrane and a cytosolic fraction (Figure 5.2, lanes 7-8; see 2.3.2). A rough quantification of the bands with ImageQuant software (version 5.1) showed that the membrane-associated and cytosolic pools of dp115 exist in a ratio of approximately 3:1.

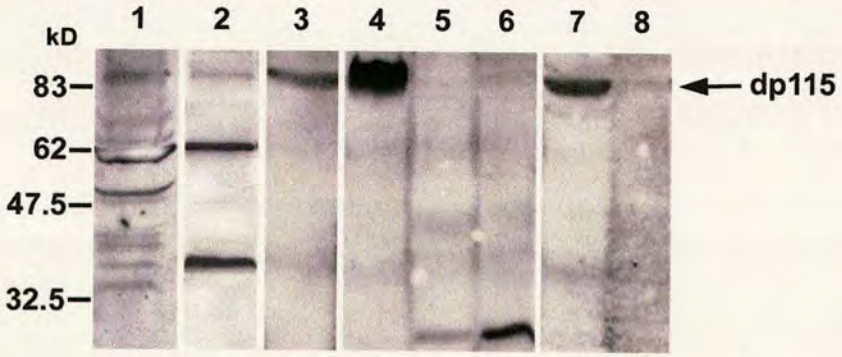

Figure 5.2: dp115 antibody characterisation. Extract from 2.5 million S2 cells (lanes 1-3), 3 third instar larvae (lane 4) or 2 adult male (lane 5) or female flies (lane 6) were prepared as described in 2.3.1. Post-nuclear supernatant from 10 million cells was fractionated into a membrane and a cytosolic fraction (100,000g for 1h). The extracts, the total membrane fraction (lane 7) and 10% of the cytosolic fraction (lane 8) were processed for Western blotting. Anti-dp115 serum (lane 1), purified antibody dp115/584-1 (lane 2) or purified antibody dp115/584-2 (lanes 3-8) were used to detect dp115.

5.3 Localisation of dp115

The localisation of dp115 was determined by IEM using the dp115/584-1 antibody (Figure 5.3), and the labelling was later corroborated using the dp115/584-2 batch of purified antibody (not shown). In S2 cells, 30±5% of the total gold particles was found in the cytoplasm. From the membrane-

associated gold, 25±8% was confined on the Golgi area, while 21±6% decorated ER cisternae. The remaining 54±7% of the labelling was associated with pleiomorphic membranes comprising tubules and vesicles (50-70 nm in diameter but also larger membrane structures) mostly found in close vicinity to the Golgi stacks (Figure 5.3A-B). A double labelling with the dSec23p sites

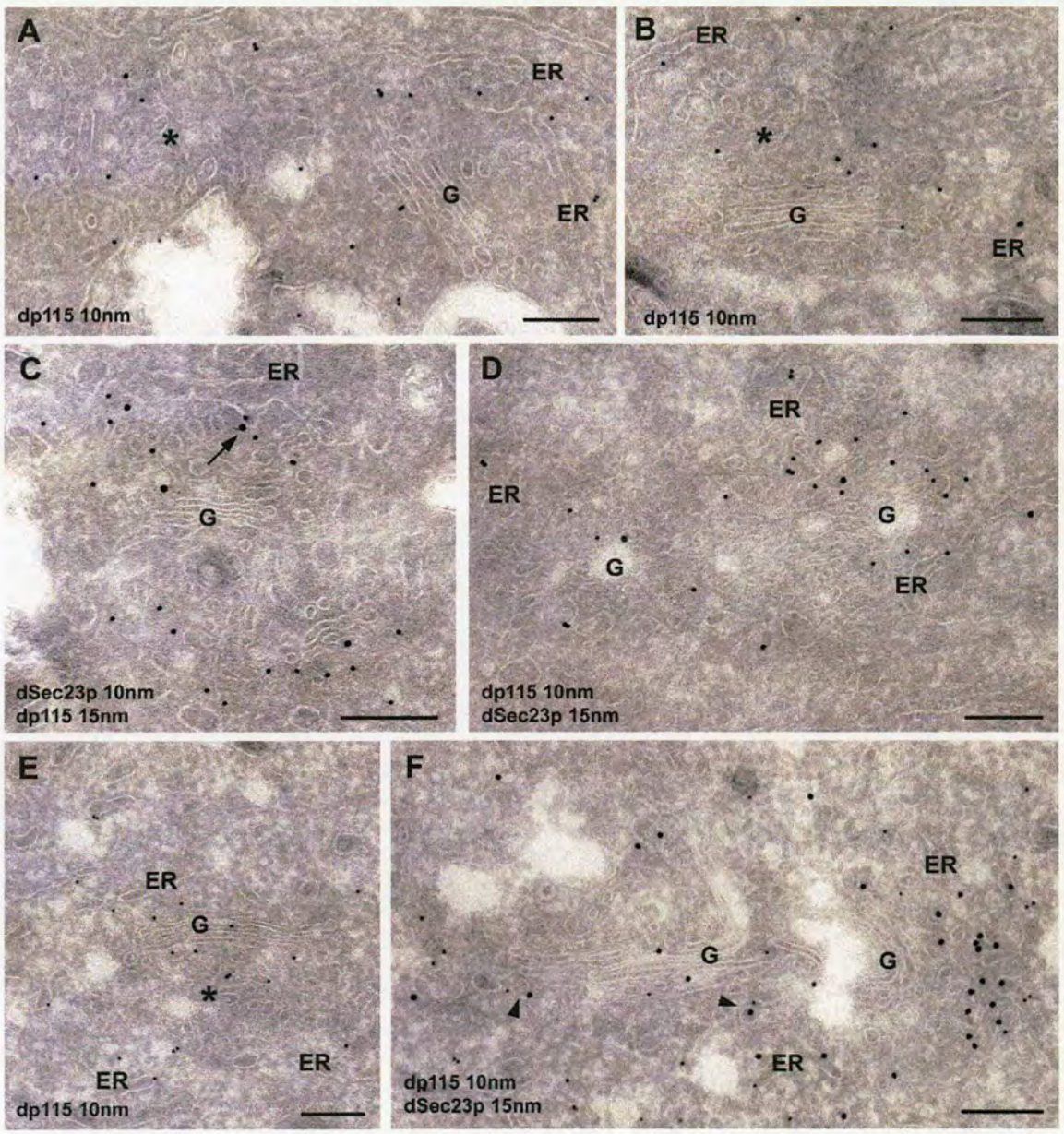

Figure 5.3: dp115 localisation. S2 cells (A-D) and salivary glands (E-F) were processed for IEM. Cryosections were labelled with dp115/584-1 (A, B, E) or double labelled with dp115/584-1 and dSec23p antibodies, followed by protein A coupled to gold (C, D, F). The sizes of the gold particles associated with each protein are mentioned in each picture. In single labellings, tER compartment is marked by asterisks. Note an ER bud (arrow in C) and coated vesicles (arrowheads in F) labelled for dp115 and dSec23p. G, Golgi stacks; ER, endoplasmic reticulum. Bars, 200nm.

antibody confirmed that these pleiomorphic membranes represented tER (Figure 5.3C-D). The linear density of gold particles over the membrane of these three compartments was estimated to be 0.57 gold particles/μm on the Golgi membrane, 0.37 on tER membrane and 0.15 on ER cisternae. Similar dp115 distribution was observed in 3rd instar larva salivary glands (Figure 5.3E-F).

5.4 Effect of dp115 depletion on Golgi stack architecture

S2 cells were depleted from dp115 by adding dsRNA corresponding to 30 nucleotides of the 5′ UTR and the first 700 nucleotides of the translated region of the only exon of dp115 gene (CG1422). As controls, mock-treated (no dsRNA added) or mock-depleted cells (dsRNA corresponding to EGFP sequence added) were used. Furthermore, the fact that no distinguishable effect had been observed in dGM130 depletion (see section 4.3) served as an additional control for the specificity of any disruption of the Golgi architecture in the other RNAi protein depletions.

dp115 RNAi was performed in S2 cells for up to 120 hours. Cell growth rate was reduced after 24h by 25±8.7%, compared to the mock-treated cells, but subsequently, it recovered to normal levels (Figure 5.4A).

Initially, due to the lack of working antibody, the efficiency of dp115 depletion was assessed by estimating dp115 mRNA with RT-PCR (Longman et al, 2000). After 48h, dp115 mRNA could not be detected and remained so up to 120h (Figure 5.4B). However, when dp115/584 antibody was raised and purified, the dp115 protein depletion was also assessed by Western blotting. The amount of dp115 appeared significantly reduced after 72h and was not detectable after 96h of incubation with dp115 dsRNA. This suggests that the protein has a relatively long half-life (probably more than 24h).

Mock-treated and ds dp115-incubated cells were processed for conventional EM. Cells incubated with ds dp115 for up to 72h did not show significant changes in their Golgi stack morphology, when compared to mock-treated cells (Figure 5.5A-B). 76.3±4.0% of the cell profiles exhibited at

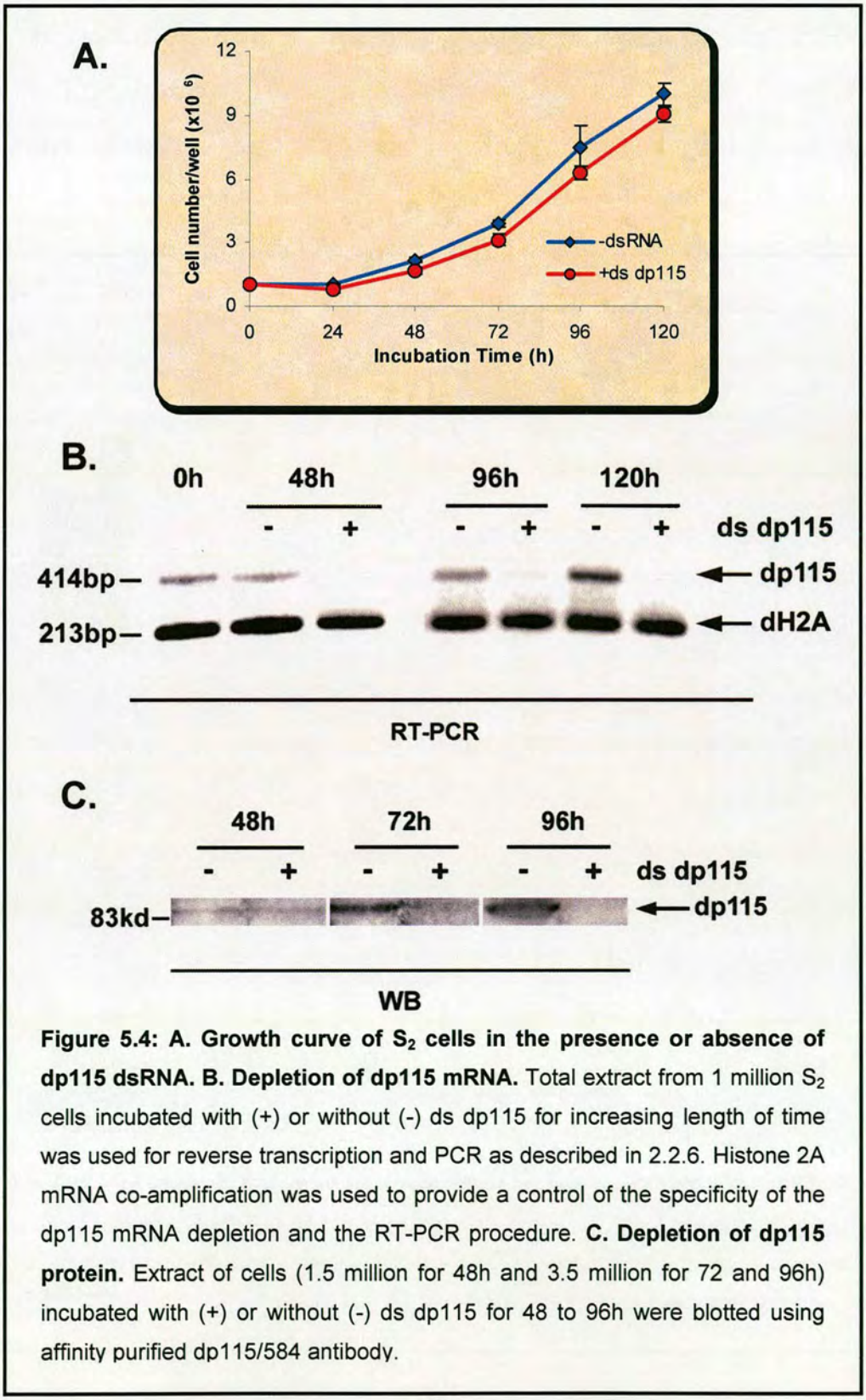

Figure 5.4: A. Growth curve of S_2 cells in the presence or absence of dp115 dsRNA. B. Depletion of dp115 mRNA. Total extract from 1 million S_2 cells incubated with (+) or without (-) ds dp115 for increasing length of time was used for reverse transcription and PCR as described in 2.2.6. Histone 2A mRNA co-amplification was used to provide a control of the specificity of the dp115 mRNA depletion and the RT-PCR procedure. **C. Depletion of dp115 protein.** Extract of cells (1.5 million for 48h and 3.5 million for 72 and 96h) incubated with (+) or without (-) ds dp115 for 48 to 96h were blotted using affinity purified dp115/584 antibody.

least one control Golgi stack (Figure 5.6A). However, this percentage decreased dramatically at 96h of incubation, when only 18±6.3% of the dp115-depleted cells showed at least one control Golgi stack (vs. 84.4±4.9% in mock-treated cells; figure 5.6A). The cisternae of these remaining Golgi stacks had also a 27% reduced cross sectional diameter (0.268±0.050 μm vs. 0.368±0.047μm in mock-treated cells) and comprised 3.2±0.4 cisternae per stack (vs. 3.7±0.8 of the mock-treated cells). The remaining 82% of cell profiles exhibited a Golgi area in the form of clusters of vesicles and tubules (Figure 5.5C-D).

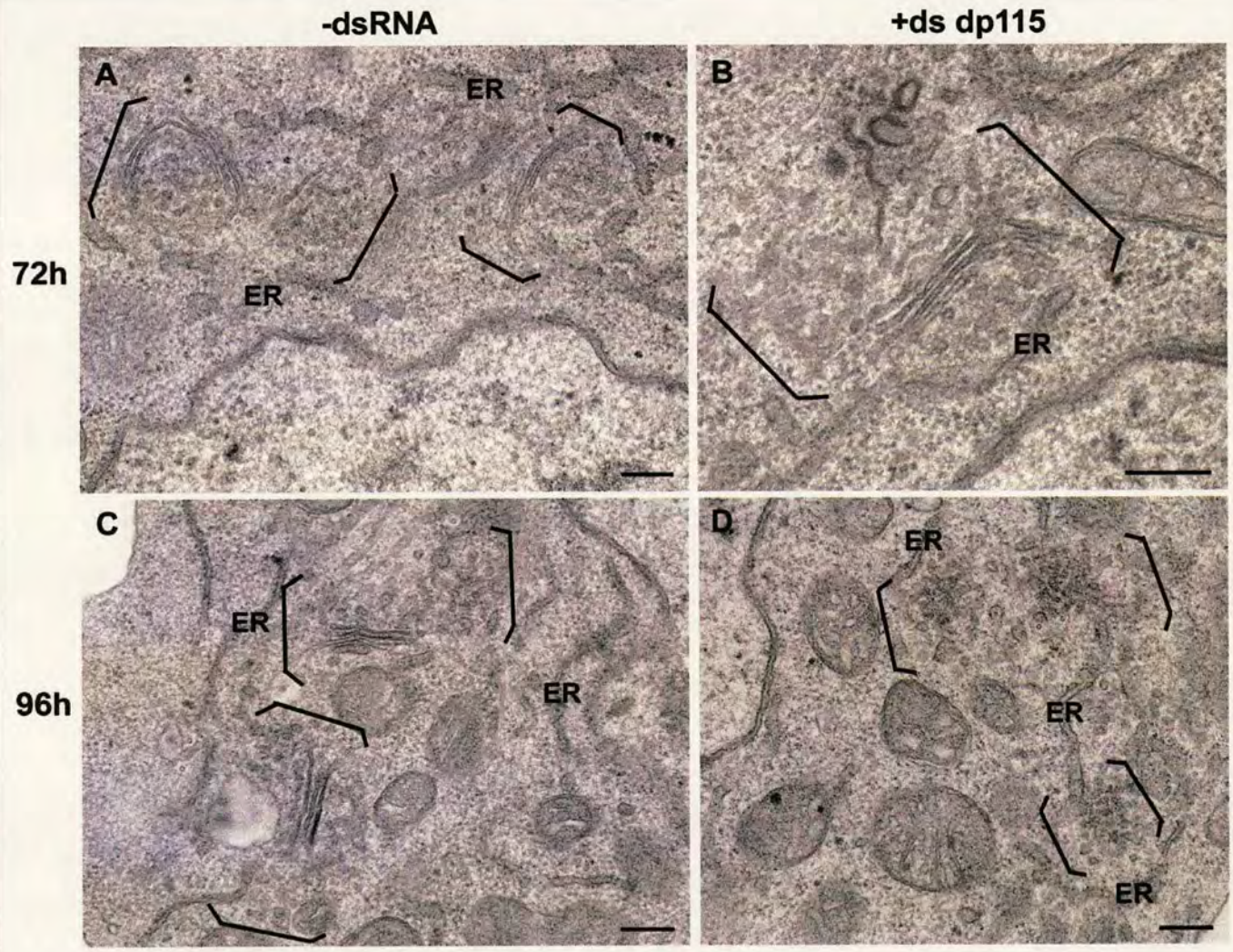

Figure 5.5: Effect of dp115 depletion on Golgi stack morphology. S_2 cells were cultured in the absence (A and C) or presence of ds dp115 (B and D) for 72h (A and B) or 96h (C and D). Golgi areas are marked between brackets. Note the Golgi stack breakdown into clusters of vesicles and tubules after 96h of dp115 RNAi. ER, endoplasmic reticulum. Bars, 200nm.

A stereological analysis was also performed on random micrographs of the cells incubated with or without ds dp115 for 72 and 96h. The percentage of Golgi membranes into total cisternae (single and stacked) decreased by 12% at 72h, while a profound reduction of 87% was observed at 96h, compared to the mock-treated cells (Figure 5.6B). This latter decrease was paralleled by a reduction in stacked cisternae and was mirrored by an increase of 32% in vesicular profiles and 50% of small tubules (Figure 5.6B). Moreover, it should be mentioned that in contrast to dGRASP- and dGRASP/dGM130-depletion, in dp115-depleted cells, the percentage of Golgi membranes in single cisternae was not significantly higher than in mock-treated cells (Figure 4.13C).

The observed decrease of total cisternal membranes in dp115-depleted cells does necessarily mean that the Golgi cisternae were converted to vesicles and tubules. For instance, similar decrease could have been a result of dilution of Golgi cisternae in incoming vesicles that would accumulate around them unable to fuse due to the lack of dp115. To rule out this possibility, the surface density of the Golgi within the cytoplasm (SD_{Go}) was estimated (see 2.4.4.2). SD_{Go} was reduced by 18% upon incubation with ds dp115 when compared to mock-depleted cells (Figure 5.6C), due to a slight reduction of the volume of the organelle within the cytoplasm (V_{Go}/V_{cyt}). The surface density of the total cisternae (SD_{cis}) (stacked and single) was also estimated and a reduction of 87% was observed (Figure 5.6C). Thus, these two parameters suggest that the striking decrease of Golgi cisternae in dp115-depleted cells was mostly due to their conversion into vesicular and tubular profiles and was not an effect of accumulating membranes in the Golgi area.

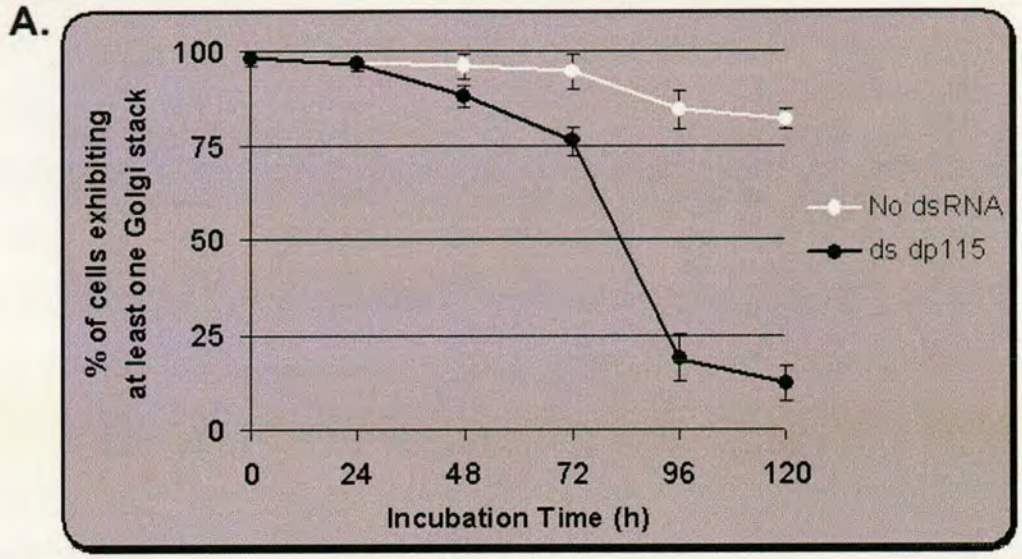

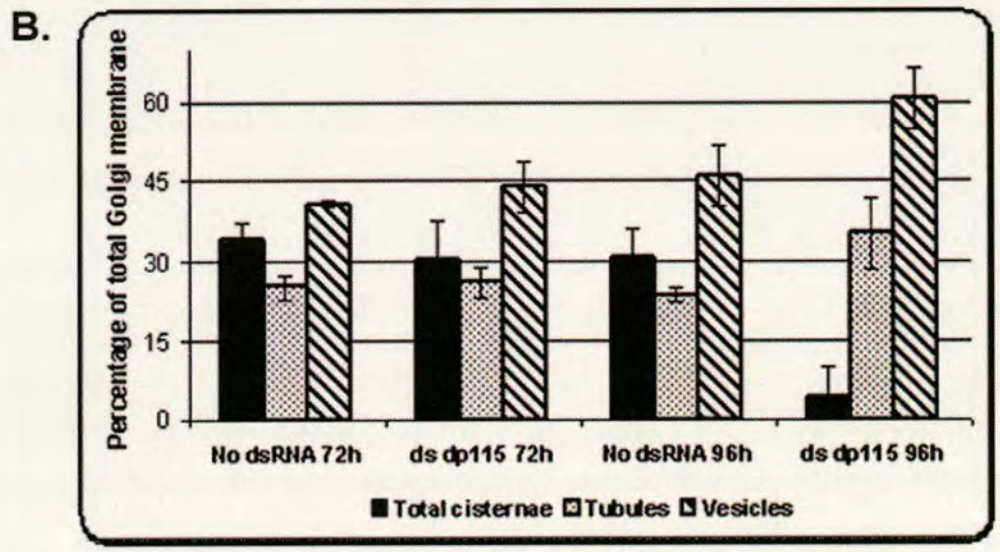

C. **Surface Density of the Golgi area (SD_{Go}) and the total cisternae (SD_{cis})**

	Mock depletion (96h)	dp115 depletion (96h)
SD_{Go}	3.64±0.44	2.97±0.29
SD_{cis}	1.25±0.17	0.16±0.07

Figure 5.6: Quantitative analysis of dp115 depletion on the morphology of the Golgi apparatus. A. The percentage of S_2 cell profiles exhibiting at least one Golgi stack in their cytoplasm was scored on ultrathin epon sections from mock-treated (white circles) and dp115-depleted cells (black circles). **B.** Random pictures of mock-treated and dp115-depleted cells at 72h and 96h were used to estimate the percentage of Golgi membrane in total cisternae (black bars), tubular (dotted bars) and vesicular profiles (lined bars). The error bars represent the SD. **C.** The surface density of the Golgi area (SD_{Go}) and the total cisternae (SD_{cis}) was estimated for mock-treated or dp115-depleted cells as described in paragraph 2.4.4.2.

5.5 Effect of dp115 depletion on transitional-ER organisation

As it was described in chapter 3, in contrast to mammalian cells, where the tER sites and the Golgi apparatus may be separated by a long distance (Hammond and Glick, 2000), in *Drosophila* S2 cells, the two compartments are located in close proximity (Figure 3.3). On the other hand, studies in two budding yeasts with different organisation in their early exocytic pathway has proposed that *Pichia pastoris*, a species that exhibits like *Drosophila* close spatial association between tER sites and Golgi stacks, may be able to sustain this organisation through the presence of a common ribosome-excluding matrix (Rossanese et al., 1999; Mogelsvang et al., 2003). This attractive hypothesis of a tER-Golgi matrix (independent of its stable or dynamic nature), together with the fact that dp115 was localised to the same extent in tER sites and the Golgi apparatus, made it interesting to examine whether dp115 depletion from S2 cells would have affected tER organisation, in addition to the profound disruption of the Golgi stacks.

As in the case of dGRASP and dGM130 depletions (see chapter 4), the tER integrity in dp115-depleted S2 cells was assessed by visualising the immunofluorescence pattern of the tER marker, dSec23p. Strikingly, after 96h of incubation with ds dp115, about 85% of the cells appeared to have lost the focused tER sites observed in mock-depleted cells (Figure 5.7, A and D). Instead of the average number of 20 focused tER sites per mock-depleted cell, dp115-depleted cells exhibited 84.5±20 small and scattered dots all over the cytoplasm (Figure 5.7D). The size of these fluorescent objects was about 3-4 times smaller than these observed in mock-depleted cells. Therefore, the effect of dp115 depletion on tER organisation seemed to coincide temporally with that Golgi stack breakdown. Moreover, morphologically, the tER

disorganisation caused by dp115 deletion was reminiscent of this following the incubation of S2 cells with the inhibitors H89 and BFA, at least at the level of light microscopy (compare figure 5.7 with figures 3.7 and 3.8).

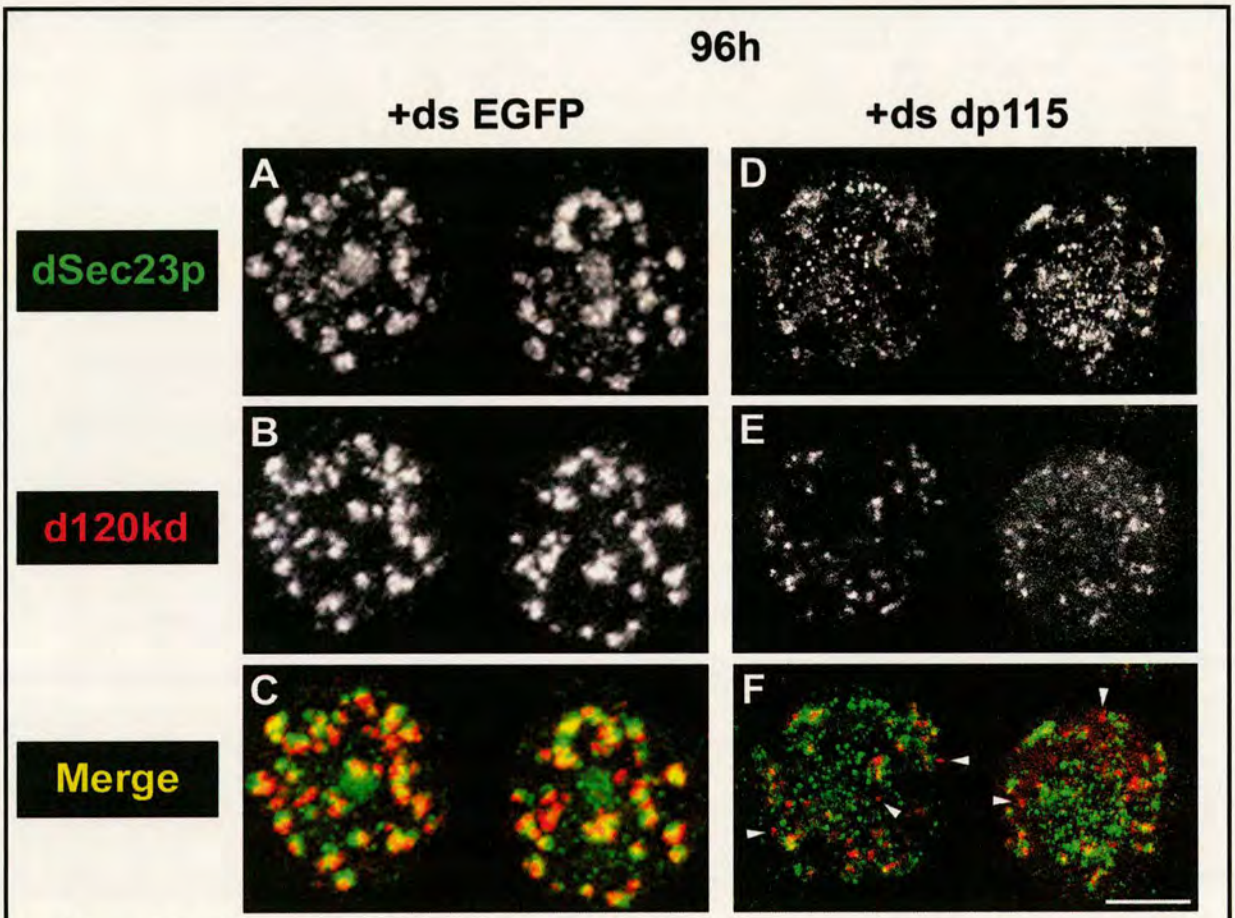

Figure 5.7: Effect of dp115 depletion on the organization of the tER sites. Mock-depleted (+ds EGFP, A-C) and dp115-depleted S_2 cells (+ds dp115, D-F) for 96h were processed for IF, and labelled for dSec23p (A and D) and d120kd (B and E). In the merged pictures (C and F), tER sites are labelled in green, Golgi membranes in red and overlapping areas in yellow. Note that in dp115-depleted cells, some of the d120kd-positive structures are situated relatively far from dSec23p-positive dots. Bar: 5µm

The fluorescence pattern of the Golgi marker d120kd also changed after dp115 depletion (Figure 5.7E), in agreement with the observed disruption in the Golgi stack architecture upon dp115 depletion, as described by EM. The number of fluorescence objects corresponding to this antigen was slightly higher than in control cells (26±7 versus 18±6 in control cells),

but their size was smaller, and the intensity of fluorescence seemed reduced, as if this antigen was dispersed (Figure 5.7, compare B with E). In addition, d120kd and dSec23p small spots did not exhibit the close spatial association to the same extent that has been described for mock-treated cells (Figure 5.7, compare C with F). Numerous dSec23p-positive spots were not associated with a d120kd-positive spot. Conversely, some of the d120kd-positive dots were also observed relatively away from dSec23p structures (see arrowheads in figure 5.7F). However, the majority still seemed to retain their close association or partial overlap with dsec23p spots (Figure 5.7F).

To establish more convincingly this novel role of dp115 in the organisation of tER sites, additional controls were carried out. First, mock- and dp115-depleted cells were fixed with stronger fixatives and for a longer period of time. The reason for this experiment is that the mild fixation normally used for IF could be adequate to preserve the tER sites and Golgi complexes in mock-depleted cells, but not in dp115-depleted cells, which might be more susceptible to extraction during IF processing. This could be a valid argument, especially if dp115 acts as a component of a matrix that may surround the tER sites and the Golgi stacks and maintain their organisation. When mock- and dp115-depleted cells were fixed with a combination of glutaraldehyde and paraformaldehyde and processed for IF, a similar tER disorganisation was observed in the dp115-depleted cells (Figure 5.8), despite the increased autofluorescence due to the use of glutaraldehyde. This suggests that the effect of dp115 depletion was not the result of a reduced stability of the tER sites under mild fixation.

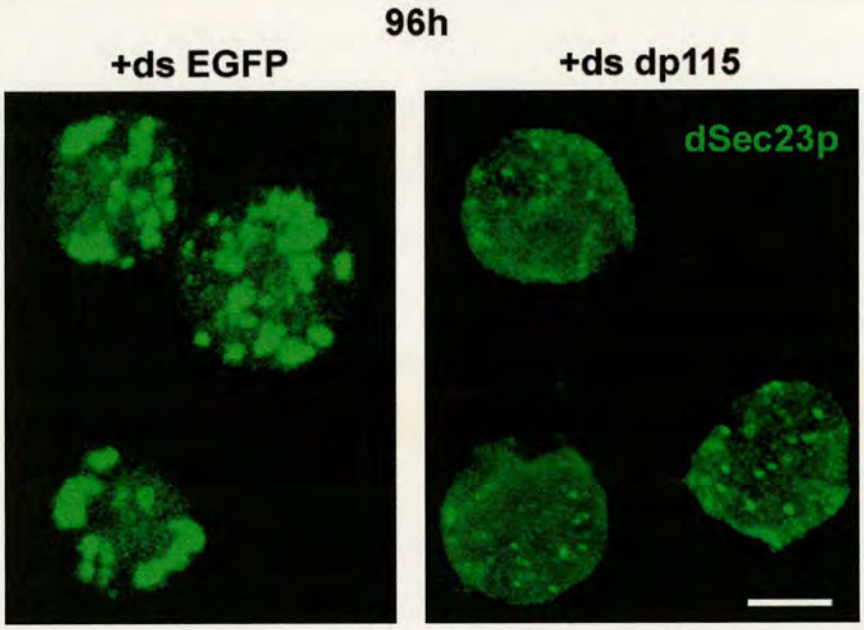

Figure 5.8: Mock- and dp115-depleted S_2 cells for 96h were fixed with 2% paraformaldehyde and 0.2% glutaraldehyde for 2h and processed for IF including an incubation for 10 minutes with $NaBH_4$ to reduce the autofluorescence. Cells were labelled for dSec23p. Bar: 5µm

Second, to rule out the possibility that dp115 depletion leads to a degradation of dSec23p or d120kd protein, Western blotting was performed in control and dp115-depleted cells. This verified that dSec23p and d120kd were not degraded upon dp115 depletion (Figure 5.9).

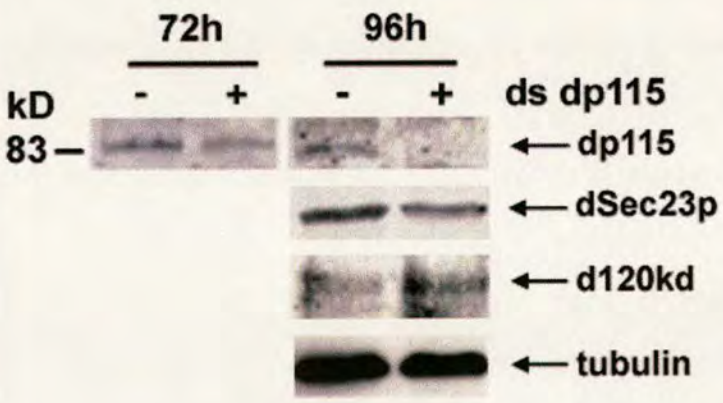

Figure 5.9: Cell extract from 1.5 million S_2 cells incubated with (+) or without (-) ds dp115 for 72 and 96h were processed for Western blotting using the affinity purified dp115/584 (dp115) and dSec23p, d120kd and anti-tubulin antibodies. Note that after incubation of the cells with ds dp115 for 96h, only dp115 is depleted.

Finally, to gain more insight into the type of structures that the observed fluorescent spots represented, dp115-depleted cells were processed

for IEM. Cells were initially viewed at low magnification to have an idea of the overall distribution of dSec23p in the cytoplasm (Figures 5.10 and 5.11). Equatorial sections of mock-depleted cells exhibited 2.7±1.5 dSec23p-positive sites per section (Figure 5.10), 90% of which were also positive for d120kd (see magnified areas in figure 5.10). In the dp115-depleted cells, dSec23p was localised in pleiomorphic membranes containing vesicles and tubules, as in the mock-depleted cells (see magnified areas in figure 5.11). However, the number of these dSec23p-positive sites per cell section increased to 6.7±2.3. Moreover, the tER sites appeared smaller than in control cells (Figure 5.11 and 5.12A), often displayed a reduced labelling density (Figure 5.12A and E), and only 20% of them were positive for d120kd (Figure 5.11 and 5.12A). These observations are in agreement with the increased number of dSec23p-positive small and scattered fluorescent dots.

The d120kd-positive fluorescent spots also represented clusters of vesicles and tubules (Figure 5.12B-F). The relative distribution of the d120kd-associated gold particles on these clusters was 73±3.6%. The remaining 27% of the membrane-associated d120kd was confined to ER cisternae (arrowheads in figure 5.12C and E), suggesting either an increased retrograde movement of Golgi resident proteins back to the ER, or an inhibition of their ER exit. Frequently, d120kd-positive structures were reminiscent of short cisternal remnants (arrows in figure 5.12D-F), implying that these clusters could have derived from Golgi stack breakdown.

Pleiomorphic membrane clusters were also labelled for both dSec23p and d120kd (Figures 5.11 and 5.12D-F), suggesting that some tER sites have remained in close proximity to the Golgi membranes, as in non-depleted cells. Noticeably, in the majority of these double-labelled clusters, the tER

and Golgi markers did not mix homogenously, but they seemed to retain a polar distribution (Figure 5.12D-F).

Figure 5.10: Mock-depleted S_2 cells were processed for IEM and labelled for dSec23p and d120kd, followed by protein A coupled to 10 and 15nm gold, respectively. In low magnification, the dSec23p-positive areas were identified and encircled in an equatorial section of a cell. Details of the labelled structures were observed in higher magnification. N, nucleus; G, Golgi stacks. Bar: 500nm

Figure 5.11: dp115-depleted S_2 cells were processed for IEM and labelled for dSec23p and d120kd, followed by protein A coupled to 10 and 15nm gold, respectively. In low magnification, the dSec23p-positive areas were identified and encircled in an equatorial section of a cell. Note their number increase and size decrease compared to the mock-depleted cells. Details of the labelled structures were observed in higher magnification. Arrows point to d120kd labelling that is observed only in few dSec23p-positive areas. N, nucleus; G, Golgi stacks. Bar: 500nm

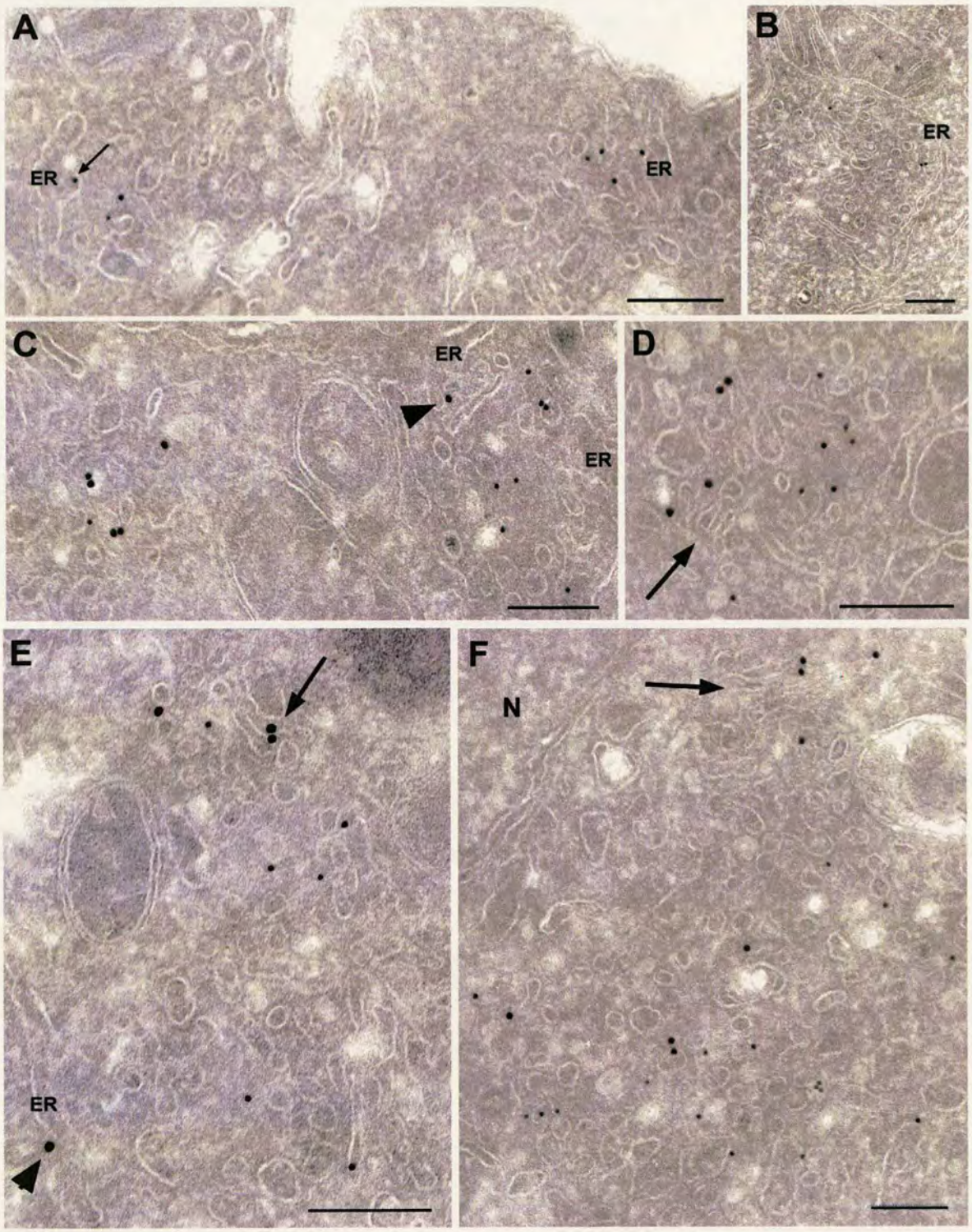

Figure 5.12: dp115-depleted S_2 cells were processed for IEM and labelled for dSec23p (10nm gold) and d120kd (15nm gold). (A and C) dSec23p-positive clusters. (B and C) d120kd-positive clusters. (D-F) Mixed clusters. Large arrows in D, E and F point to profiles reminiscent of Golgi cisternae. Arrowheads in C and E indicate d120kd gold particles associated with an ER cisterna. The small arrow in A points to an ER bud labeled for dSec23p. Note in D, E and F that the labelling for dSec23p and d120kd marks differential regions of the same cluster. ER, Endoplasmic reticulum; N, nucleus. Bars: 200nm

5.6 dp115 effects on tER site and Golgi stack organisation: causal link or 2 distinct functions?

The fact that the depletion of dp115 leads to the disorganisation of both the tER sites and the Golgi stacks could be explained by three scenarios. The first is that dp115 could be involved in the organisation of both compartments independently. A second possibility is that the breakdown of the Golgi stacks could be a consequence of the tER disorganization, which implies that dp115 could have only one role in the tER organization. Finally, a third possibility is that dp115 could have a single role in the building and/or maintenance of the Golgi stacks. Thus, its effect in the tER organisation could be indirect and caused by a disruption in membrane trafficking between the tER sites and the Golgi apparatus following the breakdown of the latter. Although the localisation of dp115 in both tER and Golgi membranes argues against the last two scenarios, the question was addressed using different approaches.

5.6.1 Kinetics of the two effects

First of all, the kinetics of the two dp115-depletion effects was tested by assessing the immunofluorescence pattern of dSec23p and d120kd in dp115-depleted S2 cells, in a time-course analysis between 72 and 96h after ds dp115 addition (Figure 5.13), when the tER and Golgi stack disorganisation seemed to take place in the majority of the cells. After 72h incubation with ds dp115, approximately 85% of the cells exhibited dSec23p and d120kd patterns almost indistinguishable from mock-treated cells (about 20 large fluorescent spots partially overlapping, that are referred to as "control patterns"). However, at 84, 88, 92 and 96h time points of dp115 RNAi, a mixture of patterns was observed. The number of cells showing control patterns decreased gradually over time to reach 12.6% after 96 hours

incubation, while the equivalent figure for mock-treated cells remained higher than 90% for all the time points tested (Figure 5.13, compare filled and open squares). Conversely, the cells exhibiting a disrupted pattern for both dSec23p and d120kd increased gradually from 17.6% to 83.8% (Figure 5.13, triangles). Finally, the percentage of cells, where the organisation of one of the two compartments was affected, was small and did not exceed 7% of the cell population, at any time point tested (Figure 5.13, circles). Furthermore, the percentage of cells where only the dSec23p pattern was disrupted (3.2±1.2%) was comparable to this, where only the d120kd pattern was disrupted (1.8%±1.1%). This result suggests that the depletion of dp115 lead to a concomitant disorganisation of the Golgi stacks and tER sites, indicating that dp115 could have a distinct role in the organisation of both structures.

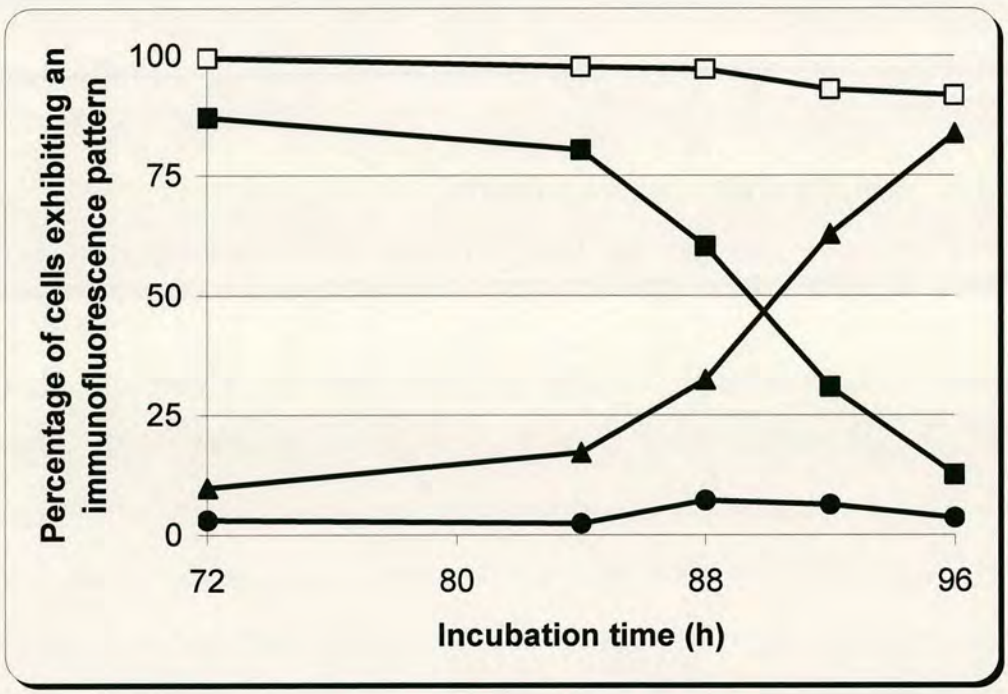

Figure 5.13: Mock-treated (open squares) and dp115-depleted S2 cells (filled symbols) were scored for their immunofluorescence pattern of dSec23p and d120kd between 72 and 96h of RNAi. Cells exhibiting control patterns for both markers are represented by squares, those with disrupted patterns for both markers are represented by triangles, while those where only one pattern was disrupted are shown by circles. Note the low percentage of cells exhibiting either tER disorganisation, or Golgi stack breakdown for all time points tested.

5.6.2 dSed5p depletion

Another way to test whether tER and Golgi stack organisation were inter-dependent, and whether dp115 function in the tER organisation was specific for this protein, was to find conditions that disrupt Golgi stack architecture without affecting the organisation of the tER sites.

An indication for the specificity of the dp115 role on the focused organisation of the tER sites derived from dGRASP/dGM130 double depletion experiments that were described in the previous chapter (see sections 4.5 and 4.6). Depletion of S2 cells from both dGM130 and dGRASP led to a quantitative breakdown of their Golgi stacks leaving the organisation of the tER sites largely unaffected. This indicated that the effect of dp115 depletion on tER organisation was specific for this protein and not a general function of the Golgi matrix proteins.

In order to investigate further this matter, additional conditions to disrupt the Golgi architecture were looked for. A good candidate protein to cause Golgi stack breakdown upon depletion was dSed5p. dSed5p is the *Drosophila* homologue of t-SNARE Syntaxin 5 (Banfield et al., 1994), and its mammalian and yeast homologues have been involved in ER to Golgi transport (Hardwick and Pelham, 1992; Dascher et al., 1994). Therefore, it was predicted that in the absence of this SNARE from S2 cells, ER-derived vesicles would be unable to fuse with their target membranes leading to Golgi disorganisation.

The protein was depleted by incubating S2 cells with dsRNA corresponding to dSed5p gene (Table 2.10) for up to 96 hours. Western blotting analysis showed more than 80% of the protein was depleted after 48 and 72 hours of incubation with the ds dSed5p, while it was below detection after 96 hours (Figure 5.14). Furthermore, after 96 hours of RNAi, the number

of dSed5p-depleted cells was 37% lower than the mock-treated cells (5.3 vs. 8.4 million cells per well). The presence of many bi-nucleated cells among the dSed5p-depleted cells (not shown) suggested that the reduced growth rate was probably due to a cytokinesis defect, which was probably the result of an arrest in anterograde transport (Xu et al., 2003; see also chapter 6).

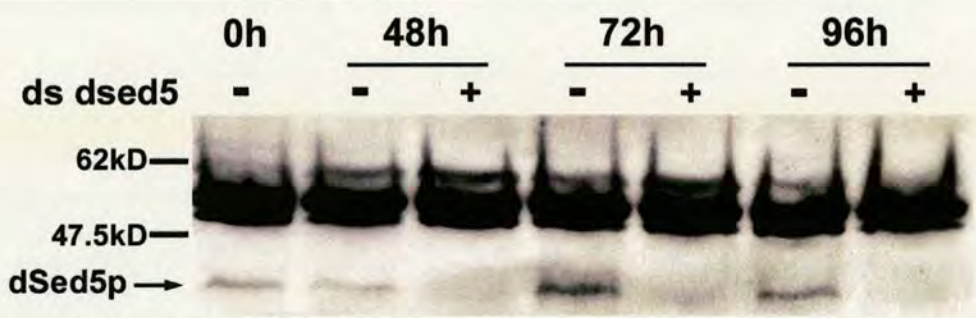

Figure 5.14: Depletion of dSed5p from S2 cells. Cells were incubated with ds dSed5p for up to 96h. Cell extracts of mock- (-) and dSed5p-depleted cells (+) were Western blotted using JSEE1 antibody (see table 2.6). Note that the 35kD band corresponding to dSed5p is detected in traces at 48 and 72h, and fully depleted after 96h.

As expected, when dSed5p-depleted cells for 72h were examined by EM, the Golgi stacks were completely vesiculated in 99% of the cell sections (Figure 5.15). The effect on the Golgi architecture was also obvious by IF labelling for d120kd. The labelling appeared weak and partly dispersed, reflecting the observed Golgi vesiculation (see inset in figure 5.15). However, larger d120kd-positive were still persisting demonstrating once more that at the IF resolution, even such an extensive Golgi stack breakdown cannot be detected with certainty.

Next, dSed5p-depleted S2 cells were labelled for dSec23p to examine the structural integrity of the tER sites. Despite the dramatic effect on the Golgi architecture, dSed5p depletion did not affect the focused organisation of the tER sites (Figure 5.16).

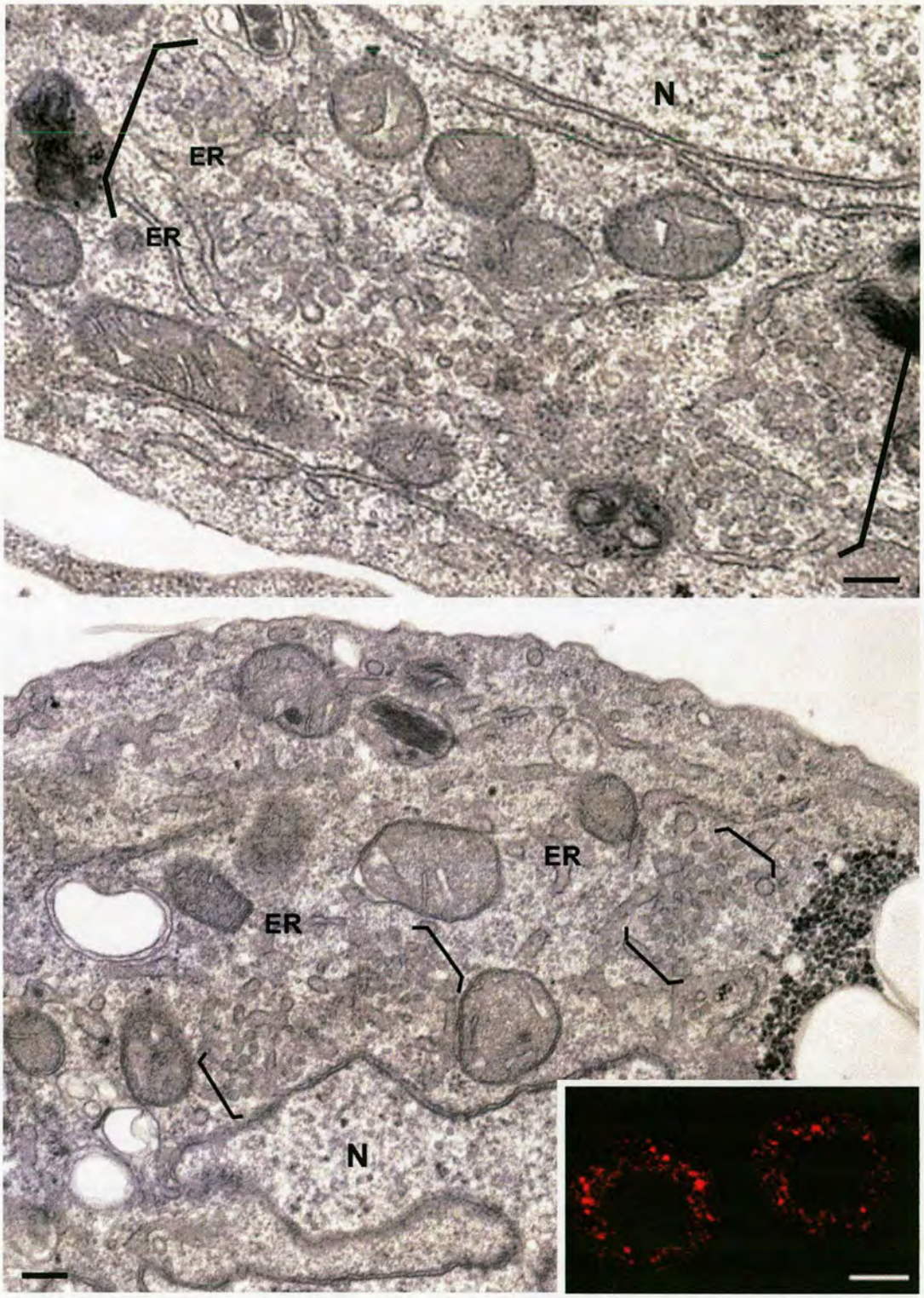

Figure 5.15: Golgi stack breakdown upon dSed5p depletion. S2 cells were incubated with ds dSed5p for 72h and processed for EM. Note the extensive vesiculation observed in areas that normally Golgi stacks are located, which are marked between brackets. In the inset, dSed5p-depleted were processed for IF and labelled for d120kd. Note in this confocal section that the Golgi marker is dispersed, but some larger spots can still be seen. ER, endoplasmic reticulum; N, Nucleus. Bars: 200nm for EM pictures; 5µm for inset.

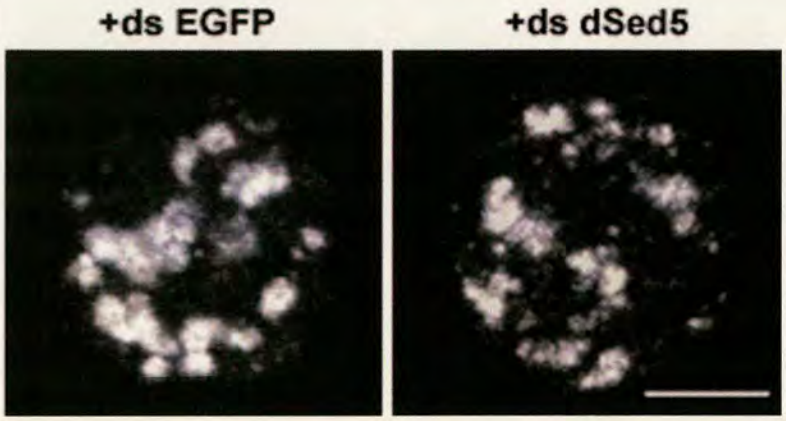

Figure 5.16: dSed5p depletion does not alter the tER organisation in S2 cells. The tER organization was monitored by IF using the anti-dSec23p antibody in mock-depleted (left), and dSed5p-depleted cells (right) for 96h. Bar: 5μm.

Collectively, these results support the notion that the role of dp115 on tER organisation is specific for this protein, since none of the other proteins tested had significant effect on it, upon their depletion. Moreover, they suggest that the processes of Golgi stack formation/maintenance and tER organisation can be dissociated. Finally, dSed5p RNAi experiment also shows that the possible SNARE complex assembly involving dSed5p recruitment by dp115 (SNARE-binding site is conserved in dp115, see discussion) is important for the Golgi stack architecture, but not for tER organisation, implying that dp115 takes part in at least two different complexes.

5.7 dp115-dGM130 double depletion

Considering the well-described interaction between mammalian p115 and GM130 (see introduction), the discrepancy between dp115 and dGM130 RNAi phenotypes was surprising. Although the biochemical interaction of the two *Drosophila* proteins is still uncertain, their possible genetic interaction was addressed by depleting both dp115 and dGM130 from S2 cells.

The incubation of S2 cells with ds dp115 and ds dGM130 combined was as efficient in depleting the two proteins as either of the single RNAi experiments (not shown). Interestingly, when dp115/dGM130 double

depleted cells were examined by EM, they exhibited a premature Golgi stack breakdown, when compared to dp115 single depleted cells (Figure 5.17). Already after 48h of treatment, 35% of the cells exhibited clusters of vesicles and tubules instead of Golgi stacks, an event never observed in dp115-depleted cells at the same time point. This phenotype became stronger after 72h of RNAi (Figure 5.18A). A common feature of these double depleted cells at early time points (48-72h) was the appearance of short stacks with cisternal diameter less than 50% of the average cisternal diameter in control cells (Figure 5.17C). These could represent Golgi fragmentation intermediates.

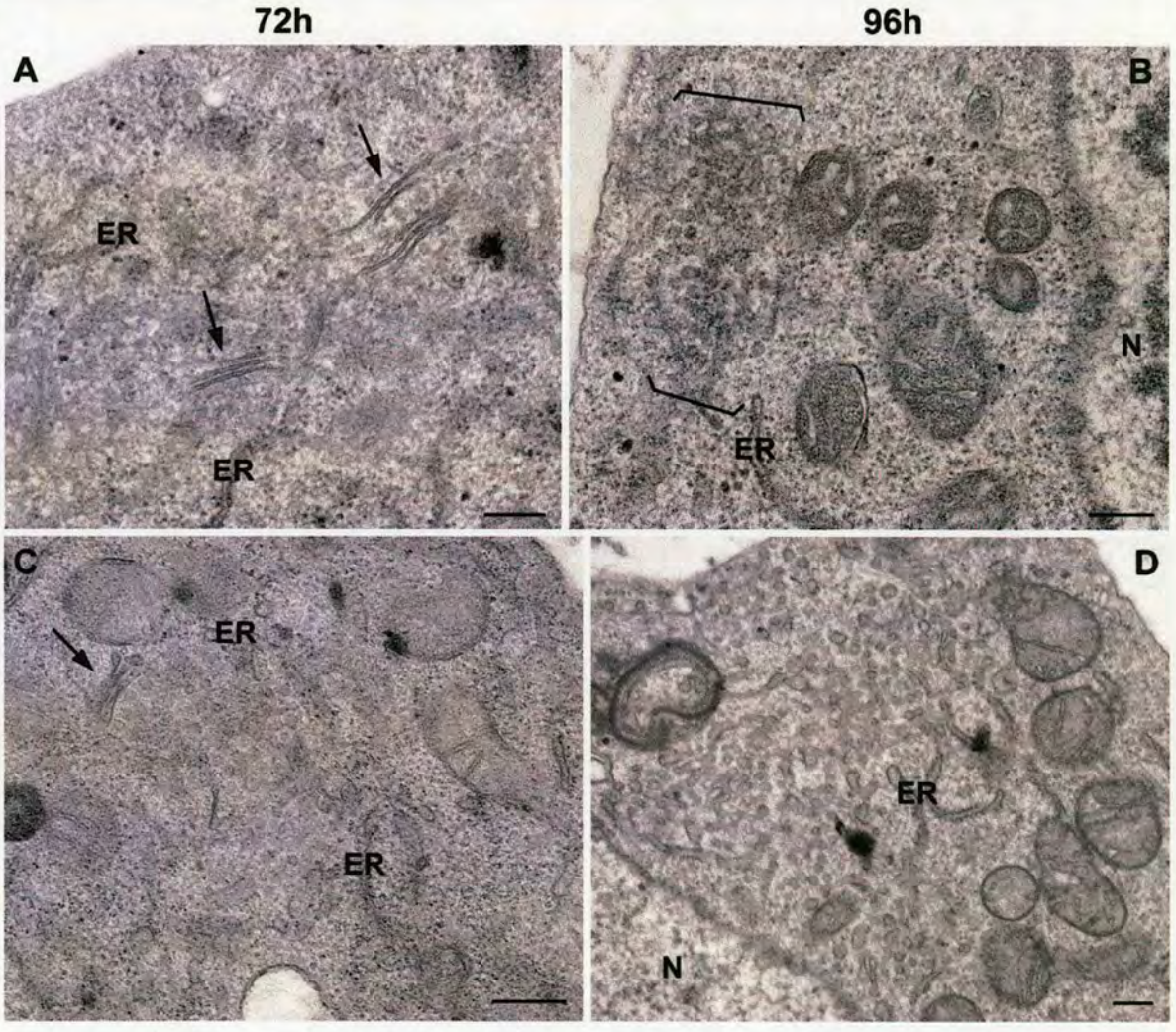

Figure 5.17: Premature Golgi stack breakdown in dp115/dGM130 double depletion. S2 cells cultured for 72h (A and C) or 96h (B and D) in the presence of ds dp115 alone (A and B) or ds dp115 and ds dGM130 (C and D) were processed for EM. Golgi is marked between brackets or with arrows. Note in C, the short cisternal diameter that is frequently observed in Golgi stacks of dp115/dGM130 depleted cells. N, nucleus; ER, endoplasmic reticulum. Bars, 200nm.

Finally, after 96h of dsRNA incubation, the extent of Golgi stack breakdown in double depleted cells was comparable to dp115-depleted cells (less than 20% cells exhibiting control Golgi stacks, Figure 5.18A).

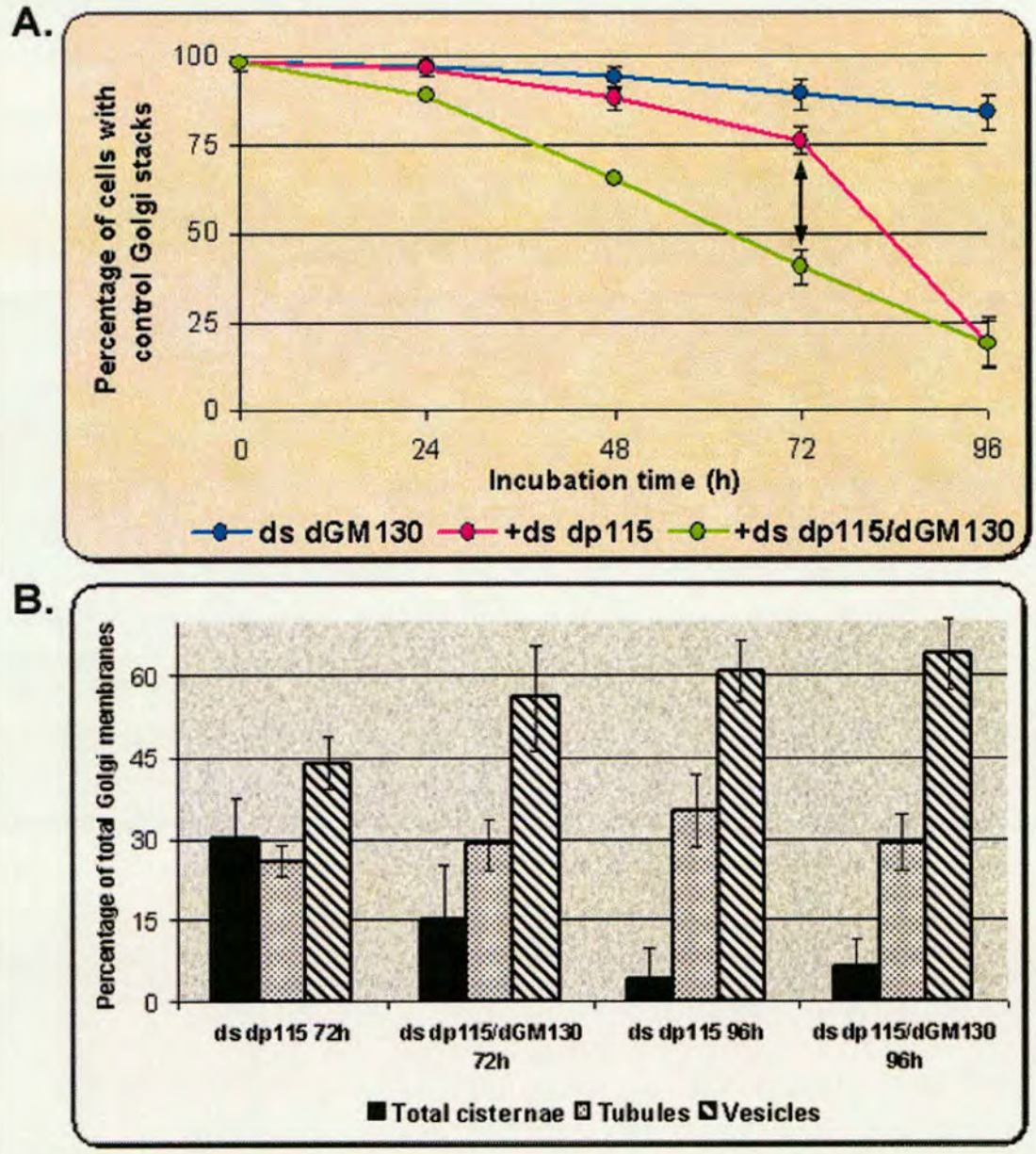

Figure 5.18: Quantitative analysis of dp115/dGM130 double depletion on Golgi morphology. A. The percentage of dp115/dGM130 depleted cells exhibiting at least one control Golgi stack in their cytoplasm was scored on ultrathin epon sections (green) and was compared to dGM130 (blue) or dp115 (pink) depleted cells. Note the premature Golgi stack breakdown at 48 and especially at 72h of dp115/dGM130 double RNAi (double arrow). **B.** The percentage of Golgi membranes in total cisternae (black bars), tubular (dotted bars) and vesicular profiles (lined bars) was compared between dp115-depleted and dp115/dGM130 double depleted cells after 72 and 96h. The error bars represent the SD.

In order to ensure that the effects observed in dp115/dGM130 double depletion were specific and not the result of technical complications due to the double dsRNA transfection, a mock double depletion was performed by incubating S2 cells with ds dp115 combined with ds EGFP. The obtained results were similar to dp115 RNAi (not shown).

Stereological analysis focused on the 72h and 96h time points, where significant conversion of Golgi stacks into clusters of vesicles and tubules was observed. In double depleted cells, a 50% reduction in total cisternal membranes after 72h demonstrates the premature effect in the Golgi stack architecture, when compared to 12% decrease for the dp115 single depletion, at the same time point (Figure 5.18B, compare the first 2 black bars). At 96h, the distribution of Golgi membranes in cisternae, tubules and vesicles was comparable between single and double depletion (Figure 5.18B).

The premature disorganisation of the Golgi stacks in dp115/dGM130 double depleted cells provided an additional means to test whether dp115 has two distinct functions at the tER sites and the Golgi stacks, or it is only involved in the organisation of the tER sites and causes indirectly the Golgi stack breakdown. A kinetic study of the tER disorganisation was performed in dp115 single and dp115/dGM130 double depleted cells. The rationale behind this experiment was that if there is a causal link between the two effects of dp115 depletion, the premature Golgi stack breakdown observed in dp115/dGM130 double depleted cells (Figure 5.18A) should be accompanied by a similar premature disruption of tER sites. The pattern of dSec23p was monitored at 72 and 96 hours after the addition of the dsRNAs (Figure 5.19). However, when the kinetics of tER disorganisation was measured, the combined depletion of dGM130 and dp115 did not seem to accelerate the

dispersal of tER sites, when compared to dp115 single depleted cells (compare 72h time point in figures 5.19 and 5.18A).

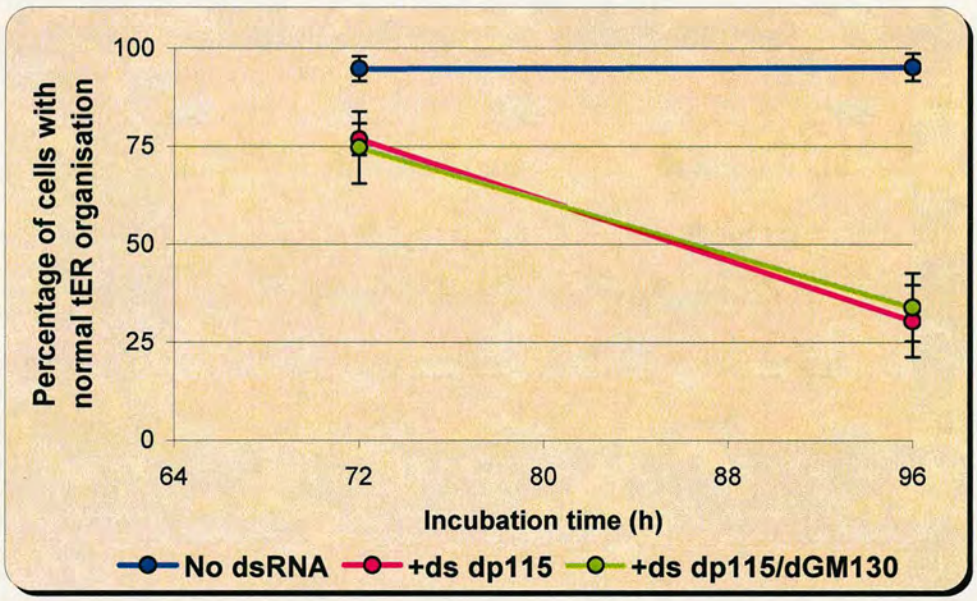

Figure 5.19: dp115 functions at tER sites and Golgi apparatus are independent. Mock-treated (blue), dp115-depleted (pink), and dp115/dGM130 double-depleted (green) S2 cells were processed for IF and labelled for dSec23p. The percentage of cells showing normal tER organisation relative to the incubation time with dsRNAs was plotted in this graph. Note that after 72h of RNAi, the double-depleted cells do not exhibit a premature disruption in the organisation of their tER sites, compared to dp115-depleted cells, as they do when Golgi stack breakdown was monitored (compare with figure 5.18A).

Thus, these results provide further support to the idea that the two processes under study are independent, and show that dp115 and dGM130 interact genetically to disrupt the Golgi stack but not the tER organisation.

Chapter Six

Effect of Golgi matrix protein depletion in anterograde protein transport in S2 Cells

6.1 Delta anterograde transport assay

Apart from their involvement in the structure of the Golgi apparatus, the Golgi matrix proteins, at least in mammalian cells, have also been implicated in several steps of intracellular transport (see introduction). However, to date, it has been difficult to establish clearly whether they have distinct functions in both the Golgi architecture and the intracellular membrane trafficking, or whether one of the two processes is primarily disrupted, and that has as consequence the disruption of the other process. For example, the Golgi stack organisation could be affected as a consequence of the inhibition in intracellular transport, and conversely, a disorganisation of the Golgi apparatus could be the cause for the observed block in transport.

In the present study, three different conditions were described, where the organisation of the exocytic pathway was disrupted quantitatively upon depletion of *Drosophila* Golgi matrix proteins. dp115 single depletion and dp115/dGM130 double depletion led to Golgi stack breakdown and dispersal of the tER sites in S2 cells, while the dGRASP/dGM130 double depletion resulted in a disorganisation of the Golgi stacks but not of the tER sites. In order to test whether anterograde protein transport was affected under the modifications imposed on the early exocytic pathway, transport of Delta to the PM was measured in all RNAi-depleted S2 cells (for description of Delta transport assay see 2.4.5 and 3.4).

6.1.1 Control experiments related to RNAi

In chapter 3, functional tests of the Delta transport assay using known anterograde transport inhibitors (BFA and H89) were described. However, some additional controls related to the RNAi methodology were carried out before estimating the efficiency of intracellular transport in Golgi matrix

protein depleted cells. First, it was confirmed that the morphological effects of the various depletions on the tER and Golgi stack organisation that were observed in wild type S2 cells, were similar in Delta S2 cells. For this reason, the EM stereological analyses presented in chapters 4 and 5 have been obtained by experiments carried out in both cell lines.

Second, it was verified that the induction and transport of Delta for as long as 2.5 hours (1h induction/90min chase protocol) did not induce the rebuilding of Golgi stacks. For example, in cells depleted of dp115 for 96h, the percentage of cells with at least one Golgi stack was the same before and after Delta induction (18.0±6.3% versus 18.9±1.2%, respectively).

In order to estimate the steady-state transport of Delta to the PM, Delta S2 cells were subjected to RNAi treatment, and subsequently they were induced with $CuSO_4$ for 1 hour, followed by a chase of 90 minutes allowing Delta reach the PM. Under these conditions, the total intensity of fluorescence at the PM is maximal (Figure 3.17) and does not increase significantly even when Delta S2 cells are induced for 2 hours and chased for 4 hours, which means that this protocol reflects accurately the steady-state rate of transport.

The sensitivity of the assay under RNAi experimental conditions was assessed in cells depleted of dsed5p (see section 5.6.2). dsed5p localises in the Golgi apparatus in S2 cells and was shown to impair transport of a GFP-tagged apical transport reporter in salivary glands of late embryos (Xu et al., 2002). Considering these results and the extensive Golgi vesiculation that was observed in dSed5p-depleted cells (Figure 5.15), dSed5p depletion was expected to block also Delta transport to the PM and was used as a positive control. Indeed, when Delta S2 cells were depleted of dSed5p, Delta labelling was retained intracellularly in 84.5±4.3% of cells (Figures 6.1 and 6.2).

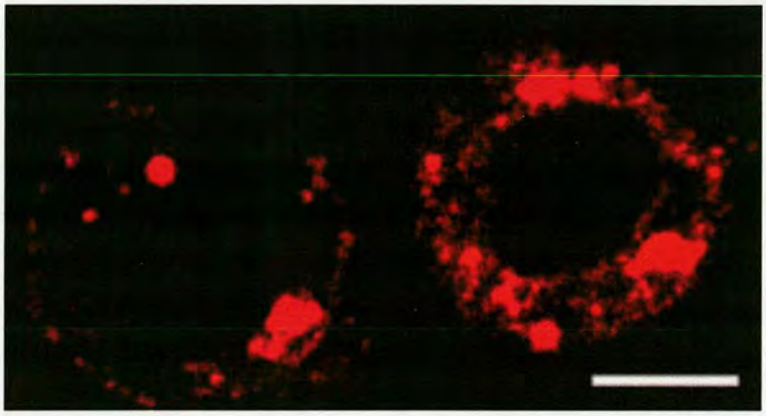

Figure 6.1: Block in Delta transport to the PM upon dSed5p depletion. Delta S2 cells depleted of dSed5p for 96h were labelled for Delta using C594.9B antibody. A confocal section is presented here. Note that Delta is retained intracellularly in induced cells. Bar: 5μm

In addition, mock-treated (no dsRNA) and mock-depleted (ds EGFP) Delta S2 cells were used as negative controls. The distribution of the mock-depleted cells into the 4 labelling categories was very similar to mock-treated cells (compare black and light green bars in figure 6.2), suggesting that the treatment of Delta S2 cells with dsRNA does not lead to a non-specific effect on Delta transport to the PM. The transport efficiency in mock-treated and mock-depleted cells was set as 100% (Figure 6.3). Steady-state transport of Delta to the PM was then calculated in dSed5p-depleted cells as a percentage of their total fluorescence intensity over the mock-treated and mock-depleted cells. Similar to BFA- and H89-treated cells, the efficiency of transport in cells devoid of dSed5p was estimated to be 12±3% (Figure 6.3).

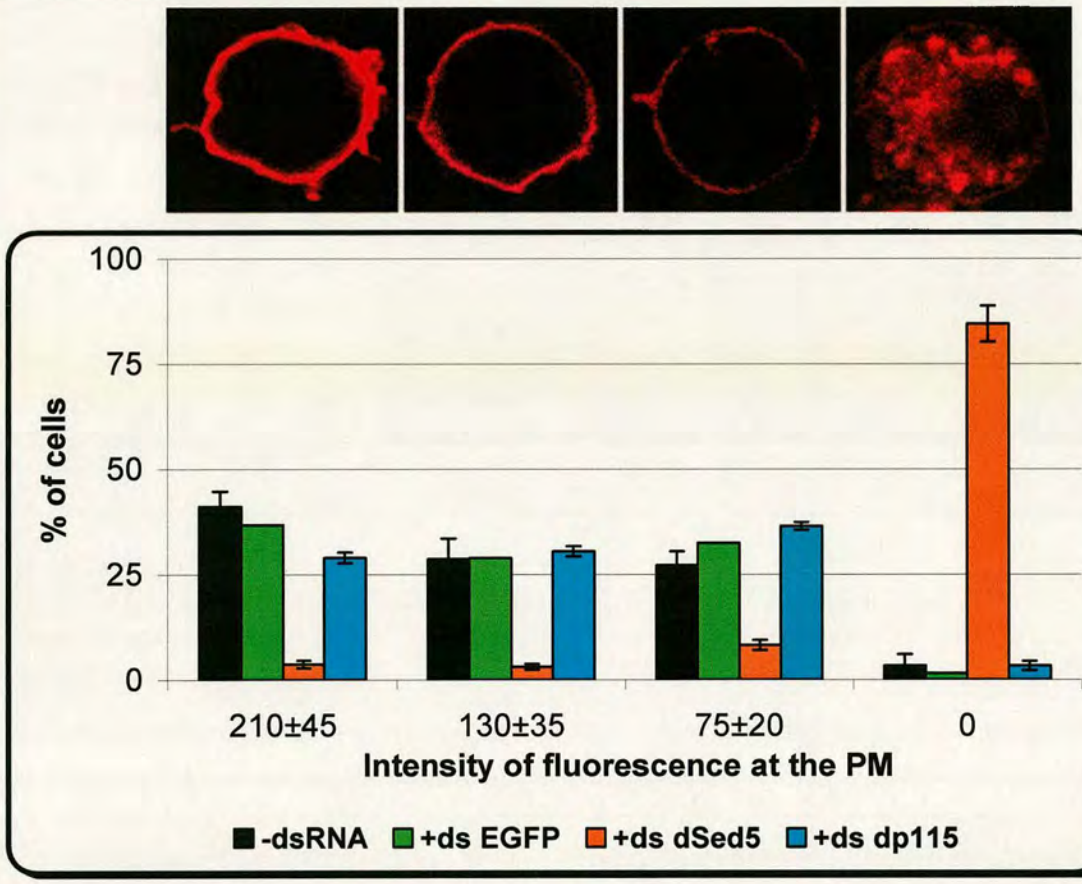

Figure 6.2: Quantification of the effect of dp115-depletion on Delta anterograde protein transport to the PM. Delta S2 cells were incubated with the indicated dsRNAs for 96 hours, and were subsequently induced for 60min using $CuSO_4$ followed by a chase of 90min. After being processed for IF and labelled for Delta, the percentage of cells exhibiting the three different intensities of plasma membrane or exclusive intracellular labelling was scored (examples of the 4 labelling categories are shown above the graph). The fluorescence intensity for each of the three categories is mentioned in x-axis. Results are expressed as a percentage of total number of cells examined (at least 500 for each condition). The error bars represent the SD. Note the small differences in distribution of cells in the 4 labelling categories between the dp115-depleted and the mock-treated or mock-depleted cells.

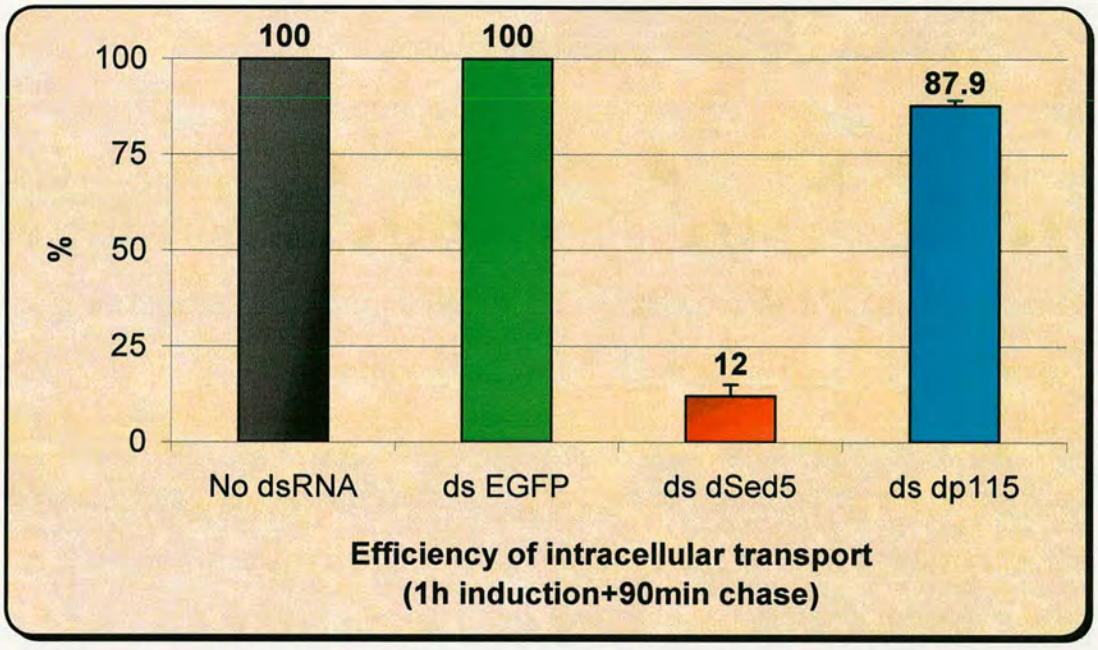

Figure 6.3: Efficiency of anterograde transport of Delta to the PM upon dp115 depletion. Total fluorescence intensity was calculated for cells incubated with ds dSed5 or ds dp115 for 96 hours, and it was expressed as a percentage compared to the total fluorescence intensity in mock-treated or mock-depleted cells, which was set as 100%. The error bars represent the SD.

6.1.2 dp115 depletion

First, Delta S2 cells depleted of dp115 were examined, since they exhibited the most profound disruption in the organisation of their early exocytic pathway. Delta transport at steady-state was measured upon dp115 depletion as described above. Surprisingly, the distribution of dp115-depleted cells in the 4 categories of PM labelling was rather similar to that of mock-treated and mock-depleted cells (Figure 6.2). A small reduction in the percentage of cells displaying high PM intensity was observed, and conversely the percentage of cells with low PM intensity was slightly increased. This was reflected in the efficiency of anterograde transport of Delta to the PM that was calculated to be 87.9±1.4%, a figure much higher

than in dSed5p-depleted cells, where anterograde transport of Delta was considered to be completely inhibited (Figure 6.3, compare the last two bars).

The lack of significant inhibition of Delta transport to the PM upon dp115 depletion was unexpected, since the mammalian p115 and the yeast homologue, Uso1p, have been shown to be required for ER to Golgi transport (Nakajima et al., 1991; Alvarez et al., 1999; Seemann et al., 2000b; Puthenveedu and Linstedt, 2001). For this reason, the initial rate of transport was measured as well, by inducing Delta expression for 25 minutes and chasing its transport to the PM for 45-90 minutes (Figure 6.4). As it was shown in figure 3.17, this protocol reflects kinetically the arrival of the bulk of Delta to the cell surface, and therefore is suitable for estimating the initial rate of transport. The initial rate of Delta transport in dp115-depleted cells was compared to that of mock-depleted cells. After 60 minutes chase the transport efficiency was lower than at steady-state (71.7±2.8% vs 87.9±1.4%), while after 90 minutes chase this figure raised to 79.7±3.1%, suggesting a convergence towards the steady-state condition. This shows that dp115 depletion only moderately inhibits anterograde transport of Delta (not more than 30%), even during the initial phase of transport.

Finally, in order to verify that the lack of transport inhibition was not due to the 20% of the dp115-depleted cells where the exocytic pathway was intact, a double labelling for dSec23p and Delta was performed. This showed that both cells exhibiting focused or disorganised tER sites could transport Delta to the PM with the same efficiency (Figure 6.5).

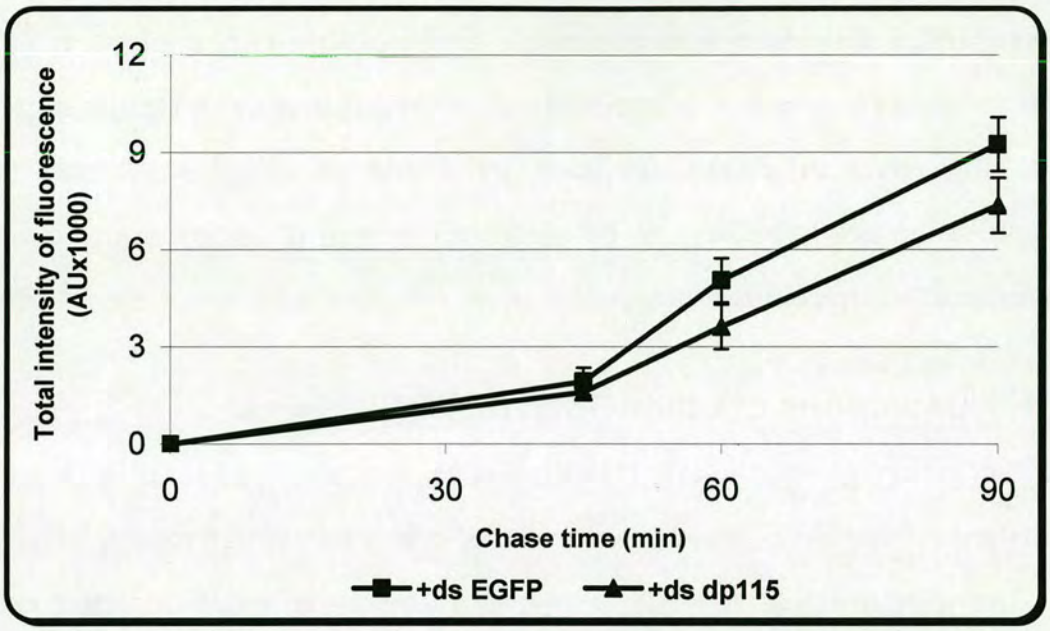

Figure 6.4: Initial rate of Delta transport to the PM in dp115-depleted cells. Delta S2 cells were incubated with ds EGFP (squares) or ds dp115 (triangles) for 96h, induced for 25min with $CuSO_4$, and Delta transport to the PM was chased for 45, 60 or 90min. Note that the efficiency of Delta transport to the PM in dp115-depleted cells is 71.7 and 79.7% compared to mock-depleted cells, after 60 and 90min chase, respectively. The error bars represent the SD

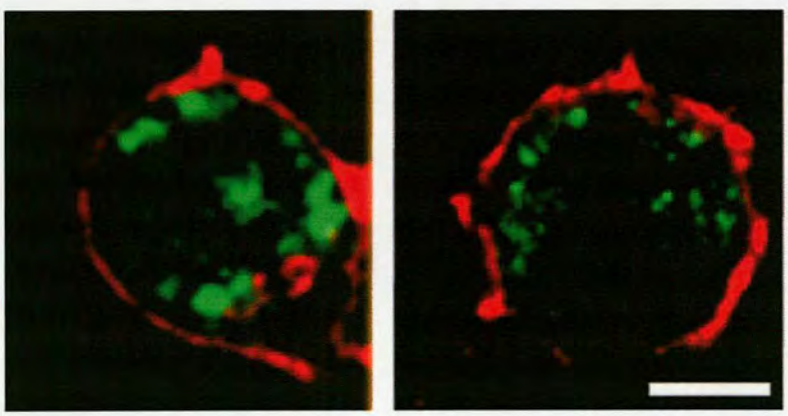

Figure 6.5: Efficiency of Delta transport to the PM is independent of the tER disorganisation. Delta S2 cells were depleted of dp115 for 96h, induced for 60min, chased for 90min, and labelled with C594.9B (red) and dSec23p (green) antibodies. A confocal section is presented here. Note that cells with focused (left) or dispersed (right) tER sites transport Delta to the PM with the same efficiency. Bar: 5µm

Although the marginal inhibition of Delta transport to the cell surface upon dp115 depletion was surprising and possible explanations will be discussed in chapter 8, it is important to point out that these results suggest that the effect of dp115 depletion by RNAi on Golgi stack and tER organisation are less likely to be secondary effects of an interference with anterograde intracellular transport.

6.1.3 Depletions of other Golgi matrix proteins

The efficiency of steady-state Delta transport was also measured in Delta S2 cells upon single or double depletion of the other Golgi matrix proteins studied (Figures 6.6 and 6.7). However, similar to dp115-depleted cells, dGM130-, dGRASP- and dGM130/dGRASP-depleted cells did not exhibit a significant decrease in Delta transport to the cell surface (Figure 6.7). A small exception were the dp115/dGM130 double depleted cells, where Delta transport was reduced by 19.9±4.3% compared to the mock-treated cells (Figure 6.7). This was due to a slight, but significant, increase in the percentage of cells displaying low and exclusively intracellular Delta labelling (Figure 6.6, red bars).

Nevertheless, in general, the conclusion drawn from the use of Delta transport assay was that the RNAi-mediated depletions of the Golgi matrix proteins tested impaired only marginally anterograde protein transport. Moreover, these results suggested that, at least in *Drosophila* S2 cells, protein transport can still be sustained almost to normal levels by a seemingly disorganised exocytic pathway, i.e. in the absence of Golgi stacks and with the tER sites being extensively dispersed.

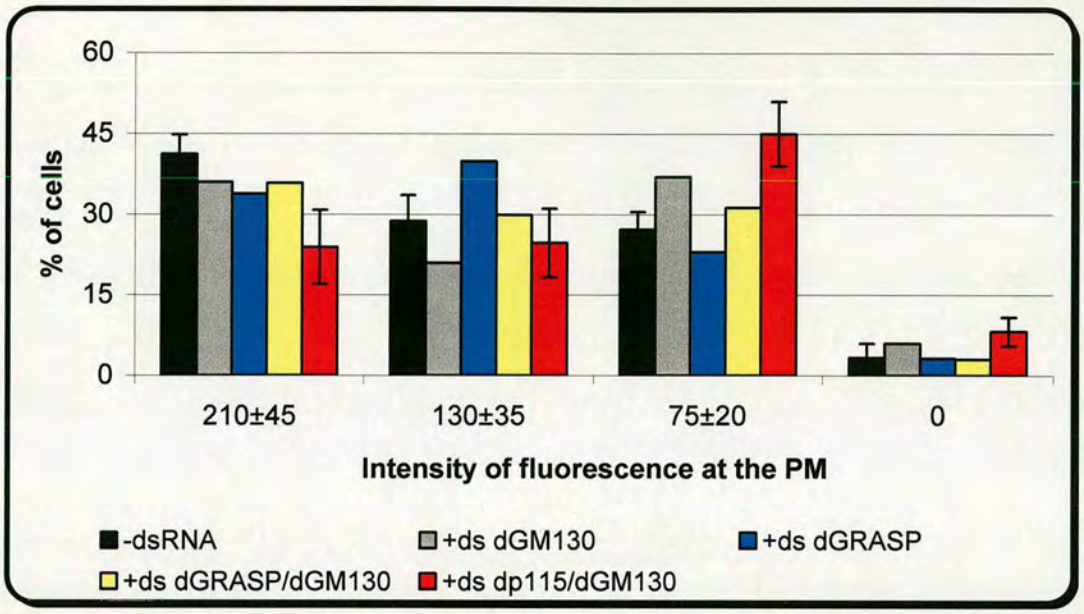

Figure 6.6: Quantification of the effect of Golgi matrix protein depletion on Delta anterograde protein transport to the PM. Delta S2 cells were incubated with the indicated dsRNAs for 96 hours, and the cells were processed and quantified as described in figure 6.2. Note the similar distribution in the 4 labelling categories between the mock-treated cells and those depleted of the Golgi matrix proteins. dp115/dGM130 double depleted cells (red bars) were an exception in that they displayed a reduced percentage of highly PM labelled cells, while cells with low and intracellular Delta labelling were increased.

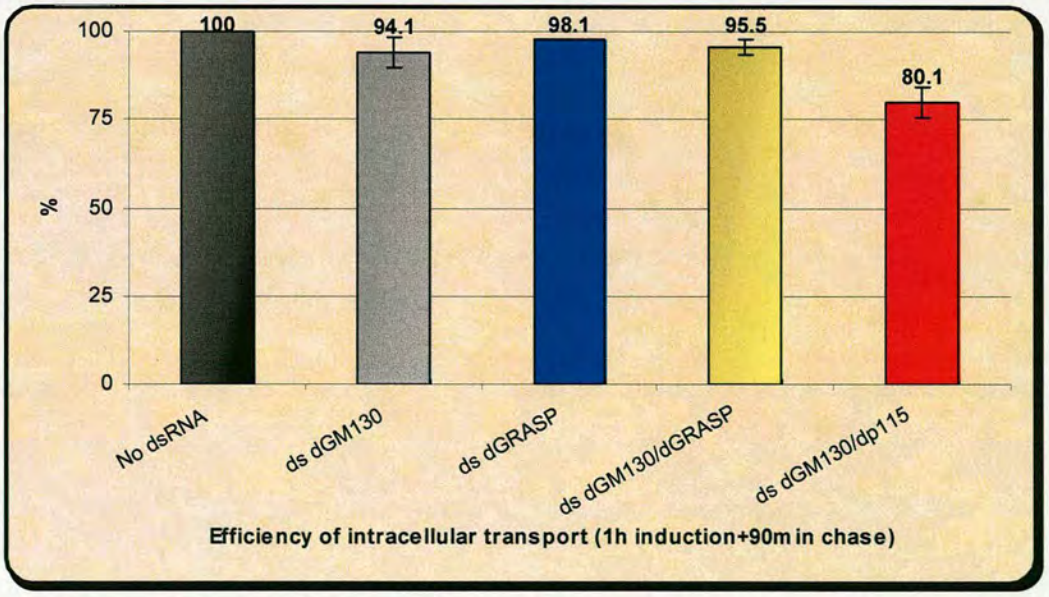

Figure 6.7: Efficiency of anterograde transport of Delta to the PM upon Golgi matrix protein depletion. Total fluorescence intensity was calculated for cells incubated with ds dGM130, ds dGRASP, dGRASP/dGM130 and ds dp115/dGM130 for 96 hours, and it was expressed as a percentage compared to the total fluorescence intensity in mock-treated cells that was set as 100%. The error bars represent the SD.

6.2 Recombinant antibody secretion assay

The unexpected lack of significant inhibition in Delta transport to the PM in S2 cells upon the depletion of *Drosophila* Golgi matrix proteins was contradictory to the reported involvement of their mammalian and yeast homologues in transport along the exocytic pathway. Therefore, the use of an independent transport assay was necessary to confirm the results obtained by Delta transport assay and to ensure that the observed marginal inhibition did not applied specifically on Delta anterograde traffic. For this reason, another stable S2 cell line, scAb-S20, was used (gift from Brian Reavy, SCRI, Dundee, UK). This cell line is transfected with a construct expressing a secreted recombinant monoclonal antibody (soluble chain variable fragment scFv) tagged with the human kappa light chain (Ck) (Reavy et al., 2000). Like in Delta S2 cells, the expression of scFv-Ck is also under the control of the metallothionein promoter, which is activated by addition of $CuSO_4$ in the culture medium.

The principle of the recombinant antibody secretion assay was similar to that of Delta transport assay. First, the cells were depleted of a given Golgi matrix protein and subsequently, synthesis of the recombinant antibody was induced by $CuSO_4$. The efficiency of scFv-Ck transport through the Golgi apparatus and its secretion to the extracellular medium was monitored by analysing a fraction of the medium by Western blotting. Unfortunately, in order to be able to detect the secreted Ck-tagged recombinant antibody in the culture media, it was necessary to induce the cells for a minimum period of 24 hours (Reavy et al., 2000). By increasing the amount of medium loaded on the SDS-PAGE gels, a signal for scFv-Ck was detectable after 16 hours of induction with $CuSO_4$.

This assay was used to investigate the efficiency of scFv-Ck secretion in dp115-depleted and dGRASP/dGM130 double depleted cells for 96 hours, which were two conditions that imposed quantitative alterations on the early exocytic pathway. First, induced and non-induced cell extracts were checked to rule out the possibility of a leaking in the expression of the recombinant antibody. As expected, no protein was detected in the lane containing the extract of non-induced cells (Figure 6.8A). Moreover, dp115-depleted cells were found to be induced at least as efficiently as mock-treated cells (Figure 6.8A). In agreement with the outcome of Delta transport assay, dp115-depleted cells secreted comparable amounts of scFv-Ck to mock-treated cells (Figure 6.8A), and quantification of the bands showed that there was a reduction of only 10% in scFv-Ck secretion. The same held true for the scAb-S20 cells depleted of both dGRASP and dGM130 for 96 hours (Figure 6.8B). The quantitation in this case showed an even smaller decrease in scFv-Ck secretion (4.8%), when compared to the mock-treated cells.

This system was not used as widely as Delta transport assay in monitoring anterograde protein transport in S2 cells, because of the long induction period that was required. This parameter could induce high over-expression of the secretion marker, which in turn could alter the morphological effects observed upon Golgi matrix protein depletions. Indeed, when cells depleted of dp115 for 96 hours and induced with $CuSO_4$ for 16 hours were examined by EM, 41.9% of them exhibited Golgi stacks (vs. 19.9% of the non-induced cells). This suggests that the high over-expression of ScFv-Ck led to a partial reversion of the Golgi stack breakdown phenotype produced by dp115 depletion. Despite this pitfall, in both cases that this secretion assay was applied, the depletion of the Golgi matrix proteins was not reverted by the long induction, and this provides strong support to the

conclusion that S2 cells depleted of these proteins by RNAi are still largely competent to sustain anterograde protein transport.

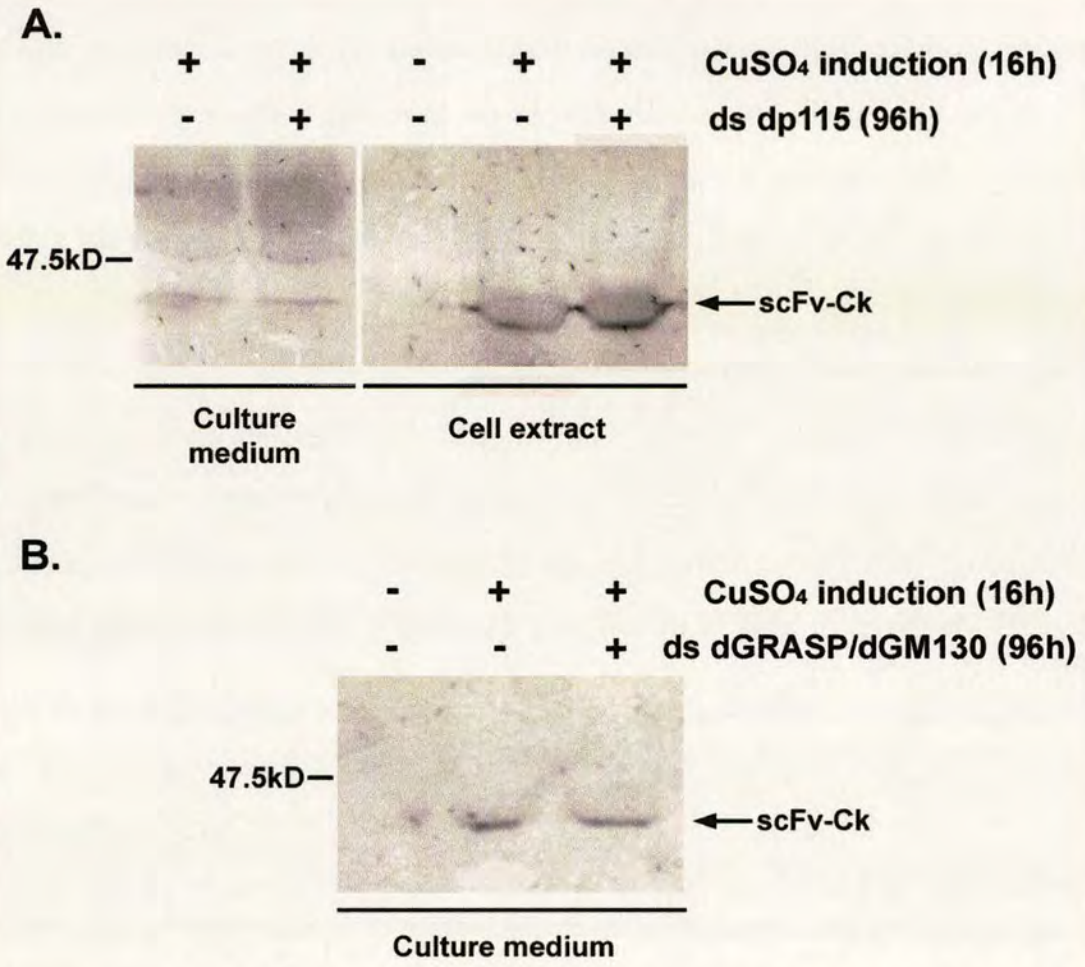

Figure 6.8: Effect of Golgi matrix protein depletions on the secretion of scFv-Ck recombinant antibody. A. scAb-S20 cells were incubated without (-) or with (+) ds dp115 for 96h and were induced (+) or not (-) with $CuSO_4$ for 16h. The cells were then separated from the cultured media, and 1.5% of the culture medium (~22µg of protein) and 3 million cells were analysed by Western blotting using the an anti-Ck antibody coupled to alkaline phosphatase. The visualisation of the bands was performed with SigmaFast NBT/BCIP substrate kit. **B.** Mock-treated and dGRASP/dGM130 double depleted cells for 96h were processed for Western blotting as mentioned in A. 1.5% of the culture medium from each sample (~24µg of protein) was analysed. Note that in both cases the secretion of scFv-Ck is comparable between control cells and cells depleted of Golgi matrix proteins.

Chapter Seven

Golgi stack biogenesis in Drosophila imaginal discs

In the previous chapters, it was described that the RNAi-mediated depletion of Golgi matrix proteins from S2 cells led in several occasions to the conversion of the Golgi stacks that are normally observed in these cells into clusters of vesicles and tubules. However, anterograde transport of a plasma membrane and a secreted marker was not significantly affected. This was surprising, because in mammalian cells the integrity of the Golgi structure is usually considered to be intrinsically linked to the essential role of the Golgi apparatus in intracellular transport. In *Drosophila*, though, there are at least two stages during development when vesicular-tubular clusters are observed instead of the typical Golgi stacks, and these are the early embryos prior and during cellularisation (Fullilove and Jacobson, 1971; Mahowald et al., 1983; Ripoche et al., 1994) and the salivary glands in early third instar larvae (Thomopoulos et al., 1992). Despite the absence of Golgi stacks, there is no evidence to suggest that intracellular transport is arrested under these conditions, since at least constitutive transport or secretion of several proteins is still essential at these developmental stages. Moreover, enzyme and immuno-histochemistry has shown that these clusters seem to carry out Golgi functions (Thomopoulos et al., 1992; Ripoche et al., 1994).

7.1 Morphometrical characterisation of Golgi stack biogenesis in imaginal discs

During the transition between the early third instar larvae to white pupae, 20-hydroxy-ecdysone (ecdysone) displays a peak in its concentration, which has been shown to be responsible for the many morphogenetic events at the end of third larval instar, through a cascade of transcription activation and repression events (Fristrom and Fristrom, 1993; see also introduction). The first phase of the imaginal disc elongation that takes place during third larval instar was thought to be a suitable developmental stage to describe the biogenesis of the Golgi stacks from vesicular-tubular clusters, since their

elaborate morphogenesis is likely to require modifications of the exocytic pathway.

The morphological studies focused on the leg and wing imaginal discs of third-instar larvae before, at, and after the onset of disc elongation. Discs from early and mid-third-instar larvae have not begun to elongate (average leg disc thickness 30–40 μm), whereas those from late third-instar larvae have (average thickness between 45 and 90 μm), and those from white pupae have completed the first phase of elongation (thickness ~240 ± 10 μm).

Discs were dissected from larvae at each developmental stage, fixed, and processed for conventional electron microscopy. The surface section of the disc cells in each developmental stage (indicating the cell size), as well as the volume density of their cytoplasm (representing the cell volume occupied by the cytoplasm), were estimated. Disc cells of the mid- and late third-instar larvae and white pupae were on average of the same size and 30% larger than the ones of early third-instar larvae, an increase largely reflecting an increase in the cytoplasmic volume. This indicates that the 6-fold increase in disc thickness could stem from the unfolding of the concentric folds (see section 1.7.2), and not from a substantial change in cell size with the exception of the initial increase.

When observed at higher magnification, the cells of early third-larval instar discs appeared dense and their endomembranes poorly developed. Although these were interphase cells, no Golgi stacked cisternae could be observed. Instead, small clusters of vesicles and tubules (Figure 7.1A and B) were present often nested in the concavity of a cup-shaped ER cisterna. The vesicles had a 50–70-nm diameter, although larger vesicular profiles and short tubules (150–200 nm in length) were also observed. The surface density of these clusters (Sorg/Vcyt) was 1.30 ± 0.07 μm^{-1} (Table 7.1). In addition, the percentage of the larval cluster membranes in vesicles, tubules, and cisternae

was calculated (Table 7.1), showing that the clusters consisted mostly of small vesicles (~81.5%) and tubules (~17.5%), but were almost devoid of cisternal profiles (1%).

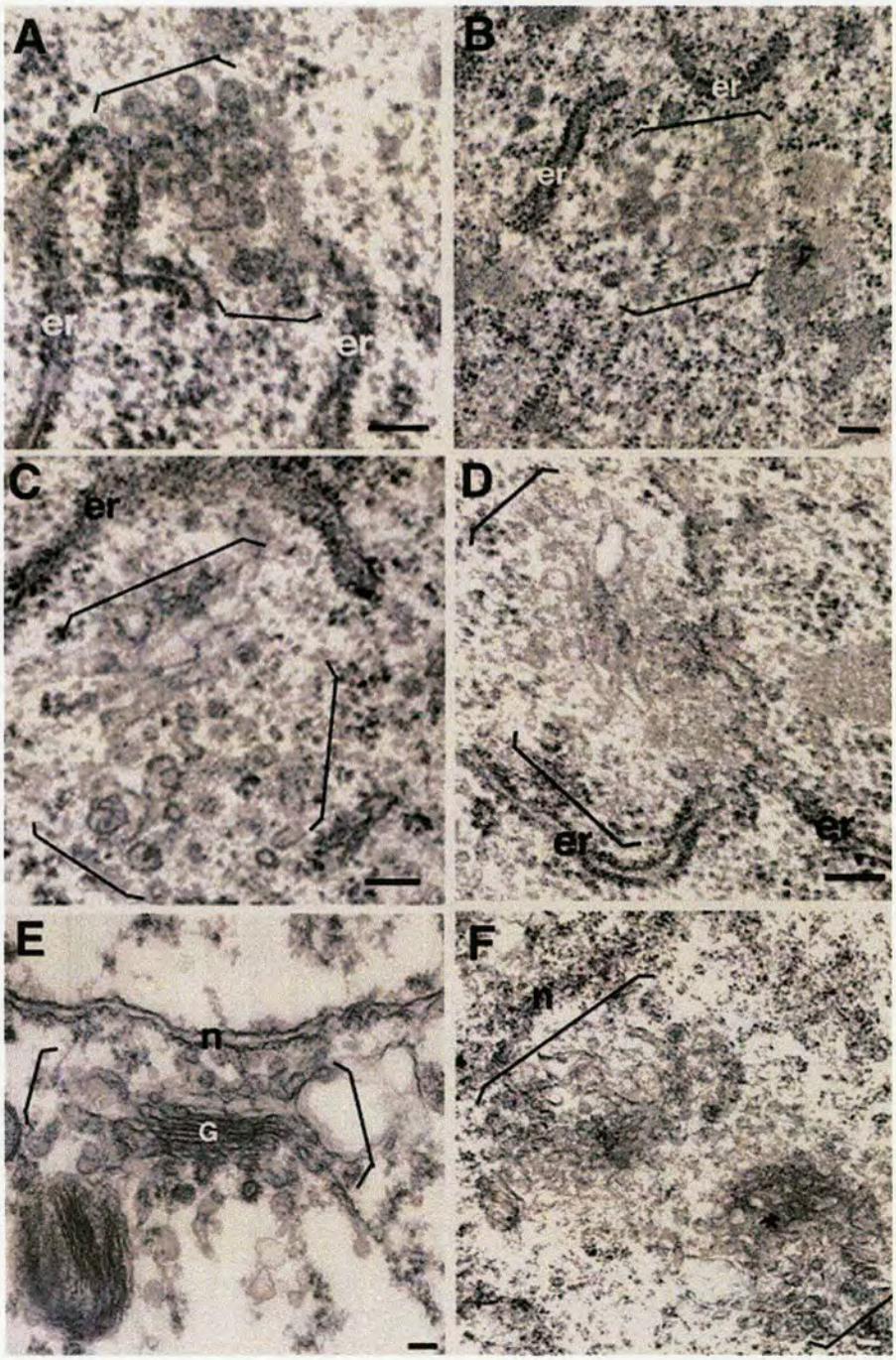

Figure 7.1: Larval clusters and Golgi areas in discs from third-instar larvae and white pupae. Imaginal discs from early (A,B), mid (C) and late third instar larvae (D), or white pupa (E,F) were fixed in 1% GA for 2h and processed for conventional EM. Larval clusters and Golgi area were visualized in leg and wing imaginal discs, and their borders are marked between brackets. Stacks are indicated with a G. In F, the asterisk indicates an *en face* view of a fenestrated cisterna. Note the proximity of the larval clusters to ER cisternae (er) in A-D. n, nuclear envelope. Bars, 100nm.

The cells of mid third larval instar discs were less dense than in the previous stage, and they exhibited clusters of vesicles and tubules again nested in ER cup-shaped cisternae in 85% of the cases. The mid-third instar larval clusters displayed a surface density of 1.56±0.05 μm^{-1} (Table 7.1). Interestingly, out of these larval clusters, the larger in size often contained cisternal elements among the observed vesicles and tubules (Figure 7.1C), which raised the percentage of cisternal membrane to 7.6% (Table 7.1).

In late third-instar larvae, the observed clusters exhibited increased surface density (3.17±0.09μm^{-1}), and contained 28.6% of their membrane in cisternae (Figure 7.1D), while the remaining membranes were vesicles and tubules (Table 7.1). At this stage, typical Golgi stacks were observed for the first time.

Finally, in the white pupal disc cells, Golgi stacks were clearly visible. The surface density of the Golgi areas within the cytoplasm was 4.87±1.10 μm^{-1} (Table 7.1), and they comprised stacked cisternae (Figure 7.1E) and extensive tubular networks around the cisternae (Figure 7.1F). The percentage of Golgi membrane found in cisternae increased to 56.8%, while 65% of them were stacked (Table 7.1).

Table 7.1. Stereological analysis of the organelle (larval clusters and Golgi areas) at the different stages of disc elongation. org refers to the larval clusters or the Golgi apparatus when clearly identifiable. Results are expressed as ±SD. Nd, not determined

				% of org membranes in			
	Sorg/Vorg in μm^{-1}	**Vorg/Vcyt**	**Sorg/Vcyt in μm^{-1}**	**Vesicular profiles**	**Tubules**	**Total cisternae**	**Stacked cisternae/Total cisternae**
Early 3rd instar	72.46±8.1	0.018±0.006	1.30±0.07	81.5±12.3	17.5.5±12.0	1.0±1.0	nd
Mid 3rd instar	70.02±4.5	0.024±0.004	1.56±0.05	57.3±11.7	35.1±13.7	7.6±3.5	nd
Late 3rd instar	66.14±2.7	0.048±0.015	3.17±0.09	28.4±12.3	43.1±10.1	28.6±10.2	0.25±0.10
White pupa	61.25±6.4	0.079±0.021	4.87±1.10	12.8±5.4	30.3±12.3	56.8±13.2	0.65±0.20

This succession of different morphological features, from vesicles and tubules in larval clusters with increasing cisternal elements to proper prepupal Golgi stacks, suggested a temporal conversion of vesicles and tubules to cisternae. However, the surface density of the organelle (larval clusters or Golgi stacks) within the cytoplasm (Sorg/Vcyt) increased as the cisternae formed. The surface density of organelle within the cytoplasm is composed of two components (see materials and methods, section 2.4.4.2): First, the surface density of organelle membranes within the volume they occupy (Sorg/Vorg) gives an indication of how packed the membranes are within a unit of volume and was comparable from one stage to the next (Table 7.1, column 1); second, the volume density of the organelle membranes within the cytoplasm (Vorg/Vcyt) reflects the cytoplasmic fraction occupied by these membranes, and was found to increase from the early third larval instar to white pupa stage (Table 7.1, column 2). This means that the amount of membrane per unit of volume was similar at the different stages, but more membrane structures were added to the organelle, leading to an increase in the volume they occupy. Because of this membrane addition, it was possible that the observed stacks would not derive from the larval clusters, but from entirely newly generated membranes. Thus, it was important to establish that the observed larval clusters were Golgi stack precursors.

7.2 Do larval clusters have Golgi identity?

7.2.1 Immuno-localisation of Golgi markers

In order to address the question of whether the larval clusters are another form of the Golgi apparatus, a number of different proteins related to the Golgi structure and function was examined for their localisation on these clusters.

First, the localisation of dGM130 was investigated by applying the MLO7 in indirect immunofluorescence experiments on wing and leg imaginal discs dissected from wild type (WT) mid-third-instar larvae. A punctate staining throughout the cytoplasm (Figure 7.2A), characteristic of the Golgi apparatus in *Drosophila* tissues was observed (Ripoche *et al.*, 1994; Stanley *et al.*, 1997; Rabouille *et al.*, 1999; Lecuit and Wieschaus, 2000; Munro and Freeman, 2000; Sisson *et al.*, 2000). In an effort to show the spatial arrangement of dGM130 staining with respect to the ER network of these very small disc cells (~5 μm in width), double labelling was performed for dGM130 (MLO7 antibody) and protein disulfide isomerase (PDI; 1D3 antibody), which is an ER resident chaperone marking the ER cisternae (Fricker et al., 1997). The 1D3 antibody was raised against the 12 C-terminal peptide of human PDI (Fricker et al., 1997), which displays 75% similarity to its *Drosophila* homologue (KDDDQKAVKDEL vs. EEEEEAPKKDEL; McKay et al., 1995). The PDI pattern was indeed reminiscent of the ER network, as the labelling extended throughout the cytoplasm surrounding the nucleus (Figure 7.2B) Additionally, small puncta were distinguishable, but the dots were smaller, more numerous, and more scattered than the dGM130 pattern. The partial colocalisation between dGM130 and the ER marker (Figure 7.2B) is also in agreement with the EM studies on S2 cells, where a portion of dGM130 was confined on ER membranes (Figure 4.3).

A very similar punctate pattern was obtained with the NN7 antibody (Figure 7.2C), which is raised against the full-length rat p115 (see table 2.6), but cross-reacts with dp115 (Kondylis et al., 2001). Furthermore, an antibody recognising δ subunit of the rat AP3 adaptor complex was used for IF in imaginal discs. δ-AP3, which has been shown to localize in the *trans*-Golgi network in mammalian cultured cells (Simpson et al., 1997), exhibits high homology to the *garnet* gene product in *Drosophila*. Similar to MLO7 and

NN7, anti-δ-AP3 antibody produced a punctate pattern reminiscent of the Golgi distribution in imaginal disc cells (Figure 7.2D). This was in line with the labelling of Golgi membranes by this antibody in S2 cells (Rabouille et al., 1999).

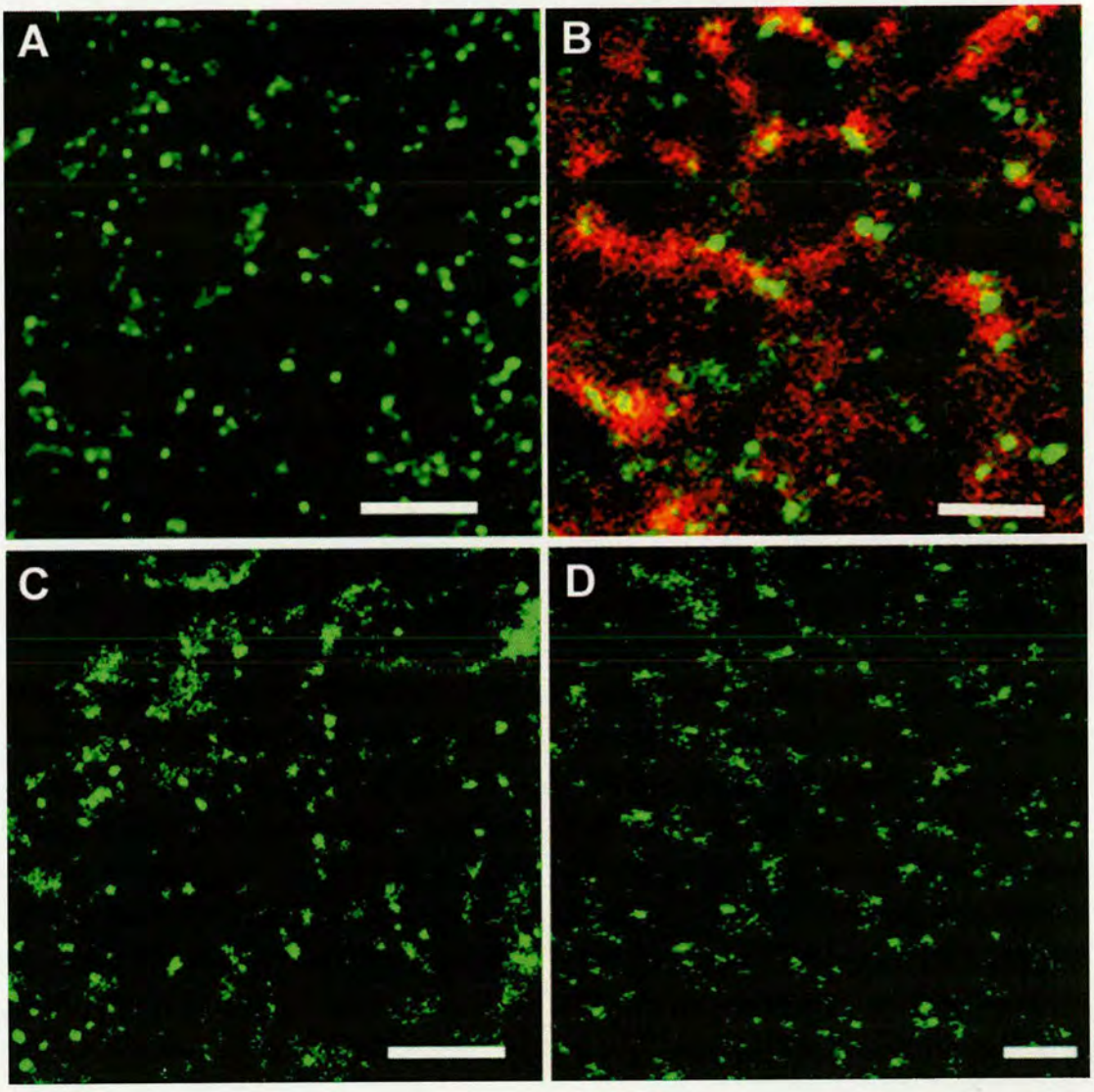

Figure 7.2: Immunofluorescence imaging of the larval clusters in imaginal disc cells. A. dGM130 immunofluorescence pattern was visualized in mid-third-instar larval leg and wing discs labelled with rabbit polyclonal MLO7 serum followed by an anti-rabbit IgG conjugated with FITC (green). Note the dots surrounding a black space (nucleus). **B.** Discs were double labelled with MLO7 and 1D3 antibodies followed by an anti-rabbit IgG conjugated with FITC (green) and an anti-mouse IgG conjugated with Texas Red (red), respectively. Note that the green dots overlap partially with the red staining representing the ER. **C.** Discs were also labelled with NN7 (anti-p115 antibody), and **D.** an anti-δ-AP3 antibody, followed by an anti-rabbit IgG conjugated with FITC. Note that the pattern in A, C, and D are similar. The pictures represent single confocal sections. Bars: 5μm.

As an alternative way to confirm the Golgi identity of the disc larval clusters, the glycosyltransferase Fringe was used, which has recently been shown to function as a Golgi glycosylation enzyme (Bruckner et al., 2000; Munro and Freeman, 2000). Homozygous transgenic flies carrying UAS-Fringe-DXD tagged with the myc epitope (stock MF919) were used for this experiment. These flies carry a transgene comprising the Fringe cDNA, in which the glycosyltransferase DDD motif has been replaced by DXD that abolishes the glycosyltransferase activity, but retains the Golgi localization (Munro and Freeman, 2000).

Male MF919 flies were crossed with female hsGAL4/Bc,Elp,Gla flies (see table 2.4), and larvae from the F1 progeny were selected against the presence of Bc gene (black cell phenotype). Prior to the collection of UAS-Fringe-DXD-myc/hsGAL4 larvae, two heat-shock treatments (each of 20min at 37°C) were performed to induce Fringe-DXD-myc expression. Mid-third-instar UAS-Fringe-DXD-myc/hsGAL4 larvae were collected, and their leg and wing discs were dissected, and processed for IF or IEM.

Fringe-DXD-myc was expressed ubiquitously at low level and its localisation was performed on ultrathin sections of unicryl-embedded discs (section 2.4.4.3) using 9E10 (monoclonal anti-myc antibody; see tables 2.5 and 2.6). Fringe-DXD-myc was localized to the larval clusters (Figure 7.3A-B) and Golgi stacks when present (Figure 7.3C). Although, normally, Golgi stacks are not observed at mid-third instar, it seems that the heat shock for the induction of Fringe drove some of the clusters to be converted into stacks. A similar effect was also observed in flies overexpressing a transgene of the *Drosophila* homologue of NSF ATPase (dNSF1; Pallanck et al., 1995), the expression of which is under the control of a heat-shock promoter. Because of the low labelling efficiency, the relative distribution of the gold particles corresponding to Fringe was performed by summing up 65 gold particles in

>20 micrographs. The labelling was confined to the ER (35%) and larval clusters or Golgi stacks (65%). No other membrane compartment was labelled except for the plasma membrane where a small percentage of gold particles was localised.

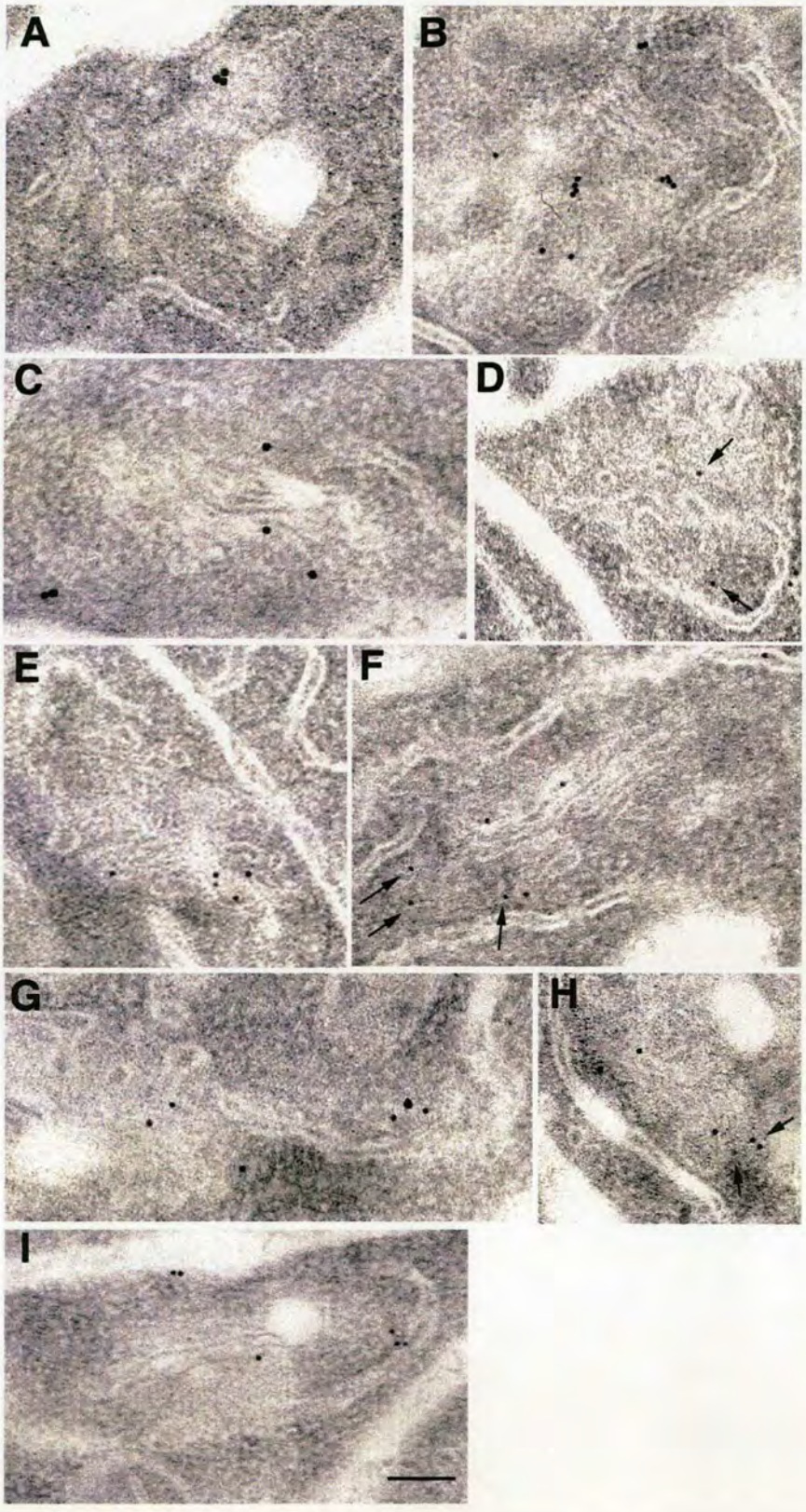

Figure 7.3: Localization of Golgi proteins on larval clusters and Golgi stacks by immuno-EM. Unicryl-embedded mid-third instar imaginal discs expressing low level of Fringe-DXD-myc were sectioned and labelled with 9E10 (anti-myc antibody) followed by anti-mouse IgG conjugated to 15-nm gold (A–C), MLO7 (anti-GM130 antibody) followed by anti-rabbit IgG conjugated to 10-nm gold (D–F), and NN7 (anti-p115 antibody) followed by anti-rabbit IgG conjugated to 10-nm gold (G–I). Note that the larval clusters (A, B, D, E, G, and H) and the Golgi areas comprising a stack (C, F, and I) were labelled by the three antibodies. The arrows in D, F, and H indicate gold particles that may be difficult to see. Bar: 100nm.

With the use of the same material, MLO7 was used to visualize dGM130 that was found in larval clusters (Figure 7.3D-E) and Golgi stacks (Figure 7.3F). Again, the only membrane compartments that were labelled were the clusters or stacks (66.6±12.8%) and the ER (33.4±9.9%) (167 gold particles counted). A similar result was obtained by applying NN7 to visualise dp115 (Figure 7.3G-I). The clusters and stacks were labelled (67.1±10.6%), as well as the ER membranes (32.9±8.6%) (147 gold particles counted). The labelling density of the Golgi stacks or the larval clusters was 9.8±3.2 times over background for Fringe-DXD-myc, 10.1±4.1 for dGM130, and 8.4±2.9 for dp115 (nuclear labelling was considered as background labelling).

In confocal immunofluorescence imaging, Fringe appeared to localise in spots surrounding the nucleus (Figure 7.4A) in a similar pattern to dGM130. Imaginal discs were also double labelled with MLO7 and 9E10. When the level of Fringe expression was low, the overlap with dGM130 was significant (Figure 7.4B-C). In 84±6% of the observed structures, there was either a complete (yellow), or partial overlap (yellow in combination with either green or red). The same pattern was obtained in discs labelled with NN7 and 9E10 (Figure 7.4D-E). 80±7.6% of Fringe-DXD-myc structures were partially or completely colocalising with dp115-positive structures.

Taken together, these results suggested that the larval clusters contained at least four Golgi markers (dGM130, dp115, Fringe, and δ subunit of AP3), and therefore, this indicated that at least a significant proportion of the membranes comprised within the larval clusters is Golgi membranes.

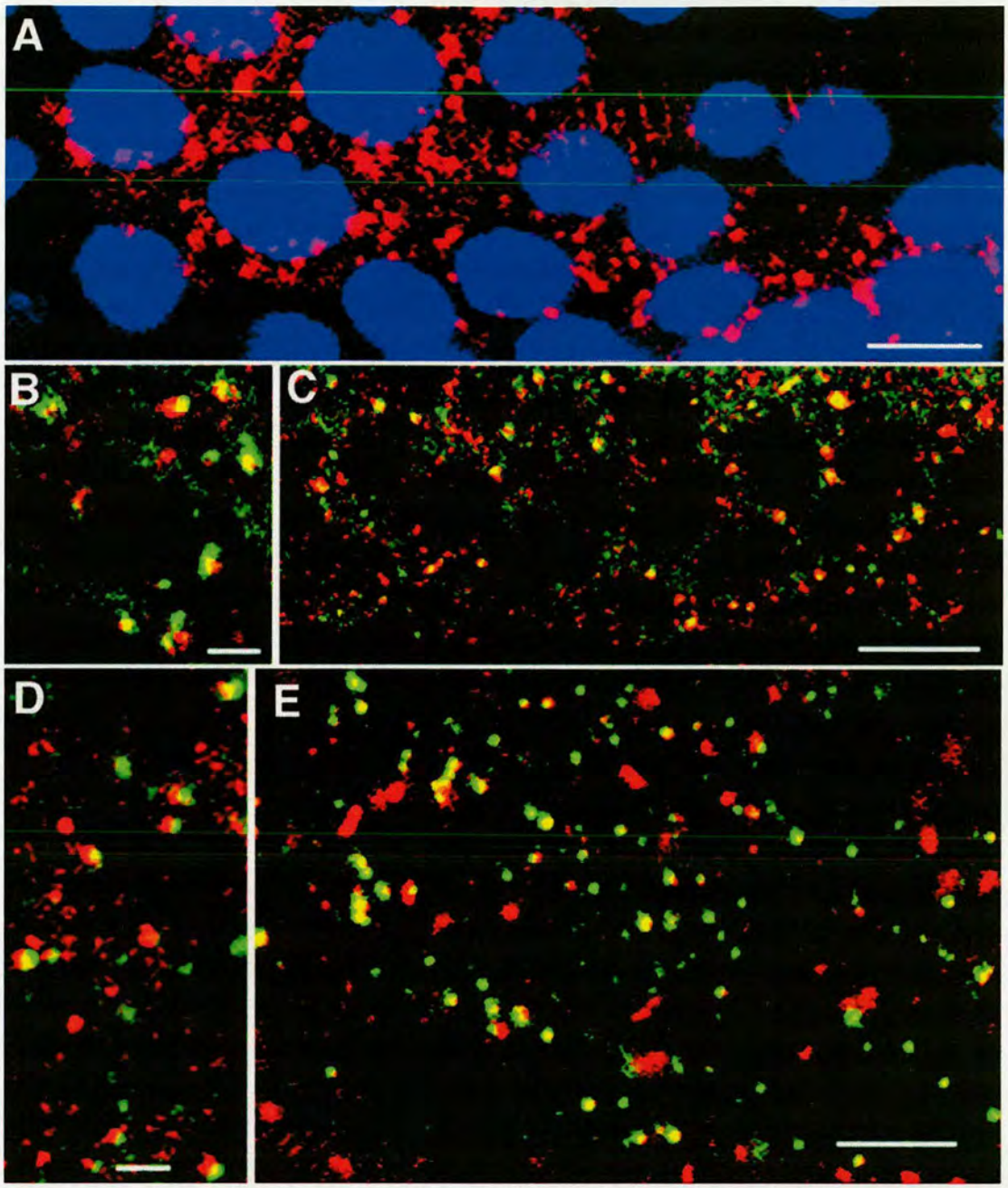

Figure 7.4: IF localisation of dGM130, dp115, and Fringe in mid-third-instar larval discs cells. UAS-Fringe-DXD-myc/hsGAL4 flies were induced by heat shock to synthesize myc-tagged Fringe-DXD. Mid-third-instar larval discs were then immuno-labelled using 9E10 monoclonal antibody followed by an anti-mouse IgG conjugated with Texas Red (red), and DAPI (blue) (A). Note the dots around the nucleus. These discs were also double labelled with 9E10 and either MLO7 (B and C) or NN7 (D and E) followed by an anti-mouse IgG conjugated with Texas Red (red) and an anti-rabbit IgG conjugated with FITC (green), respectively. Note in both cases the extensive partial (yellow, green, and red) or complete (yellow) colocalisation between the labelled proteins. The pictures represent single confocal sections. Bars: 5µm.

7.2.2 Immuno-localisation of tER markers

As it was mentioned previously, the larval clusters in early third-instar larvae consisted of >80% vesicles (Table 7.1), most of them being 50–70 nm in diameter, consistent with the geometrical features of COP I- and COPII-coated vesicles. Moreover, larval clusters were very often located in close proximity to a cup-shaped ER cisterna, which resembles the structural organisation of tER sites in S2 cells (compare figure 7.1A-B with figures depicting tER sites in chapter 3).

In order to test whether the vesicular-tubular larval clusters comprised COPII-coated membrane structures, the COPII coat subunits dSec23p and dSec31p (Barlowe, 2002) were localised using antibodies raised against the mammalian homologues of these two proteins. The immunofluorescence distribution of dSec23p and dSec31p was punctate throughout the cytoplasm, and the COPII spots colocalised partially with the ER network marker, PDI (Figure 7.5A-B). This pattern was reminiscent of that observed for dGM130 or dp115.

Mid-third-instar larval discs dissected from induced UAS-Fringe-DXD-myc/hsGAL4 flies were also labelled for dSec23p or dSec31p, and Fringe-DXD-myc (Figure 7.5C-D). When the level of Fringe expression was low, these markers exhibited approximately 60% colocalisation, approaching the figures obtained in colocalisation experiments between Fringe-DXD-myc and dGM130 or dp115. However, a significant number of the observed IF spots were solely positive for tER marker or Fringe. This could reflect two types of experimental limitations. First, the cells did not express the different proteins at the same level, and even within a cell, not all larval clusters were labelled with the same intensity. As a result, the overlap was variable and technically difficult to visualize. Second, the heat shock necessary to induce Fringe expression drove partially the conversion of some of the clusters into

Golgi stacks (Figure 7.3). In this case, it is expected that Fringe would localise mainly in the Golgi stacks, whereas dSec23p would remain at the tER sites. These subtle localisation differences could account partly for the lack of colocalisation in the IF experiments. Furthermore, it could also mean that not all ER exit sites are involved in the formation of larval clusters.

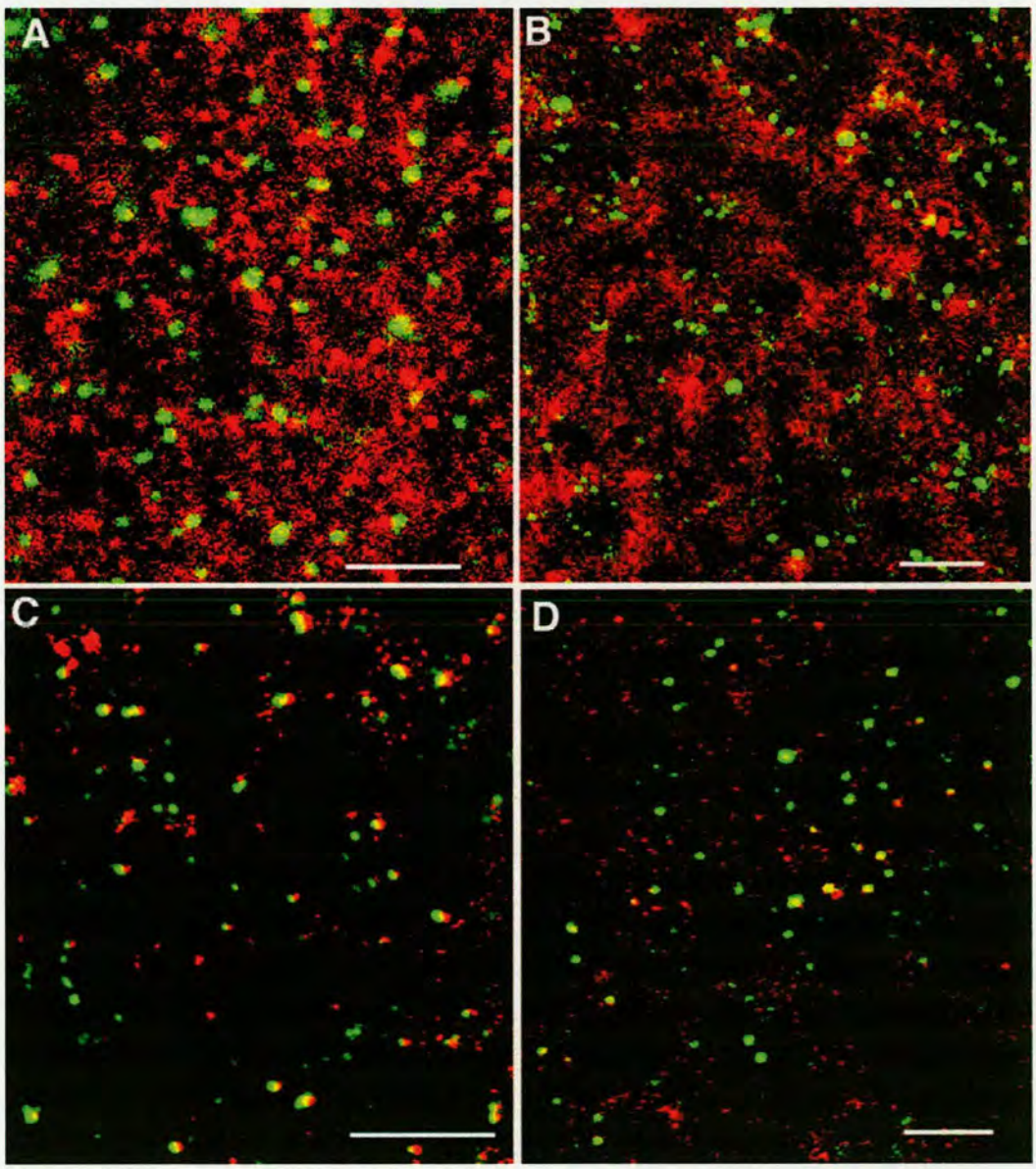

Figure 7.5: Immunofluorescence labelling of the larval clusters with components of the COPII machinery. UAS-Fringe-DXD-myc/HsGAL4 mid-third-instar larval discs were immunolabelled with the anti-Sec23p antibody (A and C) or Sec31p antibody (B and D) together with 1D3 (A and B) and 9E10 (C and D) followed by an anti-rabbit IgG conjugated with FITC and an anti-mouse IgG conjugated to Texas Red, respectively. Note in C and D structures in which dSec23p, dSec31p, and Fringe overlap completely or partially together with structures that contain only dSec23p or dSec31p or only Fringe. The pictures represent single confocal sections. Bars, 5 μm.

Overall, these results suggest that dGM130, dp115, dSec23p, dSec31p, and Fringe-DXD-myc colocalise extensively in the larval clusters, which seem to be populated by COPII-coated membranes. Nevertheless, in the absence of IEM studies, it cannot be ruled out that the COPII subunits and Fringe mark distinct membrane areas of the larval clusters.

7.3 Expression of Golgi-related proteins during the transition between mid- and late-third larval instar

A logical explanation why Golgi stacks were not observed during the early- and mid-third instar larval discs could be that the expression level of proteins necessary for building the Golgi stacks is below a functional threshold that could sustain their formation. On the contrary, at late third instar larvae, this threshold in protein expression may be reached, and therefore, this could drive the formation of Golgi cisternae and stacks. The Golgi stack biogenesis during the transition from early-third larval to white pupal stage coincides, temporally, with the prepupal peak of ecdysteroid hormone, ecdysone. Given the known activity of ecdysone as a gene expression regulator, it was hypothesised that it may trigger the expression of genes involved in the assembly of the Golgi stacks.

In order to test this hypothesis, the expression level of proteins related to Golgi structure and function were examined in imaginal discs from mid- and late-third instar larvae. To ensure that the selected larval samples were at the right stage (i.e. before and after the ecdysone pulse), in addition to larval behavioural characteristics, the morphology of the salivary glands was used as a criterion to distinguish between mid- and late-third instar larvae. More specifically, the prepupal ecdysone peak has been shown to stimulate the glue secretion into the lumen of the gland leading to its swelling, compared to its bumpy appearance during mid-third instar when the glue

granules are accumulating inside the cells (Boyd and Ashburner, 1977; Biyasheva et al., 2001; see also section 2.5.2).

The protein expression of *Drosophila* Golgi mannosidase II (dGMII), dSec23p, dGM130, dp115 and the *Drosophila* β' COP subunit was monitored. Regarding dSec23p and dGMII, a significant increase in labelling intensity was observed between the mid- and late third instar larvae wing imaginal discs (Figure 7.6) that was estimated at 4.5±1.0 fold in both cases. A similar increase in the expression of these two proteins was also detected in leg imaginal discs from the same stages. This result correlated nicely with the upregulation of dSec23p expression as measured by Western blotting (Kondylis et al., 2001). Nevertheless, it should be pointed out that the changes in the expression of the proteins were not always uniform within each imaginal disc population (see numbers accompanying each example in figure 7.6).

The protein expression of dp115 and dGM130 was slightly elevated between mid- and late-third instar larvae, and a 2.5- and 2.8-fold enhancement of the fluorescent signal was estimated, respectively (Figure 7.6). The homogeneity among the different discs of the same stage was lower compared to dSec23p and dGMII (approximately 65% homogeneity; see figure 7.6). One reason that could account for this reduced homogeneity between the imaginal discs from the same stage is the moderate increase in the expression levels in the case of dGM130 and dp115, which renders the precise developmental staging of larvae very crucial. Despite the strict criteria that were applied for larval staging, it cannot be excluded that individual flies might exhibit differences in their morphological features, which could complicate the distinction between the pre- and post-ecdysone peak third instar larvae, and therefore lead to sampling variations.

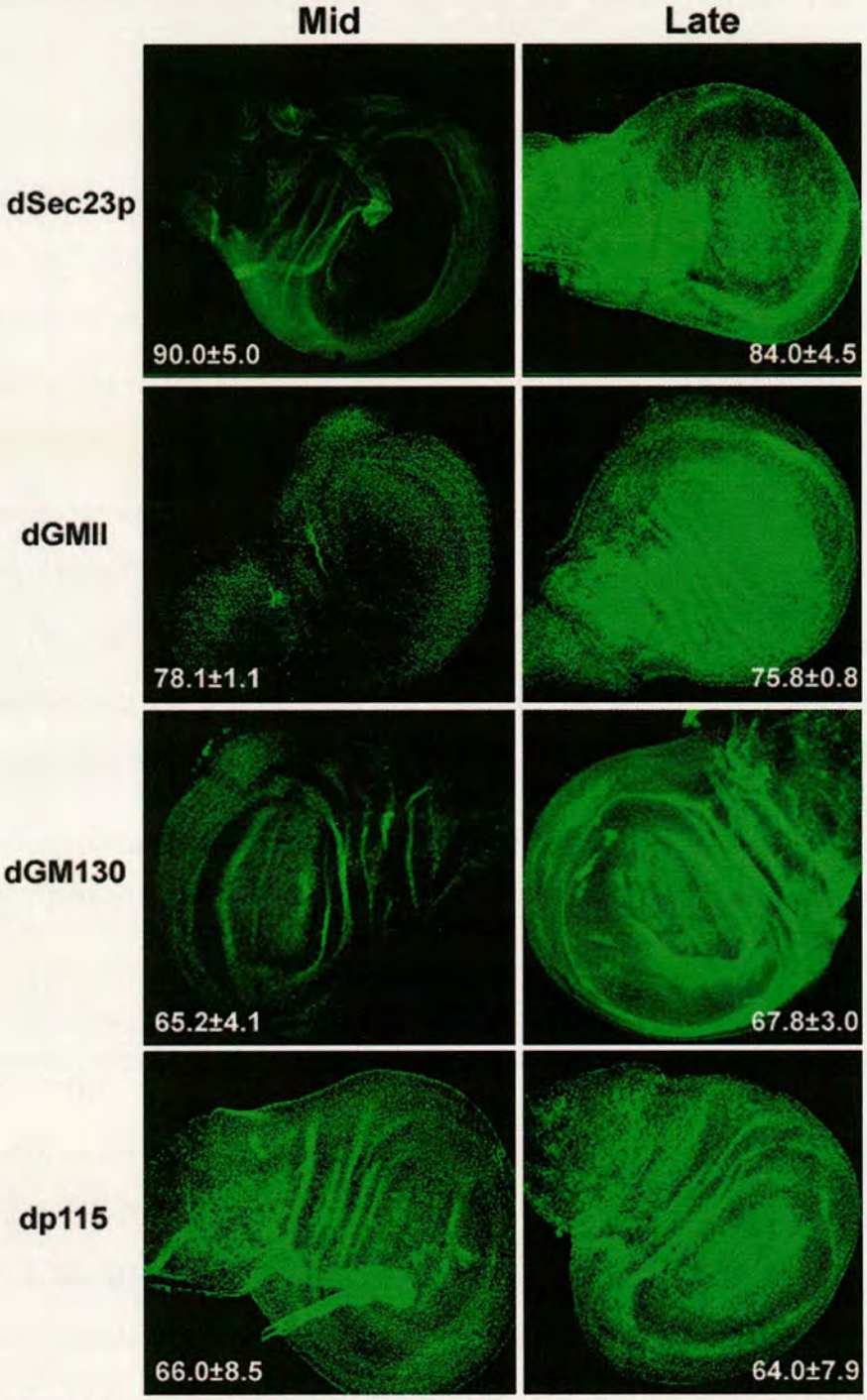

Figure 7.6: Expression of tER and Golgi-related proteins in mid- and late third instar larvae. WT mid- and late-third instar larvae were selected by using salivary gland morphology as a precise means of larval staging. Mid- (left)- and late- (right) third instar larvae were semi-dissected, processed for IF and labelled for dSec23p, dGMII, dGM130 and dp115 using the antibodies mentioned in tables 2.5 and 2.6, followed by an anti-rabbit IgG coupled to FITC. The wing imaginal discs were finely dissected, mounted in Vectashield, and observed under a Leica confocal microscope. A projection encompassing the full disc thickness is displayed. The numbers in each picture represent the percentage of imaginal discs showing the same labelling intensity with that presented in each picture, and are indicative of the homogeneity of protein expression in each group of discs. Results are expressed as ±SD.

Finally, in contrast to the other 4 protein markers, when the expression of dβ'COP (COP I coat subunit) was examined using a rabbit polyclonal antibody against the rat homologue (80% similarity), a 4- to 5-fold decrease was observed from mid- to late third instar larval discs (Dunne et al., 2002).

All proteins that displayed an increased expression between mid- and late-third instar larvae were observed in higher magnification to confirm that they localised correctly to the Golgi apparatus (punctate pattern similar to this observed in figures 7.2, 7.4 and 7.5).

Besides the regulation in the expression of Golgi-related protein after the prepupal ecdysone peak, additional evidence for the direct involvement of ecdysone in the Golgi stack biogenesis were obtained. First, the transition from larval clusters to Golgi stacks was recapitulated in a semi-intact system (Mandaron, 1971) that reconstituted the first step of imaginal disc elongation *in vitro*, by incubating dissected discs in M3 medium containing exogenous ecdysone (Kondylis et al., 2001).

Second, a mutant fly containing the *Drosophila* temperature-sensitive allele *ecdysoneless* (*ecd*^{1ts}) was also used to support the ecdysone-dependence of Golgi stack formation. At the non-permissive temperature, ecdysone production is severely inhibited in this mutant (Garen *et al.*, 1977; Redfern and Bownes, 1983), whereas at the permissive temperature, the larvae behave as wild type. Indeed, when imaginal discs dissected from larvae kept at the non-permissive temperature were incubated *in vitro* in the presence or absence of exogenous ecdysone, it was only those discs that were treated with the hormone that exhibited Golgi stack biogenesis (Kondylis et al., 2001).

Finally, an extensive study has monitored the mRNA expression of several Golgi-related genes in mid- and late-third instar larval discs by *in situ*

hybridisation (Dunne et al., 2002). The outcome of this study has suggested that ecdysone triggers the up-regulation of a subset of genes encoding Golgi-related proteins (such as dNSF1, dSec23, dSed5, and dRab1), while it down-regulates the expression of others (such as dErgic53, dβ'COP, and dRab6). Furthermore, in the case of dSec23 gene expression, the generation of imaginal disc mosaic clones using the FRT/Flp technology (Dang and Perrimon, 1992) showed that this observed mRNA up-regulation is mediated through the transcription factor Broad-complex, itself being an "early" ecdysone target (Kiss et al., 1988; Karim et al., 1993).

Collectively, these results have provided strong indications that ecdysone could be the trigger for the Golgi stack biogenesis by regulating the expression of genes that are involved in the structural organisation of the Golgi stacks, although the possibility that this event is an indirect consequence of the imaginal disc elongation cannot be excluded.

7.4 Discussion

The present study was focused on the morphological characterisation of the Golgi stack biogenesis from vesicular-tubular clusters, which takes place under physiological conditions in imaginal disc cells during the transition from early-third instar larva to white pupa stage.

7.4.1 Conversion of Golgi clusters to Golgi stacks

Two series of experiments have suggested that the membranes comprising the larval clusters observed in early- and mid-third instar imaginal discs are Golgi stack precursors. First, using immuno-electron and immunofluorescence microscopy, the larval clusters were shown to contain Golgi markers, including dGM130 and dp115, that were colocalised with a newly described *Drosophila* Golgi glycosyltransferase, Fringe, when this was expressed at low level (Bruckner et al., 2000; Munro and Freeman, 2000). The

distribution of dGM130 and dp115 was specifically confined to the larval cluster or Golgi stacks (labelling density ~10 times over the background), although approximately one-third of the labelling was associated with the ER membranes. This cellular distribution of these two proteins resembles what was observed in S2 and salivary gland cells (see sections 4.2 and 5.3), while a similar relative distribution has been reported for the Golgi enzyme dGMII (Rabouille et al., 1999).

Second, different experimental designs showed that the larval clusters are replaced by Golgi stacks of similar surface density, suggesting the conversion of the former into the latter without addition of new membrane structures. However, the possibility exists that the larval clusters could be entirely consumed and replaced by Golgi stacks, which have derived from newly generated membranes. In this case, the conservation of surface density would be coincidental. This situation seems unlikely, because if the clusters were consumed and replaced by newly formed Golgi stacks, a disappearance of the clusters would be expected in situations where they cannot be converted, i.e., in the dNSF1 and ecd^{1ts} mutants at the restrictive temperature. Nevertheless, instead of disappearing, the clusters persist in the disc cells of these mutants, since their conversion to stacks is prohibited. This issue could be definitely resolved by generating a transgenic fly containing a fluorescently tagged protein that marks the Golgi membranes, and follow its dynamics by live imaging during the transition from mid- to late-third instar larvae. In similar experiments, the dynamics of the endoplasmic reticulum during early stages of *Drosophila* development were studied by monitoring a GFP-tagged version of ER resident protein PDI (Bobinnec et al., 2003).

7.4.2 Ecdysone-dependence of Golgi stack biogenesis

The timing of the morphological transition observed in the Golgi area suggested the possible involvement of 20-hydroxyecdysone, the steroid

hormone known to trigger many morphogenetic events during puparium formation (Fristrom and Fristrom, 1993). Two lines of evidence have suggested that Golgi stack biogenesis occurring at the onset of disc elongation is also influenced by ecdysone. Using the semi-dissected disc assay, the formation of Golgi stacks from larval clusters was observed in the presence of ecdysone, while this was prevented in its absence. In support of this finding, the *in vivo* and *in vitro* conversion of larval clusters into Golgi stacks was severely reduced in imaginal discs from *ecd*^{1ts} mutant larvae.

As mentioned before, these results do not exclude the possibility that the Golgi stack biogenesis is a mere consequence of the cellular events taking place under the control of ecdysone. For example, cell rearrangement taking place during disc elongation could in turn drive Golgi stack formation. Therefore, the fact that Golgi stacks were not formed in the absence of ecdysone could simply be the result of the lack of disc elongation. The ultimate answer to this question would be to show whether Golgi stack biogenesis precedes or is concomitant with imaginal disc elongation. However, a significant number of genes, whose products are important for the Golgi structure and function, were shown to be transcriptionally regulated by ecdysone (Dunne et al., 2002). This result was also supported by studies on ecdysone-responsive gene expression with the use of microarray technology, which showed that fusion ATPase TER94 (homologue of mammalian p97; Rabouille *et al.*, 1995a) and dSec23 were among the strongly up-regulated genes by ecdysone (White et al., 1999). Considering this orchestrated transcriptional regulation of Golgi-related genes, it is likely that Golgi stack biogenesis acts as a preparative step for the exocytic pathway in order to sustain the increased need for secretion during the disc elongation.

7.4.3 What do the Golgi larval clusters represent?

In terms of morphology, the larval clusters observed in the early- and mid-third instar larval disc cells are reminiscent of the pleiomophic membrane structures consisting the tER sites in S2 cells. Moreover, they are populated with Golgi and tER protein markers (Fringe, dGM130, dp115, dSec23p and dSec31p). Thus, they could represent tER sites at an "immature" state, which might not be converted into stacks due to the absence or reduced expression of certain Golgi structural proteins, such as dp115 or others.

Alternatively, the larval clusters could represent an equivalent of the disorganised form of Golgi apparatus observed in S2 cells after RNAi-mediated depletion of dp115 (see chapter 5). For instance, the clusters could contain tER and Golgi membranes, which due to their convoluted organisation cannot be resolved. A systematic IEM characterisation using tER and Golgi markers could clarify further this issue.

7.4.4 Functional Biosynthetic Pathway in the absence of Golgi stacks

The absence of stacked cisternae in third-instar larvae raises the issue of whether these cells possess a functional biosynthetic pathway. In the imaginal discs of third-instar larvae, many important patterning processes are taking place. The dorso/ventral and anterior/posterior regions are defined and maintained by secreted signalling molecules, such as Dpp, Wingless and Hedgehog, and plasma membrane proteins, such as Smoothened and Patched (Vincent and Dubois, 2002). The need of these proteins to use a functional exocytic pathway suggests one of two possibilities; either the cells of third-instar larval discs possess a functional biosynthetic pathway in the absence of stacked cisternae, or these patterning molecules were exocytosed at an earlier developmental stage, when Golgi stacks were perhaps present, and persisted into the third-instar larval stage, where only clusters are observed.

Several observations suggest that the first possibility is more likely to be true. First, the imaginal discs of a temperature-sensitive mutant for fusion ATPase dNSF1 (comt 17; Pallanck et al., 1995) did not elongate when incubated at restrictive temperature, probably because dNSF1 was not functional in supporting exocytosis (Kondylis et al., 2001). Indeed, molecules whose lack of synthesis and transportation may inhibit disc elongation include the stubble gene product, IMP-E2 and -E3 (von Kalm et al., 1995) and integrins (Fristrom et al., 1993). Second, similar Golgi clusters have been observed in salivary glands from early third-instar larvae that are able to support at least the secretion of food digestive enzymes (Thomopoulos et al., 1992). And third, pre-cellularised embryo also contains Golgi complexes in the form of vesicular-tubular clusters (Fullilove and Jacobson, 1971; Mahowald et al., 1983; Ripoche et al., 1994) without this preventing the transport and deposition of the large amount of intracellular membranes to the plasma membrane during cellularisation. A big portion of these membranes was shown recently to originate from the exocytic pathway (Lecuit and Wieschaus, 2000; Sisson et al., 2000).

7.4.5 Biological significance of Golgi stack biogenesis

As described above, the transition from small Golgi fragments to stacked cisternae appears to be a phenomenon not confined solely to *Drosophila* larval disc development. The same transition seems to occur during *Drosophila* embryogenesis. In syntitial and gastrulating embryos, the Golgi apparatus consists of small fragments (Fullilove and Jacobson, 1971; Ripoche et al., 1994), whereas in late embryo (20h after fertilization), it acquires the typical stacked morphology (Rabouille et al., 1999). Morover, a similar change in the Golgi morphology takes place in *Drosophila* salivary glands between early and late-third-instar larvae (Thomopoulos et al., 1992).

Considering that the larval Golgi clusters appear to be functional, the question remains as to why the Golgi stacks are formed. It has been shown that the Golgi morphology changes when secretion increases in stimulated prolactin cells (Rambourg et al., 1993). In *Drosophila* salivary glands, the observed conversion of Golgi clusters to stacks occurs concomitantly to the glue synthesis and secretion (Thomopoulos et al., 1992). Therefore, in this case, the Golgi stack biogenesis could also serve an increased need for active exocytosis. By analogy, a requirement for increased synthesis and secretion of molecules involved in the complex morphogenetic changes of the imaginal discs could explain the changes in Golgi morphology observed in larval disc cells. Additionally or alternatively, the formation of a polarised stack could ensure proper differential oligosaccharide or protein processing and targeting, which might be crucial for one or more specific proteins involved in disc elongation or for the synthesis of pupal cuticle that has a different composition to larval cuticle (Riddiford, 1993). What seems certain is that, in the presence of functional Golgi clusters in *Drosophila,* the reason for the existence of the Golgi stacks in cells will occupy for long the mind of the many researchers in the field.

Chapter Eight

Discussion and Future Prospects

8.1 The organisation of the early exocytic pathway in Drosophila S2 cells

Drosophila cells are a powerful experimental system to study the organisation of the early exocytic pathway, as an alternative to mammalian cells. First, the compartments of the early exocytic pathway exhibit similar characteristics to mammalian cells in terms of their basic morphological features. Second, most of the mammalian proteins implicated in its structural organisation and functions are conserved in *Drosophila* genome (see section 1.7.3). Third, *Drosophila* together with yeast, the other widely used model system for studies on the exocytic pathway, is much easier to be genetically manipulated compared to vertebrates. However, in contrast to yeast, *Drosophila* has the advantage of being a multicellular organism. This makes flies a very useful model system, in which findings concerning the exocytic pathway can be easily related to their role in different developmental processes, thus bridging cell and developmental biology. Finally, although the basic functions taking place along the exocytic pathway are conserved both in yeast and *Drosophila* cells, its organisation seems to be simpler than mammalian cells. Therefore, comparative studies in yeast and *Drosophila* could provide important information in order to determine the fundamental aspects of the early exocytic pathway, which are conserved throughout the evolution of eukaryotes.

Organisation of the transitional-ER sites (tER sites)

In contrast to the Golgi apparatus that is an extensively studied organelle, the molecular organisation of the tER sites has only recently started to become elucidated. The reason for the increased interest in this compartment is due to its central role in the models of cisternal maturation and *de novo* Golgi formation, which have been proposed to explain how anterograde cargo

molecules move along the exocytic pathway and how Golgi apparatus is formed, respectively (see sections 1.2.1 and 1.2.2). In both models, tER sites play a crucial role, since this is where cargo exits from the ER, and moreover, they are the birthplace of membranes, which, by maturation, will give rise to the Golgi apparatus (Hammond and Glick, 2000; Glick, 2002). The most commonly used molecular markers for the characterisation of the tER sites are the components of COPII coat, which is involved in the selection of the cargo and drives the formation of their vesicular carriers (Cole et al., 1996; Rossanese et al., 1999; Hammond and Glick, 2000; Stephens et al., 2000; Antonny et al., 2001; Stephens, 2003).

In the present study, the COPII coat subunit, dSec23p, was used as a marker for the tER sites. By immuno-electron microscopy (IEM), the tER sites in *Drosophila* S2 cells appear as pleiomorphic tubular-vesicular membrane structures, and the same is true for other *Drosophila* tissues. These pleiomorphic membrane structures comprise coated vesicular profiles of ~50μm diameter, as well as budding profiles connected to the ER cisternae (Figure 3.1 and all IEM figures showing dSec23p labelling), which is similar to what has been shown in mammalian and yeast cells (Orci et al., 1991; Paccaud et al., 1996; Mogelsvang et al., 2003). However, larger tubular-vesicular profiles and more complex structures were also labelled for dSec23p. The presence of these structures could be interpreted in three ways. One explanation could be that they are still associated with ER membranes, but their connection cannot be seen, because tER sites display a highly convoluted 3-dimensional organisation extending spatially more than the 70nm thickness of an ultrathin section (Figure 8.1A). An analysis of S2 cell tER sites by 3D electron tomography could elucidate this matter. The second interpretation, which does not exclude the first one, could be that the tubules

and complex dSec23p-positive structures are separated from the ER, and have derived from the fusion of COPII-coated vesicles pinching off from the ER. This would mean that the COPII coat is not completely shed off prior to vesicle fusion (Figure 8.1B). Although this model is not supported by *in vitro* experiments on the COPII coat dynamics showing that the coat undergoes a fast disassembly after its formation (Antonny et al., 2001), it has been depicted in models describing the organisation and the formation of the early exocytic compartments (Stephens et al., 2000). The third alternative is that these complex structures could have arisen by *en bloc* protrusion from ER, as it has been described in a recent study in mammalian cells combining light and electron microscopy and electron tomography (Mironov et al., 2003). However, in the proposed model, the role attributed to the COPII coat is the selection and concentration of cargo at the tER sites, and therefore, COPII

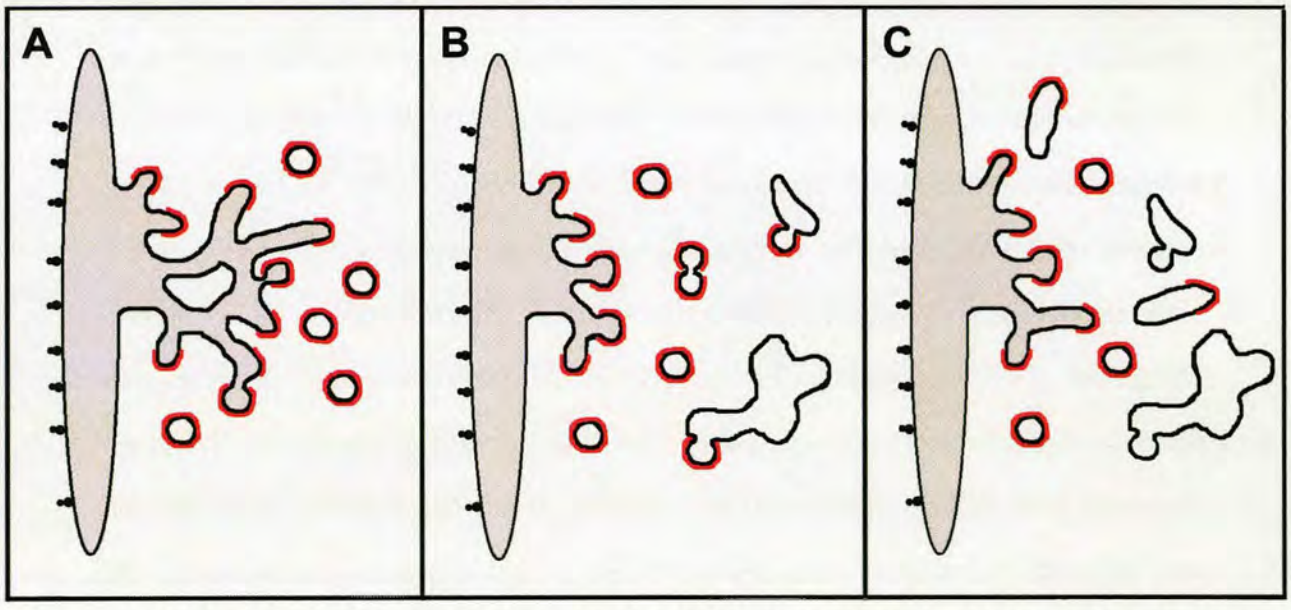

Figure 8.1: Models of tER organisation in *Drosophila* S2 cells that could explain dSec23p labelling (red) of pleiomorphic structures. A. All the non-vesicular pleiomorphic structures are still connected to the ER membranes. **B.** Some dSec23p-positive pleiomorphic membranes are not connected to the ER and could be generated by the homotypic fusion of two COPII vesicles without previously having shed completely their coat. A COPII-coated vesicle could also fuse with a larger transport intermediate. **C.** COPII-coated vesicles, but also larger COPII-coated cargo carriers, could bud from the tER sites. These three models are not mutually exclusive and a combination of the described features could be true.

subunits should not be found on any membranes not associated with ER cisternae. Furthermore, in this study, the immuno-localisation of COPII coat was not directly performed on the samples used for the tomographic reconstructions. On the contrary, recent unpublished data combining immunogold labelling on 400nm thick cryosections of wild-type HepG2 cells with analysis by 3D-tomography demonstrate that free vesicles and tubules labelled for Sec23p exist, even in some distance from the ER membranes (Dagmar Zeuschner and Judith Klumperman, personal communication). This observation could support the idea that cargo exit from the ER is mediated by COPII-coated membrane carriers that may not be necessarily vesicular (Figure 8.1C). These findings are also compatible with the possibility of COPII vesicles fusing without being completely uncoated.

Drosophila tER sites exhibit also a close spatial association with the Golgi apparatus when observed both by immuno-fluorescence (IF) and IEM (Figure 3.3). The same structural organisation between the two compartments has been described in yeast species *Pichia pastoris*, in contrast to the most widely used budding yeast S. cerevisiae, which does not have discrete tER sites and the individual Golgi cisternae that can be seen are scattered throughout the cell (Preuss et al., 1992; Rossanese et al., 1999; Mogelsvang et al., 2003). In *Pichia*, 2-4 tER sites exist on average at steady state, while in S2 cells there are 20±8 tER sites per cell. Considering that both *Pichia* and S2 cells have almost spherical shape with average diameter 3.5 and 10.7μm, respectively (nucleus diameter 1.3 and 6.5μm, respectively), S2 cell volume is estimated to be about 20 times larger than that of *Pichia* cells. This means that the density of tER sites in S2 cells is about 2-5 times higher than in *Pichia*. Despite this difference in density, the common features of the tER features in these two cell types may also reflect a similar underlying

mechanism for the structural organisation of the compartment in these two organisms.

In mammalian cells, similar close spatial tER-Golgi relationship is not observed, since about 50% of their numerous tER sites are situated at the cell periphery, while the single-copy Golgi apparatus is located at the peri-nuclear area (Cole et al., 1996; Hammond and Glick, 2000). Nevertheless, when mammalian cells are treated with microtubule-depolymerising drugs, such as nocodazole, the Golgi apparatus breaks down and small Golgi stacks appear at the cell periphery, next to the tER sites (Cole et al., 1996; Storrie et al., 1998; Hammond and Glick, 2000). Furthermore, although initially ER-Golgi transport is inhibited in nocodazole-treated cells, once this re-organisation of the exocytic pathway has taken place, anterograde transport to the plasma membrane (PM) is restored (Cole et al., 1996). This suggests that the adjacent distribution of tER sites and Golgi stacks is a conserved characteristic throughout the evolution of eukaryotes. Despite the development of the juxtanuclear Golgi ribbon of interconnected stacks and the microtubule–dependent trafficking between tER and Golgi, the nocodazole experiments demonstrate that the archetype of tER-Golgi organisation observed in more primitive eukaryotes is still inherently present in mammalian cells.

Time-lapse confocal microscopy of the tER sites in *Pichia* and mammalian cells has also shown that they exhibit similar features concerning their dynamics (Bevis et al., 2002; Stephens, 2003). In these studies, tER sites are relatively long-lived structures and their movement seems to be restricted. Fusion events between neighbouring sites have been observed, though the resulting merged tER site is immediately reduced in size, which is suggestive of an intrinsic control mechanism of their growth (Bevis et al.,

2002; Stephens, 2003). Moreover, fission events of tER sites have also been described in mammalian cells, but this does not preclude that these events reflect the optical resolution of already independent tER sites (Stephens, 2003). In S2 cells, a similar investigation of the tER dynamics has not been carried out, although comparable findings would be expected, due to the structural similarities of the *Drosophila* tER sites with those of *Pichia* and mammalian cells. However, such a study in S2 cells could help to determine whether the large dSec23p-positive spots represent individual sites or aggregation of 2 or more independent tER sites. Indicative of the later situation is the fact that occasionally two d120kd-positive spots seem to associate with one tER site. This might provide new insights in our interpretation of the effect of dp115 depletion or treatment with inhibitors, like H89, which led to fragmentation of the focused tER sites into a larger number of smaller and dispersed spots (Figures 5.7 and 3.8).

Is the intermediate compartment (IC) present in S2 cells?

The intermediate or VTC compartment has been described in mammalian cells as a separate compartment, although its borders are still difficult to determine due to its transient nature and similar morphology both with the tER sites and the CGN in electron microscopy (Bannykh et al., 1996; 1998; Farquhar and Palade, 1998; Klumperman, 2000). This distinction of the intermediate compartment is based on its different content in molecular markers (Bannykh et al., 1996; Martinez-Menarguez et al., 1999), and the long-range, microtubule-dependent, inward movement of a portion of IC elements from the peripheral tER sites, close to which they are formed, to the Golgi apparatus in the perinuclear area (Presley et al., 1997; Scales et al., 1997; Stephens et al., 2000).

In S2 cells, a distinct intermediate compartment is unlikely to exist. First, IF and electron microscopy has shown that tER sites are found closely

apposed to the Golgi stacks (Figures 3.1 and 3.3), which practically leaves no space for an additional intermediate compartment equivalent to the mammalian one. Second, the typical organisation of mammalian ER exit sites or ER export complexes (cup-shaped ER cisterna comprising coated buds and central vesicular-tubular clusters; see figure 1 in Bannykh et al., 1998) is also observed in S2 cells. However, in S2 cells, the central pleiomorphic membranes are labelled for COPII coat subunit, dSec23p, while in mammalian cells, these membranes are only labelled for COP I coat markers and not COPII (Bannykh et al., 1996; Martinez-Menarguez et al., 1999). Therefore, in S2 cells, the entire vesicular-tubular membranes are considered to represent tER sites, although the localisation of *Drosophila* homologues of proteins used as IC markers, such as ERGIC53/58, would provide a more definitive answer on this matter. A third indication suggesting the absence of an IC equivalent from *Drosophila* cells is that, in contrast to mammalian cells, ER-Golgi transport is not dependent on the microtubule network, as the experiments with microtubule-disrupting agent colchicine have shown (see section 3.4.3.1). Despite the absence of a morphologically discrete intermediate compartment, its function in segregation of anterograde from retrograde cargo and the recycling of the latter back to the ER should still take place. This is expected because proteins that need to be recycled, such as SNAREs involved in ER-Golgi transport, ERD2 (KDEL receptor) and cargo receptors (ERGIC53/58, members of the p24 family) are all conserved in *Drosophila* (see also figure 1.10).

On the other hand, a glimpse of the presence of an intermediate compartment in *Drosophila* S2 cells is suggested by the dp115 RNAi experiments. Upon depletion of dp115, Golgi stacks break down into vesicular-tubular clusters, which are often positive for both dSec23p and the

Golgi marker, d120kd (Figures 5.11 and 5.12). However, it was observed that within the same cluster the dSec23p-positive membranes were often segregated from d120kd-positive ones (Figure 5.12D-F). Thus, it is tempting to suggest that the part of the cluster that contains the Golgi marker could correspond to the *Drosophila* equivalent of the IC, which may not be as obvious when Golgi stacks are intact. From this point of view, the IC in *Drosophila* would be identical to the CGN. This has also been proposed for the mammalian IC elements originated from the juxtanuclear-located tER sites (Ladinsky et al, 1999; Hammond and Glick, 2000). Furthermore, considering that anterograde transport of PM and secreted proteins is not affected in dp115-depleted cells, these putative IC elements may represent an alternative form of Golgi apparatus, which in the presence of dp115 would get organised or mature into Golgi stacks. Such vesicular-tubular clusters carrying out proper Golgi functions are observed physiologically during certain stages of *Drosophila* development (see chapter 7).

The role of microtubule network

The inter-dependence between the microtubule network and the Golgi apparatus is well established (Thyberg and Moskalewski, 1999; Rios and Bornens, 2003). On one hand, the role of intact microtubule network and the related molecular motors in the architecture of the Golgi apparatus and the organisation of the exocytic pathway has been clearly demonstrated. In mammalian cells, the use of microtubule depolymerising agents (e.g. nocodazole) leads to a fragmentation of the Golgi ribbon and appearance of small peripheral Golgi stacks (Thyberg and Moskalewski, 1999 and references therein; see also introduction and chapter 3). Overexpression of dynamitin, a subunit of dynactin complex that is involved in dynein-dependent movement of membrane structures along microtubules, has led to a redistribution of the Golgi elements similar to nocodazole-treated cells

(Burkhardt et al., 1997). In addition, in *Schizosaccharomyces pombe* that exhibits stacked Golgi, treatment with the anti-microtubule inhibitor thiabendazole has caused unstacking of the Golgi cisternae (Ayscough et al., 1992). On the other hand, the Golgi apparatus, in addition to the centrioles, is believed to act as microtubule-nucleating point through a fraction of γ-tubulin associated with purified Golgi membranes (Chabin-Brion et al., 2001; Marsh et al., 2001). Sustaining this notion, GMAP-210, a cis-Golgi protein with characteristics of a golgin, was recently shown to anchor γ-tubulin-containing complexes on Golgi membranes (Rios et al., 2004).

Surprisingly, in *Drosophila* S2 cells, microtubule disruption with colchicine did not affect the close spatial relationship between the tER sites and the Golgi apparatus, at least at the IF level (Figure 3.10). The same held true for the anterograde transport of Delta to the PM (Figure 3.22). The lack of a discernible effect on the early exocytic pathway upon microtubule depolymerisation could be related to the fact that *Drosophila* Golgi stacks, unlike the mammalian Golgi apparatus, are not spatially associated with the centrioles that are considered as the major microtubule organising centre (MTOC). However, as it was mentioned above, there is evidence that the Golgi membranes themselves can also nucleate microtubule arrays. In S2 cells, microtubules were mostly concentrated at the cell cortex and a connection to the Golgi stacks could not be clearly detected at the IF level. Considering though that a protein bearing weak homology to GMAP-210 exist in *Drosophila*, an IEM study combined with a functional analysis of this protein would maybe shed light on whether *Drosophila* Golgi stacks can function as MTOCs.

These negative results do not mean that microtubules are not important for membrane trafficking in *Drosophila*, as their role could be

different than these described in mammalian cells, or the microtubule dependence could be cell-type specific. Two recent studies (Lecuit and Wieschaus, 2000; Sisson et al., 2000), for example, have shown that the microtubule integrity is important for the embryo cellularisation (see section 1.7.3). This process requires the deposition of large amount of membrane at the PM, the major source of which seems to be the exocytic pathway. Although in the first report, it was postulated that the transport of a PM transmembrane reporter was blocked in the Golgi upon microtubule depolymerisation (Lecuit and Wieschaus, 2000), it could not be distinguished whether this was due to a microtubule requirement for Golgi-PM transport, or due to an inhibition of the basal-apical movement of the Golgi apparatus itself during the "slow phase" of cellularisation (see section 1.7.3). The second study showed that this temporally regulated apical movement of the Golgi is dependent on microtubule network (Sisson et al., 2000), without this excluding an additional involvement of microtubules in the Golgi to PM membrane transport. Therefore, these results suggest that in *Drosophila*, the microtubule network might be involved in organelle movement rather than or in addition to membrane traffic. Similar cytoskeleton-dependent Golgi mobility has been shown in plants and yeast, albeit in this case the actin cytoskeleton is involved (Nebenführ et al., 1999; Rossanese et al., 2001).

The role of actin microfilaments

In contrast to microtubules, the actin cytoskeleton seem to be important for the organisation of the exocytic pathway in S2 cells. In the presence of cytochalasin D, an agent that disrupts actin cytoskeleton by disassembling stress fibres (Rotsch and Radmacher, 2000), a fragmentation in the IF pattern of the Golgi marker was observed (≥1.5-fold increase in the number of d120kd-positive structures, which become smaller in size; see figure 3.12). This is accompanied by a similar disruption of the tER sites. These alterations

are not likely to stem from an inhibition in intracellular transport as anterograde transport was not affected and endocytosis, which is impaired, would not be expected to cause such a drastic reorganisation in the early exocytic compartments. A more likely possibility that could explain these results would be through the interaction of actin with spectrins (de Matteis and Morrow, 2000).

In mammalian cells, specific isoforms of β-spectrin (βI sigma 1, βIII) form a membrane skeleton that surrounds the Golgi apparatus and is linked to it and all major cytoskeletal systems (Beck et al., 1994; Stankewich et al., 1998). The Golgi spectrin membrane skeleton is similar to that found underneath the PM, but in the formation of the latter, β-spectrins form heterodimers with α-spectrins (de Matteis and Morrow, 2000). Two models have been proposed to explain the function of spectrin skeleton in Golgi apparatus. The first model suggests that this scaffold could organise and stabilise the Golgi architecture and facilitate membrane transport through its capability for dynamic remodelling and its interaction with cytoskeleton. The second model postulates that the principal role of spectrin skeleton might be to regulate vesicle formation and/or transport to and from the Golgi, by interacting with adaptor proteins, such as Arf1, as well as molecular motors (Godi et al., 1998; Beck and Nelson, 1998; de Matteis and Morrow, 2000). For instance, Arp1, an actin-related protein member of the dynactin complex, has been shown to colocalise and interact directly with βIΣ1 and βIII Golgi spectrins (Holleran et al., 1996; 2001). This has provided a link between microtubule-dependent vesicular motility or Golgi positioning (through dynactin-dynein motor complex) and the Golgi spectrin skeleton.

Drosophila Golgi apparatus was shown to colocalise with spectrins during embryogenesis, but unlike mammalian cells that have only Golgi-

specific β-spectrin isoforms, in *Drosophila*, it seems that α-spectrin is also involved in the formation of the Golgi spectrin membrane skeleton (Sisson et al., 2000). Therefore, the observed fragmentation of the Golgi stacks upon cytochalasin D treatment could be because actin depolymerisation leads to a disorganisation of spectrin membrane skeleton, which maintains the structural integrity of the Golgi apparatus.

The effect of actin depolymerisation on the organisation of exocytic pathway needs to be characterised in more details in the future. In mammalian cells, cytochalasin D treatment seems to result in a compacted appearance of the Golgi ribbon, as assessed by IF, while when visualised by EM, the cells exhibited swollen cisternae containing electron dense material (Valderrama et al., 1998; di Campli et al., 1999). However, cisternal unstacking or breakdown of the Golgi ribbon was not observed (Valderrama et al., 1998). This makes the observed Golgi fragmentation in S2 cells a very interesting phenotype. First, the morphology of the fragmented Golgi membranes should be investigated by EM to determine whether they represent smaller Golgi stacks or Golgi vesicular-tubular clusters, and whether other structural changes, for example distension of cisternae, are also observed. Second, since cytochalasin D does not cause net depolymerisation of the filamentous actin (Morris and Tannenbaum, 1980), the same effect should be reproduced using other actin inhibitor that produces net depolymerisation of F-actin, such as latrunculin A or B (Valderrama et al., 2001). Third, in order to determine the mechanism by which actin exerts its effect on the Golgi organisation, the distribution of *Drosophila* α- and β-spectrin isoforms should be investigated, as the disruption of the skeleton that they form around the Golgi could be the reason for the Golgi fragmentation. Another important aspect of the

cytochalasin D effect would be to test whether the multiplication of the Golgi membranes takes place by breakdown of already existing Golgi stacks. This would be greatly facilitated by the tagging of a Golgi resident protein, like *Drosophila* Golgi Mannosidase II or Fringe (Rabouille et al., 1999; Munro and Freeman, 2000), with a fluorescent molecule, and subsequent observation of the Golgi fate upon actin depolymerisation by life cell imaging. Finally, a similar approach for tER sites would also be useful, since it will help to distinguish whether the disruption in dSec23p pattern happens concomitantly with the Golgi fragmentation, which would provide support to the notion of a common tER-Golgi matrix (see below). Alternatively, the effect on tER sites could be a consequence of the impairment of retrograde transport from Golgi to ER upon disruption of actin dynamics that has been reported in mammalian cells (Valderrama et al., 2001).

8.2 The role of Drosophila Golgi matrix proteins in the early exocytic pathway in S2 cells

In the present study, the role of three *Drosophila* homologues of mammalian Golgi matrix proteins (dGRASP, dGM130 and dp115) in the exocytic pathway of *Drosophila* S2 cells was examined. Immuno-localisation of these three proteins showed that all of them were confined to the Golgi apparatus, as expected, but also on the tER membranes marked by dSec23p and to a smaller extent on ER cisternae (see sections 4.2 and 5.3). This is in agreement with the IF localisation of p115 at peripheral spots representing tER sites or IC elements in addition to the Golgi apparatus (Nelson et al., 1998; Alvarez et al., 1999; 2001), and the proposal that GM130 and GRASP65 cycle between the ER exit sites and the Golgi apparatus (Ward et al., 2001; Stroud et al., 2003; Puri and Linstedt, 2003).

8.2.1 Building and maintenance of the Golgi stacks

The mammalian homologues of dGRASP, dGM130 and dp115 are thought to be involved in the formation and maintenance of the Golgi apparatus (see introduction section 1.5.1). Until recently, this was largely based on an *in vitro* assay making use of the Golgi stack reassembly from mitotic Golgi clusters (Rabouille et al., 1995b). However, the investigation of their *in vivo* role in the structural integrity of the Golgi apparatus has suggested that not all of them may be as important for the Golgi architecture as it was originally considered. During this project, the significance of the *Drosophila* Golgi matrix proteins for the Golgi stack organisation was tested by depleting them from S2 cells using RNA interference (RNAi).

dGRASP

Unlike mammalian cells that have two GRASP proteins (GRASP65 and GRASP55), all the other eukaryotes, including *Drosophila*, have only one GRASP homologue. dGRASP resembles both mammalian GRASPs to the same extent, and in the absence of biochemical data, it could not be determined whether it is orthologue for only one of them or performs the function of both. However, an indication that dGRASP could be a GRASP65 homologue derives from its preferential localisation at the CGN and the cis-Golgi cisterna (Shorter et al., 1999; Figure 4.4).

dGRASP seems to be involved in cisternal stacking *in vivo*, since upon its depletion, a small but significant percentage of cells exhibited single cisternae embedded into clusters of vesicles and tubules (Figure 4.9), a phenotype very rarely observed under normal conditions or in dp115 and dGM130 depletions (Figure 4.13C). The effect of the absence of dGRASP on the stacking mechanism was confirmed in dGRASP/dGM130 double depletion, where the percentage of membrane in single cisternae was 9-fold higher compared to dp115 and dGM130 depletions. These results are in

agreement with a recent study showing that injection of anti-GRASP65 antibodies in mitotic cells interfered with the post-mitotic Golgi stack reassembly, but not with the cisternal formation itself (Wang et al., 2003). In the same study, it is also postulated that GRASP65 dimers on adjacent cisternae may form trans-oligomers that could keep the Golgi cisternae stacked. However, considering the non-quantitative Golgi stack breakdown upon dGRASP depletion from S2 cells, this is unlikely to be the only mechanism that is responsible for the cisternal stacking, at least in *Drosophila*. Although the non-penetrant phenotype could be attributed to residual amounts of dGRASP that remain in RNAi-treated cells, this would not be expected for a structural protein. Instead, it is more likely that other stacking mechanisms might exist, and/or that dGRASP is part of a larger complex that remains mostly stable in its absence.

GRASP genes seem to be important for the function of eukaryotic cells, as they are conserved throughout the evolution of eukaryotes. A GRASP homologue (ECU01_0530) exists even in *Encephalitozoon cuniculi*, the protist with the smallest sequenced genome (~2.9 megabases) comprising approximately 2000 potential protein-coding DNA sequences (Katinka et al., 2001). Taking into account that this primitive eukaryote lacks a typical stacked Golgi apparatus (Franzen and Müller, 1999), the role of GRASP proteins as stacking factors is probably only one aspect of their cellular function.

dGM130

The single depletion of dGM130 did not lead to any quantitative changes in the Golgi stack morphology (Figure 4.6). Nevertheless, the fact that its depletion together with dGRASP or dp115 resulted in a more quantitative (Figure 4.13A and B) or premature breakdown of the Golgi stacks into clusters of vesicles and tubules (Figure 5.18A and B), suggests that dGM130

might be implicated in preserving the integrity of the Golgi stacks, albeit its absence alone is not crucial for the Golgi architecture.

Originally, this result was unexpected as GM130 was one of the major components of the so-called Golgi matrix, the detergent insoluble extract of purified Golgi membranes that exhibited morphology reminiscent of stacked cisternae (Slusarewicz et al., 1994; Nakamura et al., 1995). However, recent reports in mammalian cells have provided support to the observed dGM130 RNAi phenotype. Disruption of the GM130-p115 interaction, which was thought to be important for the structural integrity of the Golgi apparatus (Shorter and Warren, 1999; Linstedt, 1999; Seemann et al., 2000b), did not lead to a disorganisation of the Golgi ribbon at IF level (Puthenveedu and Linstedt, 2001). Furthermore, a temperature-sensitive CHO cell line with no detectable GM130 has apparently normal Golgi stack architecture, and the lack of GM130 only becomes critical at the non-permissive temperature (Vasile et al., 2003). Finally, down-regulation of mammalian GM130 by RNAi did not seem to affect Golgi assembly (unpublished results mentioned in Puri and Linstedt, 2003). Collectively, these observations suggest that contrary to expectations, GM130 is not likely to be an essential component of the putative template that might orchestrate the building and maintenance of the Golgi apparatus.

An interesting question is whether dGM130 is bound on the Golgi membranes through interaction with dGRASP. In mammalian cells, GRASP65 has been clearly shown to interact with GM130 through its PDZ domain, serving as the Golgi membrane receptor for GM130 (Barr et al, 1998). The genetic interaction observed between dGRASP and dGM130 in the RNAi experiments implies that, at least, the two proteins operate in the same pathway leading to the organisation of the Golgi stack. This could also reflect

a biochemical interaction, as the PDZ domain is 100% conserved in dGRASP (Figure 4.2) and could provide the means for interacting with dGM130. However, the extreme C-terminal motif in GM130 that is necessary for the interaction with this domain is not conserved in dGM130, without this excluding the possibility that they could interact via another dGM130 domain.

The existence of this putative dGRASP-dGM130 complex is also compatible with the fact that in dGRASP/dGM130 double depletion led to a significant increase in the number of cells exhibiting complete Golgi stack breakdown or short 2-cisternae Golgi stacks, when compared to dGRASP single depletion (Figure 4.12). This suggests that dGRASP might be involved in both cisternal formation and cisternal stacking by participating in two distinct complexes. The dGRASP complex involved in cisternal formation could also comprise dGM130 and other binding partners. Removal of two components (dGRASP and dGM130) of this putative complex would make it unstable and unable to sustain its function in the formation of Golgi cisternae. This could explain the more extensive Golgi stack conversion into vesicular-tubular clusters and the reduced cisternal diameter observed in dGRASP/dGM130 double depleted cells, relative to the single depletions.

dp115

Among the three *Drosophila* Golgi matrix proteins that were investigated in this study, dp115 was the one whose depletion led to the most profound fragmentation of the Golgi stack into clusters of vesicles and tubules (Figures 5.5 and 5.6). These clusters were often labelled by the Golgi marker d120kd and they seemed to contain remnants of Golgi cisternae. This suggests that, upon dp115 depletion, Golgi stacks are converted into clusters that could retain their Golgi identity and sustain anterograde transport along the exocytic pathway (Figure 6.3 and see also section 8.2.3).

The importance of p115 function for the structural organisation of the Golgi apparatus has also been demonstrated in mammalian cells. Interference with p115 function (by antibody injection or expression of truncated GM130 that does bind to p115) or down-regulation of its expression (by antibody injection or RNAi) has resulted in the fragmentation of the Golgi ribbon (Alvarez et al, 1999, Seemann et al., 2000b; Puthenveedu and Linstedt, 2001; 2004).

An important question that arises from the observed Golgi stack breakdown in dp115-depleted S2 cells is the molecular mechanism(s) that could be responsible for this effect, especially in the light of the increasing number of p115 interacting proteins. An interesting observation is that the dp115 RNAi-mediated Golgi stack breakdown seem to occur between 72 and 96h, when the percentage of S2 cells still exhibiting Golgi stacks decreases sharply from 76.3% to 18.0% (Figure 5.6A). This coincides temporally with the reduction of the dp115 expression below detection by Western blotting (Figure 5.4B). Considering that an S2 cell divides approximately once every 24-30h and that the Golgi stacks in S2 cells disassemble during mitosis (Stanley et al., 1997; Figure 3.5), it would be possible that the absence of dp115 prevented the Golgi stack reassembly at the end of the mitotic division taking place after 72h of incubation with dp115 dsRNA, when the protein is completely depleted or below a necessary threshold. This is consistent with the observation that p115 was required for NSF mediated rebuilding of Golgi cisternae from mitotic Golgi fragments *in vitro* (Rabouille et al, 1995a).

The hypothesis of dp115 inhibiting the Golgi stack formation post-mitotically, does not of course exclude an additional role of dp115 in maintaining the Golgi stacks during interphase. One possibility is that intracellular transport could be inhibited in dp115-depleted cells, and

transport intermediates could accumulate and create the membrane clusters. In mammalian cells, p115 has been involved in at least three different steps in ER to Golgi transport. First, it forms a complex with GM130 on the Golgi cisternae and giantin on the COPI vesicles, which is thought to act as tether that helps the vesicles remain in close proximity to their target membrane, enhancing their docking efficiency and fusion (Sönnichsen et al, 1998; see also figures 1.7 and 1.8). Second, p115 was shown to be recruited by activated Rab1 onto the COPII budding vesicles where p115 interacts directly with a selected set of SNARE proteins (Allan et al, 2000). Third, p115 has recently been shown to catalytically promote the syntaxin5/Gos28 SNAREpin formation, suggesting a direct role in vesicle docking during anterograde intracellular transport (Shorter et al, 2002; see section 1.5.2). Given the significant homology between dp115 and its mammalian counterpart, dp115 could have an equivalent role in intracellular transport. However, in dp115-depleted S2 cells, anterograde intracellular transport was found largely unaffected (Figure 6.3 and see also section 8.2.3), suggesting that as a sole mechanism, the reduction of docking/fusion of ER derived transport vesicles is unlikely to be sufficient to explain the observed Golgi breakdown.

Mammalian dp115 has also been proposed to take part in the building and the maintenance of the Golgi stacks, independently of its role in transport (Linstedt, 1999; see figure 1.7). More specifically, p115 was implicated in the stacking of Golgi cisternae generated by the p97 pathway *in vitro* (Shorter and Warren, 1999). The fact that cisternal stacking in this *in vitro* assay required also functional GM130 and giantin led to the proposal that the role of p115 in stacking could be through the same tripartite complex (GM130-p115-giantin), which might be able to switch from a vesicle tethering complex (role in transport) to a cisterna tethering complex (role in stacking)

(Shorter and Warren, 1999; Linstedt, 1999; see figure 1.7). However, the considerably different phenotypes generated in dp115 and dGM130 RNAi experiments argue against the idea that the same complex, if it exists in *Drosophila* (see below), would be essential for the formation of the Golgi stacks. This is consistent with recent reports showing that mammalian cells with undetectable GM130 or without functional GM130-p115 complex exhibit apparently normal Golgi stack morphology (Puthenveedu and Linstedt, 2001; Vasile et al., 2003).

Does dp115-dGM130 complex exist in S2 cells?

As it was mentioned previously, p115 and GM130 form a tripartite complex together with giantin (Dirac-Svejstrup et al., 2000), which was shown using an *in vitro* docking assay to mediate the tethering of COP I vesicles to isolated Golgi stacked membranes (Sönnichsen et al., 1998). However, the discrepancy between the observed phenotypes upon dp115 and dGM130 RNAi depletions put into question whether these two proteins interact in *Drosophila* as their mammalian counterparts do (Nakamura et al., 1997). Their sequence analysis (see sections 4.1 and 5.1) does not provide a clear answer to this question, because, although the N-terminal GM130 domain containing the p115-binding site is highly conserved in dGM130, dp115 lacks the acidic tail, which was shown to be necessary for the binding of p115 to both GM130 and giantin (Dirac-Svejstrup et al., 2000; Linstedt et al., 2000). Moreover, the fact that no obvious homologue for giantin exists in *Drosophila* genome (see section 1.7.3) makes the existence of the same mammalian complex more doubtful in *Drosophila* cells. Nevertheless, this does not preclude that an analogue of giantin exists in *Drosophila* and dp115 could interact with this and dGM130 through a different domain. Such a giantin analogue could be, for instance, Lava lamp (Lva, CG6450), a novel *Drosophila* protein (2779

amino acids long) that exhibits the typical characteristics of the golgin family (Sisson et al., 2000).

If indeed a similar to mammalian cells tethering complex exists in *Drosophila*, then three are the possible explanations why no effect was observed upon dGM130 depletion. One is that the function of dGM130 in the complex is redundant, and therefore, another protein takes over when it is depleted. The second explanation could be that the role of dGM130 in this complex is not pivotal, thus its removal alone does not destabilise the complex, while if this is combined with the removal of another protein, for example dp115, the complex is non-functional. This is in agreement with the premature Golgi stack breakdown in dp115/dGM130 double depleted cells. Finally, a third possibility is that this putative complex might have only an assisting role in anterograde transport. This could explain the marginal inhibition of transport that was observed upon dp115 and dGM130 single or double depletions. This view is also supported by a recent study performing p115 RNAi depletion in mammalian cells (Puthenveedu and Linstedt, 2004). This study shows that the Golgi fragmentation and transport inhibition caused by p115 depletion could be rescued upon expression of mutant versions of p115 lacking its phosphorylation site or the golgin-binding domain (see section 5.1). In contrast, the p115 SNARE-interacting domain was required for the reassembly of a structurally and functionally normal Golgi apparatus (Puthenveedu and Linstedt, 2004).

8.2.2 Organisation of tER sites

Considering the model deriving from yeast studies proposing that tER organisation is directly correlated to the Golgi structure (Figure 1.9) and the fact that the three *Drosophila* Golgi matrix proteins localise to a significant extent at the tER sites provided the incentive to investigate the possible role

of these proteins on the tER organisation. However, out of the three Golgi matrix proteins tested, only dp115 depletion led to a dispersal and a 4-fold increase in number of the dSec23p-positive structures (tER marker), when compared to mock-depleted cells that exhibited an average of 20 discrete large spots (Figure 5.7). This result suggests that the involvement of dp115 in the organisation of the *Drosophila* tER sites is specific for this protein and not a general role for the Golgi matrix proteins. The specificity of dp115 effect was further exemplified in dSed5p-depleted cells that, although they exhibited a complete Golgi vesiculation, their tER site organisation remained largely unaffected (Figures 5.15 and 5.16).

Despite the fact that IEM microscopy provided support to the observed dispersal of the tER sites, it could not distinguish between the two possibilities that could explain this result. The first possibility is that dp115 may be involved in the biogenesis of the tER sites or the clustering of the smaller tER sites (Figure 8.2, model A). Similar to p115, dp115 is probably bound at the tER sites by the *Drosophila* homologue of Rab1 (Allan et al., 2000), and it might recruit in turn other effectors, such as v-SNARES, which being transmembrane proteins could interact with tER putative scaffold proteins leading to the stabilisation and growth of the tER sites by recruiting more COPII coat components. In yeast, at least three different peripherally associated or transmembrane ER proteins (Sec12p, Sec16p and Sed4p) have been implicated as scaffold proteins responsible for the organisation of the tER sites (see section 1.1.2), although recent data have question the involvement of Sec12 in such a tER scaffold (Soderholm et al., 2004)[1]. If this

[1] A recent characterisation of *P. pastoris* and *S. cerevisiae* Sec12 homologues showed that although *Pichia* Sec12 is concentrated at the tER sites, its localisation is not required for the recruitment of COPII coat subunits. Exchange of the cytosolic and lumenal domains between the two homologues led to the mislocalisation of *Pichia* Sec12 in the general ER without this affecting the distribution of the COPII component Sec13p or the Golgi marker Och1p. This suggests the existence of a tER scaffold not including Sec12p as an essential component (Soderholm et al., 2004).

hypothesis were true, dp115 depletion would result in the formation of smaller tER sites, which are dispersed throughout the ER network and generate fewer vesicles per tER site (Figure 8.2, model A), a situation that is similar to the tER organisation normally observed in S. cerevisiae (Preuss et al., 1992; Rossanese et al., 1999). Therefore, although the tethering proteins and v-SNAREs are commonly thought to be recruited on the COPII vesicles to prime them for fusion with the downstream compartment of the exocytic pathway, this model implies that they might have an additional, more active role in the structural and functional organisation of the tER sites. This notion is also supported by data showing that Uso1p (yeast homologue of p115) and v-SNAREs, such as Bos1p, Bet1p and Sec22p, but not t-SNARE Sed5p, are involved in the sorting of GPI-anchored proteins from the rest of the secretory proteins upon their exit at the tER sites (Morsomme and Riezman, 2002; Morsomme et al., 2003). Moreover, the lack of sorting defect in the case of yeast Sed5p correlates nicely with the lack of tER disorganisation upon dSed5p depletion from S2 cells.

The second hypothesis that could explain the disruption of tER sites caused by dp115 depletion is based on the proposed function of p115 and Uso1p as tethering factors involved in ER-Golgi transport (Gillingham and Munro, 2003; Barr and Short, 2003). According to this model, dp115 would function as a tethering molecule keeping the COPII-coated vesicles (or carriers of different shape) in close proximity to each other, so that they can efficiently fuse and eventually give rise to the first cis-Golgi cisterna after maturation and shape flattening (Figure 8.2, model B). Alternatively, this loose tethering of COPII vesicles at the tER sites could prevent their diffusion, keeping them at a high enough local concentration to sustain the maintenance of the Golgi stacks by accelerating the formation of the new

cisternae. At the molecular level, p115 could perform this tethering role either by forming anti-parallel homodimers or by participating in a larger tethering complex.

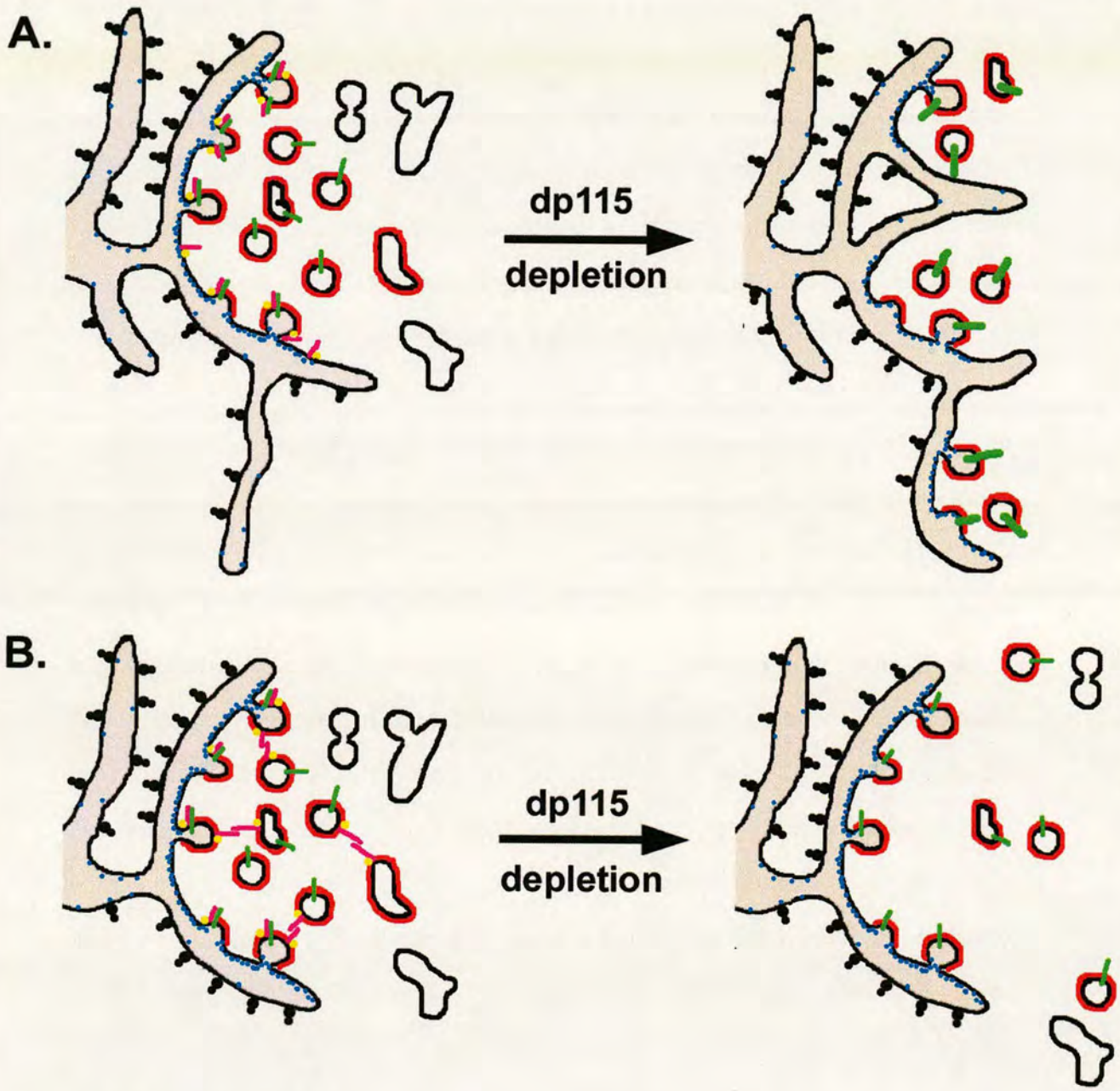

Figure 8.2: For legend see following page

Figure 8.2: Hypotheses explaining the effect of dp115 depletion on tER organisation in *Drosophila* S2 cells. Model A. dp115 (purple) is recruited on tER membranes by dRab1 (yellow). There, dp115 primes the COPII-coated vesicles (red) for docking and fusion by recruiting specific v-SNAREs (green). Additionally, directly or indirectly, dp115 could promote the local concentration of transmembrane or peripheral ER-associated proteins (blue) that act as scaffold for the functional and structural organisation of tER sites by recruiting COPII coat components. This may also lead to a merge of small neighbouring tER sites into a large one, which functions more efficiently. Upon dp115 depletion, smaller tER sites are formed in a scattered fashion throughout the ER, and fewer COPII vesicles are produced per tER site. This results in the observed increased number and reduced size of dSec23p-positive structures. **Model B.** Except for its role in recruiting v-SNAREs on the COPII vesicles, dp115 could act as a tethering molecule that keeps COPII-coated carriers in close proximity so that they can fuse with their target membranes more efficiently. This tethering function could involve homotypic interactions between dp115 molecules in the two neighbouring membranes (depicted), or the participation of dp115 in a larger tethering complex (not depicted). In the absence of dp115, the COPII-coated membranes are not tethered properly and can diffuse leading to the dispersed dSec23p pattern that was observed. However, it should be noted that the re-organisation of tER sites postulated by both models due to the dp115 depletion reduces only marginally anterograde transport.

The disruption of the tER sites upon dp115 depletion from S2 cells raised the possibility that the observed Golgi stack breakdown could be a consequence of the tER disorganisation. This is a valid argument considering that in *Pichia pastoris*, which exhibits a similar to S2 cells organisation in the early exocytic pathway, the tER sites have been shown to control Golgi biogenesis spatially and temporally (Rossanese et al., 1999; Bevis et al., 2002; Glick, 2002).

However, several observations during the course of this study strongly suggest that dp115 has at least two distinct functions, one in the organisation of the tER sites and one in the Golgi stack building and/or maintenance. First, the distribution of dp115, as it was determined by quantitative immuno-EM, showed that the protein is localised to an equal extent at both compartments (see section 5.3). Second, a kinetic study of the tER and Golgi disorganisation by IF failed to detect any significant difference in the timing between the two effects, therefore suggesting that the two processes are likely to take place concomitantly without one preceding the other (Figure 5.13). Third, dp115 is probably interacting with dSed5p, as their mammalian homologues do (Shorter et al., 2002), since the SNARE binding site is conserved in dp115 (see below). The fact that RNAi-mediated depletion of dSed5p led to Golgi vesiculation without significantly affecting the organisation of the tER sites is indicative of two distinct dp115 functions, with the recruitment of dSed5p by dp115 being important for the Golgi architecture, but not for dp115 role in tER organisation. Last, although the dp115/dGM130 double depletion led to a premature Golgi stack breakdown compared to the dp115 single depletion (Figure 5.18), a similar premature tER disruption was not observed (Figure 5.19), suggesting that dp115

interacts genetically with dGM130 for the structural organisation of the Golgi stacks, but the dp115 role at the tER organisation is dGM130-independent.

8.2.3 Anterograde intracellular transport

The role of *Drosophila* Golgi matrix proteins in anterograde transport along the exocytic pathway was investigated because of the proposed involvement of their mammalian homologues in several steps of intracellular transport (see section 1.5.2). This was performed by monitoring the transport of the transmembrane PM protein, Delta, and the secretion of scFv-Ck recombinant antibody (see chapter 6). Surprisingly, neither dp115 depletion nor any of the other Golgi matrix protein depletions (single or double) led to a significant inhibition in transport of the two reporter proteins, despite that at least three different RNAi conditions led to a quantitative disruption in the structural organisation of the early exocytic pathway. The strongest transport inhibition at steady state was observed in dp115/dGM130 depleted cells (Figure 6.7) and did not exceed 20% of the transport efficiency compared to mock-treated cells. The initial rate of Delta transport to the PM in dp115-depleted cells was also not more than 30% inhibited (Figure 6.4). Although not expected, these results were supported by the fact the cell proliferation during the course of the RNAi experiments was not affected in depleted cells relative to the mock-treated or mock-depleted cells (Figures 4.5A, 4.8A and 5.4A). This suggests that, similar to the protein markers used in our experiments, the endogenous proteins were likely to be transported as efficiently in depleted and non-depleted cells. In contrast, in dSed5p-depleted cells where transport to the PM was blocked, the cell proliferation was greatly reduced probably due to a cytokinesis defect (see section 5.6.2). This correlates nicely with a report showing that dSed5 mutant flies exhibit transport inhibition and cytokinesis defects during male spermatogenesis (Xu et al., 2003). Additionally, the fact

that transport to the plasma membrane and secretion are only marginally affected upon Golgi matrix protein depletions is in line with the observation that under physiological conditions during certain developmental stages and tissues, the presence of Golgi clusters (and not Golgi stacks) can sustain protein transport along the exocytic pathway (see chapter 7).

Golgi stack biogenesis in *Drosophila* imaginal discs and Golgi stack breakdown upon Golgi matrix protein depletion could be compared as two inverted processes. For example, dGM130 and dp115 expression levels were shown to be moderately up-regulated during the conversion of the larval clusters to Golgi stacks (Figure 7.6) is in accordance with the involvement of these two proteins in the structural preservation of the Golgi stacks in S2 cells (see chapters 4 and 5). Considering that the efficiency of RNAi-mediated depletions are usually about 90%, the dp115/dGM130 depletion from S2 cells could resemble to the situation in imaginal discs of the early- and mid-third instar larvae that seem to have basal amounts of these two proteins.

Despite this circumstantial evidence supporting the observed efficient anterograde transport in the absence of Golgi stacks in *Drosophila*, these results were surprising, especially for dp115, whose mammalian and yeast homologues have been shown to be essential for ER to Golgi transport. Injection of anti-p115 antibodies (Alvarez et al, 1999, 2001; Puthenveedu and Linstedt, 2001), interference with p115-GM130 interaction (Seemann et al, 2000b), RNAi depletion of p115 (Puthenveedu and Linstedt, 2004), as well as Uso1p mutant yeast strains (Sapperstein et al., 1995; 1996) have all resulted in significant inhibition of anterograde transport. Furthermore, mammalian GM130 has also been implicated in traffic along the early exocytic pathway (Alvarez et al, 2001).

These results raised the possibility that the early exocytic pathway in *Drosophila* S2 cells is functionally organised in a different way than in mammalian or yeast cells, or that S2 cells display a different need for Golgi matrix proteins than their proposed tethering role.

Early exocytic pathway in S2 cells behaves similar to the mammalian one upon treatment with transport inhibitors

In order to characterise the role of the *Drosophila* early exocytic pathway in anterograde transport, two known inhibitors of ER-Golgi transport, brefeldin A (BFA) and H89, were tested on S2 cells. As expected, in both cases, transport of Delta was inhibited (Figures 3.19 and 3.20), and alterations in the tER and Golgi organisation were observed by IF (Figures 3.7 and 3.8), although EM analysis will provide more information about the compartment where the transport block occurs or whether Golgi membranes are re-absorbed in the ER.

Regarding the compartment where transport of Delta is arrested in the presence of BFA, there are two possibilities. One could be that Delta exit from the ER is blocked. This is supported by the fact that in BFA-treated cells, the nuclear envelope is often strongly labelled for Delta (Figure 3.20). The large Delta-positive spots could then reflect specific ER subdomains, such as tER sites or sites where Delta could be retained by molecular chaperones due to imposed ER exit block. The other possibility could be that the arrest in transport occurs in the trafficking between Golgi and PM, and the Delta-positive structures correspond to Golgi membranes. In this case, the presence of Delta in the ER could be due to an interruption in the recycling of the ER-Golgi transport machinery that takes place through COP I-coated vesicles, the formation of which is disrupted by BFA (Jackson and Casanova, 2000). This could then indirectly inhibit or significantly impair the ER to Golgi transport of Delta and lead to an accumulation of a portion of

Delta also in the ER network. This could resemble the situation described in plant cells, where BFA does not lead to an absorbance of the Golgi back to the ER through tubulation, as in mammalian cells (Ritzanthaler et al., 2002). Instead, with the exception of the apparent loss of the cis-Golgi, the rest of the Golgi stack seems to persist forming hybrid ER-Golgi stacks (Ritzanthaler et al., 2002; Nebenführ et al., 2002).

The behaviour of Golgi resident proteins is another means of testing the behaviour of S2 cells upon BFA treatment. In mammalian cells, BFA has been shown to cause ER redistribution of the Golgi resident enzymes through the induction of retrograde tubule formation (Lippincott-Schwartz et al., 1989; Sciaky et al., 1997), while the Golgi matrix proteins are confined in punctate structures with pleiomorphic appearance (Seemann et al., 2000a; Ward et al., 2001). A Golgi-ER retrograde movement of Golgi resident proteins could also take place in S2 cells judging from the weak nuclear envelope staining observed for the Golgi marker d120kd (Figure 3.7), which is an integral protein tightly localised on the Golgi membranes under normal conditions (Figure 3.2), and could represent a Golgi resident enzyme. However, by IF, it cannot be determined whether the d120kd-positive spots that are still observed in BFA-treated S2 cells represent ER subdomains, Golgi clusters, or persisting Golgi stacks. BFA-resistant mammalian cells also exist (PtK1 and MDCK), although in these cells both Golgi structure and anterograde transport are not affected (Ktistakis et al., 1991). Therefore, a correlative live cell imaging and EM study of a Golgi marker could elucidate the effect of BFA on the exocytic pathway in *Drosophila* cells.

H89 seems to exert a similar effect to that described in mammalian cells (Lee and Linstedt, 2000; Aridor and Balch, 2000), since the tER localisation of COPII coat marker appeared to be impaired to a significant

degree (Figure 3.8). This might in turn result in the observed breakdown of the Golgi stacks, as it has been shown to happen in mammalian cells upon an ER exit block (Prescott et al., 2001; Ward et al., 2001; Miles et al., 2001; Puri and Linstedt, 2003).

Although further characterisation by EM is necessary to describe the effect of BFA and H89 in S2 cells, these results together with the transport inhibition upon dSed5p depletion suggest that the exocytic pathway in *Drosophila* is likely to be organised with similar molecular principles as in mammalian cells. Moreover, these three examples serve as positive controls for Delta transport assay and validate the marginal transport inhibition observed upon depletion of the *Drosophila* Golgi matrix proteins.

Is dp115 involved in anterograde transport?

Although the formation of a tethering complex between dp115, dGM130 and a functional orthologue of giantin is uncertain, other complexes, in which p115 was shown to take part in, are more likely to exist also in *Drosophila*. Several p115 domains involved in interactions with transport-related proteins are conserved in the dp115 molecule. First, the SNARE motif identified in mammalian p115, which bears weak homology to a conserved coiled-coil region of SNARE proteins (Weimbs et al, 1997; Shorter et al., 2002), is also present in dp115 (amino acids 660-726). This suggests that dp115 could catalyse the assembly of *Drosophila* SNARE proteins, such as dSed5p and dGos28p, as its mammalian counterpart does (Shorter et al., 2002). Second, the N-terminal head domain of p115 that is likely to contain the Rab1-binding site is also conserved in dp115 (Allan et al., 2000). Finally, the GBF1-binding domain, a recently identified p115 partner (Garcia-Mata and Sztul, 2003), is conserved in dp115, as well (amino acids 153-376). The fact that GBF1 acts as a guanine nucleotide exchange factor for Arf has

implicated p115 as a potential regulator of COP I-dependent transport events (Garcia-Mata et al., 2003).

The fact that p115 domains that are crucial for intracellular transport are conserved in dp115 protein raises the question why only a marginal inhibition in intracellular transport was observed upon its depletion. The first possibility is that dp115 is only involved in tER and Golgi structural organisation and not in transport. This would mean that the conserved domains between p115 and dp115, which were mentioned earlier, would be related in interactions solely related to dp115 structural roles.

A second more plausible explanation would be that dp115 is at least involved in the SNARE assembly. In mammalian cells, this role of p115 was shown to be catalytic at least *in vitro*. Therefore, a trace amount of dp115 could serve its function in transport. Although the expression of dp115 mRNA and protein were down-regulated below detection as assessed by RT-PCR and Western blotting, a residual amount of protein might have remained, which is a limitation of RNAi methodology, especially for proteins with long half-life, as dp115 seems to have.

A third possibility is that dp115 role in transport is only assisting and its role is only to optimise the rate of transport. This could be correlated with the formation of Golgi stacks from larval clusters in 3rd instar larvae imaginal discs, which indicates that Golgi matrix proteins could be involved in the building of Golgi stacked architecture independent of their possible role in intracellular transport, as tethering molecules (Gillingham and Munro, 2003; Barr and Short, 2003). Therefore, although an increase in transport efficiency may not be important for S2 cells, it might be critical for specific developmental processes that require rapid and extensive exocytosis, such as cellularisation during embryogenesis, glue secretion in late 3rd instar

salivary glands and cytokinesis and spermatid elongation during spermatogenesis (Thomopoulos et al., 1992; Lecuit and Wieschaus, 2000; Farkas et al., 2003).

A fourth hypothesis is that the putative role of dp115 in vesicle tethering and docking could have been overcome, because the formation of increased numbers of ER-derived vesicles would also increase the probability that the appropriate v- and t-SNAREs meet each other and assemble without the need for a role of dp115 in tethering. This is in agreement with the fact that the efficiency of the initial rate of transport is lower (~70%) than the steady state transport (~88%). Moreover, this possibility is also supported by the fact that in Ypt1p (yeast Rab1 homologue) and Uso1p mutant strains, the defect in vesicle tethering is rescued by overexpression of SNAREs involved in ER-Golgi transport (Sapperstein et al., 1996). By analogy, dp115 down-regulation might have led to an up-regulation of v- and t-SNAREs as a compensation mechanism.

Finally, the interaction between dp115 and GBF1 could also take place in *Drosophila*. However, through this complex, dp115 might modulate the function of Arf, which is related to the organisation of Golgi-based spectrin membrane skeleton (Godi et al., 1998; Garcia-Mata et al., 2003), and not the one related to the formation of the COP I vesicles. The possible involvement of spectrin in the Golgi architecture would then provide an additional mechanism for explaining the observed Golgi stack breakdown, through the action of GBF1.

8.3 Drosophila tER-Golgi units

The results obtained in the present study suggest that the early exocytic pathway in *Drosophila* cells is organised in functional tER-Golgi units (Figure 8.3). This holds true in S2 cells, as well as in several tissues that have been

examined (salivary glands, imaginal discs, spermatocytes). This organisation is comparable to that described in *Pichia pastoris* cells (Rossanese et al., 1999; Mogelsvang et al., 2003). The *Drosophila* tER-Golgi units are also embedded in a ribosome-excluding zone, which defines each unit and is thought to be preserved by a matrix of proteinaceous nature (Mollenhauer and Morre, 1978; Lucocq et al., 1987; Mogelsvang et al., 2003). This matrix has been proposed to comprise spectrin and its associated proteins, cytoskeleton elements and Golgi matrix proteins (Figure 7.3; de Matteis and Morrow, 2000; Barr and Short, 2003).

Although the proposed ribosome-excluding matrix involved in the structural organisation of the tER-Golgi unit could be capable for dynamic reorganisations, its continuous presence is at odds with the model of *de novo* formation of the Golgi apparatus (see section 1.2.2; Glick, 2002; Bevis et al., 2002). Studies in yeasts *P. pastoris* and *S. cerevisiae* have suggested that the formation of coherent Golgi stacks in *Pichia* may be a kinetic phenomenon due to the restricted COPII vesicle production at discrete tER sites (Rossanese et al., 1999; Bevis et al., 2002). In this view, a newly formed tER site gives rise to a Golgi stack by repeated rounds of COPII vesicle budding, which create new Golgi cisternae through their fusion (Figure 1.6; Glick, 2002). However, this model cannot account for the close association and regular spacing between the tER sites and the cis, medial and trans cisternae observed in an electron tomography study in *Pichia* cells (Mogelsvang et al., 2003). Moreover, in this study, tER sites associated with a single cisterna or COPII vesicle clusters was never observed, although considering their transient nature, these Golgi stack intermediates would be difficult to capture by electron microscopy (Mogelsvang et al., 2003).

In Drosophila, as it was mentioned in chapter 7, a gradual formation of Golgi stacks from COPII-positive vesicular-tubular clusters is taking place in imaginal discs of third-instar larvae, which could be consistent with the models of cisternal maturation and *de novo* Golgi formation. However, in agreement with the situation in *Pichia,* single Golgi cisternae were almost never observed under normal conditions in S2 cells, compared to the cells depleted from stacking factor dGRASP that exhibited frequently single cisternae. Moreover, several observations in S2 cells suggest that *Drosophila* Golgi stacks, at least in their architecture, can be independent of the structural and functional organisation of the tER sites (see following paragraph), without this excluding a *de novo* Golgi formation.

8.3.1 Structural independence of *Drosophila* Golgi stacks

Because the ribosome-excluding zone seems to surround both the Golgi stacks and the tER sites and several *Drosophila* Golgi matrix proteins have been localised both on Golgi and tER membranes, the possibility exists that a common structural scaffold could underlie both compartments. A putative tER matrix has been proposed to organise the tER sites in *Pichia* (Bevis et al., 2002; Glick, 2002; see also section 1.1.2). An observation that could sustain the presence of a common tER-Golgi matrix is that upon actin depolymerisation, both the Golgi stacks and the tER sites seem to undergo fragmentation in their immunofluorescence pattern. In addition, dp115 depletion from S2 cells has led to a concomitant disorganisation of both early exocytic compartments (Figure 5.13), implying that dp115 could be a component of the common matrix. This is also supported by the kinetic study of the tER and Golgi disorganisation in dp115-depleted cells, which showed that the two processes followed parallel kinetics.

However, in contrast to this proposal, there are several indications suggesting that the Golgi stacks in S2 cells behave autonomously relative to the tER site organisation and function. First, the quantitative breakdown of the Golgi stacks observed in dGRASP/dGM130- or dSed5p-depleted cells was not accompanied by a similar disruption in tER structural integrity (see sections 4.5, 4.6 and 5.6.2). Second, dp115 and dGM130 were shown to genetically interact only regarding the building/maintenance of the Golgi structure and not the tER organisation (see section 5.7). These results argue against the possibility that the putative matrix that may be involved in the Golgi architecture is common with the hypothetical tER matrix, because in this case it should be expected that its disruption would affect both the Golgi and the tER organisation. Therefore, a model that could encompass all the data from the RNAi experiments would be that dGRASP and dGM130 are only related to the Golgi matrix, while dp115 is likely to be shared by both matrices independently.

The model of the *de novo* assembly of the Golgi apparatus visualises the Golgi as a steady-state membrane structure that is maintained by the continuous membrane flow from the ER. In this view, the Golgi apparatus can be considered as an outgrowth of the ER, and not as an independent organelle (Zaal et al., 1999; Glick, 2002; see also introduction). A key prediction deriving from this model is that the biogenesis and maintenance is intrinsically linked to the ER export efficiency (Ward et al., 2001; Miles et al., 2001, Prescott et al., 2001; Puri and Linstedt, 2003), and therefore, a disruption in the Golgi stack organisation is likely to involve a disruption in membrane exit from the ER or an inhibition in ER to Golgi transport. However, the results obtained during the course of this project do not satisfy the prediction of this model. In particular, the fact that in at least three

different RNAi conditions the Golgi stacks were disorganised without the anterograde transport being significantly inhibited provides probably the strongest indication that the Golgi structure can be regulated independently of the membrane traffic from ER.

In conclusion, the *Drosophila* Golgi stacks seem to behave autonomously regarding their structural organisation, supporting the view of the Golgi apparatus as an independent organelle. Furthermore, the observation that the Golgi matrix proteins tested are involved in the Golgi architecture without this being a secondary effect of impaired transport is suggestive for the existence of a structural scaffold that could mediate the Golgi stack building and maintenance.

8.3.2 The role of Drosophila Golgi matrix proteins in tER-Golgi units

The Golgi matrix proteins are widely thought to function as tethering molecules keeping different membrane structures in close proximity, either for their structural organisation or their subsequent fusion (Gillingham and Munro, 2003). The study of dp115, dGM130 and dGRASP has confirmed the proposed from mammalian systems structural role of these Golgi matrix proteins in *Drosophila*, but has suggested that they might not be essential as tethering factors in anterograde transport, at least in S2 cells. However, this does not exclude the possibility that the tethering role of *Drosophila* Golgi matrix proteins might become critical in developmental processes that require a highly coordinated exocytic pathway. Moreover, the discrepancy in the phenotypes obtained upon their depletion combined with their high sequence diversity suggests that, despite being grouped as one protein family, each Golgi matrix protein may be differentially involved in the structural organisation of the early exocytic pathway.

Taking into consideration the experimental data described in this thesis together with observations from similar studies performed in mammalian and yeast cells, I would propose the following model to explain the organisation of the tER-Golgi units in *Drosophila* (Figure 8.3). According to this model, a structural matrix is likely to be involved in the organisation of the Golgi stacks. This matrix should be highly dynamic in nature to cope with the continuous need of the Golgi apparatus for structural re-organisation. The principal component of this structural matrix would comprise the spectrin molecules that form extensive linked mosaics with the participation of actin filaments (de Matteis and Morrow, 2000). This has been proposed in mammalian cells and seems to be also true in *Drosophila,* since spectrin isoforms were shown to colocalise with the Golgi membranes in cellularising embryos (Sisson et al., 2000). Microtubules are likely to be associated with the spectrin skeleton, but the experiments using microtubule depolymerising agents suggest that their role is not crucial for the structural integrity of the *Drosophila* Golgi apparatus. However, the microtubules could be involved in the movement and positioning of the Golgi apparatus as an organelle (see section 8.1).

The structural role of the Golgi matrix proteins could be to link the Golgi membranes with the spectrin skeleton, which in turn could be responsible for shaping up the Golgi stacks (Figure 8.3). The long coiled-coil structure that most of these proteins exhibit makes them ideal candidates to perform such a function. A protein that exemplifies this role of Golgi matrix proteins in *Drosophila* is Lva, which displays characteristics of the golgin family and was shown to interact with microtubules, microfilaments and spectrin itself (Sisson et al., 2000).

Additionally, such multiple interactions between golgins and spectrin or cytoskeleton may not only preserve the Golgi stack architecture (cisternae flattening and stacking), but also regulate the movement of Golgi membranes along cytoskeleton filaments. Bicaudal-D proteins and GMAP-210 are examples of coiled-coil, Golgi-associated proteins that are linked to the microtubule network through their association with the dynactin complex, and interference with their function has led to Golgi disassembly and intracellular transport inhibition (Infante et al., 1999; Hoogenraad et al., 2001; Pernet-Gallay et al., 2002). This type of cytoskeleton–dependent movements of Golgi elements have been shown to be important for the cellularisation in *Drosophila* embryos and the same probably holds true for other developmental stages and tissues (Lecuit and Wieschaus, 2000; Sisson et al., 2000).

Another potential indirect link between a Golgi matrix protein and spectrin skeleton is the recent demonstration that p115 recruits on Golgi membranes Arf-GEF GBF1, and therefore, it was proposed to regulate COP I-dependent transport dynamics through the interaction between GBF1 and Arf (Garcia-Mata and Sztul, 2003; Garcia-Mata et al., 2003). These data support the view of the Golgi spectrin skeleton as a network that facilitates the formation and transport of cargo carriers through interactions with adaptor complexes, such as the Arf-COP I system (de Matteis and Morrow, 2000; see also section 8.1). However, the lack of transport inhibition in dp115-depleted S2 cells has argued against this model. On the contrary, this result could be more in line with the proposed direct interaction between Arf and spectrin, which is independent of the COP I recruitment and has been postulated to be important for the Golgi architecture (Godi et al., 1998).

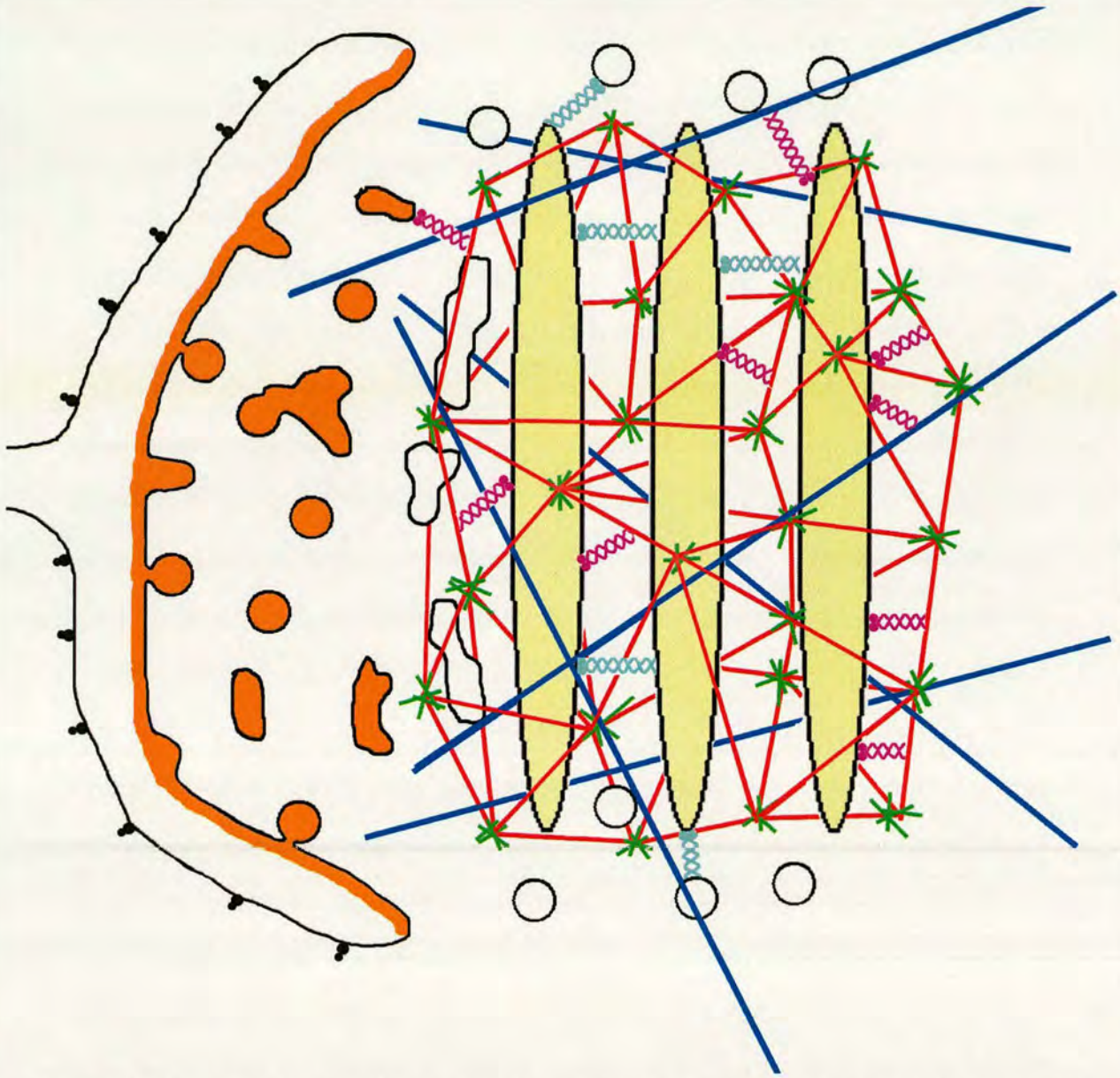

Figure 8.3: Model explaining the structural organisation of the tER-Golgi unit in *Drosophila* cells. Spectrin (red) and its associated proteins are forming a mesh-like structure around the Golgi stack (yellow), which is responsible for its organisation and stabilisation. The spectrin mosaics are linked via actin filaments (green), while connections between the spectrin skeleton and the microtubule network (blue) also exist. An important role of the Golgi matrix proteins in this structural matrix is to tether the Golgi membranes to the spectrin skeleton and the cytoskeleton elements (purple coiled-coil proteins). Additional functions of the Golgi matrix proteins concerning the Golgi architecture could involve their participation in cisternal stacking or the promotion of docking and fusion during vesicular transport (light blue coiled-coil proteins). The same Golgi structural matrix could extend to include the tER sites (orange) resulting in the observed ribosome-exclusion zone. Alternatively, tER sites may be organised by an independent tER matrix with different molecular composition, which does not exclude that certain molecules, like dp115, are shared between the two distinct matrices. It should be underlined that such matrices should be very dynamic in nature to be able to drive the continuous structural rearrangements of the early exocytic compartments.

As mentioned above, the same or a similar matrix to that underlying the Golgi stacks could also extend at the tER sites. Although morphologically, the Golgi stacks and tER sites form a tight unit, the differential effect imposed on their organisation in some RNAi experiments implies that the two compartments are likely to be organised by two independent matrices with distinct molecular composition. It is interesting to note that two of the proteins that have been thought to be part of a hypothetical tER matrix (Sec12p and Sec16p; see also introduction) seem to have homologues in *Drosophila* genome (CG5451 and CG32654, respectively), and therefore a functional study of them in S2 cells could elucidate a bit more the nature of this putative tER matrix (for Sec12p see note 1 in section 8.2.2). Moreover, a nice system to determine whether the Golgi matrix is associated with the tER sites would probably be the *Drosophila* embryo during cellularisation. The investigation of the tER organisation during the dynamic movements of the Golgi membranes at this stage (see section 1.7.3) would provide additional information whether Golgi and tER behave independently or they are restricted by a common matrix.

Drosophila Golgi matrix proteins are also likely to perform other functions in the early exocytic pathway through their multiple molecular interactions. dp115 seems to be the key protein among the family of golgins having an orchestrating role for the organisation of the early exocytic pathway. The results presented in this thesis are compatible with the proposed role for dp115 in SNARE recruitment at the tER sites (Allan et al., 2000) and do not exclude its possible involvement in promoting SNARE complex assembly (Shorter et al., 2002). Furthermore, the dp115 RNAi experiments have implied an additional role for dp115 in the structural organisation of the tER sites (see section 8.2.2; Model A in figure 8.2).

Moreover, although the disrupted tER integrity in dp115-depleted S2 cells does not affect the competence of these cells for anterograde transport of Delta, this does not rule out the possibility that transport of specific classes of proteins could be perturbed. For instance, like Uso1p, dp115 could be involved in the sorting of GPI-anchored proteins at the tER sites (Morsomme and Riezman, 2002; Morsomme et al., 2003). Therefore, it would be interesting to test whether the transport of a *Drosophila* GPI-anchored protein, such as the acetylcholinesterase (Incardona and Rosenberry, 1996), is affected in dp115-depleted cells. Finally, the Golgi matrix proteins could act as stacking factors by bridging neighbouring cisternae (Figure 8.3). This was clearly suggested for dGRASP, which although being a non-coiled-coil Golgi matrix protein, it significantly impaired cisternal stacking upon its depletion from S2 cells. Other golgins may also be involved in the stacking of Golgi cisternae.

8.3.3 Applications of the Golgi stack biogenesis in imaginal discs

The Golgi stack biogenesis in imaginal disc cells during third instar larval development could be very useful to study the role of proteins related to the architecture of the early exocytic pathway. Theoretically, a genetic screen for the identification of gene products involved in the Golgi stack formation could have as basis this transition from Golgi clusters to Golgi stacks. However, practically, this would involve immense amount of work, since it would require the examination of each mutant by electron microscopy, because in *Drosophila* cells, it is not possible to distinguish Golgi clusters from stacks by immunofluorescence, as in mammalian cells.

A more realistic approach would be to combine the Golgi stack biogenesis with the powerful technique of RNAi (see section 1.8). This methodology provides the opportunity to create transgenic flies carrying

hairpin-loop constructs with sequence specific for a particular Golgi-related gene. The production of dsRNA from this construct can be induced at specific time points and tissues if it is coupled to different GAL4 drivers, thus causing the silencing of the gene of interest only in the selected developmental stage and tissue (Tavernarakis et al., 2000; Kennerdell and Carthew, 2000; Lam and Thummel, 2000; Kalidas and Smith, 2002). In this way, the involvement of the *Drosophila* Golgi matrix proteins in the Golgi stack biogenesis can be directly addressed in imaginal discs during third-instar larval transition. Furthermore, the requirement for the different Golgi matrix proteins in different tissues can be tested. For instance, it would be interesting to examine whether the marginal transport inhibition observed upon their depletion in S2 cells is also true in tissues, such as salivary glands or spermatids, where there is need for high secretory activity. This type of experiments could help us determine whether *Drosophila* Golgi matrix proteins play only an assisting role in intracellular transport, as it is implied by the RNAi in S2 cells, and if so, in which tissues this slight reduction in transport could be critical for their development. In conclusion, the application of such an approach in *Drosophila* could greatly contribute in bridging the gap between cell and developmental biology.

References

Adams MD *et al.* 2000. The genome sequence of *Drosophila melanogaster*. *Science* 287:2185-2195.

Allan BB, Moyer BD, Balch WE. **2001.** Rab1 recruitment of p115 into a cis-SNARE complex: programming budding COPII vesicles for fusion. *Science*. 289:444-8.

Alvarez C, Fujita H, Hubbard A, Sztul E. **1999.** ER to Golgi transport: Requirement for p115 at a pre-Golgi VTC stage. *J Cell Biol.* 147:1205-22.

Alvarez C, Garcia-Mata R, Hauri HP, Sztul E. **2001.** The p115-interactive proteins GM130 and giantin participate in endoplasmic reticulum-Golgi traffic. *J Biol Chem.* 276:2693-700.

Andreeva AV, Kutuzov MA, Evans DE, Hawes CR. **1998.** Proteins involved in membrane transport between the ER and the Golgi apparatus: 21 putative plant homologues revealed by dbEST searching. *Cell Biol Int.* 22:145-60.

Andres AJ, Fletcher JC, Karim FD, Thummel CS. **1993.** Molecular analysis of the initiation of insect metamorphosis: a comparative study of Drosophila ecdysteroid-regulated transcription. *Dev Biol.* 160:388-404.

Antonny B, Madden D, Hamamoto S, Orci L, Schekman R. **2001.** Dynamics of the COPII coat with GTP and stable analogues. *Nat Cell Biol.* 3:531-7.

Appenzeller C, Andersson H, Kappeler F, Hauri HP. **1999.** The lectin ERGIC-53 is a cargo transport receptor for glycoproteins. *Nat Cell Biol.* 1:330-4.

Aridor M, Balch WE. 2000. Kinase signaling initiates coat complex II (COPII) recruitment and export from the mammalian endoplasmic reticulum. *J Biol Chem.* 275:35673-6.

Aridor M, Bannykh SI, Rowe T, Balch WE. **1995.** Sequential coupling between COPII and COPI vesicle coats in endoplasmic reticulum to Golgi transport. *J Cell Biol.* 131:875-93.

Aridor M, Fish KN, Bannykh S, Weissman J, Roberts TH, Lippincott-Schwartz J, Balch WE. **2001.** The Sar1 GTPase coordinates biosynthetic cargo selection with endoplasmic reticulum export site assembly. *J Cell Biol.* 152:213-29.

Ashburner M. 1989. Drosophila, a laboratory handbook. Cold Spring Harbor Laboratory Press, USA.

Ashrafi K, Chang FY, Watts JL, Fraser AG, Kamath RS, Ahringer J, Ruvkun G. **2003.** Genome-wide RNAi analysis of Caenorhabditis elegans fat regulatory genes. *Nature.* 421:268-72.

Axelsson MA, Warren G. 2004. Rapid, endoplasmic reticulum-independent diffusion of the mitotic Golgi haze. *Mol Biol Cell.* 15:1843-52.

Ayscough K, Hajibagheri NM, Watson R, Warren G. **1993**. Stacking of Golgi cisternae in Schizosaccharomyces pombe requires intact microtubules. *J Cell Sci.* 106:1227-37.

Babia T, Ayala I, Valderrama F, Mato E, Bosch M, Santaren JF, Renau-Piqueras J, Kok JW, Thomson TM, Egea G. **1999**. N-Ras induces alterations in Golgi complex architecture and in constitutive protein transport. *J Cell Sci.* 112:477-89.

Bainbridge SP, Bownes M. 1981. Staging the metamorphosis of Drosophila melanogaster. *J Embryol Exp Morphol.* 66:57-80.

Banfield DK, Lewis MJ, Rabouille C, Warren G, Pelham HR. **1994**. Localization of Sed5, a putative vesicle targeting molecule, to the cis-Golgi network involves both its transmembrane and cytoplasmic domains. *J Cell Biol.* 127:357-71.

Bannykh SI, Rowe T, Balch WE. **1996**. The organization of endoplasmic reticulum export complexes. *J Cell Biol.* 135:19-35.

Bannykh SI, Nishimura N, Balch WE. **1998**. Getting into the Golgi. *Trends Cell Biol.* 8:21-5.

Barlowe C. 2002. COPII-dependent transport from the endoplasmic reticulum. *Curr Opin Cell Biol.* 14:417-22.

Barlowe C. 2003. Signals for COPII-dependent export from the ER: what's the ticket out? *Trends Cell Biol.* 13:295-300.

Barlowe C, Schekman R. 1993. SEC12 encodes a guanine-nucleotide-exchange factor essential for transport vesicle budding from the ER. *Nature.* 365:347-9.

Barlowe C, Orci L, Yeung T, Hosobuchi M, Hamamoto S, Salama N, Rexach MF, Ravazzola M, Amherdt M, Schekman R. **1994**. COPII: a membrane coat formed by Sec proteins that drive vesicle budding from the endoplasmic reticulum. *Cell.* 77:895-907.

Barr FA.2002. The Golgi apparatus: going round in circles? *Trends Cell Biol.* 12:101-4.

Barr FA. 2004. Golgi inheritance: shaken but not stirred. *J Cell Biol.* 164:955-8.

Barr FA, Short B. 2003. Golgins in the structure and dynamics of the Golgi apparatus. *Curr Opin Cell Biol.* 15:405-13.

Barr FA, Puype M, Vandekerckhove J, Warren G. **1997**. GRASP65, a protein involved in the stacking of Golgi cisternae. *Cell.* 91:253-62.

Barr FA, Nakamura N, Warren G. **1998**. Mapping the interaction between GRASP65 and GM130, components of a protein complex involved in the stacking of Golgi cisternae. *EMBO J.* 17:3258-68.

Barton GM, Medzhitov R. 2002. Retroviral delivery of small interfering RNA into primary cells. *Proc Natl Acad Sci U S A.* 99:14943-5.

Beck KA, Nelson WJ. 1998. A spectrin membrane skeleton of the Golgi complex. *Biochim Biophys Acta.* 1404:153-60.

Beck KA, Buchanan JA, Malhotra V, Nelson WJ. **1994.** Golgi spectrin: identification of an erythroid beta-spectrin homolog associated with the Golgi complex. *J. Cell Biol.* 127:707-723.

Bevis BJ, Hammond AT, Reinke CA, Glick BS. **2002.** De novo formation of transitional ER sites and Golgi structures in Pichia pastoris. *Nat Cell Biol.* 4:750-6.

Bi X, Corpina RA, Goldberg J. **2002.** Structure of the Sec23/24-Sar1 pre-budding complex of the COPII vesicle coat. *Nature.* 419:271-7.

Biyasheva A, Do TV, Lu Y, Vaskova M, Andres AJ. **2001.** Glue secretion in the Drosophila salivary gland: a model for steroid-regulated exocytosis. *Dev Biol.* 231:234-51.

Blose SH, Meltzer DI, Feramisco JR. **1984.** 10-nm filaments are induced to collapse in living cells microinjected with monoclonal and polyclonal antibodies against tubulin. *J Cell Biol.* 98:847-58.

Bobinnec Y, Marcaillou C, Morin X, Debec A. **2003.** Dynamics of the endoplasmic reticulum during early development of Drosophila melanogaster. *Cell Motil Cytoskeleton.* 54:217-25.

Bonfanti L, Mironov AA Jr, Martinez-Menarguez JA, Martella O, Fusella A, Baldassarre M, Buccione R, Geuze HJ, Mironov AA, Luini A. **1998.** Procollagen traverses the Golgi stack without leaving the lumen of cisternae: evidence for cisternal maturation. *Cell.* 95:993-1003.

Bonifacino JS. 2004. The GGA proteins: adaptors on the move. *Nat Rev Mol Cell Biol.* 5:23-32.

Bonifacino JS, Glick BS. 2004. The mechanisms of vesicle budding and fusion. *Cell.* 116:153-66.

Borgese N, Brambillasca S, Soffientini P, Yabal M, Makarow M. **2003.** Biogenesis of tail-anchored proteins. *Biochem Soc Trans.* 31:1238-42.

Boutros M, Kiger AA, Armknecht S, Kerr K, Hild M, Koch B, Haas SA, Consortium HF, Paro R, Perrimon N. 2004. Genome-wide RNAi analysis of growth and viability in Drosophila cells. *Science.* 303:832-5.

Boyd M, Ashburner M. 1977. The hormonal control of salivary gland secretion in Drosophila melanogaster. Studies in vitro. *J. Insect Physiol.* 23:517-523

Bruckner K, Perez L, Clausen H, Cohen S. **2000**. Glycosyltransferase activity of Fringe modulates Notch-Delta interactions. *Nature*. 406:411-5.

Brummelkamp TR, Bernards R, Agami R. **2002**. A system for stable expression of short interfering RNAs in mammalian cells. *Science*. 296:550-3.

Brummelkamp TR, Nijman SM, Dirac AM, Bernards R. **2003**. Loss of the cylindromatosis tumour suppressor inhibits apoptosis by activating NF-kappaB. *Nature*. 424:797-801.

Burkhardt JK, Echeverri CJ, Nilsson T, Vallee RB. **1997**. Overexpression of the dynamitin (p50) subunit of the dynactin complex disrupts dynein-dependent maintenance of membrane organelle distribution. *J Cell Biol.* 139:469-84.

Burtis KC, Thummel CS, Jones CW, Karim FD, Hogness DS. **1990**. The Drosophila 74EF early puff contains E74, a complex ecdysone-inducible gene that encodes two ets-related proteins. *Cell*. 61:85-99.

Cabrera M, Muniz M, Hidalgo J, Vega L, Martin ME, Velasco A. **2003**. The retrieval function of the KDEL receptor requires PKA phosphorylation of its C-terminus. *Mol Biol Cell*. 14:4114-25.

Chabin-Brion K, Marceiller J, Perez F, Settegrana C, Drechou A, Durand G, Pous C. **2001**. The Golgi complex is a microtubule-organizing organelle. *Mol Biol Cell*. 7:2047-60.

Clemens JC, Worby CA, Simonson-Leff N, Muda M, Maehama T, Hemmings BA, Dixon JE. **2000**. Use of double-stranded RNA interference in Drosophila cell lines to dissect signal transduction pathways. *Proc Natl Acad Sci U S A*. 97:6499-503.

Clermont Y, Rambourg A, Hermo L. **1994**. Connections between the various elements of the cis- and mid-compartments of the Golgi apparatus of early rat spermatids. *Anat Rec*. 240:469-80.

Cluett EB, Brown WJ. 1992. Adhesion of Golgi cisternae by proteinaceous interactions: intercisternal bridges as putative adhesive structures. *J Cell Sci*. 103:773-84.

Cole NB, Sciaky N, Marotta A, Song J, Lippincott-Schwartz J. **1996**. Golgi dispersal during microtubule disruption: regeneration of Golgi stacks at peripheral endoplasmic reticulum exit sites. *Mol Biol Cell*. 7:631-50.

Cosson P, Letourneur F. 1994. Coatomer interaction with di-lysine endoplasmic reticulum retention motifs. *Science*. 263:1629-31.

Cosson P, Amherdt M, Rothman JE, Orci L. **2002**. A resident Golgi protein is excluded from peri-Golgi vesicles in NRK cells. *Proc Natl Acad Sci U S A*. 99:12831-4.

Dang DT, Perrimon N. 1992. Use of a yeast site-specific recombinase to generate embryonic mosaics in Drosophila. *Dev Genet*. 13:367-75.

Dascher C, Matteson J, Balch WE. **1994**. Syntaxin 5 regulates endoplasmic reticulum to Golgi transport. *J Biol Chem*. 269:29363-6.

De Matteis MA, Morrow JS. 2000. Spectrin tethers and mesh in the biosynthetic pathway. *J Cell Sci*. 113:2331-43.

Denli AM, Hannon GJ. 2003. RNAi: an ever-growing puzzle. *Trends Biochem Sci*. 28:196-201.

DePina AS, Langford GM. 1999. Vesicle transport: the role of actin filaments and myosin motors. *Microsc Res Tech*. 47:93-106.

Deschuyteneer M, Eckhardt AE, Roth J, Hill RL. **1988**. The subcellular localization of apomucin and nonreducing terminal N-acetylgalactosamine in porcine submaxillary glands. *J Biol Chem*. 263:2452-9.

Devroe E, Silver PA. 2002. Retrovirus-delivered siRNA. *BMC Biotechnol*. 2:15.

Diao A, Rahman D, Pappin DJ, Lucocq J, Lowe M. **2003**. The coiled-coil membrane protein golgin-84 is a novel rab effector required for Golgi ribbon formation. *J Cell Biol*. 160:201-12.

DiBello PR, Withers DA, Bayer CA, Fristrom JW, Guild GM. **1991**. The Drosophila Broad-Complex encodes a family of related proteins containing zinc fingers. *Genetics*. 129:385-97.

di Campli A, Valderrama F, Babia T, De Matteis MA, Luini A, Egea G. **1999**. Morphological changes in the Golgi complex correlate with actin cytoskeleton rearrangements. *Cell Motil Cytoskeleton*. 43:334-48.

Dirac-Svejstrup AB, Shorter J, Waters MG, Warren G. **2000**. Phosphorylation of the vesicle-tethering protein p115 by a casein kinase II-like enzyme is required for Golgi reassembly from isolated mitotic fragments. *J Cell Biol*. 150:475-88.

Duden R. 2003. ER-to-Golgi transport: COP I and COP II function. *Mol Membr Biol*. 20:197-207

Dunne J, Rabouille C. 2001. Lord of the flies: the Golgi in development. In: The ELSO Gazette: e-magazine of the European Life Scientist Organization (http://www.the-elso-gazette/magazines/issue3/mreviews/mreviews1.asp), issue 3 (January 1, 2001).

Dunne JC, Kondylis V, Rabouille C. **2002**. Ecdysone triggers the expression of Golgi genes in Drosophila imaginal discs via broad-complex. *Dev Biol*. 245:172-86.

Eilers U, Klumperman J, Hauri HP. **1989**. Nocodazole, a microtubule-active drug, interferes with apical protein delivery in cultured intestinal epithelial cells (Caco-2). *J Cell Biol*. 108:13-22.

Elbashir SM, Harborth J, Lendeckel W, Yalcin A, Weber K, Tuschl T. **2001.** Duplexes of 21-nucleotide RNAs mediate RNA interference in cultured mammalian cells. *Nature.* 411:494-8.

Elsner M, Hashimoto H, Nilsson T. **2003.** Cisternal maturation and vesicle transport: join the band wagon! *Mol Membr Biol.* 20:221-9.

Engqvist-Goldstein AE, Drubin DG. 2003. Actin assembly and endocytosis: from yeast to mammals. *Annu Rev Cell Dev Biol.* 19:287-332.

Espenshade P, Gimeno RE, Holzmacher E, Teung P, Kaiser CA. **1995.** Yeast SEC16 gene encodes a multidomain vesicle coat protein that interacts with Sec23p. *J Cell Biol.* 131:311-24.

Farkas RM, Giansanti MG, Gatti M, Fuller MT. **2003.** The Drosophila Cog5 homologue is required for cytokinesis, cell elongation, and assembly of specialized Golgi architecture during spermatogenesis. *Mol Biol Cell.* 14:190-200

Farmaki T, Ponnambalam S, Prescott AR, Clausen H, Tang BL, Hong W, Lucocq JM. **1999.** Forward and retrograde trafficking in mitotic animal cells. ER-Golgi transport arrest restricts protein export from the ER into COPII-coated structures. *J Cell Sci.* 112:589-600.

Farquhar MG, Hauri HP. 1997. Protein sorting and vesicular traffic in the Golgi apparatus. In The Golgi Apparatus (eds Berger, E.G. & Roth, J., Birkhauser Verlag, Basel). pp 63-129.

Farquhar MG, Palade GE. 1998. The Golgi apparatus: 100 years of progress and controversy. *Trends Cell Biol.* 8:2-10.

Featherstone C, Griffiths G, Warren G. **1985.** Newly synthesized G protein of vesicular stomatitis virus is not transported to the Golgi complex in mitotic cells. *J Cell Biol.* 101:2036-46.

Fire A, Xu S, Montgomery MK, Kostas SA, Driver SE, Mello CC. **1998.** Potent and specific genetic interference by double-stranded RNA in Caenorhabditis elegans. *Nature* 391: 806-811.

Foe VE, Alberts BM. 1983. Studies of nuclear and cytoplasmic behaviour during the five mitotic cycles that precede gastrulation in *Drosophila* embryogenesis. *J. Cell Sci.* 61:31-70.

Foe VE, Odell G, Edgar BA. **1993.** Mitosis and morphogenesis in the *Drosophila* embryo: point and counterpoint. In *The Development of Drosophila melanogaster.* (eds. Bates, M. & Martinez Arias, A., Cold Spring Harbor, NY, Cold Spring Harbor Laboratory Press). pp 149-300.

Franzen C, Muller A. 1999. Molecular techniques for detection, species differentiation, and phylogenetic analysis of microsporidia. *Clin Microbiol Rev.* 12:243-85.

Fricker M, Hollinshead M, White N, Vaux D. **1997**. Interphase nuclei of many mammalian cell types contain deep, dynamic, tubular membrane-bound invaginations of the nuclear envelope. *J Cell Biol.* 136:531-44.

Fristrom D, Fristrom JW. 1993. The metamorphic development of the adult epidermis. In *The Development of Drosophila melanogaster*. (eds. Bates, M. & Martinez Arias, A., Cold Spring Harbor, NY, Cold Spring Harbor Laboratory Press). pp 843-897.

Fullilove SL, Jacobson AG. 1971. Nuclear elongation and cytokinesis in Drosophila montana. *Dev Biol.* 26:560-77.

Garcia-Mata R, Sztul E. 2003. The membrane-tethering protein p115 interacts with GBF1, an ARF guanine-nucleotide-exchange factor. *EMBO Rep.* 4:320-5.

Garcia-Mata R, Szul T, Alvarez C, Sztul E. **2003.** ADP-ribosylation factor/COPI-dependent events at the endoplasmic reticulum-Golgi interface are regulated by the guanine nucleotide exchange factor GBF1. *Mol Biol Cell.* 14:2250-61.

Garen A, Kauvar L, Lepesant JA. **1977**. Role of ecdysone in *Drosophila* development. *Proc. Natl. Acad. Sci. USA.* 74:5099-5103.

Gartner A. 2001. Genome-wide genetic screening by RNAi – a glimpse of the future. In: The ELSO Gazette: e-magazine of the European Life Scientist Organization (http://www.the-elso-gazette/magazines/issue14/mreviews/mrevie ws3.asp), issue 14 (April, 2001).

Gillingham AK, Munro S. 2003. Long coiled-coil proteins and membrane traffic. *Biochim Biophys Acta.* 1641:71-85.

Gimeno RE, Espenshade P, Kaiser CA. **1995**. SED4 encodes a yeast endoplasmic reticulum protein that binds Sec16p and participates in vesicle formation. *J Cell Biol.* 131:325-38.

Giraudo CG, Maccioni HJ. 2003. Endoplasmic reticulum export of glycosyltransferases depends on interaction of a cytoplasmic dibasic motif with Sar1. *Mol Biol Cell.* 14:3753-66.

Glick BS. 2000. Organization of the Golgi apparatus. *Curr Opin Cell Biol.*12:450-6.

Glick BS. 2002. Can the Golgi form de novo? *Nat Rev Mol Cell Biol.* 3:615-9.

Glick BS, Malhotra V. 1998. The curious status of the Golgi apparatus. *Cell.* 95:883-9.

Glick BS, Elston T, Oster G. **1997**. A cisternal maturation mechanism can explain the asymmetry of the Golgi stack. *FEBS Lett.* 414:177-81.

Godi A, Santone I, Pertile P, Devarajan P, Stabach PR, Morrow JS, Di Tullio G, Polishchuk R, Petrucci TC, Luini A, De Matteis MA. **1998**. ADP ribosylation factor regulates spectrin binding to the Golgi complex. *Proc. Nat. Acad. Sci. USA* 95: 8607-8612.

Grishok A, Pasquinelli AE, Conte D, Li N, Parrish S, Ha I, Baillie DL, Fire A, Ruvkun G, Mello CC. **2001**. Genes and mechanisms related to RNA interference regulate expression of the small temporal RNAs that control C. elegans developmental timing. *Cell*. 106:23-34.

Hammond AT, Glick BS. 2000. Dynamics of transitional endoplasmic reticulum sites in vertebrate cells. *Mol Biol Cell*. 11:3013-30.

Hannon GJ. 2002. RNA interference. *Nature*. 418:244-51.

Hardwick KG, Pelham HR. 1992. SED5 encodes a 39-kD integral membrane protein required for vesicular transport between the ER and the Golgi complex. *J Cell Biol*. 119:513-21.

Hauri HP, Schweizer A.1992. The endoplasmic reticulum-Golgi intermediate compartment. *Curr Opin Cell Biol*. 4:600-8.

Hauri HP, Kappeler F, Andersson H, Appenzeller C. **2000**. ERGIC-53 and traffic in the secretory pathway. *J Cell Sci*. 113:587-96.

He CY, Ho HH, Malsam J, Chalouni C, West CM, Ullu E, Toomre D, Warren G. **2004**. Golgi duplication in Trypanosoma brucei. *J Cell Biol*. 165:313-21.

Hirschberg K, Miller CM, Ellenberg J, Presley JF, Siggia ED, Phair RD, Lippincott-Schwartz J. **1998**. Kinetic analysis of secretory protein traffic and characterization of golgi to plasma membrane transport intermediates in living cells. *J Cell Biol*. 143:1485-503.

Holleran EA, Tokito MK, Karki S, Holzbaur EL. **1996**. Centractin (ARP1) associates with spectrin revealing a potential mechanism to link dynactin to intracellular organelles. *J Cell Biol*. 135:1815-29.

Holleran EA, Ligon LA, Tokito M, Stankewich MC, Morrow JS, Holzbaur EL. **2001**. Beta III spectrin binds to the Arp1 subunit of dynactin. *J Biol Chem*. 276:36598-605.

Hoogenraad CC, Akhmanova A, Howell SA, Dortland BR, De Zeeuw CI, Willemsen R, Visser P, Grosveld F, Galjart N. **2001**. Mammalian Golgi-associated Bicaudal-D2 functions in the dynein-dynactin pathway by interacting with these complexes. *EMBO J*. 20:4041-54.

Hudson DF, Morrison C, Ruchaud S, Earnshaw WC. **2002**. Reverse genetics of essential genes in tissue-culture cells: 'dead cells talking'. *Trends Cell Biol*. 12:281-7.

Hurt EC, Mutvei A, Carmo-Fonseca M. **1992**. The nuclear envelope of the yeast Saccharomyces cerevisiae. *Int Rev Cytol*.136:145-84.

Infante C, Ramos-Morales F, Fedriani C, Bornens M, Rios RM. **1999**. GMAP-210, a cis-Golgi network-associated protein, is a minus end microtubule-binding protein. *J Cell Biol*. 145:83-98.

Jackson CL, Casanova JE. 2000. Turning on ARF: the Sec7 family of guanine-nucleotide-exchange factors. *Trends Cell Biol.* 10:60-7.

Jesch SA, Linstedt AD. 1998. The Golgi and endoplasmic reticulum remain independent during mitosis in HeLa cells. *Mol Biol Cell.* 9:623-35.

Jesch SA, Mehta AJ, Velliste M, Murphy RF, Linstedt AD. **2001**. Mitotic Golgi is in a dynamic equilibrium between clustered and free vesicles independent of the ER. *Traffic.* 2:873-84.

Jokitalo E, Cabrera-Poch N, Warren G, Shima DT. **2001**. Golgi clusters and vesicles mediate mitotic inheritance independently of the endoplasmic reticulum. *J Cell Biol.* 154:317-30.

Kalidas S, Smith DP. 2002. Novel genomic cDNA hybrids produce effective RNA interference in adult Drosophila. *Neuron.* 33:177-84.

Kamath RS, Ahringer J. 2003. Genome-wide RNAi screening in Caenorhabditis elegans. *Methods.* 30:313-21.

Karim FD, Guild GM, Thummel CS. **1993**. The Drosophila Broad-Complex plays a key role in controlling ecdysone-regulated gene expression at the onset of metamorphosis. *Development.* 118:977-88.

Katinka MD, Duprat S, Cornillot E, Metenier G, Thomarat F, Prensier G, Barbe V, Peyretaillade E, Brottier P, Wincker P, Delbac F, El Alaoui H, Peyret P, Saurin W, Gouy M, Weissenbach J, Vivares CP. **2001**. Genome sequence and gene compaction of the eukaryote parasite Encephalitozoon cuniculi. *Nature.* 414:450-3.

Kennerdell JR, Carthew RW. 1998. Use of dsRNA-mediated genetic interference to demonstrate that frizzled and frizzled 2 act in the wingless pathway. *Cell.* 95:1017-26.

Kennerdell JR, Carthew RW. 2000. Heritable gene silencing in Drosophila using double-stranded RNA. *Nat Biotechnol.* 18:896-8.

Kerrebrock AW, Moore DP, Wu JS, Orr-Weaver TL. **1995**. Mei-S332, a Drosophila protein required for sister-chromatid cohesion, can localize to meiotic centromere regions. *Cell.* 83:247-56.

Ketting RF, Fischer SE, Bernstein E, Sijen T, Hannon GJ, Plasterk RH. **2001**. Dicer functions in RNA interference and in synthesis of small RNA involved in developmental timing in C. elegans. Genes Dev. 15:2654-9.

Kiss I, Beaton AH, Tardiff J, Fristrom D, Fristrom JW. **1988**. Interactions and developmental effects of mutations in the Broad-Complex of Drosophila melanogaster. *Genetics.* 118:247-59.

Klausner RD, Donaldson JG, Lippincott-Schwartz J. **1992.** Brefeldin A: insights into the control of membrane traffic and organelle structure. *J Cell Biol.* 116:1071-80.

Klueg KM, Parody TR, Muskavitch MA. **1998.** Complex proteolytic processing acts on Delta, a transmembrane ligand for Notch, during Drosophila development. *Mol Biol Cell.* 9:1709-23.

Klumperman J. 2000. Transport between ER and Golgi. *Curr Opin Cell Biol.* 12:445-9.

Koelle MR, Talbot WS, Segraves WA, Bender MT, Cherbas P, Hogness DS. **1991.** The Drosophila EcR gene encodes an ecdysone receptor, a new member of the steroid receptor superfamily. *Cell.* 67:59-77.

Kondylis V, Rabouille C. 2003. A novel role for dp115 in the organization of tER sites in Drosophila. *J Cell Biol.* 162:185-98.

Kondylis V, Goulding SE, Dunne JC, Rabouille C. **2001.** Biogenesis of Golgi stacks in imaginal discs of Drosophila melanogaster. *Mol Biol Cell.* 12:2308-27.

Kornfeld R, Kornfeld S. 1985. Assembly of asparagine-linked oligosaccharides. *Annu Rev Biochem.* 54:631-64.

Ktistakis NT, Roth MG, Bloom GS. **1991.** PtK1 cells contain a nondiffusible, dominant factor that makes the Golgi apparatus resistant to brefeldin A. *J Cell Biol.* 113:1009-23.

Kuo A, Zhong C, Lane WS, Derynck R. **2000.** Transmembrane transforming growth factor-alpha tethers to the PDZ domain-containing, Golgi membrane-associated protein p59/GRASP55. *EMBO J.* 19:6427-39.

Kurihara T, Hamamoto S, Gimeno RE, Kaiser CA, Schekman R, Yoshihisa T. **2000.** Sec24p and Iss1p function interchangeably in transport vesicle formation from the endoplasmic reticulum in Saccharomyces cerevisiae. *Mol Biol Cell.* 11:983-98.

Ladinsky MS, Mastronarde DN, McIntosh JR, Howell KE, Staehelin LA. **1999.** Golgi structure in three dimensions: functional insights from the normal rat kidney cell. *J Cell Biol.* 144:1135-49.

Lam G, Thummel CS. 2000. Inducible expression of double-stranded RNA directs specific genetic interference in Drosophila. *Curr Biol.* 10:957-63.

Lecuit T, Wieschaus E. 2000. Polarized insertion of new membrane from a cytoplasmic reservoir during cleavage of the Drosophila embryo. *J Cell Biol.* 150:849-60.

Lee TH, Linstedt AD. 2000. Potential role for protein kinases in regulation of bidirectional endoplasmic reticulum-to-Golgi transport revealed by protein kinase inhibitor H89. *Mol Biol Cell.* 11:2577-90.

Lee JR, Urban S, Garvey CF, Freeman M. **2001**. Regulated intracellular ligand transport and proteolysis control EGF signal activation in Drosophila. *Cell*. 107:161-71.

Lesa GM, Seemann J, Shorter J, Vandekerckhove J, Warren G. **2000**. The amino-terminal domain of the golgi protein giantin interacts directly with the vesicle-tethering protein p115. *J Biol Chem*. 275:2831-6.

Linstedt AD. 1999. Stacking the cisternae. *Curr Biol*. 9:R893-6.

Linstedt AD, Foguet M, Renz M, Seelig HP, Glick BS, Hauri HP. **1995**. A C-terminally-anchored Golgi protein is inserted into the endoplasmic reticulum and then transported to the Golgi apparatus. *Proc Natl Acad Sci U S A*. 92:5102-5.

Linstedt AD, Jesch SA, Mehta A, Lee TH, Garcia-Mata R, Nelson DS, Sztul E. **2000**. Binding relationships of membrane tethering components. The giantin N terminus and the GM130 N terminus compete for binding to the p115 C terminus. *J Biol Chem*. 275:10196-201.

Lippincott-Schwartz J, Yuan LC, Bonifacino JS, Klausner RD. **1989**. Rapid redistribution of Golgi proteins into the ER in cells treated with brefeldin A: evidence for membrane cycling from Golgi to ER. *Cell*. 56:801-13.

Lippincott-Schwartz J, Donaldson JG, Schweizer A, Berger EG, Hauri HP, Yuan LC, Klausner RD. **1990**. Microtubule-dependent retrograde transport of proteins into the ER in the presence of brefeldin A suggests an ER recycling pathway. *Cell*. 60:821-36.

Lippincott-Schwartz J, Roberts TH, Hirschberg K. **2000**. Secretory protein trafficking and organelle dynamics in living cells. *Annu Rev Cell Dev Biol*. 16:557-89.

Longman D, Johnstone IL, Caceres JF. **2000**. Functional characterization of SR and SR-related genes in Caenorhabditis elegans. *EMBO J*. 19:1625-37.

Lowe M. 2002. Golgi complex: biogenesis de novo? *Curr Biol*. 12:R166-7.

Lowe M, Lane JD, Woodman PG, Allan VJ. **2004**. Caspase-mediated cleavage of syntaxin 5 and giantin accompanies inhibition of secretory traffic during apoptosis. *J Cell Sci*. 117:1139-50.

Lucocq JM, Pryde JG, Berger EG, Warren G. **1987**.A mitotic form of the Golgi apparatus in HeLa cells. *J Cell Biol*. 104:865-74.

Luzio JP, Brake B, Banting G, Howell KE, Braghetta P, Stanley KK. **1990**. Identification, sequencing and expression of an integral membrane protein of the trans-Golgi network (TGN38). *Biochem J*. 270:97-102.

Mahowald AP, Goralski TJ, Caulton JH. **1983**. In vitro activation of Drosophila eggs. *Dev Biol*. 98:437-45.

Makarow M. 1988. Secretion of invertase in mitotic yeast cells. *EMBO J.* 7:1475-82.

Mandaron, P. 1971. Mechanism of imaginal disk evagination in *Drosophila. Dev. Biol.* 25:581-605

Marra P, Maffucci T, Daniele T, Tullio GD, Ikehara Y, Chan EK, Luini A, Beznoussenko G, Mironov A, De Matteis MA. **2001.** The GM130 and GRASP65 Golgi proteins cycle through and define a subdomain of the intermediate compartment. *Nat Cell Biol.* 3:1101-13.

Marsh BJ, Howell KE. 2002. The mammalian Golgi--complex debates. *Nat Rev Mol Cell Biol.* 3:789-95.

Marsh BJ, Mastronarde DN, Buttle KF, Howell KE, McIntosh JR. **2001.** Organellar relationships in the Golgi region of the pancreatic beta cell line, HIT-T15, visualized by high resolution electron tomography. *Proc Natl Acad Sci U S A.* 98:2399-406.

Marsh BJ, Volkmann N, McIntosh JR, Howell KE. **2004.** Direct continuities between cisternae at different levels of the Golgi complex in glucose-stimulated mouse islet beta cells. *Proc Natl Acad Sci U S A.* 101:5565-70.

Martienssen RA, Colot V. 2001. DNA methylation and epigenetic inheritance in plants and filamentous fungi. *Science.* 293:1070-4.

Martinez-Menarguez JA, Geuze HJ, Slot JW, Klumperman J. **1999.** Vesicular tubular clusters between the ER and Golgi mediate concentration of soluble secretory proteins by exclusion from COPI-coated vesicles. *Cell.* 98:81-90.

Martinez-Menarguez JA, Prekeris R, Oorschot VM, Scheller R, Slot JW, Geuze HJ, Klumperman J. **2001.** Peri-Golgi vesicles contain retrograde but not anterograde proteins consistent with the cisternal progression model of intra-Golgi transport. *J Cell Biol.* 155:1213-24.

Matynia A, Salus SS, Sazer S. **2002.** Three proteins required for early steps in the protein secretory pathway also affect nuclear envelope structure and cell cycle progression in fission yeast. *J Cell Sci.* 115:421-31.

McKay RR, Zhu L, Shortridge RD. **1995.** A Drosophila gene that encodes a member of the protein disulfide isomerase/phospholipase C-alpha family. *Insect Biochem Mol Biol.* 25:647-54.

Melkonian M, Becker B, Becker D. **1991.** Scale formation in algae. *J Electron Microsc Tech.* 17:165-78.

Mellman I, Warren G. 2000. The road taken: past and future foundations of membrane traffic. *Cell.* 100:99-112.

Miles S, McManus H, Forsten KE, Storrie B. **2001**. Evidence that the entire Golgi apparatus cycles in interphase HeLa cells: sensitivity of Golgi matrix proteins to an ER exit block. *J Cell Biol.* 155:543-55.

Miller EA, Beilharz TH, Malkus PN, Lee MC, Hamamoto S, Orci L, Schekman R. **2003**. Multiple cargo binding sites on the COPII subunit Sec24p ensure capture of diverse membrane proteins into transport vesicles. *Cell.* 114:497-509.

Mironov AA, Mironov AA Jr, Beznoussenko GV, Trucco A, Lupetti P, Smith JD, Geerts WJ, Koster AJ, Burger KN, Martone ME, Deerinck TJ, Ellisman MH, Luini A. **2003**. ER-to-Golgi carriers arise through direct en bloc protrusion and multistage maturation of specialized ER exit domains. *Dev Cell.* 5:583-94.

Misteli T. 2001. The concept of self-organization in cellular architecture. *J Cell Biol.* 155:181-5.

Misumi Y, Misumi Y, Miki K, Takatsuki A, Tamura G, Ikehara Y. **1986**. Novel blockade by brefeldin A of intracellular transport of secretory proteins in cultured rat hepatocytes. *J Biol Chem.* 261:11398-403.

Mogelsvang S, Gomez-Ospina N, Soderholm J, Glick BS, Staehelin LA. **2003**. Tomographic evidence for continuous turnover of Golgi cisternae in Pichia pastoris. *Mol Biol Cell.* 14:2277-91.

Mollenhauer HH. 1965. An intercisternal structure in the Golgi apparatus. *J Cell Biol.* 12:439-46.

Mollenhauer HH, Morre DJ. 1978. Structural compartmentation of the cytosol: zones of exclusion, zones of adhesion, cytoskeletal and intercisternal elements. *Subcell Biochem.* 5:327-59.

Morris A, Tannenbaum J. 1980. Cytochalasin D does not produce net depolymerization of actin filaments in HEp-2 cells. *Nature.* 287:637-9.

Morsomme P, Riezman H. 2002. The Rab GTPase Ypt1p and tethering factors couple protein sorting at the ER to vesicle targeting to the Golgi apparatus. *Dev Cell.* 2:307-17.

Morsomme P, Prescianotto-Baschong C, Riezman H. **2003**. The ER v-SNAREs are required for GPI-anchored protein sorting from other secretory proteins upon exit from the ER. *J Cell Biol.* 162:403-12.

Mortensen K, Larsson LI. 2003. Effects of cytochalasin D on the actin cytoskeleton: association of neoformed actin aggregates with proteins involved in signaling and endocytosis. *Cell Mol Life Sci.* 60:1007-12.

Mossessova E, Bickford LC, Goldberg J. **2003**. SNARE selectivity of the COPII coat. *Cell.* 114:483-95.

Moyer BD, Allan BB, Balch WE. **2001**. Rab1 interaction with a GM130 effector complex regulates COPII vesicle cis--Golgi tethering. *Traffic.* 2:268-76.

Munro S. 1998. Localization of proteins to the Golgi apparatus. *Trends Cell Biol.* 8:11-5.

Munro S. 2002. More than one way to replicate the Golgi apparatus. *Nat Cell Biol.* 4:E223-4.

Munro S, Freeman M. 2000. The notch signalling regulator fringe acts in the Golgi apparatus and requires the glycosyltransferase signature motif DXD. *Curr Biol.* 10:813-20.

Munro S, Nichols BJ. 1999. The GRIP domain - a novel Golgi-targeting domain found in several coiled-coil proteins. *Curr Biol.* 9:377-80.

Murshid A, Presley JF. 2004. ER-to-Golgi transport and cytoskeletal interactions in animal cells. *Cell Mol Life Sci.* 61:133-45.

Nagai K, Oubridge C, Kuglstatter A, Menichelli E, Isel C, Jovine L. **2003**. Structure, function and evolution of the signal recognition particle. *EMBO J.* 22:3479-85.

Nakajima H, Hirata A, Ogawa Y, Yonehara T, Yoda K, Yamasaki M. **1991**. A cytoskeleton-related gene, uso1, is required for intracellular protein transport in Saccharomyces cerevisiae. *J Cell Biol.* 113:245-60.

Nakamura N, Rabouille C, Watson R, Nilsson T, Hui N, Slusarewicz P, Kreis TE, Warren G. **1995**. Characterization of a cis-Golgi matrix protein, GM130. *J Cell Biol.* 131:1715-26.

Nakamura N, Lowe M, Levine TP, Rabouille C, Warren G. **1997**. The vesicle docking protein p115 binds GM130, a cis-Golgi matrix protein, in a mitotically regulated manner. *Cell.* 89:445-55.

Nebenfuhr A, Gallagher LA, Dunahay TG, Frohlick JA, Mazurkiewicz AM, Meehl JB, Staehelin LA. **1999**. Stop-and-go movements of plant Golgi stacks are mediated by the acto-myosin system. *Plant Physiol.* 121:1127-42.

Nebenfuhr A, Ritzenthaler C, Robinson DG. **2002**. Brefeldin A: deciphering an enigmatic inhibitor of secretion. *Plant Physiol.* 130:1102-8.

Nelson DS, Alvarez C, Gao YS, Garcia-Mata R, Fialkowski E, Sztul E. **1998**. The membrane transport factor TAP/p115 cycles between the Golgi and earlier secretory compartments and contains distinct domains required for its localization and function. *J Cell Biol.* 143:319-31.

Neumann U, Brandizzi F, Hawes C. **2003**. Protein transport in plant cells: in and out of the Golgi. *Ann Bot (Lond).* 92:167-80.

Nilsson T, Pypaert M, Hoe MH, Slusarewicz P, Berger EG, Warren G. **1993**. Overlapping distribution of two glycosyltransferases in the Golgi apparatus of HeLa cells. *J Cell Biol.* 120:5-13.

Nizak C, Martin-Lluesma S, Moutel S, Roux A, Kreis TE, Goud B, Perez F. **2003**. Recombinant antibodies against subcellular fractions used to track endogenous Golgi protein dynamics in vivo. *Traffic.* 4:739-53.

Nykanen A, Haley B, Zamore PD. **2001**.ATP requirements and small interfering RNA structure in the RNA interference pathway. *Cell.* 107:309-21.

O'Neil NJ, Martin RL, Tomlinson ML, Jones MR, Coulson A, Kuwabara PE. **2001**. RNA-mediated interference as a tool for identifying drug targets. *Am J Pharmacogenomics.* 1:45-53.

Oprins A, Duden R, Kreis TE, Geuze HJ, Slot JW. **1993**. Beta-COP localizes mainly to the cis-Golgi side in exocrine pancreas. *J Cell Biol.* 121:49-59.

Orci L, Ravazzola M, Meda P, Holcomb C, Moore HP, Hicke L, Schekman R. **1991**. Mammalian Sec23p homologue is restricted to the endoplasmic reticulum transitional cytoplasm. *Proc Natl Acad Sci U S A.* 88:8611-5.

Orci L, Stamnes M, Ravazzola M, Amherdt M, Perrelet A, Sollner TH, Rothman JE. **1997**. Bidirectional transport by distinct populations of COPI-coated vesicles. *Cell.* 90:335-49.

Paccaud JP, Reith W, Carpentier JL, Ravazzola M, Amherdt M, Schekman R, Orci L. **1996**.Cloning and functional characterization of mammalian homologues of the COPII component Sec23. *Mol Biol Cell.* 7:1535-46.

Paddison PJ, Caudy AA, Hannon GJ. **2002**. Stable suppression of gene expression by RNAi in mammalian cells. *Proc Natl Acad Sci U S A.* 99:1443-8.

Palade G. 1975. Intracellular aspects of the process of protein synthesis. Science. 189:347-58.

Pallanck L, Ordway RW, Ramaswami M, Chi WY, Krishnan KS, Ganetzky B. **1995**. Distinct roles for N-ethylmaleimide-sensitive fusion protein (NSF) suggested by the identification of a second Drosophila NSF homolog. *J Biol Chem.* 270:18742-4.

Palauqui JC, Elmayan T, Pollien JM, Vaucheret H. **1997**. Systemic acquired silencing: transgene-specific post-transcriptional silencing is transmitted by grafting from silenced stocks to non-silenced scions. *EMBO J.* 16:4738-45.

Panin VM, Shao L, Lei L, Moloney DJ, Irvine KD, Haltiwanger RS. **2002**. Notch ligands are substrates for protein O-fucosyltransferase-1 and Fringe. *J Biol Chem.* 277:29945-52.

Pecot MY, Malhotra V. 2004. Golgi membranes remain segregated from the endoplasmic reticulum during mitosis in mammalian cells. *Cell.* 116:99-107.

Pelletier L, Jokitalo E, Warren G. **2000**. The effect of Golgi depletion on exocytic transport. *Nat Cell Biol.* 2:840-6.

Pelletier L, Stern CA, Pypaert M, Sheff D, Ngo HM, Roper N, He CY, Hu K, Toomre D, Coppens I, Roos DS, Joiner KA, Warren G. **2002**. Golgi biogenesis in Toxoplasma gondii. *Nature.* 418:548-52.

Pepperkok R, Lowe M, Burke B, Kreis TE. **1998**. Three distinct steps in transport of vesicular stomatitis virus glycoprotein from the ER to the cell surface in vivo with differential sensitivities to GTP gamma S. *J Cell Sci.* 111:1877-88.

Pernet-Gallay K, Antony C, Johannes L, Bornens M, Goud B, Rios RM. **2002**. The overexpression of GMAP-210 blocks anterograde and retrograde transport between the ER and the Golgi apparatus. *Traffic.* 3:822-32.

Petit V, Thiery JP. 2000. Focal adhesions: structure and dynamics. *Biol Cell.* 92:477-94.

Peyroche A, Antonny B, Robineau S, Acker J, Cherfils J, Jackson CL. **1999**. Brefeldin A acts to stabilize an abortive ARF-GDP-Sec7 domain protein complex: involvement of specific residues of the Sec7 domain. *Mol Cell.* 3:275-85.

Pothof J, van Haaften G, Thijssen K, Kamath RS, Fraser AG, Ahringer J, Plasterk RH, Tijsterman M. 2003. Identification of genes that protect the C. elegans genome against mutations by genome-wide RNAi. *Genes Dev.* 17:443-8.

Preisinger C, Short B, De Corte V, Bruyneel E, Haas A, Kopajtich R, Gettemans J, Barr FA. **2004**. YSK1 is activated by the Golgi matrix protein GM130 and plays a role in cell migration through its substrate 14-3-3{zeta}. *J Cell Biol.* 164:1009-1020.

Prescott AR, Farmaki T, Thomson C, James J, Paccaud JP, Tang BL, Hong W, Quinn M, Ponnambalam S, Lucocq J. **2001**. Evidence for prebudding arrest of ER export in animal cell mitosis and its role in generating Golgi partitioning intermediates. *Traffic.* 2:321-35.

Presley JF, Cole NB, Schroer TA, Hirschberg K, Zaal KJ, Lippincott-Schwartz J. **1997**. ER-to-Golgi transport visualized in living cells. *Nature.* 389:81-5.

Preuss D, Mulholland J, Franzusoff A, Segev N, Botstein D. **1992**. Characterization of the Saccharomyces Golgi complex through the cell cycle by immunoelectron microscopy. *Mol Biol Cell.* 3:789-803.

Puri S, Linstedt AD. 2003. Capacity of the golgi apparatus for biogenesis from the endoplasmic reticulum. *Mol Biol Cell.* 14:5011-8.

Puthenveedu MA, Linstedt AD. 2001. Evidence that Golgi structure depends on a p115 activity that is independent of the vesicle tether components giantin and GM130. *J Cell Biol.* 155:227-38.

Puthenveedu MA, Linstedt AD. 2004. Gene replacement reveals that p115/SNARE interactions are essential for Golgi biogenesis. *Proc Natl Acad Sci U S A*. 101:1253-6.

Qi H, Rand MD, Wu X, Sestan N, Wang W, Rakic P, Xu T, Artavanis-Tsakonas S. **1999**. Processing of the notch ligand delta by the metalloprotease Kuzbanian. *Science*. 283:91-4.

Rabouille C. 1999. Quantitative aspects of immunogold labeling in embedded and nonembedded sections. *Methods Mol. Biol.* 117:125-144.

Rabouille C, Jokitalo E. 2003. Golgi apparatus partitioning during cell division. *Mol Membr Biol*. 2003 20:117-27.

Rabouille C, Levine TP, Peters JM, Warren G. **1995a**. An NSF-like ATPase, p97, and NSF mediate cisternal regrowth from mitotic Golgi fragments. *Cell*. 82:905-14

Rabouille C, Misteli T, Watson R, Warren G. **1995b**. Reassembly of Golgi stacks from mitotic Golgi fragments in a cell-free system. *J Cell Biol.* 129:605-18.

Rabouille C, Hui N, Hunte F, Kieckbusch R, Berger EG, Warren G, Nilsson T. **1995c**. Mapping the distribution of Golgi enzymes involved in the construction of complex oligosaccharides. *J Cell Sci*. 108:1617-27.

Rabouille C, Kuntz DA, Lockyer A, Watson R, Signorelli T, Rose DR, van den Heuvel M, Roberts DB. **1999**. The Drosophila GMII gene encodes a Golgi alpha-mannosidase II. *J Cell Sci*. 112:3319-30.

Rambourg A, Clermont Y. 1997. Three-dimensional structure of the Golgi apparatus in mammalian cells. In The Golgi Apparatus (eds Berger, E.G. & Roth, J., Birkhauser Verlag, Basel). pp 37-61.

Rambourg A, Clermont Y, Chretien M, Olivier L. **1993**. Modulation of the Golgi apparatus in stimulated and nonstimulated prolactin cells of female rats. *Anat Rec. 235*, 353–362.

Reavy B, Ziegler A, Diplexcito J, Macintosh SM, Torrance L, Mayo M. **2000**. Expression of functional recombinant antibody molecules in insect cell expression systems. *Protein Expr Purif*. 18:221-8.

Rebay I, Fleming RJ, Fehon RG, Cherbas L, Cherbas P, Artavanis-Tsakonas S. **1991**. Specific EGF repeats of Notch mediate interactions with Delta and Serrate: implications for Notch as a multifunctional receptor. *Cell*. 67:687-99.

Redfern CPF, Bownes M. 1983. Pleiotropic effects of the "ecdysoneless-1" mutation of *Drosophila melanogaster*. *Mol. Gen. Genet.* 189:432-440.

Richards G. 1981. The radioimmune assay of ecdysteroid titres in Drosophila melanogaster. *Mol Cell Endocrinol*. 21:181-97.

Riddiford LM. 1993. Hormones and *Drosophila* development. In *The Development of Drosophila melanogaster.* (eds. Bates, M. & Martinez Arias, A., Cold Spring Harbor, NY, Cold Spring Harbor Laboratory Press). pp 843-897.

Rios RM, Bornens M. 2003. The Golgi apparatus at the cell centre. *Curr Opin Cell Biol.* 15:60-6.

Rios RM, Sanchis A, Tassin AM, Fedriani C, Bornens M. **2004.** GMAP-210 recruits gamma-tubulin complexes to cis-Golgi membranes and is required for Golgi ribbon formation. *Cell.* 118:323-35.

Ripoche J, Link B, Yucel JK, Tokuyasu K, Malhotra V. **1994.** Location of Golgi membranes with reference to dividing nuclei in syncytial Drosophila embryos. *Proc Natl Acad Sci U S A.* 91:1878-82.

Ritzenthaler C, Nebenfuhr A, Movafeghi A, Stussi-Garaud C, Behnia L, Pimpl P, Staehelin LA, Robinson DG. **2002.** Reevaluation of the effects of brefeldin A on plant cells using tobacco Bright Yellow 2 cells expressing Golgi-targeted green fluorescent protein and COPI antisera. *Plant Cell.* 14:237-61.

Roberg KJ, Crotwell M, Espenshade P, Gimeno R, Kaiser CA. **1999.** LST1 is a SEC24 homologue used for selective export of the plasma membrane ATPase from the endoplasmic reticulum. *J Cell Biol.* 145:659-72.

Rogalski AA, Singer SJ. 1984. Associations of elements of the Golgi apparatus with microtubules. *J Cell Biol.* 99:1092-100.

Rogalski AA, Bergmann JE, Singer SJ. **1984.** Effect of microtubule assembly status on the intracellular processing and surface expression of an integral protein of the plasma membrane. *J Cell Biol.* 99:1101-9.

Rossanese OW, Soderholm J, Bevis BJ, Sears IB, O'Connor J, Williamson EK, Glick BS. **1999.** Golgi structure correlates with transitional endoplasmic reticulum organization in Pichia pastoris and Saccharomyces cerevisiae. *J Cell Biol.* 145:69-81.

Rossanese OW, Reinke CA, Bevis BJ, Hammond AT, Sears IB, O'Connor J, Glick BS. **2001.** A role for actin, Cdc1p, and Myo2p in the inheritance of late Golgi elements in Saccharomyces cerevisiae. *J Cell Biol.* 153:47-62.

Roth EG. 1997. Topology of glycosylation in the Golgi apparatus. In The Golgi Apparatus (eds Berger, E.G. & Roth, J., Birkhauser Verlag, Basel). pp 131-161.

Rotsch C, Radmacher M. 2000. Drug-induced changes of cytoskeletal structure and mechanics in fibroblasts: an atomic force microscopy study. *Biophys J.* 78:520-35.

Saito-Nakano Y, Nakano A. 2000. Sed4p functions as a positive regulator of Sar1p probably through inhibition of the GTPase activation by Sec23p. *Genes Cells.* 5:1039-48.

Sanderfoot AA, Raikhel NV. 1999. The specificity of vesicle trafficking: coat proteins and SNAREs. *Plant Cell.* 11:629-42.

Sapperstein SK, Walter DM, Grosvenor AR, Heuser JE, Waters MG. **1995**. p115 is a general vesicular transport factor related to the yeast endoplasmic reticulum to Golgi transport factor Uso1p. *Proc Natl Acad Sci U S A.* 92:522-6.

Sapperstein SK, Lupashin VV, Schmitt HD, Waters MG. **1996**. Assembly of the ER to Golgi SNARE complex requires Uso1p. *J Cell Biol.* 132:755-67.

Satoh A, Wang Y, Malsam J, Beard MB, Warren G. **2003.** Golgin-84 is a rab1 binding partner involved in Golgi structure. *Traffic.* 4:153-61.

Scacheri PC, Rozenblatt-Rosen O, Caplen NJ, Wolfsberg TG, Umayam L, Lee JC, Hughes CM, Shanmugam KS, Bhattacharjee A, Meyerson M, Collins FS. **2004**. Short interfering RNAs can induce unexpected and divergent changes in the levels of untargeted proteins in mammalian cells. *Proc Natl Acad Sci U S A.* 101:1892-7.

Schekman R, Mellman I. 1997. Does COPI go both ways? *Cell.* 90:197-200.

Schlondorff J, Blobel CP. 1999. Metalloprotease-disintegrins: modular proteins capable of promoting cell-cell interactions and triggering signals by protein-ectodomain shedding. *J Cell Sci.* 112:3603-17.

Sciaky N, Presley J, Smith C, Zaal KJ, Cole N, Moreira JE, Terasaki M, Siggia E, Lippincott-Schwartz J. **1997**. Golgi tubule traffic and the effects of brefeldin A visualized in living cells. *J Cell Biol.* 139:1137-55.

Seemann J, Jokitalo E, Pypaert M, Warren G. **2000a**Matrix proteins can generate the higher order architecture of the Golgi apparatus. *Nature.* 407:1022-6.

Seemann J, Jokitalo EJ, Warren G. **2000b** The role of the tethering proteins p115 and GM130 in transport through the Golgi apparatus in vivo. *Mol Biol Cell.* 11:635-45.

Seemann J, Pypaert M, Taguchi T, Malsam J, Warren G. **2002**. Partitioning of the matrix fraction of the Golgi apparatus during mitosis in animal cells. *Science.* 295:848-51.

Segraves WA, Hogness DS. 1990. The E75 ecdysone-inducible gene responsible for the 75B early puff in Drosophila encodes two new members of the steroid receptor superfamily. *Genes Dev.* 4:204-19.

Sharp PA. 2001. RNA interference--2001. *Genes Dev.* 15:485-90.

Sheffield HG, Melton ML. 1968. The fine structure and reproduction of Toxoplasma gondii. *J Parasitol.* 54:209-26.

Shugrue CA, Kolen ER, Peters H, Czernik A, Kaiser C, Matovcik L, Hubbard AL, Gorelick F. **1999**. Identification of the putative mammalian orthologue of Sec31P, a component of the COPII coat. *J Cell Sci.* 112:4547-56.

Shima DT, Haldar K, Pepperkok R, Watson R, Warren G. **1997**. titioning of the Golgi apparatus during mitosis in living HeLa cells. *J Cell Biol.* 137:1211-28.

Shima DT, Scales SJ, Kreis TE, Pepperkok R. **1999**. Segregation of COPI-rich and anterograde-cargo-rich domains in endoplasmic-reticulum-to-Golgi transport complexes. *Curr Biol.* 9:821-4.

Short B, Barr FA. 2000. The Golgi apparatus. *Curr Biol.* 10:R583-5.

Short B, Preisinger C, Korner R, Kopajtich R, Byron O, Barr FA. **2001**. A GRASP55-rab2 effector complex linking Golgi structure to membrane traffic. *J Cell Biol.* 155:877-83.

Shorter J, Warren G. 1999. A role for the vesicle tethering protein, p115, in the post-mitotic stacking of reassembling Golgi cisternae in a cell-free system. *J Cell Biol.* 146:57-70.

Shorter J, Warren G. 2002. Golgi architecture and inheritance. *Annu Rev Cell Dev Biol.* 18:379-420.

Shorter J, Watson R, Giannakou ME, Clarke M, Warren G, Barr FA. **1999**. GRASP55, a second mammalian GRASP protein involved in the stacking of Golgi cisternae in a cell-free system. *EMBO J.* 18:4949-60.

Shorter J, Beard MB, Seemann J, Dirac-Svejstrup AB, Warren G. **2002**. Sequential tethering of Golgins and catalysis of SNAREpin assembly by the vesicle-tethering protein p115. *J Cell Biol.* 157:45-62.

Simpson F, Peden AA, Christopoulou L, Robinson MS. **1997**. Characterization of the adaptor-related protein complex, AP-3. *J Cell Biol.* 137:835-45.

Sisson JC, Field C, Ventura R, Royou A, Sullivan W. **2000**. Lava lamp, a novel peripheral golgi protein, is required for Drosophila melanogaster cellularization. *J Cell Biol.*151:905-18.

Slusarewicz P, Nilsson T, Hui N, Watson R, Warren G. **1994**. Isolation of a matrix that binds medial Golgi enzymes. *J Cell Biol.* 124:405-13.

Soderholm J, Bhattacharyya D, Strongin D, Markovitz V, Connerly PL, Reinke CA, Glick BS. **2004**. The transitional ER localization mechanism of Pichia pastoris Sec12. *Dev Cell.* 6:649-59.

Sollner T, Bennett MK, Whiteheart SW, Scheller RH, Rothman JE. **1993**. A protein assembly-disassembly pathway in vitro that may correspond to sequential steps of synaptic vesicle docking, activation, and fusion. Cell. 75:409-18.

Sönnichsen B, Lowe M, Levine T, Jamsa E, Dirac-Svejstrup B, Warren G. **1998**. A role for giantin in docking COPI vesicles to Golgi membranes. *J Cell Biol.* 140:1013-21.

Staehelin LA, Hepler PK. 1996. Cytokinesis in higher plants. *Cell.* 84:821-4.

Stafstrom JP, Staehelin LA. 1985. Dynamics of the nuclear envelope and of nuclear pore complexes during mitosis in the Drosophila embryo. *Eur J Cell Biol.* 34:179-89.

Stankewich MC, Tse WT, Peters LL, Ch'ng Y, John KM, Stabach PR, Devarajan P, Morrow JS, Lux SE. **1998**. A widely expressed betaIII spectrin associated with Golgi and cytoplasmic vesicles. *Proc Natl Acad Sci U S A.* 95:14158-63.

Stanley H, Botas J, Malhotra V. **1997**. The mechanism of Golgi segregation during mitosis is cell type-specific. *Proc Natl Acad Sci U S A.* 94:14467-70.

Steiner DF. 1998. The proprotein convertases. *Curr Opin Chem Biol.* 2:31-9.

Stephens DJ. 2003. De novo formation, fusion and fission of mammalian COPII-coated endoplasmic reticulum exit sites. *EMBO Rep.* 4:210-7.

Stephens DJ, Pepperkok R. 2001. Illuminating the secretory pathway: when do we need vesicles? *J Cell Sci.* 114:1053-9.

Stephens DJ, Lin-Marq N, Pagano A, Pepperkok R, Paccaud JP. **2000**. COPI-coated ER-to-Golgi transport complexes segregate from COPII in close proximity to ER exit sites. *J Cell Sci.* 113:2177-85.

Storrie B, White J, Rottger S, Stelzer EH, Suganuma T, Nilsson T. **1998**. Recycling of golgi-resident glycosyltransferases through the ER reveals a novel pathway and provides an explanation for nocodazole-induced Golgi scattering. *J Cell Biol.* 143:1505-21.

Stroud WJ, Jiang S, Jack G, Storrie B. **2003**. Persistence of Golgi matrix distribution exhibits the same dependence on Sar1p activity as a Golgi glycosyltransferase. *Traffic.* 4:631-41.

Tang BL, Kausalya J, Low DY, Lock ML, Hong W. **1999**. A family of mammalian proteins homologous to yeast Sec24p. *Biochem Biophys Res Commun.* 258:679-84.

Tates AD. 1971. Cytodifferentiation during spermatogenesis in *Drosophila melanogaster*: An electron microscope study. PhD Thesis. Rijksuniversiteit, Leiden.

Tavernarakis N, Wang SL, Dorovkov M, Ryazanov A, Driscoll M. **2000**. Heritable and inducible genetic interference by double-stranded RNA encoded by transgenes. *Nat Genet.* 24:180-3.

Taylor NA, Van De Ven WJ, Creemers JW. **2003**. Curbing activation: proprotein convertases in homeostasis and pathology. *FASEB J.* 17:1215-27.

Terasaki M. 2000. Dynamics of the endoplasmic reticulum and golgi apparatus during early sea urchin development. *Mol Biol Cell.* 11:897-914.

Thomas G. 2002. Furin at the cutting edge: from protein traffic to embryogenesis and disease. *Nat Rev Mol Cell Biol.* 3:753-66.

Thomopoulos GN, Neophytou EP, Alexiou M, Vadolas A, Limberi-Thomopoulos S, Derventzi A. **1992.** Structural and histochemical studies of Golgi complex differentiation in salivary gland cells during Drosophila development. *J Cell Sci.* 102:169-84.

Thyberg J, Moskalewski S. 1985. Microtubules and the organization of the Golgi complex. *Exp Cell Res* .159:1-16.

Thyberg J, Moskalewski S. 1999. Role of microtubules in the organization of the Golgi complex. *Exp Cell Res.* 246:263-79.

Tijsterman M, Ketting RF, Plasterk RH. **2002.** The genetics of RNA silencing. *Annu Rev Genet.* 36:489-519.

Ungar D, Oka T, Brittle EE, Vasile E, Lupashin VV, Chatterton JE, Heuser JE, Krieger M, Waters MG. **2002.** Characterization of a mammalian Golgi-localized protein complex, COG, that is required for normal Golgi morphology and function. *J Cell Biol.* 157:405-15.

Urban S, Lee JR, Freeman M. **2001.** Drosophila rhomboid-1 defines a family of putative intramembrane serine proteases. *Cell.* 107:173-82.

Valderrama F, Babia T, Ayala I, Kok JW, Renau-Piqueras J, Egea G. **1998.**Actin microfilaments are essential for the cytological positioning and morphology of the Golgi complex. *Eur J Cell Biol.* 76:9-17.

Valderrama F, Duran JM, Babia T, Barth H, Renau-Piqueras J, Egea G. **2001.** Actin microfilaments facilitate the retrograde transport from the Golgi complex to the endoplasmic reticulum in mammalian cells. *Traffic.* 2:717-26.

Valsdottir R, Hashimoto H, Ashman K, Koda T, Storrie B, Nilsson T. **2001.** Identification of rabaptin-5, rabex-5, and GM130 as putative effectors of rab33b, a regulator of retrograde traffic between the Golgi apparatus and ER. *FEBS Lett.* 508:201-9.

Van De Moortele S, Picart R, Tixier-Vidal A, Tougard C. **1993.** Nocodazole and taxol affect subcellular compartments but not secretory activity of GH3B6 prolactin cells. *Eur J Cell Biol.* 60:217-27.

Vasile E, Perez T, Nakamura N, Krieger M. **2003.** Structural integrity of the Golgi is temperature sensitive in conditional-lethal mutants with no detectable GM130. *Traffic.* 4:254-72.

Velasco A, Hendricks L, Moremen KW, Tulsiani DR, Touster O, Farquhar MG. **1993.** Cell type-dependent variations in the subcellular distribution of alpha-mannosidase I and II. *J Cell Biol.* 122:39-51.

Vincent JP, Dubois L. 2002. Morphogen transport along epithelia, an integrated trafficking problem. *Dev Cell.* 3:615-23.

Voeltz GK, Rolls MM, Rapoport TA. **2002.** Structural organization of the endoplasmic reticulum. *EMBO Rep.* 3:944-50.

Volchuk A, Amherdt M, Ravazzola M, Brugger B, Rivera VM, Clackson T, Perrelet A, Sollner TH, Rothman JE, Orci L. **2000.** Megavesicles implicated in the rapid transport of intracisternal aggregates across the Golgi stack. *Cell.* 102:335-48.

von Kalm L, Fristrom D, Fristrom JW. **1995.** The making of a fly leg: a model for epithelial morphogenesis. *Bioessays* 17:693702.

Walker G. 1982. Cell cycle specificity of certain antimicrotubular drugs in S. pombe. *J. Gen. Microbiol.* 128:61-71.

Wang Y, Seemann J, Pypaert M, Shorter J, Warren G. **2003.** A direct role for GRASP65 as a mitotically regulated Golgi stacking factor. *EMBO J.* 22:3279-90.

Ward TH, Polishchuk RS, Caplan S, Hirschberg K, Lippincott-Schwartz J. **2001.** Maintenance of Golgi structure and function depends on the integrity of ER export. *J Cell Biol.* 155:557-70.

Wegmann D, Hess P, Baier C, Wieland FT, Reinhard C. **2004.** Novel isotypic gamma/zeta subunits reveal three coatomer complexes in mammals. *Mol Cell Biol.* 24:1070-80.

Weide T, Bayer M, Koster M, Siebrasse JP, Peters R, Barnekow A. **2001.** The Golgi matrix protein GM130: a specific interacting partner of the small GTPase rab1b. *EMBO Rep.* 2:336-41.

Weimbs T, Low SH, Chapin SJ, Mostov KE, Bucher P, Hofmann K. **1997.** A conserved domain is present in different families of vesicular fusion proteins: a new superfamily. *Proc Natl Acad Sci U S A.* 94:3046-51.

White KP, Rifkin SA, Hurban P, Hogness DS. **1999.** Microarray analysis of Drosophila development during metamorphosis. *Science.* 286:2179-84.

Whyte JR, Munro S. 2001. The Sec34/35 Golgi transport complex is related to the exocyst, defining a family of complexes involved in multiple steps of membrane traffic. *Dev Cell.* 1:527-37.

Whyte JR, Munro S. 2002. Vesicle tethering complexes in membrane traffic. *J Cell Sci.* 115:2627-37.

Williams BR. 1999. PKR; a sentinel kinase for cellular stress. *Oncogene.* 18:6112-20.

Winston WM, Molodowitch C, Hunter CP. **2002.** Systemic RNAi in C. elegans requires the putative transmembrane protein SID-1. *Science.* 295:2456-9.

Xu H, Brill JA, Hsien J, McBride R, Boulianne GL, Trimble WS. **2002.** Syntaxin 5 is required for cytokinesis and spermatid differentiation in Drosophila. *Dev Biol.* 251:294-306.

Yamakawa H, Seog DH, Yoda K, Yamasaki M, Wakabayashi T. **1996.** Uso1 protein is a dimer with two globular heads and a long coiled-coil tail. *J Struct Biol.* 116:356-65.

Zaal KJ, Smith CL, Polishchuk RS, Altan N, Cole NB, Ellenberg J, Hirschberg K, Presley JF, Roberts TH, Siggia E, Phair RD, Lippincott-Schwartz J. **1999.** Golgi membranes are absorbed into and reemerge from the ER during mitosis. *Cell.* 99:589-601.

Zheng JY, Koda T, Fujiwara T, Kishi M, Ikehara Y, Kakinuma M. **1998.** A novel Rab GTPase, Rab33B, is ubiquitously expressed and localized to the medial Golgi cisternae. *J Cell Sci.* 111:1061-9.

Acknowledgements

When you reach the end of an important page in the book of your life and before you turn the page, it's good to have a quick look back and remember the key points of it. And while the scientifically important moments of this PhD thesis are illustrated in the chapters that have preceded, here is the place to remember all those people that have helped you to make it to the end. Therefore, I would like to use these very last pages of my thesis to thank as many people as I can think.

The beginning of my PhD was far for being ideal. It would have to use at least two more pages to describe my adventurous first trip to Edinburgh and the totally unsuccessful interview with Catherine, so I will leave the details to those who know. Catherine, I have to say a big "thank you", first of all, for taking the risk and having me in the lab, despite your justified initial doubts. I hope you still think that your instinct, that very often has guided us correctly in our experiments, was not wrong in my case. But most of all, I would like to express my deep appreciation for all your trust, continuous guidance and mentoring. During these three and a half years that I've spent as your student, I became more mature both scientifically and personally, and I can tell you now that you were a big source of experience and inspiration for me. I want you to know that all these years with you will be always kept in a special place in my mind and heart.

Jonathan, you are the second important person from my time in Edinburgh. Thanks for your precious help, especially during the first months that I was lost in the lab, and also for your excellent command in English that was so useful for Catherine and me. I hope you have a great time back in New Zealand and I wish we would meet again sometime in the future.

Alex, Xavier, Laurence and Jane, I will always remember the moments we shared in the same office. I hope I didn't annoy you much, and in case I did, I hope my cakes on Friday 4 o'clock have compensated a little bit for that.

Andreas and Ken, you have been an inspiration to me for what a devoted scientist means. I assure you that despite the long hours in the lab I have enjoyed almost every minute of it. Also, a big thanks to you, Andreas, for all your useful

comments on my thesis and for organising so nicely my viva and everything needed to be done after it.

Many thanks to all fly labs at the ICMB (Jarman, Heck, Okhura, Davis and Bownes) for the useful advice that I have been able to get from you. Be sure that all the useful discussions in our Friday fly meetings will be something that I will really miss in Utrecht, so I hope that we keep contact. Andrew, a special thank to you for being my second supervisor and all your useful comments in my first year report and my presentations, although you have nothing to do with the Golgi.

Closing the first phase of my PhD in Edinburgh, I would like to thank all the Greek community there that helped me feel like being in Greece in all those special dates in the life of a Greek person. Especially, I want to thank Takis and Dimitris for helping me overcome the shock of the first three months, when I could not even understand the Scottish accent and I felt so disappointed. Giota, thanks for your warm welcome in the ICMB and your attempt to persuade Catherine that I was not, after all, such a bad student as she might have thought originally. My favourite Alexandros, thanks for being such a good flatmate, so that when I was coming home, I did not have to deal with a messy kitchen and bathroom. I hope you manage to make us vote one day by computers. It would be so much more convenient. Argyro and Lena, with you I have laughed the most and I can assure you that this was of vital importance, especially when my mind was blocked by the continuous science. Good luck with everything you do. Sofia and Ellada, you are my strongest links in Edinburgh and I appreciate your efficiency with all the stupid administrative work that I have forced you to go through since I left for Holland. I hope you both finish successfully your PhD and continue with whatever you set as priority in your life. I don't believe that I have many good friends, but with you the standards are set high, for sure. Finally, I want to thank Matina, whose I don't know even the surname, for being the smiling person that made me for some unexplainable reason decide to stay in Edinburgh in the end of my first

week and while I had packed my things up to return to Greece. Although we never met since that day, I wish you the best of luck.

Now, I have to come to the second part of my PhD trip. I arrived in the department of Cell Biology in Utrecht, in September 2002. The place was familiar from a workshop I had attended, but to my surprise, the person in the neighbouring office desk was also familiar. Dagmar, you were definitely the most important person for me during this PhD, after Catherine. Probably, I cannot remember all the reasons for which I have to thank you, so I will only list a few. Many thanks for the numerous scientific brainstorms, and sorry for confusing you by expressing thoughts without giving some background information first. More thanks for being my taxi driver, my hairdresser, providing me with a washing machine and accompanying me in biking tours around Utrecht, to mention only some of your functions. I wish I had only a fraction of your perfect organisation skills. I hope you find what you are looking for in science and in life, even if the latter includes a goat farm in Germany or the south of France.

Ellie, Janice and Viola and George, I don't believe that there is other place in the world that a person can find accumulated so much EM experience. As long as I work next to you, I don't believe that there are difficult questions when EM is involved. Thanks for all the experience you have shared with me.

Ad, when you came in the lab, I was afraid that it would not work out with your wife as a boss. However, it seems that your chemistry with Catherine is something that everybody should look for. Thanks for your beautiful labellings while I was busy writing my thesis (see figure 4.3D) and I will be waiting for our first joint paper.

Judith, Hans, Jan-Willem and Monique, many thanks for all your useful comments on my work. I hope to gain as much as possible in the years that I will still be in the lab and I promise to do my best to keep the standards you have set for the cell microscopy centre as high as possible.

Muriel, when you came in the lab I felt a familiar Mediterranean air. Thanks for all the scientific discussions, but mostly for being such a good friend outside the lab.

Marc and Rene, while in Edinburgh, I had not appreciated the importance of having a specialist dealing with your pictures. Now that I am aware of what you can do to improve my pictures, I am sure that you will be among the persons that I will miss most the day I will leave the lab. Many thanks for all the precious work you have done for this thesis, my papers and my posters.

Bram, our projects until now were not very closely related, but I hope this will change in the future. The start has already been made. I wish all the best in your PhD and I hope you gain as much experience from Catherine as I got as her student.

Antoinette, your help with my administrative work in dutch has been invaluable. Many thanks for keeping my mind free of many troubles.

I would also like to thank the undergraduate students we had in the lab this February, who were the trigger to produce a chapter of my thesis with very interesting results in less than a month.

Finally, many thanks to all the biochemistry people in the department (Strous, van der Sluijs and Stoorvogel groups) for pushing my knowledge in biochemistry techniques a step higher. I hope to have the chance to learn much more from you in the future.

Sean, first of all, thank you for accepting being my external examiner. I really find that your comments and suggestions made me improve my thesis, but more than that, broadened my way of thinking.

Many thanks to all the people that provided our lab with reagents that were proven very useful during my PhD.

A big thanks to the Darwin Trust of Edinburgh for providing me with a scholarship that made this study possible. Especially, I would like to thank Sir Kenneth Murray for believing in me from the very first moment and managing to

persuade Catherine for the same. I wish the scientific field had more such inspiring persons. In addition, I would like to thank Mrs. Alix Fraser for all her concern for me from the first minute I arrived in Edinburgh.

Manoli and Keti, you are the best parents in the world! Without your financial and sentimental support there would be no way to be so focused on my studies. I appreciate that you gave me such a freedom to take all the decisions concerning my carrier until now, even if deep inside, you may be afraid that I may not come back to Greece again. I want you to know that I love you more than I show you sometimes.

Last, I would like to thank God for showing me first the way, and then for giving me the strength to follow it.

The PhD trip has reached the end. As C.P. Cavafis has written, in a trip, the most important thing is not the arrival at your destination, but the experience and the knowledge you gain during the trip itself. Well, looking back at my trip, it was surely worth embarking on the ship!

Appendix

Molecular Biology of the Cell
Vol. 12, 2308–2327, August 2001

Biogenesis of Golgi Stacks in Imaginal Discs of *Drosophila melanogaster*

Vangelis Kondylis, Sarah E. Goulding, Jonathan C. Dunne, and Catherine Rabouille*

The Wellcome Trust Centre for Cell Biology, Institute of Cell and Molecular Biology, University of Edinburgh, Edinburgh, EH9 3JR, Scotland, United Kingdom

Submitted December 8, 2000; Revised April 5, 2001; Accepted June 4, 2001
Monitoring Editor: Vivek Malhotra

We provide a detailed description of Golgi stack biogenesis that takes place in vivo during one of the morphogenetic events in the lifespan of *Drosophila melanogaster*. In early third-instar larvae, small clusters consisting mostly of vesicles and tubules were present in epithelial imaginal disk cells. As larvae progressed through mid- and late-third instar, these larval clusters became larger but also increasingly formed cisternae, some of which were stacked. In white pupae, the typical Golgi stack was observed. We show that larval clusters are Golgi stack precursors by 1) localizing various Golgi-specific markers to the larval clusters by electron and immunofluorescence confocal microscopy, 2) driving this conversion in wild-type larvae incubated at 37°C for 2 h, and 3) showing that this conversion does not take place in an NSF1 mutant (*comt 17*). The biological significance of this conversion became clear when we found that the steroid hormone 20-hydroxyecdysone (ecdysone) is critically involved in this conversion. In its absence, Golgi stack biogenesis did not occur and the larval clusters remained unaltered. We showed that dGM130 and sec23p expression increases approximately three- and fivefold, respectively, when discs are exposed to ecdysone in vivo and in vitro. Taken together, these results suggest that we have developed an in vivo system to study the ecdysone-triggered Golgi stack biogenesis.

INTRODUCTION

In eukaryotic cells, the Golgi apparatus consists of stacked flattened membrane-bound compartments called cisternae. Abutting each side of the stacks is a tubular/vesicular network, the *cis*- and *trans*-Golgi networks. How this architecture is built and maintained has recently been addressed by the development of in vitro and semi-intact cell assays. The in vitro assay measured the rebuilding of the Golgi apparatus from mitotic Golgi fragments (Rabouille *et al.*, 1995b). The semi-intact cell system visualized the rebuilding of the Golgi complex from illimaquinone-generated Golgi fragments (Acharya *et al.*, 1995). These assays have allowed the identification of several proteins involved in this rebuilding process, such as NEM sensitive factor (NSF) and its cofactor α soluble NSF attachment protein (a-SNAP) (Acharya *et al.*, 1995; Rabouille *et al.*, 1995a; Müller *et al.*, 1999), p97 (Acharya *et al.*, 1995; Rabouille *et al.*, 1995a), and its cofactor p47 (Kondo *et al.*, 1997). Syntaxin 5 was shown to interact with both fusion machineries (Rabouille *et al.*, 1998). p115 (Rabouille *et al.*, 1995a), Golgi matrix 130 (GM130) (Nakamura *et al.*, 1997), GRASP65 (Barr *et al.*, 1997), and GRASP55 (Shorter *et al.*, 1999) were shown to be involved.

* Corresponding author. E-mail address: C.Rabouille@ed.ac.uk.

Both in vitro assays were based on the reassembly of preexisting disassembled Golgi stacks. We therefore set out to characterize how Golgi apparatus grows and how stacked cisternae are formed in vivo. We used *Drosophila melanogaster* as a model organism primarily because it is readily amenable to genetics and cell biology. Several *Drosophila* tissues exhibit a Golgi apparatus with a morphology very similar to mammalian cells of stacked cisternae and networks of tubular membranes. The stacks are seemingly not linked to one another in a large ribbon that forms the single-copy organelle capping the nucleus typical of mammalian cells (Rabouille *et al.*, 1999). Instead, they remain dispersed throughout the cytoplasm. Several of the *Drosophila* genes encoding the proteins involved in Golgi organization have been cloned: dNSF1, one of the homologs of NSF (Ordway *et al.*, 1994; Pallanck *et al.*, 1995a); NSF2 (the other NSF homolog, Pallanck *et al.*, 1995b); TER94, one of the two homologs of p97 (Pinter *et al.*, 1998); Sed5, the homolog of syntaxin5 (Banfield *et al.*, 1994); and the *Drosophila* homolog of p115 (dp115) and GM130 (dGM130) (Adams *et al.*, 2000; Dunne and Rabouille, 2001). With the exception of TGN38/46 and giantin, almost all the known mammalian proteins related to the Golgi apparatus have homologs in *Drosophila* (Adams *et al.*, 2000; Dunne and Rabouille, 2001). Due to the large collection of mutants (EMS and P element

insertion, deletion, etc.), the study of these proteins has been made easier. This is particularly true for dNSF1 (*comt*; Siddiqi and Benzer, 1976), TER94 (Leon and McKearin, 1999), and sed5 (Ashburner *et al.*, 1999).

The first step in investigating the possible role of these proteins in Golgi stack biogenesis with the use of *Drosophila* genetics was to describe a developmental event during which the Golgi stack would acquire its typical morphology of stacked cisternae. We focused on the elongation of the leg and wing imaginal discs that takes place between the stages of early third-instar larvae and puparium formation (white pupae). Leg imaginal discs begin as concentrically folded flat sac-like structures that will give rise to adult legs. They comprise two epithelial cell layers. One is a squamous thin epithelium (peripodial membrane), the other is folded and comprises columnar cells (5 μm in diameter and up to 30 μm in height) (Fristrom and Fristrom, 1993). The binding of the steroid hormone 20-hydroxyecdysone (ecdysone) to its nuclear receptors in the disc epithelial cells during late third-instar larvae induces the more peripheral folds to constrict, pushing the central folds toward the peripodium. As a consequence leg discs lose their flattened shape and elongate (von Kalm *et al.*, 1995). Wing discs expand in a similar manner (Fristrom and Fristrom, 1993). This first phase of disc elongation is completed at puparium formation.

We show here that this organogenesis is accompanied by the biogenesis of the Golgi stacks starting with small larval clusters of vesicles and tubules in early third-instar larvae, to larger clusters that contain Golgi markers in mid- and late third-instar larvae followed by the formation of stacks of cisternae in white pupae. We show that the larval clusters contain Golgi proteins, that their conversion into Golgi stack is dependent on dNSF1, and is triggered by ecdysone.

MATERIALS AND METHODS

WT Larvae

The W^{1118} and OregonR stocks were obtained from Andrew Jarman's lab (Edinburgh, Scotland) and were both referred to as wild type (WT). They were maintained at 22°C. Early third-instar larvae were defined as those larvae that have the characteristics of a third-instar larvae (size, mouthhook, fanned anterior spiracles) but that are still burrowed in the food. Mid-third-instar larvae were defined as third-instar larvae free of the food and still wandering. The motionless third-instar larvae were late third-instar larvae. They also have swollen salivary glands and darkened everted spiracles. White pupae are the young pupae that have a white pupal case.

Fly Stocks and Experiments

comt 17 stock (gift from Barry Gunetsky, Madison, WI) is a thermosensitive allele of dNSF1 that is localized on the first chromosome. At 37°C, dNSF1 is misfolded and nonfunctional (Siddiqi and Benzer, 1976; Pallanck *et al.*, 1995a). HSN is a transgene comprising dNSF1 cDNA under the control of a heat-shock promoter. In HSN TM3, Sb/TM6 (gift from Leo Pallanck; Pallanck *et al.*, 1995a), HSN is carried on the third chromosome in association with TM3, Sb. A 37°C incubation drives the expression of dNSF1. The rescue of the *comt 17* phenotype was performed by crossing female *comt 17*/*comt 17*; +/+; +/+ flies to male +/Y; +/+; HSN TM3,Sb/TM6. Male *tubby* (associated with TM6) larvae (*comt 17*/Y; +/+; TM6/+) have the *comt 17* genotype but do not have the HSN rescue construct, whereas male non *tubby* (HSN,TM3, sb) larvae (*comt 17*/Y; +/+; HSN TM3, Sb/+) do.

Experiments with the use of these larvae were carried out in one of two ways as follows: WT and *comt 17* mid-third-instar larvae were selected and held in food vials containing 1 mM ecdysone for 1 h at 22°C followed by 2 h at 37°C in a water bath. Their leg and wing discs were dissected, fixed, and processed for conventional electron microscopy (EM) (see below). Alternatively, WT, *comt 17*, *comt 17*/Y; +/+; TM6/+, *comt 17*/Y; +/+; HSN TM3, Sb/+, mid-third-instar larvae were semidissected and incubated in vitro (see below) in the presence of 3 μM ecdysone at 37°C for 2 h. Their discs were removed, fixed, and processed for conventional EM (see below).

The stock "919" yw; P[w+, UAS-Fringe (DXD)-myc] was a gift from Matthew Freeman (Cambridge, United Kingdom). These flies carry the transgene comprising the Fringe cDNA in which the glycosyltransferase motif DDD motif has been replaced by a DXD that abolishes the glycosyltransferase activity but retains the Golgi localization (Munro and Freeman, 2000). Female flies were crossed to HsGAL4/Bc, El, Gla. We used Bc (Black Cell) as a larval marker. Two heat-shock treatments (each of 20 min at 37°C) were performed before larval collection. Mid-third-instar non Bc (UAS-Fringe-DXD-myc/HsGAL4) larvae were collected, their leg and wing discs dissected, and processed for immunofluorescence or immunoelectron microscopy (see below).

ecd^{1ts} mutants (ecd^{1ts} st ca) were a gift from Jean Antoine Lepesant (Paris, France). They are thermosensitive homozygote alleles that only produce a basal level of ecdysone at the restrictive temperature of 29°C (Garen *et al.*, 1977, Redfern and Bownes, 1983). Eggs were laid for 24 h and larvae grown for 6 d at 22°C (until second-instar/early third-instar larval stage). The vials were transferred at 29°C for 7 h. The larvae were then kept at 29°C or transferred back at 22°C for 18 h. Their discs were fixed for conventional EM.

Alternatively, after 7 h at 29°C, the discs were dissected and incubated in vitro in M3 medium (see below) in the absence or the presence of 3 μM ecdysone, omitting the fly extract in both cases. Their discs were fixed for conventional EM.

Conventional EM

Early, mid-, and late third-instar larvae and white pupae were semidissected (disks, still attached to the head and the cuticle) and fixed for 2 h in 1% glutaraldehyde in 0.2 M phosphate buffer (pH 7.4) at room temperature and rinsed three to four times in 0.1 M cacodylate buffer (pH 7.4). Leg and wing imaginal discs were dissected further to remove any other tissues and processed for conventional EM as described in Rabouille *et al.* (1995b). Sections (50–60 nm) were cut on a Leica ultramicrotome, stained with uranylacetate and lead citrate, and were viewed under a Philips biotwin electron microscope.

Immunoelectron Microscopy

Leg and wing discs were semidissected out of Fringe-DXD-myc-induced mid third-instar larvae (see above), fixed in 2% paraformaldehyde and 0.2% glutaraldehyde in 0.2 M phosphate buffer (pH 7.4) for 3 h at room temperature, and embedded in unicryl (British Biocell, Cardiff, United Kingdom) according to the standard protocol suggested by the company. Sections (50–60 nm) were cut on a Leica S4 and single labeled with 9E10 (mouse), MLO7 (rabbit), NN7 (rabbit) in 0.5% Fish skin gelatin in phosphate-buffered saline (PBS) followed by anti-rabbit IgG conjugated to 10-nm gold or anti-mouse IgG conjugated to 15-nm gold when appropriate. Sections were stained with lead citrate (5 min), 4% aqueous uranylacetate (40 min), and lead citrate (10 min) and were viewed under a Philips biotwin electron microscope.

Indirect Immunofluorescence

Leg and wing discs were semidissected out of mid third-instar WT larvae and fixed at room temperature for 20 min in 3% paraformaldehyde in 0.2 M phosphate buffer (pH 7.4) supplemented with 0.1% Triton, followed by three to four times rinsing in PBS and storage at

4°C if necessary. The immunofluorescence procedure was as described previously (Rabouille *et al.*, 1999). Briefly, discs were incubated at room temperature for 30 min in PBS supplemented with 0.1% Triton and 0.225% fish skin gelatin (PBSTG), 3 h with the primary antibodies diluted in the same buffer, rinsed three times >1 h with PBSTG and 2 h with secondary antibodies conjugated with fluorescein isothiocyanate (FITC) or Texas Red in the dark, rinsed three times >30 min in PBSTG, and stored overnight in PBS. The discs were finely dissected and mounted in Vectashield containing 4,6-diamidino-2-phenylindole (DAPI). They were viewed under a Leica confocal microscope. The pictures were processed in Adobe Photoshop.

Western Blotting

Leg and wings discs (30–50) were dissected from mid-third-instar WT larvae and homogenized directly in 100 μl of 1× SDS sample buffer (SSB) containing 5 mM dithiothreitol with the use of a motorized pestle. In one instance, 20 larval semidissected heads (including discs, brain, salivary glands, and cuticle) were homogenized in the same way.

The Kc cells were grown at 27°C in 10-cm Petri dishes containing 15 ml of M3 medium supplemented with heat-inactivated fetal bovine serum. They were harvested, spun, rinsed, and homogenized in 200 μl of buffer A (20 mM Tris-HCl, 1 mM EDTA, 10 mM $MgCl_2$, 10 mM KCl, 1 mM dithiothreitol, 0.23 M sucrose, and 1% Triton X-100). SSB was added to 1× final.

In the experiment with the use of *ecd*^{1ts} mutant, the larvae were maintained for 7 h at 29°C, the discs were dissected and incubated in vitro in M3 medium (see below) in the absence or the presence of 3 μM ecdysone, omitting the fly extract in both cases. Thirty leg and 10 wing discs were finely dissected after each incubation (plus and minus ecdysone) and homogenized in 100 μl of 1× SSB. Protein (30 μg) was loaded on the gel. They were processed further with the use of affinity-purified MLO7 (anti-GM130 antibody) and the anti-β-tubulin antibody.

The same experiment was performed with the use of WT mid-third-instar larvae that were incubated in the presence or the absence of ecdysone in M3 medium (see below). Forty leg and 10 wing discs were finely dissected after each incubation (plus or minus ecdysone) and homogenized in 100 μl of 1× SSB. Protein (30 μg) was loaded on the gel. They were processed further for Western blotting as described below with the use of the antibody anti-sec23p (gift from Jean Pierre Paccaud, Geneva, Switzerland).

Western blotting was performed as described in Hui *et al.* (1997). The rabbit anti-GM130 antiserum and affinity-purified MLO7, and the rabbit anti-p115 antiserum NN7 were detected with the use of anti-rabbit IgG coupled to horseradish peroxidase. The mouse monoclonal anti-protein disulfide isomerase (PDI) antibody and anti-β-tubulin were detected with the use of anti-mouse IgG coupled to horseradish peroxidase. The enhanced chemiluminescence (Amersham Pharmacia Biotech, Buckinghamshire, United Kingdom) system was used to visualize the bands. The prestained molecular weight markers were purchased from Bio-Rad (Richmond, CA). The intensity of the bands was estimated with the use of NIH Image, version 1.62.

In Vitro Disc Incubation

Leg and wing discs from mid-third-instar larvae of various genetic backgrounds were semidissected (still attached to the head and the cuticle) and incubated in a 3-cm plastic Petri dish for 10–18 h at 25°C in the Schneider or M3 medium (1.4 ml) supplemented by 5% hemolymph (fly extract made according to Currie *et al.* [1988] and 3 μM ecdysone (Sigma, Dorset, Poole, United Kingdom; from a 1 mM stock 10% ethanol) as described previously in Mandaron (1971). At the end of the incubation, the discs were fixed as described above for conventional electron microscopy or processed for Western blotting.

Quantitation

EM The Golgi area was defined by the Golgi stacked cisternae and immediate surrounding vesicles and tubules. Larval clusters were defined as the gathering of vesicles and tubules and cisternal profiles. To be counted as a larval cluster, at least four vesicles or tubules needed to be present and should not be >100 nm apart. In 85% of the cases the larval clusters occupied a specific location as being nested in a cup-shaped endoplasmic reticulum (ER) cisternae. Vesicles were defined as having an axial ratio of 1:1.5. Most were 50–70 nm in diameter but some were 2–3 times larger. A tubule was defined as having an axial ratio of at least 2:1 with a width of 70 nm. A cisterna has a width equal or <30 nm and was at least 200 nm in length. However, when dilated rims were linked to cisternal elements, they were considered as part of the cisternae. A cisternal stack is a profile where at least two cisternae overlap by at least 50% of their length. The cytoplasm was defined as the volume enclosed by the plasma membrane and excluding the nucleus (but including all other organelles).

Because one of the objective of this study was to define the relationship between the larval clusters and Golgi stacks, we chose the nonbiased name of organelle (org) to refer to either and both. In some instance, the org will be identifiable as Golgi area and in others, it will refer to larval clusters. The boundaries of the org were defined by the interface between the outmost membrane profiles and either the more amorphous cytoplasm or the cup-shaped ER cisternal membrane when present.

The surface density of the org within the cytoplasm (S_{org}/V_{cyt}) is the product of two distinct measurements: the surface density of the "organelle membrane" within the volume they occupy (S_{org}/V_{org}) multiplied by the volume density of the org within the cytoplasm (V_{org}/V_{cyt}).

Sorg/Vorg was estimated as follows: The boundary of the organelle (pictured at a magnification of 90 K) as well as all membrane within this boundary were marked. S_{org} was estimated with the use of the intersection method by counting the number of intersections (ΣI) between the lines of a 3-mm grid and all the membrane comprised within the organelle boundary. V_{org} was defined by the point hit method in counting the number of point hits falling within the boundary (ΣP) with the use of a 3-mm point grid. S_{org}/V_{org} was $\Sigma I/\Sigma P \times mag$ (μm^{-1}) (Rabouille, 1999). Vcyt was estimated by point hit method with the use of pictures of cells at a magnification of about 10 K and a point grid. Results are expressed ±SD.

To estimate the percentage of membrane in cisternae, tubules, or vesicles, we used a series of vertical lines spaced by 5-mm overlapping pictures at ~90 K. Each intersection between the lines and each category of profile was scored and percentage estimated (Rabouille *et al.*, 1995b). The ratio of stacked cisternae on total cisternae was determined by the same method taking only into account the cisternal profiles.

Immuno-EM. Pictures (10–20) were taken and printed at a magnification of 73 K. The relative distribution of gold particles over the ER and the organelle (either the larval clusters or the Golgi stacks when present) was established by counting the number of gold particles falling within the organelle boundary (see above) or on ER cisternae (plus nuclear envelope). One hundred percent represents the total number of gold falling on both compartments. The gold labeling corresponding to Fringe-DXD-myc was low and all gold particles summed, a method that does not give a SD. With the use of the point hit method (5-mm point grid), the nuclear background and the labeling density over the organelle was estimated (Rabouille, 1999).

Immunofluorescence. Discs from WT early and late third-instar larvae were processed for immunofluorescence with the use of the anti-GM130 antibody (see above) and the average expression was estimated with the use of NIH Image, version 1.62. All the immunofluorescence pictures used for quantitative purposes were taken

at the same settings with the 20 or 40× objectives. The raw pictures were saved as black and white and were inverted. Boxes of different sizes were used to measure the intensity of fluorescence on the discs and on the surrounding area to estimate the background. Measurements (10–15) were performed on at least three pictures from three experiments.

RESULTS

Our morphological studies focused on the leg and wing imaginal discs of third-instar larvae before, at, and after the onset of disc elongation. Discs from early and mid-third-instar larvae have not begun to elongate (average leg disc thickness 30–40 μm), whereas those from late third-instar larvae have (average thickness between 45 and 90 μm), and those from white pupae have completed the first phase of elongation (thickness ~240 ± 10 μm).

Discs were dissected from larvae at each developmental stage, fixed, and processed for conventional electron microscopy. We examined the surface section of the disc cells in each developmental stage (giving indication on the cell size) as well as the volume density of their cytoplasm (a measure of the cell volume occupied by the cytoplasm). Disc cells of the mid- and late third-instar larvae and white pupae were on average of the same size (our unpublished results) and 30% larger than the ones of early third-instar larvae represented largely by an increase in their cytoplasm. This indicates that the increase in disc thickness (600% increase) could be accounted for by the unfolding of the concentric folds (see INTRODUCTION) and was not accompanied by a substantial change in cell size except for the initial increase.

When observed at higher magnification, the cells of early third-larval instar discs appeared dense and their endomembranes poorly developed. These were interphase cells but we could not observe stacked Golgi cisternae. Instead, small clusters of vesicles and tubules (Figure 1, A and B) were observed often nested in the concavity of a cup-shaped ER cisterna. In many cases, this ER cisterna would define half to one-third of the boundaries of the clusters. The vesicles had a 50–70-nm diameter although larger profiles were also observed and the tubules were short (150–200 nm in length). The surface density of these clusters (Sorg/Vcyt) was 1.30 ± 0.07 μm^{-1} (Table 1, line 1). The percentage of cluster membranes in vesicles, tubules, and cisternae was also established (Table 1, line 1). These small larval clusters consisted mostly of small vesicles (~82.5%) and tubules (~17.5%) but were almost devoid of cisternae (1%).

The cells of mid third-larval instar discs were less dense and we observed, again nested in ER cup-shaped cisternae in 85% of the cases, two kinds of profiles whose characteristics were reminiscent of those observed in the previous stage (Table 1, lines 3 and 4). First, small clusters (Sorg/Vcyt of 1.12 μm^{-1}) mostly contained vesicles and tubules (Table 1, line 3) with only 2.8% of the clusters membrane in cisternae, almost indistinguishable from the clusters observed in the early third-instar larvae; second, medium clusters (with a Sorg/Vcyt ~1.91 μm^{-1}) (Figure 1C) contained vesicles and tubules but with 12% of the membrane in cisternal elements (Table 1, line 4).

In late third-instar larvae, large clusters (with a Sorg/Vcyt ~3.17 μm^{-1}) contained 28.6% of their membrane in cisternae (Figure 1D) (Table 1, line 5). The largest of the clusters did exhibit stacked cisternae profiles. The remainder of membrane was observed as vesicles and tubules (Table 1, line 5).

Last, white pupal disc cells were examined and Golgi stacks were clearly visible. Their surface density within the cytoplasm was large (4.87 μm^{-1}; Table 1, line 6) and they comprised stacked cisternae (Figure 1E) and large tubular networks around cisternae (Figure 1F). The percentage of Golgi membrane found in cisternae rose to ~56.8%, of which 65% were stacked (Table 1, line 6).

This succession of different morphologies, from vesicles and tubules in larval clusters with increasing cisternal elements, to proper prepupal Golgi stacks, suggested a temporal conversion of vesicles and tubules to cisternae. However, the surface density of the organelle (that refers to larval clusters or Golgi stacks) within the cytoplasm (Sorg/Vcyt) increased as the cisternae formed. The surface density of organelle within the cytoplasm is composed of two components (see MATERIALS AND METHODS): First, the surface density of organelle membranes within the volume they occupy (Sorg/Vorg) measures how packed the membranes are within a unit of volume and was found similar from one stage to the next (Table 1, first numerical column); second, the volume density of the organelle membranes within the cytoplasm (Vorg/Vcyt) measures the cytoplasmic fraction occupied by these membranes within the cytoplasm and was found to increase from one stage to the next (Table 1, second numerical column). This means that the amount of membrane per unit of volume was similar at the different stages but that more membrane structures were added to the organelle, leading to an increase in the volume they occupy. Because of this addition of membrane, it is possible that the stacks we observed were not derived from the larval clusters but from entirely newly generated membranes. It is thus important to establish that the larval clusters are Golgi stack precursors.

Drosophila Golgi Markers and Antibodies

We first addressed the question of the nature of the larval cluster membrane by localizing different Golgi proteins.

The rabbit polyclonal MLO7 antibody (gift from M. Lowe, Manchester, United Kingdom) was raised against the first 73 amino acids of human GM130 (Nakamura *et al.*, 1995; Lowe *et al.*, 1998), a Golgi peripheral membrane protein receptor for p115 (Nakamura *et al.*, 1997, see below). The corresponding 73 amino acids in the predicted *Drosophila* homolog of GM130 (AJ276417, CG11061) are 40% identical and 51% similar to human and rat GM130 with a very strong conservation in the first 25 (up to 64% identity and 84% similarity). The full-length dGM130 showed only 21% identity and 39% similarity to rat GM130 but exhibits the same overall coil-coiled structure (our unpublished results) and a similar richness in basic amino acids (such as glutamine 11.8 vs. 12.1% in rat GM130). dGM130 was mapped to 58 B7-C6 by probing a P1 array with the EST LP03286 (our unpublished results). By Western blotting with the use of either the antiserum or the affinity-purified MLO7 antibody, one strong band was revealed just above the 83-kDa marker (Figure 2A), which is slightly above the predicted molecular weight of dGM130 (790 amino acids). The same unique band was also revealed with the use of Kc cells (*Drosophila* derived tissue culture cell line) (Figure 2A).

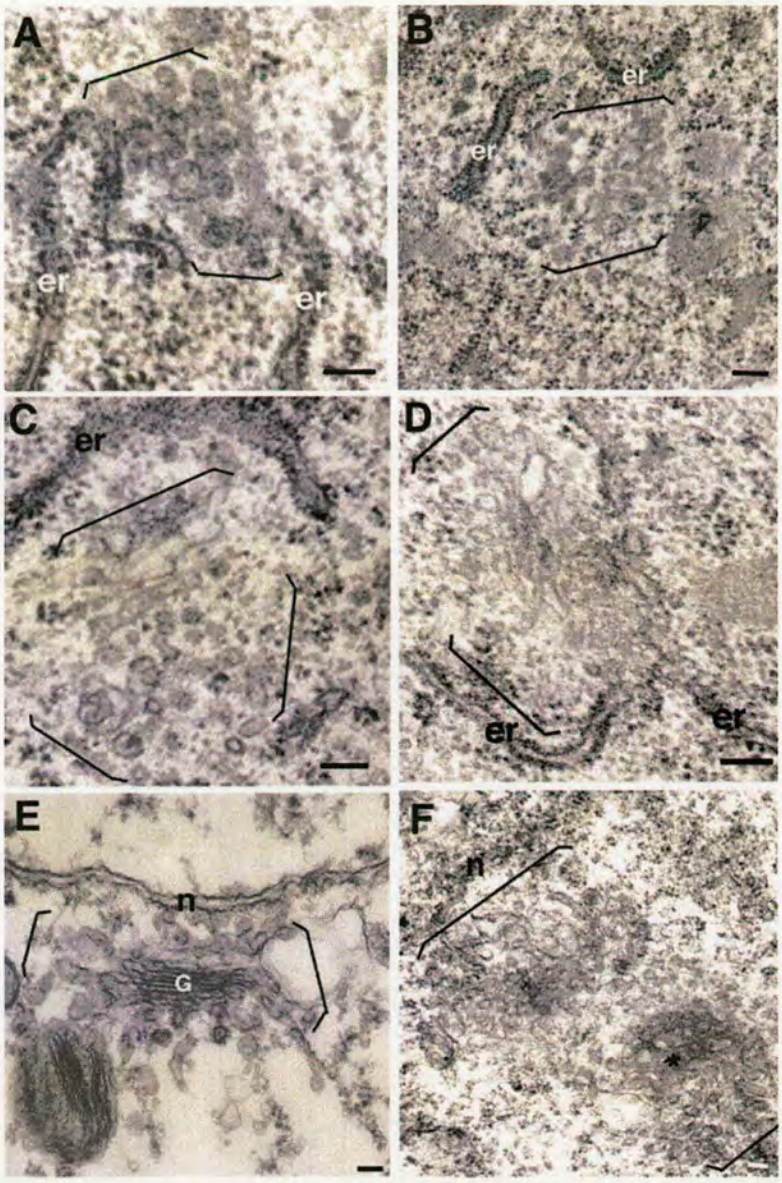

Figure 1. Larval clusters and Golgi areas in discs from third-instar larvae and white pupae. Larval clusters and Golgi area were visualized in leg and wing discs of early third-instar larvae (A and B), mid third-instar larvae (C), late third-instar larvae (D), and white pupae (E and F). Brackets mark the borders of the larval clusters and Golgi areas not bounded by ER cisternae. Stacks are marked with a G. In F, the asterisks indicate an en face view of a fenestrated cisternae. Note the proximity of the larval clusters to ER cisternae (er) in A–D. n, nuclear envelope. Bars, 100 nm.

The rabbit antiserum to p115 (NN7, gift from M. Lowe) was made against the full-length rat p115 protein (Nakamura *et al.*, 1997), a cytosolic myosin-like ligand for GM130. We cloned the *Drosophila* homolog of rat p115 (AJ272048, CG1422) by screening a *Drosophila* embryonic cDNA library (gift from Dr N. White, Edinburgh, United Kingdom) with the use of EST LD41079. A P1 clone array was also probed and dp115 was mapped to 7C6-8. dp115 is 50% identical and 67% similar to rat p115 with the same overall coil-coiled structure (our unpublished results) although the acidic tail (Dirac-Svejstrup *et al.*, 2000) is missing in dp115. When disc extracts were Western blotted with NN7 after electrophoretic separation, one band was observed at the 83-kDa molecular weight marker (Figure 2B), as expected (837 amino acids). The same band was reproduced with the use of another monoclonal antibody (mAb) against p115, 4H1 (our unpublished results).

The mouse monoclonal 1D3 antibody (1D3, gift from D. Vaux, Oxford, United Kingdom) was raised against the synthetic peptide corresponding to the 12 C terminus amino acids KDDDQKAVKDEL of human PDI that is a resident of the endoplasmic reticulum (Vaux *et al.*, 1990). In the *Drosophila* homolog of PDI (P543991, CG6988), this sequence becomes EEEEEAPKKDEL exhibiting ~60% similarity (McKay *et al.*, 1995). Used in a Western blot on a disc extract, 1D3 revealed one strong band around 50 kDa that corresponds to the predicted molecular weight of *Drosophila* PDI (496 amino acids; Figure 2B).

Table 1. Stereological analysis of the organelle (larval clusters and Golgi areas) at the different stages of disc elongation org refers to the larval clusters or the Golgi apparatus when clearly identifiable. Results are expressed as ±SD.

				% of org membrane in			
	S_{org}/V_{org}* in μm^{-1}	V_{org}/V_{cyt}*	S_{org}/V_{cyt}* in μm^{-1}	Vesicular profiles (%)	Tubules (%)	Total cisternae (%)	Stacked cisternae/total cisternae
Early third-instar larvae	72.46 ± 8.1	0.018 ± 0.006	1.30 ± 0.07	82.5 ± 12.3	17.5 ± 12	1.0 ± 1.0	nd
Mid-third-instar larvae							
Small clusters	72.35 ± 5.4	0.0155 ± 0.003	1.12 ± 0.03	77.2 ± 8.4	20.0 ± 9.3	2.8 ± 2.0	nd
Medium clusters	68.28 ± 3.8	0.028 ± 0.004	1.91 ± 0.05	35.4 ± 15	49.1 ± 18	12.0 ± 5.0	nd
Late third-instar larvae	66.14 ± 2.7	0.048 ± 0.015	3.17 ± 0.09	28.4 ± 12.3	43.1 ± 10.1	28.6 ± 10.2	0.25 ± 0.10
White pupae	61.25 ± 6.4	0.079 ± 0.021	4.87 ± 1.1	12.8 ± 5.4	30.3 ± 12.3	56.8 ± 13.2	0.65 ± 0.20

nd, not determined.

* See MATERIALS AND METHODS for details.

The rabbit anti-Sec23p antibody (gift from J.P Paccaud, Geneva, Switzerland) was raised against a human sec23A peptide (Paccaud *et al.*, 1996) that shares 69% identity and 81% similarity with the predicted *Drosophila* Sec23p (AJ276482, CG1250). Sec23 is the sar1-specific GTPase activating protein (Yoshihisa *et al.*, 1993) and is part of the coat protein complex (COP) II machinery (Barlowe *et al.*, 1994). This antibody recognizes a single band in a disc extract at the predicted molecular weight of 77 kDa (Figure 10).

The rabbit anti-Sec31p antibody (gift from F. Gorelick, West Haven, NJ) was raised against a rat Sec31 (Shugrue *et al.*, 1999). Rat Sec31 shares 33% identity and 51% similarity with *Drosophila* Sec31 (CG8266). Sec31 has been shown to be part of the COPII recruitment machinery (Schekman and Orci, 1996). This antibody recognizes a single band in a fly head extract that runs at a molecular weight consistent with a protein of 1264 amino acids (Figure 2B).

The anti-β-tubulin antibody (Sigma) and was raised against sea urchin sperm β-tubulin that shares 85% identity with the *Drosophila* counterpart. After Western blotting of disc extracts (Figure 10, C and D) and Kc cells extract (Figure 2A), one strong band was observed at the predicted molecular weight (503 amino acids).

The anti-δ-AP3 antibody (gift from M. Robinson, Cambridge, United Kingdom) was raised against the rat δ subunit of the AP3 complex that has high homology to the *garnet* gene product in *Drosophila*. δ-AP3 has been shown to localize in the *trans*-Golgi network in mammalian cultured cells (Simpson *et al.*, 1997) and in the Golgi area in S2 cells (Rabouille *et al.*, 1999).

The monoclonal mouse ascite 9E10 (gift from T. Nillson, Heidelberg, Germany) was used to detected the myc epitope (Nilsson *et al.*, 1993).

Larval Clusters Contain Golgi Proteins

MLO7 was first used in indirect immunofluorescence experiments on WT mid-third-instar larvae. A punctate staining throughout the cytoplasm (Figure 3A), characteristic of the Golgi apparatus in *Drosophila* tissues was observed (Ripoche *et al.*, 1994; Stanley *et al.*, 1997; Rabouille *et al.*, 1999; Lecuit and Wieschaus, 2000; Munro and Freeman, 2000; Sisson *et al.*, 2000). This pattern is different from mammalian cells and is more reminiscent of a plant or yeast Golgi pattern (Rabouille *et al.*, 1999). In an effort to show the spatial arrangement of dGM130 staining with respect to other subcellular compartments in these very small disc cells (~5 μm across), the ER, the microtubules, and the nucleus were labeled with the use of the 1D3, the anti-β-tubulin antibody, and DAPI, respectively. The 1D3 pattern corresponded to the ER. It was found surrounding the nucleus and was also punctate (Figure 3B), but the dots were smaller, more numerous, and more scattered than the dGM130 pattern. The same pattern was visualized with the use of CEL5C (gift from Carol Lyons, Dundee, United Kingdom), a mAb raised against human ribophorin I, a resident of the ER (our unpublished results).

When 1D3 was used in a double labeling experiment with MLO7, it revealed that dGM130 colocalized partially with the ER (Figure 3C) in agreement with our EM studies. A similar double-labeling pattern was observed when CEL5C was used instead of 1D3 (our unpublished results). A double labeling experiment with the use of β-tubulin antibody and MLO7 (Figure 3D) showed a different pattern. There was almost no overlap and no clear spatial relationship could be established. These results indicate that the dGM130 pattern was specific and exemplified the Golgi pattern. A very similar result was obtained with NN7 (an antibody to p115) (Figure 3E) and the anti-δ-AP3 antibody (Figure 3F).

The glycosyltransferase Fringe has recently been shown to be a Golgi protein (Bruckner *et al.*, 2000; Munro and Freeman, 2000). Transgenic flies carrying UAS-Fringe-DXD tagged with the myc epitope provided us with an alternative tool to confirm the Golgi nature of the disc larval clusters. Fringe localization in the fly Golgi apparatus was shown to be unaffected when the glycosyltransferase motif DDD was changed to DXD (Munro and Freeman, 2000). Fringe-DXD-myc was expressed ubiquitously at low level (see MATERIALS AND METHODS) and with the use of 9E10 (a monoclonal anti-myc antibody) on sections of unicryl-embedded discs, it was localized to larval clusters (Figure 4, A and B) and Golgi stacks (Figure 4C) when present (the heat shock necessary to induce Fringe expression has driven some of the clusters to be converted into stacks, see below; Figure 7B). The number of gold particles corresponding to Fringe

Figure 2. Western blot of *Drosophila* tissues and Kc cells. (A) Imaginal disc and Kc cell extracts were blotted with either the MLO7 serum (ser) or the MLO7 affinity-purified antibody (AP) raised against the 73 N-terminal amino acids of human GM130. One strong band just above the 83-kDa molecular weight marker is visible in all lanes. The Kc cell extract was also blotted with the anti-β-tubulin mAb and a band at 50 kDa is visible. Disc extract protein (45 μg, equivalent of 8–10 discs) and 100 μg of Kc cell extract protein were loaded on the 8% acrylamide gel. (B) Disc extract was blotted with 1D3. One band at 50 kDa (asterisk) was revealed in addition to two fainter bands just below and one above the 83-kDa marker. Disc extracts (45 μg) were also blotted with NN7 and one strong band was revealed at ~83 kDa. Disc extract protein (equivalent of 8–10 discs) was loaded on the 10% acrylamide gel. Larval head extract was blotted with an anti-Sec31p antibody. One band was revealed at ~130 kDa. Protein (40 μg) was loaded (equivalent to 5 heads) on a 6% acrylamide gel. The numbers on the left of the blots indicate the molecular weight of the prestained markers.

was low. We summed 65 gold particles in >20 pictures. The labeling was confined to the ER (35%) and larval clusters or Golgi stacks (65%). No other membrane compartment was labeled although we could see a low percentage of gold particles at the plasma membrane.

With the use of the same material, MLO7 was used to visualize dGM130 that was found in larval clusters (Figure 4, D and E) and stacks (Figure 4F). Again, the only membrane compartments that were labeled were the clusters or stacks (66.6 ± 12.8%) and the ER (33.4 ± 9.9%) (167 gold counted). This result was comparable to results obtained in WT mid-third-instar larvae (our unpublished results). A very similar result was obtained with NN7 visualizing dp115 (Figure 4, G-I). The clusters and stacks were labeled (67.1 ± 10.6%) as well as the ER (32.9 ± 8.6%) (147 gold counted). The labeling density over the stacks or the larval clusters was 9.8 ± 3.2 times over background for Fringe-DXD-myc, 10.1 ± 4.1 for dGM130, and 8.4 ± 2.9 for dp115. Similar results were also obtained with the *Drosophila* mannosidase II (our unpublished results).

Immunofluoresence imaging indicated that Fringe appeared localized in spots surrounding the nucleus (Figure 5A) in a similar manner to dGM130. Imaginal discs were labeled with MLO7 and 9E10, respectively. When the level of Fringe expression was low, the overlap with dGM130 was significant (Figure 5, B and C). 84 ± 5.7% of structures observed were either yellow (complete overlap) or were partially yellow in combination with either green or red or both. The same pattern was observed with NN7 (visualizing dp115) that also colocalized with Fringe-DXD-myc (Figure 5, D and E). 80 ± 7.6% of the structures observed were either partially or completely yellow. The lack of total overlap, we believe, is mostly due to the fact that the protein expression between clusters is not uniform even for endogenous proteins. We have found it technically difficult to visualize colocalization in situations where Fringe and either dGM130 or dp115 were expressed at very different levels. Taken together, these results suggest that the larval clusters contained at least three Golgi markers (dGM130, dp115, and Fringe), and therefore suggest that an unknown yet significant proportion of the membranes comprised within the larval clusters is Golgi membranes.

ER Exit Sites

The larval clusters in early third-instar larvae consisted of >80% vesicles most of them being 50–70 nm in diameter, consistent with the geometrical features of COPI and II vesicles. Larval clusters were also very often (85% of the cases) found in proximity to a cup-shaped ER cisterna, which resembles an ER exit site (Oprins *et al.*, 1993; Orci *et al.*, 1994). Because COPII vesicles are known to bud from ER at the ER exit sites (Barlowe *et al.*, 1994, Martinez-Menarguez *et al.*, 1999), the vesicles comprised within the larval clusters could be COPII-derived vesicles. Sec23p and Sec31p are part of the COPII machinery (Schekman and Orci, 1996) and we used antibodies raised against these two proteins to label these sites. The immunofluorescence patterns of dSec23p and dSec31p were reminiscent of that of dGM130. They were punctate, surrounded the nucleus and only colocalized partially with the ER labeled with 1D3 (Figure 6, A and B) or CEL5C (our unpublished results).

Discs were also labeled for dSec23p, dSec31p, and Fringe-DXD-myc (Figure 6, C and D). When the level of Fringe expression was low, these markers exhibited ~60% colocalization, approaching the figures obtained with dGM130, dp115, and Fringe. These results suggest that dGM130,

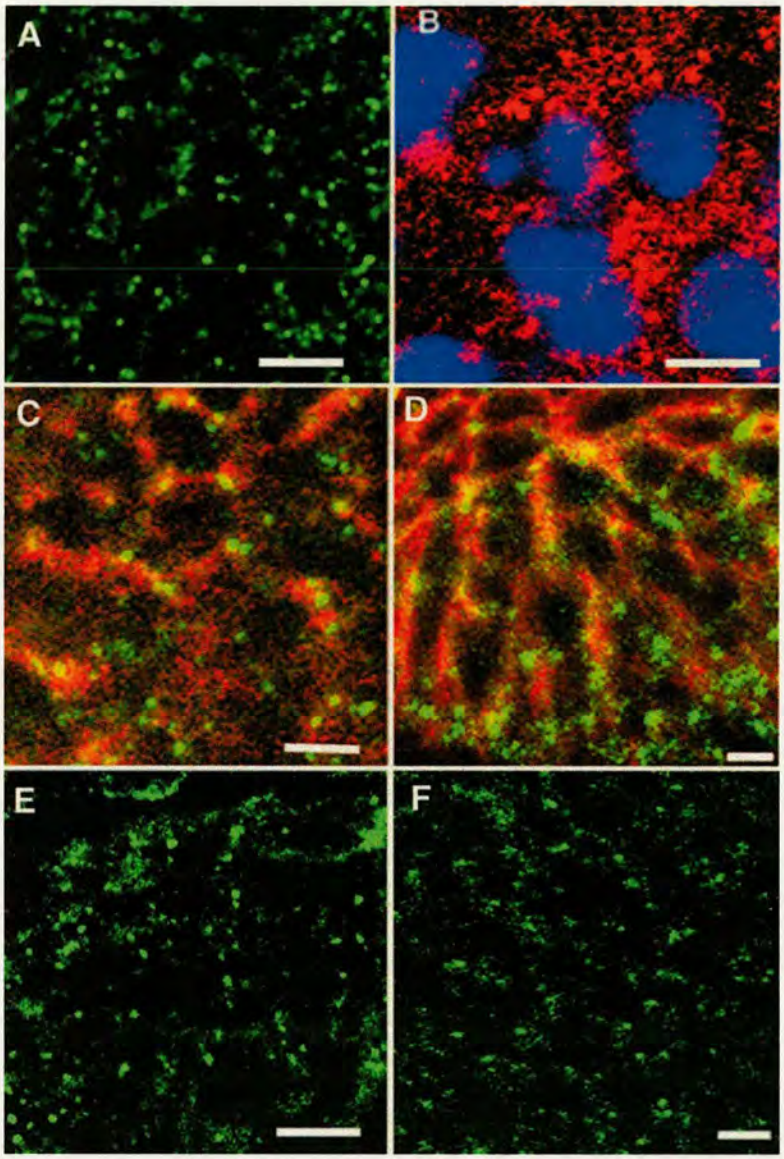

Figure 3. Immunofluorescence imaging of the larval clusters in imaginal disc cells. dGM130 immunofluorescence pattern was visualized in mid-third-instar larval leg and wing discs labeled with rabbit polyclonal MLO7 serum followed by an anti-rabbit IgG conjugated with FITC (green) (A). Note the dots surrounding a black space (nucleus). Discs were also labeled with mouse monoclonal 1D3 followed by an anti-mouse IgG conjugated with Texas Red (red), and DAPI (blue) (B). Dots are numerous and also surround the nucleus. Discs were double immunolabeled with the use of MLO7 and 1D3 followed by an anti-rabbit IgG conjugated with FITC (green) and an anti-mouse IgG conjugated with Texas Red (red) (C). Note that the green dots overlap partially with the red staining representing the ER. Discs were double immunolabeled with MLO7 and the mouse monoclonal anti-β-tubulin antibody followed by an anti-rabbit IgG conjugated with FITC (green) and an anti-mouse IgG conjugated with Texas Red (red) (D). Discs were also labeled with NN7 (the anti-p115 antibody) (E) and the anti-δ-AP3 antibody (F) followed by a anti-rabbit IgG conjugated with FITC. Note that the pattern in A, E, and F are similar. Bars, 5 μm.

dp115, dSec23p, dSec31p, and Fringe-DXD-myc localize in the same structure (the larval clusters) and that they were populated by COPII-coated vesicles.

Larval Clusters Can Be Driven to Form Stacked Cisternae

To support further the fact that the larval clusters are Golgi stack precursors, we attempted to force the conversion of these clusters into Golgi cisternae.

Mid-third-instar WT larvae were incubated at 37°C for 2 h. Under these conditions, the larvae were viable, and aged but did not become pupae. The larval clusters present in the larvae before the temperature shift consisted of tubules and vesicles with ~7% of the total membrane in cisternae and had a surface density of 1.91 μm^{-1} (Table 2). When incubated at 22°C for 2 h (Figure 7A), the larval clusters have grown a little (surface density of 2.04 μm^{-1}), and have consisted of small tubules and vesicles with 10% of membrane in cisternae (Table 2). When incubated at 37°C, however, they were replaced by small stacks of cisternae (Figure 7B) with 45% of total Golgi membrane in cisternae (Table 2) with 45% of them in stacks. Importantly, the surface density of the clusters and the resulting cisternae were not grossly modified by the 37°C incubation (3.09 μm^{-1} after incubation vs. 2.04 μm^{-1} before, a 1.51-fold difference), whereas the gain in membrane in cisternae was 6.4-fold (from 7 to 45%) (Table 2). This result suggests that most of the membrane present in larval clusters before the incubation was converted into Golgi-stacked cisternae.

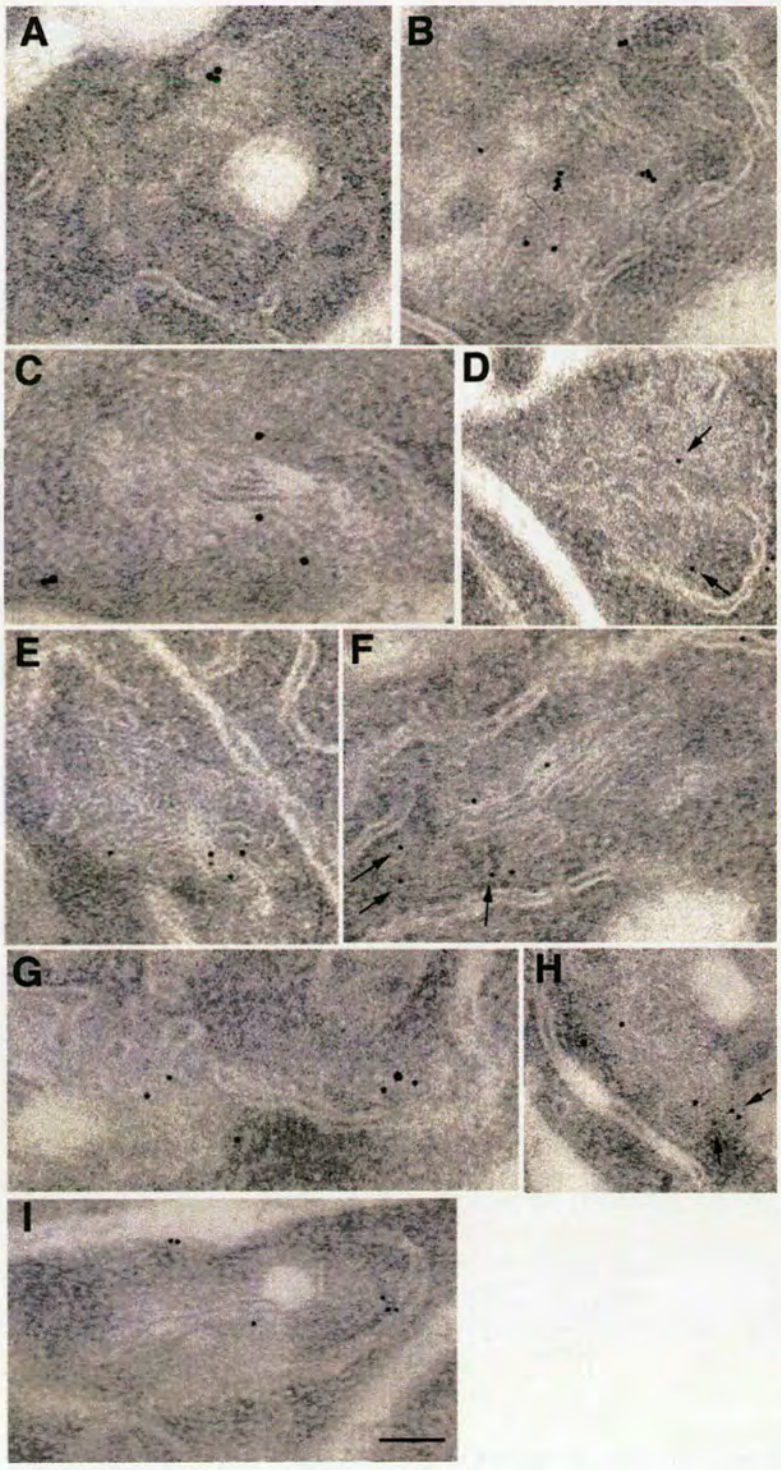

Figure 4. Immuno-EM localization of Golgi proteins on larval clusters and Golgi stacks. Unicryl-embedded mid-third-instar discs expressing low level of Fringe-DXD-myc were sectioned and labeled with 9E10 (anti-myc antibody) followed by anti-mouse IgG conjugated to 15-nm gold (A–C) MLO7 (anti-GM130 antibody) followed by anti-rabbit IgG conjugated to 10-nm gold (D–F), and NN7 (an anti-p115 antibody) followed by anti-rabbit IgG conjugated to 10-nm gold (G–I). Larval clusters (A, B, D, E, G, and H) and Golgi areas comprising a stack (C, F, and I) were labeled by the three antibodies. The arrows in D, F, and H indicate gold particles that may be difficult to see. Bar, 100 nm.

dNSF1 and Formation of Golgi Stacks

The conversion of clusters of tubules and vesicles into cisternae would imply the fusion of the former fragments into the latter as observed in the reassembly of Golgi stacks in vitro (Rabouille *et al.*, 1995b). Two ATPases are known to be involved in the reassembly of Golgi fragments into stacked

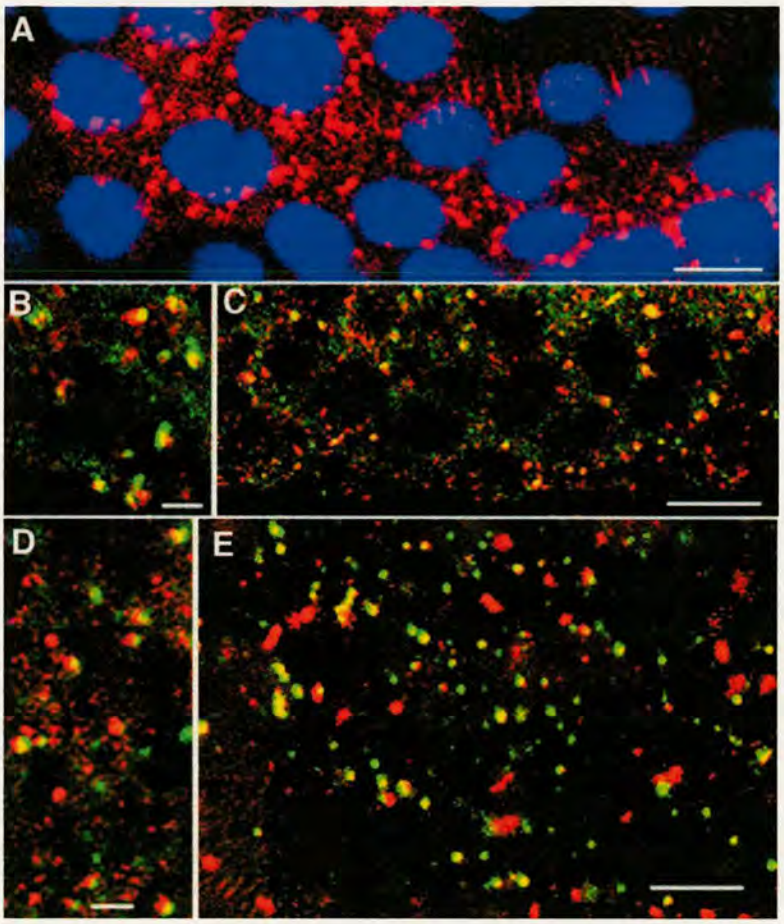

Figure 5. dGM130, dp115, and Fringe in mid-third-instar larval discs cells. UAS-Fringe-DXD-myc (stock 919)/HsGAL4 mid-third-instar larval discs were immunolabeled after heat shocking the larvae to induce the synthesis of myc-tagged Fringe-DXD. These discs were immunolabeled with the monoclonal anti-myc antibody 9E10 followed by an anti-mouse IgG conjugated with Texas Red (red), and DAPI (blue) (A). Note the dots around the nucleus. These discs were also double labeled with 9E10 and either MLO7 (B and C) or NN7 (D and E) followed by an anti-mouse IgG conjugated with Texas Red (red) and an anti-rabbit IgG conjugated with FITC (green). Note the colocalization of the two proteins (yellow) and also the structures that display all three colors (yellow, green, and red). Bars, 5 μm.

cisternae in vitro, NSF (and its cofactor αSNAP), and p97 (and its cofactor p47) (Acharya *et al.*, 1995; Rabouille *et al.*, 1995a; Kondo *et al.*, 1997). We tested the involvement of dNSF1 (one of the two *Drosophila* homologs of mammalian NSF) in the observed Golgi stack biogenesis with the use of larvae from *comt 17* homozygote stocks (gifts from Dr. B. Ganetsky). *comt 17* is a thermosensitive allele of dNSF1. At 37°C, dNSF1 is misfolded and nonfunctional (Siddiqi and Benzer, 1976; Pallanck *et al.*, 1995a). We performed parallel experiments with WT larvae as well as with larvae in which the dNSF1 mutation (*comt 17*) is rescued by a dNSF1 transgene under the control of a heat-shock promoter (HSN) (see MATERIALS AND METHODS for details). Because the production of mutant dNSF1 and the overexpression of dNSF1 were both dependent on an incubation at 37°C, all experiments were performed concurrently under equivalent conditions.

In contrast to what happened in the WT situation (Figure 7B), the formation of Golgi cisternae in *comt 17* larval discs exposed to the same conditions as WT (37°C for 2 h, see above) was blocked. The larval clusters that were present in disc cells from *comt 17* larvae before the incubation remained as tubules and vesicles (Figure 7C) with only ~17% of the total Golgi membranes in cisternae (Table 2). Furthermore, ecdysone is known to trigger disc elongation and its production by the prothoracic gland depends on the neuropeptide prothoracicotropic hormone whose secretion ultimately might depend of dNSF1. Although exogenous ecdysone was fed to the larvae to prevent any effects of the lack of production of ecdysone in the NSF mutant larvae, we also performed the experiment in vitro in the presence of exogenous ecdysone (for details, see below and MATERIALS AND METHODS). *comt 17* larvae were dissected and their discs incubated at 37°C for 2 h in the presence of ecdysone. The same results were obtained as in vivo. The larval clusters did not become Golgi stacks (Figure 7D and Table 2). The conversion of larval clusters into Golgi stacks, however, was rescued by overexpression of dNSF1. In the *comt17*/Y; HSN TM3, sb/+ larvae, the conversion from larval clusters to Golgi stacks was even more efficient than in WT (53% of membrane in cisternae, of which 64% were in stacks; Table 2 and Figure 7F). The level of dNSF1 in these larvae was at least 3 times that of the WT larvae (as estimated by fluorescent in situ hydridization; our unpublished results) and that could explained why the rescue was more efficient than the WT. The *comt 17*/Y; TM6/+ larvae (nonrescued) were very similar to the homozygote *comt 17* larvae (Figure 7E and Table 2).

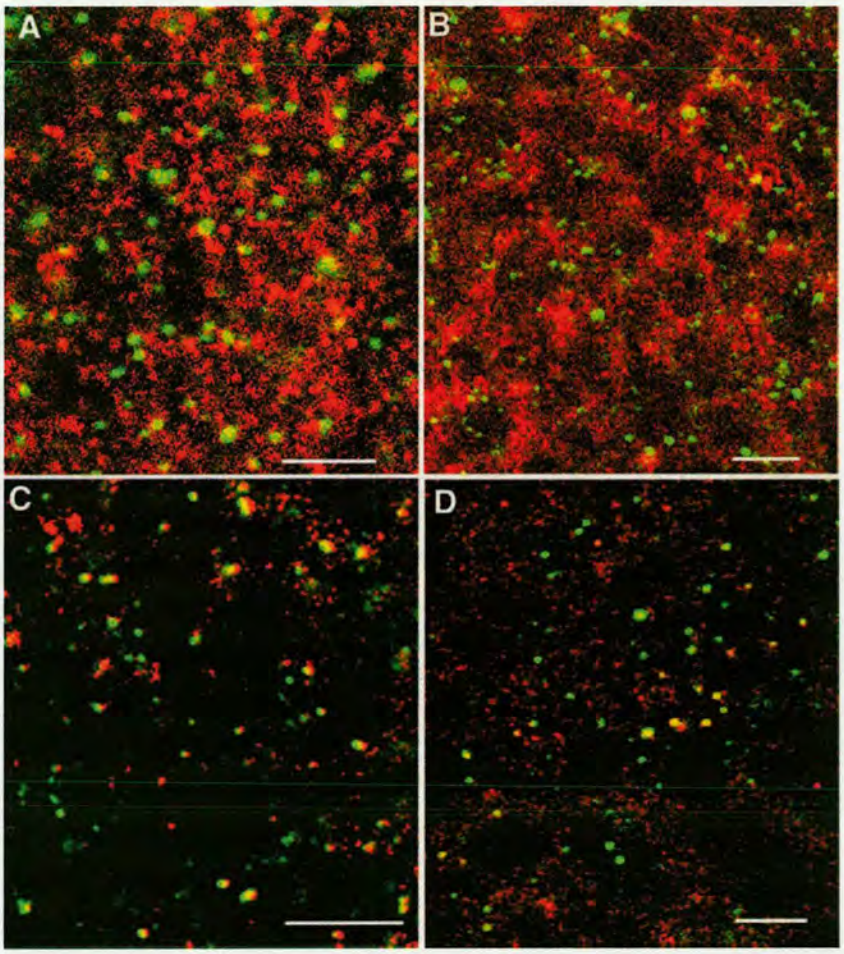

Figure 6. Immunofluorescence labeling of the larval clusters with components of the COPII machinery. UAS-Fringe-DXD-myc/HsGAL4 mid-third-instar larval discs (Fig .5) were immunolabeled with the anti-Sec23p antibody (A and C) or Sec31p antibody (B and D) together with 1D3 (A and B) and 9E10 (C and D) followed by an anti-rabbit IgG conjugated with FITC and an anti-mouse IgG conjugated to Texas Red. Note in C and D structures in which dSec23p, dSec31p, and Fringe overlap completely or partially together with structures that contain only dSec23p or dSec31p or only Fringe. Bars, 5 μm.

This series of experiments suggests that the larval clusters can be converted to stacked cisternae with only minimal addition of new membrane. This conversion was blocked in the absence of functional dNSF1 and was rescued by overexpression of functional dNSF1. Taken together, these results suggest the system we are studying could represent an in vivo system in which to study the biogenesis of Golgi stacks.

Biogenesis of Golgi Stacks Is Dependent on Ecdysone

The timing of the transition from larval clusters to stacked cisternae was suggestive of an involvement of ecdysone, the hormone that plays a crucial role in the morphogenetic event of larval-to-pupal transition (Garen *et al.*, 1977).

We first recapitulated the transition from larval clusters to Golgi stacks in a semi-intact system (Mandaron, 1971) that reconstituted disc elongation in vitro with the use of dissected discs incubated in M3 medium containing exogenous ecdysone. A 10–18-h incubation was successful in mimicking the first step of disc elongation (our unpublished results). This incubation drove the conversion of clusters of vesicles and tubules to Golgi areas comprising 58.8% cisternae (Figure 8C and Table 3), similar to figures obtained in white pupae Golgi areas (Table 1, line 6). In the absence of ecdysone, this morphological change did not occur (Figure 8, A and B, and Table 3).

These results suggest that the coupling of disc elongation and the biogenesis of the Golgi stacks can be reconstituted in vitro and that the disc culture system mimics closely the in vivo situation. Moreover, they also suggest that ecdysone could be the trigger of Golgi stack biogenesis.

To investigate the latter, we then turned toward the *ecdysoneless* mutants ecd^{1ts}, a *Drosophila* temperature-sensitive allele. At the restrictive temperature of 29°C, ecdysone production is severely inhibited (Garen *et al.*, 1977; Redfern and Bownes, 1983), whereas at 22°C, the larvae behave as WT. Six days after egg laying at 22°C, the larvae were transferred to 29°C for 7 h. After maintaining the larvae at 29°C or returning them at 22°C for 18 h, the larvae were dissected and the discs processed for electron microscopy. When maintained at 29°C, the only profiles observed were clusters of vesicles and tubules (Figure 9A). The surface density (Sorg/Vcyt) was 2.86 μm^{-1} and the percentage of mem-

Table 2. Effect of the *comt 17* mutation on the formation of Golgi stacks. org refers to the larval clusters or the Golgi when clearly identifiable. Results are expressed as ±SD.

			% of org membrane in			
		S_{org}/V_{cyt}* (μm^{-1})	Vesicular profiles (%)	Tubules (%)	Total cisternae (%)	Stacked cisternae/total cisternae
WT	Before incubation	1.91 ± 0.20	36.0 ± 8.6	57.1 ± 7.8	7.0 ± 3.5	nd
	After 2-h incubation at 21°C in vivo	2.04 ± 0.21	32.4 ± 9.3	42.5 ± 6.5	10.1 ± 3.9	nd
	After 2-h incubation at 37°C in vivo	3.09 ± 0.31	20.5 ± 4.9	34.1 ± 5.7	45.0 ± 8.2	0.45 ± 0.12
comt 17	After 2-h incubation at 37°C in vivo	3.64 ± 0.27	34.7 ± 6.8	49.3 ± 6.7	16.8 ± 9.7	nd
	After 2-h incubation at 37°C in vitro	3.65 ± 0.30	38.6 ± 5.9	45.8 ± 7.4	15.2 ± 8.6	nd
comt 17/Y; TM6/+	After 2-h incubation at 37°C in vitro	4.13 ± 0.62	35.1 ± 6.8	50.1 ± 10.3	14.8 ± 7.3	nd
comt 17/Y; HSN TM3, sb/+	After 2-h incubation at 37°C in vitro	6.99 ± 0.73	14.3 ± 7.5	32.7 ± 8.6	53.0 ± 5.4	0.64 ± 0.1

nd, not determined.

* See MATERIALS AND METHODS for details.

brane in cisternae was 7.0% (Table 3). When returned to 22°C for 18 h, the Golgi area was now neatly defined as stacked cisternae (Figure 9B). The surface density of the Golgi areas was not significantly different from the 29°C larvae (3.31 μm^{-1}; Table 3) but the percentage of membrane in cisternae was 60.9%, a highly significant increase, of which 72% in stacks (Table 4).

A similar experiment was performed in vitro. After maintaining the larvae at 29°C for 6 h, the larvae were dissected and incubated in M3 medium at 22°C in the presence or absence of ecdysone. Discs incubated without ecdysone exhibited larval clusters (Figure 9C) with a surface density of 3.24 μm^{-1} and 4.6% of membrane in cisternae (Table 3), whereas the discs incubated in the presence of ecdysone presented stacked cisternae (Figure 9D) with surface density of 2.86 μm^{-1} and 47.7% of membrane in cisternae (Table 3).

We took these results as additional evidence that the larval clusters were Golgi stack precursors. As in the in vivo experiment described above with WT larvae (Figure 7, A and B), the conversion of clustered vesicles and tubules to stacked cisternae was achieved without substantial addition of new membranes, possibly suggesting that Golgi stacks were built via consumption of the larval clusters. These results also suggest that ecdysone played an important role in the conversion of the larval clusters into Golgi stacks.

dGM130 and dSec23 Protein Expression Increases in Presence of Ecdysone

Disc elongation does not take place in the absence of ecdysone. The blockade of Golgi stack biogenesis in the absence of ecdysone could therefore be a consequence of the blockade of disc elongation. Alternatively, Golgi stack biogenesis could be an event independently triggered by ecdysone.

To address part of this issue, we investigated whether ecdysone could have an effect on the expression of Golgi-related proteins. Leg and wing discs dissected from mid-and late third-instar larvae were processed for immunofluorescence with the use of MLO7, the anti-GM130 antiserum. In mid-third-instar larvae, the general expression of dGM130 was low (Figure 10A) with no detectable pattern as observed in Figures 3 and 5. In contrast, dGM130 expression elevated in late third-instar larvae (Figure 10B), approximately three- to fourfold on average (n = 4).

Furthermore, disc were collected from either ecd^{1ts} mutant larvae maintained at 29°C or from WT mid-third-instar larvae and they were incubated in vitro in the presence or the absence of ecdysone. Western blotting of the ecd^{1ts} disc extracts with MLO7 revealed that in the presence of ecdysone the band corresponding to dGM130 has an intensity approximately threefold higher than in the absence of ecdysone (n = 2; Figure 10C). Similar results were obtained by Western blotting of WT disc extracts with MLO7 or the anti-Sec23 antibody. In the presence of ecdysone, the band corresponding to dGM130 was 2.7 times more intense (n = 2; our unpublished results) and the band corresponding to dSec23p was approximately fivefold more intense than without ecdysone (Figure 10C) for a constant expression of β-tubulin. This experiment suggests that dGM130 and dSec23 protein expression is dependent on ecdysone and that ecdysone might trigger Golgi stack biogenesis.

DISCUSSION

Golgi Stack Biogenesis In Vivo

We have shown that Golgi stack biogenesis occurs in epithelial imaginal disc cells during the first phase of disc elongation in *D. melanogaster*. As larvae become white pupae, their leg and wing imaginal discs elongate, and the morphology of the Golgi apparatus within the disc cells changes. The morphological changes begin in early third-

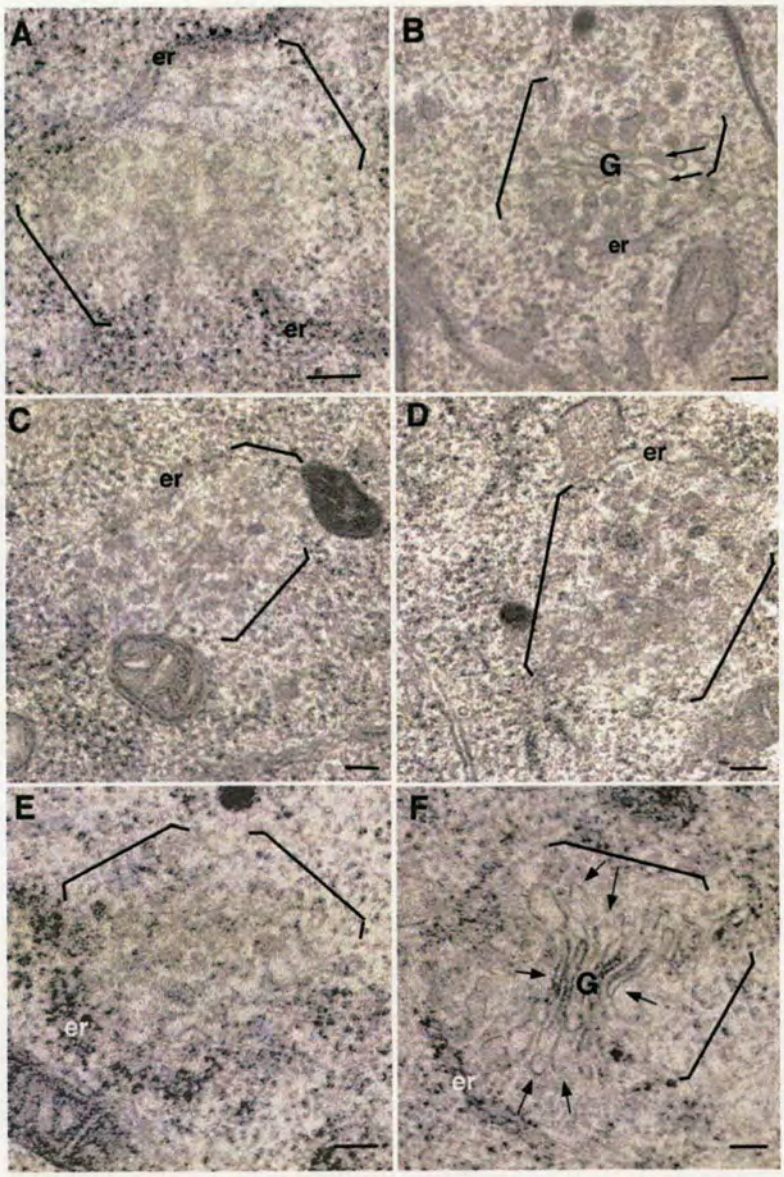

Figure 7. Effect of the *comt 17* mutation on the biogenesis of Golgi stacks. Mid-third-instar WT larvae were incubated at 22°C (A) or at 37°C (B) for 2 h. followed by dissection of their discs. *Comt17* homozygote larvae were incubated at 37°C for 2 h followed by disc dissection (C) or semidissected and incubated at 37°C for 2 h in the presence of ecdysone (D). *comt 17*/Y; TM6/+ (E) and *comt 17*/Y; TM3 HSN, Sb/+ (F) larvae were semidissected and incubated at 37°C for 2 h in the presence of ecdysone. The discs were fixed and processed for conventional EM. The larval clusters and the Golgi areas are marked between brackets when ER cisternae are not marking the natural boundaries, and the stack marked with a G. Note the cisternae in B and F (arrows). er, endoplasmic reticulum. Bars, 100 nm.

instar larvae with the presence of small larval clusters of 50–70-nm vesicles and short tubules. Through mid- to late third instar, these small clusters are gradually replaced by larger clusters of vesicles and longer tubules as well as some cisternal elements. There appears to be a correlation between the size of the clusters and the percentage of cluster membrane in cisternal profiles. And finally, in white pupae, the larval clusters are replaced by still larger Golgi-stacked cisternae of typical morphology. This succession of morphologies suggests that the small larval clusters increase in size with a concomitant formation of cisternae, up to ~60% of the Golgi membrane, of which two-thirds are in stacks.

The transition from small Golgi fragments to stacked cisternae appears to be a phenomenon not confined solely to *Drosophila* larval disc development. Rather, preliminary results suggest that the same transition occurred during *Drosophila* embryogenesis. In syntitial and gastrulating embryos, the Golgi apparatus consists of small fragments (Fullilove and Jacobson, 1971; Ripoche *et al.*, 1994; Stanley *et al.*, 1997), whereas in late embryo (20 h after fertilization), it has the typical stacked morphology (Rabouille *et al.*, 1999). A similar change in the Golgi morphology (from clusters to stacks) also occurs in *Drosophila* salivary glands (Thomopoulos *et al.*, 1992) between early and late-third-instar larvae, coinciding with glue synthesis. The apparent morphological changes could suggest that the morphological state of the Golgi apparatus are linked to the developmental state of the cell, even maybe to its commitment to differentiation.

Table 3. Stereological analysis of the effect of ecdysone on the formation of the Golgi stacks. org refers to the larval clusters or the Golgi are when clearly identifiable. Results are expressed as ±SD.

			% of org membrane in			
		S_{org}/V_{cyt}* (μm^{-1})	Vesicular profiles	Tubules	Total cisternae	Stacked cisternae/ total cisternae
WT in vitro	−ecd	2.04 ± 0.42	43.5 ± 16.6	44.0 ± 13.1	11.5 ± 5.0	nd
	+ecd	5.42 ± 1.13	13.8 ± 5.5	26.9 ± 7.9	58.8 ± 10.3	0.61 ± 0.10
Ecd^{1ts} in vivo	at 29°C	2.86 ± 0.74	28.5 ± 9.7	65 ± 14	7.0 ± 3.6	nd
	at 21°C	3.31 ± 0.50	16.1 ± 5.6	23.1 ± 10	60.9 ± 15.0	0.72 ± 0.24
Ecd^{1ts} in vitro	−ecd	3.24 ± 0.43	32.1 ± 10	63.0 ± 15	4.6 ± 4	nd
	+ecd	2.86 ± 0.20	22.6 ± 3.5	29.1 ± 8.2	47.7 ± 7	0.63 ± 0.25

nd, not determined.

* See MATERIALS AND METHODS for details.

We suggest that the clusters observed in mid-third-instar larvae are Golgi stack precursors with the use of two series of experiments. First, with the use of immunoelectron and confocal immunofluorescence microscopy, we show that the larval clusters contain Golgi markers, including dGM130 and dp115 that were colocalized with a newly described *Drosophila* Golgi protein, Fringe when it is expressed at low level. The immuno-EM was strongly indicative that these proteins were Golgi proteins (a labeling density ~10 times over background) although approximately one-third of the labeling was associated with the ER. This situation resembles closely the cellular distribution of *Drosophila* mannosidase II (Rabouille *et al.*, 1999) and could represent a characteristic of the *Drosophila* exocytic pathway. Second, we show that in different experimental designs the larval clusters are replaced by Golgi stacks of similar surface density, suggesting the conversion of the former into the latter without addition of new membrane structures. For instance, mid-third-instar larval clusters could rapidly be converted into small stacked Golgi cisternae when larvae were incubated at 37°C for 2 h. The possibility exists, however, that the clusters are consumed entirely to be replaced by Golgi stacks gener-

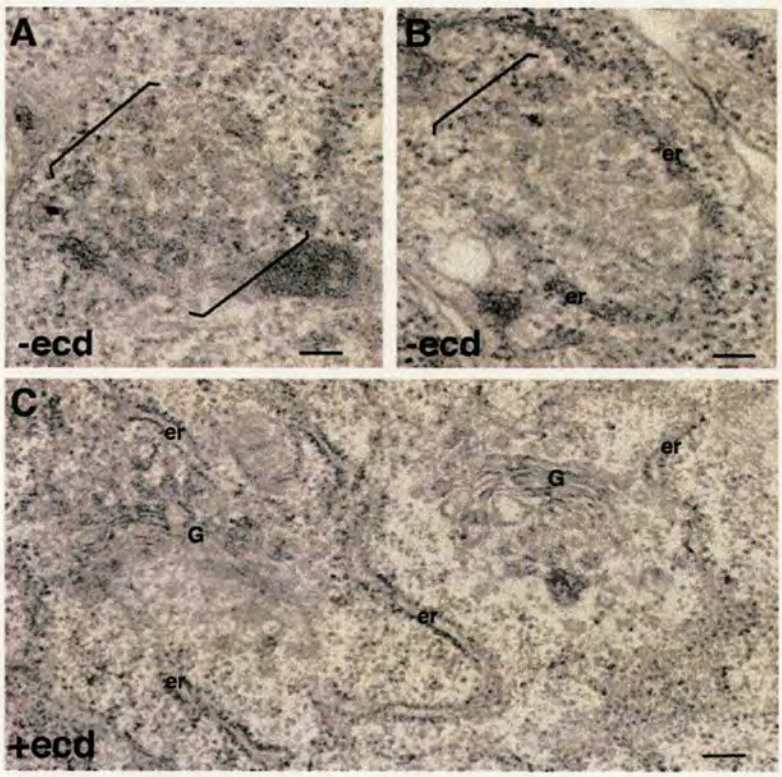

Figure 8. In vitro recapitulation of Golgi stack formation in the presence of ecdysone. WT mid-third-instar larvae were semidissected, incubated in M3 or Schneider medium either supplemented (C) with ecdysone and fly extract or without (A and B). Their discs were fixed and processed for conventional EM. The larval clusters and the Golgi areas are marked between brackets when ER cisternae are not marking the natural boundaries, and the stack marked with a G. er, endoplasmic reticulum. Bars, 100 nm.

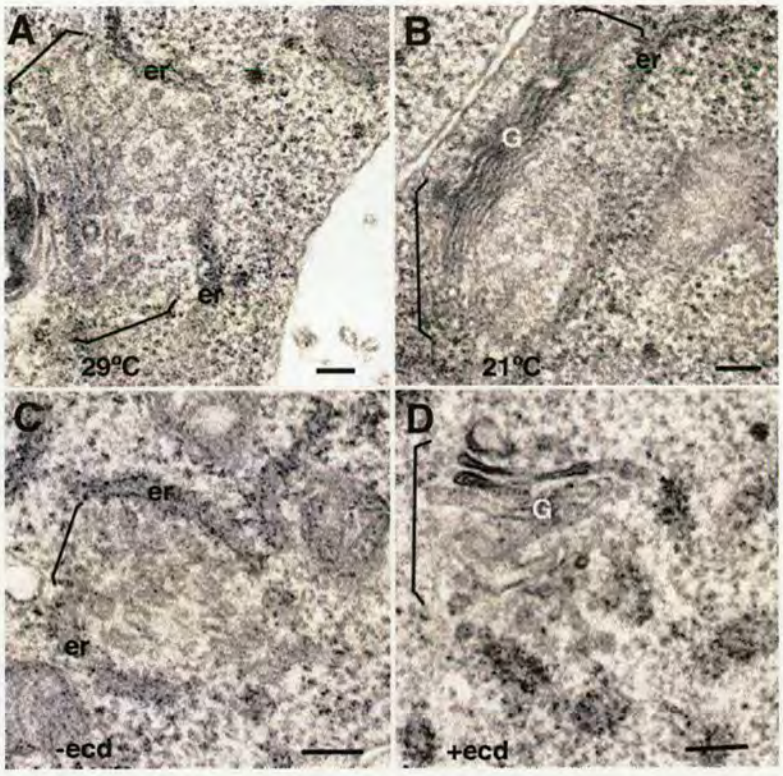

Figure 9. Effect of ecdysone on the Golgi stacks biogenesis. *ecd*^{1ts} mutant larvae were maintained at the restrictive temperature of 29°C and either kept at 29°C (A) or released at 22°C for 18 h (B). Their disks were processed for EM and Golgi areas (either Golgi stacks or larval clusters) examined. Alternatively, *ecd*^{1ts} mutant larvae maintained at 29°C were semidissected and incubated in the absence (C) or the presence (D) of 3 μM ecdysone. The larval clusters and the Golgi areas are marked between brackets when ER cisternae are not marking the natural boundaries, and the stack marked with a G. er, endoplasmic reticulum. Bars, 100 nm.

ated by a new independent mechanism. The conservation of surface density would then be coincidental. This situation seems to us unlikely. This conservation, though, also has been observed with the *ecd*^{1ts} mutants. Furthermore, if the clusters would be consumed to be replaced by newly formed Golgi stacks, we would expect to see a disappearance of the clusters in situations where they cannot be converted, i.e., in the *comt 17* and *ecd*^{1ts} mutants at restrictive temperature. Instead, we see the clusters remaining as clusters. The issue will only completely be resolved when real time experiments visualizing the membranes are carried out in a similar manner as in tissue culture cells (Mironov *et al.*, 2000).

We showed that dSec23p and dSec31p, the key components of the COPII machinery (Barlowe *et al.*, 1994; Schekman and Orci, 1996), are exhibiting a labeling pattern reminiscent of that of dGM130 and dp115 and overlap marginally with the ER. We found by immuno-EM that the larval clusters were labeled by Sec23 antibody (our unpublished results), and we also showed that dSec23p and dSec31p did colocalize substantially with Fringe (as dGM130 does), suggesting that the larval clusters derived primarily from the accumulation of COPII vesicles. This pattern is reminiscent of Sec13p colocalizing with Och1 in *Pichia pastoris* (Rossanese *et al.*, 2000). There were, however, a significant number of structures solely positive for dSec23p or dSec31p as well as structures solely positive for Fringe. This is the reflection of two types of limitations. First, cells did not express the same level of proteins and not all larval clusters within a cell were labeled to equivalent intensity. As a result, the overlap was variable and technically difficult to visualize. Second, the 20 or 40 min of heat shock necessary to induce Fringe expression also drove partially the conversion of some of the clusters into Golgi stacks (as in the WT type situation described in Figure 7B). Our preliminary immunoelectronmicroscopy results suggested that Fringe localized in the newly forming stacks, whereas dSec23p remained at the ER exit site as anticipated. These subtle localization differences could be picked up by immunofluorescence. This could also explain why dGM130, dp115, and Fringe show differential immunofluorescence patterns. Furthermore, it could also mean that not all ER exit sites are involved in the formation of larval clusters.

We found that the volume density of the larval clusters and the Golgi stacks within the cytoplasm increases from early third-instar larvae until white pupae, seemingly by accretion of newly formed vesicles. This observation suggests a mechanism whereby the dispersion of vesicles and tubules into the cytoplasm is prevented. They act as if they were anchored on a template or the "zone of exclusion" (Mollenhauer and Morré, 1978; Rabouille *et al.*, 1995b; Barr *et al.*, 1997). The anchoring of vesicles is thought to be an essential part of the formation of Golgi cisternae. It was shown in vitro that the concentration of mitotic Golgi fragments was a critical factor for their successful fusion to form cisternae (Rabouille *et al.*, 1995b). The anchoring template may play a similar role in vivo in achieving this critical concentration. Anchored vesicles would fuse together to form tubules and tubular networks, maybe under the form of vesicular tubular clusters described by Bannykh and Balch (1997). These vesicular tubular clusters would in turn

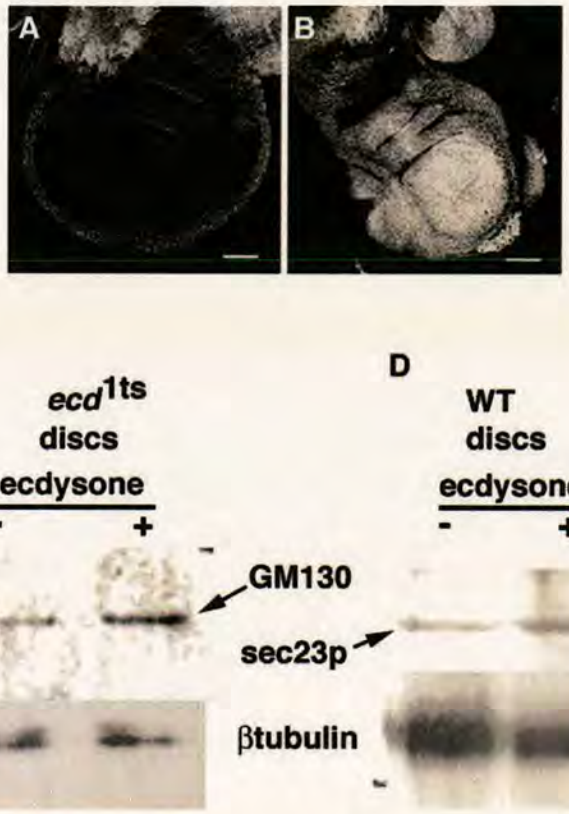

Figure 10. Effect of ecdysone on dGM130 and dSec23 protein expression. Mid- (A) and late (B) third-instar larval discs were immunolabeled with the use of MLO7 as described in Figures 3 and 5. (C) *ecd*^{1ts} mutants were maintained at 29°C, their discs dissected and incubated at 22°C in the absence (−) or the presence (+) of 3 μM ecdysone for 18 h. Thirty leg and 10 wing discs were dissected from each incubation. Disc extract protein (30 μg) was loaded on each lane of a 10% acrylamide gel. Immunoblotting was performed with the use of the affinity-purified MLO7 and the mAb to β-tubulin. (D) Mid-third-instar WT larvae were semidissected and incubated in the absence (−) or in the presence (+) of 3 μM ecdysone. Sixty leg and 20 wing discs were dissected from each incubation. 60 μg of disc extract protein was loaded on each lane of a 10% acrylamide gel. Immunoblotting was performed with the use of the rabbit polyclonal antibody to Sec23p and the mAb to β-tubulin. Bar, 30 μm (A) and 40 μm (B).

undergo further fusion, leading to the formation of the first fenestrated cisterna that could perhaps then act as the template for the stacking of next newly made cisternae. Recent studies in *Pichia* have linked Golgi stacks formation to ER exit sites (tERs), which are discrete and contain Sec13 and Sec12. The *Pichia* tERs are specific regions of the ER, and they contain additional architectural components to those of *Saccharomyces cerevisiae* where no Golgi stacks are observed (Rossanese *et al.*, 2000). These additional components could build tER scaffolds.

The fusion ATPases (dNSF1 and TER94) are present in mid-third-instar larvae (our unpublished results). Our experimental evidence indeed suggests a role for dNSF1 in the fusion of small cluster fragments to form cisternae. When NSF was rendered nonfunctional, achieved with the use of the *comt 17* thermosensitive allele at restrictive temperature, the conversion of larval clusters in Golgi stacks did not take place. This phenotype was reverted by overexpressing dNSF1 in this mutant background, showing that the mutation in the dNSF1 gene was responsible for this phenotype. NSF has been shown to be involved in Golgi stack reassembly in two in vitro mammalian assays (Acharya *et al.*, 1995; Rabouille *et al.*, 1995a). That NSF is involved in Golgi stack biogenesis in our *Drosophila* system may suggest some similarities between the two processes, although the two systems do not recapitulate the same event. The in vitro assays dealt with the reassembly of the preexisting stacks of cisternae that were disassembled and subsequently reassembled, whereas we have described the growth of stacked cisternae from precursor membranes. The two processes, we think, have NSF in common. This result is also in agreement with the requirement of Sec18 (the yeast homolog of mammalian NSF) to drive the formation of Golgi stacks in *S. cerevisiae*, one of the other model systems currently exploited to study Golgi biogenesis (Morin-Ganet *et al.*, 2000).

Comt 17 alleles have a point mutation that substitutes a glycine for an aspartic acid (G274E) in the D1 domain of the molecule. Our in vivo result is in good agreement with the results obtained by Müller *et al.* (1999) who showed that at 37°C the fusion of mitotic Golgi fragments in vitro was no longer supported by a chimeric mouse NSF cDNA in which an equivalent mutation G274E was introduced. This result is also in good agreement with the role of dNSF1 in neurotransmitter release (Tolar and Pallanck, 1998) at the nerve terminal. We do not know yet which SNAP receptors are involved. NSF has been shown to interact with numerous SNAP receptors, including syntaxin 5, Bet1p, membrin, Bos1p, Sec22p (synaptobrevin), and Gos28 (Klumperman, 2000). We could test the requirement of these molecules in the Golgi biogenetic event described here. The *Drosophila* Sec22 homologs has been cloned and Bet1, Gos28, and membrin have predicted homologs in *Drosophila* (Adams *et al.*, 2000), and there is a mutant for sed5 (Ashburner *et al.*, 1999) that we are currently using to address this issue.

The involvement of NSF in this conversion raises the question of the role of TER94. Two independent assays demonstrated that the reassembly of the Golgi stacks could be mediated by the NSF and by the p97 fusion machinery

(Acharya *et al.*, 1995; Rabouille *et al.*, 1995a). TER94 mutants are available and we are currently undertaking a series of experiments to address this question.

Ecdysone and Golgi Stack Biogenesis

The timing of the morphological transition observed in the Golgi area suggested the possible involvement of 20-hydroxyecdysone, the steroid hormone known to trigger the morphogenetic event of puparium formation. We now have two lines of evidence suggesting that Golgi stack biogenesis occurring at the onset of disc elongation is influenced by ecdysone. With the use of the semidissected disc assay, the formation of Golgi stacks from larval clusters was observed in the presence of ecdysone. In contrast, in the absence of ecdysone, Golgi stack formation was prevented. In support of this finding mutant larvae ecd^{1ts} exhibited a severely reduced conversion of larval clusters to Golgi stacks in vivo and in vitro. It seems that the ecdysone dependency of this biogenesis could shed light on its biological significance.

The possibility that the Golgi stack biogenesis is a mere consequence of the cellular events taking place under the control of ecdysone exists. For instance, cell rearrangement taking place during disc elongation could in turn drive Golgi stack formation. That Golgi stack biogenesis does not occur in the absence of ecdysone could simply be the result of the lack of disc elongation. To answer this question, it remains to be shown whether Golgi stack biogenesis precedes or is concomitant with disc elongation.

We have shown that the level of dGM130 increases by ~3 times from mid-to-late third-instar larvae. Ecdysone peaks at the late third-instar stage (~4–6 h before puparium formation) so the increased expression of dGM130 seems to be correlated with the ecdysone peak. We were able to show a causal relationship between the increased expression of dGM130 (~2.8-fold) and ecdysone with the use of discs from ecd^{1ts} mutant larvae incubated in the presence of ecdysone. A similar result was obtained for dSec23p (increase of approximately fivefold) with the use of WT discs from mid-third-instar larvae incubated in vitro. That we only have shown this relationship at the protein level opens nevertheless to the exciting possibility that Golgi stack biogenesis is an event independently triggered by ecdysone at the gene expression level.

Recently, studies of gene expression regulated by ecdysone with the use of microarrays was published by White *et al.* (1999). Of ~6240 element-containing-sequences tested (including 4500 expressed sequence tags), 465 expressed sequence tags (10.3%) were ecdysone responsive and of these, 144 (3.2%) exhibited up-regulation. Interestingly, among these were the fusion ATPase TER94 (Rabouille *et al.*, 1995a) and the component of the COPII coat Sec23A (Barlowe *et al.*, 1994). We have also observed a strong up-regulation of dSec23p expression in our disc system induced by ecdysone and together with dGM130, could be the budding and anchoring components involved in building a Golgi apparatus. It remains to be seen whether the dGM130 gene and *dsec23* are a target for ecdysone and whether other genes encoding known proteins related to the Golgi apparatus are also responsive to ecdysone. We have results that suggest that there are such genes (Dunne and Rabouille, unpublished data). It will also be important to understand whether genes encoding these Golgi proteins are primary targets for ecdysone, and if not what are the transcription activators that mediate ecdysone activity.

The control of Golgi stack biogenesis by the hormone ecdysone would create a situation where the regulated synthesis of Golgi-related proteins stimulates its biogenesis. There are other cases of organelle biogenesis due to up-regulation of genes whose products are resident of this particular organelle. An example is the unfolded protein response (Cox and Walter, 1996). In yeast and mammalian systems, the amount of ER chaperone proteins increases dramatically when cells are exposed to stress. In yeast, a transducing mechanism exists by which the concentration of unfolded proteins in the ER is sensed by an ER transmembrane kinase, Ire1, which in turn leads to the raised stability of mRNA encoding ER chaperone proteins (Cox and Walter, 1996). Importantly, other pathways have also been shown to be targeted by the unfolded protein response (Ng *et al.*, 2000), including membrane lipid synthesis and the inositol response that may lead to ER biogenesis (Cox *et al.*, 1997).

The Golgi apparatus has also been shown to be remodeled during myogenesis. The Golgi apparatus occupies a juxtanuclear polarized organization in myoblasts and a perinuclear nonpolarized distribution in myotubes. In contrast, innervated muscle of chicks or mice displayed a focal distribution of the Golgi apparatus that appears restricted to areas located underneath the motor end plates in subneural domains (Jasmin *et al.*, 1989). Interestingly, some Golgi markers (e.g., α-mannosidase II, TGN 38) present in the embryonic myotubes are no longer detected in the innervated fiber even in the subsynaptic Golgi apparatus (Antony *et al.*, 1995). Our data and the results reported in this article suggest that specific developmental events can influence the Golgi organization. This is perhaps surprising because we were rather of the view that given the important place of the Golgi apparatus in the secretory pathway, its formation should be universal and uniform during development. This seems not to be the case and we might have now at hand one signal that triggers Golgi stack formation. Our task is to understand how the Golgi stack is built at the molecular level and how ecdysone controls this process.

Functional Biosynthetic Pathway

The absence of stacked cisternae in third-instar larvae raises the issue of whether these cells possess a functional biosynthetic pathway. In the imaginal discs of third-instar larvae, many important patterning processes are taking place. The dorso/ventral and anterior/posterior regions are defined by secreted signaling molecules (Vincent, 1998) such as Dpp, Wingless and Hedgehog, and plasma membrane proteins such as Smo and Ptc. The cellular location of these proteins suggests one of two possibilities. Either the cells of third-instar larval discs possess a functional biosynthetic pathway in the absence of stacked cisternae, or these patterning molecules were exocytosed at an earlier developmental stage when Golgi stacks were perhaps present, and persisted into the third-instar larval stage where only clusters are observed. We are rather in favor of the notion that the larval clusters are functional. First, the equivalent Golgi clusters in salivary glands from early third-instar larvae are able to support the secretion of food digestive enzymes (Thomopoulos *et al.*, 1992). Second, we found that *comt 17* discs incubated at restrictive temperature did not elongate, prob-

ably because dNSF1 was not functional in supporting exocytosis (our unpublished results). Indeed, molecules whose lack of synthesis and transportation may inhibit disk elongation include the stubble gene product, IMP-E2 and -E3 (von Kalm *et al.*, 1995) and integrins (Fristrom *et al.*, 1993).

If larval clusters are functional, the question therefore remains as to why the Golgi morphology changes. It has been shown that the Golgi morphology changes when secretion increases (Rambourg *et al.*, 1993). In *Drosophila* salivary glands, the conversion of Golgi clusters to stacks was observed concomitant to glue synthesis (Thomopoulos *et al.*, 1992). A requirement for increased synthesis and secretion could explain the changes in Golgi morphology observed in larval imaginal discs. Furthermore, the formation of a polarized stack could ensure proper differential oligosaccharide or protein processing and targeting, crucial for one or more particular unidentified proteins involved in disk elongation, or for the further synthesis of pupal cuticle that has a different composition to larval cuticle (Riddiford, 1993). Regardless of the explanation, the biogenesis of Golgi stacks at puparium formation seems to be a regulated event triggered by ecdysone.

ACKNOWLEDGMENTS

We thank Leo Pallanck (Washington) for the gift of HSN transgenic lines; Barry Ganetzky for the *comt 17* allele; Matthew Freeman (Cambridge, United Kingdom) for the gift of the UAS-Fringe-DXD-myc fly line (stock 919); J.A. Lepesant (Paris, France) for the gift of the ecd^{1ts} mutant; Martin Lowe (Manchester, United Kingdom) for the gift of the MLO7 and NN7 antibodies, and for helpful comments on the manuscript; David Vaux (Oxford, United Kingdom) for the gift of the 1D3 antibody; Carol Lyons (Dundee, United Kingdom) for the anti-ribophorin I antibody; Jean Pierre Paccaud (Geneva, Switzerland) for antibody to Sec23p; Fred Gorelick (Yale, NJ) for antibody to Sec31p; Neil White (Edinburgh, United Kingdom) for the use of an embryonic cDNA library; Julie Diplexcito for cloning *Drosophila* p115; members of the Davis, Heck, Jarman, and Okhura labs for help with the flies; Marcel van den Heuvel and France Docquier for teaching and support; Graham Warren for helpful discussions; and Ken Sawin and Marcel van den Heuvel for critical comments on the manuscript. We acknowledge the use of fly base (http://flybase.bio.indiana.edu) and the Berkeley *Drosophila* Genome Project (http://www.fruitfly.org) Web sites. This study was funded by the Medical Research Council.

REFERENCES

Acharya, U., Jacobs, R., Peters, J.M., Watson, N., Farquhar, M.G., and Malhotra, V. (1995). The formation of Golgi stacks from vesiculated Golgi membranes requires two distinct fusion events. Cell *82*, 895–904.

Acharya, U., Mallabiabarrena, A., Acharya, J.K., and Malhotra, V. (1998). Signaling via mitogen-activated protein kinase kinase (MEK1) is required for Golgi fragmentation during mitosis. Cell *92*, 183–192.

Adams, M.D., et al. (2000). The genome sequence of *Drosophila melanogaster*. Science *287*, 2185–2195.

Antony, C., Huchet, M., Changeux, J.P., and Cartaud, J. (1995). Developmental regulation of membrane traffic organization during synaptogenesis in mouse diaphragm muscle. J. Cell Biol. *130*, 959–968.

Ashburner, M. et al. (1999). An exploration of the sequence of a 2.9-Mb region of the genome of *Drosophila melanogaster*: the Adh region. Genetics *153*, 179–219.

Banfield, D.K., Lewis, M.J., Rabouille, C., Warren, G., and Pelham, H.R. (1994). Localization of Sed5, a putative vesicle targeting molecule, to the cis-Golgi network involves both its transmembrane and cytoplasmic domains. J. Cell Biol. *127*, 357–371.

Bannykh, S.I., and Balch, W.E. (1997). Membrane dynamics at the endoplasmic reticulum-Golgi interface. J. Cell Biol. *138*, 1–4.

Barlowe, C., Orci, L., Yeung, T., Hosobuchi, M., Hamamoto, S., Salama, M., Rexach, M.F., Ravazzola, M., Amherdt, M., and Schekman, R. (1994). COP II - a membrane coat formed by sec proteins that drive vesicle budding from the endoplasmic-reticulum. Cell *77*, 895–907.

Barr, F.A., Puype, M., Vandekerckhove, J., and Warren, G. (1997). GRASP65, a protein involved in the stacking of Golgi cisternae. Cell *91*, 253–262.

Bruckner, K., Perez, L., Clausen, H., and Cohen, S. (2000). Glycosyltransferase activity of Fringe modulates Notch-Delta interactions. Nature *406*, 411–415.

Cox, J.S., Chapman, R.E., and Walter, P. (1997). The unfolded protein response coordinates the production of endoplasmic reticulum protein and endoplasmic reticulum membrane. Mol. Biol. Cell *8*, 1805–1814.

Cox, J.S., and Walter, P. (1996). A novel mechanism for regulating activity of a transcription factor that controls the unfolded protein response. Cell *87*, 391–404.

Currie, D.A., Milner, M.J., and Evans, C.W. (1988). The growth and differentiation in vitro of leg and wing imaginal disc cells from *Drosophila melanogaster*. Development *102*, 805–814.

Dirac-Svejstrup, A.B., Shorter, J., Waters, M.G., and Warren, G. (2000). Phosphorylation of the vesicle-tethering protein p115 by a casein kinase II-like enzyme is required for Golgi reassembly from isolated mitotic fragments. J. Cell Biol. *150*, 475–487.

Dunne, J., and Rabouille, C. (2001). Lord of the flies: the Golgi in development. In: The ELSO Gazette: e-magazine of the European Life Scientist Organization (http://www.the-elso-gazette/magazines/issue3/mreviews/mreviews1.asp), issue 3 (January 1, 2001).

Fristrom, D., and Fristrom, J.W. (1993). The metamorphic development of the adult epidermis. In: The Development of *Drosophila melanogaster*, vol II, ed. M. Bates and A. Martinez Arias, Cold Spring Harbor, NY: Cold Spring Harbor Laboratory Press, 843–897.

Fristrom, D., Wilcox, M., and Fristrom, J. (1993). The distribution of PS integrins, laminin A and F-actin during key stages in *Drosophila* wing development. Development *117*, 509–523.

Fullilove, S.L., and Jacobson, A.G. (1971). Nuclear elongation and cytokinesis in *Drosophila montana*. Dev. Biol. *26*, 560–577.

Jasmin, B.J., Cartaud, J., Bornens, M., and Changeux, J.P. (1989). Golgi apparatus in chick skeletal muscle: changes in its distribution during end plate development and after denervation. Proc. Natl. Acad. Sci. USA *86*, 7218–7222.

Garen, A., Kauvar, L., and Lepesant, J.A. (1977). Role of ecdysone in *Drosophila* development. Proc. Natl. Acad. Sci. USA *74*, 5099–5103.

Hui, N., Nakamura, N., Sonnichsen, B., Shima, D.T., Nilsson, T., and Warren, G. (1997). An isoform of the Golgi t-SNARE, syntaxin 5, with an endoplasmic reticulum retrieval signal. *8*, 1777–1787.

Klumperman, J. (2000). Transport between ER and golgi. Curr. Opin. Cell Biol. *12*, 445–449.

Kondo, H., Rabouille, C., Newman, R., Levine, T.P., Pappin, D., Freemont, P., and Warren, G. (1997). p47 is a cofactor for p97-mediated membrane fusion. Nature *388*, 75–78.

Lecuit, T., and Wieschaus, E. (2000). Polarized insertion of new membrane from a cytoplasmic reservoir during cleavage of the *Drosophila* embryo. J. Cell Biol. *150*, 849–860.

Leon, A., and McKearin, D. (1999). Identification of TER94, an AAA ATPase protein, as a Bam-dependent component of the *Drosophila* fusome. Mol. Biol. Cell *10*, 3825–3834.

Lowe, M., Rabouille, C., Nakamura, N., Watson, R., Jackman M, Jämsa, E., Rahman, D., Pappin, D.J., and Warren, G. (1998). Cdc2 kinase directly phosphorylates the cis-Golgi matrix protein GM130 and is required for Golgi fragmentation in mitosis. Cell *94*, 783–793.

Mandaron, P. (1971). Mechanism of imaginal disk evagination in *Drosophila*. Dev. Biol. *25*, 581–605.

Martinez-Menarguez, J.A., Geuze, H.J., Slot, J.W., and Klumperman, J. (1999). Vesicular tubular clusters between the ER and Golgi mediate concentration of soluble secretory proteins by exclusion from COPI-coated vesicles. Cell *98*, 81–90.

McKay, R.R., Zhu, L., and Shortridge, R.D. (1995). A *Drosophila* gene that encodes a member of the protein disulfide isomerase/phospholipase C-alpha family. Insect Biochem. Mol. Biol. *25*, 647–654.

Mironov, A.A., Polishchuk, R.S., and Luini, A. (2000). Visualizing membrane traffic in vivo by combined video fluorescence and 3D electron microscopy. Trends Cell Biol. *10*, 349–353.

Mollenhauer, H.H., and Morré, D.J. (1978). Structural compartmentation of the cytosol: zones of exclusion, zones of adhesion, cytoskeletal and intercisternal elements. Subcell. Biochem. *5*, 327–359.

Morin-Ganet, M.N., Rambourg, A., Deitz, S.B., Franzusoff, A., and Képès, F. (2000). Morphogenesis and dynamics of the yeast Golgi apparatus. Traffic *1*, 56–68.

Müller, J.M.M., Rabouille, C., Newman, R., Shorter, J., Freemont, P., Schiavo, G., Warren, G., and Shima, D.T. (1999). An NSF function distinct from ATPase-dependent SNARE disassembly is essential for Golgi membrane fusion. Nat. Cell Biol. *1*, 335–340.

Munro, S., and Freeman, M. (2000). The Notch signaling regulator fringe acts in the Golgi apparatus and requires the glycosyltransferase signature motif DXD. Curr. Biol. *10*, 813–820.

Nakamura, N., Lowe, M., Levine, T.P., Rabouille, C., and Warren, G. (1997). The vesicle docking protein p115 binds GM130, a cis-Golgi matrix protein, in a mitotically regulated manner. Cell *89*, 445–455.

Nakamura, N., Rabouille, C., Watson, R., Nilsson, T., Hui, N., Slusarewicz, P., Kreis, T.E., and Warren, G. (1995). Characterization of a cis-Golgi matrix protein, GM130. J. Cell Biol. *131*, 1715–1726.

Nilsson, T., Pypaert, M., Hoe, M.H., Slusarewicz, P., Berger, E.G., and Warren, G. (1993). Overlapping distribution of two glycosyltransferases in the Golgi apparatus of HeLa cells. J. Cell Biol. *120*, 5–13.

Ng, D.T.W., Spear, E.D., and Walter, P. (2000). The unfolded protein response regulates multiple aspects of secretory and membrane protein biogenesis and endoplasmic reticulum quality control. J. Cell Biol. *150*, 77–88.

Oprins, A., Duden, R., Kreis, T.E., Gueze, H.J., and Slot, J.W. (1993). b-COP localizes mainly to the cis-Golgi side in exocrine pancreas. J. Cell Biol. *121*, 49–59.

Orci, L., Perrelet, A., Ravazolla, M., Amherdt, M., Rothman, J.E., and Schekman, R. (1994). Coatomer-rich endoplasmic-reticulum. Proc. Natl. Acad. Sci. USA *91*, 11924–11928.

Ordway, R.W., Pallanck, L. and Ganetzky, B. (1994). Neurally expressed *Drosophila* genes encoding homologs of the NSF and SNAP secretory proteins. Proc. Natl. Acad. Sci. USA *91*, 5715–5719.

Pallanck, L., Ordway, R.W., and Ganetzky, B. (1995a). A *Drosophila* NSF mutant. Nature *376*, 25.

Pallanck, L., Ordway, R.W. Ramaswami, M., Chi, W.Y., Krishnan, K.S., and Ganetzky, B. (1995b). Distinct roles for N-ethylmaleimide-sensitive fusion protein (NSF) suggested by the identification of a second *Drosophila* homologue. J. Biol. Chem. *270*, 18742–18744.

Paccaud, J.P., Reith, W., Carpentier, J.L., Ravazzola, M., Amherdt, M., Schekman, R., and Orci, L. (1996). Cloning and functional characterization of mammalian homologues of the COPII component Sec23. Mol. Biol. Cell, *7*, 1535–1546.

Pinter, M., Jenely, G., Szepesi, R.J., Farkas, A., Theopold, U., Meyer, H.E., Lindholm, D., Nassel, D.R., Aultmark, D., and Friedrich, P. (1998). TER94, a *Drosophila* homolog of the membrane fusion protein CDC48/p97, is accumulated in nonproliferating cells, in the reproductive organs and in the brain of the imago. Insect Biochem. Mol. Biol. *28*, 91–98.

Rabouille, C. (1999). Quantitative aspects of immunogold labeling in embedded and nonembedded sections. Methods Mol. Biol. *117*, 125–144.

Rabouille, C., Kondo, H., Newman, R., Hui, N., Freemont, P., and Warren, G. (1998). Syntaxin 5 is a common component of the NSF- and p97-mediated reassembly pathways of Golgi cisternae from mitotic Golgi fragments in vitro. Cell *92*, 603–610.

Rabouille, C., Kuntz, D.A., Lockyer, A., Watson, R., Signorelli, T., Rose, D.R., van den Heuvel, M., and Roberts, D.B. (1999). The *Drosophila* GMII gene encodes a Golgi α-mannosidase II. J. Cell Sci. *112*, 3319–3330.

Rabouille, C., Levine, T.P., Peters, J.M., and Warren, G. (1995a). An NSF-like ATPase, p97, and NSF mediate cisternal regrowth from mitotic Golgi fragments. Cell *82*, 905–914.

Rabouille, C., Misteli, T., Watson, R., and Warren, G. (1995b). Reassembly of Golgi stacks from mitotic Golgi fragments in a cell-free system. J. Cell Biol. *129*, 605–618.

Rambourg, A., Clermont, Y., Chretien, M., and Olivier, L. (1993). Modulation of the Golgi apparatus in stimulated and nonstimulated prolactin cells of female rats. *235*, 353–362.

Redfern, C.P.F., and Bownes, M. (1983). Pleitropic effects of the "ecdysoneless-1" mutation of *Drosophila melanogaster*. Mol. Gen. Genet. *189*, 432–440.

Riddiford, L.M. (1993). Hormones and *Drosophila* development. In: The Development of *Drosophila melanogaster*, vol II. ed. M. Bates and A. Martinez Arias, Cold Spring Harbor, NY: Cold Spring Harbor Laboratory Press, 843–897.

Ripoche, J., Link, B., Yucel, J.K., Tokuyasu, K., and Malhotra, V. (1994). Location of Golgi membranes with reference to dividing nuclei in syncytial *Drosophila* embryos. Proc. Natl. Acad. Sci. USA *91*, 1878–1882.

Rossanese, O., Soderholm, J., Bevis, B.J., Sears, I.B., O'Connor, J., Williamson, E.K., and Glick, B.S. (2000). Golgi structure correlates with transitional endoplasmic reticulum organization in *Pichia pastoris* and *Saccharomyces cerevisiae*. J. Cell Biol. *145*, 69–81.

Schekman, R., and Orci, L. (1996). Coat proteins and vesicle budding. Science *271*, 1526–1533.

Shorter, J., Watson, R., Giannakou, M.E., Clarke, M., Warren, G., and Barr, F.A. (1999). GRASP55, a second mammalian GRASP protein involved in the stacking of Golgi cisternae in a cell-free system. EMBO J. *18*, 4949–4960.

Sisson, J.C., Field, C., Ventura, R., Royou, A., and Sullivan, W. (2000). Lava lamp. a novel peripheral Golgi protein, is required for *Drosophila melanogaster* cellularisation. J. Cell Biol. *151*, 905–918.

Siddiqi, O., and Benzer, S. (1976). Neurophysiological defects in temperature-sensitive paralytic mutants of *Drosophila melanogaster*. Proc. Natl. Acad. Sci. USA *73*, 3253–3257.

Simpson, F., Peden, A.A., Christodoulou, L., and Robinson, M.S. (1997). Characterization of the adaptor-related protein complex, AP-3. J. Cell Biol. *137*, 835–845.

Shugrue, C.A., Kolen, E.R., Peters, H., Czernik, A., Kaiser, C., Matovcik, L., Hubbard, A.L., and Gorelick, F. (1999). Identification of

the putative mammalian orthologue of Sec31P, a component of the COPII coat. J. Cell Sci. *112*, 4547–4556.

Stanley, H., Botas, J., and Malhotra, V. (1997). The mechanism of Golgi segregation during mitosis is cell type-specific. Proc. Natl. Acad. Sci. USA *94*, 14467–14470.

Thomopoulos, G.N., Neophytou, E.P., Alexiou, M., Vadolas, A., Limberi-Thomopoulos, S., and Derventzi, A. (1992). Structural and histochemical studies of Golgi complex differentiation in salivary gland cells during *Drosophila* development. J. Cell Sci. *102*, 169–184.

Tolar, L.A., and Pallanck, L. (1998). NSF function in neurotransmitter release involves rearrangement of the SNARE complex downstream of synaptic vesicle docking. J. Neurosci. *18*, 10250–10256.

Vaux, D., Tooze, J., and Fuller, S. (1990). Identification by anti-idiotype antibodies of an intracellular membrane protein that recognizes a mammalian endoplasmic reticulum retention signal. Nature *345*, 495–502.

Vincent, J.P. (1998). Compartment boundaries: where, why and how? Int. J. Dev. Biol. *42*, 311–315.

von Kalm, L., Fristrom, D., and Fristrom, J.W. (1995). The making of a fly leg: a model for epithelial morphogenesis. Bioessays *17*, 693–702.

White, K.P., Rifkin, S.A., Hurban, P., and Hogness, D.S. (1999). Microarray analysis of *Drosophila* development during metamorphosis. Science *286*, 2179–2184.

Yoshihisa, T., Barlowe, C., and Scheckman, R. (1993). Requirement for a GTPase activating protein in vesicle budding from the endoplasmic reticulum. Science *259*, 1466–1468.

Developmental Biology 245, 172–186 (2002)
doi:10.1006/dbio.2002.0632, available online at http://www.idealibrary.com on IDEAL®

Ecdysone Triggers the Expression of Golgi Genes in *Drosophila* Imaginal Discs via *Broad-Complex*

Jonathan C. Dunne, Vangelis Kondylis, and Catherine Rabouille[1]

The Wellcome Trust Centre for Cell Biology, ICMB, The Michael Swann Building, University of Edinburgh, Mayfield Road, Edinburgh, EH9 3JR, United Kingdom

One of the most significant morphogenic events in the development of *Drosophila melanogaster* is the elongation of imaginal discs during puparium formation. We have shown that this macroscopic event is accompanied by the formation of Golgi stacks from small Golgi larval clusters of vesicles and tubules that are present prior to the onset of disc elongation. We have shown that the fly steroid hormone 20-hydroxyecdysone triggers both the elongation itself and the formation of Golgi stacks (V. Kondylis, S. E. Goulding, J. C. Dunne, and C. Rabouille, 2001, *Mol. Biol. Cell*, 12, 2308). Using mRNA *in situ* hybridisation, we show here that ecdysone triggers the upregulation of a subset of genes encoding Golgi-related proteins (such as *dnsf1*, *dsec23*, *dsed5*, and *drab1*) and downregulates the expression of others (such as *dergic53*, *dβ'COP*, and *drab6*). We show that the transcription factor Broad-complex, itself an "early" ecdysone target, mediates this regulation. And we show that the ecdysone-independent upregulation of *dnsf1* and *dsnap* prior to the ecdysone peak leads to a precocious formation of large Golgi stacks. The ecdysone-triggered biogenesis of Golgi stacks at the onset of imaginal disc elongation offers the exciting possibility of advancing our understanding of the relationship between gene expression and organelle biogenesis.

Key Words: **Golgi stacks; Golgi proteins; ecdysone; Broad-complex; gene expression; *in situ* hybridisation; FISH; immunofluorescence.**

INTRODUCTION

The Golgi apparatus has a striking morphology. It comprises a series of flattened membrane-bound compartments (cisternae) that are stacked to form the so-called Golgi stack. There are multiple stacks per cell. In mammalian systems, they are connected to each other to form a single copy organelle capping the nucleus. In *Drosophila melanogaster*, the stacks are dispersed throughout the cytoplasm (Kondylis *et al.*, 2001). On each side of the Golgi stack is a membrane network, the Cis Golgi Network (CGN) and the Trans Golgi Network (TGN).

Modulation of Golgi apparatus architecture has to date been shown to be mediated via posttranslational modifications and influenced by the translational status of secretory cargo passing through the organelle. Only recently have developmental cues and processes become a parameter in this modulation.

Protein phosphorylation plays a crucial role in the remodelling of the Golgi apparatus at the onset of mitosis. Several Golgi-associated proteins, such as mammalian GM130 (Golgi matrix 130) and GRASP55 (Golgi reassembly stacking protein 55), are substrates of the phosphorylation cascade catalysed by CDC2 (Lowe *et al.*, 1998) and MEK1 (Colanzi *et al.*, 2000; Jesch *et al.*, 2001), respectively. Phosphorylation of these proteins leads to the extensive fragmentation of the Golgi complex into small clusters of vesicles and tubules (Preisinger and Barr, 2001). Conversely, GM130 dephosphorylation by protein phosphatase 2A is essential in allowing organelle reassembly at telophase (Lowe *et al.*, 2000). Lipid modifications, such as the *N*-myristoylation of mammalian GRASP65, is thought to influence the stacking of Golgi cisternae (Barr *et al.*, 1997). Lipid kinases are also seemingly involved. TGN38 is a target for PIP3 kinase and modulate TGN dynamics (Ponnambalam *et al.*, 1999). Lastly, protein processing and degradation could be other factors as they control, for instance, the number of peroxisomes in yeast (Veenhuis *et al.*, 2000) and the biogenesis of trichocysts in Paramecia (Vayssie *et al.*, 2001).

A fine example of translationally influenced Golgi mor-

[1] To whom correspondence should be addressed. Fax: 44-131-650 7360. E-mail: C.Rabouille@ed.ac.uk.

0012-1606/02 $35.00

phology is observed during larval development in *D. melanogaster*. The salivary gland glue synthesis that commences during mid-third instar larvae (TIL) is accompanied by a marked enlargement of the Golgi stacks (Thomopoulos *et al.*, 1992).

Salivary glue synthesis also provides an example of where development influences Golgi structure (Biyasheva *et al.*, 2001). Other examples are provided by mammalian hormones. For instance, prolactin is known to accelerate the production of breast milk, and the Golgi complex in the mammary gland cells is dramatically enlarged (Rambourg *et al.*, 1993). In both cases, however, the effect of the developmental cues on the enlargement of the Golgi complex is indirect and poorly understood.

Here, we provide evidence for a novel transcriptionally mediated mechanism directly modulating Golgi architecture in a developmentally controlled fashion. We have recently reported that a dramatic change in the morphology of the Golgi apparatus takes place in the cells of the *D. melanogaster* imaginal wing and leg discs at the onset of puparium formation (Kondylis *et al.*, 2001). This is the period during development when the imaginal discs begin their first phase of elongation in order to become the future adult appendages. During mid-TIL, the Golgi apparatus consists of small clusters of vesicles and tubules (called larval clusters), which become larger as the TIL progress towards puparium formation and are converted into typical Golgi stacks in white pupae.

Puparium formation is tightly controlled by the steroid hormone 20-hydroxyecdysone (ecdysone), which triggers all morphogenic events within the developing *Drosophila* larvae, including imaginal disc elongation (Fristrom and Fristrom, 1993). Many studies have focused on the prepupal peak of ecdysone at 6–8 h prior to puparium formation. This peak has been shown to activate the expression of the "early puff genes" via the heterodimeric receptor complex comprising the ecdysone receptor, EcR, and the gene product of *ultraspiracle* (Koelle *et al.*, 1991). At least three of these encode transcription factors, such as Broad complex (DiBello *et al.*, 1991; Andres *et al.*, 1993), E74 (Burtis *et al.*, 1990), and E75 (Segraves and Hogness, 1990). They self attenuate their own transcription and activate the transcription of more than 100 "late puff genes."

In light of the known activity of ecdysone as a gene expression regulator, we investigated and show that a subset of genes encoding Golgi-associated proteins are transcriptionally regulated by this hormone via the Broad-Complex transcription factor. This regulation leads to Golgi stack biogenesis during disc elongation.

MATERIALS AND METHODS

Fly Stocks

Overexpression of dNSF1 and dSNAP. The W1118 and OreR fly stocks were obtained from Andrew Jarman's lab (Edinburgh) and are both referred to as WT.

The HSN stock carries on the first chromosome a transgene comprising dNSF1 cDNA under the control of a heat shock promoter (gift from Leo Pallanck), whereby exposure at 33–37°C drives the expression of *dnsf1*.

UAS SNAP/UAS SNAP (III) is a transgenic fly stock carrying on the third chromosome a dSNAP cDNA transgene downstream of a UAS sequence (gift from Leo Pallanck). Homozygote females were crossed to hsGAL4/Bc, El, Gla to produce a genotype whereby we could drive dSNAP expression using the hsGAL4 driver. Black cell larvae (Bc) were used as control.

WT, HSN, hsGAL4/+; UAS SNAP/+ (hsGAL4 UAS SNAP) mid-TIL maintained at 22 ± 1°C were collected and heat shocked for 40 min at 37°C followed by 1 h at 33°C. The wing imaginal discs were then dissected and fixed as described below. As controls, wing imaginal discs from each fly stock above, maintained at 22°C, were dissected and processed in the same fashion.

The npr homozygote mutant clones. The *npr/npr* mosaic imaginal discs were generated as follows: Virgin female nrp l[3] w FRT18A/FM7; +/+; +/+ (Gift from Kevin Moses) were crossed to male yw/Y; +/+; hsflp, sb/TM6b,Tb. The F_1 virgin female nrp l[3] w FRT18A/+; +/+; hsflp, sb/+ were then crossed to male w[1118] P{w + piMyc} P{w + Ubi-GFP nls} P{ FRT18A}/Y for 24 h. After days 3, 5, and 6, a 20-min 37°C heat shock was given to the larvae to induce the homozygote clones. Late TIL female larvae were dissected and one in four had the desired genotype, nrp l[3] w FRT18A/W[1118] P{w + piMyc} P{w + Ubi-GFP nls} P{ FRT18A}; +/+; hsflp, sb/+.

Alkaline phosphatase RNA *in situ* hybridisation and FISH were performed by using mRNA probes for *dsec23*. The wing imaginal discs were mounted in glycerol in the case of alkaline phosphatase staining and in Vectashield in the case of FISH, and viewed under an Axioskop II epifluorescence microscope equipped with an Axiocam digital camera (Zeiss). Clones were detected by their lack of Ubi-GFP fluorescence (green channel). The *dsec23* expression was estimated within the clones by comparison with the surrounding tissue.

Tissue Preparation

Mid- and late TIL were selected in a way such that the two experimental groups straddled the ~3-h prepupal ecdysone pulse. We used salivary gland morphology as a precise and convenient means of larval staging. Glue synthesis commences during third instar in response to the slow ecdysone titre increase and continues until the prepupal ecdysone pulse (Boyd and Ashburner, 1977; Biyasheva *et al.*, 2001). This is manifest as a gradual swelling of the salivary gland cells, until the surface of the gland becomes enlarged and bumpy. The cell borders become highly visible during this stage. This salivary gland morphology was taken as an indication of mid-TIL (see Results; Fig. 1A). The prepupal ecdysone pulse triggers the rapid expulsion of the glue product into the lumen of the gland, an event that is strictly under the control of ecdysone. This is manifest as a swelling of the entire gland and a concomitant stretching of the gland cells such that they become flattened and smooth. The cell borders become considerably less visible at this stage (see Results; Fig. 1B). White pupae displayed characteristic morphology with a soft white pupal case.

Each larvae or white pupae was transected posterior to the anterior/posterior midline and the anterior portion everted such that the imaginal structures were exposed and visible under a dissecting stereoscope. These larvae are what we term "semidissected." When used for *in situ* hybridisation, the carcasses were immediately fixed in 3.7% formaldehyde in PBT (DEPC treated

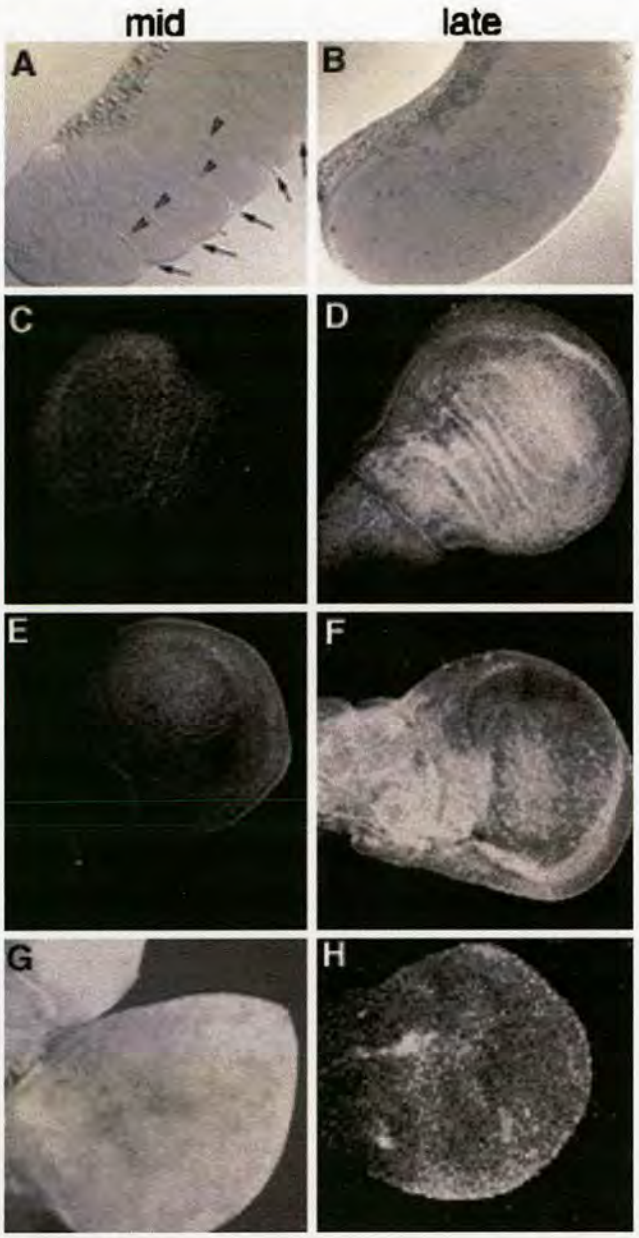

FIG. 1. Expression of Golgi proteins in mid- and late third instar larvae. WT mid- and late TIL were selected by using salivary gland morphology as a precise and convenient means of larval staging. During mid-third instar (A), the salivary gland cells are slightly swollen and as such the gland appears bumpy and the cell borders are clearly visible (arrows). The prepupal ecdysone pulse triggers the rapid expulsion of the glue product into the lumen of the gland. At late third instar, the entire gland becomes swollen and each cell becomes flattened and smooth (B). The cell borders become considerably less visible. WT mid (C, E, G)- and late TIL (D, F, H) were processed for indirect immunofluorescence by using a rabbit anti-dGMII antiserum (C, D), a rabbit anti-human Sec23 antibody (E, F), and a rabbit anti-rat β'COP (G, H) followed by an anti-rabbit IgG coupled to FITC. The wing imaginal discs were dissected, mounted in Vectashield, and observed under a Leica confocal microscope. A section projection encompassing the full disc thickness is displayed.

PBS supplemented by 0.1% Tween) for 1 h on a gently rotating wheel. This was followed by sequential dehydration to 100% EtOH. Tissue was then stored at −20°C until required for *in situ* hybridisation. *In situ* hybridisation for each mRNA probe tested consisted of a single group of tissue from each developmental time point (defined as an experimental group). In three cases, the everted larval carcasses from all three developmental time points were fixed and processed in the same tube so as to check avoidance of processing artifacts (see Results).

Indirect Immunofluorescence

WT mid- and late TIL were semidissected and fixed as described in Kondylis *et al.* (2001) and labelled with either an anti-Sec23 antibody that cross reacts with dSec23 (Kondylis *et al.*, 2001), an anti-dGMII antiserum (Rabouille *et al.*, 1999), or an anti-rat β'COP antibody (gift from Martin Lowe) followed by an anti-rabbit IgG antibody conjugated to FITC. The wing imaginal discs were dissected, mounted in Vectashield containing DAPI, and viewed under a confocal LEICA microscope. A series of optical sections (2-μm thickness) were obtained from mid- and late TIL imaginal discs at 40× by using identical laser settings. The appropriate laser intensity was chosen, using the late TIL so as to avoid optical saturation. A section projection was created, and the resulting image is presented.

In Situ Hybridisation

The templates used to synthesise the mRNA probes are described in Table 2. Each digoxigenin (Dig)-labelled mRNA antisense probe was synthesised with an *in vitro* transcription kit (Roche) using the 3′ digested template (see Table 2), the appropriate T7 or T3 promoter (see Table 2), and a nucleotide mixture including Dig-UTP. The *in situ* hybridisation protocol was as previously described (Goulding *et al.*, 2000). Anti-Dig-alkaline phosphatase Fab fragments (Roche) were used to visualise the Dig-labelled mRNA, and we used NBT (4-nitroblue tetrazolium chloride) and X-phosphate (5-bromo-4-chloro-3-indolyl-phosphate) as substrates. Anti-Dig-peroxidase Fab fragments were also used in the FISH experiments. In this case, we used the Cyanine 3-labelled Tyramide Signal Amplification System (NEN) to visualise the Dig-labelled mRNA. Following *in situ* hybridisation, the wing imaginal discs were dissected free from the carcasses and mounted in 80% glycerol in PBS or Vectashield (containing DAPI) and viewed under a Zeiss Axioskop II (as above) using DIC or fluorescence microscopy.

Disc Culture Assay

For this experiment, mid-TIL were required to be old enough to respond to exogenous ecdysone but not so old as to have been exposed to endogenous ecdysone. These larvae were again selected on the basis of their salivary gland morphology, which exhibited bumpy salivary glands with moderate cell size, slightly larger than the mid-TIL used for the *in vivo* experiments but not too large (for fear of selecting larvae that have been exposed to endogenous ecdysone) but have not yet extruded the glue into the canal there is approximately a 6-h gap between the two events.

They were semidissected and incubated at 22°C for 16 h in a 30-mm plastic culture dish containing 1.4 ml Schneider medium supplemented with 2 μM 20-hydroxyecdysone (Sigma; 5 mM stock in 10% ethanol). As a control, equivalent larvae were incubated in the same conditions in the absence of ecdysone. Upon conclusion of the incubation period, the carcasses were removed from the

culture medium and fixed immediately as above, sequentially dehydrated to 100% EtOH, and stored at −20°C.

Quantitation of Immunofluorescence and in Situ Hybridisation Labelling

An experimental group is defined as tissue of equal developmental age assayed for a given Golgi-related mRNA or protein. All the immunofluorescence and *in situ* hybridisation pictures used for quantitative purposes were captured at the same exposure settings within one experimental group. We used the 20× objective of the upright Zeiss Axioskop II equipped with epifluorescence and DIC and a Zeiss Axiocam digital camera. Images were transferred to Adobe Photoshop 5.5 and converted to black and white.

The labelling intensity was quantitated by using NIH Image Version 1.62 (publicly available at http://rsb.info.nih.gov/nih-image/). Approximately 20 boxes of various sizes were used to estimate the mean labelling intensity within at least 8 images per experimental group. In some cases, staining was more intense in specific areas of the wing imaginal disc, and as such an estimation of the labelling was performed for the specific region.

We also estimated the difference in labelling intensity by using FISH experiments. We achieved this by artificially matching labelling intensities through manipulation of camera exposure times. For each mRNA probe, we chose the sample that displayed the lower labelling intensity. We then set and recorded the exposure time required to obtain an image that is within the dynamic range of the camera. We then repeated the same procedure with the other samples such that the images displayed equivalent labelling intensities. The exposure time was also recorded. The ratio of the two exposure times provided an estimation of the ratio of labelling intensity. This technique gave very similar results to those obtained with the NIH Image software. When possible, the results from both techniques were combined and are expressed ± SD.

The quantitation of EM pictures was performed according to Kondylis *et al.* (2001).

RESULTS

Expression of Golgi Proteins in Mid- and Late Third Larval Instar

In the wing and leg imaginal discs of *D. melanogaster*, Golgi stack biogenesis takes place towards the onset of puparium formation and is dependent on the steroid hormone ecdysone (Kondylis *et al.*, 2001).

We reasoned that Golgi stack formation is not observed earlier (i.e., during mid-TIL) because the expression level of proteins necessary for building the Golgi apparatus is below a functional threshold. It is plausible to expect that the expression level of these proteins must reach this threshold before cisternae could be built and Golgi stacks assembled. Given the known activity of ecdysone as a gene expression regulator, we made the hypothesis that it triggers the expression of genes involved in this assembly.

We first set out to investigate whether ecdysone triggered the increased expression of Golgi-associated proteins. Mid- and late TIL and white pupae discs were labelled with specific antibodies to proteins of interest. Mid- and late TIL were selected in such a way that the two experimental groups straddled the ~3-h prepupal ecdysone pulse. We used salivary gland morphology as a precise and convenient means of larval staging (see Materials and Methods; Figs. 1A and 1B). White pupae displayed characteristic morphology with a soft white pupal case.

It was critically important to ensure that the above larval selection criterion was suitable for larval staging. Thus, we established the percentage homogeneity of each experimental group (Table 1). An experimental group was defined as tissue of equal developmental age assayed for a given Golgi-related protein or mRNA. Homogeneity was achieved when ≥75% of the discs displayed the same level of labelling intensity, which was the case for 44 of 52 experimental groups.

We first tested the protein expression of *Drosophila* Golgi mannosidase II (dGMII) and dSec23 (Table 2) in the imaginal discs of the different larval stages. There was a significant increase in labelling intensity between the mid- and late TIL wing imaginal discs (Figs. 1C–1F) that was estimated at 4.5 ± 1.0 fold in both cases. This result correlates nicely with that from our Western blots for dSec23 (Kondylis *et al.*, 2001), though changes in labelling intensity were not always uniform within individual wing imaginal discs.

The protein expression of dp115 and dGM130 (Kondylis *et al.*, 2001) was elevated 2.5- and 2.8-fold, respectively (not shown), between mid- and late TIL. This quantitation is somewhat tenuous in that only 65% homogeneity could be achieved for each experimental group using either anti-sera. The protein expression of dβ'COP (a COPI subunit; Table 2) was examined by using a rabbit polyclonal antibody raised against the rat protein (80% homology) and was found to be downregulated 4- to 5-fold from mid- to late TIL (Figs. 1G and 1H).

All proteins that display an increase in protein expression level between mid- and late TIL were observed to be correctly localised to the Golgi apparatus (not shown) as observed previously (Kondylis *et al.*, 2001).

Expression of mRNA Encoding Golgi-Associated Proteins in Mid- and Late Third Larval Instar

We investigated whether the expression dynamics of Golgi-related proteins were mimicked by changes at the transcriptional level. Using RNA *in situ* hybridisation coupled with alkaline phosphatase and/or FISH, we first assessed the expression dynamics of *dsec23* (see Figs. 4A and 4B) in WT mid- and late TIL and white pupae. Using the quantitative methods described in Materials and Methods and given the homogeneity of each group (Table 1), we found that *dsec23* expression increased 4.0 ± 0.6-fold between mid- and late TIL (see Fig. 3).

Encouraged by this result, we raised RNA probes to a host of other genes encoding Golgi proteins ("Golgi genes," a total of 15; Table 2). These are *Drosophila* homologues of mammalian genes whose products have been implicated in Golgi function and Golgi biogenesis (Table 2). Three expression patterns became apparent (see Fig. 3).

TABLE 1
Estimation of the Homogeneity of Labelling

	Immunofluorescence		Alkaline phosphatase *in situ* hybridisation		
Genes/gene products	Mid-TIL discs	Late TIL discs	Mid-TIL discs	Late TIL discs	White pupae discs
dGMII	78.1 ± 1.1	75.8 ± 0.8			
dnsf1			80.0 ± 0.0	85.0 ± 1.0	91.5 ± 8.5
dSec23/*dsec23*	90.0 ± 5.0	84.0 ± 4.5	100 ± 0.0	100 ± 0.0	93.7 ± 6.2
dsed5			97.2 ± 2.7	100 ± 0.0	96.6 ± 3.3
drab1			93.5 ± 6.5	76.0 ± 1	100 ± 0
dsnap			90.0 ± 1.0	84.0 ± 1	84.5 ± 1.5
dsar1			94.0 ± 2.0	85.0 ± 4.0	100 ± 0.0
dgos28			78.0 ± 5.0	83.0 ± 2.0	100 ± 0.0
dGM130/*dgm130*	65.2 ± 4.1	67.8 ± 3.0	92	80	66
dp115/*dp115*	66.0 ± 8.5	64.0 ± 7.9	71.2 ± 21.2	100 ± 0.0	95.0 ± 5.0
ter94			78.5 ± 11.5	86.65 ± 13.5	62.5 ± 12.5
dp47			87.5 ± 12.5	100 ± 0.0	66.0 ± 20.0
dergic53			75	81.25	100
drab6			80.0 ± 5.0	95.0 ± 5.0	74.5 ± 8.5
dβ'COP/*dβ'cop*	75.0 ± 6.0	60.0 ± 10.0	85	79	100

Note. Results are expressed as the percentage of imaginal discs that are of the same labelling intensity within one group (mid- or late TIL or white pupae) labelled for one mRNA probe. "100%" represents a result where all discs exhibit the same labelling intensity. No indication is made here as the to absolute level of staining intensity. "80%" represents a result where 80% of the discs are of the same labelling intensity and 20% are either above or below this intensity. 75% is deemed the lower limit for homogeneity of any one group.

The first is that exhibited by *dgos28* (Figs. 2A and 2B), *dsec23* (see Figs. 4A and 4B), *dnsf1* (see Figs. 6A and 6B), *dsnap* (see Figs. 6E and 6F), *dsed5*, *drab1*, and *dsar1*. These mRNA probes indicate a very low expression level within mid-TIL imaginal wing discs, and a 3.5- to 4-fold higher level within those of late TIL (Fig. 3). The results obtained for *dsec23* correlate nicely with those observed at the protein level by immunofluorescence (Figs. 1E and 1F) and Western blot (Kondylis *et al.*, 2001). The strong expression increase was most apparent within the leading edge, distal portion, and intermediate folds of the wing discs, which are the areas that mostly contribute to the first phase of disc elongation (Cohen, 1993). The mRNA expression within white pupal wing discs was found to be equal to (*dgos28*, *dsec23*, *dnsf1*, *dsnap*, *dsed5*, and *drab1*) or more intense than (*dsar1*) expression in late TIL discs. We also tested the expression of *dnsf2*, encoding the second *Drosophila* homologue of mammalian NSF (Pallanck *et al.*, 1995) in imaginal discs. We could not detect any labelling in this tissue, whereas muscles of late embryos were very positively labelled (not shown).

The second expression pattern is characterised by *dgm130* (Figs. 2C and 2D), *dp115*, *ter94*, and *dp47*. This group of genes exhibited an mRNA expression increase between 1.5- and 2-fold (Fig. 3). The mRNA expression in white pupae wing discs for 3 out of 4 groups tested was mixed. Some discs exhibited as strong a labelling intensity as in late TIL while others were clearly not, and as a consequence, homogeneity within white pupae wing discs for these probes was reduced (Table 1).

The third expression pattern is that exhibited by *dergic53* (Figs. 2E and 2F), *dβ'cop*, and *drab6*. These mRNA are downregulated by ~4-fold between mid- and late TIL (Fig. 3). This expression pattern is in stark contrast to that of the first group described above. Interestingly, mRNA expression levels increased between late TIL and white pupae for all three genes tested.

The expression dynamics of this last group of mRNA indicate that transcriptional upregulation between mid- and late TIL is not a general feature of Golgi genes in the imaginal wing discs of *D. melanogaster*.

The possibility that these observations are a result of discrepancies in the *in situ* hybridisation protocol was addressed by combining samples of all three developmental time points, processing as one, and restaging them using salivary glands morphology prior to visualisation. Three mRNA were tested in this manner (*drab1*, *drab6*, and *dp115*), and in all cases, the expression dynamics were identical to previous results.

The possibility that the results observed here are a result of ubiquitous and thus nonspecific mRNA expression dynamics is negated by the observation that in all but one instance (*dnsf1*) the larval brain does not mimic the expression dynamics seen in imaginal wing discs (data not shown). This is also the case in larval salivary glands for all but two of the mRNA tested (*dgm130* and *dsec23*).

The Role of Ecdysone

The temporal dynamics of Golgi gene expression suggested to us a possible involvement of the ecdysone in the transcriptional regulation of these genes. To address this

TABLE 2
Reagents Used for the *in Situ* Hybridisation Experiments

Genes	EST[a]/cDNA	Vector	Antisense Dig-labelled probe	Gene products	References
dβ'cop (CG6699/P35606)	LD 07733	pBS	*Kpn*I/T7	dβ'COP: Putative subunit of the COPI coat	Gad fly/Fly base
dergic53 (CG6822/*rhea*)	GH 16748	pOT2	*Xho*I/T7	dERGIC53: Putative mannose binding protein cycling between the ER and the cis Golgi cisternae	Gad fly/Fly base; Prout *et al.* (1997)
dgm130 (CG11061)	LD 07754	pBS	*Eco*RI/T7	dGM130: Putative tethering protein	Gad fly/Fly base; Kondylis *et al.* (2001)
dgos28 (CG7700)	RE 64493	PFlc1	*Xho*I/T3	dGos28: Putative Golgi v-SNARE	Gad fly/Fly base
dnsf1 (CG1618/comt)	clone dN20	pBS	*Xba*I/T7	dNSF1: Fusion ATPase	Ordway *et al.* (1994); Kondylis *et al.* (2001)
dnsf2 (CG9931)	clone dN2.14	pBS	*Xba*I/T3	dNSF2: Fusion ATPase	Pallanck *et al.* (1995)
dp115 (CG1422)	clone 1.P2	PBK-CMV	*Sal*I/T7	dp115: Putative tethering protein	Kondylis *et al.* (2001)
dp47 (CG11139)	GH 01724	pOT2	*Xho*I/T7	dp47: Putative cofactor for TER94	Gad fly/Fly base
drab1 (CG3320)	LD 14676	pBS	*Sma*I/T7	dRab1: Small GTPase Rab1 involved in ER to Golgi transport	Gad fly/Fly base; Satoh *et al.* (1997)
drab6 (CG6601)	GH 09086	pOT2	*Xho*I/T7	dRab6: Putative small GTPase Rab6 involved in intra-Golgi transport	Gad fly/Fly base
dsar1 (CG7073)	GH 06356	pOT2	*Xho*I/T7	dSar1: Putative GTPase involved in the formation of the COPII complex	Gad fly/Fly base
dsec23 (CG1250)	GH 23373	pOT2	*Xho*I/T7	dSec23: Putative Sar1-specific GTPase activating protein part of COPII machinery	Gad fly/Fly base; Kondylis *et al.* (2001)
dsed5 (CG4214)	clone SD1	subcloned in pBS	*Eco*RI/T7	dSed5: Golgi t-SNARE	Banfield *et al.* (1994)
dsnap (CG7809)	LP 04493	pOT2	*Xho*I/T7	dSNAP: Cofactor of dNSF1	Gad fly/Fly base; Ordway *et al.* (1994)
ter94 (CG2331)	clone Ab14	pBK CMV	*Bam*HI/T7	TER94: Homologue of p97, a fusion ATPase	Pinter *et al.* (1998); Leon and McKearin (1999)

Note. The references for the inferred function are in Klumperman (2000); Rabouille and Warren (1997); Pfeffer (1999); Roche and Monsigny (2001); Dunne and Rabouille (2001). See also Discussion.

[a] All the EST were from Research Genetics.

possibility, we turned to a disc culture assay (Kondylis *et al.*, 2001) in which semidissected mid-TIL are incubated *in vitro* in the presence or absence of exogenously applied ecdysone. An important aspect of this culture assay was the requirement of the TIL imaginal discs to be responsive, yet not endogenously exposed, to ecdysone. We again used salivary gland morphology to select suitable larvae and selected mid-TIL larvae that exhibited moderate but not extreme salivary gland cell swelling (see Materials and Methods). These larvae were semidissected and incubated in Schneider medium between 9 and 16 h in the presence or absence of 2 μM 20-hydroxyecdysone.

Using RNA *in situ* hybridisation, we assessed the mRNA expression of *dsec23* as a representative of the first expression group as described above. *In vitro* incubation up to 9 h elicited no significant increase in *dsec23* mRNA expres-

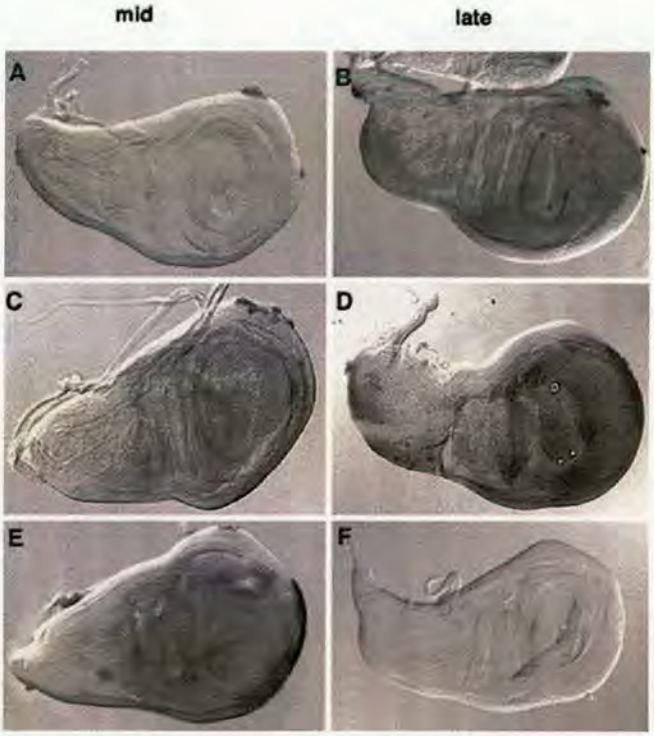

FIG. 2. mRNA expression in WT mid- and late third instar larvae. WT mid- and late TIL were selected according to salivary gland morphology, semidissected, and processed for RNA *in situ* hybridisation by using digoxigenin (DIG)-labelled mRNA probes for *dgos28* (A, B), *dgm130* (C, D), and *dergic53* (E, F). Wing imaginal discs were dissected, mounted, and viewed under a Zeiss Axioskop II microscope equipped with DIC using the 20× objective. Pictures were captured by using the Axiocam digital camera at equal settings for mid- and late TIL discs labelled for the same probe. Note the clear difference in staining intensity between mid- and late TIL for two of the three mRNA probes.

sion. A 12-h incubation led to a small but insignificant increase, and after 16 h, the increase in labeling intensity was equivalent to that observed *in vivo* (5.2-fold) (Figs. 4C and 4D). This mRNA expression increase was accompanied by a change in the disc morphology that was not observed *in vivo*. In view of the fact that the prepupal ecdysone pulse is ~2–3 h in duration, we mimicked this pulse by incubating the semidissected mid-TIL in the presence or absence of ecdysone for 3 h followed by 16 h of ecdysone-free incubation. This protocol elicited equivalent *dsec23* mRNA expression increase and wing disc morphological changes as continuous ecdysone exposure (data not shown).

The disc culture assay did not completely mimic the *in vivo* situation and we therefore investigated the involvement of Juvenile hormone (JH), the other hormone present *in vivo* in TIL (Riddiford, 1996). Using the disc culture assay in the presence of exogenous JH for 16 h, we verified that JH played no role in the increased expression of *dsec23* (not shown).

Broad Complex

The response duration of the ecdysone induced *dsec23* mRNA expression increase *in vitro* was suggestive of an intermediate factor that mediates the ecdysone signal. Ecdysone is known to bind to its nuclear heterodimer receptor (Koelle *et al.*, 1991) and induce the transcriptional activation of a set of genes known as "early genes" (Ashburner, 1990; Thummel, 1990), most them being transcription modulators themselves. *Broad Complex* (*Br-C*) is among these early genes (Kiss *et al.*, 1988), has a number of known tissue-specific isoforms (containing one to four Zinc finger domains; DiBello *et al.*, 1991), and has been shown to mediate ecdysone-regulated gene expression (Karim *et al.*, 1993; Fletcher and Thummel, 1995).

We first used a hypomorphic viable allele of *Br-C* called *br-1*. We semidissected *br-1* homozygote mid- and late TIL and processed them for RNA *in situ* hybridisation by using a *dsec23* mRNA probe. *dsec23* mRNA expression was considerably reduced when compared with WT larvae of equivalent developmental status. More importantly, no increase in *dsec23* mRNA expression was observed between *br-1* mid- and late TIL (Figs. 4E and 4F). This result is in stark contrast to that obtained using WT larvae (Figs. 4A and 4B), where an ~4-fold increase was observed. Similar results were obtained with *drab1* mRNA expression (not shown).

We next utilised the *npr* (*non pupariating*) mutant, that lacks all the isoforms of Br-C (Brennan *et al.*, 2001). *npr* is homozygous lethal. Thus, we generated mosaic imaginal discs using the FRT/Flp technology (Dang and Perrimon, 1992; see Materials and Methods). The majority of the disc cells are heterozygous mutant for npr (*npr*/ubi-GFP) and are thus marked by the expression of ubi-GFP. Within these discs were clonal clusters of cells (marked by DAPI staining; Fig. 5E) that were homozygous mutant for *npr* where the ubi-GFP is absent (Figs. 5A and 5C). Alkaline phosphatase RNA *in situ* hybridisation and FISH were performed on these discs by using an mRNA probe for *dsec23* (Figs. 5B and 5D). The mRNA labelling of *dsec23* was significantly reduced in the *npr* homozygous clones by using both visualisation techniques, indicating that the increased expression of *dsec23* observed in late TIL is mediated by *Broad complex*.

dNSF1 and dSNAP

The ~4-fold mRNA expression increase for *dnsf1*, *dsnap*, and others of the "first expression pattern" (Fig. 3) is in good temporal correlation with the formation of Golgi stacks *in vivo* (Kondylis *et al.*, 2001). The larval clusters that are present in mid-TIL begin enlarging during late third instar; cisternae become visible and Golgi stacks are only observed in white pupae discs.

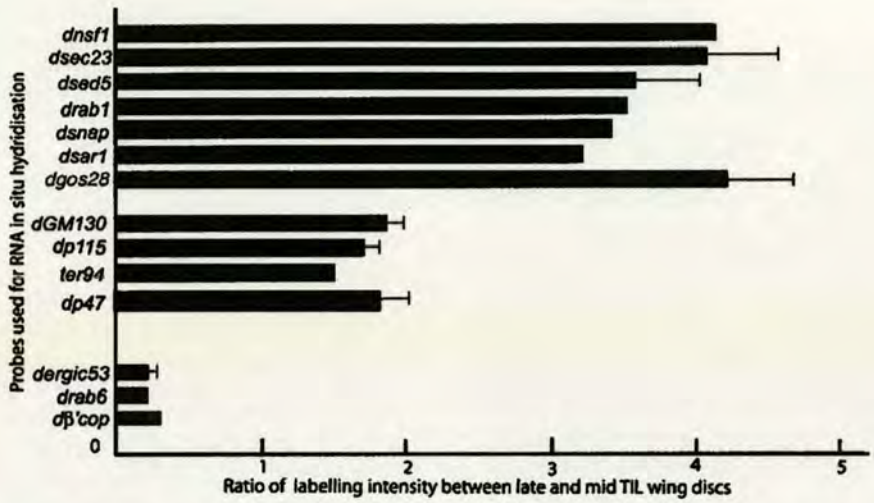

FIG. 3. mRNA expression dynamics in the wing imaginal discs of developing WT TIL. Wing imaginal disc labelling intensity was quantitated as described in Materials and Methods. Results are expressed ± SD. A ratio of 1 indicates no change in labelling intensity between mid- and late TIL. A ratio greater than 1 indicates an increased expression from mid- to late TIL. A ratio less than 1 indicates an expression decrease from mid- to late TIL.

Our mRNA expression dynamics observations support the possibility that the Golgi morphology observed at the onset of puparium formation is not observed earlier (i.e., during mid-TIL) because the expression level of proteins necessary for building the Golgi apparatus is below a functional threshold. It is plausible to expect that the expression level of these proteins must reach this threshold, via ecdysone-induced upregulation, before cisternae could be built and Golgi stacks assembled.

We tested this hypothesis by investigating whether the experimental upregulation of Golgi proteins could trigger Golgi stack biogenesis independently of ecdysone.

We first used a transgenic fly that carries a transgene comprising dNSF1 cDNA under the control of a heat shock promoter, HSN (gift from Leo Pallanck; Ordway *et al.*, 1994). We heat shocked WT and HSN mid-TIL and assessed the level of *dnsf1* mRNA expression using FISH. *dnsf1* expression was 7-fold increased in HSN over WT (compare Figs. 6C and 6D). *dnsf1* expression was 2-fold increased in heat shocked HSN vs HSN late TIL maintained at 21°C (compare Figs. 6B and 6D). The heat shock also led to a 1.3-fold increase in the *dnsf1* expression in WT mid-TIL (compare Figs. 6A and 6C).

As a control, we monitored the expression of *dsec23* mRNA. Heat shock treatment of WT and HSN mid-TIL elicited a 1.8-fold increase in *dsec23* expression compared with the same larvae maintained at 21°C (vs 1.3 for *dnsf1*), but there was no difference between WT and HSN. This contrasted markedly to the 7-fold increase observed for *dnsf1*.

A similar experiment was performed by using a transgenic fly stock carrying the cDNA of dSNAP under the control of UAS (gift from Leo Pallanck; Ordway *et al.*, 1994). This stock was crossed to hsGAL4 (see Materials and Methods). We heat shocked the WT and hsGAL4 UAS-SNAP mid-TIL and assessed the level of *dsnap* mRNA expression using FISH. *dsnap* expression was 5-fold increased in hsGAL4 UAS-SNAP vs WT (compare Figs. 6G and 6H). *dsnap* expression was 1.25-fold increased in heat shocked vs non heatshocked late TIL hsGAL4 UAS-SNAP (compare Figs. 6F and 6H). The heat shock also led to a 1.4-fold increase in the *dsnap* expression in WT mid-TIL (compare Figs. 6E and 6G).

We then observed the morphology of the Golgi area in the WT, HSN, UAS SNAP, and hsGAL4 UAS SNAP mid-TIL discs subjected to temperature treatment. Nontreated WT mid-TIL were used as control. The Golgi area in WT mid-TIL disc cells comprised clusters of vesicles and tubules with only about 10% of membrane in cisternae (Fig. 7A; Table 3), none of them stacked. After exposure to the temperature treatment, the percentage of Golgi membrane in cisternae increased to 30.3% (Fig. 7B; Table 3). A similar percentage was achieved in the noninduced UAS SNAP larvae (34.3%; Table 3). The percentage of stacked cisternae was 30 and 29%, respectively (Table 3).

When HSN mid-TIL were subjected to the temperature treatment, the Golgi area comprised 56.3% of membrane in cisternae, 70% of them stacked (Fig. 7C; Table 3). Similar results was obtained with the hsGAL4-induced UAS SNAP larvae (Fig. 7D). The percentage of membrane in cisternae reached 55.5%, 68% of them in stacks (Table 3). These latter figures are very similar to those obtained in the white pupae *in vivo* (Kondylis *et al.*, 2001). Furthermore, the volume density of Golgi membrane in the overexpressing discs after temperature treatment was increased by 2.7 ± 0.4 times when compared with the WT under the same conditions. This was not

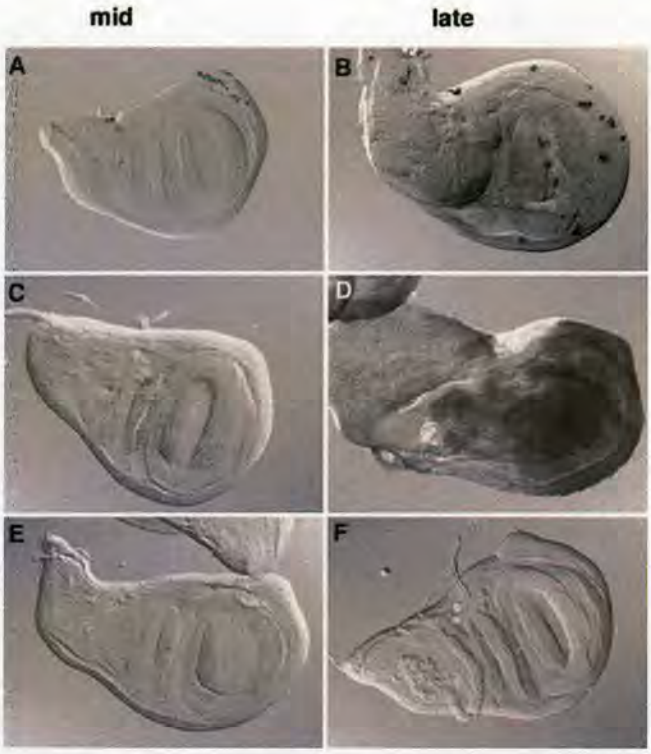

FIG. 4. The role of ecdysone and *Broad-Complex* in *dsec23* mRNA expression regulation. *In vivo dsec23* mRNA expression in WT mid (A)- and late TIL (B) was assayed as described in the legend for Fig. 2. WT mid-TIL were semidissected and incubated at 22°C for 16 h in a 30-mm culture dish containing 1.4 ml of Schneider medium supplemented with (C), or free of (D), 2 μM ecdysone. *In situ* hybridisation was performed on the incubated larvae by using a *dsec23* mRNA probe. Broad-Complex homozygous mutant *br1* mid (E)- and late TIL (F) were selected and processed for *in situ* hybridisation by using a *dsec23* mRNA probe. Note the significant *dsec23* mRNA expression increase in the presence vs absence of ecdysone. Also note the abolishment of *dsec23* mRNA increase between mid- and late TIL in the *br-1* homozygous mutant.

due to a change in the density of the Golgi membrane, but to an increase in the total membrane present.

This 2.7-fold increase, together with the doubling in the percentage of membrane in total and stacked cisternae, shows that Golgi biogenesis can be driven by increasing the expression of dNSF1 and dSNAP. This may also be the case for other Golgi genes of the "first expression pattern." Since the expression level of these is under the control of ecdysone, this suggests that ecdysone provides a developmental timing mechanism so that Golgi stack biogenesis takes place during, and not prior to, puparium formation.

DISCUSSION

Here, we show that transcriptional regulation of a number of *Drosophila* Golgi genes directly controls Golgi apparatus architecture. We believe this provides evidence of a novel mechanism of developmentally controlled organelle biogenesis, mediated by ecdysone and the transcription factor Broad-Complex.

Developmental Implications

We show that Golgi genes are subjected to developmental control by ecdysone, adding to the long list of known ecdysone targets (White *et al.*, 1999). Ecdysone activates the transcription of early puffs genes (see Introduction; and Riddiford, 1993), such as Broad complex (DiBello *et al.*, 1991; Andres *et al.*, 1993), E74 (Burtis *et al.*, 1990), and E75 (Segraves and Hogness, 1990), which in turn activate the transcription of more than 100 "late puff genes."

A recent microarray analysis (White *et al.*, 1999) examined the expression pattern of 4500 *Drosophila* genes in the third larval instar and pupae. The expression of approximately 12% of these was modulated by ecdysone and approximately 6% were upregulated (170 out of 4500). Ecdysone-responsive genes were grouped into clusters according to their pattern of regulation. Among these are genes that we also have identified, such as *dsec23* (cluster 28) and *ter94* (cluster 29). We found *dpdi* to have a constant expression within the time frame of our experiment, and that was confirmed by the microarray analysis (cluster 26). *dβ'cop* was found in cluster 27 of genes whose mRNA expression is reduced at the onset of pupation, supporting our results. Interestingly, their study also revealed that *clathrin* (cluster 0) is strongly upregulated, suggesting an increased endosomal activity. This raises the possibility that ecdysone also controls the biogenesis of the endocytic pathway in addition to Golgi stack biogenesis.

We have shown that ecdysone triggers its transcriptional activity through *Broad-complex*, itself a well-known ecdysone target (Karim *et al.*, 1993; Fletcher and Thummel, 1995). *Br-C* encodes a family of transcription factors differing in their zinc finger motif (Z1 to Z4) (DiBello *et al.*, 1991). We have utilised a BR-C null mutant *npr* lacking all four Br-C isoforms, to show that the *dsec23* mRNA expression increase observed between WT mid- and late TIL is dependent on the activity of at least one of the four Br-C isoforms. A switch from the Z1 to Z2 isoform has been implicated in the progression of the morphogenetic furrow in *Drosophila* eye imaginal discs (Brennan *et al.*, 2001). Further experiments will be needed to clarify the activity of one or more isoforms in the increased expression of Golgi genes.

We cannot exclude the possibility that Br-C does not directly regulate the expression of Golgi genes but rather induces the synthesis of another transcription factor(s), such as the *crooked leg* gene product (D'avino and Thummel, 1998). This issue will need to be investigated further.

There is one other example of developmentally associated Golgi remodelling, though the regulation of this event is not known. The expression of alpha-mannosidase II and TGN 38 (two Golgi resident proteins) has been shown to be

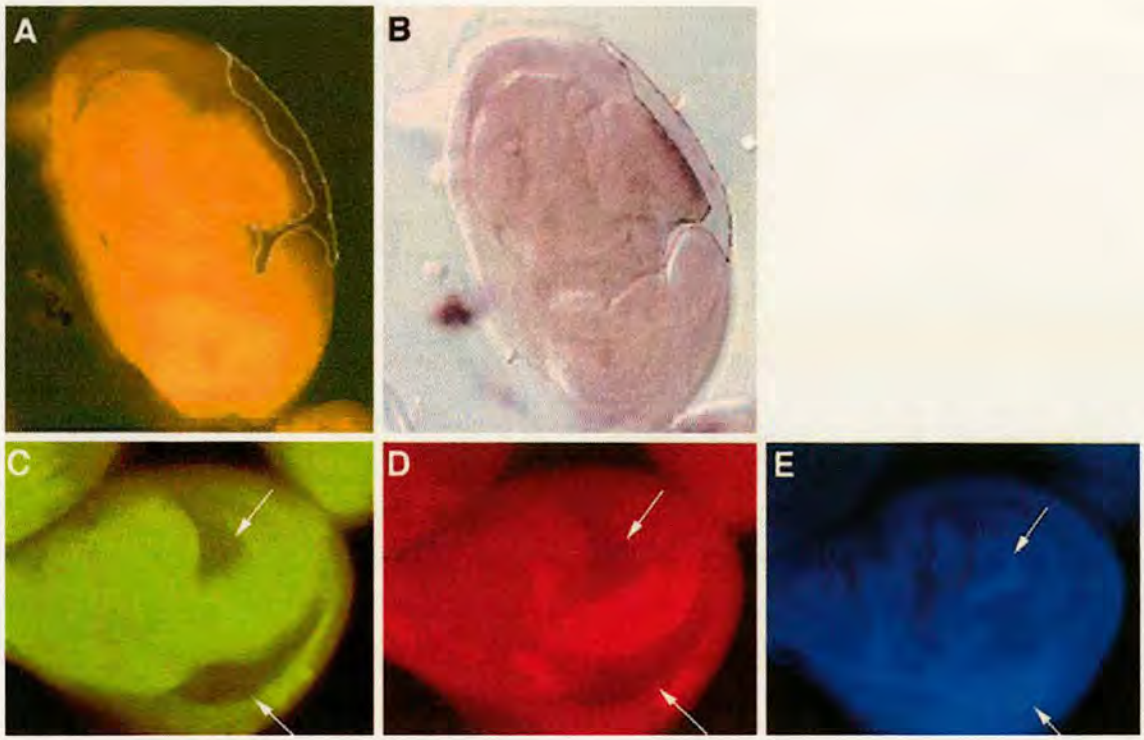

FIG. 5. Broad-Complex is the transcription factor mediating ecdysone-induced mRNA expression. Broad Complex (*npr*) homozygote mutant clones were induced as described in Materials and Methods. The *npr/npr* clones were marked by the absence of ubi-GFP marker (A, C) (white arrows, and doted line in A). *dsec23* mRNA expression was assessed by using alkaline phosphatase (B) and FISH (D). DAPI staining (E) was used to assess the viability of the homozygous mutant clonal tissue. Note that the clone borders are slightly different. This is due to differences in the visualisation techniques (epifluorescence picture, A) encompassing the full thickness of the disc and the clone, and DIC (B) creating an optical section. Note the absence of *dsec23* mRNA expression within the homozygote mutant clones.

regulated during vertebrate myogenesis. Both proteins were present in the embryonic myotubes but absent in the innervated muscle fibre (Antony *et al.*, 1995), during which time the Golgi apparatus is remodelled and relocated under the neuromuscular junction (Jasmin *et al.*, 1989). This and our results suggest that Golgi proteins could have a role in development.

There is mounting evidence that this is the case (reviewed in Dunne and Rabouille, 2001). In addition, genes encoding members of the p24 family (resident of the ER-Golgi intermediate compartment) have recently been shown to be genetic interactors of Dpp (Decapentaplegic), encoding a secreted protein that is crucial for proper *Drosophila* embryonic development (Bartoszewki *et al.*, 2001). The formation of the embryonic muscles and myoepidermal junction in *Drosophila* embryos has been shown to be significantly impaired in *rhea* mutants due to the strong genetic interactions between dERGIC53 (a mannose-binding protein resident of the *ER* to *G*olgi *I*ntermediate *C*ompartment) and PS integrins (Prout *et al.*, 1997). Further, the knockout of the mouse alpha-mannosidase II (a Golgi resident enzyme) results in dyserythropoietic anaemia (Chui *et al.*, 1997).

Taken together, our results strengthen the argument that Golgi gene expression is developmentally controlled and that Golgi stack formation at puparium formation could be implicated in development.

How Does Golgi Gene Expression Drive Golgi Stack Biogenesis?

At the onset of disc elongation, small larval Golgi clusters comprising vesicles and tubules grow in size to finally be converted to Golgi stacks in white pupae.

During this period, *dsar1*, *dsec23*, *drab1*, *dnsf1*, *dsnap*, *dsed5*, and *dgos28* genes and dSec23 protein were shown to be upregulated by ecdysone. To us, these results suggest a possible model involving the activation of three pathways leading to the formation of large Golgi stacks from small larval clusters: a COPII vesicle budding pathway (dSec23/dSar1) leading to increased ER-derived membrane (Barlowe *et al.*, 1994); a docking mechanism involving dRab1 (Allan *et al.*, 2000; Moyer *et al.*, 2001) leading to increased vesicle tethering prior to fusion; and a fusion pathway (dNSF1 and dSNAP, dSed5 and dGos28) mediating fusion of vesicles and tubules to form Golgi cisternae.

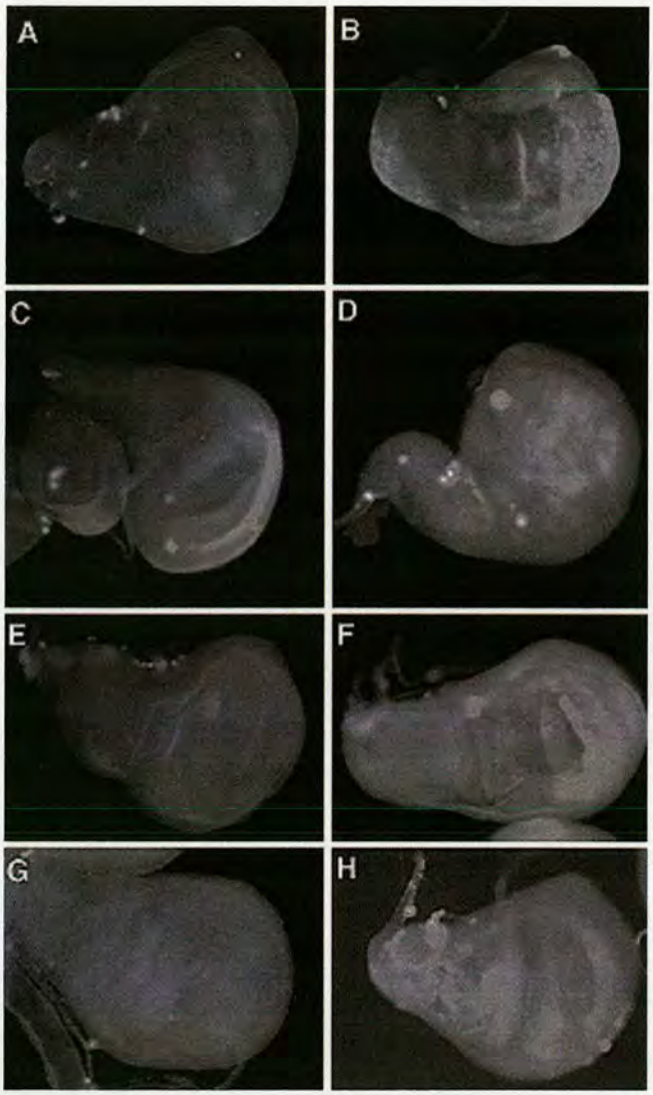

FIG. 6. Expression of *dnsf1* and *dsnap* in TIL and in transgenic flies. WT mid (A, E)- and late (B, F) TIL were semidissected and processed for FISH by using an mRNA probe for *dnsf1* (A, B) and *dsnap* (E, F). WT (C, G), HSN (D), and hsGAL4/+; UAS SNAP/+ (H) mid-TIL were heat shocked at 37°C for 40 min followed by 1 h at 33°C and processed for FISH by using a mRNA probe for *dnsf1* (C, D) and *dsnap* (G, H). Imaginal wing discs were viewed under an upright epifluorescence microscope AxioskopII by using the 20× objective. Note that the images in (B), (D), (F), and (H) were taken at 250-ms exposure time, whereas the photographs in (A), (C), (E), and (G) were taken at 800 ms.

We have shown previously that larval clusters grow in size between mid- and late TIL (their surface density increases ~3-fold; Kondylis *et al.*, 2001), and we have shown that ~60% of the larval clusters in the TIL are populated with COPII-derived vesicles. These findings could be explained by our present results. *dsec23* and *dsar1* are transcriptionally activated between mid- and late TIL (and dSec23 protein is being synthesised). This activation could be expected to activate the COPII budding pathway leading to more vesicles generated at ER exit sites. Interestingly, concomitant to the COPII budding mechanism being stimulated, observations of mRNA and protein expression dynamics of dβ'COP suggest that the COPI budding mechanism is downregulated from mid- to late TIL. Together, these results suggest that, during late TIL, the COPII budding mechanism dominates over the COPI. Con-

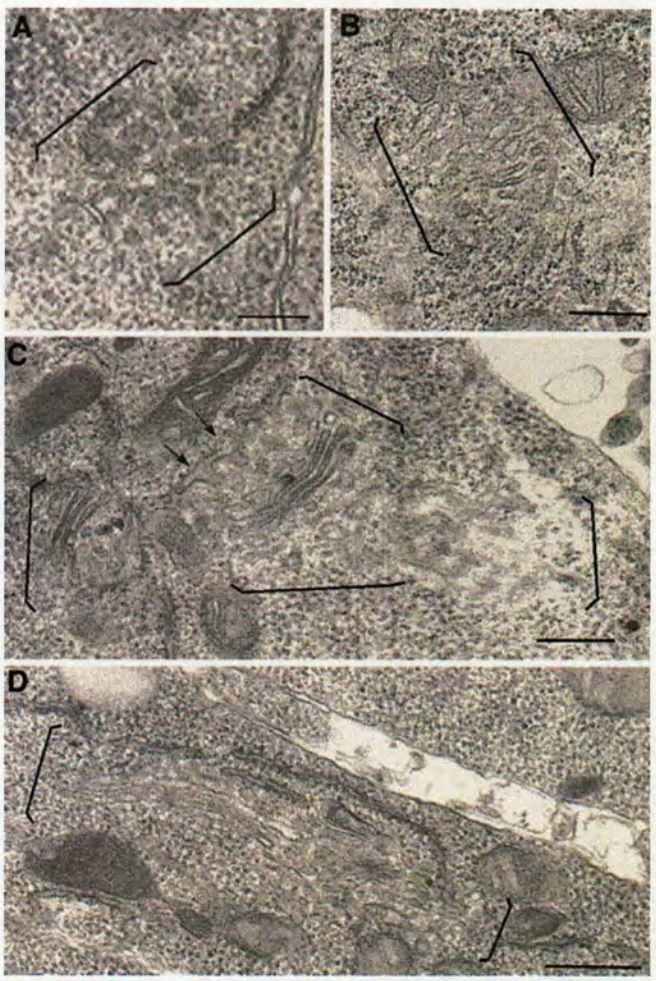

FIG. 7. Effect of dNSF1 and dSNAP overexpression on Golgi stack morphology. WT (A) mid-TIL were maintained at 21°C. WT (B), HSN (C), and hsGAL4/+; UAS-SNAP/+ (D) mid-TIL were heat shocked as described in the legend for Fig. 6. Wing and leg imaginal discs were immediately dissected, fixed, and processed for conventional electron microscopy as described in Kondylis *et al.* (2001). The Golgi area is marked between brackets. The arrow in (C) points to budding profiles from the surrounding ER cisternae. Note the considerable difference in the Golgi stack formation between the WT, HSN, and hsGAL4/+; UAS SNAP/+ cells after temperature treatment. Bars, 200 nm.

TABLE 3
Effect of dNSF1 and dSNAP Overexpression on the Formation of Golgi Stacks

	Percentage of total Golgi membranes in:			
	Total cisternae (%)	Tubules (%)	Vesicles (%)	Stacked/nonstacked
WT mid-TIL at 21°C for 1 h 40 min	10.0 ± 6.0	48.0 ± 17.5	38.0 ± 16.4	nd
WT mid-TIL after temperature treatment[a]	30.3 ± 8.2	42.1 ± 5.7	35.5 ± 4.9	0.30 ± 0.05
HSN mid-TIL after temperature treatment[a]	56.3 ± 10.1	23.4 ± 8.7	23.6 ± 7.7	0.70 ± 0.15
Noninduced UAS SNAP mid-TIL after temperature treatment[a]	34.3 ± 3.3	45.8 ± 5.6	19.8 ± 5.0	0.29 ± 0.06
hsGAL-induced UAS SNAP mid-TIL after temperature treatment[a]	55.5 ± 9.2	30.1 ± 5.3	14.4 ± 3.5	0.68 ± 0.13

Note. The percentage of membrane in each category has been estimated as described in Materials and Methods and Kondylis *et al.* (2001).
[a] The temperature treatment consists of exposing the larvae to 37°C for 40 min followed by 1 h at 33°C.

versely, the dβ'COP downregulation suggests that the COPI budding mechanism dominates during mid-third instar. This model requires that the Golgi larval clusters present in the mid-TIL would comprise predominantly COPI-derived vesicles and the enlargement of larval clusters observed in late TIL imaginal discs could be accounted for by COPII vesicles. Our immunofluorescence studies provide circumstantial evidence that this is the case, but further work needs to be undertaken to clarify the process.

Rab1 is part of the Ras superfamily of small GTPases and has been shown to have a role in vesicular transport between the ER and the cis face of the Golgi stack. Between mid- and late TIL, we found that *drab1* expression increases about 3.7-fold. This result represents the activation of a possible docking mechanism of the newly budded COPII vesicles. Recently, mammalian Rab1 has been shown to recruit p115 (Allan *et al.*, 2000) and GM130 (Moyer *et al.*, 2001), two proteins known to be involved in vesicle tethering and docking (Nakamura *et al.*, 1997; Sönnichsen *et al.*, 1998).

Although in *Drosophila* a similar interaction has yet to be characterised, the role for dRab1 could be as follows. The expression of *dp115* and *dGM130* was found to be elevated throughout the third larval instar. During mid-TIL, their gene products could serve a tethering mechanism (as it does in mammalian systems; Sönnichsen *et al.*, 1998; Pfeffer, 1999) for the COPI vesicles present in the larval clusters. During late third instar, dRab1 would switch dp115 and dGM130 function from tethering the COPI vesicles to docking and priming the newly formed COPII vesicles prior to their fusion to form Golgi cisternae.

The upregulation of *drab1* was specific. Indeed, *drab6* (involved in retrograde transport in mammalian systems; Martinez *et al.*, 1994) was downregulated ~4-fold.

The fusion machinery including the SNAREs dSed5 and dGos28, and the fusion ATPase dNSF1 and cofactor dSNAP is also upregulated ~4-fold at the mRNA level. This upregulation would provide the machinery necessary for COPII vesicle fusion and cisternae formation. This correlates well with our earlier results showing that dNSF1 is required for the conversion in Golgi morphology (Kondylis *et al.*, 2001). A similar activity has also been shown *in vitro* by using a Golgi stack reassembly assay from mitotic Golgi fragments (Rabouille *et al.*, 1995).

A second homologue of mammalian NSF was identified in *Drosophila* (dNSF2; Pallanck *et al.*, 1995) that is expressed from the end of embryogenesis to adulthood. Throughout our study, *dnsf2* was not detected in TIL imaginal discs, contrary to previous reports (Boulianne and Trimble, 1995).

We are therefore left with the possible role of TER94 and cofactor dp47 that we found are not substantially regulated but present at all stages of disc elongation. This second fusion machinery has also been shown *in vitro* to be involved in Golgi stack reassembly (Rabouille *et al.*, 1995; Acharya *et al.*, 1995). Nevertheless, because of the constant level of expression, we tend to favour the hypothesis according to which this complex is not involved in Golgi stack biogenesis at puparium formation. Our previous work indicates that Golgi clusters are not converted to Golgi stacks in the absence of dNSF1, using the *comt 17* mutant maintained at restrictive temperature (Kondylis *et al.*, 2001). Taken together, these results suggest to us that the dNSF1 fusion pathway is the major and possible sole contributor to the formation of Golgi stacks in disc cells. Only a hypomorphic ter94 mutant will solve the puzzle, and we are currently engaged in these experiments. p97, the mammalian homologue of TER94 has been shown to bind at least two other cofactors, ufd1 (required for ubiquitine degradation) and nlp4 (implicated in nuclear transport) (Meyer *et al.*, 2000). Its presence in imaginal disc cells might reflect the activity of these two other pathways.

Finally, we have shown that the overexpression of either dNSF1 or dSNAP leads to the precocious formation of Golgi

stacks from larval clusters that were comparable to pupal profiles (Kondylis *et al.*, 2001). That the overexpression of either proteins was sufficient to stimulate Golgi stack biogenesis encouraged us to investigate whether *dsec23* expression was influenced by the overexpression of dNSF1 or dSNAP. *dsec23* expression was 1.8-fold increased, but resulted from the heat shock and not from the overexpression of either protein. This result argues against a direct cross talk between dNSF1 and dSNAP (protein or mRNA), and *dsec23*. Other genes will be investigated.

The direct involvement of dNSF1 and dSNAP in the formation of active COP II vesicles could account for this biogenesis, especially the 2.7-fold increase in volume density. This has been shown before in mammalian systems for the COPI vesicles (Wattenberg *et al.*, 1992) and for clathrin-coated vesicles in the endocytic pathway (Steel *et al.*, 1996). The data presented here support the hypothesis that transcriptional regulation of a variety of Golgi genes is a significant factor contributing to Golgi stack biogenesis. The direct transcriptional activation of the budding, docking, and fusion pathways are likely to lead to the construction of Golgi stacks.

Until present, experimental evidence has indicated that modulation of organelle architecture is mostly influenced and/or regulated by modifications at the translational and posttranslational level (see Introduction). Here, we show for the first time that changes in the expression of genes known to participate in the building of the Golgi apparatus exert a direct effect on Golgi biogenesis. Furthermore, for the first time, we demonstrate that this gene expression regulation is developmentally controlled by the steroid hormone ecdysone. This novel mechanism is likely to be common to other organisms.

ACKNOWLEDGMENTS

We thank Martin Lowe (Manchester, UK) for his gift of the β'COP antibody; J. P. Paccaud (Geneva, Switzerland) for his gift of the Sec23 antibody; Kevin Moses (Atlanta, GA) for his gift of the npr-FRT18/FM7 stock; Leo Pallanck (Seattle, WA) for his gift of the HSN and the UAS SNAP flies stocks and of the dNSF1 and dNSF2 clones; Julie Diplexcito for cloning dp115 and Steve Christie for subcloning dsed5 into PBSK; Marianna Pinter (Tucson, AZ) for the TER94 cDNA clone Ab14; Andy Jarman for critically reading the manuscript; Members of the Davis, Jarman, and Heck's lab (ICMB, Edinburgh) for their helpful discussions. We acknowledge the use of fly base (http://flybase.bio.indiana.edu) and the Berkeley *Drosophila* Genome Project (http://www.fruitfly.org) web sites. This study was funded by the Medical Research Council. V.K. is funded by the Darwin Trust of Edinburgh.

REFERENCES

Allan, B. B., Moyer, B. D., and Balch, W. E. (2000). Rab1 recruitment of p115 into a cis-SNARE complex: Programming budding COPII vesicles for fusion. *Science* **289**, 444–448.

Acharya, U., Jacobs, R., Peters, J. M., Farquhar, M. G., and Malhotra, V. (1995). The formation of Golgi stacks from vesiculated Golgi membranes requires two distinct fusion events. *Cell* **82**, 895–904.

Andres, A. J., Fletcher, J. C., Karim, F. D., and Thummel, C. S. (1993). Molecular analysis of the initiation of insect metamorphosis: A comparative study of *Drosophila* ecdysteroid-regulated transcription. *Dev. Biol.* **160**, 388–404.

Antony, C., Huchet, M., Changeux, J. P., and Cartaud, J. (1995). Developmental regulation of membrane traffic organization during synaptogenesis in mouse diaphragm muscle. *J. Cell Biol.* **130**, 959–968.

Ashburner, M. (1972). Ecdysone induction of puffing in polytene chromosomes of *Drosophila melanogaster*. Effects of inhibitors of RNA synthesis. *Exp. Cell Res.* **71**, 433–440.

Ashburner, M. (1990). Puffs, genes, and hormones revisited. *Cell* **61**, 1–3.

Banfield, D. K., Lewis, M. J., Rabouille, C., Warren. G., and Pelham, H. R. (1994). Localization of Sed5, a putative vesicle targeting molecule, to the cis-Golgi network involves both its transmembrane and cytoplasmic domains. *J. Cell Biol.* **127**, 357–371.

Barlowe, C., Orci, L., Yeung, T., Hosobuchi, M., Hamamoto, S., Salama, N., Rexach, M. F., Ravazzola, M., Amherdt, M., and Schekman, R. (1994). COP II: A membrane coat formed by sec proteins that drive vesicle budding from the endoplasmic-reticulum. *Cell* **77**, 895–907.

Barr, F. A., Puype, M., Vanderckhove, J., and Warren, G. (1997). GRASP65, a protein involved in the stacking of Golgi cisternae. *Cell* **91**, 253–262.

Bartoszewki, S., Luschnig, S., Desjeux, I., and Nusslein-Volhard, C. (2001). *Drosophila* p24 homologues, *ecl* and *Bai*, are necessary for membrane localisation of maternally expressed Tkv receptor. Abstract from the "17th European *Drosophila* Research Conference," Edinburgh.

Biyasheva, A., Do, T. V., Lu, Y., Vaskova, M., and Andres, A. J. (2001). Glue secretion in the *Drosophila* salivary gland: A model for steroid-regulated exocytosis. *Dev. Biol.* **231**, 234–251.

Boulianne, G. I., and Trimble, W. S. (1995). Identification of a second homologue of N-ethylmaleimide-sensitive fusion protein that is expressed in the nervous system and secretory tissues of *Drosophila*. *Proc. Natl. Acad. Sci. USA* **92**, 7095–7099.

Boyd, M., and Ashburner, M. (1977). The hormonal control of salivary gland secretion in *Drosophila melanogaster*: Studies in vitro. *J. Insect Physiol.* **23**, 517–523.

Brennan, C. A., Li, T. R., Bender, M., Hsiung, F., and Moses, K. (2001). Broad-Complex, but not ecdysone receptor, is required for progression of the morphogenetic furrow in the *Drosophila* eye. *Development* **128**, 1–11.

Burtis, K. C., Thummel, C. S., Jones, C. W., Karim, F. D., and Hogness, D. S. (1990). The *Drosophila* 74EF early puff contains E74, a complex ecdysone-inducible gene that encodes two ets-related proteins. *Cell* **61**, 85–99.

Chui, D., Oh-Eda, M., Liao, Y. F., Panneerselvam, K., Lal, A., Marek, K. W., Freeze, H. H., Moremen, K. W., Fukuda, M. N., and Marth, J. D. (1997). Alpha-mannosidase-II deficiency results in dyserythropoiesis and unveils an alternate pathway in oligosaccharide biosynthesis. *Cell* **90**, 157–167.

Cohen, S. (1993). Imaginal disc development. In "The Development of *Drosophila melanogaster*," Volume II. (M. Bates and A. Martinez Arias, Eds.), pp. 843–897. Cold Spring Harbor Laboratory Press, Cold Spring Harbor, NY.

Colanzi, A., Deerinck, T. J., Ellisman, M. H., and Malhotra, V. (2000). A specific activation of the mitogen-activated protein

kinase kinase 1 (MEK1) is required for Golgi fragmentation during mitosis. *J. Cell Biol.* **149,** 331–339.

Dang, D. T., and Perrimon, N. (1992). Use of a yeast site-specific recombinase to generate embryonic mosaics in *Drosophila*. *Dev. Genet.* **13,** 367–375.

D'avino, P. P., and Thummel, C. S. (1998). crooked legs encodes a family of zinc finger proteins required for leg morphogenesis and ecdysone-regulated gene expression during *Drosophila* metamorphosis. *Development* **125,** 1733–1745.

DiBello, P. R., Withers, D. A., Bayer, C. A., Fristrom, J. W., and Guild, G. M. (1991). The *Drosophila* Broad-Complex encodes a family of related proteins containing zinc fingers. *Genetics* **129,** 385–397.

Dunne, J. C., and Rabouille, C. (2001). Lord of the flies? The Golgi apparatus in development. In "The ELSO Gazette: E-magazine of the European Life Scientist Organization" (http://www.the-elsogazette/magazines/issue3/mreviews/mreviews1. asp), Issue 3 (1 January 2001).

Fletcher, J. C., and Thummel, C. S. (1995). The ecdysone-inducible Broad-complex and E74 early genes interact to regulate target gene transcription and *Drosophila* metamorphosis. *Genetics* **141,** 1025–1035.

Fristrom, D., and Fristrom, J. W. (1993). The metamorphic development of the adult epidermis. In "The Development of *Drosophila melanogaster*," Volume II. (M. Bates and A. Martinez Arias, Eds.), pp. 843–897. Cold Spring Harbor Laboratory Press, Cold Spring Harbor, NY.

Goulding, S. E., zur Lage, P., and Jarman, A. P. (2000). Amos, a proneural gene for *Drosophila* olfactory sense organs that is regulated by lozenge. *Neuron* **25,** 69–78.

Jasmin, B. J., Cartaud, J., Bornens, M., and Changeux, J. P. (1989). Golgi apparatus in chick skeletal muscle: Changes in its distribution during end plate development and after denervation. *Proc. Natl. Acad. Sci. USA* **86,** 7218–7222.

Jesch, S. A., Lewis, T. S., Ahn, N. G., and Linstedt, A. D. (2001). Mitotic phosphorylation of. Golgi reassembly stacking protein 55 by mitogen-activated protein kinase ERK2. *Mol. Biol. Cell* **12,** 1811–1817 .

Karim, F. D., Guild, G. M., and Thummel, C. S. (1993). The *Drosophila* Broad-Complex plays a key role in controlling ecdysone-regulated gene expression at the onset of metamorphosis. *Development* **118,** 977–988.

Kiss, I., Beaton, A. H., Tardiff, J., Fristrom, D., and Fristrom, J. W. (1988). Interactions and developmental effects of mutations in the Broad-Complex of *Drosophila melanogaster*. *Genetics* **118,** 247–259.

Klumperman, J. (2000). Transport between ER, and Golgi. *Curr. Opin. Cell Biol.* **12,** 445–449.

Koelle, M., Talbot, W. S., Segraves, W. A., Bender, M. T., Cherbas, P., and Hogness, D. S. (1991). The *Drosophila* EcR gene encodes an ecdysone receptor, a new member of the steroid receptor superfamily. *Cell* **67,** 59–77.

Kondo, H., Rabouille, C., Newman, R., Levine, T. P., Pappin, D., Freemont P., and Warren, G. (1997). p47 is a co-factor for p97-mediated membrane fusion. *Nature* **388,** 75–78.

Kondylis, V., Goulding, S. E., Dunne, J. C., and Rabouille, C. (2001). The biogenesis of the Golgi stacks in the imaginal discs of *Drosophila melanogaster*. *Mol. Biol. Cell* **12,** 2308–2327.

Leon, A., and McKearin, D. (1999). Identification of TER94, an AAA ATPase protein, as a Bam-dependent component of the *Drosophila* fusome. *Mol. Biol. Cell* **10,** 3825–3834.

Lowe, M., Gonatas, N. K., and Warren, G. (2000). The mitotic phosphorylation cycle of the cis-Golgi matrix protein GM130. *J. Cell Biol.* **149,** 341–356.

Lowe, M., Rabouille, C., Nakamura, N., Watson, R., Jackman, M., Jämsa, E., Rahman, D., Pappin, D. J., and Warren, G. (1998). Cdc2 kinase directly phosphorylates the cis-Golgi matrix protein GM130 and is required for Golgi fragmentation in mitosis. *Cell* **94,** 783–793.

Martinez, O., Schmidt, A., Salamero, J., Hoflack, B., Roa, M., and Goud, B. (1994). The small GTP-binding protein rab6 functions in intra-Golgi transport. *J. Cell Biol.* **127,** 1575–1588.

Meyer, H. H., Shorter, J. G., Seemann, J., Pappin, D., and Warren, G. (2000). A complex of mammalian ufd1 and npl4 links the AAA-ATPase, p97, to ubiquitin and nuclear transport pathways. *EMBO J.* **19,** 2181–2192.

Moyer, B. D., Allan, B. B., and Balch, W. E. (2001). Rab1 interaction with a GM130 effector complex regulates COPII vesicle cis-Golgi tethering. *Traffic* **2,** 268–276.

Ordway, R. W., Pallanck, L., and Ganetzky, B. (1994). Neurally expressed *Drosophila* genes encoding homologs of the NSF and SNAP secretory proteins. *Proc. Natl. Acad. Sci. USA* **91,** 5715–5719.

Nakamura, N., Lowe, M., Levine, T. P., Rabouille, C., and Warren, G. (1997). The vesicle Docking Protein p115 binds GM130, a cis-Golgi Matrix protein, in a mitotically regulated manner. *Cell* **89,** 445–455.

Pallanck, L., Ordway, R. W., Ramaswami, M., Chi, W. Y., Krishnan, K. S., and Ganetzky, B. (1995). Distinct roles for N-Ethylmaleimide-Sensitive Fusion Protein (NSF) suggested by the identification of a second *Drosophila* homologue. *J. Biol. Chem.* **270,** 18742–18744.

Pfeffer, S. R. (1999). Transport-vesicle targeting: Tethers before SNAREs. *Nat. Cell Biol.* **1,** E17–E22.

Pinter, M., Jekely, G., Szepesi, R. J., Farkas, A., Theopold, U., Meyer, H. E., Lindholm, D., Nassel, D. R., Hultmark, D., and Friedrich, P. (1998). TER94, a *Drosophila* homolog of the membrane fusion protein CDC48/p97, is accumulated in nonproliferating cells, in the reproductive organs and in the brain of the imago. *Insect Biochem. Mol. Biol.* **28,** 91–98.

Ponnambalam, S., Clough, S., Downes, C. P., Lucocq, J. M., McLauchlan, H. J., and Towler, M. C. (1999). Lipid kinases and trans-Golgi network membrane dynamics. *Biochem. Soc. Trans.* **27,** 670–673.

Preisinger, C., and Barr, F. A. (2001). Signaling pathways regulating Golgi structure and function. *Sci. STKE* **2001,** PE38.

Prout, M., Damania, Z., Soong, J., Fristrom, D., and Fristrom, J. W. (1997). Autosomal mutations affecting adhesion between wing surfaces in *Drosophila melanogaster*. *Genetics* **146,** 275–285.

Rabouille, C., Levine, T., Peters, J. M., and Warren, G. (1995). An NSF-like ATPase, p97, and NSF mediates cisternal regrowth from mitotic Golgi fragments. *Cell* **82,** 905–914.

Rabouille, C., and Warren, G. (1997). The changes in the architecture of the Golgi apparatus during mitosis. In "The Golgi Apparatus" (E. G. Berger and Roth, Eds.). Birkhäuser Verlag Basel/Switzerland.

Rabouille, C., Kuntz, D. A., Lockyer, A., Watson, R., Signorelli, T., Rose, D. R., Van den Heuvel, M., and Roberts, D. B. (1999). The *Drosophila GMII* gene encodes Golgi α-mannosidase II. *J. Cell Sci.* **112,** 3319–3330.

Rambourg, A., Clermont, Y., Chretien, M., and Olivier, L. (1993). Modulation of the Golgi apparatus in stimulated and non stimulated prolactin cells in female rats. *Anat. Rec.* **235,** 353–362.

Riddiford, L. M. (1993). Hormone receptors and the regulation of insect metamorphosis. *Receptor* **3,** 203–209.

Riddiford, L. M. (1996). Juvenile hormone: The status of its "status quo" action. *Arch. Insect Biochem. Physiol.* **32,** 271–286.

Roche, A. C., and Monsigny, M. (2001). MR60/ERGIC-53, a mannose-specific shuttling intracellular membrane lectin. *Results Probl. Cell Differ.* **33,** 19–38.

Satoh, A., Tokunaga, F., Kawamura, S., and Ozaki, K. (1997). In situ inhibition of vesicle transport and protein processing in the dominant negative Rab1 mutant of *Drosophila*. *J. Cell Sci.* **110,** 2943–2953.

Segraves, W. A., and Hogness, D. S. (1990). The E75 ecdysone-inducible gene responsible for the 75B early puff in *Drosophila* encodes two new members of the steroid receptor superfamily. *Genes Dev.* **4,** 204–219.

Sönnichsen, B., Lowe, M., Levine, T., Jämsa, E., Dirac-Svejstrup, B., and Warren, G. (1998). A role for giantin in docking COPI vesicles to Golgi membranes. *J. Cell Biol.* **140,** 1013–1021.

Steel, G. J., Tagaya, M., and Woodman, P. G. (1996). Association of the fusion protein NSF with clathrin-coated vesicle membranes. *EMBO J.* **15,** 745–752.

Thomopoulos, G. N., Neophytou, E. P., Alexiou, M., Vadolas, A., Limberi-Thomopoulos, S., and Derventzi, A. (1992). Structural and histochemical studies of Golgi complex differentiation in salivary gland cells during *Drosophila* development. *J. Cell Sci.* **102,** 169–184.

Thummel, C. S. (1990). Puffs and gene regulation: Molecular insights into the *Drosophila* ecdysone regulatory hierarchy. *BioEssays* **12,** 561–568.

Vayssie, L., Garreau de Loubresse, N., and Sperling, L. (2001). Growth and form of secretory granules involves stepwise assembly but not differential sorting of a family of secretory proteins in Paramecium. *J. Cell Sci.* **114,** 875–886.

Veenhuis, M., Salomons, F. A., and Van Der Klei, J. J. (2000). Peroxisome biogenesis and degredation in yeast: A structure/function analysis. *Microsc. Res. Tech.* **51,** 584–600.

Wattenberg, B. W., Raub, T. J., Hiebsch, R. R., and Weidman, P. J. (1992). The activity of Golgi transport vesicles depends on the presence of the N-ethylmaleimide-sensitive factor (NSF) and a soluble NSF attachment protein (alpha SNAP) during vesicle formation. *J. Cell Biol.* **118,** 1321–3132.

White, K. P., Rifkin, S. A., Hurban, P., and Hogness, D. S. (1999). Microarray analysis of *Drosophila* development during metamorphosis. *Science* **286,** 2179–2184.

Received for publication October 16, 2001
Revised January 22, 2002
Accepted February 14, 2002
Published online April 14, 2002

JCB Article

A novel role for dp115 in the organization of tER sites in *Drosophila*

Vangelis Kondylis[1,2] and Catherine Rabouille[1,2]

[1]The Wellcome Trust Centre for Cell Biology, Institute for Cell and Molecular Biology, University of Edinburgh, Edinburgh, UK
[2]Department of Cell Biology, University Medical Centre Utrecht, Academic Ziekenhuis Utrecht, 3584CX Utrecht, Netherlands

Here, we describe that depletion of the *Drosophila* homologue of p115 (dp115) by RNA interference in *Drosophila* S2 cells led to important morphological changes in the Golgi stack morphology and the transitional ER (tER) organization. Using conventional and immunoelectron microscopy and confocal immunofluorescence microscopy, we show that Golgi stacks were converted into clusters of vesicles and tubules, and that the tERs (marked by Sec23p) lost their focused organization and were now dispersed throughout the cytoplasm. However, we found that this morphologically altered exocytic pathway was nevertheless largely competent in anterograde protein transport using two different assays. The effects were specific for dp115. Depletion of the *Drosophila* homologues of GM130 and syntaxin 5 (dSed5p) did not lead to an effect on the tER organization, though the Golgi stacks were greatly vesiculated in the cells depleted of dSed5p. Taken together, these studies suggest that dp115 could be implicated in the architecture of both the Golgi stacks and the tER sites.

Introduction

The Golgi apparatus exhibits a unique membrane architecture comprising Golgi stacked cisternae. There is accumulating evidence, particularly from yeast studies, suggesting a relationship between the presence of the Golgi stacks and a focused organization of the transitional ER (tER)* sites (Glick, 2002). tER sites are defined as specialized ER subdomains at which proteins destined for the Golgi apparatus are packaged into transport vesicles. They are defined by the presence of COPII vesicles, which carry the secretory cargo out of the ER. Cells contain many tER sites, where the COPII components Sec23p, Sec13p, and Sar1p have been localized (Orci et al., 1991; Barlowe et al., 1994). tER sites often display an elaborate architecture of clustered pleiomorphic membranes comprising one cup-shaped ER cisternae where budding profiles can be observed, small 50–70-nm vesicles (sometimes coated), and short tubules (Bannykh et al., 1996). However, the molecular mechanism that generates them is still mysterious (Rossanese et al., 1999).

In yeast *Pichia pastoris*, the Golgi apparatus exhibits stacked cisternae with established polarity, and the pattern of Sec13–GFP representing the tERs comprised two to six spots surrounding the nucleus. In contrast, *Saccharomyces cerevisiae* exhibits a Golgi apparatus in a form of multiple single cisternal elements surrounded by vesicles and tubules, which represent either the cis or the trans side of the Golgi (Preuss et al., 1992). Sec13–GFP appears in multiple fluorescent dots, indicating that the tER sites are dispersed throughout the ER. The reasoning sustaining the relationship between the tER organization and the presence of polarized Golgi stacks is that the concentration of vesicles budding from focused tER sites would remain high enough, maybe due to the presence of a tER matrix, to allow cisternal formation and stacking (Rossanese et al., 1999; Bevis et al., 2002), whereas the membrane derived from dispersed tERs is too low in concentration for proper cisternal formation and further stacking. However, the nature of the tER matrix is far from being clear.

On the other hand, studies performed in mammalian cells have established a number of so-called "Golgi matrix proteins," most of them Golgins such as p115, GM130, and giantin, that are involved in the building and maintenance of the Golgi stacks (Shorter and Warren, 2002). These proteins were characterized by the fact that they are not relocated to the ER upon brefeldin A treatment (Seemann et al., 2000a). These proteins have been shown and/or postulated to help

The online version of this article includes supplemental material.

Address correspondence to Catherine Rabouille, Department of Cell Biology, University Medical Centre Utrecht, AZU Room G02.525, Heidelberglaan 100, 3584CX Utrecht, Netherlands. Tel.: 31-30-250 9280. Fax: 31-30-254 1797. E-mail: C.Rabouille@lab.azu.nl

*Abbreviations used in this paper: GA, glutaraldehyde; IEM, immunoelectron microscopy; RNAi, RNA interference; tER, transitional ER.

Key words: *Drosophila* S2 cells; Golgi apparatus; tER sites; RNAi; p115

The Journal of Cell Biology, Volume 162, Number 2, July 21, 2003 185–198
http://www.jcb.org/cgi/doi/10.1083/jcb.200301136

the Golgi stacks adopt this typical architecture of stacked cisternae (see Discussion).

Golgi matrix proteins have been localized in mammalian cells to the Golgi area but also in earlier secretory compartments, rather away from the Golgi complex. p115, for instance, has been localized in the intermediate compartment and has been involved in ER to Golgi transport (Nelson et al., 1998; Alvarez et al., 1999, 2001). p115 has also been shown to be recruited on COPII vesicles by Rab1 and prime them for fusion with the Golgi membranes by recruiting a SNARE protein complex (Allan et al., 2000). Finally, Uso1p, the yeast functional orthologue of p115, has been implicated in early transport events such as ER-derived vesicle tethering and proper protein sorting (Sapperstein et al., 1995; Morsomme and Riezman, 2002), indicating that it could be localized in this part of the exocytic pathway. This opens the possibility that, in addition to its role in the different transport steps, p115 could also have a role in the organization of the tER sites.

In fly, the organization of the exocytic pathway is slightly different from the mammalian one. Golgi stacks are not interconnected to form a single copy organelle capping the nucleus. Instead, they remain dispersed in the cytoplasm (Rabouille et al., 1999), as is the case in plants and *Pichia*. The simplified organization observed in *Drosophila* provides us with the possibility to examine the molecular mechanisms underlying both structures in relation to each other. This could allow us to investigate whether the architecture of the Golgi apparatus in *Drosophila* S2 cells is a direct consequence of the tER organization or whether their structural organization is regulated independently of each other.

In the present study, we show that depletion of the *Drosophila* homologue of p115, dp115, which is localized both in the Golgi stacks and in dSec23p-positive tERs, led to a quantitative breakdown of Golgi stacks that are converted into Golgi clusters of vesicles and tubules and strongly affected the general organization of the tER sites. In addition, we show that despite the presence of a morphologically modified exocytic pathway, the intracellular transport was largely unaffected, suggesting that the disorganized tER and the Golgi clusters still form a functional exocytic pathway.

Results

The localization of dp115 in *Drosophila* S2 cells

Drosophila p115 (dp115) exhibits 60% similarity to its rat counterpart (Fig. 1 A). dp115 does not possess the acidic stretch of the 50 COOH-terminal amino acids that has been shown in rat p115 to be involved in binding GM130 and giantin (Dirac-Svejstrup et al., 2000). In dp115, there are only a few acidic amino acids scattered along the last 100 COOH-terminal portion of the protein. Besides *Neurospora*, the tail of *Caenorhabditis elegans* and *Arabidopsis* p115 homologues is not acidic either, except for the last 5 and 15 amino acids, respectively (our search). However, the domain in GM130 that binds p115 is conserved in dGM130 (Kondylis et al., 2001; Fig. 1 A), suggesting that both *Drosophila* proteins could bind each other (albeit possibly through a different domain in dp115).

Despite the high level of homology between mammalian and *Drosophila* p115, we were interested to verify the localization of the *Drosophila* homologue. dp115 has been shown to localize to the Golgi apparatus and Golgi clusters in *Drosophila* imaginal discs by an antibody raised against rat p115 that cross reacted with dp115 (Kondylis et al., 2001). We raised an antibody against a dp115-specific peptide (dp115/584) that recognizes three bands by Western blotting (Fig. 1 B), one at 40 kD (resulting from the secondary antibody, because it is present in the absence of primary antibody; unpublished data), one at 65 kD, and one at 85 kD (Fig. 1 B, lane 1), which has the predicted molecular mass for dp115. We fractionated the S2 cell extract into cytosolic and membrane fractions. After blotting, the 85-kD band seemed only associated with the membrane fraction (lane 3), although its absence from the cytoplasmic fraction (lane 2) might be due to insufficient loading. In larval extract, this band was the major one, and the 65-kD band was much weaker (lane 5). The 65-kD band was considered nonspecific because Western blotting of embryo extracts did not show any bands at 85-kD but revealed a 65-kD band with the same intensity as the larval extract (lane 4). Furthermore, the intensity of this band did not vary according to the amount of protein loaded (unpublished data), and it was present in other Western blots using different primary antibodies.

When used in immunoelectron microscopy (IEM), the dp115/584 antibody gave a specific signal (Fig. 1, C–F). In S2 cells, 30 ± 5% of the gold particles were on the cytoplasm. The Golgi area was labeled by 25 ± 8% of the membrane-associated gold particles. The ER cisternae were decorated by 21 ± 6%. Pleiomorphic membranes (Fig. 1, C and D, asterisk) comprising tubules and vesicles (50–70 nm in diameter, but also larger vessels) close to the Golgi stacks or in their neighborhood contained 54 ± 7% of the membrane-associated labeling. A double labeling with an antibody recognizing the *Drosophila* homologue of Sec23p (dSec23p; Fig. 1, E and F) suggested that these pleiomorphic membranes represented tERs (see Fig. 5). The linear density of gold particles over the membrane of these three compartments was estimated to be 0.57 gold/μm on the Golgi membrane, 0.37 on tER membrane, and 0.15 on ER cisternae. A similar pattern of distribution was observed when salivary glands of third instar larvae were labeled with the same antibody (Fig. 1 D).

dGM130 has been described in Kondylis et al. (2001) and localizes to the Golgi apparatus in *Drosophila* imaginal discs. When MLO7 (a polyclonal antibody directed against the first 73 amino acids of GM130; a gift from Martin Lowe, University of Manchester, Manchester, UK) was used in S2 cells for indirect immunofluorescence, it labeled dGM130 in a Golgi-specific manner (unpublished data).

Effect of depleting dp115 and dGM130 on Golgi stack morphology

We depleted S2 cells of dGM130 using a dsRNA corresponding to the second exon of dGM130 (ds dGM130). When samples were analyzed by Western blotting, two bands were detected, one very faint, which was neglected (Fig. 2, top, lane C), and a strong one. The strong band

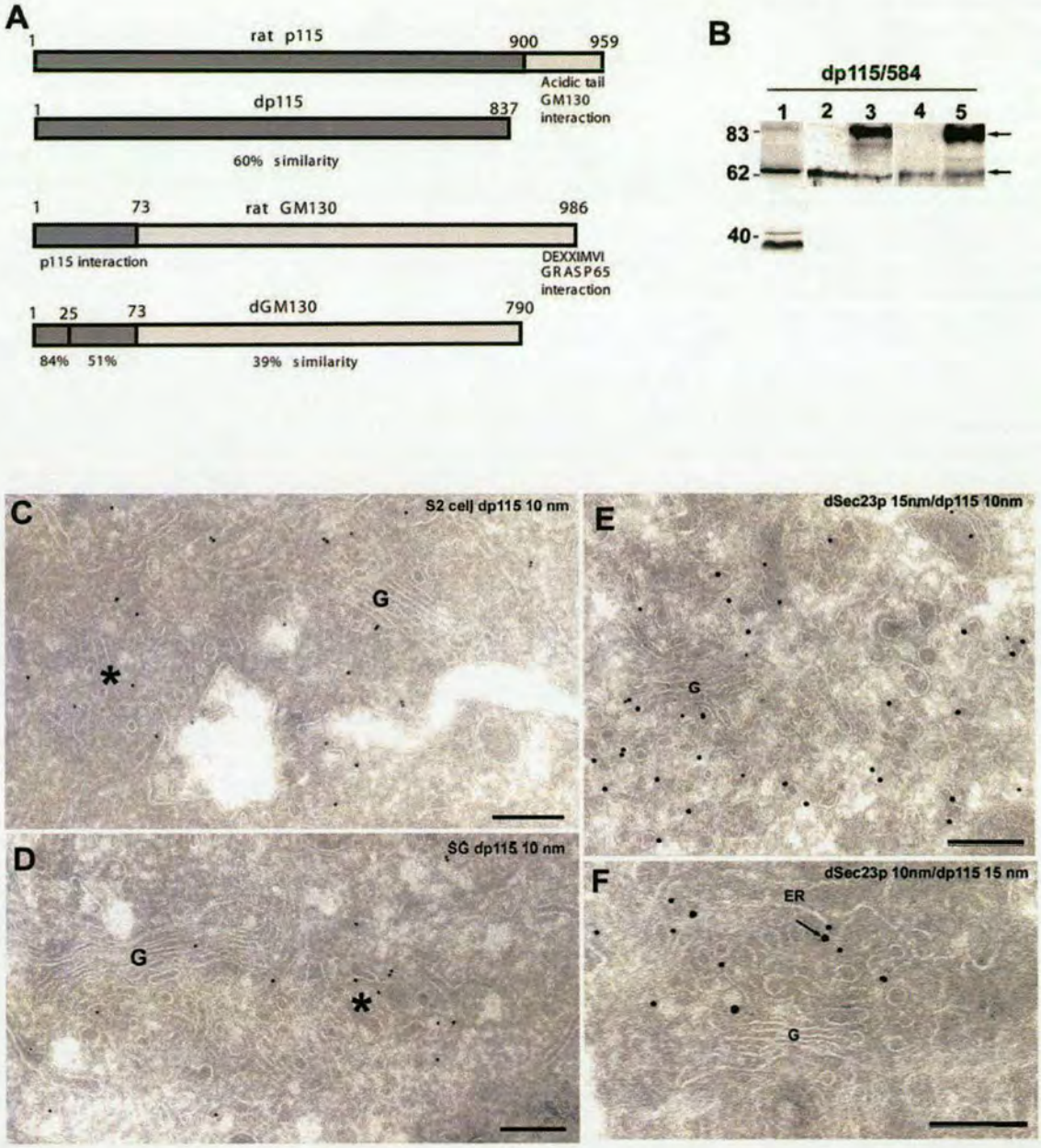

Figure 1. **dp115 in *Drosophila* S2 cells.** (A) dGM130 and dp115 proteins were compared with their rat homologues, and the domains of highest homology are painted in dark gray. (B) Western blotting using the affinity-purified dp115/584 of total S2 cell extract corresponding to 2,000,000 cells (lane 1), 4% of the cytosolic fraction of 10,000,000 cells (lane 2), the total membrane corresponding to 10,000,000 cells (lane 3), total extract corresponding to 20 embryos (lane 4), one third instar larva (lane 5). Two bands were recognized (small arrows on the right). Molecular mass markers are indicated on the left. (C–F) IEM of dp115 on *Drosophila* cells and tissues. Cryosections of PFA (C and E) and PFA/GA (F) fixed S2 cells and *Drosophila* third instar larvae salivary glands (D) were incubated with the affinity-purified dp115/584 and 10-nm protein A gold. (E) S2 cell sections were double labeled with the dp115/584 antibody followed by 10-nm protein A gold, and the Sec23p antibody followed by 15-nm protein A gold. (F) The same labeling was performed but the gold sizes are inverted. Golgi stacks are marked by a G, and pleiomorphic membranes are marked by an asterisk in C and D. The arrow indicates dp115 in an ER bud in F. Bars, 200 nm.

migrated at the predicted position for a protein of the mass of dGM130 (arrow) and was reduced below detectable level after 48 h (Fig. 2, top) and remained so up to 120 h of incubation. This depletion, however, did not lead to any effect on Golgi stack morphology, as assessed by EM (Fig. 3 B).

The percentage of cell sections exhibiting at least one Golgi stack per cell profile was scored. 100% of mock-treated (incubated without dsRNA) and mock-depleted cells (incubated with ds EGFP) exhibited at least one Golgi stack per cell profile (Fig. 3 A). This percentage decreased slightly to 85% for incubations up to 96 and 120 h. On average,

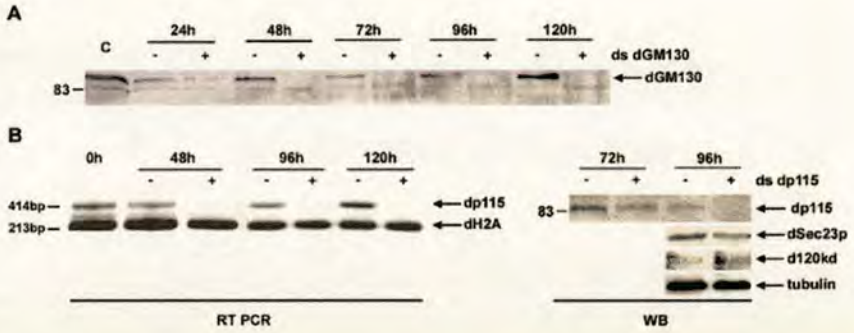

Figure 2. **Depletion of dGM130 protein and dp115 mRNA.** (A) Western blotting using MLO7 (anti-GM130 antibody) of the extract of S2 cells incubated with (+) or without (−) ds dGM130 for increasing lengths of time. C corresponds to time 0 (3,000,000 cells). 1,500,000 cells were used for lanes 24–72 h, and 2,500,000 for lanes 96–120 h. From the two bands the antibody recognizes, the stronger upper band is specifically depleted (arrow). (B) The dp115 mRNA was measured by RT-PCR from total RNA extract from 1,000,000 cells incubated with (+) or without (−) ds dp115 for 48–120 h. Amplification of histone 2A mRNA was used as control of the specific depletion of dp115 mRNA and as a loading control. Western blotting of the extract of cells (1,500,000) incubated with (+) or without (−) ds dp115 for 72 and 96 h using the dp115/584 antibody (dp115), the Sec23p antibody (dSec23p), the antibody recognizing the 120-kD *Drosophila* antigen (d120kd), and α-tubulin. Note that only dp115 is depleted.

these Golgi stacks had a cross-sectional diameter of 0.368 ± 0.047 μm and 3.7 ± 0.8 cisternae per stack.

In cells depleted of dGM130, the percentage of cells exhibiting Golgi stacks (Fig. 4 A), the number of cisternae per stack, and the mean diameter of the stacks were comparable to the figures obtained for mock-treated cells (diameter of 0.347 ± 0.078 μm and 3.5 ± 1.6 cisternae per stack).

We depleted S2 cells of dp115. dsRNA corresponding to the NH_2-terminal portion of dp115 (ds dp115) was added to S2 cells for up to 120 h. We first assessed the depletion of dp115 mRNA by RT-PCR using primers corresponding to the 5′ end of the dp115 gene (Fig. 2 B, RT PCR). After 48 h, dp115 mRNA could not be detected and remained so up to 120 h. Western blotting with the dp115/584 antibody showed that the 85-kD band disappeared after 96 h of incubation with ds dp115 (Fig. 2 B, WB).

Cells depleted of dp115 up to 72 h did not show significant changes in their Golgi stack morphology when compared with controls (Fig. 3 C). 76.3 ± 4.0% exhibited at least one Golgi stack per cell section (Fig. 4 A). However, this percentage decreased sharply in the cells incubated for 96 h. In only 18 ± 6.3% of the cell sections, one or more

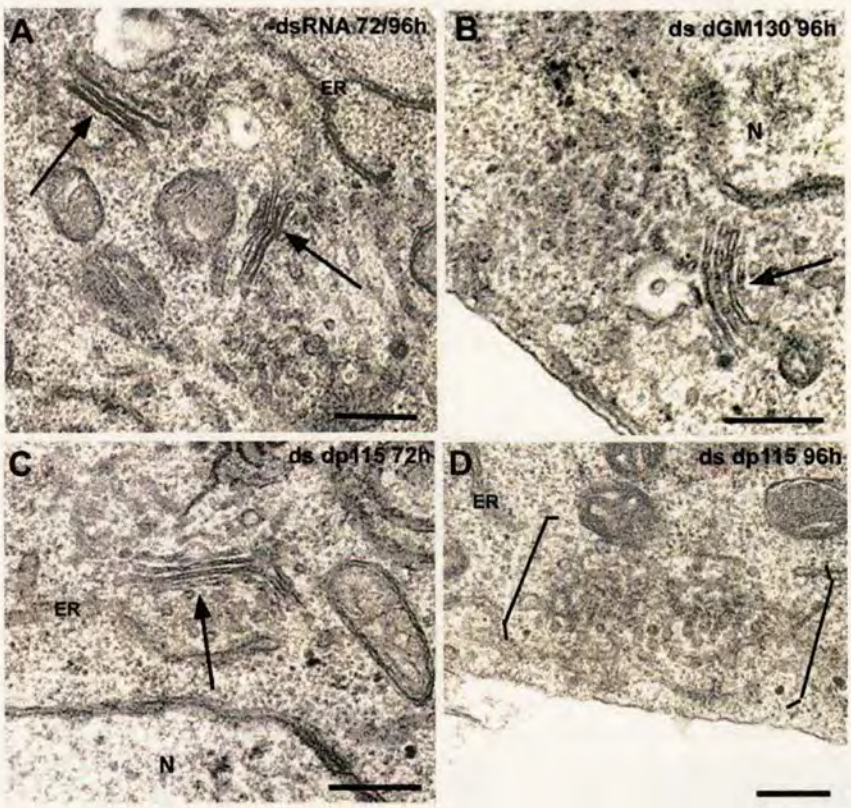

Figure 3. **Effect of depleting dp115 and dGM130 on the Golgi stack morphology.** *Drosophila* S2 cells were cultured (A) in the absence (−dsRNA) or (B) presence of ds dGM130 for 96 h, or (C) in the presence of ds dp115 for 72 or (D) 96 h. Cells were collected and processed for conventional EM. Golgi stacks are indicated with a long arrow, and clusters of vesicles and tubules are marked between brackets. N, nucleus. Bars, 200 nm.

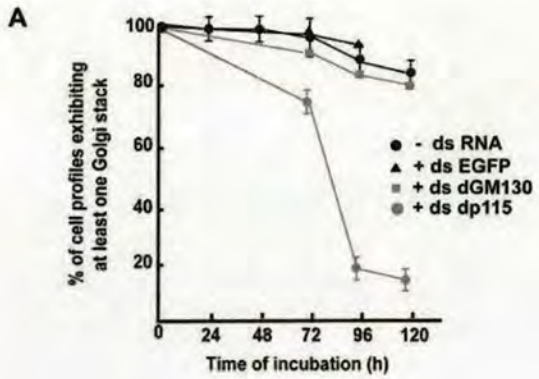

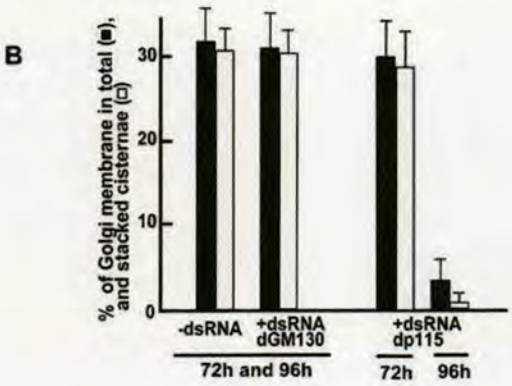

C

Estimation of the surface density of the Golgi area (SDgo) and the total cisternae (SDcis).

	Mock depleted 96h	dp115 depleted 96h
SD go	3.64 ± 0.44	2.97±0.29
SD cis	1.25±0.17	0.16±0.07

Figure 4. **Quantitative analysis of the morphological effects after protein depletion.** (A) Percentage of Golgi stacks in profiles of S2 cells depleted of dp115 and dGM130. S2 cells were incubated for 24 to 120 h with the different dsRNAs, processed for EM, and scored for the presence of at least one Golgi stack per cell profile. The results obtained are presented as a percentage of the total number of cells examined for each condition (~300). (B) Stereological analysis of the Golgi area after protein depletion. Representative EM pictures of mock-treated cells and cells depleted of dGM130 and dp115 at 72 and 96 h were used to estimate the percentage of Golgi membrane in total cisternae (black bars) and stacked cisternae (white bars). The error bars represent the SD. (C) Estimation of the surface density of the Golgi area (SDgo) and the total cisternae (stacked and single) (SDcis) in mock- and dp115-depleted cells for 96 h. Results are expressed in μm^{-1} and ± represents SD.

Golgi stacks were visible (Fig. 4 A). These stacks were also smaller than in mock-depleted cells with a mean diameter of 0.268 ± 0.050 μm and 3.2 ± 0.4 cisternae/stack. The remaining 82% of the cell sections exhibited a Golgi area under the form of clusters of vesicles and tubules (Fig. 3 D). The percentage of membrane in cisternae per Golgi area decreased by 12% at 72 h, and by 87% at 96 h, when compared with control (Fig. 4 B). This latter decrease was paralleled by a decrease in stacking (Fig. 4 B) and was mirrored by an increase of 32% in vesicular profiles and an increase of 50% of small tubules.

The surface density of the Golgi area (SDgo) and total cisternae (SDcis) (stacked and single) was estimated in mock- and dp115-depleted cells. A reduction of 21% of SDgo was observed after dp115 depletion together with a reduction of 88% of the SDcis (Fig. 4 C), suggesting that cisternal profiles were lost or not merely diluted, for instance, by incoming vesicles that would accumulate around them, unable to fuse due to lack of dp115.

Effect of dp115 depletion on the tER organization

Given the impact of dp115 depletion on the structure of the Golgi stacks, the proposed relationship between the tER organization and the presence of Golgi stacks, and the presence of dp115 at the tERs, we were prompted to look at the organization of the tER sites in cells depleted of dp115.

For this purpose, two antibodies were used. First, a polyclonal antibody raised against a rat Sec23p peptide (conserved in *Drosophila*) was used for IEM on S2 cell cryosections. This antibody decorated pleiomorphic membrane populated with 50–70-nm vesicular profiles (some coated; Fig. 5, D and E), ER coated buds, as well as larger vesicular and tubular membrane structures, often contained in the concavity of an ER cisterna (Fig. 5, A and C–E). These structures are reminiscent of those described by Bannykh et al. (1996), referred to as vesicular tubular clusters (VTCs). Since then, the VTC terminology has been used to describe other structures in the intermediate compartment. To avoid a possible misunderstanding, we refer to our membrane structures as tER sites on the basis of their dSec23p labeling and their colocalization with a transport cargo, such as the plasma membrane protein Delta (Fig. 5 F; see below). The gold labeling density on the tER sites was six to seven times higher than in the surrounded cytoplasm. Furthermore, 10 ± 3% of the gold particles decorated the ER cisternae.

Second, a monoclonal antibody recognizing a 120-kD *Drosophila* Golgi membrane antigen (d120kd; Stanley et al., 1997) was tested by IEM. The gold labeling was specific to the Golgi apparatus. 55% labeled the Golgi stacks, and 35% labeled vesicles and tubules abutting the Golgi stack (Fig. 5, B and C), a result in agreement with immunofluorescence data (Stanley et al., 1997; Munro and Freeman, 2000).

In immunofluorescence, these two antibodies gave similar patterns. The dSec23p pattern corresponded to 20 ± 8 large fluorescent objects dispersed in the cytoplasm (Fig. 6 A). The d120kd pattern corresponded to 18 ± 7 similar large fluorescent objects (Fig. 6 B). These two patterns overlapped partially (Fig. 6 C). By IEM, the region of overlap corresponded to the interface between the Golgi stack and the tER where the two antigens are in close proximity (Fig. 5 C).

In cells depleted of dp115 for 96 h, however, both patterns were differentially affected. In 90% of the cells, the immunofluorescence pattern of dSec23p appeared as numerous scattered small dots all over the cytoplasm (84.5 ± 20/cell; Fig. 6 D). The size of these fluorescent objects was approxi-

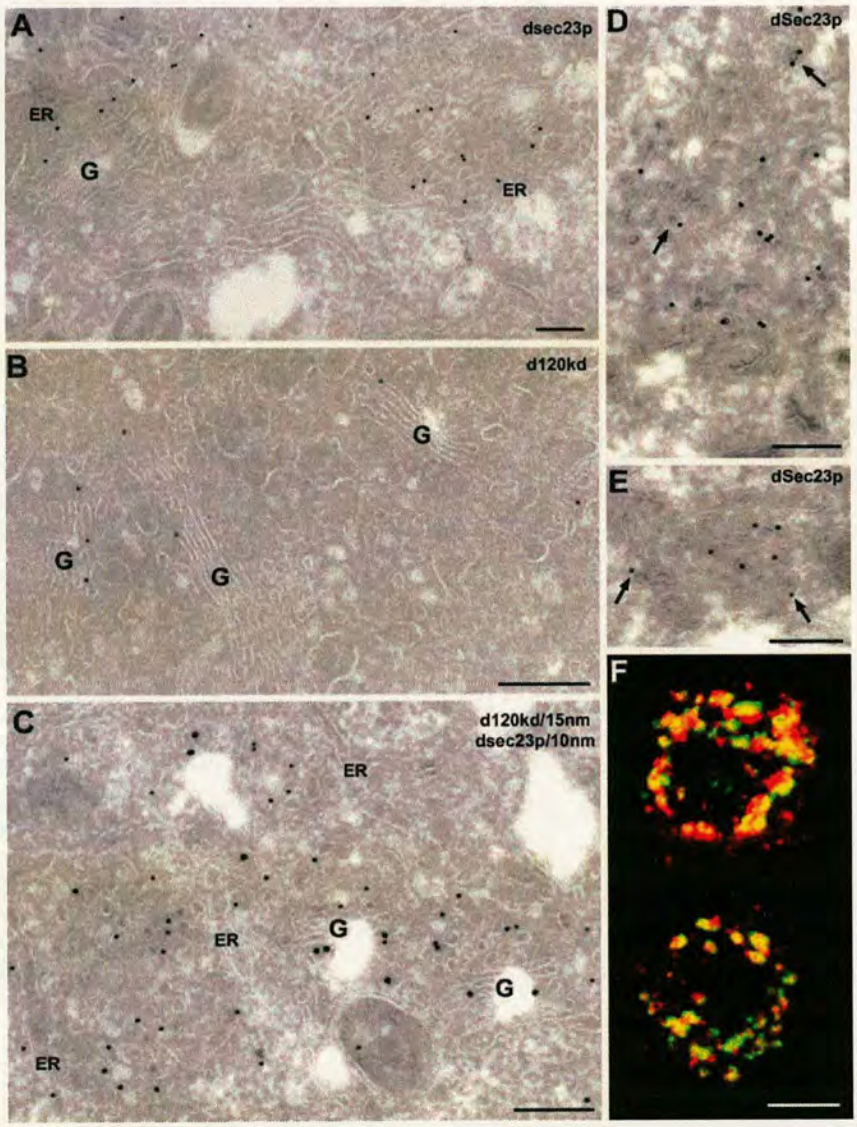

Figure 5. **Localization of d120kd and dSec23p in S2 cells.** Cryosections of *Drosophila* S2 cells, fixed with PFA/GA (A–C) or PFA alone (D and E), were labeled (A, D, and E) with a polyclonal anti-Sec23p antibody (10-nm gold) or (B) a monoclonal antibody against d120kd (10-nm gold). (C) Sections were double labeled with the d120kd antibody (15-nm gold) and the anti-Sec23p antibody (10-nm gold). (F) Delta S2 cells were induced with CuSO4 for 25 min and processed for immunofluorescence. Delta and dSec23p were labeled using C594.9B (red) and the anti-Sec23p antibody (green), respectively. The merge projections of 30 confocal sections are presented, and the overlap is yellow. The COPII coats labeled for dSec23p are indicated with an arrow. G, Golgi stacks. Bars: (A–E) 200 nm; (F) 5 μm.

mately three to four times smaller when compared with mock-depleted cells. The d120kd pattern of fluorescence also changed after dp115 depletion (Fig. 6 E). The number of fluorescent objects corresponding to this antigen was slightly higher than in control cells (26 ± 7 vs. 18 ± 6 in control cells), but their size was smaller, and the intensity of fluorescence reduced, as if this antigen was dispersed. d120kd and dSec23p immunofluorescence patterns did not overlap as much as in mock-treated cells. Numerous dSec23p dots seemed to be free of d120kd, and ~50% of the d120kd-positive dots were also observed free of dSec23p (Fig. 6 F). Similar changes in patterns were also observed when the cells were fixed with stronger fixatives and for a longer period of time, suggesting that the observed effects were not due to mild fixation (see Fig. S1, available at http://www.jcb.org/cgi/content/full/jcb.200301136/DC1). Furthermore, dSec23p and d120kd were not degraded upon dp115 depletion (Fig. 2 B), suggesting that this was not the cause of the change in patterns.

In dp115-depleted cells observed by IEM, the dSec23p-positive small and scattered dots observed in immunofluorescence represented pleiomorphic membranes containing vesicles and tubules, reminiscent of those observed in control cells, but with a smaller size (compare Fig. 5 A with Fig. 7, A and B; see Fig. S2, A and B, available at http://www.jcb.org/cgi/content/full/jcb.200301136/DC1). They appeared more dispersed throughout the cytoplasm than in control cells and sometimes exhibited a reduced labeling density (Fig. 7, B and E). The number of these dSec23p-positive sites per cell section was 6.7 ± 2.3, and only 20% of them were positive for d120kd. This is to be compared with 2.7 ± 1.5 dSec23p-positive sites per section of mock-depleted cells, 90% of them also positive for d120kd (Fig. 5 C), suggesting that small tER sites have been generated that lack the spatial relationship with Golgi areas.

The d120kd-positive dots that were observed in immunofluorescence represented clusters of vesicles and tubules labeled by 73 ± 3.6% of the gold particles associated with

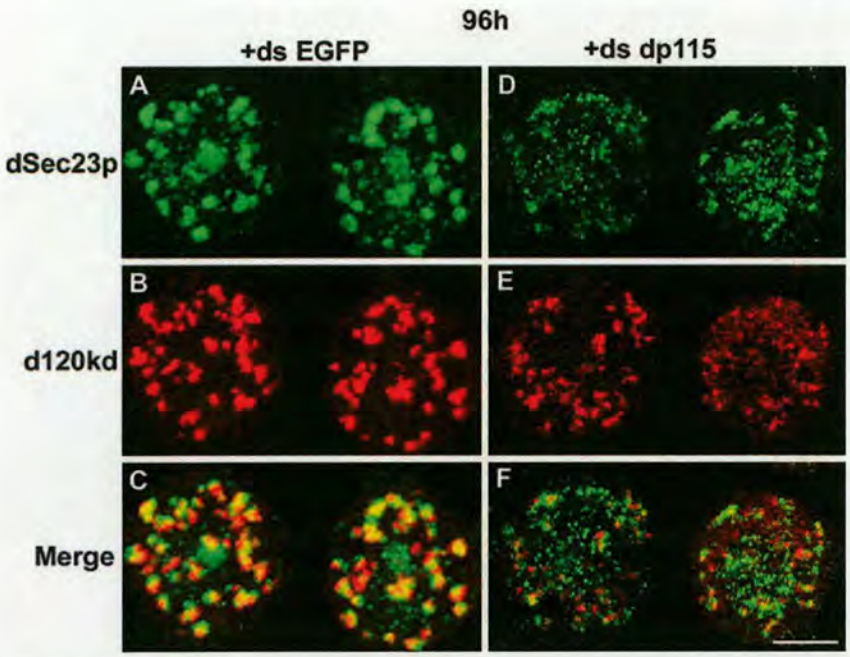

Figure 6. **Effect of dp115 depletion on the organization of the tER sites.** S2 cells were processed for confocal immunofluorescence microscopy using the anti-Sec23p antibody (green; A and D) and the d120kd antibody (red; B and E) in mock-depleted (+ds EGFP; A–C) and dp115-depleted cells (+ds dp115; D–F). Projections of 30 sections are presented, and in merge images (C and F), the overlap is yellow. Note that in mock-depleted cells, almost every dSec23p-positive structure is found in close proximity to a d120kd-positive one. Bar, 5 μm.

d120kd (Fig. 7, C–F). In these clusters, we could observe profiles reminiscent of short cisternal remnants (Fig. 7, D–F, arrows), indicating that these clusters could derive from Golgi stack breakdown. d120kd also labeled the ER cisternae (27 ± 3.6%; Fig. 7 E, arrowhead), suggesting perhaps a retrograde movement of Golgi membrane to the ER.

Pleiomorphic membranes of vesicles and tubules were also labeled by both dSec23p and d120kd, showing that some tERs have remained in close proximity to the Golgi membrane, as they were in nondepleted cells. In some cases, these two markers did not label the pleiomorphic membrane homogeneously and seemed to retain their original polarity (Fig. 7, D–F).

Overall, this experiment shows that the depletion of dp115 leads to the disorganization of both the tER sites and the Golgi stacks, suggesting that dp115 could be involved in the organization of both. Alternatively, the disorganization of the tERs could lead to the destabilization on the Golgi stacks. dp115 could thus have only one role in tER organization. To test this hypothesis, we assessed the immunofluorescence pattern of dSec23p and d120kd in dp115-depleted S2 cells between 72 and 96 h after ds dp115 addition (see Fig. S3, available at http://www.jcb.org/cgi/content/full/jcb.200301136/DC1). After a 72-h incubation with ds dp115, both dSec23p and d120kd patterns were almost indistinguishable from mock-treated cells (~20 large fluorescent objects partially overlapping, which we will refer to as "control patterns"). However, after 84, 88, and 92 h incubation, a mixture of patterns was observed. The number of cells exhibiting control patterns decreased gradually over time to reach 12.6% after 96 h incubation. Conversely, the cells exhibiting a pattern where both dSec23p and d120kd were affected increased gradually from 17.6 to 83.8%. The percentage of cells where only the dSec23p pattern was affected was roughly the same (2.3%) as that of cells where only the d120kd pattern was affected (0.9%). This result suggests that depletion of dp115 leads to a concomitant loss of Golgi stacks and tER organization, indicating that dp115 could have a distinct role in the organization of both structures.

These effects were specific for dp115 depletion. dGM130 depletion did not have any effect either on the structure of the Golgi complex (Fig. 3 B) or on tER organization (Fig. 8 E). On the other hand, depletion of dSed5p, the *Drosophila* homologue of mammalian syntaxin 5 (Banfield et al., 1994), had a very strong effect on the Golgi stack morphology (complete and quantitative vesiculation; Fig. 8, A and B), but the organization of the tERs was kept intact (Fig. 8 D) when compared with mock-depleted cells (Fig. 8 C). The fragmentation of the Golgi stacks therefore did not cause the redistribution of the tER sites.

Effect of the depletion of dp115 and dGM130 on anterograde protein transport

Depletion of dp115 led to quantitative breakdown of the Golgi stacks and dispersal of the tER sites. That prompted us to test whether this morphologically modified exocytic pathway was still functional.

We used an S2 cell line stably transfected with a construct expressing the full-length plasma membrane protein Delta (Klueg et al., 1998), referred to as Delta S2 cells. Delta is a glycosylated *Drosophila* ligand of Notch (Panin et al., 2002) that uses the exocytic pathway for its plasma membrane deposition (Fig. 5 F; see Fig. S4, available at http://www.jcb.org/cgi/content/full/jcb.200301136/DC1). The expression of Delta in this cell line is under the control of a metallothionein promoter, and addition of $CuSO_4$ drives its expression. The morphological effects of the various depletions were strictly similar in Delta S2 cells and in wild-type S2 cells, and all our stereological analyses have been obtained with both cell lines.

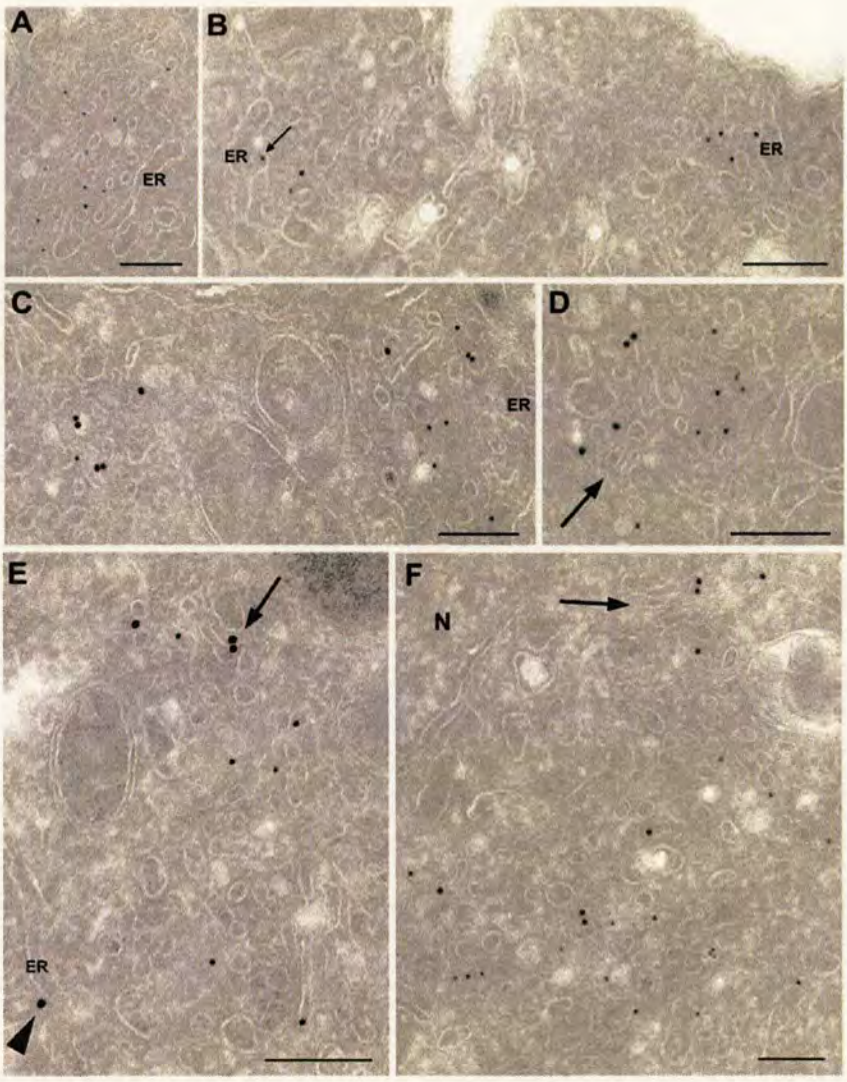

Figure 7. **Localization of dSec23p and d120kd in dp115-depleted cells.** S2 cells depleted of dp115 were processed for IEM and double labeled for dSec23p (10-nm gold) and d120kd (15-nm gold), as described in the legend of Fig. 5. (A–C) dSec23p-positive clusters. (C) d120kd-positive clusters. (D–F) Mixed clusters. A small arrow in B points to an ER bud labeled for dSec23p. Large arrows in D–F point to profiles reminiscent of Golgi cisternal remnants. Arrowhead in E points to a gold particle corresponding to d120kd associated with an ER cisterna. Note that in D–F, the labeling for dSec23p and d120kd marks differential regions of the same cluster. N, nucleus. Bars, 200 nm.

We verified that the induction and transport of Delta for as long as 2.5 h did not induce the rebuilding of Golgi stacks. In cells depleted of dp115 for 96 h, the percentage of cells with at least one Golgi stack was the same before and after Delta induction (18.0 ± 6.3 vs. 18.9 ± 1.2%, respectively).

We first induced Delta expression for 1 h followed by a 90-min chase as a way of measuring steady-state transport. In mock-treated and mock-depleted cells, a large majority of the staining was found at the plasma membrane (Fig. 9 A). Only 3.3 ± 2.5% of the cells exhibited exclusively intracellular (Fig. 9 B), with no plasma membrane, labeling.

The intensity of surface labeling at the plasma membrane varied considerably (Fig. 9 A). The estimation of the percentage of cells exhibiting the different labeling intensities allowed the calculation of the total intensity of the mock-treated cells (Fig. 9 D; Table I). This was set as 100% and was 90% inhibited by brefeldin A (Fig. 9, B and C; Table I), a known inhibitor of transport in the early exocytic pathway. Furthermore, an 89% transport inhibition was also obtained when cells were depleted of dSed5p, a protein largely documented for its role in intracellular transport (Fig. 9 C; Table I), suggesting that our transport assay was sufficiently sensitive to monitor an inhibition in transport and that Delta was a suitable marker for anterograde transport.

Depletion of dGM130 had only a negligible effect on the steady-state transport of Delta (Fig. 9 C; Table I). Surprisingly, depletion of dp115 reduced steady-state transport to a very small extent (~12%; Fig. 9 C; Table I).

The initial rate of transport in cells depleted for dp115, measured by inducing Delta expression for 25 min (minimal induction period to detect expression of the protein by Western blotting; unpublished data) and chasing for 45–90 min, was found to be reduced by 30.5 ± 3% when compared with mock-depleted cells (Fig. 9 D). The distribution of plasma membrane intensity was essentially the same in mock- and dp115-depleted cells where the exocytic pathway was largely modified (Fig. 9, compare E with F). This suggests that the large modifications to the morphology of the Golgi stacks and the tER organization caused by dp115 depletion did not make the cells incompetent for transport.

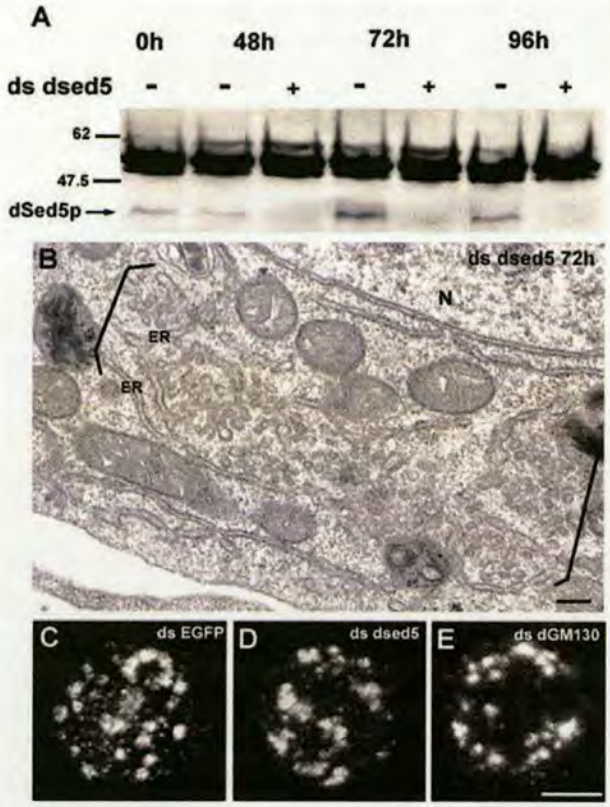

Figure 8. **Effect of dSed5p depletion on the Golgi stack morphology and tER organization.** (A) S2 cells were incubated with ds dsed5 up to 96 h. Extracts of mock- and dSed5p-depleted S2 cells were Western blotted using JSEE1 antibody. The 35-kD band corresponding to dSed5p is efficiently depleted (arrow). (B) The Golgi stack morphology in depleted cells was assessed by conventional EM. The cells exhibited no Golgi stacks, but extended areas completely vesiculated in >95% of the profiles examined. (C) The tER organization was monitored by immunofluorescence using the anti-Sec23p antibody, as described in the legend of Fig. 6, in control cells, (D) in cells depleted of dSed5p, and (E) in cells depleted of dGM130. N, nucleus. Bars: (B) 200 nm; (C–E) 5 μm.

Last, using a second S2 cell line where the expression of a secreted marker could be induced and monitored, we showed that the depletion of dp115 and dGM130 did not affect the secretion of this marker (unpublished data). This result strengthens the notion that the disorganization of the exocytic pathway does not lead to a significant decrease in transport efficiency.

Discussion

We have used *Drosophila* S2 cells to perform depletion of dp115 and dGM130 by RNA interference (RNAi). Despite small differences with mammalian cells, *Drosophila* cells are a novel, but adequate, biological system to investigate the issues related to membrane traffic and organelle structure.

dp115 localization

dp115 was localized on dSec23p-positive pleiomorphic membrane structures representing tERs, on the Golgi area, and on the ER cisternae. This distribution is slightly different from that in mammalian cells, where p115 has been localized in the cis Golgi, the Golgi stack, and the intermediate compartment (Nelson et al., 1998; Alvarez et al., 1999, 2001). Its localization on the tER sites was inferred only by the role it plays in priming COPII vesicles for fusion (Allan et al., 2000). This difference could be explained by the fact that the region between the ER and the Golgi stack comprised more layers in mammalian cells, including one positive for ERGIC53 that does not overlap with Sec13p (Hammond and Glick, 2000). In contrast, in S2 cells, the tER sites were found abutting the Golgi stack itself, as if the intermediate compartment was missing (a situation that seems similar to yeast where sec12/sec13 labeling seems to overlap with the Golgi apparatus; Rossanese et al., 1999; Bevis et al., 2002) or compressed into a single layer.

Golgi stacks are breaking down upon dp115 depletion

Depletion of dp115 in S2 cells led to the fragmentation of their Golgi stacks into clusters of vesicles and tubules. These clusters were labeled by a fraction of d120kd that, in mock-treated cells, preferentially marked the Golgi stacks. Some of them also seemed to contain remnants of Golgi cisternae. Furthermore, the Golgi stacks, in the small percentage of cells where they could still be observed, were 30% shorter than control. This suggests that upon dp115 depletion, Golgi stacks are fragmented into clusters retaining Golgi identity and function (see below). Similar results have been reported in mammalian cells that exhibited a fragmented

Table I. **Effect of depleting S2 cells of dp115, dGM130, and dSed5p on the efficiency of Delta intracellular transport to the plasma membrane**

Conditions	Efficiency of intracellular transport	
	Steady state (60 min/90 min)	Initial rate (25 min/45–90 min)
Mock treated	100%	100%
Mock depleted	100%	100%
dGM130 depleted	94.1 ± 4.5% (n = 2)	ND
dp115 depleted	87.9 ± 1.4% (n = 2)	69.5 ± 3%
Brefeldin A treated	10% (n = 1)	ND
dSed5p depleted	11 ± 1% (n = 3)	ND

Transport was measured after depletion of the various proteins for 96 h. The efficiency of transport (initial and steady state) in the mock-treated cells was set at 100%. The results of the steady-state transport efficiency obtained after the various depletions are expressed as a fraction of the "steady-state" efficiency of mock-treated cells. The results of the "initial rate" obtained after dp115 depletion are expressed as a fraction of the "initial" rate of the mock-treated cells. The results are expressed ± SD.

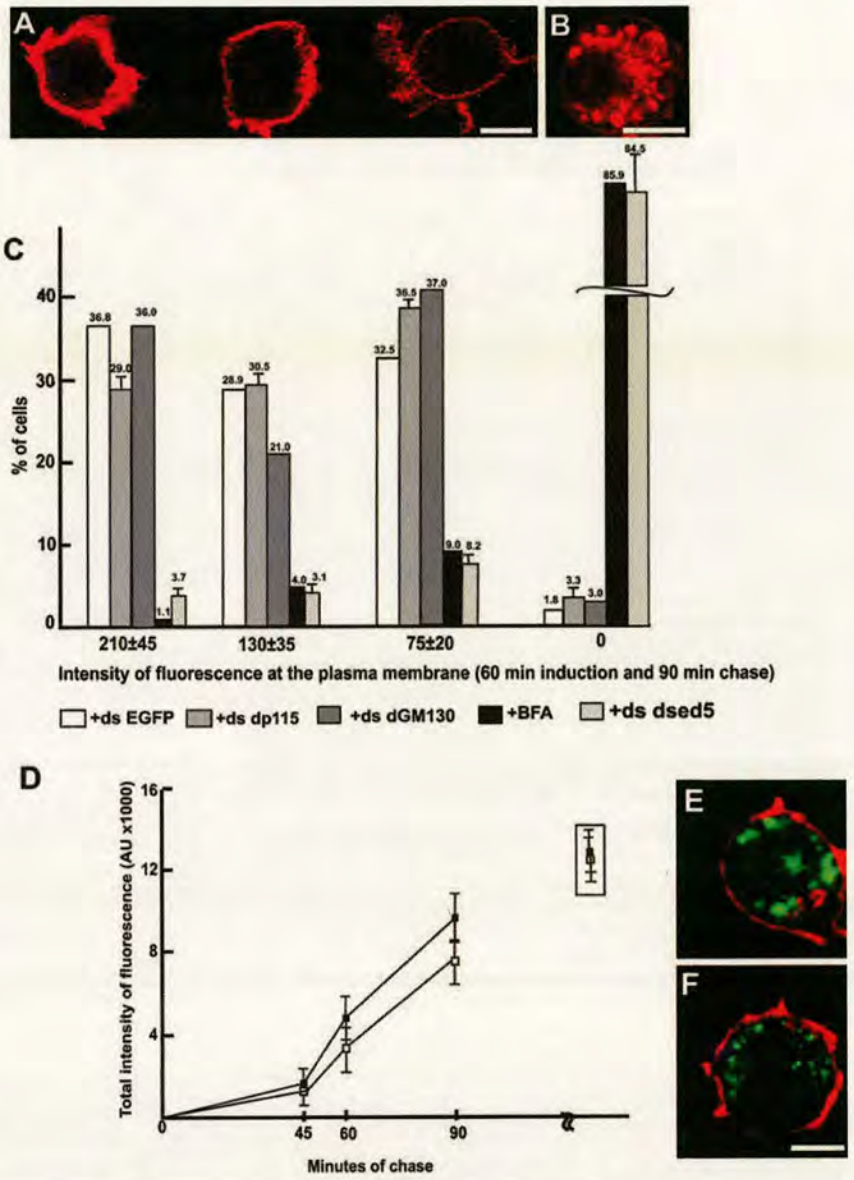

Figure 9. **Effect of protein depletion on Delta anterograde protein transport to the plasma membrane.** Delta S2 cells were incubated for 96 h with ds EGFP, ds dp115, ds dGM130, and ds dsed5, or treated with brefeldin A (BFA) (see Materials and methods). (A) Representation of the three categories of plasma membrane labeling intensity, after a 1-h induction of Delta followed by a 90-min chase. One confocal section is presented. (B) Example of exclusive intracellular Delta labeling. (C) Percentage of cells exhibiting the three different intensities of plasma membrane or exclusive intracellular labeling after Delta induction for 1 h followed by 90 min of chase. Results obtained with mock-depleted cells (+ds EGFP), cells depleted of dp115 (+ds dp115), dGM130 (+ds dGM130), or dSed5p (+ds dsed5), or cells treated with brefeldin A are expressed as the percentage of total number of cells examined. The error bars represent the SD. (D) Initial rate of transport in dp115-depleted (empty symbols) and mock-depleted (filled symbols) cells induced for 25 min followed by 45, 60, and 90 min of chase. The intensity of Delta labeling at the plasma membrane was estimated as described in the Materials and methods and plotted against the chase time. The boxed results represent the total intensity obtained after a 1-h induction and 90-min chase. Immunofluorescence picture of a mock-depleted cell (E) with a control dSec23p pattern (green) and Delta at the plasma membrane (red), and of a dp115-depleted cell (F) with a fragmented dSec23p pattern (green) and the same amount of Delta at the plasma membrane (red). One confocal section is presented. Bar, 5 μm.

Golgi ribbon upon depletion of p115 by antibody injection (Alvarez et al., 1999; Puthenveedu and Linstedt, 2001).

What could be the mechanism? Intracellular transport could be inhibited in dp115-depleted cells, and transport intermediates could accumulate and create the membrane clusters. In mammalian cells, p115 has been shown to have a role in intracellular transport by at least three mechanisms. First, it forms a complex with GM130 on the Golgi cisternae, and giantin on the COPI vesicles, that helps the vesicles to be in close proximity to their target membrane, enhancing docking efficiency and fusion (Nakamura et al., 1997; Sönnichsen et al., 1998). Second, p115 is recruited by activated rab1 onto the COPII budding vesicles, priming them for fusion (Allan et al., 2000). Third, p115 has recently been shown to catalytically promote the syntaxin5/Gos28 SNAREpin formation, suggesting a direct role in vesicle docking and fusion (Shorter et al., 2002). Given the significant homology between dp115 and its mammalian counterpart, dp115 could have an equivalent role in intracellular transport. However, we found that anterograde intracellular transport was largely unaffected (see below), suggesting that as a sole mechanism, the reduction of docking/fusion of ER-derived transport vesicles is unlikely to be sufficient to explain the observed Golgi breakdown.

Mammalian p115 has also been involved in the building and maintenance of the Golgi stacks, independent of its role in transport (Puthenveedu and Linstedt, 2001; Shorter and Warren, 2002). First, in vitro NSF-mediated rebuilding of Golgi cisternae was shown to require p115 (Rabouille et al., 1995) (though that could due to its role in SNARE pairing). p115 was also involved in the in vitro stacking of the p97-mediated Golgi cisternae (Shorter and Warren, 1999). Last, it has been identified as a binding partner of GM130 in the GM130/GRASP65 complex (Barr et al., 1998). This tripar-

tite complex is proposed to be involved in the stacking of Golgi cisternae (Barr et al., 1997; Linstedt, 1999).

dp115 could be involved in a similar complex. Our unpublished results show that dp115 and dGM130 interact genetically and could therefore form a complex, perhaps with dGRASP, the single homologue of GRASP65 and 55. If the stacking mechanism were impaired by the removal of dp115, this would affect the morphology of the Golgi area. However, we did not observe single cisternae, suggesting that dp115 might have an additional role in the maintenance of the cisternae themselves, maybe in preventing their fission into smaller fragments. Furthermore, we have shown that depletion of dGM130 does not affect Golgi stack architecture, in agreement with Puthenveedu and Linstedt (2001) and Vasile et al. (2003). That dGM130, and its mammalian counterpart, has a direct role in the structure of the Golgi stack remains to be shown.

Depletion of dp115 affects tER organization

The alteration in the tER organization that we demonstrated in S2 cells depleted of dp115 could contribute to the breakdown of the Golgi stack architecture (see Introduction; Rossanese et al., 1999; Ward et al., 2001). Instead of the focused organization observed in control cells, the tERs were scattered into a multitude of smaller sites in dp115-depleted S2 cells. The organization of the tER/Golgi stacks in our mock-treated cells was reminiscent of that in *Pichia pastoris* (see Fig. 6 B in Rossanese et al., 1999), whereas in dp115-depleted S2 cells, it resembles *S. cerevisiae* (see Fig. 5 in Rossanese et al., 1999). Given our results, a differential localization of Uso1p or a binding partner between *Pichia* and *S. cerevisiae* could perhaps explain the difference in the organization of their exocytic pathways.

dp115 could therefore only have a role in tER organization. If that were the case, the dispersion of the tER sites would precede the change in the Golgi stack. Despite intensive searching for such profiles, only a very small percentage of cells fit these criteria, and to the same extent as cells in which the Golgi stack organization was lost while still exhibiting a normal tER pattern. Of course, the effect of the tER disorganization on the Golgi stack morphology could be very rapid. Only video microscopy could lead to a definitive answer on that issue. Nevertheless, this result suggests that dp115 is involved in Golgi stack morphology independently of its role in tER organization.

We propose that in *Drosophila*, dp115 has a role in both tER and Golgi stack organization. dp115 could be involved in at least two different complexes, one in the tERs (with unknown partners; Nelson et al., 1998) and one in the Golgi stacks (with perhaps dGM130). These two complexes could either form part of a common matrix underlying both the tERs and the Golgi stacks, as is the case in *Pichia* (Mogelsvang et al., 2003). The fact that in cells depleted of dSed5p, the Golgi stacks are completely vesiculated while the tER organization is intact leads us to propose that there are two independent matrices that have dp115 as a common component. Furthermore, it has been proposed that tERs and Golgi stacks would operate as a positive feedback loop on each other's organization by exchanging membrane and molecules (Hammond and Glick, 2000). dp115 could be an important part of this exchange program.

The dispersion of the tERs could also contribute to Golgi stack breakdown, by allowing the dispersion of budded vesicles that would not participate in the homeostasis/building of Golgi stacked cisternae. Whether Golgi stacks can form in cells comprising dispersed tER sites remains to be shown.

Intracellular transport is only marginally reduced in cells depleted of dp115

The anterograde protein transport in cells depleted of dp115, in which both the Golgi stacks and the tER sites are disorganized, was only marginally affected, shown by two independent assays. Supporting this result, cell proliferation was not affected in dp115 depletion (unpublished data), suggesting that, as for the protein markers used in our experiments, endogenous proteins were likely to be transported as efficiently in depleted cells.

This result is different from those recently published where the injection of a p115 antibody in mammalian cells disrupts the Golgi ribbon and strongly inhibits the ER to Golgi transport (Alvarez et al., 1999, 2001). Furthermore, the injection of a GM130 cDNA encoding a form of GM130 lacking its p115 binding domain also inhibited anterograde transport by 65% (Seemann et al., 2000b). The same holds true for the depletion of dGM130 that did not lead to an inhibition of intracellular transport in our assay, contrary to mammalian cell studies (Alvarez et al., 2001). These differences could be explained by the methodology used for the depletion or perhaps suggest that dp115 and dGM130, unlike their mammalian counterparts, do not have a role in intracellular transport.

However, we find it quite surprising. A strong structural similarity between dp115 and mammalian p115 exists. The SNARE motif identified in mammalian SNARES (Weimbs et al., 1997) is also present in dp115 (amino acids 664–729; unpublished data), suggesting that like its mammalian counterpart, it could also catalyze SNAREpin assembly between dSed5p and dGos28, which also contains a SNARE motif (Weimbs et al., 1997; unpublished data). Given that the role of p115 is catalytic at least in vitro, a trace amount of dp115 could serve its function in transport. Although we show that the dp115 mRNA and protein were successfully depleted, we think that trace amounts of protein remain, a limitation of RNAi techniques. Therefore, we instead conclude that the role of dp115 in contributing to the Golgi stack structure and tER organization can be separated from its role in intracellular transport.

We show here, as is the case in yeast, that *Drosophila* intracellular transport can be sustained by more than one type of exocytic pathway, including dispersed tERs and fragmented Golgi stacks. Clearly, smaller and multiple tER sites and Golgi clusters of vesicles and tubules can efficiently perform this transport function. This could explain the existence of developmental stages in *Drosophila* in which cells do not exhibit Golgi stacks but exhibit clusters of vesicles and tubules instead, as in the case of the third instar larval imaginal discs (Kondylis et al., 2001). Perhaps this flexibility is not offered to mammalian cells, with their unique organization of the

Golgi complex involving the formation of the single copy Golgi ribbon.

Thus, what is the role of Golgi stacks if efficient anterograde transport can take place in their absence? Golgi stacks (but not Golgi clusters) could have a role in retrograde transport, in the proper and complete maturation of protein-born O- and N-linked oligosaccharide moieties and the addition of sorting signals. This is for further investigation.

Materials and methods

Double-stranded RNA

dp115 cDNA was cloned by screening an embryonic cDNA library with a DNA probe made using the EST LD41079. The dp115 cDNA (1P2C1) was used to PCR a 682-bp fragment with flanking T7 RNA polymerase binding sites using the 5′ primer TAATACGACTCACTATAGGGAGA(T7)-acccagaataagac and the 3′ primer T7-tcaaaaaggcggtca. The 774-bp T7-dGM130 template was obtained by PCR from the clone p5.6KK (provided by Terry Orr-Weaver, Whitehead Institute, Cambridge, MA) containing the MeiS332 gene (Kerrebrock et al., 1995) and the coding sequence of dGM130 using the 5′ primer T7-cgccagcaacaacaa and the 3′ primer T7-tgctccttgtcctgcgtt. The 635-bp T7/T3-EGFP template (gift from Thomas Vaccari, European Molecular Biology Laboratory [EMBL], Heidelberg, Germany) was obtained using the 5′ primer T7-taaacggccacaagttcag and the 3′ primer AATTAACCCTCACTAAAGGGAGA(T3)-gtgatcgcgcttctcgttg. Finally, the 733-bp T7/T3-dsed5 template (gift from Thomas Vaccari) was obtained using the 5′ primer T7-gcttatttgatgacagac and the 3′ primer T3-aatatgagaacgccgaag.

The various T7 and T3 templates were purified from the agarose gel using the GFX PCR DNA and gel band purification kit (Amersham Biosciences). The purified products were used as templates for dsRNA synthesis using the MEGASCRIPT T7 and T3 transcription kit (Ambion) according to manufacturer's standard protocol.

Cell cultures and dsRNA interference

S2 cells were grown in Schneider's insect medium supplemented with 10% heat-inactivated and insect-tested FBS at 27°C in a humidified atmosphere. Delta-WTNdeMYC S2 cells (Delta S2 cells) were a gift from Kris Klueg (Indiana University, Bloomington, IN). Delta S2 is a stable cell line expressing the full-length Delta protein at the plasma membrane upon induction with 1 mM $CuSO_4$ (Klueg et al., 1998). The Delta S2 cell line was cultured in the presence of 2×10^{-6} M methotrexate (ICN Biomedicals).

RNAi was performed in both cell lines as described in Clemens et al. (2000). 1,000,000 cells/well in DES serum-free medium (Invitrogen) were incubated with 20–30 μg of the various dsRNAs for 30 min at room temperature followed by the addition of 2 ml of Schneider's medium containing FBS and methotrexate in the case of Delta S2 cells. Mock-treated and mock-depleted cells were treated in the same way except that no dsRNA or ds EGFP was added, respectively. They were considered as controls.

Antibodies

dGM130 was detected using a rabbit polyclonal antibody directed against the first 73 amino acids of human GM130 (MLO7; gift from Martin Lowe), as described in Kondylis et al. (2001). dp115 was detected with a rabbit polyclonal antibody raised against the peptide (G)CSKLAEVSRHEAYSRA, which corresponds to amino acids 584–599 from dp115 (Biosynthesis), and purified against the peptide coupled to EAH–Sepharose 4B (Amersham Biosciences) activated by Sulfo-MBS cross-linker (Pierce Chemical Co.) (dp115/584). dSec23p was detected using a rabbit polyclonal antibody raised against the first 18 amino acids of mammalian Sec23p (Affinity BioReagents, Inc.), sharing 90% identity with the equivalent peptide of dSec23p. d120kd was detected with a mouse monoclonal antibody recognizing a 120-kD integral Golgi membrane protein in *Drosophila* (Calbiochem). dSed5p was detected using a rabbit polyclonal antibody raised against mammalian syntaxin 5 (JSEE1; gift from Martin Lowe). Delta was detected using C594.9B, a mouse monoclonal antibody raised against its extracellular domain (DSHB; University of Iowa).

Western blotting

The same number of cells (typically from 1,000,000 to 2,500,000) incubated with or without dsRNA for each time point was harvested, spun, and homogenized in 25 μl buffer containing 20 mM Tris-HCl, 1 mM EDTA, 10 mM $MgCl_2$, 10 mM KCl, 10 mM NaCl, 1 mM DTT, 0.23 M sucrose, and 1% Triton X-100 and protease inhibitors using a motorized pestle. In the case of dp115 detection, cells were homogenized in the absence of Triton and with protease inhibitor cocktail (Roche). The SDS sample buffer was added to a 1× final concentration. The membrane fraction was prepared as follows. 10,000,000 cells were cracked using a 30-gauge needle in the homogenization buffer and protease inhibitors. After a short spin to remove cell debris and nuclei, the extract was spun for 1 h at 100,000 *g* to separate the cytosol from the membrane. The membrane pellet was recovered in 40 μl 1× SDS sample buffer. Total extract of one third instar *Drosophila* larvae and 20 embryos was prepared by homogenization using a motorized pestle in 40 μl of the homogenization buffer. The total extract, the membrane pellets, and 4% of the cytosolic fraction were fractionated on a 10% acrylamide gel and detected by Western blots using MLO7, the affinity-purified dp115 antibody, JSEE1, Sec23p antibody, and d120kd antibody, followed by the appropriate secondary antibody coupled to HRP (Vector Laboratories). ECL (Amersham Biosciences) was used for the visualization of the bands.

RT-PCR

Total RNA was extracted from 1,000,000 S2 cells using the Purescript RNA isolation kit (Flowgen). The RT reactions were performed with the Superscript II reverse transcriptase kit (Invitrogen) according to the company's protocol and using 1 μg of total RNA.

The RT products were diluted 1/20 and were used in the PCR reaction with the 5′ primer agttcctgaagagtggcatcaa and the 3′ primer gctatctggacgaatacgat for dp115, leading to a 414-bp fragment (corresponding to the 5′ end of the dp115 gene), and the 5′ primer gtggaaaaggtggcaaagtgaa and 3′ primer atgctggtgacaacaagaa for histone 2A (H2A), leading to a 213-bp fragment. The four primers were added in the same reaction.

Conventional EM

Cells were fixed for 2 h in 1% glutaraldehyde in 0.2 M phosphate buffer (pH 7.4) and processed for conventional EM as described in Kondylis et al. (2001).

IEM

Control or depleted S2 cells (96 h) were fixed in 2% PFA and 0.2% glutaraldehyde (GA) (2 h at room temperature) or 4% PFA alone (overnight at 4°C) in 0.2 M phosphate buffer, pH 7.4. Oregon R third instar salivary glands were dissected as described in Dunne et al. (2002), fixed in 2% PFA and 0.2% GA overnight at 4°C in the same buffer as described above. Both cells and tissues were processed for IEM as described previously (Liou et al., 1996). In brief, immunolabeling was performed using the described primary antibodies followed directly by protein A conjugated to gold particles (protein A gold), in the case of rabbit antibodies. In the case of a mouse antibody, a bridging step of rabbit anti–mouse IgG was used followed by protein A gold.

Stereology

The Golgi area was defined by the Golgi stacked cisternae and immediate surrounding vesicles and tubules. When Golgi stacks were not observed, the Golgi area was defined as the clusters of vesicles and tubules occupying the position where Golgi stacks are normally found, nested near an ER cisterna in 80% of the cases. Vesicles, tubules, cisternae, and Golgi stacks are defined in Kondylis et al. (2001).

The percentage of cell profiles exhibiting at least one Golgi stack was estimated by randomly analyzing under the transmission electron microscope >100 cell profiles taken from at least two grids and two different experiments. The percentage of membrane in cisternae, tubules, or vesicles per Golgi area and the surface density of the Golgi area and total cisternae were estimated as described in Kondylis et al. (2001). The linear density was determined by the intersection method.

Delta transport assay

Delta S2 cells plated on glass coverslips were treated with dsRNA for given periods of time to deplete the protein of interest, typically 96 h. 1 mM $CuSO_4$ was added to the culture media to induce the production of Delta. After 25 min at 27°C, the media were replaced with new Schneider's media without $CuSO_4$, and the transport of Delta to the plasma membrane was chased for up to 90 min (initial transport of Delta). We also induced the synthesis of Delta for 60 min followed by a chase of 90 min (steady-state transport of Delta). Delta transport was also measured in cells treated with 50 μM brefeldin A for 30 min at 37°C, followed by induction with $CuSO_4$ and chase at 27°C in the presence of brefeldin A.

Indirect immunofluorescence

S2 cells were fixed for 20 min in 3% PFA in PBS at room temperature and processed for immunofluorescence (Rabouille et al., 1999) after permeabi-

lization with Triton. dSec23p and d120kd were detected using the antibodies described above followed by anti–rabbit IgG coupled to Alexa 488 and anti–mouse IgG coupled to Alexa 568 (Molecular Probes), respectively. Delta S2 cells were processed in the same way. Delta protein was labeled using C594.9B antibody followed by an anti–mouse IgG coupled to Texas red (Vector Laboratories). Cells were viewed under a Leica confocal microscope. A series of 30 sections through the cells were collected, and projections were reconstituted and presented unless otherwise stated.

Quantitation of Delta transport to the plasma membrane

Equatorial sections of random cells from each sample were captured with the Leica confocal microscope using a 63× water lens. Control cells were analyzed first so that the highest intensity of labeling was within the dynamic range of the laser. This set up was maintained for the analysis of the depleted cells.

The surface labeling intensity was estimated using the Leica software, which is able to measure and display the intensity of labeling along a line that is drawn perpendicular to the plasma membrane. In this way, the intensity peak as well as the thickness of the labeled plasma membrane were estimated. Typically, cells induced for 1 h followed by a 90-min chase displayed a large range of intensity and were ranked into three categories: 210 ± 45, 130 ± 35, and 75 ± 20 intensity units per plasma membrane cross section. The intensity was essentially constant around the perimeter of the cell.

About 300–500 cells for each condition were quantitated, and the results were expressed as a percentage of cells exhibiting each of the three categories of intensity. The total intensity in each condition was calculated using an arithmetic sum $\Sigma I \times N \times p$, where I is the intensity, N is the percentage of cells exhibiting intensity I, and p is the perimeter length of the plasma membrane. The perimeter length was not taken into account because both control and depleted cells had similar mean diameters and their almost spherical shape did not change. The total intensity was considered as 100% for the control cells, while the efficiency of intracellular transport in treated/depleted cells was expressed as a ratio of their total intensity versus that of the control cells. The same procedure was reproduced for cells induced for 25 min and chased for 45, 60, and 90 min. Again the intensity of labeling at the plasma membrane was measured as described above and ranked into three categories that vary slightly with the time of chase. The total intensity was calculated as an absolute value.

Online supplemental material

The supplemental material (Figs. S1–S4) is available at http://www.jcb.org/cgi/content/full/jcb.200301136/DC1. A concise description of the data presented in each supplementary figure is introduced upon citation in the text. Details on the experimental procedure and further comments on data reported can be found in the legends.

We wish to thank Martin Lowe for his gift of antibodies, Kris Klueg for her gift of the Delta cell line, Terry Orr-Weaver for the cDNA clone containing dGM130 sequence, Jonathan Dunne for critically reading and editing the manuscript, Elly van Donselaar for her help with IEM, Dagmar Zeuschner for her help with the affinity purification of the dp115 antiserum, and Thomas Vaccari and Anne Ephrussi (EMBL) for their gift of EGFP and dsed5 primers. We acknowledge the use of Flybase, the Berkeley *Drosophila* genome project, and Gadfly.

V. Kondylis was supported by the Darwin Trust of Edinburgh. C. Rabouille was supported by a fellowship from the Medical Research Council (UK) and by the Department of Cell Biology, Utrecht.

Submitted: 30 January 2003
Revised: 15 May 2003
Accepted: 3 June 2003

References

Allan, B.B., B.D. Moyer, and W.E. Balch. 2000. Rab1 recruitment of p115 into a cis-SNARE complex: programming budding COPII vesicles for fusion. *Science.* 289:444–448.

Alvarez, C., H. Fujita, A. Hubbard, and E. Sztul. 1999. ER to Golgi transport: requirement for p115 at a pre-Golgi VTC stage. *J. Cell Biol.* 147:1205–1222.

Alvarez, C., R. Garcia-Mata, H.P. Hauri, and E. Sztul. 2001. The p115-interactive proteins GM130 and giantin participate in endoplasmic reticulum-Golgi traffic. *J. Biol. Chem.* 276:2693–2700.

Banfield, D.K., M.J. Lewis, C. Rabouille, G. Warren, and H.R. Pelham. 1994. Localization of Sed5, a putative vesicle targeting molecule, to the cis-Golgi network involves both its transmembrane and cytoplasmic domains. *J. Cell Biol.* 127:357–371.

Bannykh, S.I., T. Rowe, and W.E. Balch. 1996. The organization of endoplasmic reticulum export complexes. *J. Cell Biol.* 135:19–35.

Barlowe, C., L. Orci, T. Yeung, M. Hosobuchi, S. Hamamoto, N. Salama, M.F. Rexach, M. Ravazzola, M. Amherdt, and R. Schekman. 1994. COPII: a membrane coat formed by Sec proteins that drive vesicle budding from the endoplasmic reticulum. *Cell.* 77:895–907.

Barr, F.A., M. Puype, J. Vandekerckhove, and G. Warren. 1997. GRASP65, a protein involved in the stacking of Golgi cisternae. *Cell.* 91:253–262.

Barr, F.A., N. Nakamura, and G. Warren. 1998. Mapping the interaction between GRASP65 and GM130, components of a protein complex involved in the stacking of Golgi cisternae. *EMBO J.* 17:3258–3268.

Bevis, B.J., A.T. Hammond, C.A. Reinke, and B.S. Glick. 2002. De novo formation of transitional ER sites and Golgi structures in *Pichia pastoris*. *Nat. Cell Biol.* 4:750–756.

Clemens, J.C., C.A. Worby, N. Simonson-Leff, M. Muda, T. Maehama, B.A. Hemmings, and J.E. Dixon. 2000. Use of double-stranded RNA interference in *Drosophila* cell lines to dissect signal transduction pathways. *Proc. Natl. Acad. Sci. USA.* 97:6499–6503.

Dirac-Svejstrup, A.B., J. Shorter, M.G. Waters, and G. Warren. 2000. Phosphorylation of the vesicle-tethering protein p115 by a casein kinase II–like enzyme is required for Golgi reassembly from isolated mitotic fragments. *J. Cell Biol.* 150:475–487.

Dunne, J.C., V. Kondylis, and C. Rabouille. 2002. Ecdysone triggers the expression of Golgi genes in *Drosophila* imaginal discs via broad-complex. *Dev. Biol.* 245:172–186.

Hammond, A.T., and B.S. Glick. 2000. Dynamics of transitional endoplasmic reticulum sites in vertebrate cells. *Mol. Biol. Cell.* 11:3013–3030.

Glick, B.S. 2002. Can the Golgi form de novo? *Nat. Rev. Mol. Cell Biol.* 3:615–619.

Kerrebrock, A.W., D.P. Moore, J.S. Wu, and T.L. Orr-Weaver. 1995. Mei-S332, a *Drosophila* protein required for sister-chromatid cohesion, can localize to meiotic centromere regions. *Cell.* 83:247–256.

Klueg, K.M., T.R. Parody, and M.A. Muskavitch. 1998. Complex proteolytic processing acts on Delta, a transmembrane ligand for Notch, during *Drosophila* development. *Mol. Biol. Cell.* 9:1709–1723.

Kondylis, V., S.E. Goulding, J.C. Dunne, and C. Rabouille. 2001. The biogenesis of the Golgi stacks in the imaginal discs of *Drosophila melanogaster*. *Mol. Biol. Cell.* 12:2308–2327.

Linstedt, A.D. 1999. Stacking the cisternae. *Curr. Biol.* 9:R893–R896.

Liou, W., H.J. Geuze, and J.W. Slot. 1996. Improving structural integrity of cryosections for immunogold labeling. *Histochem. Cell Biol.* 106:41–58.

Mogelsvang, S., N. Gomez-Ospina, J. Soderholm, B.S. Glick, and L.A. Staehelin. 2003. Tomographic evidence for continuous turnover of Golgi cisternae in *Pichia pastoris*. *Mol. Biol. Cell.* 14:2277–2291.

Morsomme, P., and H. Riezman. 2002. The Rab GTPase Ypt1p and tethering factors couple protein sorting at the ER to vesicle targeting to the Golgi apparatus. *Dev. Cell.* 2:307–317.

Munro, S., and M. Freeman. 2000. The Notch signalling regulator fringe acts in the Golgi apparatus and requires the glycosyltransferase signature motif DXD. *Curr. Biol.* 10:813–820.

Nakamura, N., M. Lowe, T.P. Levine, C. Rabouille, and G. Warren. 1997. The vesicle docking protein p115 binds GM130, a cis-Golgi matrix protein, in a mitotically regulated manner. *Cell.* 89:445–455.

Nelson, D.S., C. Alvarez, Y.S. Gao, R. Garcia-Mata, E. Fialkowski, and E. Sztul. 1998. The membrane transport factor TAP/p115 cycles between the Golgi and earlier secretory compartments and contains distinct domains required for its localization and function. *J. Cell Biol.* 143:319–331.

Orci, L., M. Ravazzola, P. Meda, C. Holcomb, H.P. Moore, L. Hicke, and R. Schekman. 1991. Mammalian Sec23p homologue is restricted to the endoplasmic reticulum transitional cytoplasm. *Proc. Natl. Acad. Sci. USA.* 88:8611–8615.

Panin, V.M., L. Shao, L. Lei, D.J. Moloney, K.D. Irvine, and R.S. Haltiwanger. 2002. Notch ligands are substrates for protein O-fucosyltransferase-1 and Fringe. *J. Biol. Chem.* 277:29945–29952.

Preuss, D., J. Mulholland, A. Franzusoff, N. Segev, and D. Botstein. 1992. Characterization of the *Saccharomyces* Golgi complex through the cell cycle by immunoelectron microscopy. *Mol. Biol. Cell.* 3:789–803.

Puthenveedu, M.A., and A.D. Linstedt. 2001. Evidence that Golgi structure depends on a p115 activity that is independent of the vesicle tether compo-

nents Giantin and GM130. *J. Cell Biol.* 155:227–238.

Rabouille, C., T.P. Levine, J.M. Peters, and G. Warren. 1995. An NSF-like ATPase, p97, and NSF mediate cisternal regrowth from mitotic Golgi fragments. *Cell.* 82:905–914.

Rabouille, C., D.A. Kuntz, A. Lockyer, R. Watson, T. Signorelli, D.R. Rose, M. Van den Heuvel, and D.B. Roberts. 1999. The *Drosophila GMII* gene encodes Golgi α-mannosidase II. *J. Cell Sci.* 112:3319–3330.

Rossanese, O.W., J. Soderholm, B.J. Bevis, I.B. Sears, J. O'Connor, E.K. Williamson, and B.S. Glick. 1999. Golgi structure correlates with transitional endoplasmic reticulum organization in *Pichia pastoris* and *Saccharomyces cerevisiae*. *J. Cell Biol.* 145:69–81.

Sapperstein, S.K., D.M. Walter, A.R. Grosvenor, J.E. Heuser, and M.G. Waters. 1995. p115 is a general vesicular transport factor related to the yeast endoplasmic reticulum to Golgi transport factor uso1p. *Proc. Natl. Acad. Sci. USA.* 92:522–526.

Seemann, J., E. Jokitalo, M. Pypaert, and G. Warren. 2000a. Matrix proteins can generate the higher order architecture of the Golgi apparatus. *Nature.* 407: 1022–1026.

Seemann, J., E. Jokitalo, and G. Warren. 2000b. The role of the tethering proteins p115 and GM130 in transport through the Golgi apparatus in vivo. *Mol. Biol. Cell.* 11:635–645.

Shorter, J., and G. Warren. 1999. A role for the vesicle tethering protein, p115, in the post-mitotic stacking of reassembling Golgi cisternae in a cell-free system. *J. Cell Biol.* 146:57–70.

Shorter, J., and G. Warren. 2002. Golgi architecture and inheritance. *Annu. Rev. Cell Dev. Biol.* 18:379–420.

Shorter, J., M.B. Beard, J. Seemann, A.B. Dirac-Svejstrup, and G. Warren. 2002. Sequential tethering of Golgins and catalysis of SNAREpin assembly by the vesicle-tethering protein p115. *J. Cell Biol.* 157:45–62.

Sönnichsen, B., M. Lowe, T. Levine, E. Jämsa, A.B. Dirac-Svejstrup, and G. Warren. 1998. A role for giantin in docking COPI vesicles to Golgi membranes. *J. Cell Biol.* 140:1013–1021.

Stanley, H., J. Botas, and V. Malhotra. 1997. The mechanism of Golgi segregation during mitosis is cell type-specific. *Proc. Natl. Acad. Sci. USA.* 94:14467–14470.

Vasile, E., T. Perez, N. Nakamura, and M. Krieger. 2003. Structural integrity of the Golgi is temperature sensitive in conditional-lethal mutants with no detectable GM130. *Traffic.* 4:254–272.

Ward, T.H., R.S. Polishchuk, S. Caplan, K. Hirschberg, and J. Lippincott-Schwartz. 2001. Maintenance of Golgi structure and function depends on the integrity of the ER export. *J. Cell Biol.* 155:557–570.

Weimbs, T., S.H. Low, S.J. Chapin, K.E. Mostov, P. Bucher, and K. Hofmann. 1997. A conserved domain is present in different families of vesicular fusion proteins: a new superfamily. *Proc. Natl. Acad. Sci. USA.* 94:3046–3051.